CURRENT CHALLENGES FOR TARGETING BROWN FAT THERMOGENESIS TO COMBAT OBESITY

EDITED BY: Takeshi Yoneshiro, Matthias Johannes Betz, Patrick C. N. Rensen and Rosalia Rodriguez-Rodriguez

PUBLISHED IN: Frontiers in Endocrinology

frontiers Research Topics

frontiers

ISSN 1664-8714
ISBN 978-2-88966-282-1
DOI 10.3389/978-2-88966-282-1

About Frontiers

Frontiers is more than just an open-access publisher of scholarly articles: it is a pioneering approach to the world of academia, radically improving the way scholarly research is managed. The grand vision of Frontiers is a world where all people have an equal opportunity to seek, share and generate knowledge. Frontiers provides immediate and permanent online open access to all its publications, but this alone is not enough to realize our grand goals.

Frontiers Journal Series

The Frontiers Journal Series is a multi-tier and interdisciplinary set of open-access, online journals, promising a paradigm shift from the current review, selection and dissemination processes in academic publishing. All Frontiers journals are driven by researchers for researchers; therefore, they constitute a service to the scholarly community. At the same time, the Frontiers Journal Series operates on a revolutionary invention, the tiered publishing system, initially addressing specific communities of scholars, and gradually climbing up to broader public understanding, thus serving the interests of the lay society, too.

Dedication to Quality

Each Frontiers article is a landmark of the highest quality, thanks to genuinely collaborative interactions between authors and review editors, who include some of the world's best academicians. Research must be certified by peers before entering a stream of knowledge that may eventually reach the public - and shape society; therefore, Frontiers only applies the most rigorous and unbiased reviews.
Frontiers revolutionizes research publishing by freely delivering the most outstanding research, evaluated with no bias from both the academic and social point of view. By applying the most advanced information technologies, Frontiers is catapulting scholarly publishing into a new generation.

What are Frontiers Research Topics?

Frontiers Research Topics are very popular trademarks of the Frontiers Journals Series: they are collections of at least ten articles, all centered on a particular subject. With their unique mix of varied contributions from Original Research to Review Articles, Frontiers Research Topics unify the most influential researchers, the latest key findings and historical advances in a hot research area! Find out more on how to host your own Frontiers Research Topic or contribute to one as an author by contacting the Frontiers Editorial Office: researchtopics@frontiersin.org

CURRENT CHALLENGES FOR TARGETING BROWN FAT THERMOGENESIS TO COMBAT OBESITY

Topic Editors:
Takeshi Yoneshiro, The University of Tokyo, Japan
Matthias Johannes Betz, University Hospital of Basel, Switzerland
Patrick C. N. Rensen, Leiden University Medical Center, Netherlands
Rosalia Rodriguez-Rodriguez, International University of Catalonia, Spain

Citation: Yoneshiro, T., Betz, M. J., Rensen, P. C. N., Rodriguez-Rodriguez, R., eds. (2020). Current Challenges for Targeting Brown Fat Thermogenesis to Combat Obesity. Lausanne: Frontiers Media SA. doi: 10.3389/978-2-88966-282-1

Table of Contents

frontiers in Endocrinology

EDITORIAL
published: 27 October 2020
doi: 10.3389/fendo.2020.600341

Editorial: Current Challenges for Targeting Brown Fat Thermogenesis to Combat Obesity

Takeshi Yoneshiro[1,2]*, *Rosalía Rodríguez-Rodríguez*[3], *Matthias Johannes Betz*[4] *and Patrick C. N. Rensen*[5,6]

[1] Division of Metabolic Medicine, Research Center for Advanced Science and Technology, The University of Tokyo, Tokyo, Japan, [2] Diabetes Center, University of California, San Francisco, San Francisco, CA, United States, [3] Basic Sciences Department, Faculty of Medicine and Health Sciences, Universitat Internacional de Catalunya, Barcelona, Spain, [4] Department of Endocrinology, Diabetes and Metabolism, University Hospital Basel and University of Basel, Basel, Switzerland, [5] Division of Endocrinology, Department of Medicine, Leiden University Medical Center, Leiden, Netherlands, [6] Einthoven Laboratory for Experimental Vascular Medicine, Leiden University Medical Center, Leiden, Netherlands

Keywords: brown adipose tissue, beige adipocytes, energy metabolism, thermogenesis, obesity, type 2 diabetes

Editorial on the Research Topic

Current Challenges for Targeting Brown Fat Thermogenesis to Combat Obesity

INTRODUCTION

Just over a decade has passed since metabolically active brown adipose tissue (BAT) was unequivocally identified in healthy adult humans. Since then, researchers have provided evidence of expression of the thermogenic molecule uncoupling protein 1 (UCP1) in human BAT, as well as its energy dissipating capacity. Additionally, clinical cross-sectional analysis suggested that a decline in BAT activity with aging, as judged from [^{18}F]FDG-PET/CT, coincides with the development of obesity and insulin resistance. These major observations provided a rationale to investigate BAT as a potential target for preventing obesity. Indeed, several studies have demonstrated that cold exposure and adrenomimetic agents strongly activate BAT thermogenesis, and thus energy expenditure in humans. However, the extent to which stimulating BAT thermogenesis decreases adiposity in humans remains unclear. Moreover, therapeutic strategies aimed at general stimulation of the sympathetic nervous system (SNS) and adrenergic receptors involved may not be applicable for obese and diabetic patients, because of potential negative side-effects on cardiovascular function.

While implementation in humans remains challenging, recent studies in mice have yielded insights in molecular mechanisms underlying thermogenic regulation of brown and brown-like (brite/beige) adipocytes, highlighting their ability to reduce insulin resistance and atherosclerosis (1). These include identification of UCP1-independent thermogenesis as well as peripheral organ-derived endocrine factors and metabolites capable of triggering adipocyte thermogenesis. Activating these non-canonical mechanisms through genetic manipulation or pharmacological agents suppresses obesity and its associated complications in mice. The major challenge remains translating preclinical scientific advances to humans. To bridge basic research with clinical investigation, this Research Topic reviews the current advances in human BAT pathophysiology, novel molecular mechanisms regulating adipose thermogenesis, and remaining challenges in this field.

OPEN ACCESS

Edited and reviewed by:
Katherine Samaras,
St Vincent's Hospital Sydney, Australia

***Correspondence:**
Takeshi Yoneshiro
yoneshiro.takeshi@lsbm.org

Specialty section:
This article was submitted to Obesity, a section of the journal Frontiers in Endocrinology

Received: *29 August 2020*
Accepted: *07 October 2020*
Published: *27 October 2020*

Citation:
Yoneshiro T, Rodríguez-Rodríguez R, Betz MJ and Rensen PCN (2020) Editorial: Current Challenges for Targeting Brown Fat Thermogenesis to Combat Obesity. Front. Endocrinol. 11:600341. doi: 10.3389/fendo.2020.600341

PHYSIOLOGY AND PATHOLOGY OF BAT

Numerous studies have confirmed the contribution of BAT to cold-induced thermogenesis (CIT) in mice and humans. Additionally, diet-induced thermogenesis (DIT), another component of non-shivering thermogenesis, has demonstrated reliance on BAT in mice—evidence in humans is limited. The review article by Saito et al. gathers the recent advancements in human BAT physiology, focusing on the contribution of BAT to DIT. The authors provide an overview of the mechanisms by which food intake triggers BAT thermogenesis, including the SNS, bile acids, secretin, and ghrelin.

Another physiological stimulus of thermogenesis in BAT and white adipose tissue (WAT) is exercise. Vidal and Stanford provide an overview of the molecular mechanisms underlying exercise-induced adipose thermogenesis. The authors also discuss how exercise-induced release of lipokine 12,13-diHOME from BAT can stimulate fatty acid metabolism in skeletal muscle. Notably, environmental factors, such as ambient temperature, mediate the effects of exercise on adipose thermogenesis. Aldiss et al. demonstrate that in rats, exercise does not induce browning at thermoneutrality but instead induces a muscle-like signature in BAT, which might be relevant to the previously uncharacterized UCP1-independent thermogenesis in BAT. Because of the divergent results between rodents and humans, further studies in both species are needed to fully understand the physiological meaning, molecular mechanisms, and clinical significance of adipose tissue adaptation in response to exercise.

In addition to exercise, intriguingly, certain disease states have also been shown to mediate BAT activity. Increased BAT activity in patients with cancer is a known aspect of cachexia-induced body-weight loss. Conversely, BAT thermogenesis may possibly be impaired in patients with a different disease, narcolepsy type 1, caused by the destruction of orexin-producing neurons in the hypothalamus (Straat et al.). Orexin-producing neurons control the wake-sleep cycle and appetite, but also participate in SNS-mediated BAT activation. Although patients with narcolepsy type 1 exhibit increased adiposity, convincing evidence in humans demonstrating impaired BAT function with narcolepsy type 1 is still lacking.

Chronic inflammation in adipose tissue poses a significant metabolic challenge, as it impairs BAT thermogenesis and exacerbates insulin resistance. Omran and Christian comprehensively review the effect of inflammatory cells, such as macrophages and mast cells, on the function of thermogenic adipocytes. The activity of inflammatory cells is mediated by proinflammatory cytokines, generating an inflammatory microenvironment.

METHODOLOGICAL ADVANCEMENTS

[^{18}F]FDG-PET/CT has emerged as the gold standard for assessing the metabolic activity of BAT in humans. However, given the challenges in performing repeated [^{18}F]FDG-PET/CT including exposure to ionizing radiation, methodological advances to estimate BAT activity are highly desirable.

Wu et al. extensively describe the currently available modalities to non-invasively probe BAT volume and/or metabolic activity, especially focusing on magnetic resonance imaging (MRI) and spectroscopy (MRS) methods. MR techniques have enabled assessment of the lipid content, microstructure, and the mitochondrial oxidative capacity of BAT. The authors also discuss the inherent limitations in quantifying BAT by MR. To this end, Abreu-Vieira et al. demonstrate the fundamental importance of adjusting fat fraction thresholds to accurately determine cold-induced changes in BAT *via* MR. Another novel methodology for estimating BAT in humans is near-infrared time-resolved spectroscopy (NIR_{TRS}), which measures absolute concentration of hemoglobin (Hamaoka et al.). As BAT is highly vascularized, NIR_{TRS} parameters are indicative of BAT volume/activity.

In addition to the aforementioned imaging techniques, BAT functionality might be estimated from the circulating BAT-derived secretome (i.e. "batokines") or microRNAs, although the utility of these metrics is debated. Similarly, BAT-associated metabolites may well be indicative of BAT activity. In this regard, oxygenated polyunsaturated fatty acid metabolites (oxylipins), could be a surrogate marker for BAT activity and/or amount, as Dieckmann et al. show that murine BAT is distinguishable from WAT by oxylipin profiling.

These advances in non-invasive methodology are potentially valuable in performing future cross-sectional studies with large numbers of participants as well as longitudinal studies with repeated BAT measurements, thereby facilitating investigations into BAT biology in humans.

NEW THERMOGENIC MECHANISMS

The identification of novel molecular circuits involved in BAT thermogenesis may lead to the discovery of targetable pathways for the development of practicable pharmacotherapies for adiposity and related cardiometabolic diseases. Recent studies in small rodents have contributed to substantial advances in this regard. While thermogenesis in brown adipocytes largely relies on UCP1 function, brite/beige adipocytes residing in WAT can utilize alternative pathways that are independent of UCP1. Ikeda and Yamada review the current evidence of UCP1-independent thermogenic pathways involved in creatine-substrate cycling and calcium cycling. It remains essential to determine the contribution of non-canonical thermogenesis to whole-body energy homeostasis in humans.

The β-adrenergic receptor (β-AR) is the crucial gatekeeper of adipose thermogenesis. Several studies have unveiled additional signaling pathways mediated by adenosine and mineralocorticoid receptors as reviewed by Pan et al. Subsequently, they introduce β-AR-independent mechanisms by which cold exposure induces a unique type of thermogenic adipocyte with enhanced glucose oxidative capacity, so-called "glycolytic beige", contributing to systemic glucose homeostasis in mice.

New insights also include novel transcription factors and related molecules involved in adipose thermogenesis. Müller et al. identify the orphan nuclear factor estrogen related receptor gamma (ESPRG), and the transcriptional factor PGC1 and ESRR-induced regulator in muscle 1 (PERM1) as modulators of cold-induced browning of

WAT. They show ESPRG and PERM1 positively regulate UCP1 expression and mitochondrial components, respectively.

METABOLITES REGULATE THERMOGENESIS

The SNS is undoubtedly a central regulator of adipose thermogenesis. A concept gaining increasing attention is that non-neuronal systems can also trigger adipose thermogenesis. Indeed, peripheral organ-derived endocrine factors and metabolites can play a role in adipose thermogenesis through transcriptional control and non-genomic post-translational modification. In this context, Herz and Kiefer describe that intracellular retinoids stringently control browning of WAT through the regulation of *Ucp1* transcription and protein retinoylation. Retinoid action can be stimulated by norepinephrine, implying the importance of retinoids in cold-induced adipose thermogenesis.

Moreover, the review by Bast-Habersbrunner et al. provides an in-depth overview of intracellular mechanisms by which cytosolic purine nucleotides control UCP1 function. Purine nucleotides such as ATP, ADP, GTP, and GDP have been proven to be constitutive inhibitors of UCP1-mediated proton conductance. Adrenergic stimulation dramatically reduces cytosolic purine nucleotides, facilitating UCP1-mediated thermogenesis. Further elucidation of the signaling cascade of the adrenergic receptor-mediated control of cytosolic purine nucleotides may help establish approaches to directly modulate BAT thermogenesis.

PERSPECTIVES

It is clear that thermogenic adipocytes and their precursors, once thought monolithic, are composed of various, distinct cell populations (2, 3). For instance, although conventional brite/beige adipocytes arise from $MyoD^-$ progenitors, the glycolytic beige adipocytes arise from $MyoD^+$ progenitors (Pan et al.). Due to the complex heterogeneity, the developmental origin and pathways remain insufficiently understood. A better understanding of this heterogeneity may lead to the development of new approaches to specifically activate certain subpopulations of thermogenic cells without unfavorable side-effects.

In addition, mechanisms governing the generation of precursors committed to thermogenic adipocyte cell fate are still poorly understood. Given the difficulty of obtaining an abundant source of human progenitors for study, pluripotent stem cells (PSCs), as implemented by Yao et al., are promising tools to elucidate such mechanisms. However, several challenges have been presented, including the weak efficacy of thermogenic differentiation, which precludes greater utilization. Another future challenge will be the generation of efficient *in vitro* models resembling human adipose tissue, in which an efficient interplay between the various cell types involved is likely important.

From a clinical perspective, further studies to translate the proofs of concept generated in rodent models to clinical investigation are crucial. Although there are many similarities between rodent and human BAT depots, notable differences also exist. Whereas the activation of murine BAT is mediated by β3-AR, a recent study revealed that β2-AR is the relevant adrenoceptor which activates human BAT (4). This underscores the need for caution when translating new advances generated by preclinical studies to humans. Future research should focus on the cardiometabolic benefits of long-term activation of β2-AR, preferably BAT-specific, in obese patients.

Lastly, further methodological improvements in visualization and evaluation of BAT metabolic activity in humans are warranted to define the actual contribution to whole-body nutrient turnover and energy expenditure. Of note, given that mouse studies suggest the uptake by BAT of triglyceride-derived fatty acids may be higher than that of glucose, and lipoprotein lipase is crucial for murine BAT thermogenesis, development of a PET-compatible lipoprotein-triglyceride tracer may be valuable to accurately estimate the total energy dissipating capacity of human BAT.

In conclusion, the original and review articles published in this Research Topic have provided significant insights in the field of thermogenic fat biology, emphasizing new aspects of pathophysiology and molecular control of BAT thermogenesis both in preclinical and clinical settings. We also emphasize the need for further investigation of the physiological significance of human BAT, methodological advances in estimating BAT functionality, novel non-canonical thermogenic pathways, and the heterogeneity of thermogenic adipocytes. Pursuing these issues may open opportunities to develop effective strategies utilizing adipose tissue thermogenesis to combat obesity and cardiometabolic diseases in humans.

AUTHOR CONTRIBUTIONS

TY wrote the manuscript. RR-R, MB, and PCNR edited the manuscript. All authors contributed to the article and approved the submitted version.

FUNDING

TY is supported by the research fellowship from the Uehara Memorial Foundation. RR-R is supported by the Spanish Ministry of Economy, Industry and Competitiveness (SAF2017-82813-C3-3R) and Joint Bilateral Project Japan-Spain/Agencia Estatal de Investigación (PCI2018-092997/AEI). MB is supported by the Swiss National Science Foundation (PZ00P3_167823). PCNR is supported by the Netherlands CardioVascular Research Initiative (CVON-GENIUS-II).

ACKNOWLEDGMENTS

We are grateful to all the authors and reviewers for their contributions to this Research Topic. We thank Zachary Brown at University of California, San Francisco for editing a draft of this manuscript.

REFERENCES

1. Berbée JF, Boon MR, Khedoe PP, Bartelt A, Schlein C, Worthmann A, et al. Brown fat activation reduces hypercholesterolaemia and protects from atherosclerosis development. *Nat Commun* (2015) 6:6356. doi: 10.1038/ncomms7356
2. Chen Y, Ikeda K, Yoneshiro T, Scaramozza A, Tajima K, Wang Q, et al. Thermal stress induces glycolytic beige fat formation via a myogenic state. *Nature* (2019) 565:180–5. doi: 10.1038/s41586-018-0801-z
3. Oguri Y, Shinoda K, Kim H, Alba DL, Bolus WR, Wang Q, et al. CD81 controls beige fat progenitor cell growth and energy balance via FAK signaling. *Cell* (2020) 182:563–77. doi: 10.1016/j.cell.2020.06.021
4. Blondin DP, Nielsen S, Kuipers EN, Severinsen MC, Jensen VH, Miard S, et al. Human brown adipocyte thermogenesis is driven by β2-AR stimulation. *Cell Metab* (2020) 32:287–300. doi: 10.1016/j.cmet.2020.07.005

Conflict of Interest: The authors declare that the research was conducted in the absence of any commercial or financial relationships that could be construed as a potential conflict of interest.

frontiers in Endocrinology

ORIGINAL RESEARCH
published: 09 January 2020
doi: 10.3389/fendo.2019.00898

Human Brown Adipose Tissue Estimated With Magnetic Resonance Imaging Undergoes Changes in Composition After Cold Exposure: An *in vivo* MRI Study in Healthy Volunteers

Gustavo Abreu-Vieira[1†], Aashley S. D. Sardjoe Mishre[1,2†], Jedrzej Burakiewicz[2], Laura G. M. Janssen[1], Kimberly J. Nahon[1], Jari A. van der Eijk[2], Titia T. Riem[1], Mariëtte R. Boon[1], Oleh Dzyubachyk[3], Andrew G. Webb[2], Patrick C. N. Rensen[1] and Hermien E. Kan[2]*

[1] Division of Endocrinology and Einthoven Laboratory for Experimental Vascular Medicine, Department of Medicine, Leiden University Medical Center, Leiden, Netherlands, [2] Department of Radiology, C.J. Gorter Center for High Field MRI, Leiden University Medical Center, Leiden, Netherlands, [3] Division of Image Processing (LKEB), Department of Radiology, Leiden University Medical Center, Leiden, Netherlands

OPEN ACCESS

Edited by:
Massimiliano Caprio, Università Telematica San Raffaele, Italy

Reviewed by:
Valeria Guglielmi, University of Rome Tor Vergata, Italy
Rossella Canese, Istituto Superiore di Sanità (ISS), Italy

***Correspondence:**
Hermien E. Kan
h.e.kan@lumc.nl

[†] *These authors share first authorship*

Specialty section:
This article was submitted to Obesity, a section of the journal Frontiers in Endocrinology

Received: *08 October 2019*
Accepted: *09 December 2019*
Published: *09 January 2020*

Citation:
Abreu-Vieira G, Sardjoe Mishre ASD, Burakiewicz J, Janssen LGM, Nahon KJ, van der Eijk JA, Riem TT, Boon MR, Dzyubachyk O, Webb AG, Rensen PCN and Kan HE (2020) Human Brown Adipose Tissue Estimated With Magnetic Resonance Imaging Undergoes Changes in Composition After Cold Exposure: An in vivo MRI Study in Healthy Volunteers. Front. Endocrinol. 10:898. doi: 10.3389/fendo.2019.00898

Aim: Magnetic resonance imaging (MRI) is increasingly being used to evaluate brown adipose tissue (BAT) function. Reports on the extent and direction of cold-induced changes in MRI fat fraction and estimated BAT volume vary between studies. Here, we aimed to explore the effect of different fat fraction threshold ranges on outcomes measured by MRI. Moreover, we aimed to investigate the effect of cold exposure on estimated BAT mass and energy content.

Methods: The effects of cold exposure at different fat fraction thresholding levels were analyzed in the supraclavicular adipose depot of nine adult males. MRI data were reconstructed, co-registered and analyzed in two ways. First, we analyzed cold-induced changes in fat fraction, T2* relaxation time, volume, mass, and energy of the entire supraclavicular adipose depot at different fat fraction threshold levels. As a control, we assessed fat fraction differences of deltoid subcutaneous adipose tissue (SAT). Second, a local analysis was performed to study changes in fat fraction and T2* on a voxel-level. Thermoneutral and post-cooling data were compared using paired-sample *t*-tests ($p < 0.05$).

Results: Global analysis unveiled that the largest cold-induced change in fat fraction occurred within a thermoneutral fat fraction range of 30–100% (−3.5 ± 1.9%), without changing the estimated BAT volume. However, the largest cold-induced changes in estimated BAT volume were observed when applying a thermoneutral fat fraction range of 70–100% (−3.8 ± 2.6%). No changes were observed for the deltoid SAT fat fractions. Tissue energy content was reduced from 126 ± 33 to 121 ± 30 kcal, when using a 30–100% fat fraction range, and also depended on different fat fraction thresholds.

Voxel-wise analysis showed that while cold exposure changed the fat fraction across nearly all thermoneutral fat fractions, decreases were most pronounced at high thermoneutral fat fractions.

Conclusion: Cold-induced changes in fat fraction occurred over the entire range of thermoneutral fat fractions, and were especially found in lipid-rich regions of the supraclavicular adipose depot. Due to the variability in response between lipid-rich and lipid-poor regions, care should be taken when applying fat fraction thresholds for MRI BAT analysis.

Keywords: brown adipose tissue, lipid metabolism, cold exposure, thermogenesis, magnetic resonance imaging, fat fraction

INTRODUCTION

The main function of brown adipose tissue (BAT) is to convert chemical energy stored within lipids into thermal energy (heat). Exposure to low temperatures is the main physiological stimulus for BAT activation (1). Upon adrenergic stimulation by sympathetic nerves, intracellular lipolysis takes place within brown adipocytes (2), and the resulting free fatty acids bind to uncoupling protein 1 (UCP1), which, in turn, functions as a molecular gate that dissipates the generated mitochondrial proton gradient as heat. To replenish the intracellular lipid stores, BAT takes up glucose and fatty acids from the systemic circulation (3, 4). In rodents, visualization of BAT by magnetic resonance imaging (MRI) was first reported almost three decades ago (5), and soon the technique was shown to accurately reflect the tissue structure (6) as well as histological changes due to temperature acclimatization (7). More recently, with research being expanded toward human physiology, several studies explored this ionizing-radiation-free method with the aim of understanding BAT function (8). From preclinical models it is known that the chemically-assessed fat content of tissues matches the fat mass estimated by MRI (9) and that fat fraction (FF) correlates negatively with the amount of UCP1-expressing cells in BAT (10) and positively with adipocyte size (11). In the intrascapular BAT of rodents kept on regular chow and at room temperature (circa 21°C), MRI estimations of FF vary between 20 and 50%, depending on the depth of the tissue (12). However, FF can reach up to almost 80% when animals are kept at thermoneutrality (13). In infants, BAT resembles the classic intrascapular depot found in rodents, both in morphology and function (14). In adults, however, there is a remarkable lack of easily distinguishable borders for e.g., the supraclavicular depot, which makes it difficult for a consensus to be reached on the optimal FF thresholds that should be used for specific BAT imaging (15). As a consequence, FF within human BAT has variously been described as circa 60% (16), 65% (17), 80% (18, 19), and 94% (20) in elderly adults and different FF threshold levels have been used to segment BAT (19, 21–24). Only one recent study explored the effect of specific FF threshold levels (0–100, 40–100, and 50–100%) on the cold-induced response in FF (25), but no analyses on other MR outcome parameters were explored. The relaxation time T2* has also been studied as an indirect MRI measure of BAT activity (16, 21, 24, 26, 27). It has been demonstrated that the T2* of BAT is shorter compared to white adipose tissue (WAT), which is most likely due to the abundant iron-rich mitochondria present in brown adipocytes. Cold-induced BAT activation increases oxygen consumption due to increased metabolic activity, which in turn increases blood perfusion. The latter increases T2*, whereas oxygen consumption shortens T2* (21). Different reports exist on the direction of changes in T2* during cold exposure, most likely due to these conflicting effects (17, 28, 29). BAT is naturally heterogeneous: on a molecular scale, this is manifested in differences in UCP-1 protein expression of adjacent cells, which after immunostaining create a multicolored pattern termed the "harlequin phenomenon" (30). The lack of homogeneity between adipose tissue depots within a single organism has also been noted at the functional level (31–33). Although structural heterogeneity has been noted in BAT imaging studies (34–37), it is generally seen as a confounding factor. Moreover, while the major goal of BAT medical research is to understand and manipulate energy fluxes, the quantification of tissue mass as caloric equivalents is rare. There are a few interesting examples of such a concept being applied, e.g., by matching body composition to potential energy storages and predicting whole-body energy expenditure (38, 39) or inferences concerning BAT energy uptake by estimating the energy content in labeled macromolecules (40). To our knowledge, however, an estimation of BAT energy storages *in vivo* has not been performed yet. Given the importance of BAT in current metabolic research, we aimed to explore the effect of different fat fraction threshold ranges on multiple outcomes measured by MRI. Moreover, for the first time, we aimed to investigate the effect of cold exposure on BAT mass and energy content. To this end, we first assessed estimated BAT volumes at thermoneutral and cold conditions to establish a lower FF threshold for the exclusion of non-fatty voxels. Subsequently, we determined

Abbreviations: BAT, Brown adipose tissue; FF, Fat fraction; FF_{Glob}, Supraclavicular adipose tissue fat fraction estimated by global analysis; FF_{Loc}, Fat fraction on a voxel-level; FF_{SAT}, Fat fraction of the subcutaneous adipose tissue depot; MRI, Magnetic resonance imaging; ROIs, Regions of interest; T2*, Mono-exponential effective transverse relaxation time; $T2^*_{Glob}$, Mono-exponential effective transverse relaxation time estimated by global analysis; $T2^*_{Loc}$, Mono-exponential effective transverse relaxation time estimated on a voxel-level; Vol_{BAT}, Estimated BAT volume; WAT, White adipose tissue; SAT, Subcutaneous adipose tissue.

estimated BAT volume, FF, T2*, mass and energy content, and explored the effect of different FF thresholds on these parameters. Finally, we assessed local changes in FF and T2* upon cold exposure on a voxel-level. We demonstrate the importance of the high-lipid areas of the tissue and suggest that the conceptual framework of this work could further aid investigations on BAT as a target for obesity and metabolic disorders in humans.

MATERIALS AND METHODS

Subjects

Ten healthy, non-smoking, lean (BMI 18–25 kg/m^2) Europid male volunteers, born in the Netherlands and aged between 18 and 30 years, were recruited as part of a larger intervention study that investigated the effect of cold exposure and the β3-receptor agonist mirabegron on BAT (Clinical Trials number: NCT03012113). The study was conducted in accordance with the principles of the revised Declaration of Helsinki (41) and with approval from the local medical ethics committee. Exclusion criteria were recent excessive weight change (>3 kg within the last 3 months), vigorous exercise, use of any medication known to affect lipid and/or glucose metabolism, BAT activity, cardiac function or QT interval time, smoking and any relevant chronic disease. Contraindications for undergoing an MRI scan were the presence of non-MR-safe metal implants or objects in the body (i.e., a pacemaker, neurostimulator, hydrocephalus or drug pump, non-removable hearing aid or large recent tattoos), and a history of claustrophobia, tinnitus, or hyperacusis.

Study Design and BAT Activation Protocol

Subjects were instructed to withhold from alcohol and caffeine for 24 h and to fast overnight for 10 h, prior to the experiment. Subjects remained fasted until the end of the experiment. To activate BAT, a personalized cooling protocol was conducted as previously described (42). Each subject was placed between water-perfused temperature-controlled mattresses with water initially circulating at 32°C. The water temperature was gradually reduced during the first hour until reaching 9°C or reporting of shivering by the subject. In either case the temperature was raised by 3°C and the subject laid for one additional hour under these conditions. In the case of renewed shivering, the temperature was raised slightly to stop shivering and to assure that BAT remained the dominant source of heat production (2). MRI scans were acquired before and after the cooling protocol on a 3 T MRI scanner (Philips Ingenia, Philips Healthcare, Best, The Netherlands). Subjects were positioned supine and head-first in the scanner. Scans were conducted at the same time of day in all participants (before cooling: in the morning, after cooling: in the afternoon).

Image Acquisition

A three-dimensional six-point chemical-shift encoded gradient-echo acquisition using a 16-channel anterior array, 12-channel posterior array and the posterior section of the 16-channel head and neck coil was used to image the supraclavicular adipose depot (**Figure 1**). The following imaging parameters were used: repetition time TR = 15 ms, first echo time TE = 1.98 ms, echo time separation ΔTE = 1.75 ms, flip angle = 8°, field-of-view of 480 × 300 × 90 mm^3 (Right-Left, Foot-Head, Anterior-Posterior), 1.1 mm isotropic resolution, four signal averages. Averaging was done post-acquisition; in the case of significant subject motion the corresponding averages were rejected. Bulk motion due to either shivering or subject discomfort was the major source of motion. The total imaging time was 12 min. To increase the reproducibility of subject positioning, the participants were asked to reach as far as possible with their fingers toward their feet after being placed on the scanner table and to relax their shoulders afterwards.

Data Reconstruction and Analysis

Data Reconstruction

Quantitative water and fat images were reconstructed off-line using an in-house water-fat separation algorithm based on the known frequencies of the multi-peak fat spectrum and assuming a mono-exponential T2*, combined with a region-growing scheme to mitigate strong main field inhomogeneity effects. Initially, a low-resolution reconstruction was performed by using an estimate for the main magnetic field inhomogeneity. Subsequently, a region growing scheme was used to extrapolate the solution from correctly reconstructed parts in order to acquire the reconstructed water and fat images at high resolution (43–46). FF maps were generated according to the following equation, where x, y, and z denote the position of a voxel in the image.

$$\textit{Signal fat fraction}\,(x,y,z) = \frac{\textit{Signal}_{Fat}(x,y,z)}{\textit{Signal}_{Fat}(x,y,z) + \textit{Signal}_{Water}(x,y,z)}$$

Image Registration and ROI Delineation

Registration was performed using the open-source image registration toolbox Elastix (47, 48). The first echo of the thermoneutral image stack was registered to that of the post-cooling stack by first pre-aligning them in an affine manner followed by deformable registration with a three-dimensional B-spline transform with a 10 × 10 × 10 mm^3 grid. In both cases, an adaptive stochastic gradient descent with two resolutions for optimization and Mattes mutual information was used as the similarity measure. Region masks, defined as the sampled part of each image stack, were used during the registration. The parameter files that were used for performing the registration can be downloaded from http://elastix.bigr.nl/wiki/index.php/Par0048. Regions of interest (ROIs) encompassing the known location of the left supraclavicular adipose depot (49) (**Figure 1**) were drawn manually on the thermoneutral scans by one observer. Additionally, to ensure that potential changes in FF of the supraclavicular BAT depot were specific to this region, regions of interest comprising deltoid subcutaneous adipose tissue (SAT) were manually delineated on both the thermoneutral and post-cooling scans (**Supplemental Figure S1**). To exclude potential bias caused by the direction of registration, we also performed the registration in the reverse direction (post-cooling

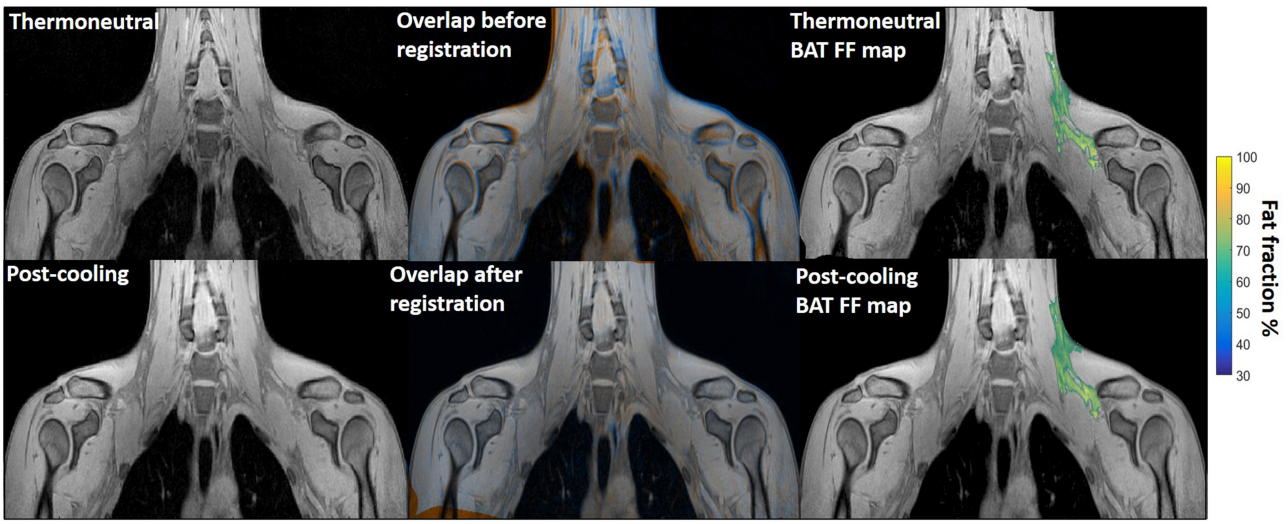

FIGURE 1 | Example of image registration and a reconstructed fat fraction map before and after cooling. The first column shows thermoneutral and post-cooling images (one slice from the first echo in the acquisition). In the second column, the overlay of the same images before (top) and after registration (bottom) is shown. The images are colored orange (thermoneutral) and blue (post-cooling) for better visualization of differences between the scans. The third column shows the thermoneutral and post-cooling fat fraction maps of the supraclavicular adipose depot, overlaid on the corresponding images. Lipid content in the supraclavicular region is color-mapped over a 30–100% fat fraction range.

→ thermoneutral) and obtained results (not shown) that were virtually identical to the ones reported below.

Data Analysis

Cold-induced changes to the supraclavicular adipose depot were assessed using two complementary analyses. First, changes in FF, T2*, volume, mass, and energy content of the supraclavicular adipose depot were assessed using a global analysis. As this analysis only uses the deformation field for ROI mapping on the post-cooling image, this allows not only assessment of FF, but also any changes in estimated BAT volume. Assessment of BAT volume was recently shown to be highly dependent on segmentation criteria in [^{18}F]FDG PET-CT studies (50). Therefore, we decided to explore the influence of FF segmentation criteria on both estimated BAT volume and FF using MRI.

The estimated BAT volume was determined by multiplying the volume of a single voxel (0.548 μL) by the number of voxels that fall within a certain fat fraction segmentation range (e.g., 30–100% FF). For example: when using a 30–100% FF segmentation threshold range, 93275 voxels were segmented from the thermoneutral image. Multiplied by the volume of a single voxel (0.548 μL), the estimated BAT volume would be 51 mL. Data from this analysis were also used to explore different FF thresholds. Secondly, we performed a local analysis to study changes in FF and the T2* relaxation time on a voxel-level. As this method directly deforms the thermoneutral images and ROIs to post-cooling image coordinates, no conclusions regarding the true volume can be inferred Details of the methods are outlined below. Due to excessive movement during image acquisition, MRI data from one participant could not be reconstructed and were excluded from all analyses.

I. Global analysis : FF_{Glob}, FF_{SAT}, $T2^*_{Glob}$, and Vol_{BAT}

Global analysis of supraclavicular adipose tissue FF (FF_{Glob}), T2* relaxation time ($T2^*_{Glob}$) and estimated BAT volume (Vol_{BAT}) was performed by mapping the defined ROIs to the post-cooling image coordinates. To this end, the calculated deformation field from the registration was used to transform the thermoneutral ROIs to the post-cooling scan coordinates. The deformation field of the ROIs was converted to the floating point image type. This enabled performing the analysis on raw (non-interpolated) data. The distribution of thermoneutral and post-cooling Vol_{BAT} across the FF range was assessed using volume histograms with FF bins of 0.5%. This was then assessed statistically by determining at which FF ranges (10% intervals), estimated BAT volume was significantly changed after cold exposure. To explore the effect of different upper and lower FF thresholds for BAT analysis, cold-induced changes in Vol_{BAT}, FF_{Glob}, and $T2^*_{Glob}$ were quantified at all FF threshold options. To illustrate these effects, we tested for specific FF ranges: 30–100, 50–100, and 70–100% whether Vol_{BAT}, FF_{Glob}, and $T2^*_{Glob}$ changed significantly after cold exposure. Voxels below the selected lower FF thresholds (i.e., 30, 50, or 70%) were excluded in both the thermoneutral and post-cooling ROIs. By plotting the ROIs using different lower FF segmentation thresholds, we observed that voxels within a 10–30% FF interval were mostly located at the boundaries of the supraclavicular adipose depot, which are adjacent to muscle (**Supplemental Figure S2**). Therefore, to avoid inclusion of non-fatty tissue and minimize partial volume effects, a lower FF threshold of 30% was adopted for the subsequent analyses. ROIs comprising deltoid SAT were manually delineated on both thermoneutral and post-cooling scans to preclude analysis bias arising from difficulty

registering ROIs located at the interface of tissue and air (**Supplemental Figure S1**). The average FF of the deltoid SAT depots (FF_{SAT}) was determined using a 70–100% FF interval before and after cooling to avoid voxels containing muscle and air and to minimize partial volume effects.

II. Global analysis: estimation of BAT mass and energy content

To estimate BAT mass and energy content, the FF was used to calculate water and fat mass, and, subsequently, the total tissue energy was estimated similarly to (38–40). 1 µl of lipid was assumed to represent 0.92 mg in mass, corresponding to 9.4×10^{-3} kcal. Lean mass measurements were derived from the water MR signal and represent a combination of water-bound structures, such as proteins, glucose and intra- extracellular fluids. Lean mass of 1 µl corresponded to 1.06 mg and 1.0×10^{-3} kcal, correspondingly. Energy variation and lean/fat mass changes were calculated from the FF. Therefore, a voxel of 1 µl with a FF of 50% is equivalent to 0.5 µl lean mass and 0.5 µl fat, which, after adjustments for density, represented 0.455 mg fat and 0.540 mg lean mass.

III. Voxel-wise analysis: FF_{Loc} and $T2^*_{Loc}$

For voxel-wise analysis of the supraclavicular adipose depot, the deformation field from the registration was used to transform the thermoneutral ROIs, FF and T2* maps to the post-cooling image coordinates to compare the FF and T2* on a voxel-level (FF_{Loc} and $T2^*_{Loc}$). To compensate for potential bias due to interpolation of the moving image and small-scale inconsistencies between the co-registered images, each voxel of both thermoneutral and post-cooling image stacks was assigned a mean value from its 3 × 3 voxel neighborhood.

FF maps were generated to visualize FF composition changes across the supraclavicular adipose depot on a voxel-wise level. Cold-induced FF changes on a voxel level (FF_{Loc}) were further studied using two-dimensional joint histograms. In these plots, for every voxel its initial FF was plotted against its change in FF after cold exposure, and the number of voxels belonging to each combination was added to represent the counts (color scale). Similar voxel density plots were used to assess (i) the relation between thermoneutral $T2^*_{Loc}$ and FF_{Loc}, (ii) the relation between $\Delta T2^*_{Loc}$ after cold exposure and thermoneutral FF measurements, and (iii) the relation between $\Delta T2^*_{Loc}$ and ΔFF_{Loc} after cold exposure. The distributions of thermoneutral FF_{Loc}, ΔFF_{Loc}, and $\Delta T2^*_{Loc}$ after cold exposure were assessed using K-means clustering. The Elbow method (51) was used to obtain the optimal cluster number by evaluating the percentage of explained variance as a function of the number of clusters. The explained variance percentage was determined as the ratio of the between-group variance to the total variance. In general, when the explained variance is plotted against cluster number, the first few clusters will add information (explain variance), so these can be observed as jumps from one k-value to another. However, at a certain k-value little information is added, which results in a knee point. For analyzing the voxel distributions, the optimal k-value was determined by visual inspection and implementing a 95% explained variance cut-off value.

Statistical Analysis

Data were tested for a normal distribution according to the Shapiro-Wilk test. For the global analysis, comparisons between thermoneutral and post-cooling data were performed by paired Student's *t*-tests with results deemed statistically significant when $p < 0.05$. No correction for multiple comparisons was performed. For the local analysis we used a voxel-wise comparison, and performed k-means clustering for the analysis. As this approach uses an unsupervised learning algorithm that simply visualizes underlying clusters in the voxel distribution without providing any details regarding the significance of the different clusters, no correction for multiple comparisons is needed (51). Linear regression was used to assess the relation between supraclavicular adipose tissue mass and volume using a 0.05 significance level and the R-squared is given. Data analysis including statistical analysis

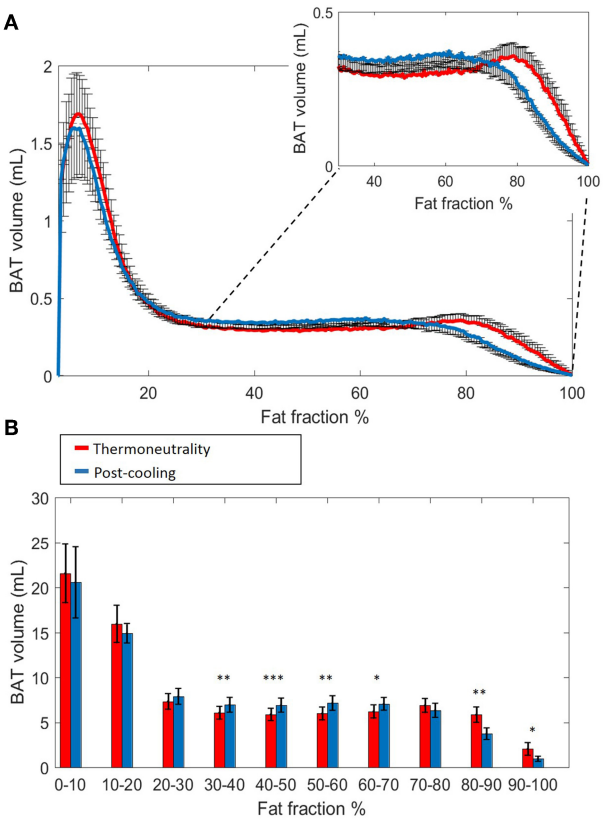

FIGURE 2 | Estimated volumetric BAT analysis. Thermoneutral and post-cooling volume histograms as a function of fat fraction with bin size 0.5%: thermoneutral volumes are shown in red and post-cooling volumes in blue **(A)**. Cold-induced volume changes plotted as a function of fat fractions (10% FF interval) **(B)**. Data are represented as mean ± SEM for $n = 9$. In **(B)**, a paired sample *t*-test was used to analyze the changes in volume after cold exposure. $^*p < 0.05$, $^{**}p < 0.01$, and $^{***}p < 0.001$.

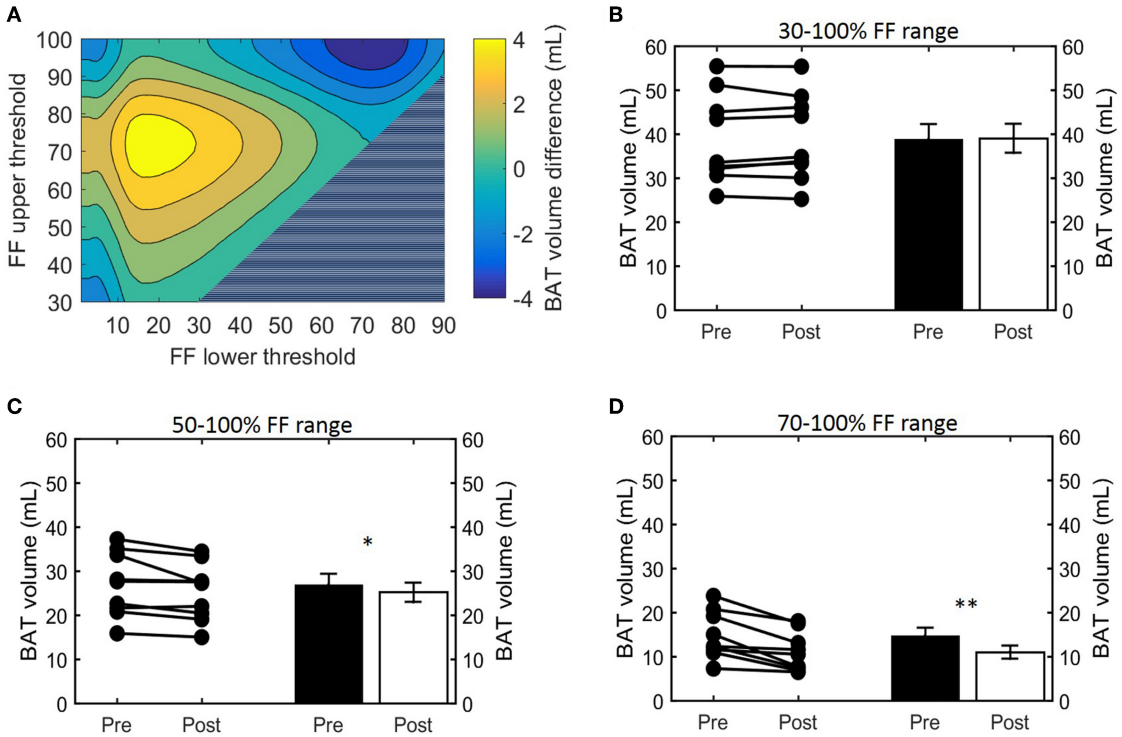

FIGURE 3 | Effect of FF thresholds on estimated BAT volume differences. Heatmap of the effect of different FF segmentation thresholds on estimated BAT volume differences after cooling. The color (second y-axis) depicts the estimated BAT volume difference for each lower (x-axis) and upper left (y-axis) threshold. The largest decrease in estimated BAT volume is present with a lower threshold of 72% and no upper threshold. The triangle in the lower right corner indicates invalid FF threshold options, as we implemented a minimum FF threshold of 30%. **(A)** Cold-induced volume changes analyzed using the paired sample *t*-test (*$p < 0.05$, **$p < 0.01$) at different threshold ranges: 30–100% **(B)**, 50–100% **(C)**, and 70–100% **(D)**. Data is represented as mean ± SEM for all participants ($n = 9$).

was performed in MATLAB (version R2018b). Data are presented as mean ± SEM.

RESULTS

Volumetric Changes in Estimated BAT Volume After Cold-Exposure

Histogram analysis of the changes in Vol_{BAT} showed an overall shift of the estimated post-cooling BAT volume from higher FFs toward lower FFs (**Figure 2A**). When binned into 10% FF intervals, this resulted in significant increases in estimated BAT volume above a FF of 30%, while the estimated BAT volume was significantly decreased above a FF of 80% (**Figure 2B**). Interestingly, Vol_{BAT} did not change significantly within the 70–80% FF range, which is at the intersection of the thermoneutral and post-cooling histograms (inset of **Figure 2A**). The effect of different FF threshold options on cold-induced changes in Vol_{BAT} is shown in **Figure 3A**. For a lower FF threshold of 30% and upper FF threshold of 100%, no clear change in Vol_{BAT} occurred. However, with increasing lower FF threshold values, Vol_{BAT} decreased upon cold exposure. This was subsequently tested for statistical significance for FF ranges with a relatively low (30–100%), intermediate (50–100%), and high (70–100%) lower threshold. For the broadest FF range (30–100%), no significant change was detected in Vol_{BAT} after cold exposure (**Figure 3B**). For the intermediate FF range (50–100%), Vol_{BAT} lowered from 26.9 ± 2.4 to 25.2 ± 2.2 mL (−1.8%; $p = 0.031$, **Figure 3C**) after cold exposure. For the 70–100% FF range, Vol_{BAT} decreased from 14.7 ± 1.8 to 11.0 ± 1.5 mL (−3.8%; $p = 0.0022$, **Figure 3D**) after cold exposure.

FF_{SAT} and the Effect of FF Thresholds on Global FF and T2*

Next, we studied how lower and upper FF thresholds affected the cold-induced change in FF_{Glob} (ΔFF_{Glob}; post-cooling minus pre-cooling) and FF_{SAT} (ΔFF_{SAT}; post-cooling minus pre-cooling), as well as $T2^*_{Glob}$ ($\Delta T2^*_{Glob}$; post-cooling minus pre-cooling). The largest decrease in FF_{Glob} occurred at a lower FF threshold of 34% and upper FF threshold of 100% (**Supplemental Figure S3**). This decrease in FF became smaller when shifting the lower FF threshold toward higher values. This was further tested for statistical significance for the following FF ranges: 30–100, 50–100, and 70–100%. When applying the 30–100% FF range, FF_{Glob} decreased from 62.0 ± 1.6 to 58.5 ± 1.3% (−3.5%; $p = 5.0e\text{-}4$, **Figure 4A**). With an intermediate threshold of 50–100%, FF_{Glob} decreased from 71.6

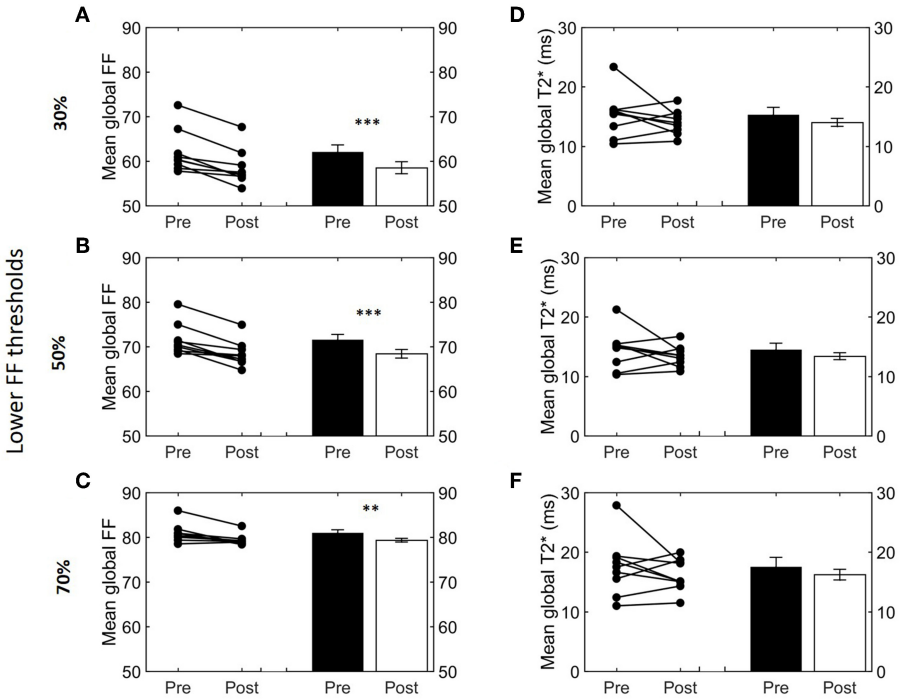

FIGURE 4 | Effect of different FF thresholds on global supraclavicular adipose tissue FF and T2*. Cold-induced FF and T2* changes analyzed using the paired *t*-test at different threshold ranges: 30–100% **(A,D)**, 50–100% **(B,E)**, and 70–100% **(C,F)**. Data are represented as mean ± SEM for $n = 9$. The paired sample *t*-test was used to analyze the changes in volume after cold exposure (**$p < 0.01$ and ***$p < 0.001$).

± 1.2 to 68.4 ± 1.0% (−3.2%; 5.6e-4, **Figure 4B**). When a lower threshold of 70% was assumed, FF_{Glob} decreased from 81.0 ± 0.7 to 79.3 ± 0.4% (−1.6%; $p = 0.006$, **Figure 4C**). In contrast, no significant changes were noted in FF_{SAT} after cold exposure (**Supplemental Figure S1B**). For $T2^*_{Glob}$, no clear changes were seen as a function of different threshold options (**Supplemental Figure S3**, **Figures 4D–F**).

Estimation of BAT Lipid and Lean Mass After Cold

Having defined the effect of cold exposure on Vol_{BAT}, FF_{Glob}, and $T2^*_{Glob}$, we set out to characterize the subtle changes that take place within the tissue composition. Supraclavicular adipose tissue is composed of two compartments distinguishable by MRI: fat mass and lean mass. While fat mass comprises the accumulated lipid droplets, lean mass corresponds to water-rich structures, a broad category that includes blood, cytoplasm and hydrophilic structures, such as glycogen storages and proteins. Here we used the FF of each voxel to separate the underlying lean and fat masses (**Figure 5A**, see "Methods" section for details). Interestingly, we observed a biphasic effect of cold exposure on supraclavicular adipose tissue mass (**Figure 5B**). There was an apparent decrease in the number of voxels with a high FF, most pronouncedly observed as a decrease in lipid mass on the right side of the plot (i.e., 70–100% FF). Lean mass was also decreased in this range, albeit to a lesser extent. When the left side of the plot was taken into account (i.e., voxels included in the FF range below 70%), lean and fat masses were increased to a similar extent. Both lean mass and fat mass explained a large part of the variance of the total supraclavicular adipose volume, with slight dominance of lipid mass ($R^2 = 0.92$) over lean mass ($R^2 = 0.85$) (**Figure 5C**). The discrepancy between loss and gain was quantified in the total mass variation of the tissue, where total lean mass was increased from 15.7 ± 1.6 to 17.2 ± 1.7 g (+1.5 g; $p = 0.001$) and total lipid mass in the supraclavicular depot decreased from 22.1 ± 1.9 to 21.0 ± 1.7 g (−1.2 g; $p = 0.02$) (**Figure 5D**).

Tissue Energy Storages Are Decreased After Cold Exposure

The main function of BAT is to convert chemical energy into thermal energy. Estimation of metabolic energy content in lean and fat masses has been validated in well-controlled experiments measuring whole-body energy intake and expenditure (38), and the concept of energy equivalence has been used to quantify the energy influx to BAT during cold exposure (40). In addition, because BAT does not contain significant amounts of bone mineral or air and the tissue water is bound to proteins, its total mass can be taken as the potential energy substrate for heat generation. Therefore, we set out to quantify the cold-induced change in energy storages. BAT is composed of a mixture of lean and lipid masses, but its chemical energy storage equivalence is largely dominated by the lipid component (**Figure 6A**). When analyzed from this bioenergetic perspective, the variation in lean mass previously observed by us (**Figure 5B**) became insignificant,

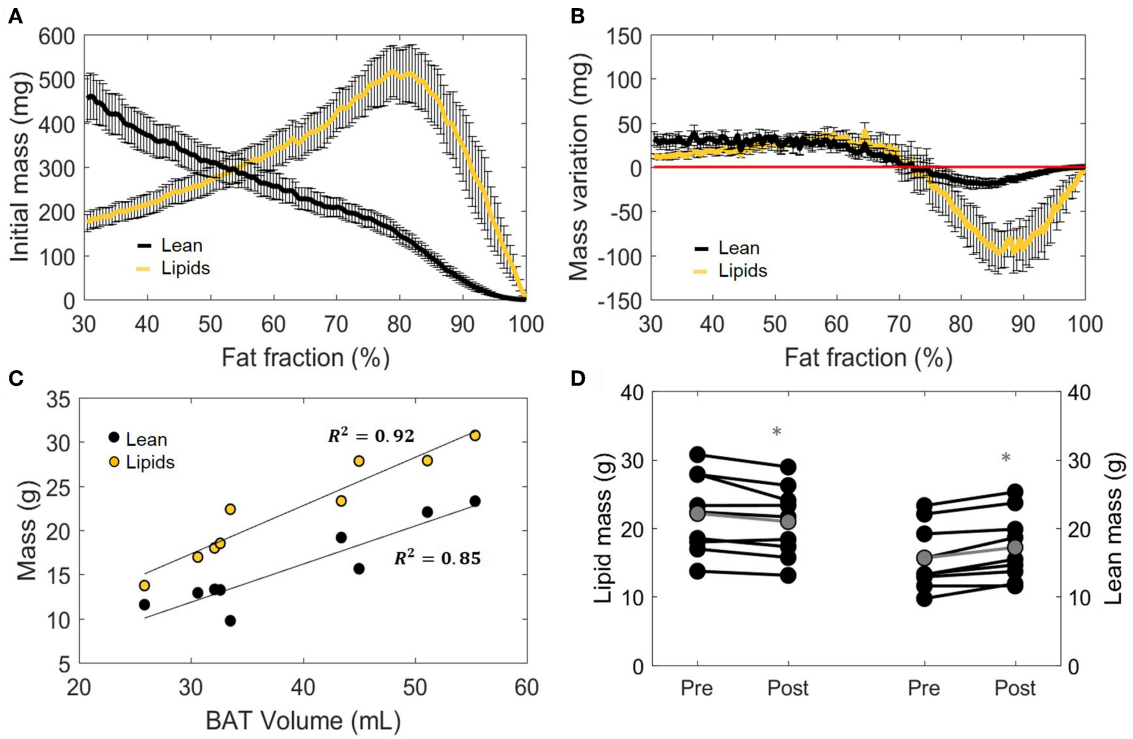

FIGURE 5 | Distinction between lean and lipid masses within supraclavicular adipose tissue. Lean and lipid masses were estimated as described in the "Methods" section and represented as a function of their specific fat fractions **(A)**. Cold exposure decreased both lean and fat masses to in the upper fat fractions (above 70%) and slightly increased these in the lower fat fractions **(B)**. **(C)** Correlation between total estimated BAT volume and lipid or lean mass analyzed using linear regression (R^2 is reported). Change in total lipid and lean mass after cold exposure, analyzed with the paired sample *t*-test **(D)**. Data in **(A,B,D)** represent mean ± SEM for $n = 9$ volunteers. *$p < 0.05$.

as cold-induced changes in energy content attributed to lean mass was substantially lower compared to energy variations in lipid mass (**Figure 6B**). Here, the significant decrease in fat mass was reflected in a diminished energy storage in the supraclavicular depot, which decreased from 126 ± 11 to 121 ± 10 kcal (−5 kcal; $p = 0.03$, **Figure 6C**). It was noticeable that this variation was not uniform in the volume histogram, but instead there were losses in the initial high-lipid area and gains in initially leaner parts of the tissue. To better visualize this effect, a contour plot was created to represent different thresholding possibilities for the analysis of energy variation (**Figure 6D**). When the higher FFs of the tissue were chosen, a large decrease in energy content was inferred. On the other hand, an analysis focusing on the FF interval between 30 and 70%, for example, would have resulted in the opposite conclusion that the tissue increased its chemical energy storage after cold exposure.

Local Assessment of the Supraclavicular Adipose Tissue FF Distribution After Cold Exposure

Voxel-wise thermoneutral and post-cooling FF maps unveiled that the supraclavicular adipose tissue is composed of a juxtaposition of low-and high lipid zones, as exemplified in **Figures 7A,B**. After cold exposure, which is generally shown to decrease BAT lipid content, we found a high spatial variability in responses since several areas presented the expected reduction in lipids, while in contrast, other tissue areas increased their lipid content (**Figure 7C**). Lipid maps of the other eight subjects are presented in **Supplemental Figure S4**. Local FF changes were evaluated using a 2D joint histogram, where every voxel had its initial FF used as a reference to define the variation in FF that it underwent upon cold exposure, and the number of voxels belonging to each combination was added to represent the counts (color scale; **Figure 7D**). Assuming the vertical line as zero change, we observed FF changes along the entire thermoneutral FF range, with a clear increase in voxel-density in the higher FF range. To quantify this, K-means clustering was applied with the optimal cluster number equal to four. The results are shown in **Supplemental Figure S5**. Cluster analysis indeed revealed that for the high thermoneutral FF range, FF decreases were observed especially within cluster C1 (average thermoneutral FF: 76.0 ± 11.2%). The average FF decrease after cold-exposure that corresponded to this cluster was −3.5 ± 2.2%.

The Association Between Supraclavicular Adipose Tissue FF and T2* on a Local Level

Using voxel-wise analysis, we then studied the relation of the baseline T2* relaxation time to tissue FF (**Figure 8A**). $T2^*_{Loc}$

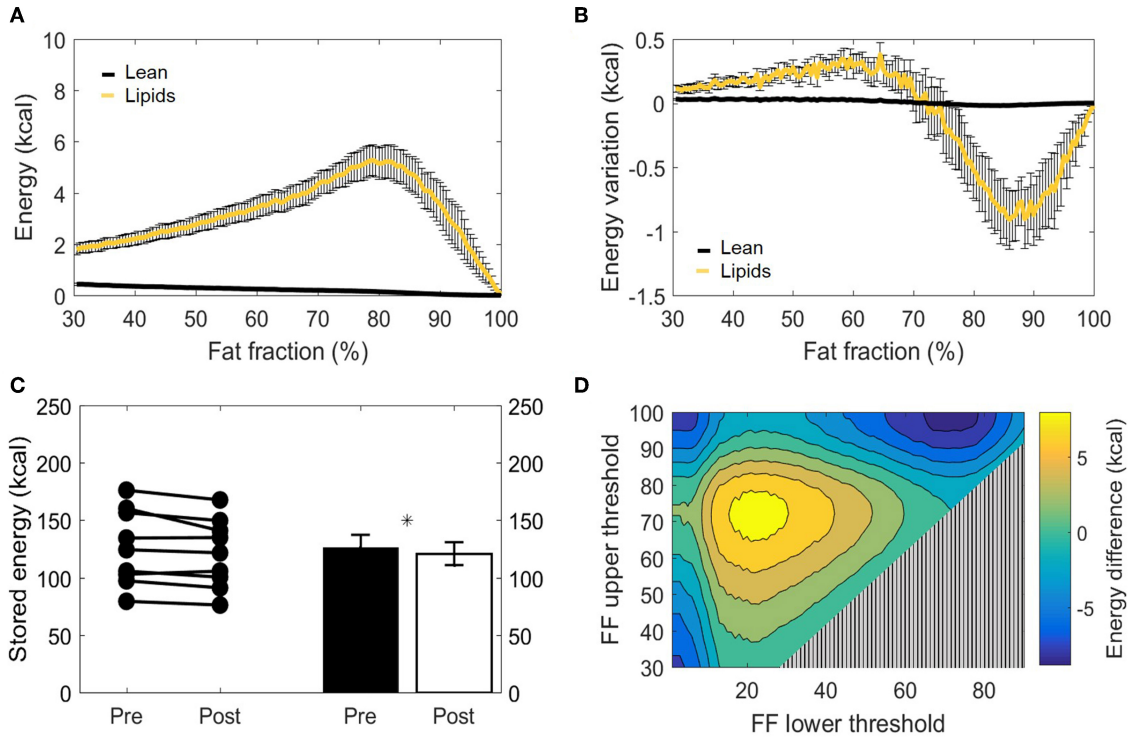

FIGURE 6 | Metabolizable energy content in the supraclavicular adipose depot. Representation of energy content in the supraclavicular depot at thermoneutrality, with specific values attributed to lean tissue or lipids **(A)**. Changes in energy content attributed to lean or fat masses, represented over different fat fraction ranges **(B)**. Total energy storages (kcal) before and after cold exposure analyzed, by using the paired *t*-test **(C)**. Heatmap of the effect of different FF segmentation thresholds on estimated energy content differences after cooling. The color (second y-axis) depicts the estimated energy content difference for each lower (x-axis) and upper left (y-axis) threshold. The largest decrease in estimated energy is present with a lower threshold of 70% and no upper threshold. The triangle in the lower right corner indicates invalid FF threshold options, as we implemented a minimum FF threshold of 30% **(D)**. Data represent mean ± SEM of all participants ($n = 9$). *$p < 0.05$.

values were near 10 ms at the lower FFs and circa 20–25 ms at the highest FFs. However, there was no clear relation between the baseline FF_{Loc} and $T2^*_{Loc}$ values. Also, when the cold-induced changes in $T2^*_{Loc}$ were plotted against baseline FF_{Loc}, no clear association was observed (**Figure 8B**). Regarding the changes in $T2^*_{Loc}$ and FF_{Loc} in response to cold exposure, for most voxels FF_{Loc} decreases were accompanied by increases in $T2^*_{Loc}$ (**Figure 8C**). The voxel distribution was analyzed using k-means clustering. Cluster C1 included the highest voxel counts per data point (**Supplemental Figure S5**). For this cluster, the average $T2^*_{Loc}$ and FF_{Loc} changes were 1.4 ± 1.5 ms and −2.2 ± 4.0%, respectively.

DISCUSSION

In this study, we show that reductions in volume, mass and energy of the supraclavicular adipose tissue depot during cold exposure are heterogeneous and take place most prominently within lipid-rich regions of the tissue, whereas no significant changes were observed in the SAT FF. Leaner areas of the supraclavicular adipose tissue depot (defined by a low thermoneutral FF), however, tended to gain volume, mass, and energy following cold exposure. We also showed that the location and width of the FF interval can alter the apparent size and direction of cold-induced changes of MRI-derived parameters used for BAT analysis. The maximum FF change to the entire supraclavicular adipose depot was obtained by implementing a 34–100% FF range. Finally, local changes in FF occurred over the entire thermoneutral FF range (30–100%) in both directions (i.e., increase and decrease).

The Upper FF Threshold Range for BAT FF Analysis

The classical distinction between unilocular WAT and multilocular BAT suggests that a clear division based on FF should exist between both tissues. From this perspective, the range where FF is higher than 70% has previously been assumed to be above the BAT threshold (52). For this reason, we found it remarkable that, in our results, these high-lipid areas of the supraclavicular adipose depot actually showed the largest decrease in lipid and energy content after cold exposure, which is in agreement with recent findings (25). These data suggest that, in fact, one should not use 70% as an upper threshold, and voxels showing up to 100% FF should be used in the analysis [e.g., as performed in (22, 53)]. Unfortunately, it was not possible to infer whether these regions comprised unilocular white

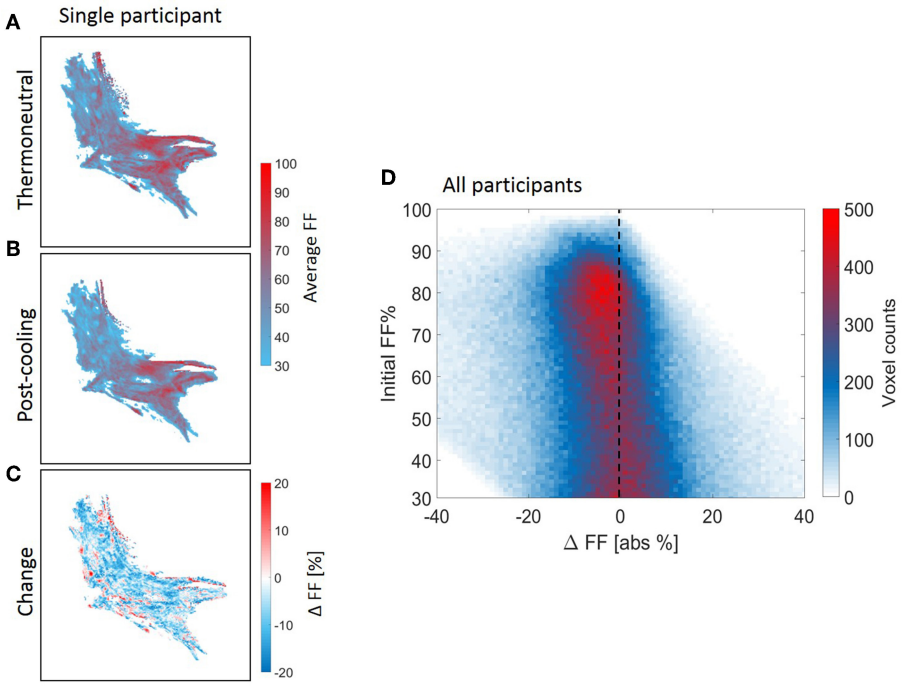

FIGURE 7 | Structural heterogeneity of brown adipose tissue in the supraclavicular region during cold exposure. Example of a reconstructed fat fraction map with merged z-slices before and after cooling **(A,B)** and cold-induced change (post-minus pre) **(C)** for $n = 1$. The 2D joint voxel histogram representing variation in change in lipid content of each voxel in relation to its thermoneutral FF from the voxel-wise analysis, wherein the colors represent the number of voxels belonging to each combination **(D)** for all participants ($n = 9$). Cold colors indicate decreases in fat fraction and warm colors indicate increases in fat fraction.

adipocytes that partially donated their lipids for combustion by surrounding "leaner" brown adipocytes. Alternatively, this region could englobe unilocular UCP1-expressing cells capable of thermogenesis. In both scenarios, the lobular distribution of high-fat zones, intercalated by regions of lower lipid content, suggests that human BAT should be taken as a morphologically diverse organ, and care should be used before excluding areas from its analysis. T2* analysis did not provide any additional information in establishing lower and upper FF thresholds for BAT segmentation.

The Lower FF Threshold Range for BAT Analyses of FF and Volume

Both the global and local analyses showed that changes occurred across the entire baseline FF range (30–100%), with the greatest apparent FF decrease when using a 34–100% FF range. The largest FF decrease we observed (i.e., 3.5%) is in the range of values reported in literature (19, 21, 23), but also much smaller (22) and larger decreases (25) have been reported. This could be due to the use of different thresholds, but also differences in the cooling protocols can play an important role (54, 55). Raising the lower threshold above 34% decreases the extent of FF differences upon cold exposure, as we excluded voxels that fell below the threshold in both the thermoneutral and post-cooling scan in order to avoid partial volume artifacts and to enable volumetric analysis. For example, when a lower FF threshold of 70% is used, voxels below 70% FF are excluded in both the thermoneutral and post-cooling ROIs. Hence, regions in the post-cooling ROIs that shifted from high thermoneutral FFs (>70%) to FFs below 70% upon cold exposure are excluded, but are still present in the thermoneutral ROIs. These lower FF regions can, therefore, not contribute to the reduction of FF_{Glob} in the post-cooling ROIs. A recent report where the use of FF thresholds were also explored showed an opposite effect, as a larger effect on FF was shown using a 50% threshold compared to a 40% threshold. In their approach, FF thresholds were only applied to the thermoneutral ROIs (25), which could have enabled measuring larger FF differences with increasing lower thresholds because voxels in the post-cooling scans were not excluded. This indicates that care should be taken before excluding low-lipid areas from the analysis.

The total estimated BAT volume showed an opposite trend compared to FF, where increasing the lower FF threshold enlarged the differences. This is expected, as most prominent volume reductions take place above a FF of about 70%.

On the Heterogeneity of Human Supraclavicular Adipose Tissue

In this work, we expanded the idea of supraclavicular adipose tissue heterogeneity by visualizing its structure, its complex distribution of lipids and described the variations in the lipid content (increased and decreased in the same depot) after cold exposure. These data strongly suggest that BAT acutely modulates lipid influx and combustion divergently, here exemplified by the supraclavicular areas that gained lipids after thermogenic activation by cold exposure, which was also shown

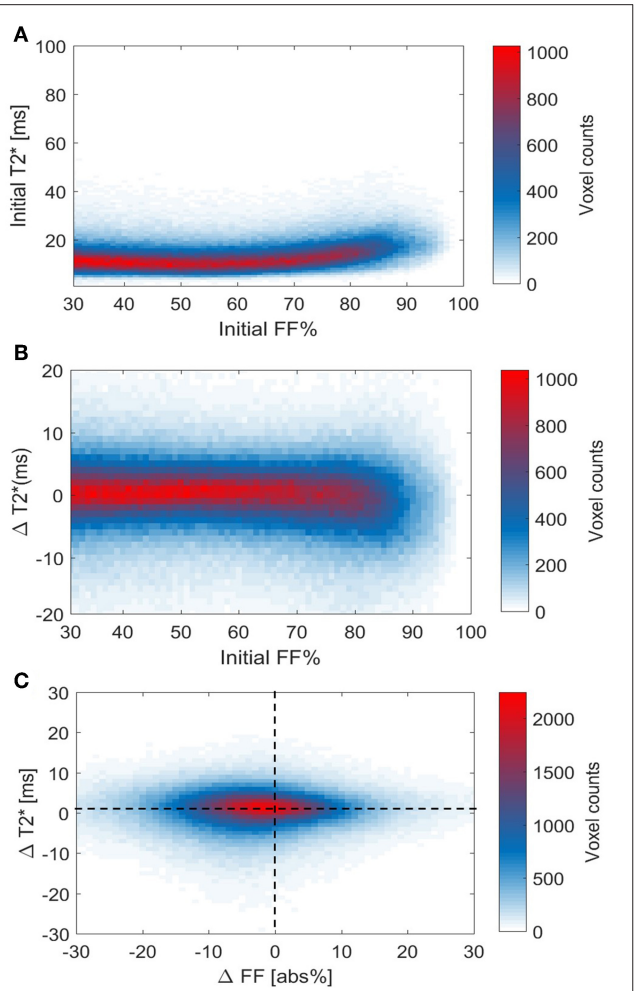

FIGURE 8 | Voxel histograms representing the relation between thermoneutral values and cold-induced changes in T2* and FF. Thermoneutral measurements of T2* against thermoneutral fat fractions **(A)**. Relation between the cold-induced changes in T2* and thermoneutral fat fractions **(B)**. The association between cold-induced changes in both T2* and FF **(C)**. Data is presented as the mean of all participants ($n = 9$).

in a recent study (25). This example goes against expectations of BAT only decreasing its lipid content, an idea so broadly accepted that the loss of lipids during cooling has been used as a condition sine qua non for the identification of BAT (23). The guiding factors behind the cold-induced lipid gain in some BAT areas are unclear. We speculate that an increase in lipids is also possible due to *de novo* lipogenesis taking place after glucose uptake (56).

Mass Quantification Within the Supraclavicular Adipose Depot

In the present work, we estimated the absolute amounts of lean and fat masses within the supraclavicular adipose depot. This provided the insight that, at least in our lean young subjects, fat and lean masses (conceptualized as representing the lipid storages and the metabolically-active components of the tissue, respectively) had a high linear correlation with total tissue volume. Therefore, we assume that estimated BAT size in its simplest measure is likely to be correlated to its total potential thermogenic function. The cold-induced decrease in total lipid mass seen in our study was expected because of the thermogenic activation of BAT, which leads to increased β-oxidation (57, 58), and is in agreement with other imaging studies using FF as an outcome (19, 21, 25, 59). This was accompanied by an increase in lean mass, which is unlikely to be caused by acute protein synthesis, since our entire experiment took place in a few hours. The increase in blood perfusion expected to happen in BAT during cold exposure (2, 22, 60–63) could contribute to an increase in water signal. However, it was recently postulated that FF reductions immediately after cold-exposure are too large to be solely achieved by increasing the blood volume fraction (25). Additionally, cold-induced FF decreases were shown to be maintained even after reheating the subject, which does not coincide with the fast dynamics of perfusion (19, 25). These findings support the rationale that the observed decrease in lipid mass and increase in lean mass are prominently caused by the intracellular lipid depletion in brown adipocytes. This results from the very general classification of lean mass as a collection of structures richly bound to water, which makes it susceptible to acute changes in hydration levels (64).

In a broader context of metabolic studies, lean mass is generally understood to be the major determinant of whole-body basal metabolic rate. Because the contribution of specific organs to the whole-body basal metabolic rate can be estimated based on their total mass (65–67), we predict that the evaluation of the specific lean mass of organs (such as performed in our study) may contribute to the generation of better allometric models to infer on organ-specific metabolic rates and their influence on whole-body energy expenditure.

Energy Variation Following Thermogenic Activation

The supraclavicular adipose tissue composition analysis demonstrated the dominance of fat mass on energy dynamics during cold exposure. Critically, although lean mass comprised almost half of the tissue, even significant variations in its mass are not likely to play a major role in metabolic energy storage. We can only speculate on whether this reflects a decreased volume of larger lipid droplets due to combustion, increased lipid droplet formation due to lipid uptake from the bloodstream, or a combination of both phenomena. Based on the principle of energy conservation, it can be postulated that, if the nutrient uptake by the tissue perfectly matches its combustion rates, the fat energy loss and gain within different FF of the organ will be equal to zero. Results differing from zero can be interpreted as an uncompensated or overcompensated lipid (or glucose) uptake from the bloodstream (in relation to BAT expenditure during cooling). Most importantly, while our setup did not allow us to estimate the total energy flux of the tissue, it did provide an important conceptual milestone for the quantification of BAT-specific energy expenditure. Because expenditure can be estimated based on combinatory measurements of glucose and lipid uptake and variations in tissue composition, we predict that the method employed in our study [allied to energy uptake

estimations by Virtanen et al. (40)] will make it possible to finally infer concerning the energy combusted by BAT during activation and to more accurately quantify the specific contribution of BAT depots to whole-body metabolism.

General Conceptual Applications of the Method

The application of the bioenergetic framework presented here is not confined to the analysis of BAT during cooling. It can also be used for the analysis of metabolic content in any tissue where energy storages are crucial for pathophysiological processes. These include muscles, where changes in energy availability can modify the long-term maintenance of the mass, as well as the liver, where excessive energy storages in the form of lipid droplets are thought to be causal to insulin resistance and metabolic diseases.

Limitations

We could only partially infer about the dynamic changes in tissue composition due to the limited number of time-points, i.e., one before and after cooling. Dynamic scans would possibly provide more insights into changes in lipid composition within the supraclavicular adipose depot. In our study, we used six echoes for the mono-exponential T2* fit. Recently, a study has shown that the accuracy of the fit enhances with increasing echo number (26), and therefore in future studies the echo number will be increased to improve T2* measurement in BAT. We did not perform respiratory triggering in acquisition, which could have led to motion artifacts. We mitigated this by using a 3×3 smoothing kernel after registration. In addition, a recent study that employed similar MR methodology without respiratory triggering demonstrated an error of less than one pixel after image registration (25). This study included a relatively homogeneous study population (young, male, healthy, lean white Dutch natives). Therefore, caution should be used when extrapolating our results to a more general population. Instead, it is recommended to assume our results as representing those of a control population and as a demonstration of methodological possibilities to track alterations in obesity, disease or drug testing. The extent of cold-induced FF changes that have been reported in literature and in this study are quite modest. It has been also shown that there is only a small, albeit statistically difference in supraclavicular FF between individuals with and without BAT activity on [^{18}F]FDG PET-CT (68). BAT activity assessed by glucose uptake in PET/CT and by FF differences upon cold exposure, however, are not measuring the same exact response. This is not unexpected, as in [18F]FDG PET glucose is used as a tracer, while in fat-water MRI we are assessing the fat content directly. Future studies including multiple MR sequences each tuned to a different aspect of physiology will hopefully further elucidate this issue.

CONCLUSION

The supraclavicular adipose depot in humans is highly heterogeneous with respect to basal lipid content, and lipid-rich areas are intercalated with lipid-poor regions. After thermogenic activation by cooling, areas of the tissue with a high FF tend to lose more lipids, while an increase in mass is noticeable in the leaner regions. Cold-induced loss of metabolic energy is more noticeable in the high 70–100% FF range. Overall, cold exposure decreases absolute lipid mass and tissue energy content, which is associated with an increase in lean mass, but does not significantly change tissue volume. Due to variability of the supraclavicular adipose depot when responding to cold exposure, the choice of MRI thresholding highly affects the estimated magnitude and direction of changes. Overall, we found that by increasing the lower FF threshold level, global FF differences became less pronounced, whereas estimated BAT volume differences became larger in magnitude. This emphasizes that the selection of FF threshold levels can affect parameters differently.

DATA AVAILABILITY STATEMENT

Data is available from the corresponding author on reasonable request.

ETHICS STATEMENT

The studies involving human participants were reviewed and approved by METC Leiden-Den Haag-Delft, The Netherlands. The patients/participants provided their written informed consent to participate in this study.

AUTHOR CONTRIBUTIONS

KN and LJ designed the study, collected and analyzed the data, and revised the manuscript for intellectual content. GA-V conceptualized, analyzed and interpreted the data, and drafted the manuscript. AS reanalyzed the data and drafted the manuscript. JB analyzed and interpreted the data, developed the MRI acquisition protocol and post-processing algorithms, and drafted and revised the manuscript for intellectual content. OD contributed to the methods (data analysis) and revised the manuscript for intellectual content. JE contributed to the post-processing algorithms. TR analyzed and interpreted the data. AW revised the manuscript for intellectual content. HK, PR, and MB conceptualized and designed the study, interpreted the data, contributed to the discussion, reviewed and edited the manuscript.

FUNDING

This work was supported by a Prof. J. Terpstra Award to KN, a Dutch Diabetes Research Foundation Fellowship to MB (grant 2015.81.1808). JB and HK were partially supported by the European Union's Seventh Framework Programme for research, technological development, and demonstration under grant agreement no 602485. Partial funding was supplied by the European Research Council (NOMA-MRI 670629) to AW. OD

was supported by Dutch Technology Foundation STW (as part of the STW 502 project 12721: Genes in Space under the IMAGENE perspective program).

ACKNOWLEDGMENTS

Parts of the data in this manuscript were presented at the MRI of Obesity & Metabolic Disorders in 2019 and at The European Society for Magnetic Resonance in Medicine and Biology (ESMRMB) Congress in 2019.

SUPPLEMENTARY MATERIAL

The Supplementary Material for this article can be found online at: https://www.frontiersin.org/articles/10.3389/fendo.2019.00898/full#supplementary-material

REFERENCES

1. Cannon B, Nedergaard J. Brown adipose tissue: function and physiological significance. *Physiol Rev*. (2004) 84:277–359. doi: 10.1152/physrev.00015.2003
2. Blondin DP, Frisch F, Phoenix S, Guérin B, Turcotte ÉE, Haman F, et al. Inhibition of intracellular triglyceride lipolysis suppresses cold-induced brown adipose tissue metabolism and increases shivering in humans. *Cell Metab*. (2017) 25:438–47. doi: 10.1016/j.cmet.2016.12.005
3. Bartelt A, Bruns OT, Reimer R, Hohenberg H, Ittrich H, Peldschus K, et al. Brown adipose tissue activity controls triglyceride clearance. *Nat Med*. (2011) 17:200–6. doi: 10.1038/nm.2297
4. Olsen JM, Csikasz RI, Dehvari N, Lu L, Sandström A, Öberg AI, et al. β3-Adrenergically induced glucose uptake in brown adipose tissue is independent of UCP1 presence or activity: mediation through the mTOR pathway. *Mol Metab*. (2017) 6:611–9. doi: 10.1016/j.molmet.2017.02.006
5. Osculati F, Leclercq F, Sbarbati A, Zancanaro C, Cinti S, Antonakis K. Morphological identification of brown adipose tissue by magnetic resonance imaging in the rat. *Eur J Radiol*. (1989) 9:112–4.
6. Osculati F, Sbarbati A, Leclercq F, Zancanaro C, Accordini C, Antonakis K, et al. The correlation between magnetic resonance imaging and ultrastructural patterns of brown adipose tissue. *J Submicrosc Cytol Pathol*. (1991) 23:167–74.
7. Sbarbati A, Baldassarri AM, Zancanaro C, Boicelli A, Osculati F. *In vivo* morphometry and functional morphology of brown adipose tissue by magnetic resonance imaging. *Anat Rec*. (1991) 231:293–7. doi: 10.1002/ar.1092310302
8. Hu HH. Magnetic resonance of brown adipose tissue: a review of current techniques. *Crit Rev Biomed Eng*. (2015) 43:161–81. doi: 10.1615/CritRevBiomedEng.2015014377
9. Hu HH, Li Y, Nagy TR, Goran MI, Nayak KS. Quantification of absolute fat mass by magnetic resonance imaging: a validation study against chemical analysis. *Int J Body Compos Res*. (2011) 9:111–22.
10. Branca RT, Zhang L, Warren WS, Auerbach E, Khanna A, Degan S, et al. *In vivo* noninvasive detection of brown adipose tissue through intermolecular zero-quantum MRI. *PLoS ONE*. (2013) 8:e0074206. doi: 10.1371/journal.pone.0074206
11. Peng XG, Ju S, Fang F, Wang Y, Fang K, Cui X, et al. Comparison of brown and white adipose tissue fat fractions in ob, seipin, and Fsp27 gene knockout mice by chemical shift-selective imaging and 1H-MR spectroscopy. *Am J Physiol Endocrinol Metab*. (2013) 304:E160–7. doi: 10.1152/ajpendo.00401.2012
12. Lunati E, Marzola P, Nicolato E, Fedrigo M, Villa M, Sbarbati A. *In vivo* quantitative lipidic map of brown adipose tissue by chemical shift imaging at 4.7 tesla. *J Lipid Res*. (1999) 40:1395–400.
13. Smith DL, Yang Y, Hu HH, Zhai G, Nagy TR. Measurement of interscapular brown adipose tissue of mice in differentially housed temperatures by chemical-shift-encoded water-fat MRI. *J Magn Reson Imaging*. (2013) 38:1425–33. doi: 10.1002/jmri.24138
14. Lidell ME, Betz MJ, Dahlqvist Leinhard O, Heglind M, Elander L, Slawik M, et al. Evidence for two types of brown adipose tissue in humans. *Nat Med*. (2013) 19:631–4. doi: 10.1038/nm.3017
15. Chen KY, Cypess AM, Laughlin MR, Haft CR, Hu HH, Bredella MA, et al. Brown Adipose Reporting Criteria in Imaging STudies (BARCIST 1.0): recommendations for standardized FDG-PET/CT experiments in humans. *Cell Metab*. (2016) 24:210–22. doi: 10.1016/j.cmet.2016.07.014
16. Gifford A, Towse TF, Walker RC, Avison MJ, Welch EB. Characterizing active and inactive brown adipose tissue in adult humans using PET-CT and MR imaging. *Am J Physiol Endocrinol Metab*. (2016) 311:E95–104. doi: 10.1152/ajpendo.00482.2015
17. van Rooijen BD, van der Lans AA, Brans B, Wildberger JE, Mottaghy FM, Schrauwen P, et al. Imaging cold-activated brown adipose tissue using dynamic T2*-weighted magnetic resonance imaging and 2-deoxy-2-[^{18}F]fluoro-d-glucose positron emission tomography. *Invest Radiol*. (2013) 48:708–14. doi: 10.1097/RLI.0b013e31829363b8
18. Franssens BT, Hoogduin H, Leiner T, van der Graaf Y, Visseren FLJ. Relation between brown adipose tissue and measures of obesity and metabolic dysfunction in patients with cardiovascular disease. *J Magn Reson Imaging*. (2017) 46:497–504. doi: 10.1002/jmri.25594
19. Lundström E, Strand R, Johansson L, Bergsten P, Ahlström H, Kullberg J. Magnetic resonance imaging cooling-reheating protocol indicates decreased fat fraction via lipid consumption in suspected brown adipose tissue. *PLoS ONE*. (2015) 10:e0126705. doi: 10.1371/journal.pone.0126705
20. Franz D, Karampinos DC, Rummeny EJ, Souvatzoglou M, Beer AJ, Nekolla SG, et al. Discrimination between brown and white adipose tissue using a 2-point dixon water-fat separation method in simultaneous pet/MRI. *J Nucl Med*. (2015) 56:1742–7. doi: 10.2967/jnumed.115.160770
21. Deng J, Neff LM, Rubert NC, Zhang B, Shore RM, Samet JD, et al. MRI characterization of brown adipose tissue under thermal challenges in normal weight, overweight, and obese young men. *J Magn Reson Imaging*. (2018) 47:936–47. doi: 10.1002/jmri.25836
22. Holstila M, Pesola M, Saari T, Koskensalo K, Raiko J, Borra RJ, et al. MR signal-fat-fraction analysis and T2* weighted imaging measure BAT reliably on humans without cold exposure. *Metabolism*. (2017) 70:23–30. doi: 10.1016/j.metabol.2017.02.001
23. Stahl V, Maier F, Freitag MT, Floca RO, Berger MC, Umathum R, et al. *In vivo* assessment of cold stimulation effects on the fat fraction of brown adipose tissue using DIXON MRI. *J Magn Reson Imaging*. (2017) 45:369–80. doi: 10.1002/jmri.25364
24. Gashi G, Madoerin P, Maushart CI, Michel R, Senn JR, Bieri O, et al. MRI characteristics of supraclavicular brown adipose tissue in relation to cold-induced thermogenesis in healthy human adults. *J Magn Reson Imaging*. (2019) 50:1160–8. doi: 10.1002/jmri.26733
25. Coolbaugh CL, Damon BM, Bush EC, Welch EB, Towse TF. Cold exposure induces dynamic, heterogeneous alterations in human brown adipose tissue lipid content. *Sci Rep*. (2019) 9:13600. doi: 10.1038/s41598-019-49936-x
26. Franz D, Diefenbach MN, Treibel F, Weidlich D, Syväri J, Ruschke S, et al. Differentiating supraclavicular from gluteal adipose tissue based on simultaneous PDFF and T2* mapping using a 20-echo gradient-echo acquisition. *J Magn Reson Imaging*. (2019) 50:424–34. doi: 10.1002/jmri.26661
27. Hui SCN, Ko JKL, Zhang T, Shi L, Yeung DKW, Wang D, et al. Quantification of brown and white adipose tissue based on Gaussian mixture model using water–fat and T2* MRI in adolescents. *J Magn Reson Imaging*. (2017) 46:758–68. doi: 10.1002/jmri.25632
28. Khanna A, Branca RT. Detecting brown adipose tissue activity with BOLD MRI in mice. *Magn Reson Med*. (2012) 68:1285–90. doi: 10.1002/mrm.24118
29. Chen YC, Cypess AM, Chen YC, Palmer M, Kolodny G, Kahn CR, et al. Measurement of human brown adipose tissue volume and activity using anatomic MR imaging and functional MR imaging. *J Nucl Med*. (2013) 54:1584–7. doi: 10.2967/jnumed.112.117275

30. Cinti S, Cancello R, Zingaretti MC, Ceresi E, De Matteis R, Giordano A, et al. CL316,243 and cold stress induce heterogeneous expression of UCP1 mRNA and protein in rodent brown adipocytes. *J Histochem Cytochem*. (2002) 50:21–31. doi: 10.1177/002215540205000103
31. de Jong JM, Larsson O, Cannon B, Nedergaard J. A stringent validation of mouse adipose tissue identity markers. *Am J Physiol Endocrinol Metab*. (2015) 308:E1085–105. doi: 10.1152/ajpendo.00023.2015
32. Jeffery E, Wing A, Holtrup B, Sebo Z, Kaplan JL, Saavedra-Peña R, et al. The adipose tissue microenvironment regulates depot-specific adipogenesis in obesity. *Cell Metab*. (2016) 24:142–50. doi: 10.1016/j.cmet.2016.05.012
33. Grandl G, Müller S, Moest H, Moser C, Wollscheid B, Wolfrum C. Depot specific differences in the adipogenic potential of precursors are mediated by collagenous extracellular matrix and Flotillin 2 dependent signaling. *Mol Metab*. (2016) 5:937–47. doi: 10.1016/j.molmet.2016.07.008
34. Branca RT, He T, Zhang L, Floyd CS, Freeman M, White C, et al. Detection of brown adipose tissue and thermogenic activity in mice by hyperpolarized xenon MRI. *Proc Natl Acad Sci USA*. (2014) 111:18001–6. doi: 10.1073/pnas.1403697111
35. Bhanu Prakash KN, Verma SK, Yaligar J, Goggi J, Gopalan V, Lee SS, et al. Segmentation and characterization of interscapular brown adipose tissue in rats by multi-parametric magnetic resonance imaging. *Magn Reson Mater Phys Biol Med*. (2016) 29:277–86. doi: 10.1007/s10334-015-0514-3
36. Hu HH, Smith DL, Nayak KS, Goran MI, Nagy TR. Identification of brown adipose tissue in mice with fat-water IDEAL-MRI. *J Magn Reson Imaging*. (2010) 31:1195–202. doi: 10.1002/jmri.22162
37. Hu HH, Wu TW, Yin L, Kim MS, Chia JM, Perkins TG, et al. MRI detection of brown adipose tissue with low fat content in newborns with hypothermia. *Magn Reson Imaging*. (2014) 32:107–17. doi: 10.1016/j.mri.2013.10.003
38. Ravussin Y, Gutman R, LeDuc CA, Leibel RL. Estimating energy expenditure in mice using an energy balance technique. *Int J Obes*. (2013) 37:399–403. doi: 10.1038/ijo.2012.105
39. Heymsfield SB, Peterson CM, Thomas DM, Hirezi M, Zhang B, Smith S, et al. Establishing energy requirements for body weight maintenance: validation of an intake-balance method NCT01672632 NCT. *BMC Res Notes*. (2017) 10:220. doi: 10.1186/s13104-017-2546-4
40. U Din M, Raiko J, Saari T, Kudomi N, Tolvanen T, Oikonen V, et al. Human brown adipose tissue [^{15}O]O_2 PET imaging in the presence and absence of cold stimulus. *Eur J Nucl Med Mol Imaging*. (2016) 43:1878–86. doi: 10.1007/s00259-016-3364-y
41. General Assembly of the World Medical. World Medical Association Declaration of Helsinki: ethical principles for medical research involving human subjects. *J Am Coll Dent*. (2014) 81:14–8. doi: 10.1001/jama.2013.281053
42. Bakker LE, Boon MR, van der Linden RA, Arias-Bouda LP, van Klinken JB, Smit F, et al. Brown adipose tissue volume in healthy lean south Asian adults compared with white Caucasians: a prospective, case-controlled observational study. *Lancet Diabetes Endocrinol*. (2014) 2:210–7. doi: 10.1016/S2213-8587(13)70156-6
43. Yu H, Reeder SB, Shimakawa A, Brittain JH, Pelc NJ. Field map estimation with a region growing scheme for iterative 3-point water-fat decomposition. *Magn Reson Med*. (2005) 54:1032–9. doi: 10.1002/mrm.20654
44. Reeder SB, Wen Z, Yu H, Pineda AR, Gold GE, Markl M, et al. Multicoil dixon chemical species separation with an iterative least-squares estimation method. *Magn Reson Med*. (2004) 51:35–45. doi: 10.1002/mrm.10675
45. Yu H, McKenzie CA, Shimakawa A, Vu AT, Brau AC, Beatty PJ, et al. Multiecho reconstruction for simultaneous water-fat decomposition and T2* estimation. *J Magn Reson Imaging*. (2007) 26:1153–61. doi: 10.1002/jmri.21090
46. Reeder SB, Pineda AR, Wen Z, Shimakawa A, Yu H, Brittain JH, et al. Iterative decomposition of water and fat with echo asymmetry and least-squares estimation (IDEAL): application with fast spin-echo imaging. *Magn Reson Med*. (2005) 54:636–44. doi: 10.1002/mrm.20624
47. Klein S, Staring M, Murphy K, Viergever MA, Pluim JP. Elastix: a toolbox for intensity-based medical image registration. *IEEE Trans Med Imaging*. (2010) 29:196–205. doi: 10.1109/TMI.2009.2035616
48. Shamonin DP, Bron EE, Lelieveldt BP, Smits M, Klein S, Staring M, et al. Fast parallel image registration on CPU and GPU for diagnostic classification of Alzheimer's disease. *Front Neuroinform*. (2014) 7:50. doi: 10.3389/fninf.2013.00050
49. Sacks H, Symonds ME. Anatomical locations of human brown adipose tissue: functional relevance and implications in obesity and type 2 diabetes. *Diabetes*. (2013) 62:1783–90. doi: 10.2337/db12-1430
50. Martinez-Tellez B, Nahon KJ, Sanchez-Delgado G, Abreu-Vieira G, Llamas-Elvira JM, van Velden FHP, et al. The impact of using BARCIST 1.0 criteria on quantification of BAT volume and activity in three independent cohorts of adults. *Sci Rep*. (2018) 8:8567. doi: 10.1038/s41598-018-26878-4
51. Madhulatha TS. An overview on clustering methods. *IOSR J Eng*. (2012) 2:719–25. doi: 10.9790/3021-0204719725
52. Hu HH, Perkins TG, Chia JM, Gilsanz V. Characterization of human brown adipose tissue by chemical-shift water-fat MRI. *Am J Roentgenol*. (2013) 200:177–83. doi: 10.2214/AJR.12.8996
53. McCallister A, Zhang L, Burant A, Katz L, Branca RT. A pilot study on the correlation between fat fraction values and glucose uptake values in supraclavicular fat by simultaneous PET/MRI. *Magn Reson Med*. (2017) 78:1922–32. doi: 10.1002/mrm.26589
54. Sun L, Verma S, Michael N, Chan SP, Yan J, Sadananthan SA, et al. Brown adipose tissue: multimodality evaluation by PET, MRI, infrared thermography, and whole-body calorimetry (TACTICAL-II). *Obesity*. (2019) 27:1434–42. doi: 10.1002/oby.22560
55. Ong FJ, Ahmed BA, Oreskovich SM, Blondin DP, Haq T, Konyer NB, et al. Recent advances in the detection of brown adipose tissue in adult humans: a review. *Clin Sci*. (2018) 132:1039–54. doi: 10.1042/CS20170276
56. Irshad Z, Dimitri F, Christian M, Zammit VA. Diacylglycerol acyltransferase 2 links glucose utilization to fatty acid oxidation in the brown adipocytes. *J Lipid Res*. (2017) 58:15–30. doi: 10.1194/jlr.M068197
57. Yu XX, Lewin DA, Forrest W, Adams SH. Cold elicits the simultaneous induction of fatty acid synthesis and β-oxidation in murine brown adipose tissue: prediction from differential gene expression and confirmation *in vivo*. *FASEB J*. (2002) 16:155–68. doi: 10.1096/fj.01-0568com
58. Blondin DP, Labbé SM, Tingelstad HC, Noll C, Kunach M, Phoenix S, et al. Increased brown adipose tissue oxidative capacity in cold-acclimated humans. *J Clin Endocrinol Metab*. (2014) 99:E438–46. doi: 10.1210/jc.2013-3901
59. Koskensalo K, Raiko J, Saari T, Saunavaara V, Eskola O, Nuutila P, et al. Human brown adipose tissue temperature and fat fraction are related to its metabolic activity. *J Clin Endocrinol Metab*. (2017) 102:1200–7. doi: 10.1210/jc.2016-3086
60. Abreu-Vieira G, Hagberg CE, Spalding KL, Cannon B, Nedergaard J. Adrenergically stimulated blood flow in brown adipose tissue is not dependent on thermogenesis. *Am J Physiol Endocrinol Metab*. (2015) 308:E822–9. doi: 10.1152/ajpendo.00494.2014
61. Muzik O, Mangner TJ, Leonard WR, Kumar A, Granneman JG. Sympathetic innervation of cold-activated brown and white fat in lean young adults. *J Nucl Med*. (2017) 58:799–806. doi: 10.2967/jnumed.116.180992
62. Muzik O, Mangner TJ, Leonard WR, Kumar A, Janisse J, Granneman JG. 15O PET measurement of blood flow and oxygen consumption in cold-activated human brown fat. *J Nucl Med*. (2013) 54:523–31. doi: 10.2967/jnumed.112.111336
63. Orava J, Nuutila P, Lidell ME, Oikonen V, Noponen T, Viljanen T, et al. Different metabolic responses of human brown adipose tissue to activation by cold and insulin. *Cell Metab*. (2011) 14:272–9. doi: 10.1016/j.cmet.2011.06.012
64. Thomsen TK, Jensen VJ, Henriksen MG. *In vivo* measurement of human body composition by dual-energy X-ray absorptiometry (DXA). *Eur J Surg*. (1998) 164:133–7. doi: 10.1080/110241598750004797
65. Wang Z, Ying Z, Bosy-Westphal A, Zhang J, Schautz B, Later W, et al. Specific metabolic rates of major organs and tissues across adulthood: evaluation by mechanistic model of resting energy expenditure. *Am J Clin Nutr*. (2010) 92:1369–77. doi: 10.3945/ajcn.2010.29885
66. Kaiyala KJ. Mathematical model for the contribution of individual organs to non-zero y-intercepts in single and multi-compartment

linear models of whole-body energy expenditure. *PLoS ONE*. (2014) 9:e0103301. doi: 10.1371/journal.pone.0103301

67. Gallagher D, Belmonte D, Deurenberg P, Wang Z, Krasnow N, Pi-Sunyer FX, et al. Organ-tissue mass measurement allows modeling of ree and metabolically active tissue mass. *Am J Physiol Endocrinol Metab*. (1998) 275:E249–58. doi: 10.1152/ajpendo.1998.275.2.E249
68. Jones TA, Wayte SC, Reddy NL, Adesanya O, Dimitriadis GK, Barber TM, et al. Identification of an optimal threshold for detecting human brown adipose tissue using receiver operating characteristic analysis of IDEAL MRI fat fraction maps. *Magn Reson Imaging*. (2018) 51:61–8. doi: 10.1016/j.mri.2018.04.013

Conflict of Interest: The authors declare that the research was conducted in the absence of any commercial or financial relationships that could be construed as a potential conflict of interest.

frontiers in Endocrinology

REVIEW
published: 21 January 2020
doi: 10.3389/fendo.2019.00932

Human Pluripotent Stem Cells: A Relevant Model to Identify Pathways Governing Thermogenic Adipocyte Generation

*Xi Yao, Vincent Dani and Christian Dani**

Université Côte d'Azur, iBV, UMR CNRS/INSERM, Faculté de Médecine, Nice, France

Brown and brown-like adipocytes (BAs) are promising cell targets to counteract obesity thanks to their potential to drain and oxidize circulating glucose and triglycerides. However, the scarcity of BAs in human adults is a major limitation for energy expenditure based therapies. Enhanced characterization of BA progenitor cells (BAPs) and identification of critical pathways regulating their generation and differentiation into mature BAs would be an effective way to increase the BA mass. The identification of molecular mechanisms involved in the generation of thermogenic adipocytes is progressing substantially in mice. Much less is known in humans, thus highlighting the need for an *in vitro* model of human adipocyte development. Pluripotent stem cells (PSCs), i.e., embryonic stem cells and induced pluripotent stem cells, help gain insight into the different phases in the development of multiple cell types. We will discuss the capacity of human PSCs to differentiate into BAs in this review. Several groups, including ours, have reported low spontaneous adipocyte generation from PSCs. However, factors governing the differentiation of induced pluripotent stem cell-derived BA progenitors cells were recently identified, and the TGFβ signaling pathway has a pivotal role. The development of new relevant methods, such as the differentiation of hPSC-BAPs into 3D adipospheres to better mimick the lobular structure of human adipose tissue, will also be discussed. Differentiation of human PSCs into thermogenic adipocytes at high frequency provides an opportunity to characterize new targets for anti-obesity therapy.

Keywords: human induced pluripotent stem cells, brown adipocytes, adipocyte progenitors, drug discovery, cell-based therapy, obesity

OPEN ACCESS

Edited by:
Takeshi Yoneshiro, University of California, San Francisco, United States

Reviewed by:
Igor Slukvin, University of Wisconsin-Madison, United States
Marc Thibonnier, AptamiR Therapeutics. Inc., United States

****Correspondence:***
Christian Dani
dani@unice.fr

Specialty section:
This article was submitted to Obesity, a section of the journal Frontiers in Endocrinology

Received: *21 November 2019*
Accepted: *20 December 2019*
Published: *21 January 2020*

Citation:
Yao X, Dani V and Dani C (2020) Human Pluripotent Stem Cells: A Relevant Model to Identify Pathways Governing Thermogenic Adipocyte Generation. Front. Endocrinol. 10:932. doi: 10.3389/fendo.2019.00932

INTRODUCTION

The development of obesity and associated metabolic disorders such as diabetes and heart diseases is a major health issue. Obesity results from an imbalance between calorie intake and energy expenditure. The scientific community is focusing attention on white adipose tissue (WAT) that stores energy, and on means to fight its expansion. However, modern lifestyles are often not

compatible with a reduction in energy intake. Current anti-obesity drugs to reduce energy intake may have major side effects for the patients. Bariatric surgery has proven efficient for obesity, although long-term complications and obesity relapse may occur. The identification of new anti-obesity targets is thus urgently required. In contrast to WAT, classical brown adipocytes and brown-like adipocytes (BAs) dispersed in WATs, mainly in subcutaneous fat depots, are specialized in energy expenditure thanks to their high content of mitochondria expressing the uncoupling protein-1 (UCP1) (1). Upon activation, BAs consume metabolic substrates and burn fat and sugars via uncoupling of oxidative phosphorylation, in turn inhibiting ATP synthesis (2). The ability of BAs to actively drain circulating glucose and triglycerides to oxidize them can prevent hyperglycemia and hypertriglyceridemia. BAs secrete adipokines that may also contribute to metabolic effects (3). BAs are therefore promising cell targets to counteract obesity and type-2 diabetes. However, major obstacles hamper BA-based treatment of obesity, including the scarcity of BAs in adult humans.

HOW TO INCREASE THE MASS OF BROWN-LIKE ADIPOCYTES IN OBESE PATIENTS?

Brown adipocytes present at birth persist only around deep organs in healthy adult humans. In addition, BA activity is lower in overweight and obese individuals than in lean ones (4). The proof-of-concept of the beneficial effects of brown fat transplantation has been achieved in rodents, where normoglycemia was restored in diabetic mice and obesity reduced in Ob/Ob mice (5–7). This has given rise to the notion of increasing the BA mass in obese patients as a therapeutic approach to counteract obesity and its associated metabolic complications. A challenge now is to identify an abundant source of human BA progenitors (BAPs) for transplantation. The generation of induced pluripotent stem cells from obese patients as an unlimited source of BAPs that could be expanded for autologous transplantation is a recently discussed option [(8–10) and see below]. Another option that we discuss in the present review is to promote endogenous BA generation in obese patients. Understanding the mechanisms governing the commitment of human pluripotent stem cells toward the brown-like adipogenic lineage, as well as the differentiation of BAPs into functional BAs, should help addressing this issue.

HUMAN CELL MODELS AVAILABLE FOR INVESTIGATING BROWN-LIKE ADIPOCYTE BIOLOGY

The identification of molecular mechanisms involved in thermogenic adipocyte generation is progressing substantially in mice. However, much less is known in humans, thus highlighting the need for an *in vitro* model of human adipocyte development. Because of the rareness of BAs in adult humans, immortalized cell lines or multipotent stem cells derived from adipose tissues of young donors (hMADS cells) are the main cellular models used to identify pathways critical for adipogenesis. PAZ6 cells are preadipocytes derived from the vascular stromal fraction of infant BAT which have been immortalized *ex vivo* using the SV40T and t antigens (11). Human preadipocytes from adult BAT localized in deep neck fat can also be immortalized, as recently described (12). hMADS cell lines have been isolated from adipose tissues of young donors in our laboratory. They are not immortalized cells, but can be maintained for several passages *in vitro* thanks to the intrinsic high self-renewal capacity of stem cells (13, 14). Interestingly, hMADS cells can be converted into functional brown-like adipocytes (15). However, the features of infant hMADS dramatically decrease with aging. In addition, these cells are already committed in the adipose lineage, thus precluding the possibility of investigating the earliest steps of adipogenesis.

PLURIPOTENT STEM CELLS REPRESENT A POWERFUL MODEL TO IDENTIFY PATHWAYS GOVERNING THERMOGENIC ADIPOCYTE DEVELOPMENT

Pluripotent stem cells (PSCs), i.e., embryonic stem cells (ESCs) and induced pluripotent stem cells (iPSCs), display a quasi-unlimited self-renewal capacity and are an abundant source of multiple cell types of therapeutic interest. Some papers in the early 2000s reported the potential of human ES cells to generate adipocytes (16–18). These observations suggested that PSCs could be a valuable tool to identify pathways regulating the different steps of adipogenesis, i.e., from the generation of adipose progenitors to their differentiation into mature adipocytes. Then, Taura et al. demonstrated that human iPSCs have an adipogenic potential comparable to that of human ES cells (19). However, these authors did not address the adipogenesis efficiency and the phenotype of adipocytes generated. Surprisingly, a cocktail of hematopoietic factors allowed Nishio and colleagues to report, for the first time, the capacity of human iPSCs to generate substantial BAs (20). These findings support the idea that, as previously shown in mice (21), the BMP signaling pathway plays a critical role in human brown adipocyte generation. However, Nishio did not purify BAPs from differentiating hiPSCs and there was no evidence that the stem cells progressed through a complete adipogenic program to generate adipocytes. Ahfeldt et al. purified hiPSC-derived fibroblasts that were able to undergo differentiation into white adipocytes or BAs following forced expression of adipogenic master genes (22). This strategy allows the generation of human BAs and may be a powerful tool for drug discovery, but the question arises as to whether these cells with ectopic expression of adipogenic master genes faithfully reflect physiological adipogenesis. More recently, a procedure to isolate expandable BAPs from hiPSCs and to generate high levels of functional BAs with no gene transfer was described (8, 23, 24). West and colleagues clonally derived several white- and brown- adipocyte progenitors

from hES cell lines and assessed their adipogenic potential when encapsulated in a biocompatible matrix approved for use in human clinical studies (25). These models provide an opportunity to make effective use of hiPSC features to identify critical pathways governing the development of brown-like adipocytes.

HUMAN PLURIPOTENT STEM CELL COMMITMENT TOWARD THE BROWN-LIKE ADIPOGENIC LINEAGE IS NEGATIVELY REGULATED BY THE RETINOIC ACID PATHWAY

Mohsen-Kanson and colleagues, in our laboratory, investigated factors involved in the commitment of pluripotent stem cells toward adipogenic lineages (23). Four hiPS cell lines and one hES cell line were studied for that purpose. Adipogenic markers, including *UCP1*, *Dio2*, *PGC1α*, and *PRDM16,* were detected in differentiated cultures, indicating that cells having a brown-like adipocyte gene program were spontaneously generated during differentiation. However, the adipogenesis efficiency was weak. Indeed, adipocytes were co-stained with LipidTox (for triglyceride staining) and CD73 (an adipocyte cell surface marker), and then quantified by flow cytometry (26). The data showed that the number of LipidTox$^+$/CD73$^+$ cells represented only 2% of cells in the differentiated cultures. Small-scale drug screening to uncover signaling pathways regulating the earliest steps of human adipogenesis revealed that the retinoic acid (RA) pathway promoted hiPSCS commitment toward the adipogenic lineage by increasing the number of LipidTox$^+$/CD73$^+$ cells to 15%. In contrast, expression of the brown adipocyte specific marker *UCP1* was inhibited in RA-treated cultures. Together, these data support the hypothesis that RA pathway activation at an early development stage dramatically promotes the differentiation of human PSCs into the UCP1-negative adipocyte lineage, while inhibiting UCP1-positive adipocyte generation (see **Figure 1**). This observation is reminiscent of the critical role of RA in the early steps of mouse ES cell white adipogenesis (27, 28). The identification of RA targets could provide a means to uncover genes involved in the earliest steps of adipogenesis. The combination of computational and experimental approaches in mouse ES cells revealed an extensive network of transcription factors that might coordinate the expression of genes essential for the acquisition of adipocyte characteristics (29). This could represent a unique comprehensive resource that could be further explored to investigate human adipocye development.

CRITICAL ROLE OF THE TGFβ PATHWAY IN HIPSC-BA PROGENITOR DIFFERENTIATION

Several research groups, including ours, have reported that hiPSC-BAPs display a low adipogenic capacity that hamper their use in cell-based therapy and basic research. In fact, Chen et al. first underlined the limited capacity of hiPSC-derived progenitors to undergo adipocyte differentiation, a feature that is often observed by authors but not always

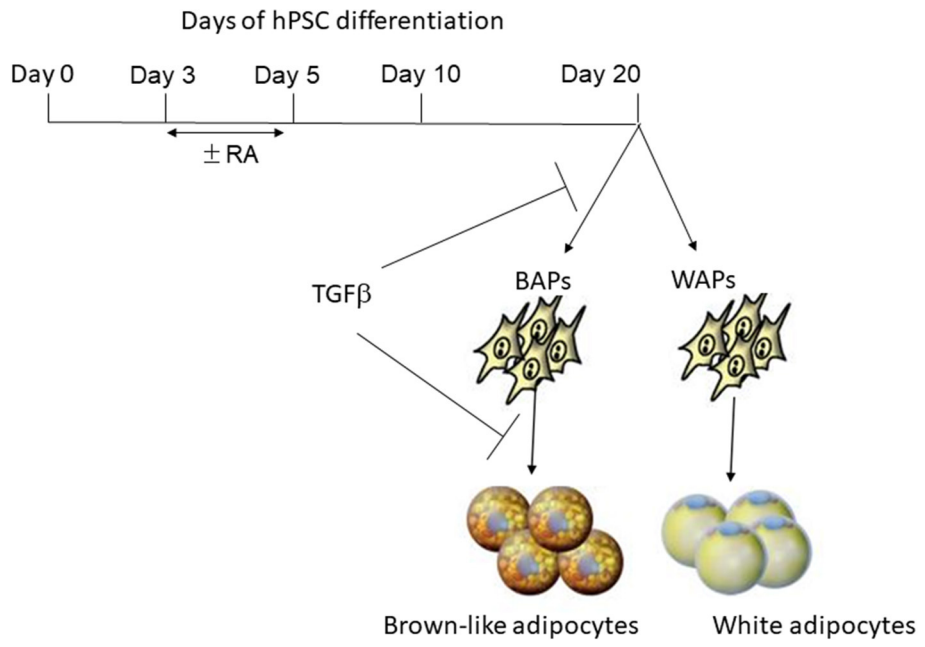

FIGURE 1 | Regulation of brown-like adipose progenitor generation by RA and TGFβ pathways. Treatment of early differentiated hPSCs with retinoic acid (RA) for a short period of time (between days 3–5) inhibits the generation of brown-like adipose progenitors (BAPs) while promoting the generation of white adipose progenitors (WAPS). The TGFβ pathway inhibits both the generation of BAPs and their differentiation into mature adipocytes.

pointed out (30). Interestingly, the low adipogenic differentiation potential is not restricted to hiPSC-derived cells as cells derived from human hESCs display the same feature, thus ruling out the possibility that the low hiPSC-adipogenic capacity could be due to incomplete reprogramming. The low adipogenic potential of adipose progenitors is also not dependent on the methods used to derive them from PSCs (31). Overall, these observations indicated that appropriate culture conditions had to be set up to unlock hPSC-BAP adipogenesis. Ascorbic acid, EGF, hydrocortisone, activin A and IL4 have been shown to regulate hiPSC-BAPs differentiation (8, 23, 24, 32) (see **Table 1**). However, TGFβ signaling has a pivotal role. The TGFβ pathway has emerged as a critical anti-adipogenic player through the Smad 2/3 activation (33–35). Deletion of TGFβ receptor 1 in mice has been shown to promote brown-like adipogenesis within white adipose tissue, thus supporting a model where TGFβ receptor signaling plays a role in regulating the pool of BAPs (36). The Smad2/3 pathway was found to be active during hiPSC-BAP differentiation, suggesting that bioactive TGFβ family members were secreted, which might lock differentiation (24). In agreement with this hypothesis, Su et al. showed more recently that the expression of TGFβ-ligands and -receptors increased during the differentiation of FOXF1 mesoderm progenitors toward adipocytes during hiPSCs development (8). The anti-adipogenic role of the TGFβ pathway has also been functionally demonstrated via use of the TGFβ inhibitor SB431542 (37). Inhibition of the active Smad 2/3 pathway upon SB431542 addition during hiPSC-BAP differentiation induced a sharp increase in *UCP1* expression and in the number of mature BAs (8, 24, 38). **Figure 1** illustrates the regulation of brown-like adipocyte generation from hPSCs by the retinoic acid and TGFβ pathways. Wankhade and colleagues proposed that negative regulation of PGE2/Cox-2 by TGFβ is involved in the recruitment of brown-like adipose progenitors (36). Interestingly, inhibition of the TGFβ pathway is not a prerequisite for adult adipose tissue-derived adipose progenitor differentiation. The low hiPSC-BAP adipogenic capacity compared to human adult-BAPs is reminiscent of the findings of Wang et al. who described distinct mechanisms regulating differentiation of embryonic-like and adult adipose progenitors in mice (39). Our hypothesis is that several pathways inhibit the development of PSC-BAs, which means that small molecules must be used to unlock differentiation. We also hypothesize that the current 2D culture conditions are not effective in promoting hiPSC-BAP differentiation. The development of new *in vitro* culture methods better mimicking the structure of human adipose tissue could now help decipher relevant regulators of BA adipogenesis.

TABLE 1 | Pathways regulating brown/brown-like adipocyte generation from human pluripotent stem cells.

hPSCs	Pathways/facors	References
hESCs, hiPSCs	BMP7, VEGFA, FLT3LG, IL6, IGF2	Nishio et al. (20)
hESCs, hiPSCs	Retinoic acid	Mohsen-Kanson et al. (24)
hiPSCs	BMP7, activin A	Guenantin et al. (32)
hiPSCs	Ascorbic acid, hydrocortisone, EGF	Hafner et al. (38)
hiPSCs	IL4	Su et al. (8)
hiPSCs	TGFβ	Hafner et al. (38) Su et al. (8)

THE NEXT STEPS TOWARD GAINING GREATER INSIGHT INTO THE DEVELOPMENT OF HUMAN BAs: 3D ADIPOSPHERES GENERATION

The weak efficacy of hiPSC-BAP differentiation might partially be explained by the culture conditions, which do not mimic the physiological microenvironment in which cells normally reside within adipose tissue. Cells are conventionally grown as monolayers in 2D, which is out of line with the *in vivo* situation. Adipose tissue exhibits a complex lobular architecture that plays a functional role in adipogenesis (40). Indeed, adipose tissue is highly vascularized and made up of lobules, corresponding to clusters of adipocytes, separated from each other by a structured extracellular matrix (41). Interestingly, it has been proposed that the adipocyte browning phenomenon specifically occurs in these lobules (42). In an effort to enhanced the physiological relevance of *in vitro* studies, 3D culture technologies and bioengineering methods for seeding different cell types in an organoid-like structure are highly promising (43–46). 3D cultures represent a bridge between traditional cell culture and live tissue. But, could these new technologies be applied to hiPSC-BAPs maintenance and differentiation? It is interesting to note that hiPSC-BAs have been generated by several teams via the formation of hiPSC-embryoids in suspension (20, 22, 23, 38). This strongly suggests that hiPSC-BAPs could be maintained in 3D culture conditions. The next challenge will be the generation of 3D hiPSC-brown-like adipospheres resembling human adipose tissue. The challenges will include to enrich hiPSC-brown-like adipospheres with endothelial cells and macrophages embedded in an extracellular matrix allowing functional bidirectional interactions between the microenvironment and adipocytes.

CONCLUSIONS

Human pluripotent stem cells provide an opportunity to characterize pathways that play a role in the different steps of thermogenic adipocyte development. Some factors have been identified, but their impact on other hiPSC-derived cells of interest such as white adipocytes, endothelial cells and macrophages, has yet to be determined and integrated in a relevant model. 3D culture of hiPSC-adipospheres in which BAs interact with cell types that are present in the adipose tissue microenvironment will provide a more suitable physiological *in vitro* condition that should lead to the identification of druggable pathways to counteract obesity and its associated metabolic disorders.

AUTHOR CONTRIBUTIONS

XY, VD, and CD contributed to the conception and design of the review. XY and VD generated the data shown. CD wrote the manuscript. All authors approved the submitted version.

FUNDING

Research related to this review in Dani's team was supported by the French National Research Agency (grant number ANR-18-CE18-0006-01) and through the Investments for the Future (LABEX SIGNALIFE: program reference # ANR-11-LABX-0028-01).

REFERENCES

1. Rosen ED, Spiegelman BM. What we talk about when we talk about fat. *Cell*. (2014) 156:20–44. doi: 10.1016/j.cell.2013.12.012
2. Himms-Hagen J. Brown adipose tissue thermogenesis: interdisciplinary studies. *Faseb J*. (1990) 4:2890–8. doi: 10.1096/fasebj.4.11.2199286
3. Villarroya F, Giralt M. The beneficial effects of brown fat transplantation: further evidence of an endocrine role of brown adipose tissue. *Endocrinology*. (2015) 156:2368–70. doi: 10.1210/en.2015-1423
4. van Marken Lichtenbelt WD, Vanhommerig JW, Smulders NM, Drossaerts JM, Kemerink GJ, Bouvy ND, et al. Cold-activated brown adipose tissue in healthy men. *N Engl J Med*. (2009) 360:1500–8. doi: 10.1056/NEJMoa0808718
5. Stanford KI, Middelbeek RJ, Townsend KL, An D, Nygaard EB, Hitchcox KM, et al. Brown adipose tissue regulates glucose homeostasis and insulin sensitivity. *J Clin Invest*. (2013) 123:215–23. doi: 10.1172/JCI62308
6. Liu X, Wang S, You Y, Meng M, Zheng Z, Dong M, et al. Brown adipose tissue transplantation reverses obesity in Ob/Ob mice. *Endocrinology*. (2015) 156:2461–9. doi: 10.1210/en.2014-1598
7. Min SY, Kady J, Nam M, Rojas-Rodriguez R, Berkenwald A, Kim JH, et al. Human 'brite/beige' adipocytes develop from capillary networks, and their implantation improves metabolic homeostasis in mice. *Nat Med*. (2016) 22:312–8. doi: 10.1038/nm.4031
8. Su S, Guntur AR, Nguyen DC, Fakory SS, Doucette CC, Leech C, et al. A renewable source of human beige adipocytes for development of therapies to treat metabolic syndrome. *Cell Rep*. (2018) 25:3215–28 e3219. doi: 10.1016/j.celrep.2018.11.037
9. Brown AC. Brown adipocytes from induced pluripotent stem cells-how far have we come? *Ann N Y Acad Sci*. (2019). doi: 10.1111/nyas.14257. [Epub ahead of print].
10. Yao X, Salingova B, Dani C. Brown-like adipocyte progenitors derived from human ips cells: a new tool for anti-obesity drug discovery and cell-based therapy? *Handb Exp Pharmacol*. (2019) 251:97–105. doi: 10.1007/164_2018_115
11. Kazantzis M, Takahashi V, Hinkle J, Kota S, Zilberfarb V, Issad T, et al. PAZ6 cells constitute a representative model for human brown pre-adipocytes. *Front Endocrinol*. (2012) 3:13. doi: 10.3389/fendo.2012.00013
12. Xue R, Lynes MD, Dreyfuss JM, Shamsi F, Schulz TJ, Zhang H, et al. Clonal analyses and gene profiling identify genetic biomarkers of the thermogenic potential of human brown and white preadipocytes. *Nat Med*. (2015) 21:760–8. doi: 10.1038/nm.3881
13. Rodriguez A-M, Pisani D, Dechesne CA, Turc-Carel C, Kurzenne J-Y, Wdziekonski B, et al. Transplantation of a multipotent cell population from human adipose tissue induces dystrophin expression in the immunocompetent mdx mouse. *J Exp Med*. (2005) 201:1397–405. doi: 10.1084/jem.20042224
14. Zaragosi LE, Ailhaud G, Dani C. Autocrine fibroblast growth factor 2 signaling is critical for self-renewal of human multipotent adipose-derived stem cells. *Stem Cells*. (2006) 24:2412–9. doi: 10.1634/stemcells.2006-0006
15. Elabd C, Chiellini C, Carmona M, Galitzky J, Cochet O, Petersen R, et al. Human multipotent adipose-derived stem cells differentiate into functional brown adipocytes. *Stem Cells*. (2009) 27:2753–60. doi: 10.1002/stem.200
16. Xiong C, Xie CQ, Zhang L, Zhang J, Xu K, Fu M, et al. Derivation of adipocytes from human embryonic stem cells. *Stem Cells Dev*. (2005) 14:671–5. doi: 10.1089/scd.2005.14.671
17. van Harmelen V, Astrom G, Stromberg A, Sjolin E, Dicker A, Hovatta O, et al. Differential lipolytic regulation in human embryonic stem cell-derived adipocytes. *Obesity*. (2007) 15:846–52. doi: 10.1038/oby.2007.595
18. Hannan NR, Wolvetang EJ. Adipocyte differentiation in human embryonic stem cells transduced with Oct4 shRNA lentivirus. *Stem Cells Dev*. (2009) 18:653–60. doi: 10.1089/scd.2008.0160
19. Taura D, Noguchi M, Sone M, Hosoda K, Mori E, Okada Y, et al. Adipogenic differentiation of human induced pluripotent stem cells: comparison with that of human embryonic stem cells. *FEBS Lett*. (2009) 583:1029–33. doi: 10.1016/j.febslet.2009.02.031
20. Nishio M, Yoneshiro T, Nakahara M, Suzuki S, Saeki K, Hasegawa M, et al. Production of functional classical brown adipocytes from human pluripotent stem cells using specific hemopoietin cocktail without gene transfer. *Cell Metab*. (2012) 16:394–406. doi: 10.1016/j.cmet.2012.08.001
21. Tseng YH, Kokkotou E, Schulz TJ, Huang TL, Winnay JN, Taniguchi CM, et al. New role of bone morphogenetic protein 7 in brown adipogenesis and energy expenditure. *Nature*. (2008) 454:1000–4. doi: 10.1038/nature07221
22. Ahfeldt T, Schinzel RT, Lee YK, Hendrickson D, Kaplan A, Lum DH, et al. Programming human pluripotent stem cells into white and brown adipocytes. *Nat Cell Biol*. (2012) 14:209–19. doi: 10.1038/ncb2411
23. Mohsen-Kanson T, Hafner AL, Wdziekonski B, Takashima Y, Villageois P, Carriere A, et al. Differentiation of human induced pluripotent stem cells into brown and white adipocytes: role of Pax3. *Stem Cells*. (2014) 32:1459–67. doi: 10.1002/stem.1607
24. Hafner AL, Contet J, Ravaud C, Yao X, Villageois P, Suknuntha K, et al. Brown-like adipose progenitors derived from human induced pluripotent stem cells: Identification of critical pathways governing their adipogenic capacity. *Sci Rep*. (2016) 6:32490. doi: 10.1038/srep32490
25. West MD, Chang CF, Larocca D, Li J, Jiang J, Sim P, et al. Clonal derivation of white and brown adipocyte progenitor cell lines from human pluripotent stem cells. *Stem Cell Res Ther*. (2019) 10:7. doi: 10.1186/s13287-018-1087-7
26. Schaedlich K, Knelangen JM, Navarrete Santos A, Fischer B, Navarrete Santos A. A simple method to sort ESC-derived adipocytes. *Cytometry A*. (2010) 77:990–5. doi: 10.1002/cyto.a.20953
27. Dani C, Smith A, Dessolin S, Leroy P, Staccini L, Villageois P, et al. Differentiation of embryonic stem cells into adipocytes *in vitro*. *J Cell Sci*. (1997) 110:1279–85.
28. Kawaguchi J, Mee PJ, Smith AG. Osteogenic and chondrogenic differentiation of embryonic stem cells in response to specific growth factors. *Bone*. (2005) 36:758–69. doi: 10.1016/j.bone.2004.07.019
29. Billon N, Kolde R, Reimand J, Monteiro MC, Kull M, Peterson H, et al. Comprehensive transcriptome analysis of mouse embryonic stem cell adipogenesis unravels new processes of adipocyte development. *Genome Biol*. (2010) 11:R80. doi: 10.1186/gb-2010-11-8-r80
30. Chen YS, Pelekanos RA, Ellis RL, Horne R, Wolvetang EJ, Fisk NM. Small molecule mesengenic induction of human induced pluripotent stem cells to generate mesenchymal stem/stromal cells. *Stem Cells Transl Med*. (2012) 1:83–95. doi: 10.5966/sctm.2011-0022
31. Hafner AL, Dani C. Human induced pluripotent stem cells: a new source for brown and white adipocytes. *World J Stem Cells*. (2014) 6:467–72. doi: 10.4252/wjsc.v6.i4.467
32. Guenantin AC, Briand N, Capel E, Dumont F, Morichon R, Provost C, et al. Functional human beige adipocytes from induced pluripotent stem cells. *Diabetes*. (2017) 66:1470–8. doi: 10.2337/db16-1107
33. Zaragosi LE, Wdziekonski B, Villageois P, Keophiphath M, Maumus M, Tchkonia T, et al. Activin a plays a critical role in proliferation and differentiation of human adipose progenitors. *Diabetes*. (2010) 59:2513–21. doi: 10.2337/db10-0013

34. Zamani N, Brown CW. Emerging roles for the transforming growth factor-β superfamily in regulating adiposity and energy expenditure. *Endocr Rev*. (2011) 32:387–403. doi: 10.1210/er.2010-0018
35. Bourlier V, Sengenes C, Zakaroff-Girard A, Decaunes P, Wdziekonski B, Galitzky J, et al. TGFβ family members are key mediators in the induction of myofibroblast phenotype of human adipose tissue progenitor cells by macrophages. *PLoS ONE*. (2012) 7:e31274. doi: 10.1371/journal.pone.0031274
36. Wankhade UD, Lee JH, Dagur PK, Yadav H, Shen M, Chen W, et al. TGF-β receptor 1 regulates progenitors that promote browning of white fat. *Mol Metab*. (2018) 16:160–71. doi: 10.1016/j.molmet.2018.07.008
37. Inman GJ, Nicolas FJ, Callahan JF, Harling JD, Gaster LM, Reith AD, et al. SB-431542 is a potent and specific inhibitor of transforming growth factor-β superfamily type I activin receptor-like kinase (ALK) receptors ALK4, ALK5, and ALK7. *Mol Pharmacol*. (2002) 62:65–74. doi: 10.1124/mol.62.1.65
38. Hafner AL, Mohsen-Kanson T, Dani C. Differentiation of brown adipocyte progenitors derived from human induced pluripotent stem cells. *Methods Mol Biol*. (2018) 1773:31–9. doi: 10.1007/978-1-4939-7799-4_4
39. Wang QA, Tao C, Jiang L, Shao M, Ye R, Zhu Y, et al. Distinct regulatory mechanisms governing embryonic versus adult adipocyte maturation. *Nat Cell Biol*. (2015) 17:1099–111. doi: 10.1038/ncb3217
40. Esteve D, Boulet N, Belles C, Zakaroff-Girard A, Decaunes P, Briot A, et al. Lobular architecture of human adipose tissue defines the niche and fate of progenitor cells. *Nat Commun*. (2019) 10:2549. doi: 10.1038/s41467-019-09992-3
41. Wassermann F. The development of adipose tissue. *Compr Physiolo*. (1965). 87 (Suppl. 15):100.
42. Barreau C, Labit E, Guissard C, Rouquette J, Boizeau ML, Gani Koumassi S, et al. Regionalization of browning revealed by whole subcutaneous adipose tissue imaging. *Obesity*. (2016) 24:1081–9. doi: 10.1002/oby.21455
43. Horvath P, Aulner N, Bickle M, Davies AM, Nery ED, Ebner D, et al. Screening out irrelevant cell-based models of disease. *Nat Rev Drug Discov*. (2016) 15:751–69. doi: 10.1038/nrd.2016.175
44. Takebe T, Zhang B, Radisic M. Synergistic engineering: organoids meet organs-on-a-chip. *Cell Stem Cell*. (2017) 21:297–300. doi: 10.1016/j.stem.2017.08.016
45. Langhans SA. Three-dimensional *in vitro* cell culture models in drug discovery and drug repositioning. *Front Pharmacol*. (2018) 9:6. doi: 10.3389/fphar.2018.00006
46. Liu C, Oikonomopoulos A, Sayed N, Wu JC. Modeling human diseases with induced pluripotent stem cells: from 2D to 3D and beyond. *Development*. (2018) 145:dev156166. doi: 10.1242/dev.156166

Conflict of Interest: The authors declare that the research was conducted in the absence of any commercial or financial relationships that could be construed as a potential conflict of interest.

frontiers in Endocrinology

ORIGINAL RESEARCH
published: 21 February 2020
doi: 10.3389/fendo.2020.00073

Fatty Acid Metabolite Profiling Reveals Oxylipins as Markers of Brown but Not Brite Adipose Tissue

Sebastian Dieckmann[1,2,3], *Stefanie Maurer*[1,2,3], *Tobias Fromme*[1,2,3], *Cécilia Colson*[4], *Kirsi A. Virtanen*[5], *Ez-Zoubir Amri*[4] *and Martin Klingenspor*[1,2,3]*

[1] Chair for Molecular Nutritional Medicine, TUM School of Life Sciences, Technical University of Munich, Freising, Germany, [2] EKFZ - Else Kröner-Fresenius Center for Nutritional Medicine, Technical University of Munich, Freising, Germany, [3] ZIEL Institute for Food and Health, TUM School of Life Sciences, Technical University of Munich, Freising, Germany, [4] Université Côte d'Azur, CNRS, Inserm, iBV, Nice, France, [5] Turku PET Centre, Turku University Hospital, University of Turku, Turku, Finland

Metabolites of omega-6 and omega-3 polyunsaturated fatty acids are important signaling molecules implicated in the control of adipogenesis and energy balance regulation. Some of these metabolites belonging to the group of oxylipins have been associated with non-shivering thermogenesis in mice mediated by brown or brite adipose tissue. We aimed to identify novel molecules with thermogenic potential and to clarify the relevance of these findings in a translational context. Therefore, we characterized and compared the oxylipin profiles of murine and human adipose tissues with different abundance of brown or brite adipocytes. A broad panel of 36 fatty acid metabolites was quantified in brown and white adipose tissues of C57BL/6J mice acclimatized to different ambient temperatures and in biopsies of human supraclavicular brown and white adipose tissue. The oxylipin profile of murine brite adipose tissue was not distinguishable from white adipose tissue, suggesting that adipose tissue browning *in vivo* is not associated with major changes in the oxylipin metabolism. Human brown and white adipose tissue also exhibited similar metabolite profiles. This is in line with previous studies proposing human brown adipose tissue to resemble the nature of murine brite adipose tissue representing a heterogeneous mixture of brite and white adipocytes. Although the global oxylipin profile served as a marker for the abundance of thermogenic adipocytes in bona fide brown but not white adipose tissue, we identified 5-HETE and 5,6-EET as individual compounds consistently associated with the abundance of brown or brite adipocytes in human BAT and murine brite fat. Further studies need to establish whether these candidates are mere markers or functional effectors of thermogenic capacity.

Keywords: adipose tissue, browning, thermogenesis, PUFA (polyunsaturated fatty acid), n-6 fatty acid, n-3 fatty acid, oxylipin

OPEN ACCESS

Edited by:
Matthias Johannes Betz, University Hospital of Basel, Switzerland

Reviewed by:
Denis Richard, Laval University, Canada
Christian Wolfrum, ETH Zürich, Switzerland

***Correspondence:**
Martin Klingenspor
mk@tum.de

Specialty section:
This article was submitted to Obesity, a section of the journal Frontiers in Endocrinology

Received: *29 November 2019*
Accepted: *03 February 2020*
Published: *21 February 2020*

Citation:
Dieckmann S, Maurer S, Fromme T, Colson C, Virtanen KA, Amri E-Z and Klingenspor M (2020) Fatty Acid Metabolite Profiling Reveals Oxylipins as Markers of Brown but Not Brite Adipose Tissue. Front. Endocrinol. 11:73. doi: 10.3389/fendo.2020.00073

INTRODUCTION

Obesity is one of today's major health burdens with a steadily increasing prevalence. It is characterized by excessive fat accumulation and unhealthy expansion of white adipose tissue (WAT) associated with severe comorbidities such as type 2 diabetes and cardiovascular diseases. Obesity is the consequence of a chronic positive energy balance, a state where energy intake

exceeds energy expenditure. A major obstacle of obesity management is the maintenance of a given body weight loss, since weight loss is accompanied by a notable and persistent decrease in energy expenditure (1, 2). This decrease in energy expenditure is hardly compensated by physical activity, the only available strategy to increase energy expenditure so far. Consequently, other means to increase energy expenditure are in demand. Thermogenic tissues such as brown (BAT) and brite adipose tissue are promising targets. Brite adipose tissue, in contrast to BAT, is an inducible type of fat originating from the recruitment of brown-like, so called brite (or beige) cells with thermogenic properties in WAT. Both tissues dissipate chemical energy from fatty acids and glucose to generate heat, thus increasing energy expenditure. This non-shivering thermogenesis is mediated by uncoupling protein 1 (UCP1). It is naturally activated upon cold exposure to defend body temperature and during eating to promote meal termination (3). Although the presence of functional BAT has been confirmed in adult humans (4–6), humans mostly live under thermoneutral conditions (7). Therefore, BAT activation in humans is mostly associated with food intake, whereas cold-induced activation is less prevalent. BAT volume and activity negatively correlate with BMI (8), suggesting a lower abundance of active BAT in overweight and obese compared to lean subjects. Consequently, the therapy of obesity by means of BAT and brite fat not only requires strategies to activate it but also to increase its abundance. Several natural compounds and drugs are associated with the activation and recruitment of BAT in mice and humans (9, 10). Among these are metabolites of omega-6 and omega-3 polyunsaturated fatty acids (PUFA). Oxygenated PUFA metabolites, belonging to the group of oxylipins, are important signaling molecules implicated in the control of adipogenesis and energy balance regulation (11). These potent and short-lived metabolites are generated by a series of enzymatic steps involving one of three enzyme classes—cyclooxygenase (COX), lipoxygenase (LOX) or cytochrome P450 (CYP) (12). Some oxylipins have been associated with the browning of adipose tissues. The COX derived ARA metabolites prostaglandin E2 (PGE2) and prostacyclin (PGI2) facilitate the formation of brite adipocytes *in vitro* (13–16). The oxylipin 12-hydroxyeicosapentaenoic acid (12-HEPE), identified in a PUFA metabolite screen in murine serum samples, facilitates glucose uptake into brown adipocytes (17). In a similar approach, increased levels of 12,13-dihydroxy-9Z-octadecenoic acid (12,13-diHOME) were identified in oxylipin profiles of human serum after cold acclimatization (18). This oxylipin increases fatty acid uptake into brown adipocytes and presumably UCP1 expression (18). Furthermore, a second class of PUFA derived metabolites, the endocannabinoids, are suggested to be involved in the negative regulation of BAT activity in mice (19). Thus, several lines of evidence suggest PUFA-derived metabolites to be involved in the recruitment and activity of thermogenic cells in mice and humans. The aim of the current study was to characterize the oxylipin profiles of murine and human adipose tissues with different abundance of brown and brite adipocytes to identify novel molecules with thermogenic potential in a translational context.

We quantified a panel of 36 fatty acid metabolites in brown and white adipose tissues of C57BL/6J mice acclimatized to different ambient temperatures and in biopsies of human supraclavicular brown and white adipose tissue. Our results reveal the global oxylipin profile of bona fide brown but not brite adipose tissue as a marker for the abundance of brown adipocytes. Moreover, we identified 5-HETE and 5,6-EET as individual compounds associated with the abundance of brown or brite adipocytes in both human BAT and murine brite fat.

MATERIALS AND METHODS

Animal Experiments

Eight-week-old male C57BL/6J mice were housed in climate cabinets (HPP750 life, Memmert) at 23°C and 55% humidity with a 12/12 h light/dark cycle. Mice were provided *ad libitum* access to water and a control diet (Ssniff, Cat# S5745-E720). After an adaptation phase of 3 weeks, mice were assigned to one of two groups and transferred to preconditioned cabinets at 5 or 30°C. After 1 week, mice were killed by CO_2 exposure and tissues were immediately dissected, snap frozen in liquid nitrogen, and stored at −80°C until further processing. The experiment was performed according to the German animal welfare law with permission from the district government of Upper Bavaria (Regierung von Oberbayern, reference number ROB-55.2-2532.Vet_02-16-166).

Human Subjects

Paired biopsies of BAT and WAT were obtained from the supraclavicular region of 14 healthy male and female subjects. A detailed description of the biopsy procedure and of anthropometric characteristics of this study cohort has been published previously (20). Depending on the size of the specimens obtained, BAT and WAT were either entirely subjected to RNA isolation or grinded in liquid nitrogen to obtain aliquots used for both metabolite analysis and RNA isolation.

Oxylipin and Endocannabinoid Profiling

Murine interscapular BAT, inguinal WAT and human supraclavicular fat biopsies were grinded in liquid nitrogen. Aliquots of 23–140 mg were subjected to oxylipin and endocannabinoid analysis, which was conducted at the Metatoul lipidomic platform (INSERM UMR1048, Toulouse, France), certified to ISO 9001:2015 standards. Metabolite abundance was normalized to tissue mass.

RNA Isolation and Quantitative Real-Time PCR (qRT-PCR)

RNA isolation from murine inguinal WAT and supraclavicular BAT as well as human adipose tissues was performed with TRIsure™ (Bioline, Cat# BIO-38032) according to the manufacturer's instructions. Precipitated RNA was transferred to spin columns (SV Total RNA Isolation System, Promega, Cat# Z3105), centrifuged for 1 min with 12,000 × g and further processed according to the supplier's instructions. RNA concentration was determined spectrophotometrically (Infinite 200 PRO NanoQuant, Tecan). Generation of cDNA was performed with 1 μg RNA (SensiFAST™ cDNA Synthesis

Kit, Bioline, Cat# BIO-65053). qRT-PCR was performed in a 384 well plate format with the LightCylcer 480 system (Roche Diagnostics) in a total reaction volume of 12.5 µl containing 6.25 µl 2x SensiMix SYBR no-ROX (Bioline, Cat# QT650-05), 250 nM forward and reverse primers and 1 µl template cDNA. Murine primers (Ucp1 5′-TCTCTGCCAGGACAGTACCC-3′ and 5′-AGAAGCCCAATGATGTTCAG-3′, Tf2b 5′-TGGAGA TTTGTCCACCATGA-3′ and 5′-GAATTGCCAAACTCATCA AAACT-3′) and human primers (UCP1 5′-GGAGGCCTTTGT GAAAAACA-3′ and 5′-CTTGAAGAAAGCCGTTGGTC-3′, TF2B 5′-GCTGTGGAACTGGACTTGGT-3′ and 5′-AGTTTG TCCACTGGGGTGTC-3′) were produced by Eurofins MWG Operon. Expression of Ucp1 was normalized to transcription factor 2b (Tf2b) expression.

Statistical Analysis

All statistical analyses were performed using R-Studio (version 1.2.5019) with R version 3.6.1. Principal component analysis was performed with the R packages factoextra (version 1.0.5) and FactoMineR (version 1.42). Other statistical tests were calculated with the R package ggpubr (version 0.2.3). Wilcoxon test was performed for all group comparisons, after checking the assumption of normal distribution with Shapiro–Wilk test. $P < 0.05$ were deemed statistically significant. The appropriate statistical test, paired, or unpaired is mentioned for each figure.

RESULTS

Adaptive, non-shivering thermogenesis is the key functional difference that discriminates mammalian BAT and WAT. Since almost a decade, the rediscovery of functional BAT in adult humans has intensified efforts to characterize the molecular properties of human adipose tissues and to identify novel thermogenic effectors intended for therapeutic use. Within this scope, oxylipins appear to be a promising class of endogenous compounds affecting the function and recruitment of thermogenic adipocytes in cultured cells of human and murine origin (11). In the course of this study, we further elucidated the association of these metabolites with the recruitment of thermogenic brown and brite adipocytes in a translational context. To this end, we subjected BAT and WAT of murine and human origin to metabolite profiling and analyzed the data in consideration of the tissues' thermogenic properties. Human BAT and WAT biopsies were obtained from the supraclavicular region subsequent to PET imaging under cold-exposed conditions (20). Humans live within thermoneutral conditions most of their life (7). Thus, for a more appropriate comparison between mice and humans we acclimatized C57BL/6J mice to 30°C for 1 week to mimic the thermal environment of humans. In order to confirm the thermogenic potential of BAT vs. WAT in both humans and mice, Ucp1 mRNA expression was quantified as a surrogate marker for the abundance of thermogenic competent adipocytes. As expected, all BAT specimens were characterized by considerably higher Ucp1 mRNA levels compared to WAT with a wide range of inter-individual variation (**Figures 1A,B**). However, mean Ucp1 mRNA expression in human and murine BAT was 544- and 255-fold higher compared to WAT, respectively. Consequently, human and murine BAT harbor more brown adipocytes than WAT.

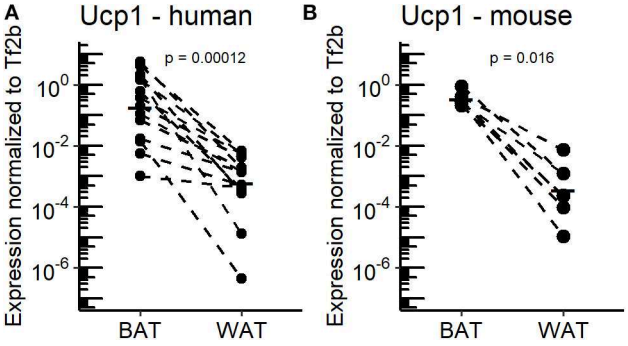

FIGURE 1 | Ucp1 expression in BAT and WAT of the murine and human study cohorts. **(A)** Uncoupling protein 1 (Ucp1) mRNA expression in supraclavicular brown adipose tissue (BAT) and white adipose tissue (WAT) of human subjects ($n = 14$). **(B)** Ucp1 mRNA expression in inguinal WAT and supraclavicular BAT of mice housed at 30°C for 1 week ($n = 7$). *P*-values are derived from paired Wilcoxon test.

The Abundance of Adipose Tissue Oxylipins Differs Between Mice and Humans

To elucidate the regulation of oxylipin production in BAT and WAT, we quantified a broad panel of 33 metabolites representing major oxylipin classes produced by mammalian tissues. Additionally, we quantified the levels of 3 AA-derived endocannabinoids. The oxylipin panel encompasses COX, LOX and CYP-derived metabolites generated by the conversion of arachidonic acid (AA), its n-6 precursor linoleic acid (LA), and the n-3 fatty acids eicosapentaenoic acid (EPA) and docosahexaenoic acid (DHA). Within this setting, LA-derived metabolites were most abundant, while n-3 derived metabolites had a relatively low abundance in inguinal WAT and interscapular BAT of mice (**Figure 2A**). This high abundance of LA-derived metabolites was reflected in a high percentage of LOX-derived metabolites (**Figure 2A**). In human adipose tissues, the relative abundance followed a slightly different pattern. In both human BAT and WAT, AA-derived metabolites produced via the COX-pathway accounted for a higher percentage of total oxylipin abundance compared to murine fat, which proportionally reduced the relative levels of LA and DHA-derived metabolites (**Figures 2A,B**). The contribution of EPA-derived oxylipins to the oxylipins pool was negligible in adipose tissues of both species. Of note, the contribution of CYP derived oxylipins in mice was higher in interscapular BAT compared to inguinal WAT while in humans no notable difference was observed. Despite this similar composition of the oxylipin pools in WAT and BAT, the total abundance of all oxylipins in BAT vs. WAT in mice was significantly lower while it was significantly higher in human BAT vs. WAT (**Figures 2C,D**). These differences are primarily attributed to changes in the abundance of the LA-derived oxylipins 9- and 13-HODE. These two oxylipins are the predominant species in WAT and BAT, accounting

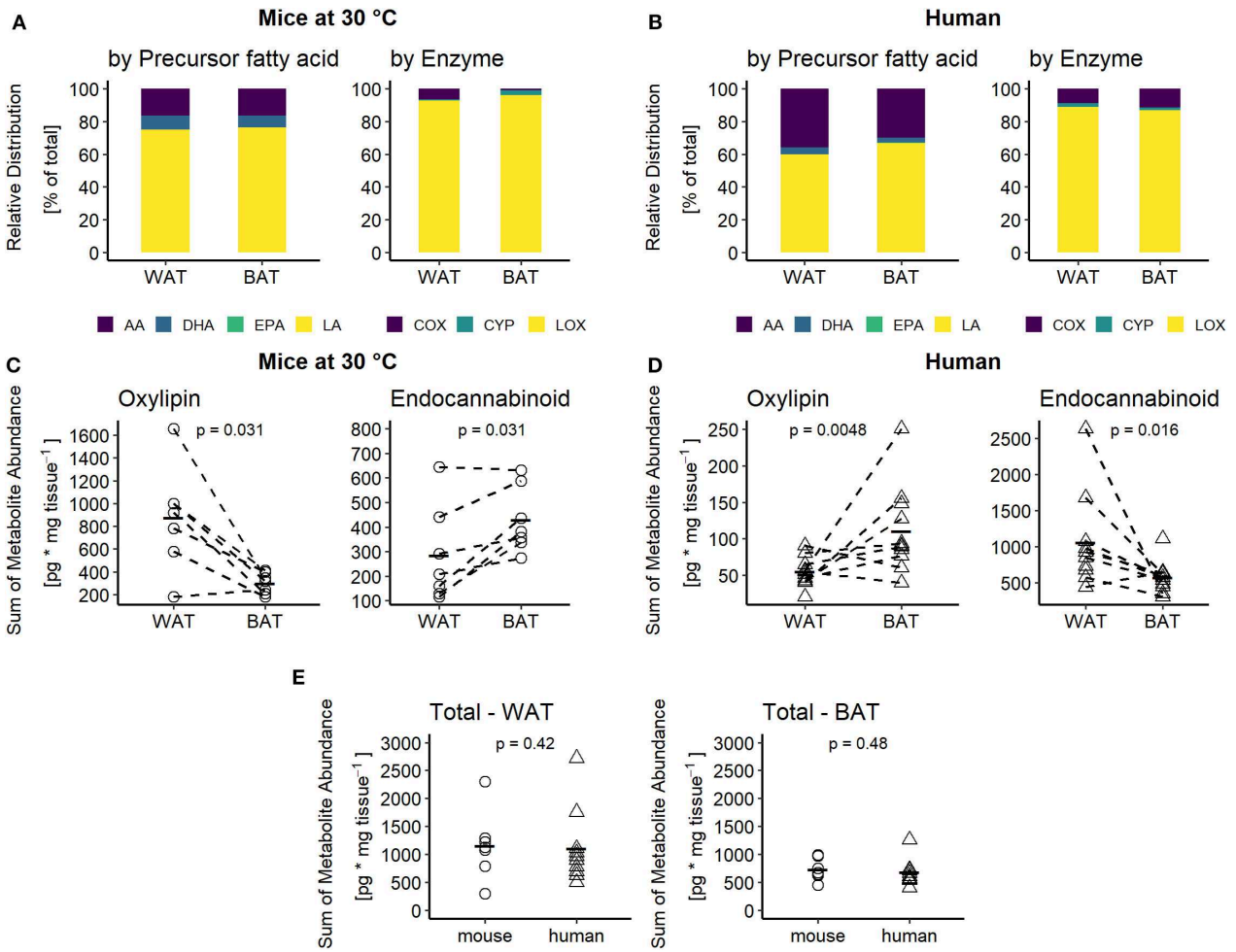

FIGURE 2 | Adipose tissues of mice and men are comparable in terms of oxylipins composition but not abundance. Relative distribution of oxylipins categorized by their common fatty acid progenitor (left) or enzymatic synthesis pathway (right) for **(A)** mice at 30°C and **(B)** humans. Total sum of oxylipins (left) or endocannabinoids (right) for each individual **(C)** mouse ($n = 7$) or **(D)** human subject ($n = 10$ for WAT and $n = 11$ for BAT). **(E)** Total sum of combined oxylipins and endocannabinoids in murine and human WAT and BAT. Statistical analysis paired Wilcoxon test **(C)** and unpaired Wilcoxon test **(D,E)**.

for at least 60% of the total oxylipin pool in adipose tissues of both species (**Figures 2A,B**). Endocannabinoids represent another class of fatty acid metabolites with potential effects on Ucp1 dependent thermogenesis (19). Interestingly, the total abundance of the three endocannabinoids was lower in murine WAT vs. BAT but higher in human WAT vs. BAT, while we observed the exact opposite for total oxylipin abundance (**Figures 2C,D**). Ultimately, considering the combined pool of oxylipins and endocannabinoids there was no difference in total metabolite abundance between murine and human WAT or BAT (**Figure 2E**). Conclusively, mice and humans are similar in terms of the total production of PUFA metabolites. However, these tissues seem to differ in the partitioning of PUFA metabolism.

The Global Oxylipin Profile Is a Surrogate Marker for the Abundance of Brown but Not Brite Adipocytes

As oxylipin abundance differs between WAT and BAT in both mice and humans, we investigated, whether oxylipins may serve as discriminative markers for the two tissues. Therefore, we applied principal component analysis (PCA) on the metabolite data of BAT and WAT. In mice, principal components 1 and 2 together explained 82.8% of the variability between WAT and BAT. In a continuum of these principal components, murine WAT and BAT formed distinct and separate clusters (**Figure 3A**). Thus, murine BAT and WAT can be distinguished by their characteristic oxylipin patterns. In humans, principal components 1 and 2 explained considerably less of the variation between BAT and WAT (54.5%). A distinction of human BAT and WAT according to their specific oxylipin patterns was not possible (**Figure 3B**). This was reflected in the analysis of the combined human and murine data set. In this analysis the two species formed distinct clusters separating the murine tissues while human BAT and WAT could not be distinguished (**Supplementary Figure 1A**). In contrast to murine BAT, human BAT constitutes a complex, interwoven mixture of both brown and white adipocytes. Consequently, oxylipin patterns established from human tissues may not represent differences on the cellular level of individual brown

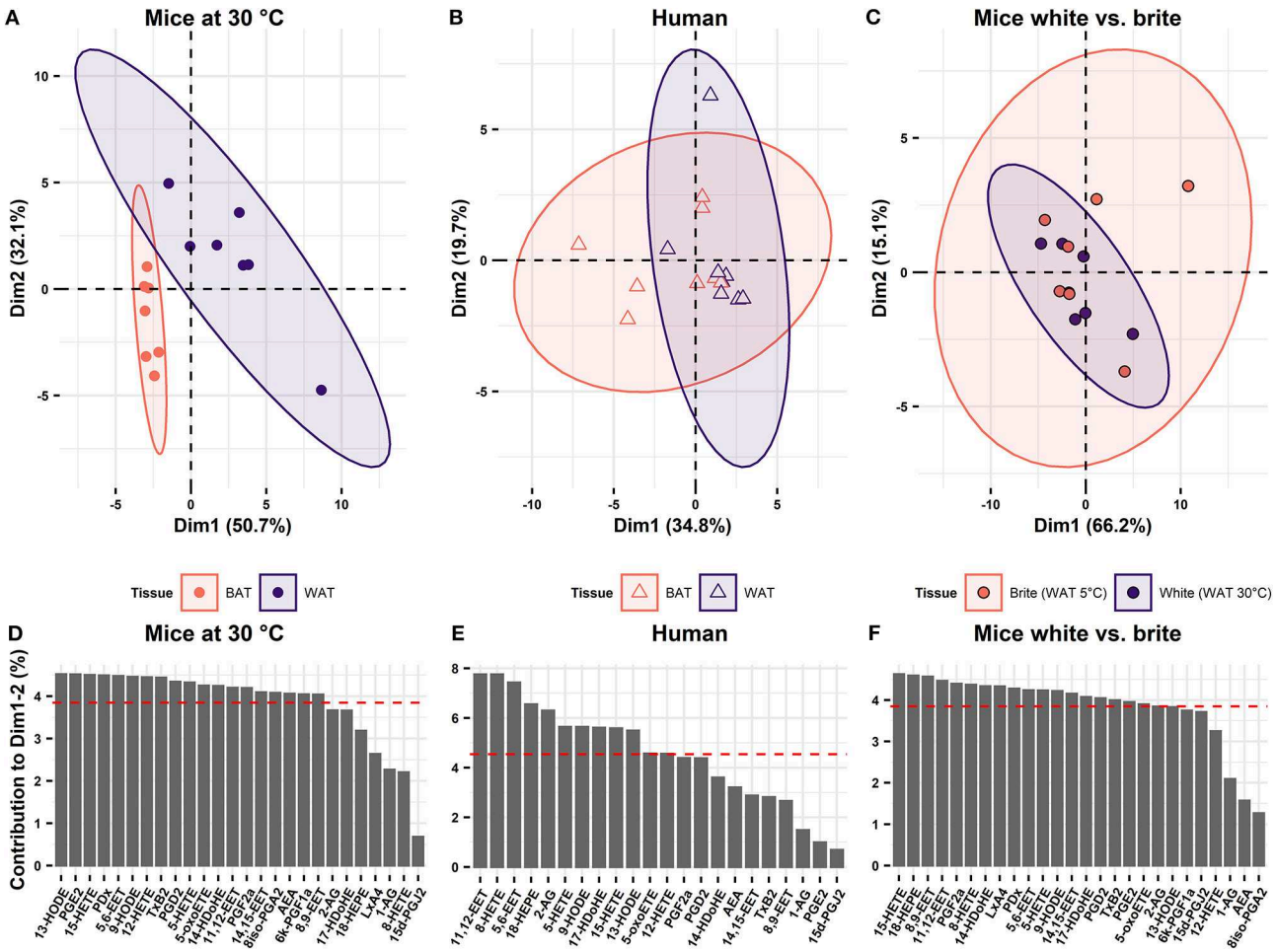

FIGURE 3 | Oxylipin profiles distinguish BAT but not brite adipose tissue from WAT. Principal component analysis of the oxylipins in BAT and WAT showing the two first principal components (Dim1 and Dim2) in **(A)** mice at 30°C ($n = 7$) and **(B)** human ($n = 8$). **(C)** Principal component analysis of oxylipins in murine WAT acclimatized to 5 or 30°C ($n = 7$). Contribution of the single variables to Dim1 and Dim2 for **(D)** mice at mice at 30°C, **(E)** human, and **(F)** murine WAT acclimatized to 5 or 30°C for 1 week. Red dashed line indicates the average contribution of all variables.

and white adipocytes and lack discriminative power (**Figure 3B**). To overcome this limitation, we transferred oxylipin patterns established from murine BAT and WAT and plotted human oxylipin levels according to these murine principal components. However, human BAT and WAT remained indistinguishable (**Supplementary Figure 1B**). Surprisingly, the reverse strategy, i.e., plotting murine oxylipin levels according to principal components of human oxylipin variation, murine BAT and WAT could be well-separated (**Supplementary Figure 1C**). This indicates that oxylipins in humans do not *per se* lack the variability observed in murine tissues but fail to sharply distribute into the categories BAT and WAT. The lack of discrimination of human supraclavicular BAT and WAT oxylipin patterns are in line with the observation that human supraclavicular BAT does not resemble the characteristics of classical BAT in conventional laboratory mice but rather displays a brite phenotype (7, 21). Indeed, brite adipose tissue obtained from mice housed at 5°C for 1 week and human supraclavicular BAT were both characterized by increased UCP1 expression compared to WAT (**Supplementary Figure 2** and **Figure 1A**). Murine brite adipose tissue contained a mixed population of unilocular white and multilocular brown/brite cells (**Supplementary Figure 3**), similarly to the phenotype reported from human supraclavicular BAT (7). We investigated this by comparing oxylipin profiles of inguinal WAT of mice acclimatized to either 30°C (white adipose tissue) or 5°C (brite adipose tissue). In this comparison, the principal components 1 and 2 explained a large proportion (81.3%) of the variation between brite and white adipose tissue (**Figure 3C**). However, murine brite and white adipose tissue could not be separated from one another by oxylipin patterns (**Figure 3C**), although both formed distinct populations separate from BAT (**Supplementary Figure 1D**). Interestingly, BAT of mice acclimatized to 5 or 30°C also formed distinguishable populations (**Supplementary Figure 1D**). This suggests the global BAT oxylipin profile as surrogate marker of the abundance of brown adipocytes, since BAT of 5°C acclimatized mice

contained more multilocular brown adipocytes than BAT of mice housed at 30°C. Conclusively, the oxylipin profiles of adipose tissues allow the discrimination of bona fide BAT and WAT composed of homogenous populations of brown and white adipocytes, respectively. However, it is either unsuitable to distinguish tissues harboring both types of cells or unable to distinguish brite from white adipocytes. Thus, the oxylipin profile can serve as a surrogate marker for brown adipocyte abundance in murine BAT but not murine brite fat or human BAT.

The Oxylipins 5-HETE and 5,6-EET Are Potential Markers of Brown Adipocyte Abundance in BAT in Mice and Humans

The oxylipin profile serves as a potential surrogate measure for the abundance of brown but not brite adipocytes. We asked which metabolites contributed the most to this phenomenon and whether we could identify novel oxylipins associated with the recruitment of brown and brite adipocytes. Therefore, we investigated the contribution of individual oxylipins to the principal components 1 and 2. In the murine adipose tissues, more than two-thirds of the measured fatty acid metabolites contribute higher-than-average to the first two principal components (**Figures 3D,F**). In contrast, less than half of the compounds did so in the human tissues (**Figure 3E**). Interestingly, several compounds previously associated with the recruitment of brown and brite adipocytes, namely 9- and 13-HODE (22), the PGI2 degradation product 6k-PGF1α (14, 15), 12-HETE (17) as well as PGE2 (13, 14) contributed higher-than-average in the murine BAT/WAT comparison (**Figure 3D**). Among those, only 9- and 13-HODE consistently contributed to the discrimination of BAT and brite adipose tissue from WAT (**Figures 3D–F**), suggesting an association of individual metabolites with the abundance of thermogenic competent adipocytes in a translational context. In line with this notion, the AA-derivatives 11,12-EET and 5,6-EET generated by the CYP pathway, and the LOX pathway products 15-HETE, 5-HETE and its active form 5-oxoETE contributed above-average in all three conditions (**Figures 3D–F**). However, the abundance of most of these metabolites was exclusively different in murine BAT vs. WAT but not in the other comparisons (**Figures 4A–C**), confirming the limited discriminative potential of the oxylipin profile in these settings. Only the abundance of 13-HODE in humans and 5-oxoETE in the murine brite vs. white comparison were significantly different in brown and brite adipose tissue compared to WAT, respectively (**Figures 4B,C**). Interestingly, 11,12-EET, 5,6-EET, and 5-HETE were significantly higher in murine BAT than in WAT (**Figure 4A**), contradicting the overall trend toward higher total oxylipin abundance in WAT (**Figure 2C**). This suggests an involvement of these three metabolites in regulation of BAT function. We identified 5,6-EET and 5-HETE as the only two metabolites significantly more abundant in murine BAT compared to WAT that showed at least a similar trend toward a higher abundance in murine brite and human BAT vs. WAT (**Figures 4B,C**). In line with this regulation, 5-oxoETE, the oxidation product of 5-HETE, also tended to be more abundant in these tissues. Consequently, 5-HETE and 5,6-EET constitute novel oxylipins associated with the abundance of brown and brite adipocytes in a translational context.

DISCUSSION

Activation of NST in BAT and brite adipose tissue increases energy expenditure and therefore is a potential therapeutic strategy to treat obesity. Within this scope, metabolites of PUFA (especially oxylipins) are discussed as potential effectors. Several studies have associated selected oxylipins with improved BAT functionality (17, 18) or the recruitment of brite adipocytes (13–15) in mice. However, evidence in the human context is scarce. Only the prostaglandin PGI2 has been shown to increase UCP1 expression in cultured murine and human adipocytes (14, 16). Therefore, we screened the abundance of 36 omega-6 or omega-3 PUFA-derived metabolites in human and murine adipose tissues to identify novel compounds associated with abundance of brown and brite adipocytes in a translational context. Based on their respective PUFA metabolite pattern, murine but not human BAT could be distinguished from WAT. Indeed, it has been argued that human supraclavicular BAT resembles murine brite adipose tissue rather than murine BAT, thus comprising a mixture of white and brite adipocytes (7, 23). This is in line with our finding that in mice the oxylipin profiles of brite adipose tissue induced by cold exposure and WAT at thermoneutrality could also not be distinguished. We think of two possible explanations for this observation. First, the oxylipin profile could be a surrogate marker for the thermogenic activity of the respective adipose tissues, since only BAT but not WAT shows increased metabolic activity in cold acclimatized mice (24). However, we did not measure thermogenic activity in our study, and thus lack direct experimental evidence. Second, the oxylipin profile could be a surrogate marker for the abundance of brown or brite adipocytes that markedly increase in abundance upon cold exposure in both BAT and WAT of mice, respectively. However, we speculate that the relative abundance of interspersed brown or brite adipocytes in human BAT and murine brite adipose tissue, respectively, is not sufficient to notably alter the oxylipin metabolite profiles of the whole tissue.

We therefore checked individual oxylipins with discriminative potential between murine BAT and WAT. A set of seven oxylipins with high potential to explain variability between BAT or brite adipose tissue and WAT in mice and humans was identified. Within this set, we could confirm previously reported oxylipins associated with the recruitment of BAT and browning of WAT. As such, LA-derived 9- and 13- HODE were the most abundant oxylipins in both human and murine adipose tissues and had a high discriminative potential. When used at very high concentrations, both compounds sensitize murine white adipocyte progenitors to β_3-receptor agonist treatment, consequently increasing UCP1 expression in the presence of isoproterenol (22). In our study, the abundance of 9- and 13-HODE in murine adipose tissues gradually decreased with the

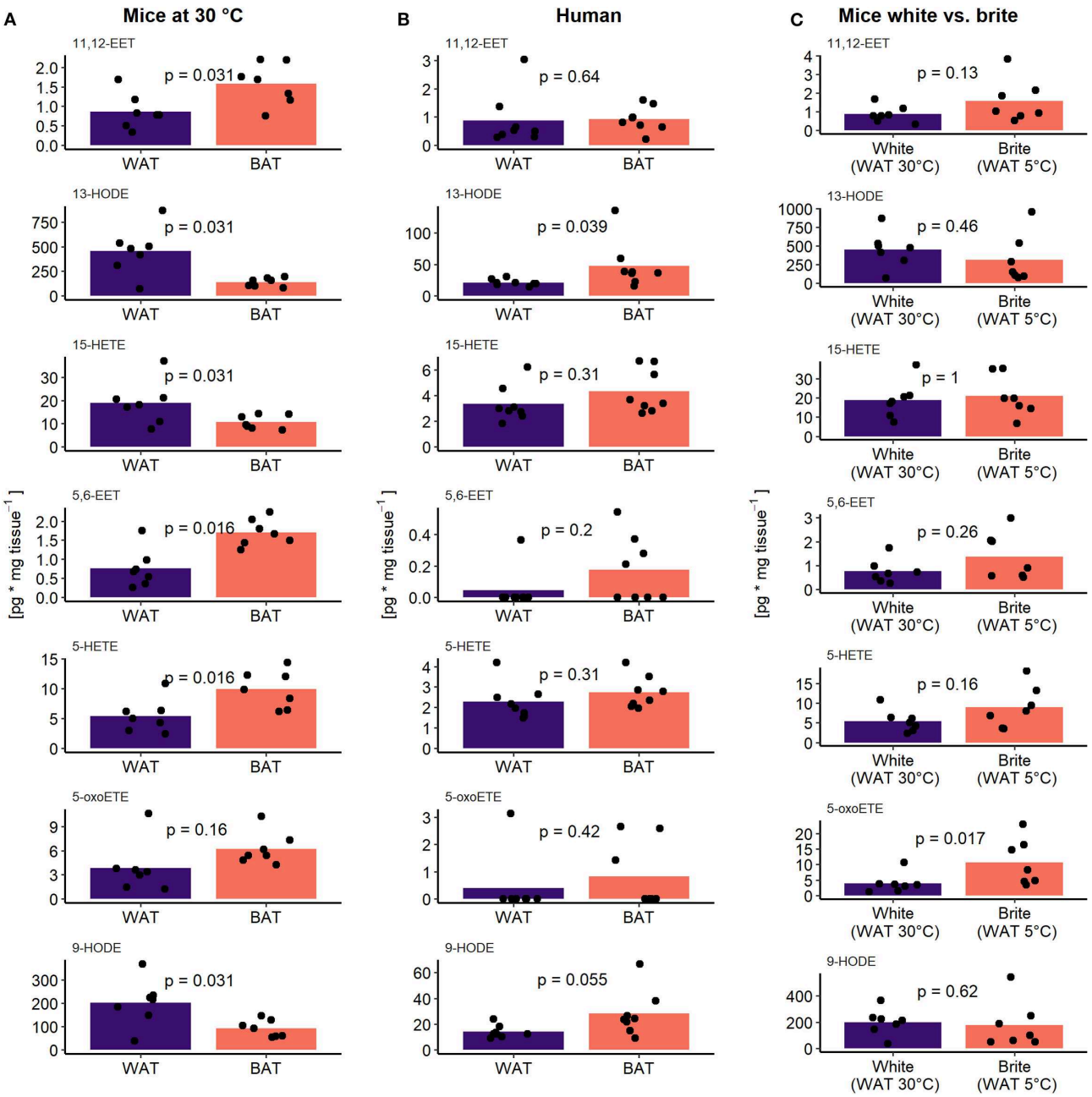

FIGURE 4 | 5-HETE and 5,6-EET are regulated similar between adipose tissues. The concentration of the seven higher than average contributing oxylipins in **(A)** murine BAT and WAT ($n = 7$), **(B)** human BAT and WAT ($n = 8$), and **(C)** murine white and brite adipose tissue ($n = 7$). Bars represent mean values and p-values are derived from paired **(A,B)** or unpaired **(C)** Wilcoxon test.

abundance of brown and brite adipocytes from white to brite to brown. This phenotype may indicate a coordinated regulation of 9- and 13-HODE production to contain thermogenic capacity on reasonable levels upon prolonged β-adrenergic stimulation (1 week at 5°C). However, the sensitizing effect of 9- and 13-HODE was achieved with supraphysiological concentrations of 68 μM (22). Furthermore, the decreasing abundance of 9- and 13-HODE in increasingly thermogenic competent tissues might simply reflect an increased consumption of precursor fatty acids caused by the higher lipolytic and oxidative activity. Consequently, the relevance of 9- and 13-HODE in a physiological context needs further experimental validation. Interestingly, 12-HETE and 14-HDoHE, two LOX products reported to be upregulated in murine interscapular BAT and inguinal WAT upon cold simulation (17), were also high contributors explaining variability between murine BAT and WAT in our study. In contrast to previously

published observations, 14-HDoHE was not only lower at 5°C compared to 30°C in BAT but also lacked regulation in WAT (**Supplementary Figure 4**). Additionally, 12-HETE concentrations were not different between 5 and 30°C in BAT or WAT (**Supplementary Figure 4**). We cannot exclude an effect of diets differing in the fatty acid composition altering the supply of oxylipin precursor fatty acids. However, we speculate that the lack of regulation of 12-HETE and 14-HDoHE especially in WAT upon cold stimulation indicates that both oxylipins are not implicated in the process of WAT browning *in vivo*.

In line with the scope of our study, we could identify two novel metabolites, which have not been associated with the recruitment of brown and brite adipocytes. Following a translational pattern, the oxylipins 5-HETE and 5,6-EET were more abundant in BAT and brite adipose tissue compared to WAT in mice and humans. 5,6-EET is directly synthesized from AA via the CYP pathway and can activate transient receptor potential vanilloid 4 (TRPV4) channels (25). In contrast, 5-HETE synthesis from AA is a multi-step process involving 5-LOX and glutathione peroxidases (26). Expression of CYP isoforms responsible for 5,6-EET production has been reported for murine adipocytes (27). Further 5-LOX is expressed in human and murine adipose tissue (28–30). Thus, it is possible that both 5-HETE and 5,6-EET are generated endogenously in adipose tissues, although their tissue-specific abundance may be influenced by plasma levels. Considering the different number of brown adipocytes and levels of Ucp1 expression in BAT and WAT, both compounds might be associated with thermogenic capacity. Indeed, both 5-HETE and 5,6-EET are linked to signaling pathways with the potential to regulate the recruitment of thermogenic capacity in adipose tissue. Although 5-HETE is a rather inactive metabolite that and needs further conversion by 5-hydroxyeicosanoid dehydrogenase (5-HEDH) to the active metabolite 5-oxo-ETE, the latter one activates the OXE receptor and PPARγ (31). Activation of PPARγ is one of the strongest inducers of Ucp1 expression (32). Consequently, 5-HETE could by conversion to 5-oxo-ETE activate PPARγ and regulate adipogenesis and Ucp1 expression. Nevertheless, not all PPARγ agonists are able to increase Ucp1 expression in brown or white adipose tissue. As such, the oxylipin and PPARγ agonist 15d-PGJ2 has no effect on the recruitment of Ucp1 in human adipocytes (33). This in in line with our finding that 15d-PGJ2 was virtually undetectable in BAT as well as WAT and did not contribute to the variation in human adipose tissue samples. In contrast to 5-HETE, 5,6-EET could have a negative regulatory effect on the browning of adipose tissues by binding to the TRPV4 channel. This receptor constitutes a negative regulator of thermogenic capacity as mice with a knockout of TRPV4 show increased expression of Ucp1 in WAT in addition to increased total energy expenditure (34). Although 5-HETE and 5,6-EET have the potential to affect browning of adipose tissues, these effects remain to be demonstrated in *in vitro* and *in vivo* studies aiming to clarify the role both oxylipins for the recruitment and function of brown and brite adipocytes.

In summary, we show that bona fide BAT vs. WAT are distinguishable by their global oxylipin profile. Furthermore, we identify 5-HETE and 5,6-EET as novel compounds associated with the recruitment of brown and brite adipocytes in mice and humans. Further studies need to establish whether these oxylipins are mere markers or functional effectors of thermogenic capacity.

DATA AVAILABILITY STATEMENT

The datasets generated for this study are available on request to the corresponding author.

ETHICS STATEMENT

The studies involving human participants were reviewed and approved by the ethical review board of the Hospital District of Southwest Finland. The patients/participants provided their written informed consent to participate in this study. The animal study was reviewed and approved by the district government of Upper Bavaria (Regierung von Oberbayern) Reference number ROB-55.2-2532.Vet_02-16-166.

AUTHOR CONTRIBUTIONS

SD performed the molecular analysis, data analysis, interpreted the results, and drafted the manuscript. SM conceived and designed the study, performed the mouse experiment, contributed to the molecular analysis and data interpretation, and revised the manuscript. MK conceived and designed the study, contributed to data interpretation, and revised the manuscript. TF contributed to data analysis and interpretation and revised the manuscript. E-ZA conceived and designed the study, contributed to data interpretation, and revised the manuscript. CC contributed to data interpretation and revised the manuscript. KV provided human tissue samples and revised the manuscript.

FUNDING

This work was supported by joint grant Nutribrite Deutsche Forschungsgemeinschaft ID: KL973/13-1 and French Agence Nationale de la Recherche ANR-15-CE14-0033.

ACKNOWLEDGMENTS

We thank Pauline Le Faouder and Justine Bertrand-Michel from the METATOUL platform (Toulouse, France) for oxylipin and endocannabinoid analysis.

SUPPLEMENTARY MATERIAL

The Supplementary Material for this article can be found online at: https://www.frontiersin.org/articles/10.3389/fendo.2020.00073/full#supplementary-material

REFERENCES

1. Hall KD, Kahan S. Maintenance of lost weight and long-term management of obesity. *Med Clin North Am*. (2018) 102:183. doi: 10.1016/j.mcna.2017.08.012
2. Rosenbaum M, Hirsch J, Gallagher DA, Leibel RL. Long-term persistence of adaptive thermogenesis in subjects who have maintained a reduced body weight. *Am J Clin Nutr*. (2008) 88:906–12. doi: 10.1093/ajcn/88.4.906
3. Li Y, Schnabl K, Gabler SM, Willershäuser M, Reber J, Karlas A, et al. Secretin-activated brown fat mediates prandial thermogenesis to induce satiation. *Cell*. (2018) 175:1561–74.e12. doi: 10.1016/j.cell.2018.10.016
4. Cypess AM, Lehman S, Williams G, Tal I, Rodman D, Goldfine AB, et al. Identification and importance of brown adipose tissue in adult humans. *Obstet Gynecol Surv*. (2009) 64:519–20. doi: 10.1097/OGX.0b013e3181ac8aa2
5. Virtanen KA, Lidell ME, Orava J, Heglind M, Westergren R, Niemi T, et al. Functional brown adipose tissue in healthy adults. *N Engl J Med*. (2009) 360:1518–25. doi: 10.1056/NEJMoa0808949
6. Nedergaard J, Bengtsson T, Cannon B. Unexpected evidence for active brown adipose tissue in adult humans. *Am J Physiol Metab*. (2007) 293:E444–52. doi: 10.1152/ajpendo.00691.2006
7. de Jong JMA, Sun W, Pires ND, Frontini A, Balaz M, Jespersen NZ, et al. Human brown adipose tissue is phenocopied by classical brown adipose tissue in physiologically humanized mice. *Nat Metab*. (2019) 1:830–43. doi: 10.1038/s42255-019-0101-4
8. van Marken Lichtenbelt WD, Vanhommerig JW, Smulders NM, Drossaerts JMAFL, Kemerink GJ, Bouvy ND, et al. Cold-activated brown adipose tissue in healthy men. *N Engl J Med*. (2009) 360:1500–8. doi: 10.1056/NEJMoa0808718
9. Mukherjee J, Baranwal A, Schade NK. Classification of therapeutic and experimental drugs for brown adipose tissue activation: potential treatment strategies for diabetes and obesity. *Curr Diabetes Rev*. (2016) 12:414–28. doi: 10.2174/1573399812666160517115450
10. Yoneshiro T, Matsushita M, Saito M. Translational aspects of brown fat activation by food-derived stimulants. *Handb Exp Pharmacol*. (2019) 251:359–79. doi: 10.1007/164_2018_159
11. Maurer SF, Dieckmann S, Kleigrewe K, Colson C, Amri E-Z, Klingenspor M. Fatty acid metabolites as novel regulators of non-shivering thermogenesis. In: Pfeifer A, Klingenspor M, Herzig S, editors. *Handbook of Experimental Pharmacology*. Berlin; Heidelberg; Springer (2018). p. 1–32.
12. Gabbs M, Leng S, Devassy JG, Monirujjaman M, Aukema HM. Advances in our understanding of oxylipins derived from dietary PUFAs. *Adv Nutr*. (2015) 6:513–40. doi: 10.3945/an.114.007732
13. García-Alonso V, Titos E, Alcaraz-Quiles J, Rius B, Lopategi A, López-Vicario C, et al. Prostaglandin E2exerts multiple regulatory actions on human obese adipose tissue remodeling, inflammation, adaptive thermogenesis and lipolysis. *PLoS ONE*. (2016) 11:e0153751. doi: 10.1371/journal.pone.0153751
14. Vegiopoulos A, Muller-Decker K, Strzoda D, Schmitt I, Chichelnitskiy E, Ostertag A, et al. Cyclooxygenase-2 controls energy homeostasis in mice by de novo recruitment of brown adipocytes. *Science*. (2010) 328:1158–61. doi: 10.1126/science.1186034
15. Bayindir I, Babaeikelishomi R, Kocanova S, Sousa IS, Lerch S, Hardt O, et al. Transcriptional pathways in cPGI2-induced adipocyte progenitor activation for browning. *Front Endocrinol*. (2015) 6:129. doi: 10.3389/fendo.2015.00129
16. Ghandour RA, Giroud M, Vegiopoulos A, Herzig S, Ailhaud G, Amri EZ, et al. IP-receptor and PPARs trigger the conversion of human white to brite adipocyte induced by carbaprostacyclin. *Biochim Biophys Acta*. (2016) 1861:285–93. doi: 10.1016/j.bbalip.2016.01.007
17. Leiria LO, Wang C-H, Lynes MD, Yang K, Shamsi F, Sato M, et al. 12-Lipoxygenase Regulates Cold Adaptation and Glucose Metabolism by Producing the Omega-3 Lipid 12-HEPE from Brown Fat. *Cell Metab*. (2019)1–16. doi: 10.1016/j.cmet.2019.07.001
18. Lynes MD, Leiria LO, Lundh M, Bartelt A, Shamsi F, Huang TL, et al. The cold-induced lipokine 12,13-diHOME promotes fatty acid transport into brown adipose tissue. *Nat Med*. (2017) 23:631–7. doi: 10.1038/nm.4297
19. Krott LM, Piscitelli F, Heine M, Borrino S, Scheja L, Silvestri C, et al. Endocannabinoid regulation in white and brown adipose tissue following thermogenic activation. *J Lipid Res*. (2016) 57:464–73. doi: 10.1194/jlr.M065227
20. Din UM, Saari T, Raiko J, Kudomi N, Maurer SF, Lahesmaa M, et al. Postprandial oxidative metabolism of human brown fat indicates thermogenesis. *Cell Metab*. (2018) 28:207–16.e3. doi: 10.1016/j.cmet.2018.05.020
21. Chechi K, van Marken Lichtenbelt W, Richard D. Brown and beige adipose tissues: phenotype and metabolic potential in mice and men. *J Appl Physiol*. (2018) 124:482–96. doi: 10.1152/japplphysiol.00021.2017
22. Lee Y-H, Kim S-N, Kwon H-J, Maddipati KR, Granneman JG. Adipogenic role of alternatively activated macrophages in β-adrenergic remodeling of white adipose tissue. *Am J Physiol Integr Comp Physiol*. (2016) 310:R55–65. doi: 10.1152/ajpregu.00355.2015
23. Sharp LZ, Shinoda K, Ohno H, Scheel DW, Tomoda E, Ruiz L, et al. Human BAT possesses molecular signatures that resemble beige/brite cells. *PLoS ONE*. (2012) 7:e49452. doi: 10.1371/journal.pone.0049452
24. Labbé SM, Caron A, Chechi K, Laplante M, Lecomte R, Richard D. Metabolic activity of brown, "beige," and white adipose tissues in response to chronic adrenergic stimulation in male mice. *Am J Physiol Metab*. (2016) 311:E260–8. doi: 10.1152/ajpendo.00545.2015
25. Watanabe H, Vriens J, Prenen J, Droogmans G, Voets T, Nilius B. Anandamide and arachidonic acid use epoxyeicosatrienoic acids to activate TRPV4 channels. *Nature*. (2003) 424:434–8. doi: 10.1038/nature01807
26. Rådmark O, Werz O, Steinhilber D, Samuelsson B. 5-Lipoxygenase, a key enzyme for leukotriene biosynthesis in health and disease. *Biochim Biophys Acta*. (2015) 1851:331–9. doi: 10.1016/j.bbalip.2014.08.012
27. Graves JP, Gruzdev A, Bradbury JA, DeGraff LM, Li H, House JS, et al. Quantitative polymerase chain reaction analysis of the mouse Cyp2j subfamily: Tissue distribution and regulation. *Drug Metab Dispos*. (2015) 43:1169–80. doi: 10.1124/dmd.115.064139
28. Mehrabian M, Schulthess FT, Nebohacova M, Castellani LW, Zhou Z, Hartiala J, et al. Identification of ALOX5 as a gene regulating adiposity and pancreatic function. *Diabetologia*. (2008) 51:978–88. doi: 10.1007/s00125-008-1002-3
29. Heemskerk MM, Giera M, el Bouazzaoui F, Lips MA, Pijl H, van Dijk KW, van Harmelen V. Increased PUFA content and 5-lipoxygenase pathway expression are associated with subcutaneous adipose tissue inflammation in obesewomen with type 2 diabetes. *Nutrients*. (2015) 7:7676–90. doi: 10.3390/nu7095362
30. Horrillo R, González-Périz A, Martínez-Clemente M, López-Parra M, Ferré N, Titos E, et al. 5-Lipoxygenase activating protein signals adipose tissue inflammation and lipid dysfunction in experimental obesity. *J Immunol*. (2010) 184:3978–87. doi: 10.4049/jimmunol.0901355
31. Shiraki T, Kamiya N, Shiki S, Kodama TS, Kakizuka A, Jingami H. α,β-Unsaturated ketone is a core moiety of natural ligands for covalent binding to peroxisome proliferator-activated receptor γ. *J Biol Chem*. (2005) 280:14145–53. doi: 10.1074/jbc.M500901200
32. Petrovic N, Shabalina IG, Timmons JA, Cannon B, Nedergaard J. Thermogenically competent nonadrenergic recruitment in brown preadipocytes by a PPARγ agonist. *Am J Physiol Metab*. (2008) 295:E287–E296. doi: 10.1152/ajpendo.00035.2008
33. Bartesaghi S, Hallen S, Huang L, Svensson PA, Momo RA, Wallin S, et al. Thermogenic activity of UCP1 in human white fat-derived beige adipocytes. *Mol Endocrinol*. (2015) 29:130–9. doi: 10.1210/me.2014-1295
34. Ye L, Kleiner S, Wu J, Sah R, Gupta RK, Banks AS, et al. TRPV4 is a regulator of adipose oxidative metabolism, inflammation, and energy homeostasis. *Cell*. (2012) 151:96–110. doi: 10.1016/j.cell.2012.08.034

Conflict of Interest: The authors declare that the research was conducted in the absence of any commercial or financial relationships that could be construed as a potential conflict of interest.

The handling Editor declared a past co-authorship with the E-ZA.

frontiers in Endocrinology

MINI REVIEW
published: 10 March 2020
doi: 10.3389/fendo.2020.00118

Purine Nucleotides in the Regulation of Brown Adipose Tissue Activity

Andrea Bast-Habersbrunner[1,2] *and Tobias Fromme*[1,2*]

[1] *Chair of Molecular Nutritional Medicine, TUM School of Life Sciences, Technical University of Munich, Munich, Germany,*
[2] *EKFZ - Else Kröner-Fresenius Center for Nutritional Medicine, Technical University of Munich, Munich, Germany*

Non-shivering thermogenesis in mammalian brown adipose tissue is a powerful mechanism to defend normothermia in cold climates. To minimize the loss of chemical energy, the central functional component, mitochondrial uncoupling protein 1, UCP1, must be tightly regulated. The canonical pathway of UCP1 activation includes lipolytic release of free fatty acids in response to an adrenergic signal. Activating fatty acids overcome constitutive inhibition of UCP1 by the di- and triphosphate forms of purine nucleotides, i.e., ATP, ADP, GTP, and GDP. Cellular concentrations of inhibitory, free nucleotides are subject to significant, adrenergically induced alterations. The regulatory components involved may constitute novel drug targets to manipulate brown fat thermogenesis and thereby organismic energy balance. We here review evidence for and against a dominant role of nucleotides in thermogenic control, describe conceptual routes to endogenously and pharmacologically alter free nucleotide pool size, speculate on a signaling role of degradation products released from active brown fat, and highlight gaps in our understanding of signaling and metabolic pathways involved.

Keywords: brown adipose tissue, uncoupling protein 1, nucleotides, non-shivering thermogenesis, mitochondria, GMP reductase, AMP deaminase

OPEN ACCESS

Edited by:
Takeshi Yoneshiro,
University of California, San Francisco, United States

Reviewed by:
Andrea Armani,
San Raffaele Pisana (IRCCS), Italy
Lei Zhang,
Garvan Institute of Medical Research, Australia

***Correspondence:**
Tobias Fromme
fromme@tum.de

Specialty section:
This article was submitted to Obesity, a section of the journal Frontiers in Endocrinology

Received: *27 November 2019*
Accepted: *24 February 2020*
Published: *10 March 2020*

Citation:
Bast-Habersbrunner A and Fromme T (2020) Purine Nucleotides in the Regulation of Brown Adipose Tissue Activity. Front. Endocrinol. 11:118. doi: 10.3389/fendo.2020.00118

INTRODUCTION

Brown adipose tissue (BAT) provides a mechanism for adaptive, non-shivering thermogenesis to endotherm mammals [reviewed in (1)]. Isolated mitochondria from this tissue display intense oxygen consumption in the absence of ATP production, i.e., uncoupled respiration. The di- and triphosphate forms of purine nucleotides (ATP, ADP, GTP, and GDP) have long been known to restore respiratory control to such mitochondrial preparations (2–4). The nucleotide binding site was found to reside within the central thermogenic protein of the mitochondrial inner membrane later named uncoupling protein 1 (UCP1) (5–7). Nucleotides proved a constitutive inhibitor of UCP1 mediated proton conductance of the mitochondrial inner membrane and thus constitute the default shut-off mechanism in the absence of thermogenic demand. Upon BAT activation by the sympathetic nervous system, lipolytically liberated free fatty acids are thought to displace nucleotides from UCP1 in a competitive manner to act as thermogenic activators (8–10). Challenging this concept of mere competitive relief of UCP1 inhibition, several lines of evidence support an additional, active regulation of purine nucleotides in response to adrenergic stimulation.

NUCLEOTIDES ARE ACTIVELY CONTROLLED REGULATORS OF UCP1 MEDIATED THERMOGENESIS

For decades, the divergent roles of actively controlled free fatty acid levels as UCP1 activators and passively acting nucleotides as constitutively present inhibitors remained the widely accepted model

of thermogenic regulation in BAT. The arguments seemed obvious enough: millimolar cytosolic concentration of ATP alone seemed sufficient to fully and efficiently shut down UCP1 function at all times, exceeding the nanomolar or low micromolar dissociation constant by several orders of magnitude (11–13). To actively release the inhibitory effect of purine nucleotides on UCP1, their concentrations would need to be tremendously reduced, which seemed prohibitively wasteful, as resynthesis of one nucleotide would demand an energy investment equivalent to 50 ATP (14). However, considerable degradation of nucleotides also occurs routinely in contracting muscle, where ADP is degraded in order to preserve the ATP/ADP ratio in conditions of high ATP hydrolysis (15, 16). Furthermore, in active brown adipocytes, where large amounts of chemical energy are released as heat instead of being converted into ATP, energy efficiency does not appear a priority.

Remaining doubts were convincingly countered and brought to the point in a publication by Klingenberg, in which he finds that "the conclusion that nucleotides do not play a role in intracellular regulation of UCP1 because of a too high affinity, seems to be unfounded" (17). Arguments put forward were, first, the phospholipid composition of the mitochondrial inner membrane is very different from the phosphatidylcholine proteoliposomes in which UCP1 was initially characterized (11). Adding phosphatidylserine and especially cardiolipin not only changed absolute UCP1 activity but in particular attenuated the inhibitory potential of purine nucleotides in a dose dependent manner (17). At the 12% molar amount cardiolipin typically found in the inner membrane of BAT mitochondria (18, 19), the dissociation constant must be expected to be increased by more than an order of magnitude. Second and even more important, UCP1 is only inhibited by free, non-complexed nucleotides (20). The preferred form to be used as substrate by ATPases, however, is a complex with one of the divalent cations magnesium and calcium and accordingly, the vast majority of cytosolic purine nucleotides is cation complexed and irrelevant for the inhibition of UCP1 (21, 22). Furthermore, total purine nucleotide concentration is relatively low in brown adipocytes, e.g., by a factor of two to six compared to white adipocytes or skeletal muscle cells, respectively (23). Taking into account both a higher than anticipated dissociation constant and a lower than anticipated free nucleotide concentration, further modulation of nucleotide levels appears a plausible regulator of UCP1 activity.

If active regulation of free nucleotides is assumed to be implicated in the activation of UCP1 mediated non-shivering thermogenesis, brown adipocytes require a mechanism to reduce their concentration in response to an adrenergic stimulus, either by a shift in the balance between free and complexed nucleotides or by an altered overall amount. There is evidence for both.

Complexation of purine nucleotides with magnesium increases with increasing cytosolic pH, which is indeed elevated upon α-adrenergic stimulation of brown adipocytes (21, 24–26). In addition, the inhibitory potency of free purine nucleotides on UCP1 is also a function of pH, with decreased purine affinity in response to pH elevation (20, 24). Furthermore, after thermogenic activation of brown adipocytes, total calcium content of these cells increases 15-fold by uptake from the external medium (23). Cytosolic concentrations of both calcium and magnesium sharply increase, both by uptake from the extracellular medium and release from intracellular stores (27–30). The concentration of remaining free, non-complexed purine nucleotides will strongly decrease accordingly (**Figure 1**).

A first indication for cold induced changes in BAT purine nucleotide concentrations themselves came from the observation of drastic changes in the transcript abundance of purine metabolism gene products. For instance, GMP reductase (Gmpr) expression is strongly and very quickly induced in BAT by cold exposure, both on the transcript and the protein level (31, 32). At peak expression after ∼24 h of cold exposure, Gmpr is among the 50 most abundant transcripts in murine BAT, together with core functional components including Ucp1, citrate synthase and subunits of respiratory chain complexes [GEO accession GSE119452 (23)]. These changes in gene expression are far from incidental. Total nucleotide pool size is essentially a function of nucleotide monophosphate degradation, because mono-, di- and triphosphate forms are mutually interconvertible not only by classical ATPases, but dominantly by multiple, widely expressed adenylate- and guanylate kinases. These enzymes bi-directionally convert two diphosphates into one tri- and one monophosphate, thereby constantly rearranging the ratios between mono-, di- and triphosphate nucleotides (33). Indeed, an adrenergic stimulus leads to a loss of purine nucleotides specifically in brown adipocytes, especially ATP, ADP, and GTP. The sum of UCP1-inhibiting di- and triphosphate purine nucleotides drops to nearly one half of control levels. In accordance with gene expression data, this loss is not merely a transition toward GMP and AMP, but an actual decrease in total purine nucleotide pool size associated with a release of the respective breakdown products [(23); **Figure 1**].

In summary, even under control conditions, inhibitory purine nucleotide concentrations in the cytosol of brown adipocytes are in the range of their UCP1 dissociation constant. Adrenergic stimulation of non-shivering thermogenesis decreases both total pool size by enzymatic degradation and the fraction of inhibitory free nucleotides by changes in calcium concentration and pH. Activation of UCP1 includes the concerted action of both free fatty acid liberating and nucleotide degrading processes.

CONTROL OF NUCLEOTIDE METABOLISM IN BROWN ADIPOCYTES

Adrenergic stimulation leads to degradation of purine nucleotides in brown adipocytes contributing to the activation of UCP1 mediated thermogenesis. Enzymes involved in purine metabolism are targets of a large number of approved and experimental drugs for indications as diverse as gout [e.g., allopurinol (34)], viral infection [e.g., ribavirin (35)], post-transplantive immunosuppression [e.g., mycophenolate (36)], and Alzheimer's disease [e.g., lumacaftor (37)]. Some of these are widely used, well-studied and feature favorable safety profiles. At least for mycophenolate, we demonstrated interference with thermogenic activation in brown adipocytes (23). Whether this phenomenon is an unexpected side effect of this and other such

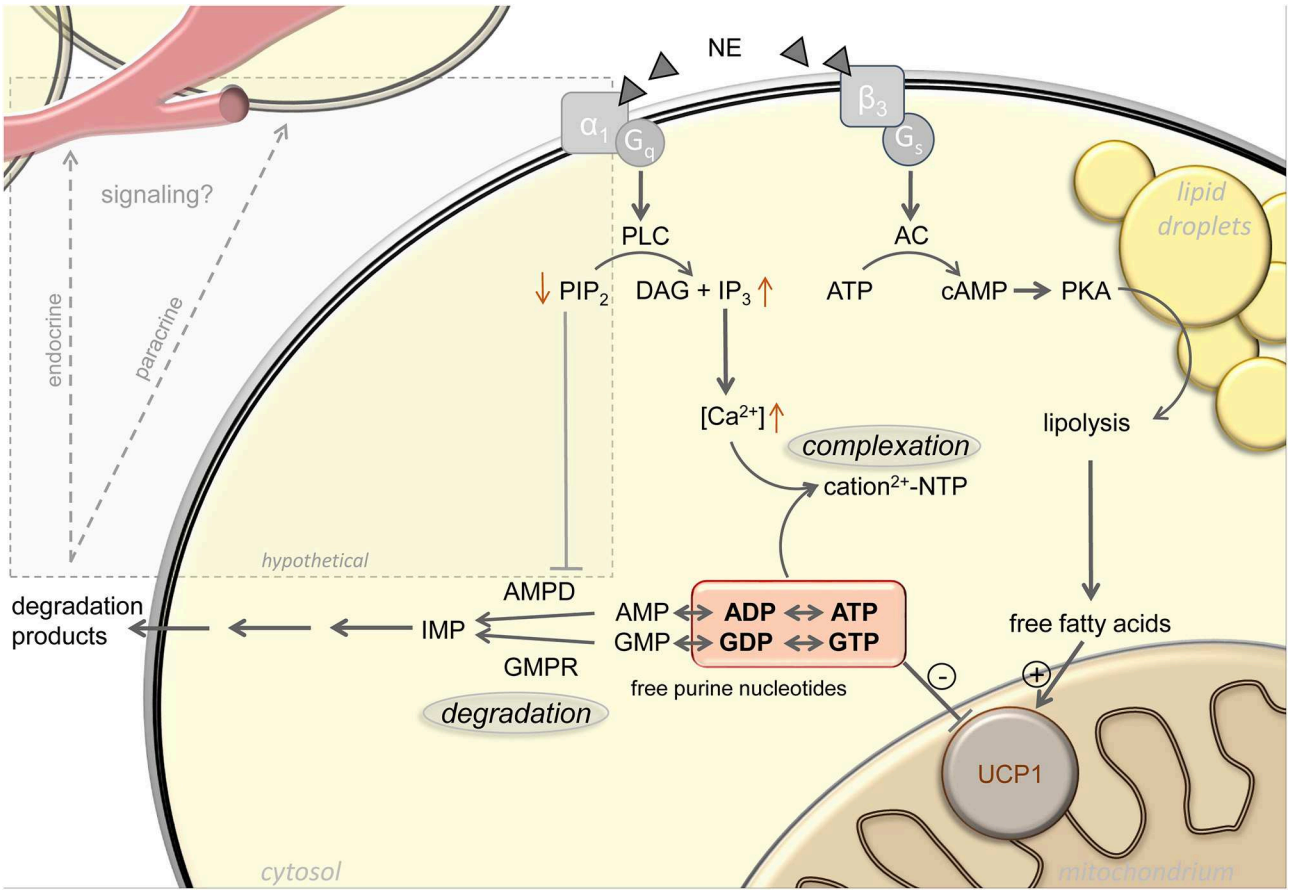

FIGURE 1 | Active regulation of free purine nucleotides upon adrenergic stimulation of brown adipocytes. Norepinephrine (NE) stimulation of brown adipocytes mediates activation of uncoupling protein 1 (UCP1) via increasing free fatty acid and decreasing free purine nucleotide levels. Lipolytic release of free fatty acids occurs in response to G_s-coupled β_3-adrenergic receptor activation. The pool of free purine nucleotides is regulated via complexation and degradation mediated by G_q-coupled α_1-adrenergic receptor signaling. Phospholipase C (PLC), phosphatidylinositol 4,5-bisphosphate (PIP2), diacylglycerol (DAG), inositol 1,4,5-trisphosphate (IP3), adenylyl cyclase (AC), protein kinase A (PKA), AMP deaminase (AMPD), GMP reductase (GMPR), inosine monophosphate (IMP), adenosine mono-/di-/triphosphate (AMP/ADP/ATP), guanosine mono-/di-/triphosphate (GMP/GDP/GTP). Black arrows represent established signaling pathways, gray box and arrows indicate hypothetical pathways.

drugs *in vivo* remains to be studied. If so, inhibitors of human brown fat thermogenesis may be considered for the treatment of cachexia, a progressive body mass loss in cancer patients recently linked to brown fat energy wasting (38–40).

Therapeutic targeting of human brown fat thermogenesis, however, is more often discussed in the context of metabolic disease and envisions activation, not inhibition, of the immense oxidative capacity of this tissue. At least young adults feature an amount of brown adipose tissue that, fully activated, would cause a sizeable negative shift in energy balance (41), potentially exploitable to combat obesity (42), diabetes (10, 43, 44), dyslipidemia (45), and hyperphagia (46). Neither thermogenic activation, nor brown adipose tissue specific action is plausibly achieved with inhibitors of purine nucleotide metabolism. More promising targets may be found in the intracellular signaling components connecting adrenergic receptors with purine degrading enzymes, a pathway completely unresolved and of immense interest for future study.

Adrenergic stimulation leads to purine nucleotide loss in brown adipocytes. Mere changes in phosphorylation state between ADP/ATP and GDP/GTP can bi-directionally be caused by a large variety of enzymes and pathways. Similarly, the monophosphate forms AMP and GMP are readily formed or converted back to diphosphates by adenylate and guanylate kinases. Immediately upon thermogenic activation, formation of the second messengers cAMP and cGMP may, to some extent, contribute to a reduction in ATP and GTP concentration before being eliminated to AMP and GMP (47). Since cytosolic ATP/GTP and ADP/GDP together are orders of magnitude more abundant than AMP, any meaningful change in these UCP1-inhibting nucleotides by dephosphorylation alone would cause a most dramatic AMP accumulation impossible to overlook but not observed (23). Thus, total pool size of all adenine and guanine nucleotides must decrease. In order to leave the total pool of adenine and guanine nucleotides entirely, metabolites have to pass one of the two gatekeeper enzymes

GMPR or AMP deaminase (AMPD), respectively (**Figure 1**). These two enzymes must be considered central players in Ucp1 regulation, and expression of both is indeed cold induced (31, 32).

Since full activation of UCP1 mediated thermogenesis and changes in nucleotide concentration occur rapidly upon adrenergic stimulation (23, 48, 49), the activity of gatekeepers GMPR and AMPD must be expected to be regulated on the post-translational level. To our knowledge, the regulation of mammalian GMPR activity is poorly understood, at least by anything beyond its substrate, product and highly related metabolites, in particular not by any known protein modifications or interactors (50). With its prominent role in preserving ATP/ADP ratio in contracting skeletal muscle, AMPD regulation is far better studied and understood (15, 16, 51, 52). Isoforms of AMPD are expressed from three genes, all of which well-detectable in brown adipose tissue on the transcript level [GEO accession GSE119452 (53)]. Similar to GMPR, AMPD activity is a function of nucleotide concentrations, i.e., it is activated by ADP, inhibited by ATP and therefore effectively regulated by changes in ATP/ADP ratio. Adrenergically stimulated uncoupling of respiration from ATP synthesis in brown adipocytes drastically reduces mitochondrial ATP synthesis, reducing the ATP/ADP ratio and increasing GMPR and AMPD activities, thereby enhancing nucleotide degradation (54). In striated muscle, multiple protein-protein interactions have been reported, mostly with dominant functional component of muscle contraction, e.g., myosin and troponin, some of which appear to modify kinetic properties [reviewed in (55)]. While these interactions are a plausible mechanism to couple AMPD activity to contraction, and thus rapid ATP loss, in muscle where they are exceedingly abundant, they seem unlikely to mediate adrenergically induced activity changes in brown fat.

More promisingly, facultative binding of AMPD to the plasma membrane strongly impedes catalytic activity (56), a phenomenon mediated by the inhibitory binding to phosphoinositides, especially phosphatidylinositol 4,5-bisphosphate (PIP2) [(57); **Figure 1**]. Intriguingly, membrane sequestered AMPD thereby forms a pool of inactive enzyme rapidly mobilizable by the action of phospholipases. In parallel to the well-known Gs-coupled β3-adrenoreceptor cascade, brown adipocytes strongly express Gq-coupled α1-adrenoreceptors that activate phospholipase C to hydrolyze PIP2 into inositol 1,4,5-trisphosphate and diacylglycerol (58). The second messenger inositol 1,4,5-trisphosphate is already responsible for the resulting increase in cytosolic calcium and thus for the sequestration of free UCP1-inhibitory nucleotides into non-inhibitory complexes (59). It is conceivable that in parallel, phospholipase C hydrolysis of PIP2 rapidly converts membrane-bound, inactive AMPD into soluble, active enzyme to decrease adenine nucleotide pool size in response to an adrenergic signal, as observed (23). If corroborated, pharmacological targeting of Gq-coupled α1-adrenoreceptors and their downstream signal transduction cascade may prove a valid alternative to the classical β-adrenergic pathway in the endeavor to identify safe activators of brown fat thermogenesis. For decades, it has been attempted to pharmacologically target the β3-receptor to treat aspects of human metabolic syndrome, to date without clinical breakthrough (60–62). The inherent challenge, i.e., unintended effects from receptor expression outside the target tissue, must be expected to be similar for α-agonists. Considered together with a completely different and partly unresolved intracellular second messenger cascade, α-adrenergic recruitment of nucleotide metabolism enzymes may prove a complementary approach worthwhile to follow.

SUMMARY AND OUTLOOK

The significance of purine nucleotides in the control of non-shivering thermogenesis was one of the first milestones in the mechanistic understanding of brown adipose tissue mitochondria, predating the identification of their target, uncoupling protein 1. As a means of acute thermogenic activation, nucleotides have long been neglected as passive inhibitors being displaced by actively regulated free fatty acid levels. In fact, cytosolic free purine nucleotide concentrations are adrenergically modified by several routes acting in concert, including calcium complex formation and enzymatic nucleotide degradation. The signaling cascade connecting norepinephrine and purine metabolic enzymes remains unresolved, and at least in the case of adenine nucleotides, plausibly relies on α1-adrenoreceptors and phospholipase C. Beyond the diligence work of elaborating these unknown pathways, the release of degradation products by active brown adipocytes presents the fascinating opportunity to discover novel markers and endogenous indicators of non-shivering thermogenesis (**Figure 1**). While the well-established endocrine/paracrine agents adenosine and ATP (63) are not detectably released from brown adipocytes, abundant guanosine, inosine, and AMP have all been reported to act as non-canonical transcellular messengers through known purinergic or novel receptors (64–69). Taken together, novel targets to manipulate or detect brown fat thermogenesis may be found both up- and downstream of the thermogenic modulation conferred by purine nucleotide metabolism.

AUTHOR CONTRIBUTIONS

AB-H and TF wrote this review article in concert. All authors read and approved the final manuscript.

FUNDING

AB-H received support from a grant by the German Research Foundation (DFG KL973/12). TF received support from a grant by the German Research Foundation (DFG FR3628/2-1).

REFERENCES

1. Klingenspor M, Andrea B, Florian B, Yongguo L, Stefanie M, Sabine S, et al. Brown adipose tissue. In: Michael Symonds E, editor. *Adipose Tissue Biology*. Cham: Springer International Publishing (2017). doi: 10.1007/978-3-319-52031-5_4
2. Hohorst HJ, Rafael J. [Oxidative phosphorylation by mitochondria from brown adipose tissue]. *Hoppe Seylers Z Physiol Chem*. (1968) 349:268–70.
3. Rafael J, Ludolph HJ, Hohorst HJ. [Mitochondria from brown adipose tissue: uncoupling of respiratory chain phosphorylation by long fatty acids and recoupling by guanosine triphosphate]. *Hoppe Seylers Z Physiol Chem*. (1969) 350:1121–31. doi: 10.1515/bchm2.1969.350.2.1121
4. Pedersen JI. Coupled endogenous respiration in brown adipose tissue mitochondria. *Eur J Biochem*. (1970) 16:12–18. doi: 10.1111/j.1432-1033.1970.tb01047.x
5. Heaton GM, Wagenvoord RJ, Kemp AJr, Nicholls DG. Brown-adipose-tissue mitochondria: photoaffinity labelling of the regulatory site of energy dissipation. *Eur J Biochem*. (1978) 82:515–21. doi: 10.1111/j.1432-1033.1978.tb12045.x
6. Ricquier D, Gervais C, Kader JC, Hemon P. Partial purification by guanosine-5-diphosphate–agarose affinity chromatography of the 32,000 molecular weight polypeptide from mitochondria of brown adipose tissue. *FEBS Lett*. (1979) 101:35–8. doi: 10.1016/0014-5793(79)81289-2
7. Lin CS, Klingenberg M. Isolation of the uncoupling protein from brown adipose tissue mitochondria. *FEBS Lett*. (1980) 113:299–303. doi: 10.1016/0014-5793(80)80613-2
8. Shabalina IG, Jacobsson A, Cannon B, Nedergaard J. Native UCP1 displays simple competitive kinetics between the regulators purine nucleotides and fatty acids. *J Biol Chem*. (2004) 279:38236–48. doi: 10.1074/jbc.M402375200
9. Bertholet AM, Kirichok Y. The mechanism FA-dependent H(+) transport by UCP1. *Handb Exp Pharmacol*. (2019) 251:143–59. doi: 10.1007/164_2018_138
10. Schweizer S, Oeckl J, Klingenspor M, Fromme T. Substrate fluxes in brown adipocytes upon adrenergic stimulation and uncoupling protein 1 ablation. *Life Sci Alliance*. (2018) 1:e201800136. doi: 10.26508/lsa.201800136
11. Klingenberg M, Winkler E. The reconstituted isolated uncoupling protein is a membrane potential driven H+ translocator. *EMBO J*. (1985) 4:3087–92. doi: 10.1002/j.1460-2075.1985.tb04049.x
12. Rial E, Poustie A, Nicholls DG. Brown-adipose-tissue mitochondria: the regulation of the 32000-Mr uncoupling protein by fatty acids and purine nucleotides. *Eur J Biochem*. (1983) 137:197–203. doi: 10.1111/j.1432-1033.1983.tb07815.x
13. Cannon B, Sundin U, Romert L. Palmitoyl coenzyme A: a possible physiological regulator of nucleotide binding to brown adipose tissue mitochondria. *FEBS Lett*. (1977) 74:43–6. doi: 10.1016/0014-5793(77)80748-5
14. Lynch M, Marinov GK. The bioenergetic costs of a gene. *Proc Natl Acad Sci U S A*. (2015) 112:15690–5. doi: 10.1073/pnas.1514974112
15. Parnas JK. Über die Ammoniakbildung im Muskel und ihren Zusammenhang mit Funktion und Zustandsänderung. VI. Mitteilung: der Zusammenhang der Ammoniakbildung mit der Umwandlung des Adeninnucleotids zu Inosinsäure. *Biochem Zschr*. (1929) 206:16–38.
16. Hancock CR, Brault JJ, Terjung RL. Protecting the cellular energy state during contractions: role of AMP deaminase. *J Physiol Pharmacol*. (2006) 57(Suppl. 10):17–29.
17. Klingenberg M. Cardiolipin and mitochondrial carriers. *Biochim Biophys Acta*. (2009) 1788:2048–58. doi: 10.1016/j.bbamem.2009.06.007
18. Goubern M, Chapey MF, Senault C, Laury MC, Yazbeck J, Miroux B, et al. Effect of sympathetic de-activation on thermogenic function and membrane lipid composition in mitochondria of brown adipose tissue. *Biochim Biophys Acta*. (1992) 1107:159–64. doi: 10.1016/0005-2736(92)90342-J
19. Senault C, Yazbeck J, Goubern M, Portet R, Vincent M, Gallay J. Relation between membrane phospholipid composition, fluidity and function in mitochondria of rat brown adipose tissue. Effect of thermal adaptation and essential fatty acid deficiency. *Biochim Biophys Acta*. (1990) 1023:283–9. doi: 10.1016/0005-2736(90)90424-M
20. Klingenberg M. Nucleotide binding to uncoupling protein. Mechanism of control by protonation. *Biochemistry*. (1988) 27:781–91. doi: 10.1021/bi00402a044
21. Luthi D, Gunzel D, McGuigan JA. Mg-ATP binding: its modification by spermine, the relevance to cytosolic Mg^{2+} buffering, changes in the intracellular ionized Mg^{2+} concentration and the estimation of Mg^{2+} by 31P-NMR. *Exp Physiol*. (1999) 84:231–52. doi: 10.1017/S0958067099017996
22. Corkey BE, Duszynski J, Rich TL, Matschinsky B, Williamson JR. Regulation of free and bound magnesium in rat hepatocytes and isolated mitochondria. *J Biol Chem*. (1986) 261:2567–74.
23. Fromme T, Kleigrewe K, Dunkel A, Retzler A, Li Y, Maurer S, et al. Degradation of brown adipocyte purine nucleotides regulates uncoupling protein 1 activity. *Mol Metab*. (2018) 8:77–85. doi: 10.1016/j.molmet.2017.12.010
24. Chinet A, Friedli C, Seydoux J, Girardier L. Does cytoplasmic alkalinization trigger mitochondrial energy dissipation in the brown adipocyte? *Experientia Suppl*. (1978) 32:25–32. doi: 10.1007/978-3-0348-5559-4_2
25. Lee SC, Hamilton JS, Trammell T, Horwitz BA, Pappone PA. Adrenergic modulation of intracellular pH in isolated brown fat cells from hamster and rat. *Am J Physiol*. (1994) 267:C349–C356. doi: 10.1152/ajpcell.1994.267.2.C349
26. Giovannini P, Seydoux J, Girardier L. Evidence for a modulating effect of Na^+/H^+ exchange on the metabolic response of rat brown adipose tissue. *Pflugers Arch*. (1988) 411:273–7. doi: 10.1007/BF00585114
27. Hayato R, Higure Y, Kuba M, Nagai H, Yamashita H, Kuba K. beta(3)-Adrenergic activation of sequential $Ca(^{2+})$ release from mitochondria and the endoplasmic reticulum and the subsequent $Ca(^{2+})$ entry in rodent brown adipocytes. *Cell Calcium*. (2011) 49:400–14. doi: 10.1016/j.ceca.2011.02.011
28. Wilcke M, Nedergaard J. Alpha 1- and beta-adrenergic regulation of intracellular Ca^{2+} levels in brown adipocytes. *Biochem Biophys Res Commun*. (1989) 163:292–300. doi: 10.1016/0006-291X(89)92134-7
29. Nedergaard J. Effects of cations on brown adipose tissue in relation to possible metabolic consequences of membrane depolarisation. *Eur J Biochem*. (1981) 114:159–67. doi: 10.1111/j.1432-1033.1981.tb06187.x
30. Connolly E, Nanberg E, Nedergaard J. Na^+-dependent, alpha-adrenergic mobilization of intracellular (mitochondrial) Ca^{2+} in brown adipocytes. *Eur J Biochem*. (1984) 141:187–93. doi: 10.1111/j.1432-1033.1984.tb08173.x
31. Salvatore D, Bartha T, Larsen PR. The guanosine monophosphate reductase gene is conserved in rats and its expression increases rapidly in brown adipose tissue during cold exposure. *J Biol Chem*. (1998) 273:31092–6. doi: 10.1074/jbc.273.47.31092
32. Watanabe M, Yamamoto T, Kakuhata R, Okada N, Kajimoto K, Yamazaki N, et al. Synchronized changes in transcript levels of genes activating cold exposure-induced thermogenesis in brown adipose tissue of experimental animals. *Biochim Biophys Acta*. (2008) 1777:104–12. doi: 10.1016/j.bbabio.2007.10.014
33. Panayiotou C, Solaroli N, Karlsson A. The many isoforms of human adenylate kinases. *Int J Biochem Cell Biol*. (2014) 49:75–83. doi: 10.1016/j.biocel.2014.01.014
34. Yue TF, Gutman AB. Effect of allopurinol (4-hydroxypyrazolo-(3,4-D)pyrimidine) on serum and urinary uric acid in primary and secondary gout. *Am J Med*. (1964) 37:885–98. doi: 10.1016/0002-9343(64)90131-7
35. Hedstrom L. IMP dehydrogenase: structure, mechanism, and inhibition. *Chem Rev*. (2009) 109:2903–28. doi: 10.1021/cr900021w
36. Allison AC, Eugui EM. Mycophenolate mofetil and its mechanisms of action. *Immunopharmacology*. (2000) 47:85–118. doi: 10.1016/S0162-3109(00)00188-0
37. Liu HD, Luo K, Luo DH. Guanosine monophosphate reductase 1 is a potential therapeutic target for Alzheimers disease. *Scientific Rep*. (2018) 8:2759. doi: 10.1038/s41598-018-21256-6
38. Kir S, White JP, Kleiner S, Kazak L, Cohen P, Baracos VE, et al. Tumour-derived PTH-related protein triggers adipose tissue browning and cancer cachexia. *Nature*. (2014) 513:100–4. doi: 10.1038/nature13528
39. Petruzzelli M, Schweiger M, Schreiber R, Campos-Olivas R, Tsoli M, Allen J, et al. A switch from white to brown fat increases energy expenditure in cancer-associated cachexia. *Cell Metab*. (2014) 20:433–47. doi: 10.1016/j.cmet.2014.06.011
40. Tsoli M, Moore M, Burg D, Painter A, Taylor R, Lockie SH, et al. Activation of thermogenesis in brown adipose tissue and dysregulated lipid metabolism associated with cancer cachexia in mice. *Cancer Res*. (2012) 72:4372–82. doi: 10.1158/0008-5472.CAN-11-3536

41. Gerngross C, Schretter J, Klingenspor M, Schwaiger M, Fromme T. Active brown fat during 18FDG-PET/CT imaging defines a patient group with characteristic traits and an increased probability of brown fat redetection. *J Nucl Med*. (2017) 58:1104–10. doi: 10.2967/jnumed.116.183988
42. Poher AL, Altirriba J, Veyrat-Durebex C, Rohner-Jeanrenaud F. Brown adipose tissue activity as a target for the treatment of obesity/insulin resistance. *Front Physiol*. (2015) 6:4. doi: 10.3389/fphys.2015.00004
43. Maurer SF, Fromme T, Mocek S, Zimmermann A, Klingenspor M. Uncoupling protein 1 and the capacity for non-shivering thermogenesis are components of the glucose homeostatic system. *Am J Physiol Endocrinol Metab*. (2019) 318:E198–215. doi: 10.1152/ajpendo.00121.2019
44. Stanford KI, Middelbeek RJ, Townsend KL, An D, Nygaard EB, Hitchcox KM, et al. Brown adipose tissue regulates glucose homeostasis and insulin sensitivity. *J Clin Invest*. (2013) 123:215–23. doi: 10.1172/JCI62308
45. Bartelt A, Bruns OT, Reimer R, Hohenberg H, Ittrich H, Peldschus K, et al. Brown adipose tissue activity controls triglyceride clearance. *Nat Med*. (2011) 17:200–5. doi: 10.1038/nm.2297
46. Li Y, Schnabl K, Gabler SM, Willershauser M, Reber J, Karlas A, et al. Secretin-activated brown fat mediates prandial thermogenesis to induce satiation. *Cell*. (2018) 175:1561–74.e12. doi: 10.1016/j.cell.2018.10.016
47. Jennissen K, Haas B, Kunz WS, Pfeifer A. cGMP and cAMP differentially regulate differentiation and function of brown adipocytes. *BMC Pharmacol*. (2011) 11:P37. doi: 10.1186/1471-2210-11-S1-P37
48. Li Y, Fromme T, Klingenspor M. Meaningful respirometric measurements of UCP1-mediated thermogenesis. *Biochimie*. (2017) 134:56–61. doi: 10.1016/j.biochi.2016.12.005
49. Li Y, Fromme T, Schweizer S, Schottl T, Klingenspor M. Taking control over intracellular fatty acid levels is essential for the analysis of thermogenic function in cultured primary brown and brite/beige adipocytes. *EMBO Rep*. (2014) 15:1069–76. doi: 10.15252/embr.201438775
50. Spector T, Jones TE, Miller RL. Reaction mechanism and specificity of human GMP reductase. Substrates, inhibitors, activators, and inactivators. *J Biol Chem*. (1979) 254:2308–15.
51. Chapman AG, Atkinson DE. Stabilization of adenylate energy charge by the adenylate deaminase reaction. *J Biol Chem*. (1973) 248:8309–12.
52. Sahlin K, Broberg S. Adenine nucleotide depletion in human muscle during exercise: causality and significance of AMP deamination. *Int J Sports Med*. (1990) 11(Suppl. 2):S62–S67. doi: 10.1055/s-2007-1024856
53. Morisaki T, Sabina RL, Holmes EW. Adenylate deaminase. A multigene family in humans and rats. *J Biol Chem*. (1990) 265:11482–6.
54. Ronca-Testoni S, Raggi A, Ronca G. Muscle AMP aminohydrolase. 3. A comparative study on the regulatory properties of skeletal muscle enzyme from various species. *Biochim Biophys Acta*. (1970) 198:101–12. doi: 10.1016/0005-2744(70)90038-0
55. Sabina RL, Mahnke-Zizelman DK. Towards an understanding of the functional significance of N-terminal domain divergence in human AMP deaminase isoforms. *Pharmacol Ther*. (2000) 87:279–83. doi: 10.1016/S0163-7258(00)00040-1
56. Pipoly GM, Nathans GR, Chang D, Deuel TF. Regulation of the interaction of purified human erythrocyte AMP deaminase and the human erythrocyte membrane. *J Clin Invest*. (1979) 63:1066–76. doi: 10.1172/JCI 109376
57. Sims B, Mahnke-Zizelman DK, Profit AA, Prestwich GD, Sabina RL, Theibert AB. Regulation of AMP deaminase by phosphoinositides. *J Biol Chem*. (1999) 274:25701–7. doi: 10.1074/jbc.274.36.25701
58. Bronnikov GE, Zhang SJ, Cannon B, Nedergaard J. A dual component analysis explains the distinctive kinetics of cAMP accumulation in brown adipocytes. *J Biol Chem*. (1999) 274:37770–80. doi: 10.1074/jbc.274.53.37770
59. Leaver EV, Pappone PA. Beta-adrenergic potentiation of endoplasmic reticulum $Ca(^{2+})$ release in brown fat cells. *Am J Physiol Cell Physiol*. (2002) 282:C1016–C1024. doi: 10.1152/ajpcell.00204.2001
60. Cypess AM, Weiner LS, Roberts-Toler C, Franquet Elia E, Kessler SH, Kahn PA, et al. Activation of human brown adipose tissue by a beta3-adrenergic receptor agonist. *Cell Metab*. (2015) 21:33–8. doi: 10.1016/j.cmet.2014.12.009
61. Lowell BB, Flier JS. Brown adipose tissue, beta 3-adrenergic receptors, and obesity. *Annu Rev Med*. (1997) 48:307–16. doi: 10.1146/annurev.med.48.1.307
62. Himms-Hagen J, Danforth E. The potential role of beta3 adrenoceptor agonists in the treatment of obesity and diabetes. *Curr Opin Endocrinol Diab*. (1996) 3:59–65. doi: 10.1097/00060793-199602000-00010
63. Tozzi M, Novak I. Purinergic receptors in adipose tissue as potential targets in metabolic disorders. *Front Pharmacol*. (2017) 8:878. doi: 10.3389/fphar.2017.00878
64. Tilley SL, Wagoner VA, Salvatore CA, Jacobson MA, Koller BH. Adenosine and inosine increase cutaneous vasopermeability by activating A(3) receptors on mast cells. *J Clin Invest*. (2000) 105:361–7. doi: 10.1172/JCI8253
65. Guinzberg R, Cortes D, Diaz-Cruz A, Riveros-Rosas H, Villalobos-Molina R, Pina E. Inosine released after hypoxia activates hepatic glucose liberation through A3 adenosine receptors. *Am J Physiol Endocrinol Metab*. (2006) 290:E940–51. doi: 10.1152/ajpendo.00173.2005
66. Volpini R, Marucci G, Buccioni M, Dal Ben D, Lambertucci C, Lammi C, et al. Evidence for the existence of a specific g protein-coupled receptor activated by guanosine. *ChemMedChem*. (2011) 6:1074–80. doi: 10.1002/cmdc.201100100
67. Rittiner JE, Korboukh I, Hull-Ryde EA, Jin J, Janzen WP, Frye SV, et al. AMP is an adenosine A1 receptor agonist. *J Biol Chem*. (2012) 287:5301–9. doi: 10.1074/jbc.M111.291666
68. Lanznaster D, Dal-Cim T, Piermartiri TC, Tasca CI. Guanosine: a neuromodulator with therapeutic potential in brain disorders. *Aging Dis*. (2016) 7:657–79. doi: 10.14336/AD.2016.0208
69. Welihinda AA, Kaur M, Greene K, Zhai Y, Amento EP. The adenosine metabolite inosine is a functional agonist of the adenosine A2A receptor with a unique signaling bias. *Cell Signal*. (2016) 28:552–60. doi: 10.1016/j.cellsig.2016.02.010

Conflict of Interest: The authors declare that the research was conducted in the absence of any commercial or financial relationships that could be construed as a potential conflict of interest.

frontiers in Endocrinology

ORIGINAL RESEARCH
published: 20 March 2020
doi: 10.3389/fendo.2020.00097

Exercise Training in Obese Rats Does Not Induce Browning at Thermoneutrality and Induces a Muscle-Like Signature in Brown Adipose Tissue

Peter Aldiss[1], Jo E. Lewis[2], Irene Lupini[3], Ian Bloor[1], Ramyar Chavoshinejad[1], David J. Boocock[4], Amanda K. Miles[4], Francis J. P. Ebling[2], Helen Budge[1] and Michael E. Symonds[1,5]**

[1] The Early Life Research Unit, Division of Child Health, Obstetrics and Gynaecology, School of Medicine, University of Nottingham, Nottingham, United Kingdom, [2] School of Life Sciences, Queen's Medical Centre, University of Nottingham, Nottingham, United Kingdom, [3] School of Biosciences and Veterinary Medicine, University of Camerino, Camerino, Italy, [4] John van Geest Cancer Research Centre, Nottingham Trent University, Nottingham, United Kingdom, [5] Nottingham Digestive Disease Centre and Biomedical Research Unit, School of Medicine, University of Nottingham, Nottingham, United Kingdom

OPEN ACCESS

Edited by:
Patrick C. N. Rensen,
Leiden University Medical Center, Netherlands

Reviewed by:
Milena Schönke,
Leiden University Medical Center, Netherlands
David Wright,
University of Guelph, Canada

***Correspondence:**
Peter Aldiss
peter.aldiss@nottingham.ac.uk
Michael E. Symonds
michael.symonds@nottingham.ac.uk

Specialty section:
This article was submitted to Obesity, a section of the journal Frontiers in Endocrinology

Received: 18 November 2019
Accepted: 14 February 2020
Published: 20 March 2020

Citation:
Aldiss P, Lewis JE, Lupini I, Bloor I, Chavoshinejad R, Boocock DJ, Miles AK, Ebling FJP, Budge H and Symonds ME (2020) Exercise Training in Obese Rats Does Not Induce Browning at Thermoneutrality and Induces a Muscle-Like Signature in Brown Adipose Tissue. Front. Endocrinol. 11:97. doi: 10.3389/fendo.2020.00097

Aim: Exercise training elicits diverse effects on brown (BAT) and white adipose tissue (WAT) physiology in rodents housed below their thermoneutral zone (i.e., 28–32°C). In these conditions, BAT is chronically hyperactive and, unlike human residence, closer to thermoneutrality. Therefore, we set out to determine the effects of exercise training in obese animals at 28°C (i.e., thermoneutrality) on BAT and WAT in its basal (i.e., inactive) state.

Methods: Sprague-Dawley rats ($n = 12$) were housed at thermoneutrality from 3 weeks of age and fed a high-fat diet. At 12 weeks of age half these animals were randomized to 4-weeks of swim-training (1 h/day, 5 days per week). Following a metabolic assessment interscapular and perivascular BAT and inguinal (I)WAT were taken for analysis of thermogenic genes and the proteome.

Results: Exercise attenuated weight gain but did not affect total fat mass or thermogenic gene expression. Proteomics revealed an impact of exercise training on 2-oxoglutarate metabolic process, mitochondrial respiratory chain complex IV, carbon metabolism, and oxidative phosphorylation. This was accompanied by an upregulation of multiple proteins involved in skeletal muscle physiology in BAT and an upregulation of muscle specific markers (i.e., Myod1, CkM, Mb, and MyoG). UCP1 mRNA was undetectable in IWAT with proteomics highlighting changes to DNA binding, the positive regulation of apoptosis, HIF-1 signaling and cytokine-cytokine receptor interaction.

Conclusion: Exercise training reduced weight gain in obese animals at thermoneutrality and is accompanied by an oxidative signature in BAT which is accompanied by a muscle-like signature rather than induction of thermogenic genes. This may represent a new, UCP1-independent pathway through which BAT physiology is regulated by exercise training.

Keywords: adipose tissue, exercise training, obesity, housing temperature, browning

INTRODUCTION

During obesity, the accumulation of excess lipid and subsequent hypertrophy of adipocytes leads to adipose tissue (AT) dysfunction (1). These deleterious alterations in obese AT include macrophage infiltration and apoptosis, an increase in, and secretion of, inflammatory cytokines, hypoxia, and insulin resistance, all of which contribute to systemic cardiometabolic risk (1–3).

Given that sustainable weight loss is hard to achieve, improving the AT phenotype is one potential avenue to preventing the onset of diseases associated with obesity. Exercise training elicits diverse effects on both general metabolic parameters (i.e., improved insulin sensitivity) and on the AT phenotype (4–7). Following exercise training, there is a switch from a pro-inflammatory M1 to a M2 macrophage phenotype where inflammation is inhibited (8). Increased vascular endothelial growth factor A and reduced AT lactate following exercise suggest an induction of AT angiogenesis and reduction in AT hypoxia whilst improving AT adipokine secretion, oxidative stress, mitochondrial biogenesis and insulin sensitivity (4–6, 9).

More recently, there has been a focus on the role of exercise training to regulate the thermogenic programme in brown (BAT) and white AT (WAT) (10). BAT has a high oxidative capacity similar to skeletal muscle, utilizing glucose and free fatty acids (FFA) as substrates for cold and diet-induced thermogenesis following the activation of uncoupling protein (UCP)1 (11). Yet, how exercise training regulates BAT physiology is unclear. Exercise has been shown to induce a "whitening" of BAT and reduce insulin-stimulated glucose uptake, whilst promoting the appearance of "beige/brite" adipocytes in classical WAT (12–14). This adaptation has been attributed to a range of mechanisms including the downstream actions of various myokines (e.g., meteorin-like) (15), hepatokines (e.g., fibroblast growth factor 21) (16), and metabolites (e.g., β-aminoisobutyric acid) (17). Importantly, this occurs regardless of exercise modality (i.e., treadmill, swim training, and voluntary wheel running) (18).

An important caveat, however, is that rodents subjected to exercise are typically housed at c.20°C, a temperature well below their thermoneutral zone (19). This impacts on a number of physiological processes including adaptive thermogenesis, cardiovascular function, and immune cell metabolism (19, 20). In particular, it is an important consideration when studying BAT, which is chronically active at 20°C with UCP1+ adipocytes readily seen in WAT (21). Importantly, BAT from obese mice housed chronically at thermoneutrality, closer resembles human BAT and this model of "physiologically humanized BAT" represents the best choice for modeling BAT physiology (22). Therefore, we used chronic thermoneutrality (i.e., 28°C from weaning) to closer mimic human physiology and study AT in the basal state (i.e., when UCP1 is inactive). We analyzed the effects of exercise training on animals kept at thermoneutrality on both interscapular (BAT) and perivascular (PVAT) BAT, having previously shown these depots to exhibit a divergent response to brief nutrient excess (23), as well as IWAT hypothesizing that exercise induced "browning" would be absent under these conditions. Finally, we sought to identify how the AT proteome responds to exercise training to better understand the molecular adaptations of BAT to training at thermoneutrality.

METHODS

Animals, Exercise Protocol, and Metabolic Assessment

All studies were approved by the University of Nottingham Animal Welfare and Ethical Review Board, were carried out in accordance with the UK Animals (Scientific Procedures) Act of 1986. Twelve male Sprague-Dawley rats aged 3 weeks were obtained from Charles River (Kent, UK) and housed (3 per cage) immediately at thermoneutrality (c.28°C) under a 12:12-h reverse light-dark cycle (lights off at 08:00 a.m./ZT12, on at 20:00 p.m./ZT0) so as to closer mimic human physiology (21), minimize animal stress and maximize data quality and translatability (24). Animals were fed a high-fat diet (45%, 824018 SDS, Kent, UK) *ad-libitum* with body weight monitored weekly throughout. Half of the animals were then randomized (http://www.graphpad.com/quickcalcs/randomize1.cfm) to 4 weeks of exercise training (Ex) at 12 weeks of age. Then, the Ex group were acclimatized to water (c.35°C) for a 3-day period (10–20 min per day) at the beginning of the dark phase (i.e., ZT13). After acclimatization, the Ex group underwent the 4-week swim training programme (1 h/day for 5 days/week at ZT13). As described by the American Physiological Society, "Continuous swimming involves continuous movement of the rat's forelimbs and hindlimbs while maintaining its snout above the waterline" (25). We confirmed this behavior, and the ability of each animal to swim, prior to commencing the training programme. Following each session, animals were towel dried and placed back in their home cage underneath a heat lamp.

Animals were individually placed in an open-circuit calorimeter (CLAMS: Columbus Instruments, Linton Instrumentation, UK) for 48 h following training and prior to tissue collection. Assessment of whole body metabolism was performed as previously described (23), after which all animals were weighed and fasted overnight prior to euthanasia at ZT12-ZT15 by rising CO_2 gradient. BAT, IWAT, PVAT from the thoracic aorta and portion of the central liver lobe were then rapidly dissected, weighed, snap-frozen in liquid nitrogen and stored at −80°C for subsequent analysis. All fat depots were excised and weighed to calculate total fat mass.

Histology

Brown and inguinal adipose tissue samples were fixed in formalin for 96 h and embedded in paraffin wax using an Excelsior ES tissue processor (Thermo-Fisher). Sections were cut from each sample at 8 μm, mounted on Superfrost Plus slides (Fisher Scientific) and stained using haematoxylin and eosin (Sigma-Aldrich). Three to five randomly selected sections per sample were imaged and calibrated using an Olympus BX40 microscope with a charge-coupled device high-speed color camera (Micropublisher 3.3RTV; QImaging) at 10x magnification using Volocity v6.1 software (Perkin Elmer). BAT

and WAT cell area was determined using Adiposoft (26), an automated image analyzing java plugin for Image J (Fiji).

Gene Expression Analysis

Total RNA was extracted from each fat depot using the RNeasy Plus Micro extraction kit (Qiagen, West Sussex, UK) following an adapted version of the single step acidified phenol-chloroform method. RT-qPCR was carried out as previously described (23) using rat-specific oligonucleotide primers (Sigma-Aldrich) or FAM-MGB Taqman probes (see **Supplementary Table 1** for primer list). Gene expression was determined using the GeNorm algorithm against two selected reference genes; *RPL19:RPL13a in BAT* and IWAT (stability value M = 0.26 in BAT and 0.224 in IWAT) and RPL19:HPRT1 in PVAT (stability value M = 0.209).

Serum and Liver Analysis

Blood was taken by cardiac puncture and allowed to clot for ∼30 min at room temperature. Samples were then centrifuged at 2000G for 10 min and the serum removed and stored at −80°C until use. Serum was thawed gently on ice. Concentrations of glucose (GAGO-20, Sigma-Aldrich, Gillingham, UK), triglycerides (LabAssay™ Triglyceride, Wako, Neuss, Germany), non-esterified fatty acids (NEFA-HR(2), Wako, Neuss, Germany), insulin (80-INSRT-E01, Alpco, Salem, NH, USA), and leptin (EZRL-83K, Merck, Darmstadt, Germany) were measured following manufacturers' instructions. HOMA-IR was determined by calculating fasting insulin (μ U/mL) x fasting glucose (mg/dl)/405. Hepatic triglycerides were quantified using the Triglyceride Quantification Assay Kit (Colorimetric/Fluorometric) (ab65336).

Adipose Tissue Proteomics

Protein extraction, clean up and trypsinisation was carried out as previously described (23). Briefly, 50–100 mg of frozen BAT and IWAT was homogenized in 500 μL CellLytic MT cell lysis buffer (Sigma-Aldrich, C3228) prior to removal of lipid and other non-protein components using the ReadyPrep 2D clean up Kit (Biorad, 1632130). Samples (n = 4/group) were then subjected to reduction, alkylation and overnight trypsinisation, following which they were dried down at 60°C for 4 h and stored at −80°C before resuspension in LCMS grade 5% acetonitrile in 0.1% formic acid for subsequent analysis. Analysis by mass spectrometry was performed on a SCIEX TripleTOF 6600 instrument as previously described (27). Briefly, samples were analyzed in both SWATH (Data Independent Acquisition) and IDA (Information Dependent Acquisition) modes for quantitation and spectral library generation respectively. IDA data was searched using ProteinPilot 5.0.2 to generate a spectral library and SWATH data was analyzed using Sciex OneOmics software (28) extracted against the locally generated library as described previously (23). The mass spectrometry proteomics data have been deposited to the ProteomeXchange Consortium via the PRIDE partner repository with the dataset identifier PXD017306 (29).

Statistical Analyses

Statistical analyses were performed in GraphPad Prism version 8.0 (GraphPad Software, San Diego, CA). Data are expressed as Mean ± SEM with details of specific statistical tests in figure legends. Functional analysis of the proteome (fold change ± 0.5 and OneOmics confidence score cut-off of 0.75) was performed using the Advaita Bioinformatic iPathwayGuide software (www.advaitabio.com/ipathwayguide.html). Significantly-impacted biological processes, molecular interactions, and pathways were analyzed in the context of pathways obtained from the Kyoto Encyclopedia of Genes and Genomes database (Release 84.0+/10-26, Oct 17) (30) and the Gene Ontology Consortium database (2017-Nov) (31). The Elim pruning method, which removes genes mapped to a significant GO term from more general (higher level) GO terms, was used to overcome the limitation of errors introduced by considering genes multiple times (32). Analysis of protein-protein interactions (PPI) and GO term enrichment of these PPI networks was performed using NetworkAnalyst (www.networkanalyst.ca). Differentially regulated proteins were imported into NetworkAnalyst (https://www.networkanalyst.ca/NetworkAnalyst/home.xhtml) and protein-protein interactions were determined using the STRING interactome database with a confidence score cut-off of 900 and requirement of experimental evidence.

RESULTS

Exercise Training Increases BAT Mass and Regulates Thermogenic Genes in Perivascular BAT and Inguinal WAT

Swim training in diet-induced obesity did not affect body weight, subcutaneous fat mass or total fat mass (i.e., the weight of all dissected fat depots) but significantly attenuated weight gain during the 4-week intervention period (HFD: 78.6 ± 5.3 vs. Ex: 52 ± 7.7g, p = 0.03; **Figures 1A–C, E**) without effect on serum insulin or metabolites (**Figures 1J–O**), hepatic weight or hepatic triglycerides (**Figures 1P,Q**) (**Supplementary Data**). We attribute this attenuation in weight-gain to a trend in both EI (p = 0.08, **Figure 1I**) and RER (p = 0.09, **Figure 1F**) to decline given there is no effect on VO_2 or ambulatory activity (**Figures 1G,H**). Despite attenuated weight gain, BAT mass increased along with a significant increase in lipid droplet size (**Figures 1D** and **2D,E**) although no difference in key thermogenic (e.g., UCP1) or lipogenic (FASN) mRNA levels (**Figure 2A**) was detected. Interestingly, UCP1 was upregulated in PVAT along with PGC1α, a marker of mitochondrial biogenesis and P2RX5, a purinergic receptor and brown/beige adipocyte cell surface marker (**Figure 2B**). Similarly, mRNA's governing fatty-acid oxidation (PPARA) and lipogenesis (FASN) were upregulated in PVAT. With regards to "browning," UCP1 mRNA was undetectable in IWAT and was not induced with exercise training despite an upregulation of PGC1a, ADRB3, DIO2 and PPARA (**Figure 2C**). Morphologically, BAT was characterized by a heterogeneous mixture of classic, BAT-like tissue, small multilocular lipid droplets and small to large adipocytes with exercise training driving a significant

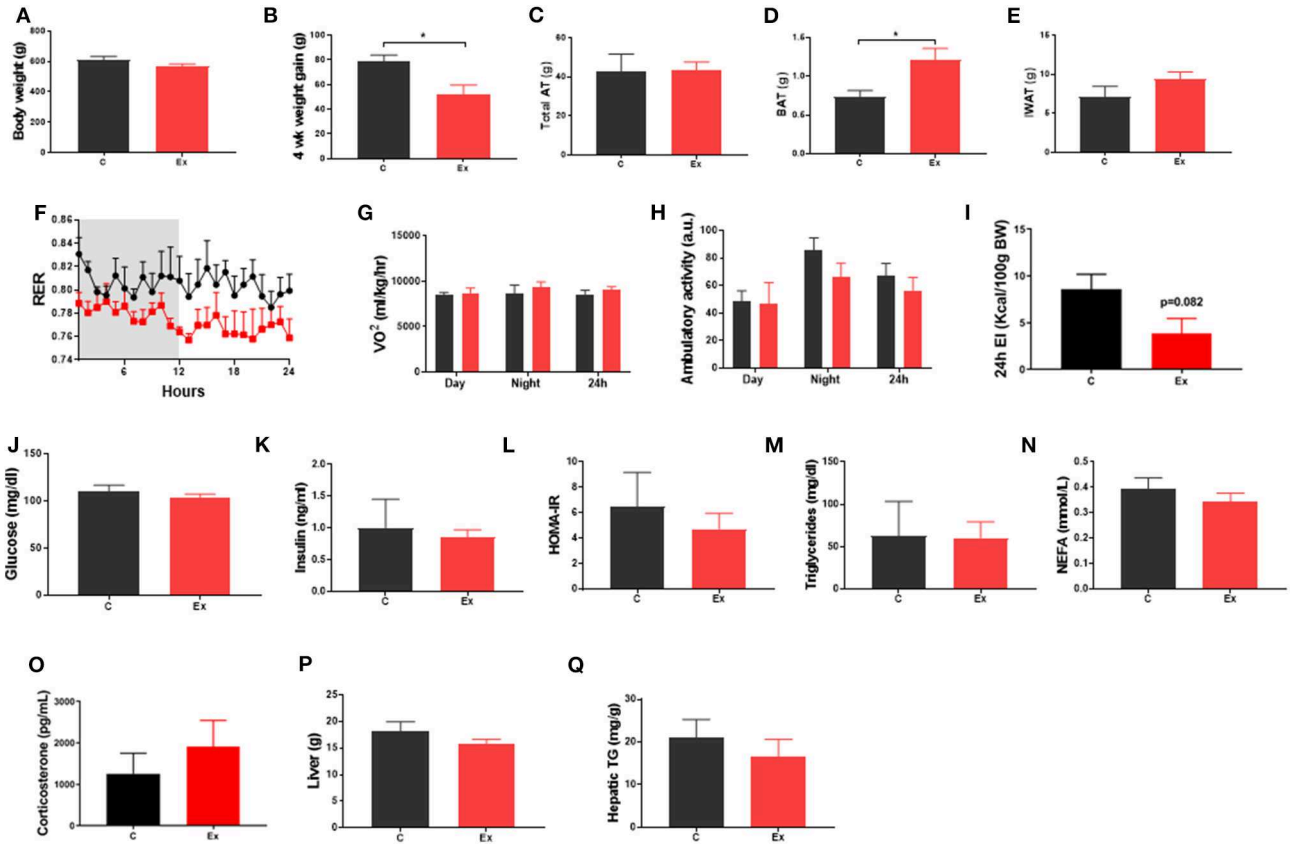

FIGURE 1 | Exercise training (Ex) attenuated weight gain and increased brown adipose tissue (BAT) mass but had no effect on insulin, glucose, triglycerides, or non-esterified fatty acids compared to no training **(C)**. **(A)** Final body weight, **(B)** 4 week intervention weight gain, **(C)** total fat mass, **(D)** BAT mass, **(E)** inguinal white adipose tissue (IWAT) mass, **(F)** respiratory exchange ratio (RER), **(G)** oxygen consumption (VO_2), **(H)** ambulatory activity. **(I)** 24h energy intake **(J)** serum glucose, **(K)** insulin, **(L)** HOMA-IR, **(M)** triglycerides, **(N)** NEFA and **(O)** Corticosterone, **(P)** liver weight and **(Q)** hepatic triglycerides. Data **(F–I)** obtained from CLAMs metabolic cages. All data expressed as mean ± SEM, $n = 4$–5 per group. For comparison, data was analyzed by either Students *t*-test **(A–E, I–P)** or two-way ANOVA **(F–H)** and Sidak *post-hoc* tests. Significance denoted as $^*p < 0.05$.

increase in lipid droplet size (**Figures 2D,E**) whereas there was no discernable difference in IWAT (**Figures 2F,G**) which was characterized by large adipocytes and no sign of multilocular, beige adipocytes as is evident in WAT at lower ambient temperatures.

Identification of Differentially Regulated Proteins in BAT and IWAT in Response to Swim-Training

We then sought to determine the exercise-induced effects on the proteome of these BAT and IWAT depots. We identified 353 differentially regulated proteins in BAT (**Table 1**: Top 20 proteins; **Supplementary Table 1**: Full list). The most significantly altered proteins were involved in mitochondrial ATP synthesis (ATP5E), nucleopore (NUP35), ADP ribosylation (ARF1 and SCOC), and progesterone binding (PGMRC2). Among the proteins most upregulated in BAT were those involved in assembly of the skeletal muscle cytoskeleton (PDLIM3 and MYH4), muscle contraction (TNNI2), and muscle-specific phosphoglycerate mutase metabolism (PGAM2). Proteins involved in calcium sensing in the lumen of the sarcoplasmic reticulum (CASQ1) and beta adrenergic signaling (CAPN1 and PSMB7) were found to be the most downregulated in BAT. Conversely, only 189 proteins were differentially regulated in IWAT after exercise. The most significantly altered proteins (**Table 2**: Top 20 proteins; **Supplementary Table 2**: Full list) were involved in the trafficking of GLUT4 (TUSC5), the mitochondrial electron transport chain (NDUFS6), beta adrenergic signaling (PSMB7), TLR4 signaling (LRRFIP2), and apoptosis (ATG7 and BIN1). Proteins with the greatest fold change were those involved in cell adhesion (CD44 and VCAN), FFA and lipoprotein metabolism (FABP3 and APOC1), TGF-beta signaling (TSC22D1), purine and mitochondrial metabolism (LHPP and COX6A1), and the acetylation of nucleosomes and DNA binding (HET and HMGB1).

Exercise Training Enriches Mitochondrial and Skeletal Muscle Related GO Terms and Pathways in BAT

We then carried out functional analysis of the BAT and IWAT proteome. The differentially regulated proteins in BAT enriched GO terms (**Table 3**; **Supplementary Table 3**: Full list) including *2-oxoglutarate metabolic process, generation of precursor metabolites, cytochrome-c oxidase activity,*

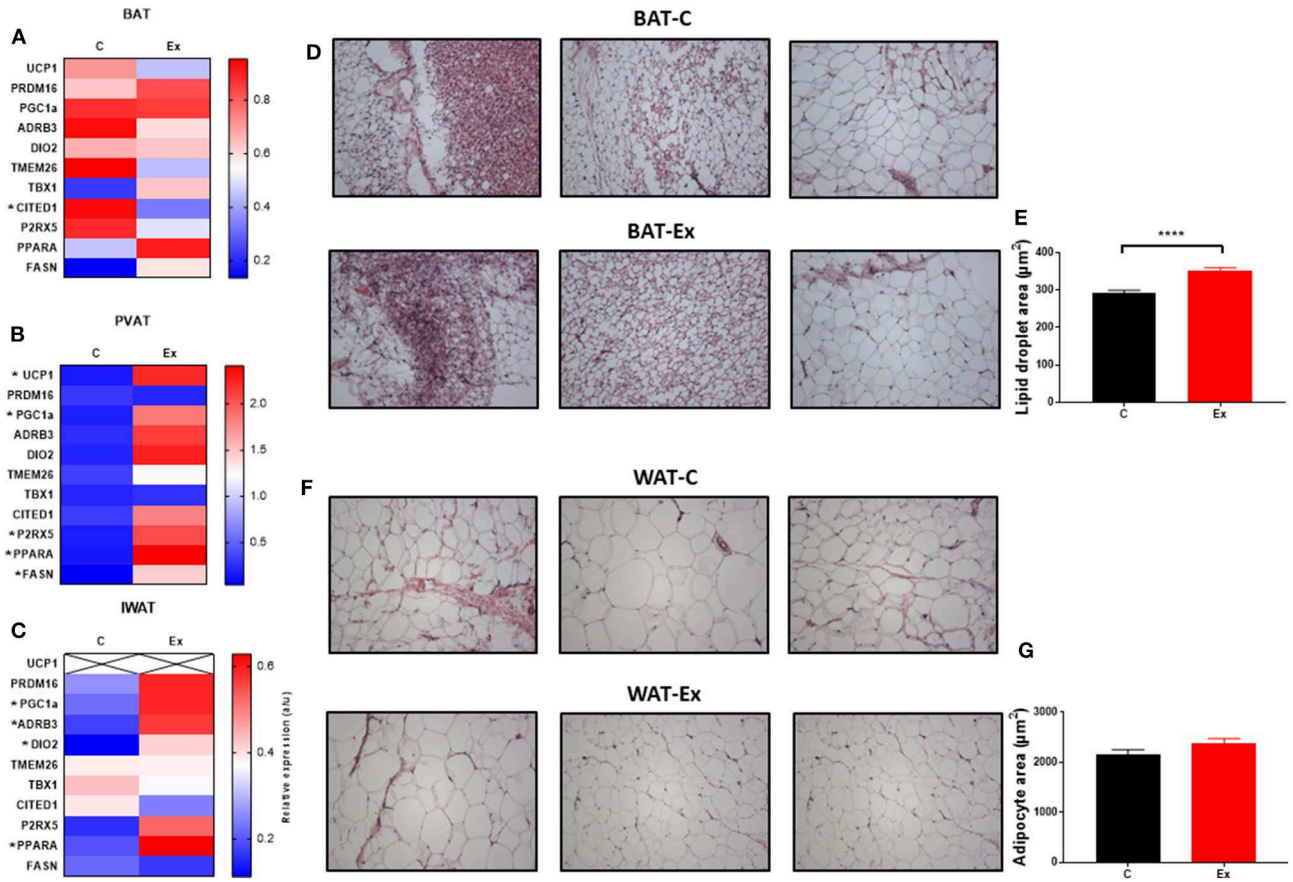

FIGURE 2 | Exercise training (Ex) regulates thermogenic genes in a depot-specific manner. **(A–C)** thermogenic mRNA in BAT, PVAT, and IWAT, **(D,E)** histological analysis of BAT and lipid droplet size and **(F,G)** histological analysis of WAT and adipocyte size. Data expressed as mean ± SEM, $n = 4$–5 per group. Adipocyte/lipid droplet area quantified using Adiposoft (BAT-C, $n = 8{,}949$ and Ex, $n = 8{,}234$; WAT-C, $n = 750$ and Ex – $n = 555$). For comparison, data was analyzed by Students *t*-test. Significance denoted as $^{*}p < 0.05$ and $^{****}p < 0.0001$.

mitochondrial respiratory chain complex IV and proton transporting ATP synthase activity (**Figures 3A–D**). There was also an enrichment of GO terms related to skeletal muscle physiology including *sarcomere, myosin complex, and skeletal muscle tissue development* (**Figures 3E–G**). This enrichment was associated with a significant upregulation of skeletal muscle markers (**Figure 3H**) including Myoglobin, Myogenic differentiation 1 (MYOD1) and Myogenin (MYOG). In IWAT, (**Table 4**; **Supplementary Table 4** for full list) the differentially regulated proteins enriched GO terms including *positive regulation of apoptotic process, positive regulation of ATPase activity* and *lipid droplet* (**Figures 4A–C**). In addition, a number of GO terms associated with RNA processing were enriched including *spliceosomal complex and negative regulation of transcription from RNA polymerase II promoter* (**Figure 4D**).

Impact analysis, which combines classical overrepresentation analysis with the perturbation of a pathway, highlighted several metabolic pathways modified by exercise (**Supplementary Table 5**) in BAT *carbon metabolism*, *Alzheimer's disease,* and *oxidative phosphorylation* (**Figures 5A–C**). In IWAT, the impacted pathways (**Figures 5D,E**) included the *spliceosome and Fc gamma R-mediated phagocytosis*.

Characterization of the "Interactome" in Exercise-Trained Brown and White Adipose Tissues

To better understand how our differentially altered proteins affect downstream signaling pathways, we characterized the "interactome" of BAT and IWAT through analysis of protein-protein interactions. NetworkAnalyst generated 28 sub-networks (i.e., the main "continent" and 27 "islands") in BAT with the main network consisting of 1,091 proteins (**Figure 6**). Hub proteins (pink unless specified and labeled if high ranking) in this main network included the ribosomal proteins (i.e., RPL27a and RPL10a), the mitochondrial elongation factor GFM1, AKT Serine/Threonine Kinase 2 (Akt2) and mitogen-activated protein kinase 1 (MAPK1). Further analysis demonstrated interacting proteins (purple unless specified) in this main network enriched 30 biological processes (**Supplementary Data**

TABLE 1 | Top 20 differentially regulated proteins in BAT.

Symbol	Entrez	Logfc	adjpv
Picalm	89816	−1.77605	3.83E-06
Scoc	364981	−1.84724	7.37E-05
Trim72	365377	0.773012	0.000139
Arf1	64310	−2.72857	0.00015
Rbbp9	29459	−1.79555	0.000168
Rps26	27139	−0.57111	0.000217
Pgrmc2	361940	−1.29142	0.00027
Atp5e	245958	1.29928	0.000345
Ruvbl1	65137	−2.89092	0.000414
Serpinb1a	291091	−0.6765	0.000424
Rnmt	291534	2.861109	0.000447
Nup35	295692	1.47585	0.000704
Ggcx	81716	0.762945	0.00088
Rpl21	79449	−3.79095	0.000976
Farsa	288917	−2.23967	0.001057
Pon1	84024	1.269484	0.001358
Vars	25009	0.905263	0.001382
Slc3a2	50567	1.68137	0.001386
Acox1	50681	−1.05358	0.001481
Rab7a	29448	−0.56428	0.001598

Entrez gene ID (Entrez), log fold change (Logfc) where minus symbol equals downregulation, adjusted P value (adjPval).

TABLE 2 | Top 20 differentially regulated proteins in IWAT.

Symbol	Entrez	Logfc	adjpv
Lrrfip2	301035	−1.62311	7.61E-06
RGD1311739	311428	0.886759	0.000023
Psmb7	85492	2.732771	0.000195
Ndufs6	29478	2.213416	0.000496
Ezr	54319	−0.7888	0.0005
Orm1	24614	1.11547	0.001359
Bin1	117028	−3.21998	0.001856
Stk3	65189	−1.51626	0.001979
Gna11	81662	0.563094	0.002852
Sult1a1	83783	0.868093	0.003031
Sod3	25352	0.639222	0.003225
Atg7	312647	−2.31741	0.004631
Rpl38	689284	−1.10403	0.006447
Pip4k2a	116723	−1.89092	0.006578
Tusc5	360576	0.802222	0.007389
Usp7	360471	−0.81645	0.00841
Cd14	60350	0.942401	0.008533
Pdcd10	494345	−0.80063	0.009051
Timm8a1	84383	−1.10352	0.010498
EGF	25313	3.510509	0.01074

Entrez gene ID (Entrez), log fold change (Logfc) where minus symbol equals downregulation, adjusted P value (adjPval).

TABLE 3 | GO terms enriched in BAT.

Go Id	goName	countDE	countAll	pv_elim
BIOLOGICAL PROCESS				
GO:0003151	Outflow tract morphogenesis	4	4	0.0053
GO:0006103	2-oxoglutarate metabolic process	6	8	0.0064
GO:0051304	Chromosome separation	5	6	0.0067
GO:0007093	Mitotic cell cycle checkpoint	6	9	0.0148
GO:0014075	Response to amine	6	9	0.0148
GO:0014044	Schwann cell development	5	7	0.0182
GO:0018198	Peptidyl-cysteine modification	5	7	0.0182
GO:2000273	Positive regulation of receptor activity	5	7	0.0182
GO:0006091	Generation of precursor metabolites and energy	31	82	0.0189
GO:0000132	Establishment of mitotic spindle orientation	4	5	0.0209
MOLECULAR FUNCTION				
GO:0004129	Cytochrome-c oxidase activity	6	7	0.002
GO:0004029	Aldehyde dehydrogenase (NAD) activity	6	8	0.0061
GO:0035255	Ionotropic glutamate receptor binding	5	6	0.0064
GO:0019905	Syntaxin binding	6	9	0.0142
GO:0046933	Proton-transporting ATP synthase activity, rotational mechanism	6	9	0.0142
GO:0070628	Proteasome binding	3	3	0.0192
GO:0072341	Modified amino acid binding	10	20	0.022
GO:0008026	ATP-dependent helicase activity	6	11	0.0471
GO:0030170	Pyridoxal phosphate binding	6	11	0.0471
GO:0016769	Transferase activity, transferring nitrogenous groups	4	6	0.0479
MOLECULAR FUNCTION				
GO:0005751	Mitochondrial respiratory chain complex IV	6	8	0.0065
GO:0030017	Sarcomere	20	47	0.0147
GO:0002080	Acrosomal membrane	3	3	0.0199
GO:0000275	Mitochondrial proton-transporting ATP synthase complex, catalytic core F(1)	4	5	0.0211
GO:0031201	SNARE complex	4	5	0.0211
GO:0005774	Vacuolar membrane	17	40	0.0241
GO:0016459	Myosin complex	7	13	0.0369
GO:0000922	Spindle pole	8	16	0.0424
GO:0090543	Flemming body	3	4	0.0635
GO:0005765	Lysosomal membrane	14	35	0.0655

GO term ID (gold), GO term name (goName), number of differentially regulated proteins (countDE), total number of proteins associated with GO term (countAll) and p-value based on Elim pruning method (pv_elim).

PPI, **Table 2**) including *chromatin assembly or disassembly, developmental growth and muscle organ development* and 30 molecular functions (**Figure 5**) including *RNA binding* (yellow), *steroid dehydrogenase activity* (green), *neuropeptide hormone activity* (orange), and *transcription cofactor activity* (light blue).

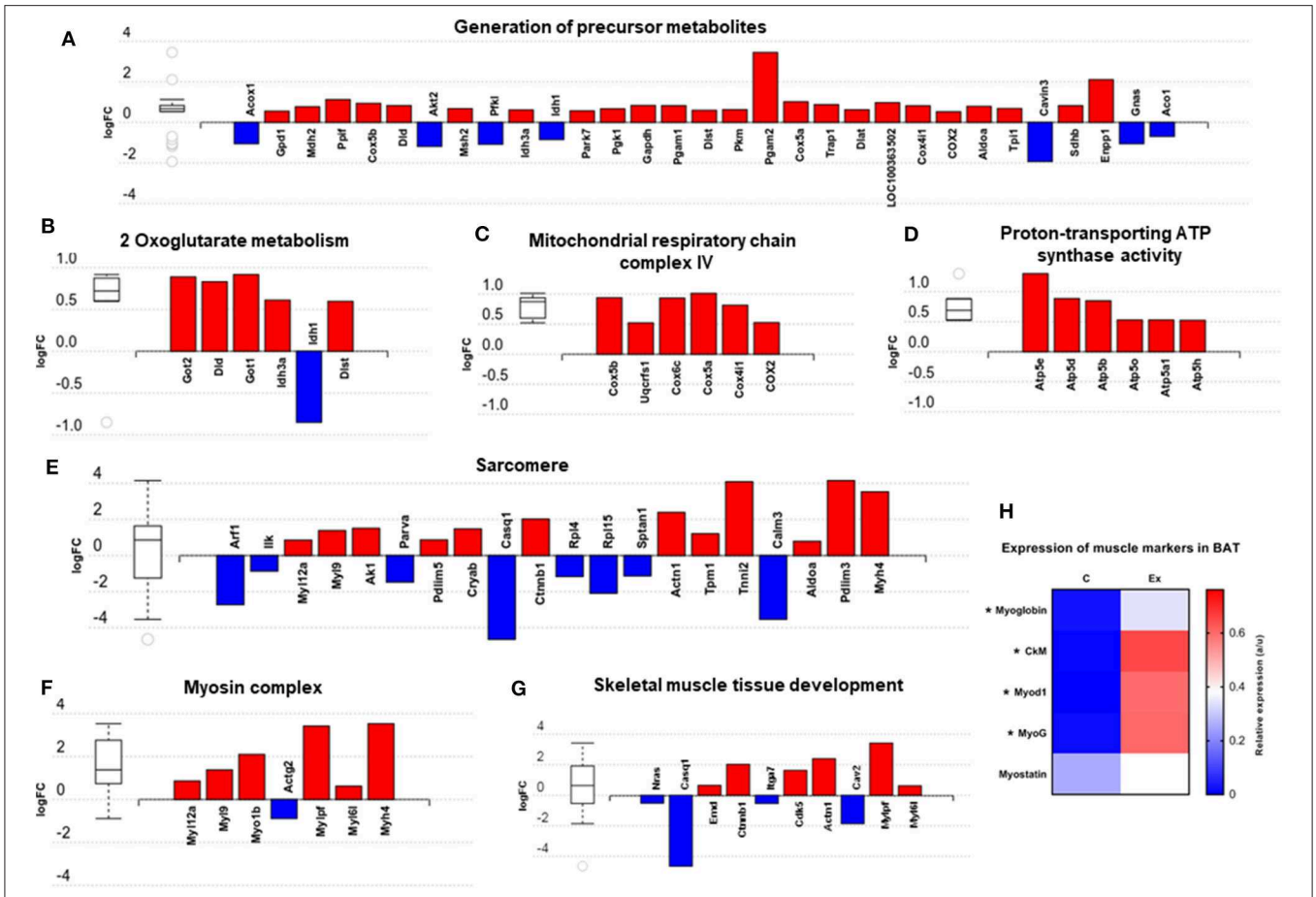

FIGURE 3 | Overview of enriched metabolic and skeletal muscle related gene ontology (GO) terms in brown adipose tissue **(A–G)** and expression of myogenic markers **(H)**. Figures created with AdvaitaBio IPathway Guide. *N* = 4–5/group, for analysis see methods section.

In IWAT, the "interactome" was smaller, consisting of 19 sub-networks (i.e., 1 "continent" and 18 "islands") with the main network made up of 488 proteins (**Figure 7**). Hub proteins (pink unless specified and labeled if high ranking) in the main network again included multiple ribosomal proteins (i.e., RPL27a and RPL4) in addition to Proteasome subunit B10 (PSMB10) and the spliceosomal protein mago homolog, exon junction complex subunit (MAGOH). Further analysis demonstrated that the interacting proteins (purple unless specified) in this main network were involved in 6 biological processes (Supplementary data PPI, **Supplementary Table 6**) including *chromatin assembly or disassembly, sensory taste perception* and *RAS protein signal transduction* and 5 molecular functions (**Figure 6**) including *RNA binding (yellow), transcription cofactor activity (light blue),* and nucleotide *binding (green)*.

DISCUSSION

The vast majority of studies investigating the function of BAT in rodents have been carried out at temperatures (i.e., c.20–22°C) which are well below thermoneutrality (i.e., c.28–33°C). These environmental differences have diverse effects on physiology, immunity and metabolism (19, 20). Whilst the use of thermoneutrality has been suggested as the optimal environment to mimic human physiology there is ongoing debate as to "how high" we should go (19, 33, 34). It was recently demonstrated that BAT from mice housed chronically at thermoneutrality and fed an obesogenic diet closer resembles human BAT with it suggested that this model of "physiologically humanized BAT" represents the ideal model of BAT physiology (22). Here, under these conditions (i.e., chronic thermoneutrality and diet induced obesity), we show exercise training induces an oxidative phenotype in BAT of obese animals that is associated with an enrichment of GO terms involved in skeletal muscle physiology, pathways associated with altered mitochondrial metabolism (i.e., oxidative phosphorylation) and increased lipid content. Unlike studies conducted at sub-thermoneutrality (18, 35), we show UCP1 mRNA is absent in IWAT of obese animals raised at thermoneutrality and is not induced with exercise training. Instead, IWAT in exercise trained animals exhibits a reduction in apoptotic proteins and perturbations in the spliceosomal pathway.

A Thermogenic Response in PVAT and Adipocyte-to-Myocyte Switch in BAT

Despite no induction of thermogenic mRNA's in BAT, an upregulation of these markers in PVAT suggests an uncoupling of the response to exercise training in anatomically distinct BAT depots. A downregulation of thermogenic genes and "whitening" of thermogenic AT has previously been attributed to increases in core body temperature with exercise training (10). This would seem not to be the case, however, given an increase of these genes in PVAT which plays a critical role in heating blood prior to circulation (36). The physiological role of these alterations in PVAT is unclear but may represent depot-specific adaptations to exercise training which are potentially linked to cardiovascular alterations occurring with training. A "whitening" of BAT is evident however and is associated with a shift toward a muscle-like signature.

A myogenic signature in brown adipocytes was first established in 2007 when it was shown that the expression of myogenic genes in differentiating brown adipocytes was a characteristic that clearly distinguished them from white adipocytes (37). It was subsequently shown that both BAT and skeletal muscle derive from the same Pax7+ / Myf5+ progenitor cells and that the transcription factor PRDM16 drives the fate of these progenitors to committed brown adipocytes (38). Despite these shared characteristics, a definitive physiological role for these skeletal muscle associated proteins in BAT has not been demonstrated. In WAT, blockade of the β3-receptors induces myogenesis with (a) the emergence of MyoD+ mononucleated cells which undergo myogenesis even under adipogenic conditions and (b) the fusion of stromal cells which form multinucleated myotubes that "twitch" and express myosin-heavy chain (MHC) (39). A subset of UCP1+ beige adipocytes (c.15% of total beige adipocytes) in Myod1-CreERT2 reporter mice are derived from MyoD+ cells located adjacent to the microvasculature, and this "glycolytic" beige fat exhibits enhanced glucose metabolism compared to typical beige adipocytes.

Given that exercise training drives myogenesis in skeletal muscle, it may have a similar impact on BAT given their shared developmental origins and, whilst the prevalence of muscle cells (i.e., Pax7+) residing in BAT needs to be directly assessed in future studies an upregulation of markers including MYOD1, MYOG, and Myoglobin points toward an induction of myogenesis in BAT following exercise training. The enrichment of pathways involved in amino acid metabolism (i.e., *biosynthesis of amino acids*; *glycine, serine, threonine, arginine and proline metabolism*), and their known role in protein synthesis and muscle hypertrophy may point toward this and explain, in part, the increase in BAT mass though this could be attributed solely to increased lipid content. Mice lacking interferon regulatory factor 4 (IRF4) in BAT (BATI4KO) exhibit reduced exercise capacity at both low and high-intensity treadmill running, and display selective myopathy (40). Interscapular BAT of these exercise intolerant mice is characterized by an upregulation of genes governing skeletal muscle physiology, including MyoD1, troponin T1, and myostatin. This suggests that myogenesis in BAT may have an adverse effect on whole body physiology. Alongside the induction of muscle-related proteins was an upregulation of proteins involved in the *generation of precursor metabolites* and *energy and mitochondrial respiration*. Phosphoglycerate mutase 2 is a key muscle-specific

TABLE 4 | GO terms enriched in IWAT.

Go Id	goName	countDE	countAll	pv_elim
BIOLOGICAL PROCESS				
GO:0000381	Regulation of alternative mRNA splicing, via spliceosome	6	12	0.0029
GO:0032781	Positive regulation of ATPase activity	6	12	0.0029
GO:0032760	Positive regulation of tumor necrosis factor production	5	10	0.0066
GO:0042742	Defense response to bacterium	6	14	0.0073
GO:0043065	Positive regulation of apoptotic process	18	73	0.0074
GO:0000122	Negative regulation of transcription from RNA Polymerase II promoter	11	37	0.0083
GO:0000077	DNA damage checkpoint	3	4	0.0093
GO:0001960	Negative regulation of cytokine-mediated Signaling pathway	3	4	0.0093
GO:0002828	Regulation of type 2 immune response	3	4	0.0093
GO:0010799	Regulation of peptidyl-threonine phosphorylation	3	4	0.0093
MOLECULAR FUNCTION				
GO:0070573	Metallodipeptidase activity	3	3	0.0026
GO:0019955	Cytokine binding	4	6	0.0043
GO:0051015	Actin filament binding	12	40	0.0058
GO:0060590	ATPase regulator activity	4	7	0.009
GO:0005080	Protein kinase C binding	6	15	0.0112
GO:0003727	Single-stranded RNA binding	6	16	0.0159
GO:0004180	Carboxypeptidase activity	4	9	0.0258
GO:0036002	Pre-mRNA binding	4	9	0.0258
GO:0003697	Single-stranded DNA binding	5	14	0.0341
GO:0003725	Double-stranded RNA binding	6	19	0.0376
CELLULAR COMPONENT				
GO:0071013	Catalytic step 2 spliceosome	7	16	0.0032
GO:0031528	Microvillus membrane	4	6	0.0041
GO:0005811	Lipid droplet	8	24	0.0113
GO:0005681	Spliceosomal complex	10	22	0.0346
GO:0030315	T-tubule	4	10	0.037
GO:0005885	Arp2/3 protein complex	3	6	0.0372
GO:0016604	Nuclear body	11	46	0.0412
GO:0000776	Kinetochore	5	15	0.0437
GO:0016607	Nuclear speck	7	26	0.0548
GO:0022626	Cytosolic ribosome	12	54	0.0562

GO term ID (gold), GO term name (goName), number of differentially regulated proteins (countDE), total number of proteins associated with GO term (countAll) and p-value based on Elim pruning method (pv_elim).

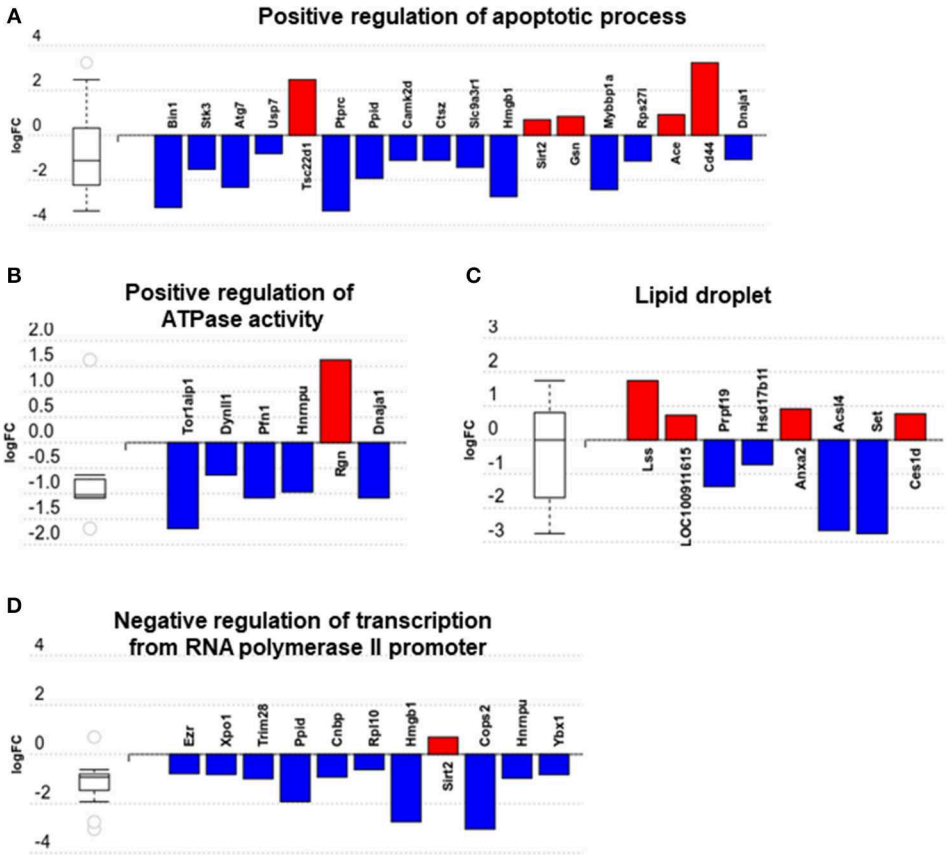

FIGURE 4 | Overview of enriched gene ontology (GO) terms in inguinal white adipose tissue **(A–D)**. Figures created with AdvaitaBio IPathwayGuide. *N* = 4/group, for analysis see methods section.

enzyme in which mutations (i.e., muscle phosphoglycerate deficiency) cause tubular aggregates and exercise intolerance. An upregulation of this protein in BAT further strengthens the idea of a switch toward a muscle phenotype. An enrichment of multiple mitochondria associated metabolic pathways including OXPHOS further suggests that, despite no demonstrable impact on UCP1 in BAT, the metabolic activity of this tissue has potentially increased. On the other hand, no change in UCP1 mRNA alongside a significant increase in tissue mass could also suggest a net increase in the thermogenic capacity of the depot i.e., 50% more BAT expressing similar levels of UCP1. Structural and mechanical proteins, such as the actomyosin machinery in BAT, are crucial for the induction of oxidative metabolism and thermogenesis (41). BAT responds mechanically to adrenergic stimulation and actomyosin mediated tension with type-II myosins in particular facilitating uncoupled respiration. The induction of structural, and actomyosin related proteins seen in BAT with training could therefore facilitate an increased metabolic capacity in this tissue, which would support the upregulation of mitochondrial proteins. A downregulation of CASQ1, calcium sensor and regulator in the mitochondria and CALM3, a calcium binding protein suggest that exercise training may perturb calcium signaling in BAT which may be of particular functional importance for the SERCA2b-RyR2 pathway which can drive UCP1-independent thermogenesis (42–44). Whilst further work is needed to validate and corroborate this data, and to determine the functional role of specific proteins, we propose this muscle-like signature as a novel, UCP1-independent pathway through which exercise regulates BAT metabolism.

A Role for Exercise in the Attenuation of Adipose Tissue Apoptosis

Whilst prior work has demonstrated an induction of thermogenic genes in WAT following exercise training, we show that UCP1 mRNA is absent in IWAT of animals raised at thermoneutrality from weaning. Instead, there are alterations to apoptotic and spliceosomal proteins. Dysregulated apoptotic processes are associated with AT inflammation and insulin resistance (45, 46). Here, we show one potential benefit of exercise training on IWAT is a downregulation of multiple proteins governing the "*positive regulation of apoptotic process.*" Bridging integrator 1, for instance, is a MYC proto-oncogene interacting factor that activates caspase-independent apoptosis in cancer cells, though its role in AT immunometabolism is unknown (47). Autophagy-related (ATG)7 is a ubiquitin activating enzyme which forms a complex with caspase-9 to cross-regulate autophagy and apoptosis (48). Adipocyte specific ATG7 k/o mice are lean with reduced fat mass, increased insulin sensitivity, an increase in

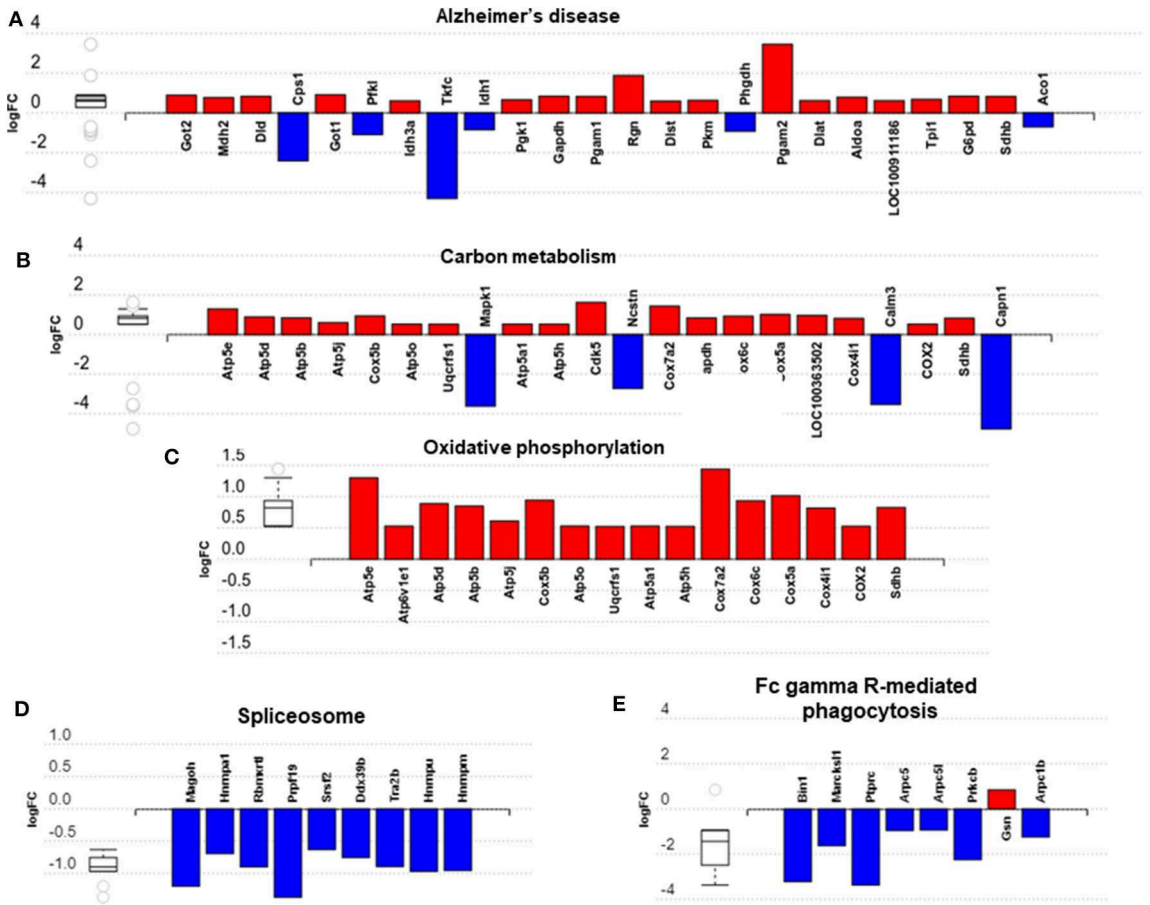

FIGURE 5 | Overview of significantly impacted pathways in brown adipose tissue **(A–C)** and inguinal white adipose tissue **(D,E)**. **(A–E)** created with AdvaitaBio IPathwayGuide. *N* = 4/group, for analysis see methods section.

BAT thermogenesis and are resistant to diet-induced obesity (49, 50). Other proteins of particular interest include MYB binding protein (MYBBP)1a and CD44. MYBBP1a is a SIRT7 interacting protein which regulates nucleolar stress and ribosome biogenesis that is increased in visceral AT of obese mice and negatively regulates adipogenesis (51, 52). Downregulation of MYBBP1a by exercise training may be a putative mechanism whereby physical activity and/or exercise regulates adipocyte number and size. Finally, CD44 mRNA is 3-fold higher in AT of insulin-resistant humans and correlates with CD68 and IL6, whilst CD44 k/o mice are phenotypically healthier and exhibit reduced AT inflammation (53, 54). These changes in apoptotic proteins occurred alongside an enrichment of proteins involved in the regulation of lipid droplets, including Lanosterol Synthase (LSS) and Carboxylesterase 1 (CES1) which regulate the synthesis of cholesterol, and the metabolism of cholesterol esters. Alongside a downregulation of Acyl-CoA Synthetase Long Chain Family Member 4 (ACSL4) this could point to exercise induced changes to the lipidome of WAT though how the lipidome of physiologically humanized animals following exercise training differs to animals at standard housing conditions remains to be determined (55).

Impact analysis demonstrated a number of significantly perturbed pathways. Epidermal growth factor (EGF) was the single protein differentially regulated in pathways including melanoma, phospholipase D signaling and PI3K-Akt signaling pathways. The role of EGF in adipogenesis is well-described with EGF receptor (ErbB1) abundance reduced in insulin resistant women with Type 2 diabetes. Importantly, EGF exerts insulin-like effects on adipocytes and skeletal muscle and this exercise-induced increase may be one way in which physical exercise potentiates insulin-sensitizing effects in these tissues (56). The most impacted pathway, however, was the spliceosome. This multi-megadalton ribonucleoprotein complex removes introns from RNA polymerase II transcripts (pre mRNAs) and is a crucial step in mRNA synthesis (57). Given that c.95% of genes are subject to alternative splicing, a downregulation of proteins involved in the spliceosome pathway would likely have major downstream effects on AT function, and may be driving the alterations observed in the proteome (58). Perturbation of the spliceosomal pathway was associated with an enrichment of the GO term "*regulation of RNA metabolic process*" in which 36 of 44 proteins were reduced. Why exercise training downregulates large numbers of proteins involved in pre-mRNA

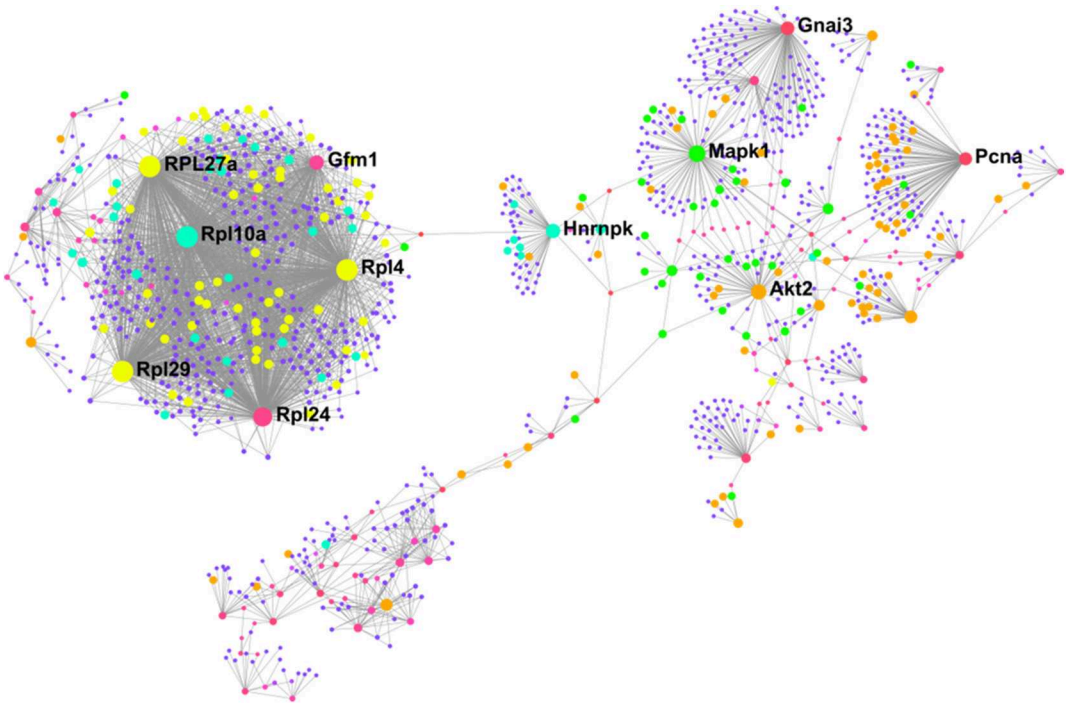

FIGURE 6 | Protein-protein interaction network in BAT created using NetworkAnalyst showing hub proteins (bold) and proteins involved in *RNA binding* (yellow), *steroid dehydrogenase activity* (green), *neuropeptide hormone activity* (orange), and *transcription cofactor activity* (light blue). The pink/purple dots represent topological representation of other hub/seed proteins. $N = 4$/group, for analysis see methods section.

synthesis and in RNA metabolism is, however, unclear and merits further investigation.

Characterizing the Exercise Interactome in BAT and WAT

Analysis of protein-protein interactions is an important step in understanding the communication between proteins and identification of putative signaling pathways occurring in specific tissues following an intervention. Here, we have identified multiple ribosomal proteins (i.e., RPL27a and RPL10a), AKT2 and MAPK1 as important hub proteins controlling regulation of chromatin assembly, muscle organ development and steroid hormone dehydrogenase activity in exercised BAT. It has been suggested that increased ribosomal biogenesis plays a major role in skeletal muscle hypertrophy and though a number of these ribosomal proteins were downregulated (i.e., RPL21, RPL29, RPL15, RPL10a, RPL27a, and RPL4) we propose that these specific ribosomal hub proteins may play an important role in the shift toward a muscle-like signature in BAT through their interacting proteins (59). Further, ribosomal proteins are regulated by growth factors, and that IGF1 specifically regulates muscle hypertrophy through both the PI3K-AKT-mTOR and MAPK signaling pathways, with the latter playing a key role in regulating ribosomal biogenesis (59–61). These adaptations could also be a response to physiological stress, with ribosomal proteins involved in numerous functions beyond the ribosome including immune signaling, inflammation, and development (62). It is not clear at present whether the changes to ribosomal proteins in BAT impacts on ribosomal biogenesis or, extra ribosomal functions however, proteostasis is essential for the adaptation of BAT, and mice to cold and obesity and the same may apply to exercise training. PCNA, is a cell cycle protein, whose upregulation suggests satellite cells have entered the cell cycle (63, 64). That AKT2, MAPK1, and PCNA are identified as hub proteins suggests that both of them, and the proteins interacting with them, could be important to the induction of muscle-related proteins in BAT. These proteins and their downstream targets offer novel insight into the induction of muscle-related proteins in BAT and the regulation of BAT physiology with exercise. The identification of ribosomal proteins as both hub and interacting proteins in WAT suggests they are also important in the general regulation of adipose tissue physiology by exercise training, though their role in WAT is less clear. To date, no functional role for these hub proteins in AT has been shown though the identification of MAGOH as a hub protein suggests it may play a key role in the regulation of the spliceosome pathway. Functional studies of these hub proteins and signaling pathways in AT is needed to better understand how exercise regulates WAT biology.

Strengths, Limitations, and Future Perspectives

We acknowledge that there are several limitations to this work. First, despite showing a trend toward reduced energy intake and RER we recognize that at ∼500–600 g these animals are likely to

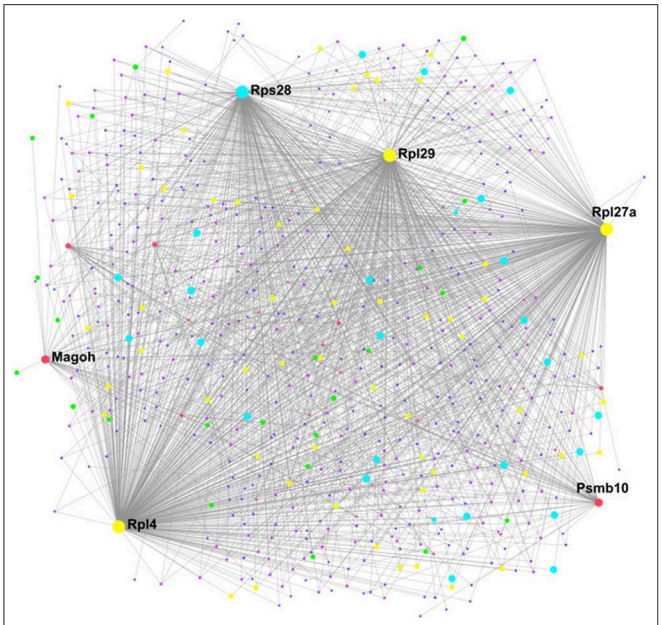

FIGURE 7 | Protein-protein interaction network in WAT created using NetworkAnalyst showing hub proteins (bold) and proteins involved in *RNA binding (yellow), transcription cofactor activity (light blue),* and nucleotide *binding (green)*. The pink/purple dots represent topological representation of other hub/seed proteins. *N* = 4/group, for analysis see methods section.

be near the maximum capacity of the metabolic cages, and that home cage systems would obtain more accurate physiological data (65). Second, whether the effects we see here occur in lean animals remains to be established. Whilst not directly comparable, recent work by Raun et al. and McKie et al. (66, 67) shows an attenuated effect of exercise on thermogenic genes in lean 8 to 10 week-old mice acclimated to Tn for just 1–2 weeks. Whilst it needs testing, it is feasible to suggest the lack of effect on UCP1 seen here would also be absent in lean animals raised at Tn from weaning given the extended time spent at thermoneutrality. Thermoneutrality also impacts on running volume, the diurnal rhythm of RER and attenuates metabolic adaptations including glucose homeostasis and insulin action and it could also be suggested that the complete lack of an effect on multiple metabolites and physiological parameters seen here could be attributed to chronic thermoneutrality from weaning (66, 67). It will also need to be determined whether the effects we see here are applicable to other modalities of exercise training such as wheel and treadmill running. However, given "browning" is not restricted to a single exercise type it is not a given that other modalities would induced thermogenic genes in IWAT (18). Further, we opted for swim training as there is a reduced risk of injuries (i.e., foot/leg) and, whilst there is evidence to suggest that rats "float" in water when air is caught in their fur we noted that fur thickness was greatly reduced compared to what we typically see in animals of a similar age housed at 20°C. Though we did not place the control group in shallow water to control for any specific effect of water temperature, or stress, on thermogenesis this would be unlikely to mimic many of the effects seen in fully submerged, swimming animals but is worthy of future consideration. Furthermore, adipose tissue proteomics was a secondary, unbiased analysis in the absence of a thermogenic effect and, whilst validation is needed in larger studies, we consider this to be an important data set given it is the first work to analyse the proteome in animals raised, and trained under these conditions.

CONCLUSION

We propose that BAT is dormant at thermoneutrality and that exercise training drives a muscle-like signature. The physiological relevance of this adaptation is unclear and BAT-muscle crosstalk, in particular, merits further investigation. Meanwhile, WAT exhibits a reduction in apoptotic proteins and a wholesale downregulation of proteins involved in pre-mRNA synthesis and RNA metabolism.

DATA AVAILABILITY STATEMENT

The datasets used and analyzed during the current study are available from the corresponding author on reasonable request.

ETHICS STATEMENT

The animal study was reviewed and approved by University of Nottingham Animal Welfare and Ethical Review Board.

AUTHOR CONTRIBUTIONS

PA, HB, and MS conceived the study and attained the funding. PA and MS developed and designed the experiments. PA, JL, IL, AM, IB, RC, and DB performed the experiments. PA, AM, and DB analyzed the data. PA and MS wrote the paper which was revised critically by DB, HB, FE, and JL for important intellectual content. All authors read and approved the final manuscript.

FUNDING

The study was funded by the British Heart Foundation [grant number FS/15/4/31184/].

SUPPLEMENTARY MATERIAL

The Supplementary Material for this article can be found online at: https://www.frontiersin.org/articles/10.3389/fendo.2020.00097/full#supplementary-material

REFERENCES

1. Klöting N, Blüher M. Adipocyte dysfunction, inflammation and metabolic syndrome. *Rev Endocr Metab Disord.* (2014) 15:277–87. doi: 10.1007/s11154-014-9301-0
2. Grant RW, Dixit VD. Adipose tissue as an immunological organ. *Obesity.* (2015) 23:512–8. doi: 10.1002/oby.21003
3. Nakamura K, Fuster JJ, Walsh K. Adipokines: a link between obesity and cardiovascular disease. *J Cardiol.* (2014) 63:250–9. doi: 10.1016/j.jjcc.2013.11.006
4. Trevellin E, Scorzeto M, Olivieri M, Granzotto M, Valerio A, Tedesco L, et al. Exercise training induces mitochondrial biogenesis and glucose uptake in subcutaneous adipose tissue through eNOS-dependent mechanisms. *Diabetes.* (2014) 63:2800–11. doi: 10.2337/db13-1234
5. Disanzo BL, You T. Effects of exercise training on indicators of adipose tissue angiogenesis and hypoxia in obese rats. *Metabolism.* (2014) 63:452–5. doi: 10.1016/j.metabol.2013.12.004
6. Sakurai T, Ogasawara J, Shirato K, Izawa T, Oh-Ishi S, Ishibashi Y, et al. Exercise training attenuates the dysregulated expression of adipokines and oxidative stress in white adipose tissue. *Oxid Med Cell Longev.* (2017) 2017:9410954. doi: 10.1155/2017/9410954
7. Joyner MJ, Green DJ. Exercise protects the cardiovascular system: effects beyond traditional risk factors. *J Physiol.* (2009) 587:5551–8. doi: 10.1113/jphysiol.2009.179432
8. Kawanishi N, Yano H, Yokogawa Y, Suzuki K. Exercise training inhibits inflammation in adipose tissue via both suppression of macrophage infiltration and acceleration of phenotypic switching from M1 to M2 macrophages in high-fat-diet-induced obese mice. *Exerc Immunol Rev.* (2010) 16:105–18.
9. Stallknecht B, Vinten J, Ploug T, Galbo H. Increased activities of mitochondrial enzymes in white adipose tissue in trained rats. *Am J Physiol.* (1991) 261:E410–4. doi: 10.1152/ajpendo.1991.261.3.E410
10. Aldiss P, Betts J, Sale C, Pope M, Budge H, Symonds ME. Exercise-induced 'browning' of adipose tissues. *Metabolism.* (2018) 81:63–70. doi: 10.1016/j.metabol.2017.11.009
11. Cannon B, Nedergaard J. Brown adipose tissue: function and physiological significance. *Physiol Rev.* (2004) 84:277–359. doi: 10.1152/physrev.00015.2003
12. Wu MV, Bikopoulos G, Hung S, Ceddia RB. Thermogenic capacity is antagonistically regulated in classical brown and white subcutaneous fat depots by high fat diet and endurance training in rats: impact on whole-body energy expenditure. *J Biol Chem.* (2014) 289:34129–40. doi: 10.1074/jbc.M114.591008
13. Larue-Achagiotis C, Rieth N, Goubern M, Laury MC, Louis-Sylvestre J. Exercise-training reduces BAT thermogenesis in rats. *Physiol Behav.* (1995) 57:1013–7.
14. Sepa-Kishi DM, Ceddia RB. Exercise-mediated effects on white and brown adipose tissue plasticity and metabolism. *Exerc Sport Sci Rev.* (2016) 44:37–44. doi: 10.1249/JES.0000000000000068
15. Rao RR, Long JZ, White JP, Svensson KJ, Lou J, Lokurkar I, et al. Meteorin-like is a hormone that regulates immune-adipose interactions to increase beige fat thermogenesis. *Cell.* (2014) 157:1279–91. doi: 10.1016/j.cell.2014.03.065
16. Giralt M, Gavaldà-Navarro A, Villarroya F. Fibroblast growth factor-21, energy balance and obesity. *Mol Cell Endocrinol.* (2015) 418 (Pt 1):66–73. doi: 10.1016/j.mce.2015.09.018
17. Kammoun HL, Febbraio MA. Come on BAIBA light my fire. *Cell Metab.* (2014) 19:1–2. doi: 10.1016/j.cmet.2013.12.007
18. Lehnig AC, Stanford KI. Exercise-induced adaptations to white and brown adipose tissue. *J Exp Biol.* (2018) 221:jeb161570. doi: 10.1242/jeb.161570
19. Gordon CJ. The mouse thermoregulatory system: Its impact on translating biomedical data to humans. *Physiol Behav.* (2017) 179:55–66. doi: 10.1016/j.physbeh.2017.05.026
20. Hylander BL, Repasky EA. Thermoneutrality, mice, and cancer: a heated opinion. *Trends Cancer.* (2016) 2:166–75. doi: 10.1016/j.trecan.2016.03.005
21. Kalinovich AV, de Jong JM, Cannon B, Nedergaard J. UCP1 in adipose tissues: two steps to full browning. *Biochimie.* (2017) 134:127–37. doi: 10.1016/j.biochi.2017.01.007
22. de Jong JMA, Sun W, Pires ND, Frontini A, Balaz M, Jespersen NZ, et al. Human brown adipose tissue is phenocopied by classical brown adipose tissue in physiologically humanized mice. *Nat Metab.* (2019) 1:830–43. doi: 10.1038/s42255-019-0101-4
23. Aldiss P, Lewis JE, Boocock DJ, Miles AK, Bloor I, Ebling FJP, et al. Interscapular and perivascular brown adipose tissue respond differently to a short-term high-fat diet. *Nutrients.* (2019) 11:1065. doi: 10.3390/nu11051065
24. Hawkins P, Golledge HDR. The 9 to 5 Rodent - Time for Change? Scientific and animal welfare implications of circadian and light effects on laboratory mice and rats. *J Neurosci Methods.* (2018) 300:20–5. doi: 10.1016/j.jneumeth.2017.05.014
25. American Physiological Society. *Resource Book for the Design of Animal Exercise Protocols.* (2006). Available online at: https://www.the-aps.org/docs/default-source/science-policy/animalresearch/resource-book-for-the-design-of-animal-exercise-protocols.pdf?sfvrsn=43d9355b_12
26. Galarraga M, Campión J, Muñoz-Barrutia A, Boqué N, Moreno H, Martínez JA, et al. Adiposoft: automated software for the analysis of white adipose tissue cellularity in histological sections. *J Lipid Res.* (2012) 53:2791–6. doi: 10.1194/jlr.D023788
27. Mele L, Paino F, Papaccio F, Regad T, Boocock D, Stiuso P, et al. A new inhibitor of glucose-6-phosphate dehydrogenase blocks pentose phosphate pathway and suppresses malignant proliferation and metastasis *in vivo*. *Cell Death Dis.* (2018) 9:572. doi: 10.1038/s41419-018-0635-5
28. Lambert JP, Ivosev G, Couzens AL, Larsen B, Taipale M, Lin ZY, et al. Mapping differential interactomes by affinity purification coupled with data-independent mass spectrometry acquisition. *Nat Methods.* (2013) 10:1239–45. doi: 10.1038/nmeth.2702
29. Perez-Riverol Y, Csordas A, Bai J, Bernal-Llinares M, Hewapathirana S, Kundu DJ, et al. The PRIDE database and related tools and resources in 2019: improving support for quantification data. *Nucleic Acids Res.* (2019) 47:D442–50. doi: 10.1093/nar/gky1106
30. Kanehisa M. The KEGG database. *Novartis Found Symp.* (2002) 247:91–101; discussion 101–3, 119–28, 244–152.
31. Ashburner M, Ball CA, Blake JA, Botstein D, Butler H, Cherry JM, et al. Gene ontology: tool for the unification of biology. The Gene Ontology Consortium. *Nat Genet.* (2000) 25:25–9. doi: 10.1038/75556
32. Alexa A, Rahnenführer J, Lengauer T. Improved scoring of functional groups from gene expression data by decorrelating GO graph structure. *Bioinformatics.* (2006) 22:1600–7. doi: 10.1093/bioinformatics/btl140
33. Keijer J, Li M,Speakman JR. What is the best housing temperature to translate mouse experiments to humans? *Mol Metab.* (2019) 26:1–3. doi: 10.1016/j.molmet.2019.04.001
34. Fischer AW, Cannon B,Nedergaard J. The answer to the question "What is the best housing temperature to translate mouse experiments to humans?" is: thermoneutrality. *Mol Metab.* (2019) 25:168–76. doi: 10.1016/j.molmet.2019.05.006
35. Lehnig AC, Dewal RS, Baer LA, Kitching KM, Munoz VR, Arts PJ, et al. Exercise training induces depot-specific adaptations to white and brown adipose tissue. *iScience.* (2019) 11:425–39. doi: 10.1016/j.isci.2018.12.033
36. Chang L, Villacorta L, Li R, Hamblin M, Xu W, Dou C, et al. Loss of perivascular adipose tissue on peroxisome proliferator-activated receptor-gamma deletion in smooth muscle cells impairs intravascular thermoregulation and enhances atherosclerosis. *Circulation.* (2012) 126:1067–78. doi: 10.1161/CIRCULATIONAHA.112.104489
37. Timmons JA, Wennmalm K, Larsson O, Walden TB, Lassmann T, Petrovic N, et al. Myogenic gene expression signature establishes that brown and white adipocytes originate from distinct cell lineages. *Proc Natl Acad Sci USA.* (2007) 104:4401–6. doi: 10.1073/pnas.0610615104
38. Seale P, Bjork B, Yang W, Kajimura S, Chin S, Kuang S, et al. PRDM16 controls a brown fat/skeletal muscle switch. *Nature.* (2008) 454:961–7. doi: 10.1038/nature07182
39. Chen Y, Ikeda K, Yoneshiro T, Scaramozza A, Tajima K, Wang Q, et al. Thermal stress induces glycolytic beige fat formation via a myogenic state. *Nature.* (2019) 565:180–5. doi: 10.1038/s41586-018-0801-z
40. Kong X, Yao T, Zhou P, Kazak L, Tenen D, Lyubetskaya A, et al. Brown adipose tissue controls skeletal muscle function via the secretion of myostatin. *Cell Metab.* (2018) 28:631–43 e633. doi: 10.1016/j.cmet.2018.07.004

41. Tharp KM, Kang MS, Timblin GA, Dempersmier J, Dempsey GE, Zushin PH, et al. Actomyosin-mediated tension orchestrates uncoupled respiration in adipose tissues. *Cell Metab*. (2018) 27:602–15 e604. doi: 10.1016/j.cmet.2018.02.005
42. Jensen HH, Brohus M, Nyegaard M, Overgaard MT. Human calmodulin mutations. *Front Mol Neurosci*. (2018) 11:396. doi: 10.3389/fnmol.2018.00396
43. Ikeda K, Kang Q, Yoneshiro T, Camporez JP, Maki H, Homma M, et al. UCP1-independent signaling involving SERCA2b-mediated calcium cycling regulates beige fat thermogenesis and systemic glucose homeostasis. *Nat Med*. (2017) 23:1454–65. doi: 10.1038/nm.4429
44. Scorzeto M, Giacomello M, Toniolo L, Canato M, Blaauw B, Paolini C, et al. Mitochondrial Ca2+-handling in fast skeletal muscle fibers from wild type and calsequestrin-null mice. *PLoS ONE*. (2013) 8:e74919. doi: 10.1371/journal.pone.0074919
45. Fischer-Posovszky P, Wang QA, Asterholm IW, Rutkowski JM, Scherer PE. Targeted deletion of adipocytes by apoptosis leads to adipose tissue recruitment of alternatively activated M2 macrophages. *Endocrinology*. (2011) 152:3074–81. doi: 10.1210/en.2011-1031
46. Alkhouri N, Gornicka A, Berk MP, Thapaliya S, Dixon LJ, Kashyap S, et al. Adipocyte apoptosis, a link between obesity, insulin resistance, and hepatic steatosis. *J Biol Chem*. (2010) 285:3428–38. doi: 10.1074/jbc.M109.074252
47. Elliott K, Ge K, Du W, Prendergast GC. The c-Myc-interacting adaptor protein Bin1 activates a caspase-independent cell death program. *Oncogene*. (2000) 19:4669–84. doi: 10.1038/sj.onc.1203681
48. Han J, Hou W, Goldstein LA, Stolz DB, Watkins SC, Rabinowich H. A Complex between Atg7 and Caspase-9: a novel mechanism of cross-regulation between autophagy and apoptosis. *J Biol Chem*. (2014) 289:6485–97. doi: 10.1074/jbc.M113.536854
49. Singh R, Xiang Y, Wang Y, Baikati K, Cuervo AM, Luu YK, et al. Autophagy regulates adipose mass and differentiation in mice. *J Clin Invest*. (2009) 119:3329–3339, doi: 10.1172/JCI39228
50. Zhang Y, Goldman S, Baerga R, Zhao Y, Komatsu M, Jin S. Adipose-specific deletion of autophagy-related gene 7 (atg7) in mice reveals a role in adipogenesis. *Proc Natl Acad Sci USA*. (2009) 106:19860–5. doi: 10.1073/pnas.0906048106
51. Karim MF, Yoshizawa T, Sato Y, Sawa T, Tomizawa K, Akaike T, et al. Inhibition of H3K18 deacetylation of Sirt7 by Myb-binding protein 1a (Mybbp1a). *Biochem Biophys Res Commun*. (2013) 441:157–63. doi: 10.1016/j.bbrc.2013.10.020
52. Ota A, Kovary KM, Wu OH, Ahrends R, Shen WJ, Costa MJ, et al. Using SRM-MS to quantify nuclear protein abundance differences between adipose tissue depots of insulin-resistant mice. *J Lipid Res*. (2015) 56:1068–78. doi: 10.1194/jlr.D056317
53. Liu LF, Kodama K, Wei K, Tolentino LL, Choi O, Engleman EG, et al. The receptor CD44 is associated with systemic insulin resistance and proinflammatory macrophages in human adipose tissue. *Diabetologia*. (2015) 58:1579–86. doi: 10.1007/s00125-015-3603-y
54. Kang HS, Liao G, DeGraff LM, Gerrish K, Bortner CD, Garantziotis S, et al. CD44 plays a critical role in regulating diet-induced adipose inflammation, hepatic steatosis, and insulin resistance. *PLoS ONE*. (2013) 8:e58417. doi: 10.1371/journal.pone.0058417
55. May FJ, Baer LA, Lehnig AC, So K, Chen EY, Gao F, et al. Lipidomic adaptations in white and brown adipose tissue in response to exercise demonstrate molecular species-specific remodeling. *Cell Rep*. (2017) 18:1558–72. doi: 10.1016/j.celrep.2017.01.038
56. Gogg S, Smith U. Epidermal growth factor and transforming growth factor alpha mimic the effects of insulin in human fat cells and augment downstream signaling in insulin resistance. *J Biol Chem*. (2002) 277:36045–51. doi: 10.1074/jbc.M200575200
57. Will CL, Lührmann R. Spliceosome structure and function. *Cold Spring Harb Perspect Biol*. (2011) 3:a003707. doi: 10.1101/cshperspect.a003707
58. Chen M, Manley JL. Mechanisms of alternative splicing regulation: insights from molecular and genomics approaches. *Nat Rev Mol Cell Biol*. (2009) 10:741–54. doi: 10.1038/nrm2777
59. Figueiredo VC, McCarthy JJ. Regulation of ribosome biogenesis in skeletal muscle hypertrophy. *Physiology*. (2019) 34:30–42. doi: 10.1152/physiol.00034.2018
60. Schiaffino S, Mammucari C. Regulation of skeletal muscle growth by the IGF1-Akt/PKB pathway: insights from genetic models. *Skelet Muscle*. (2011) 1:4. doi: 10.1186/2044-5040-1-4
61. James MJ, Zomerdijk JC. Phosphatidylinositol 3-kinase and mTOR signaling pathways regulate RNA polymerase I transcription in response to IGF-1 and nutrients. *J Biol Chem*. (2004) 279:8911–8. doi: 10.1074/jbc.M307735200
62. Zhou X, Liao WJ, Liao JM, Liao P, Lu H. Ribosomal proteins: functions beyond the ribosome. *J Mol Cell Biol*. (2015) 7:92–104. doi: 10.1093/jmcb/mjv014
63. Ishido M, Kami K, Masuhara M. Localization of MyoD, myogenin and cell cycle regulatory factors in hypertrophying rat skeletal muscles. *Acta Physiol Scand*. (2004) 180:281–9. doi: 10.1046/j.0001-6772.2003.01238.x
64. Johnson SE, Allen RE. Proliferating cell nuclear antigen (PCNA) is expressed in activated rat skeletal muscle satellite cells. *J Cell Physiol*. (1993) 154:39–43. doi: 10.1002/jcp.1041540106
65. Lewis JE, Brameld JM, Hill P, Cocco C, Noli B, Ferri GL, et al. Hypothalamic over-expression of VGF in the Siberian hamster increases energy expenditure and reduces body weight gain. *PLoS ONE*. (2017) 12:e0172724. doi: 10.1371/journal.pone.0172724
66. Raun SH, Henriquez Olguín C, Karavaeva I, Ali M, Møller LLV, Kot W, et al. Housing temperature influences exercise training adaptations in mice. *bioRxiv [Preprint]*. (2019) 651588. doi: 10.1101/651588
67. McKie GL, Medak KD, Knuth CM, Shamshoum H, Townsend LK, Peppler WT, et al. Housing temperature affects the acute and chronic metabolic adaptations to exercise in mice. *J Physiol*. (2019) 597:4581–600. doi: 10.1113/JP278221

Conflict of Interest: The authors declare that the research was conducted in the absence of any commercial or financial relationships that could be construed as a potential conflict of interest.

frontiers in Endocrinology

REVIEW
published: 24 March 2020
doi: 10.3389/fendo.2020.00156

Inflammatory Signaling and Brown Fat Activity

Farah Omran[1] *and Mark Christian*[2]*

[1] Warwick Medical School, University of Warwick, Coventry, United Kingdom, [2] Department of Biosciences, School of Science and Technology, Nottingham Trent University, Nottingham, United Kingdom

Obesity is characterized by a state of chronic inflammation in adipose tissue mediated by the secretion of a range of inflammatory cytokines. In comparison to WAT, relatively little is known about the inflammatory status of brown adipose tissue (BAT) in physiology and pathophysiology. Because BAT and brown/beige adipocytes are specialized in energy expenditure they have protective roles against obesity and associated metabolic diseases. BAT appears to be is less susceptible to developing inflammation than WAT. However, there is increasing evidence that inflammation directly alters the thermogenic activity of brown fat by impairing its capacity for energy expenditure and glucose uptake. The inflammatory microenvironment can be affected by cytokines secreted by immune cells as well as by the brown adipocytes themselves. Therefore, pro-inflammatory signals represent an important component of the thermogenic potential of brown and beige adipocytes and may contribute their dysfunction in obesity.

Keywords: inflammation, brown adipose tissue (BAT), cytokine, beige adipocyte, white adipose tissue

OPEN ACCESS

Edited by:
Rosalia Rodriguez-Rodriguez, Universitat Internacional de Catalunya, Spain

Reviewed by:
Alexander Bartelt, Ludwig Maximilian University of Munich, Germany
Marta Giralt, University of Barcelona, Spain

***Correspondence:**
Mark Christian
mark.christian@ntu.ac.uk

Specialty section:
This article was submitted to Obesity, a section of the journal Frontiers in Endocrinology

Received: *05 February 2020*
Accepted: *06 March 2020*
Published: *24 March 2020*

Citation:
Omran F and Christian M (2020) Inflammatory Signaling and Brown Fat Activity. Front. Endocrinol. 11:156. doi: 10.3389/fendo.2020.00156

INTRODUCTION

Obesity is generally associated with a systemic low-grade inflammation with adipocytes able to produce and release signaling proteins that contribute to this condition (1–4). Many pathologies are associated with this inflamed state, including cancer, heart disease, type 2 diabetes (T2DM), and neurodegenerative diseases. Additionally, inflammation has been shown to impact the function of BAT with thermogenic activity inhibited by TNFα-induced insulin resistance and proinflammatory cytokines secreted from macrophages (5–8).

Adipose tissue (AT) functions as the body's main organ to maintain energy homeostasis (9). Mammals have two main classes of AT; brown AT (BAT) and white (WAT) that act together to maintain a balance between fat accumulation and energy expenditure (10). AT is characterized by the presence of mature lipid-storing adipocytes and pre-adipocytes (11). However, it is heterogeneous in nature and composed of a wide range of additional cell types including macrophages, neutrophils, lymphocytes, endothelial cells, and nerve endings (12–14). With its secretion of over 100 different adipokines, cytokines, and chemokines, AT is the largest endocrine organ and links metabolism and immunity (15). Undesirable changes in adipokine expression including up-regulation of inflammatory markers and down-regulation of adiponectin are linked to obesity (16).

BAT dissipates energy through the process of non-shivering thermogenesis (10). This is facilitated by a large number of mitochondria, which express high levels of UCP1 (uncoupling protein 1) in the inner membrane (10). In brown adipocytes, the nucleus occupies a central position and triglycerides (TGs) are stored in many small multilocular lipid droplets (LDs) (17, 18). This provides a large LD surface accessible to lipases, which facilitates the rapid lipid consumption for

adaptive thermogenesis (18). In contrast, WAT acts as a storage repository with white adipocytes maintaining TG in a single large LD that occupies a central position (16, 19). Its nucleus is located on the periphery and the cell possesses fewer mitochondria than brown adipocytes (16). Adipocytes with brown characteristics located within WAT are known as BRITE (brown-in-white) or beige adipocytes, and are found under conditions such as in response to cold or other stimuli (20–22). Evidence indicates that beige adipocytes are mostly derived from a different cellular lineage to that of classical brown adipocytes and have the capacity to reversibly transition between white and beige adipocytes (23). Due to the widespread prevalence of obesity and its associated diseases, there is considerable research interest in factors that modulate BAT thermogenesis and the beige phenotype to enhance weight loss and reduce morbidity risk. BAT itself has recently being recognized to practice an endocrine role. It can secrete multiple factors which could contribute to the systemic consequences of BAT activity. This also forms an interesting aspect of obesity research as it could lead to the identification of novel brown fat factors to direct drug discovery approaches and ultimately improve metabolic health (24).

The presence of BAT is associated with metabolic health and the amount of BAT is reduced in obesity (25–29). Higher BAT content and activation, such as by BAT transplantation in mice, positively affects glucose and insulin metabolism and body mass and plays a protective role against obesity pathogenesis and associated metabolic disorders such as hyperglycaemia and hyperlipidaemia (30–38). Cold induced thermogenesis, glucose uptake rates and insulin stimulation is severely impaired in BAT in the adiposity state (29, 39–41). Despite the studies showing that reduced BAT in obesity is associated with many negative metabolic consequences, understanding of the underlying mechanisms is limited. Chronic inflammation represents an important mechanism behind the dysfunction of BAT and browning of white adipocytes in obesity.

INFLAMMATORY CELLS IN BROWN ADIPOSE TISSUE

Although mainly composed of brown adipocytes and pre-adipocytes BAT also contains a variety of immune cells such as macrophages, neutrophils and lymphocytes (42–44). Inflammation due to infiltration by macrophages and other immune cells is recognized as a key contributor to WAT pathophysiology in adiposity including insulin resistance and other alterations in metabolism (45, 46). Recent studies have identified infiltrated immune cells in BAT and inflammatory processes as contributors to BAT dysfunction in obesity and associated metabolic disorders. Similar to WAT, it is thought that recruitment of immune cells in BAT is a result of lipolysis and the release of fatty acids from stored TG (47). In diet-induced obese mice, after 6 months, BAT presents an increase in immune responses, including genes that indicate broad infiltration of leukocytes, monocytes, M1-macrophages, and cytokine release (48–51). However, BAT appears to be more resistant to macrophage infiltration than WAT in diet induced obese mice as these cells take longer to appear and have a more limited influence on BAT (50, 51). Also, the expression of inflammatory markers is lower in BAT than WAT regardless of diet (52) providing further support that BAT is generally more resistant to inflammation. Ultimately, inflammatory changes and higher expression of inflammation markers (including TNFα and F4/80) are evident in BAT after a persistent high burden of calorie intake (39, 52–54).

Enhanced inflammation is suggested to play a major role in the whitening of BAT that occurs after prolonged exposure to high fat diet at thermoneutrality. This transformation of brown adipocytes to unilocular cells similar to white adipocytes, is a result of a combination of various factors that include triggering macrophage infiltration, brown adipocyte death, and crown-like structure (CLS) formation. Whitened BAT shows CLS formation surrounding adipocytes that contain enlarged endoplasmic reticulum, cholesterol crystals, some degenerating mitochondria, and become surrounded by an increased number of collagen fibrils. BAT gene expression analysis shows that whitened BAT is associated with a strong inflammatory response and activation of nucleotide-binding oligomerization domain-like receptor-3 inflammasome (NLRP3) (72). In addition, the multimodular adaptor protein p62 is involved in multiple functions including inflammation, and it contributes to regulating energy metabolism via control of mitochondrial function in BAT which is another indicator of the importance of inflammation and immune cells pathways in BAT biology (73).

The enhancement in BAT inflammation is considered to be largely a result of the existence and active participation of infiltrated pro-inflammatory immune cells which are listed and reviewed below:

MACROPHAGES

Macrophages are immune cells that serve an important role in the coordination of inflammatory processes (74). Classically activated macrophages (M1) secrete high levels of pro-inflammatory cytokines including TNF-α, MCP-1, IL-1β, and IL-6, whereas alternatively activated macrophages (M2) produce anti-inflammatory cytokines including IL-4 (2). In subcutaneous fat (scWAT), positive roles are reported for M2 macrophages in adaptive thermogenesis. Adipocyte-derived adiponectin signals to activate M2 macrophage proliferation during chronic cold exposure and the depletion of macrophages or adiponectin leads to resistance to cold-induced browning in scWAT (75). M2 macrophage activation also contributes to the beiging effects of adrenomedullin 2 (ADM2) and subsequent increased UCP1 expression in adipocytes (76). ADM2 can be produced by white adipocytes, and its expression is down-regulated in adipose tissues of obese mice (76). M2 macrophage activation is also stimulated by meteorin-like (Metrnl) supporting the link between adaptive thermogenic responses and anti-inflammatory gene programs in fat (77).

In the lean state BAT resident macrophages which are mostly the M2 subtype (78, 79). In obesity, however, BAT

is infiltrated with (M1) macrophages which are suggested to play a crucial role in controlling adaptive thermogenesis. Inflammation of BAT caused by infiltrated macrophages reduces thermogenesis and UCP1 activation (39, 43). However, how macrophages affect thermogenesis and BAT biology is controversial (78). Initially, cold-induced thermogenesis was thought to be dependent on the secretion of the cytokines IL-4 and IL-13 by innate lymphoid cells and eosinophils that signal to macrophages as deletion of these cytokines receptors was found to diminish UCP1 expression and heat generation (77, 80). It was also suggested that M2 macrophages participate in this mechanism by secreting catecholamines (77, 80–82). However, this concept was recently challenged (83). It was found that adipose resident macrophages do not express tyrosine hydroxylase (the rate limiting enzyme for the catecholamine synthesis) and chronic treatment of wild type, UCP1$^{-/-}$, and IL-4 receptor knockout mice with IL-4 failed to increase energy expenditure. In addition, incubation of adipocytes with conditioned medium from IL-4 stimulated macrophages did not induce UCP1 protein expression (83). These data indicate that any role of macrophages in brown fat activation is not through IL-4 stimulated secretion of catecholamines. However, a role of macrophages should not be completely ruled out in thermogenesis.

The main pathway for thermogenesis activation in BAT is via the sympathetic nervous system. It has recently been demonstrated that macrophages play a role in the control of BAT innervation; as selective depletion of the nuclear transcription factor Mecp2 (methyl-CpG- binding protein 2) in macrophages, a murine model of Rett syndrome, leads to spontaneous obesity with compromised homeostatic energy expenditure and thermogenesis of BAT. Specifically, deficiency of Mecp2 in BAT-macrophages causes a reduction of UCP1 gene expression levels that appears to result from impaired sympathetic innervation (43). Moreover, adipose tissue resident macrophages are reported to express a set of genes, or have a subpopulation attached to sympathetic neurons, which regulate norepinephrine levels by controlling its degradation which influences adipose tissue thermogenesis (84, 85).

MAST CELLS

Mast cells are immunological classic mediators of allergic reactions and the main secretors of histamine (86). They are present in both WAT and BAT and their number increases in obesity (87, 88). Similar to some macrophages, they are closely associated with the vasculature (88). Brown adipocytes have high levels of histamine contained in mast cells and it is reported to play a role in thermogenesis through the H2-receptor. This action appears to be independent of any effect on noradrenaline stimulated oxygen consumption in isolated brown adipocytes (89). In response to colder temperatures, mast cells secrete histamine, IL-4 and other factors that promote UCP1 expression and the beiging response of WAT (90). Furthermore, it is proposed that acute cold exposure recruits mast cells to the WAT of lean subjects and enhances their degranulation and histamine secretion in both lean and obese subjects. As degranulation positively correlates with UCP1 suggests thermogenesis and beiging enhancement through histamine and secretion of other factors (91). However, these positive associations between mast cells and thermogenesis/beiging of WAT has been challenged. Zhang et al. reported that mast cell deficiency or pharmacological inhibition in mice increases browning of WAT by increasing beige adipocyte differentiation. It has also been demonstrated that mast cell-derived serotonin inhibits WAT browning and systemic energy expenditure (92). The mouse model used for this study has a mutation in c-kit tyrosine kinase and a degree of caution in the interpretation of the outcomes is required. Several alternative (c-kit-independent) genetic models of mast cell depletion have found that there is essentially no effect of mast cells in obesity and related pathologies. That is because diet-induced obese mice with either deficiency or proficiency of mast cells exhibits similar profiles of weight gain, glucose tolerance, insulin sensitivity, metabolic parameters, and AT or liver inflammation (93, 94). Further research is needed to fully understand the role of mast cells in brown and beige adipocytes especially in humans.

T LYMPHOCYTES: T_{REG} AND ILC2S CELLS

T_{reg} cells are a small subset of T lymphocytes and are considered to be one of the most crucial defense mechanisms in maintaining appropriate immune responses including roles in autoimmunity and inflammation (95). T_{reg} cells appear to be reduced in obesity and also required to maintain a normal adaptive thermogenesis response to cold (96, 97). Depletion of this type of immune cell impairs BAT function which was demonstrated by decreased oxygen consumption and prevention of the activation of thermogenic genes coincident with enhanced inflammation and the invasion of proinflammatory macrophages (96).

ILC2s (IL-33/Group 2 innate lymphoid cells) are a subtype of innate lymphoid cells. ILC2s are activated by epithelial cell-derived cytokines IL-33 and IL-25 as well as thymid stromal lympoiphoidin (TSLP) in response to allergens. In WAT, it has been found that white adipocytes themselves (98) and endothelial cells (99) can express IL-33. ILC2s control eosinophil and pro inflammatory macrophages to initiate type 2 immune responses that prevent helminth infection or promote pathologic allergic inflammation (100). They are found in WAT and their number is decreased in obese mice and humans (101). These cells essentially release IL-5 which maintains macrophage responses and IL-13 which controls eosinophil responses. Both of these cytokines appear to play an indirect role as mediators of beiging of WAT (100). In addition, ILC2s produce an opioid-like peptide, methionine-enkephalin (MetEnk) peptide, which appears to directly upregulate UCP1 in WAT and induces the beiging process (101). The cytokine IL-33 limits the development of spontaneous obesity by increasing numbers of ILC2s and eosinophils. This coincides with beiging and energy expenditure in the WAT of mice by but not BAT. Deletion of IL-33 leads to opposite effects (100, 102, 103).

IMPACT OF INFLAMMATION AND INFLAMMATORY MEDIATORS ON BROWN ADIPOCYTE FUNCTION

Obesity mediated upregulation of inflammatory cytokines has been extensively studied in WAT, while relatively little is known about the cytokines involved in the adiposity inflammatory state in BAT and how it affects BAT function and thermogenesis. However, there is an increasing amount of evidence that inflammation directly alters the thermogenic activity of brown fat by impairing its energy expenditure mechanism and glucose uptake. Pro-inflammatory cytokines can affect thermogenesis in BAT (104–106) and also determine the capacity of WAT browning (106, 107). It has been clearly demonstrated that infiltrated macrophages and other immune cells in subcutaneous WAT negatively impact the ability of precursor cells to differentiate into thermogenically active beige adipocytes because of pro-inflammatory cytokine secretion and generating an inflammatory microenvironment (108).

In BAT, the increased expression of inflammatory markers such as TNFα and MCP-1 in obese murine models is accompanied by a decrease in the expression of UCP1 and other markers of thermogenesis as well as lack of fatty acids which are needed as substrate for thermogenesis (49, 109). Also, it is reported that IL-1b reduces the cAMP-mediated induction of UCP1 expression (104), cold-induced thermogenesis in adipocytes *in vivo* via sirtuin-1 inhibition (SIRT1) (110) and WAT browning (111). Furthermore, Fractalkine, which is an adipocyte-synthesized chemokine, appears to contribute to enhancement of the pro-inflammatory status of BAT and reduced thermogenic gene expression in diet-induced obese mice (59). In contrast, IL-13, which has anti-inflammatory properties, induces GDF15 (growth differentiation factor 15) expression which is found to protect against obesity by inducing thermogenesis, lipolysis, and oxidative metabolism in mice (112, 113), and prevent inflammation through inhibition of M1 macrophage activation (71).

Oncostatin M, a macrophage proinflammatory cytokine impairs BAT thermogenesis and browning capacity of subcutaneous WAT *in vivo*. Furthermore, it inhibits brown adipocyte differentiation *in vitro* (114, 115). The pro-inflammatory phenotype induced by Oncostatin M is indicated as a mechanism of downregulating UCP1 expression. The significance of inflammation-driven inhibition of beige adipogenesis in obesity has been highlighted by studies of the interaction between α4-integrin receptor on pro-inflammatory macrophages and VCAM-1 (vascular cell adhesion molecule-1) on adipocytes. This interaction resulted in reduced UCP1 gene expression via the ERK (extracellular signal-regulated kinase) pathway and blockage of α4 integrin led to elevated beige adipogenesis and prevented metabolic dysregulation of the obese AT (113). This mechanism establishes a self-sustained cycle of inflammation driven impairment of the beige phenotype in obesity.

Another inflammatory candidate that might affect BAT biology and thermogenesis is the macrophage secreted factor GDF3 (growth differentiation factor-3) which increases in obesity. It is suggested that GDF3 is responsible for inhibition of β3-adrenoceptors which can lead to reduced lipolysis and consequently the impaired release of fuel for thermogenesis (84). However, although thermogenic gene expression was not restored after deleting activin-like kinase-7 (Alk7) which is the GDF3 receptor (84, 116, 117), deleting Alk7 led to reduced obesity. The metabolic benefit of Alk7 deletion may be attributed to enhanced mitochondrial biogenesis and increased levels of fatty acid oxidation found in this mouse model (116) as browning did not occur.

BAT can respond to immune and inflammatory pathways by the expression of cytokine receptors, Toll like receptors (TLRs), and nucleotide-oligomerization domain-containing proteins (NODs). Activation of these receptors by immune and metabolic signals mediates a negative impact of proinflammatory signaling on BAT thermogenesis (53). In this respect, both LPS and TNFα are found to impair UCP1 in BAT in mice *in vivo* and *in vitro* studies (110, 118). In addition, TLR4 activation inhibits β3-adrenergic-induced browning of WAT, whereas TLR4-deletion maintains thermogenic capacity (111). Some inflammatory inducers can lead to greater disruption of WAT browning compared to affecting thermogenesis in BAT. This may be indicative of a greater inflammatory response of WAT compared BAT. For example, depletion of the intestinal microbiota leads to greatly enhanced WAT browning while having only a minor effect on typical BAT (119). Also, LBP (LPS-binding protein) depletion similarly enhances WAT browning (120). This might be explained by a higher basal level of inflammation in subcutaneous WAT compared to BAT (51, 106, 107).

On the molecular level, IKKε (IκB kinase ε) and IRF3 (interferon regulatory factor-3) are among the main inflammation regulators in obesity (121, 122). Deletion of IKKε or IRF3 results in a reduction of inflammatory markers in adipose tissues and enhanced WAT browning with UCP1 expression and energy expenditure increased, while there are only minor effects on BAT (122, 123). The Nod-like receptor 3 (NLRP3) inflammasome multiprotein complex regulates inflammation and macrophage activity by cleaving IL-1b and IL-18 precursors into their active forms. Activation of NLRP3 in macrophages attenuates UCP1 and adaptive thermogenesis induction of white adipocytes and mitochondrial respiration, while NLRP3 deletion prevents UCP1 reduction. The action is through IL-1 as blocking the IL-1 receptor in adipocytes protected thermogenesis activity (111). IEX-1, an immediate early gene, is highly expressed in macrophages in obesity and is responsible for the majority of the obesity associated inflammation in humans and mice and its deletion had profound effects on the browning of WAT. Knockout of IEX-1 prevents HFD-induced inflammation, insulin resistance, and obesity by elevated browning and increasing thermogenic gene expression in WAT. This results from the promotion of M2 macrophages in WAT, but not BAT (124): and further highlights the different immune responses of white and brown adipose tissues.

There is a link between inflammatory stress pathways and the accompanied activation of endoplasmic reticulum (ER) in conditions of disruption of systemic metabolic homeostasis like obesity (125, 126). Brown adipocytes have a relatively small ER content and restricted ER surface area compared to other cell types. Thus, ER adaptation in these cells may require alternative pathways to conventional mechanisms such as chaperone-mediated protein folding and ER expansion (127, 128). In fact, some of the canonical ubiquitin-proteasome system molecules, for example X-box binding protein 1, appear to be dispensable in adipocytes (129). To maintain ER homeostasis and cellular integrity increased proteasomal activity in brown adipocytes is reported to be essential for thermogenic adaptation. This occurs via induction of the induction of the ER-localized transcription factor nuclear factor erythroid-2, like-1 (Nfe2l1, also known as Nrf1) (130). Deletion of Nfe2l1, specifically in brown adipocytes, results in ER stress, inflammation, mitochondrial dysfunction, insulin resistance, and whitening of the BAT (130, 131).

In addition to the direct effects that proinflammatory cytokines may have on brown adipocytes, some of these factors may inhibit activation of adrenergic receptors, stimulation of sympathetic nervous activity and thus local secretion of noradrenaline. As this is the main mechanism of inducing BAT thermogenesis activity and WAT browning, in response to cold and diet, it should be considered when evaluating effects on browning.

BROWN ADIPOCYTES SECRETE PRO/ANTI-INFLAMMATORY MEDIATORS

In addition to the cytokine mediators secreted by infiltrated immune cells, such cytokines may also be secreted by brown adipocytes themselves. **Table 1** summarizes what has been studied in BAT.

Chemerin is an adipokine associated with inflammation markers (e.g., IL-6, TNFα, Leptin) and components of the metabolic syndrome in WAT. It modulates chemotaxis and activation of dendritic cells and macrophages (132–134). Chemerin was found to be secreted by brown adipocytes. Its gene expression levels are increased in obesity and decreased with cold induced thermogenesis and could potentially play a key role as an inflammatory modulator in BAT. However, the lack of correlation between expression levels in BAT and circulating levels make it unclear whether it plays an endocrine role in attracting immune cells (55). At present, it remains to be determined how Chemerin expression is controlled and what is its function in BAT.

Endothelin-1 (ET-1) has pro-inflammatory effects by activating macrophages, resulting in the secretion of pro-inflammatory and chemotactic mediators including TNFα, IL-1, IL-6, and IL-8 (135, 136). ET-1 levels were found to be increased in obesity and enhance lipolysis thereby linking it to insulin resistance in WAT (137). ET-1 is released by brown adipocytes and its secretion is inhibited during adrenergic stimulation (56). Data implicates that it can inhibit thermogenesis via induction of Gq signaling. However, the contribution of ET-1 to inflammation of BAT and the mechanism of thermogenesis repression remains to be fully investigated.

Vascular endothelial growth factor A (VEGFA) is a proangiogenic cytokine. The reported findings concerning VEGFA levels in WAT in obesity are controversial. Deletion of VEGFA in WAT leads to little or no change in the expression of inflammatory markers that contribute to systemic insulin resistance, such as EGF-like module-containing mucin-like hormone receptor-like 1 (Emr1), TNF-α, and MCP-1. Nor were there detectable changes in the expression of mitochondrial genes in WAT (138, 139). In contrast, in BAT VEGFA can induce thermogenic activity and deletion of VEGFA results in reduction of BAT mass, vessel density, and eventually loss of thermogenesis through mitochondrial dysfunction (68, 138). Hence, ablation of VEGFA results in the whitening of BAT. However, the direct effect of VEGFA on inflammatory markers in brown adipocytes is currently unknown.

Retinol-Binding Protein 4 (RBP4) is an adipokine and circulating transporter of vitamin A (retinol) that induces inflammation and promotes the secretion of proinflammatory molecules (140). There has been some controversy regarding the associations and/or causality in the context of obesity and metabolic syndrome. However, in adipocytes, RBP4 appears to have a relevant role in obesity and the development of insulin resistance and diabetes (141). Brown adipocytes release RBP4 when exposed to a thermogenic, noradrenergic activation, but the mechanism associated with this release is unclear. Lipocalin 2 (Lcn2) has been implicated in the release of RBP4 as Lnc2 KO adipose tissue shows increased RBP4 levels while circulating levels are reduced (142). Also, BAT released RBP4 may not be associated with insulin resistance given that cold-induced activation of BAT is associated with insulin sensitization (57).

Fibroblast growth factor 21 (FGF21) is a brown adipokine and a key factor in the regulation of energy homeostasis. In WAT, it induces browning and participates in improving glucose metabolism and weight regulation. Cold induced thermogenesis and adrenergic activation induces FGF21 release from brown adipocytes. In addition to this mechanism, WAT-resident anti-inflammatory invariant natural killer T (iNKT) cells promote the release of FGF-21 by adipocytes and the browning process (143–145). Prevention of hyperglycaemia and hyperlipidaemia is associated with high levels of FGF21 in line with high BAT activity and enhanced energy expenditure (146, 147). Although FGF21 is reported to have anti-inflammatory effects on white adipocytes (148) it remains to be determined if it has a similar action in brown adipocytes.

CXCL14 is a member of the CXC chemokine family and exerts chemoattractive activity for activated macrophages, immature dendritic cells and natural killer cells. In WAT, CXCL14 participates in glucose metabolism (149, 150). It is reported to be secreted by brown adipocytes in response to thermogenic activation. CXCL14 appears to attract M2 macrophages and its deletion leads to impaired BAT thermogenesis activity and low recruitment of macrophages into BAT. CXCL14 enhances the browning of white fat via type 2 cytokine signaling (67).

Fractalkine (CX3CL1) is a chemokine produced by brown adipocytes that plays a role in the recruitment of leukocytes

TABLE 1 | Summary of brown adipocyte secreted inflammatory mediators.

Inflammatory mediator	Role in brown/beige adipocytes	Inflammation		Cold-regulated	References
		Pro-	Anti-		
Chemerin	↑ Chemerin expression in brown adipocytes in obesity ↑ Chemerin gene expression in brown adipocytes through differentiation Chemerin predicted to increase triglyceride accumulation	✓		↓	(55)
Endothelin 1 (ET-1)	ET-1 inhibits adipogenesis Adrenergic activation inhibits ET-1 secretion	✓ (?)		↓	(56)
Retinol-Binding Protein 4 (RBP4)	↑ RBP4 expression in BAT with thermogenic, noradrenergic activation	✓ (?)		↑	(57)
Growth differentiation factor (GDF8/myostatin)	Myostatin leads to ↓ thermogenesis and browning and ↓ metabolic activity in BAT	✓		(?)	(58)
Classic pro-inflammatory cytokines such as MCP1, TNFα, IL-1.	The increase in these cytokines is accompanied with ↓ thermogenesis genes and ↓ mitochondrial respiration in BAT	✓		↓	(53)
Fractalkine (CX3CL1)	Enhanced CX3CL1 secretion leads to ↑ pro-inflammatory status and ↓ thermogenesis gene expression in BAT	✓		(?)	(59)
Insulin-Like Growth Factor-1 (IGF-1)	IGF-1 leads to ↑ proliferation and differentiation of preadipocytes	✓	✓	↑	(60, 61)
IL-6	↑ IL-6 expression in BAT with adrenergic stimulus	✓	✓	↑	(62)
Fibroblast growth factor 21 (FGF21)	FGF21 leads to ↑ thermogenesis		✓	↑	(63, 64)
Follistatin (Fst)	Fst leads to ↑ thermogenesis and browning Fst leads to ↑ adipocyte differentiation		✓	↑	(65)
C-terminal fragment of SLIT2 protein (SLIT2-C)	SLIT2-C leads to ↑ browning		✓	↑ (acute) - (Chronic)	(66)
C-X-C motif chemokine ligand-14 (CXCL14)	CXCL14 leads to ↑ browning and ↑ (M2) macrophages in BAT		✓	↑	(67)
Vascular endothelial growth factor A (VEGFA)	VEGFA leads to ↑ thermogenesis and browning		✓	↑	(68, 69)
Lipocalin prostaglandin D synthase (L-PGDS)	L-PGDS leads to ↑ basal metabolic rates and ↑ lipid utilization in BAT		✓	↑	(70)
Growth and differentiation factor 15 (GDF15)	↑ GDF15 gene expression and release with noradrenergic, cAMP-mediated thermogenic activation of brown adipocytes Inhibits local inflammatory pathways originated from macrophages		✓	↑	(71)

through the fractalkine receptor. Its action seems to be to promote an inflammatory state as deficiency of the fractalkine receptor prevents BAT accumulation of macrophages and leads to reduced expression of pro inflammatory genes (Tnfα, Il1α, and Ccl2) in mice exposed to HFD. Furthermore, the BAT of fractalkine receptor deficient mice shows increased expression of lipolytic enzymes such as adipose triglyceride lipase (Atgl), lipase, hormone-sensitive (Hsl) and monoglyceride lipase (Mgtl) and upregulation of UCP1 and other thermogenesis genes (59). This indicates that fractalkine serves a key role in the local inflammation of BAT tissue and the remodeling on HFD affecting metabolism.

Follistatin (FST) is a soluble glycoprotein that has the capacity to modulate the activities of multiple members of the transforming growth factor (TGF) family, specifically activin A and myostatin (GDF8). TGF-β superfamily cytokines play pivotal roles in regulation of tissue functions including inflammation (151–153). Blockade of TGF-β/Smad3 signaling enhances insulin sensitivity and prevents diet-induced obesity, promotes the browning of WAT with reduced levels of inflammatory cytokines

and less inflammatory macrophage infiltration (154–156). FST is upregulated in BAT in response to cold, and is potentially a positive regulator of BAT function by blocking TGF-β signaling pathways, GDF8 actions, and exerting anti-inflammatory effects (65, 157, 158). However, these actions are yet to be explored.

Myostatin (GDF8) is a key member of the transforming growth factor-β (TGF-β) super family and has an essential role in the regulation of overall fat content in mice. Loss of GDF8 leads to a significant increase in lean mass, total energy expenditure, protection against diet-induced obesity, and insulin resistance. GDF8 levels increase in obesity and it is reported to suppresses Irisin leading to activation of inflammatory cytokines and insulin resistance in WAT. GDF8 secretion from brown adipocytes is stimulated by activation of hunger-related neural circuits. It negatively regulates BAT thermogenesis as well as WAT browning, and metabolic activity. Data clearly indicates that GDF8 inhibits brown fat gene expression (157), however, further research is needed to investigate its inflammatory related effects in this tissue (58, 156, 157, 159–161).

Growth and differentiation factor 15 (GDF15) is also known as macrophage inhibiting cytokine-1 and is a member of the TGF-β superfamily (162). GDF15 is suggested to be a reliable predictor of disease progression in certain tumors, inflammatory diseases, cardiovascular disease, and obesity (162). It is reported to decrease food intake, body weight and adiposity, and to improve glucose tolerance under normal and obesogenic diets (163). Furthermore, systemic overexpression of GDF15 was shown to prevent obesity and insulin resistance by increasing the expression of the main thermogenic and lipolytic genes and oxidative metabolism in BAT and WAT (164). It is identified as one of the factors secreted by brown adipocytes through protein kinase A-mediated mechanisms, and highly induced in response to thermogenic activity following stimulus by cold, norepinephrine, and cAMP. GDF15 acts on macrophages in BAT and may mediate inhibition of local inflammatory pathways under conditions of enhanced BAT activity (71).

C-terminal fragment of SLIT2 protein (SLIT2-C) belongs to the Slit family of secreted proteins that play important roles in various physiologic and pathologic activities including inflammatory cell chemotaxis where it exercises an anti-inflammatory role (66, 165). SLIT2-C expression is regulated by PRDM16 and is secreted from beige/brown adipocytes. It induces thermogenesis, WAT browning, and metabolic processes associated with substrate supply to fuel thermogenesis. The pathway for the induction of thermogenesis is independent of β-adrenergic activation, but requires activation of protein kinase A signaling (66). The protease that generates the SLIT2-C fragment as well as the receptor in BAT that binds it are important areas for future investigation.

Lipocalin prostaglandin D synthase (L-PGDS) is expressed in BAT where it has a key role in energy substrate utilization. It is also localized in the central nervous system and it is involved in inflammatory modulations amongst other functions (166). Deletion of L-PGDS leads to inadequate thermogenesis in BAT because of impairment in switching of substrate utilization from glucose to lipids (70, 167). In addition, L-PGDS deficiency induces obesity possibly through the regulation of inflammatory responses (168). However, if that is the case in brown adipocytes, it is yet to be elucidated.

Insulin-Like Growth Factor-1 (IGF-1) appears to play pleiotropic functions and provides signals to macrophages to sustain adipose tissue development and homeostasis. IGF1 signaling integrates immune-metabolic interactions to facilitate macrophage activation status. Cold exposure stimulates elevation of IGF-1 expression in the BAT of rats (169). However, Myeloid-specific ablation of IGF-1 receptor worsens diet induced obesity but not cold induced thermogenesis (170, 171). It is suggested that IGF-1 is released by brown adipocytes and involved in proliferation and differentiation of brown preadipocytes (60, 61, 172). IGF-1 upregulation due to BAT transplantation is proposed to abolish type I diabetes in this experimental model and negatively correlates with glucose, glucagon, and inflammatory cytokines in rodents (31, 173). However, the detailed role of IGF-1 in brown adipocytes inflammation regulation remains an area to be investigated.

Interleukin 6 (IL-6) is secreted by brown adipocytes upon β-adrenergic activation (62). Chronic elevation of IL-6 in the CNS leads to increased UCP1 in BAT, but not in denervated BAT tissue which suggest a central role in IL-6-dependent promotion of thermogenesis (174). Signaling by IL-6 promotes M2 macrophage polarization in BAT (175). Evidence indicates that IL-6 is released from WAT during the differentiation of human beige adipocytes to facilitate the commitment of adipocyte precursors toward beigeing and enhancement of thermogenesis capacity in an autocrine manner (176). The deletion of IL-6 in mice leads to inefficient BAT transplantation with sustained obesity and insulin resistance, and blunted FGF21 increase (33). These data suggest beneficial effects of IL-6 in regulation of BAT metabolism possibly directly or indirectly related to FGF21 actions. However, this contrasts with the action of IL-6 as a potent pro-inflammatory cytokine. This aspect can be demonstrated by plasma IL-6 being elevated in obesity and diabetes, in addition to reduced levels in weight loss (177–179). Furthermore, it is also found to play a major role as a pro-inflammatory cytokine in obese adipose tissue, macrophage polarization, and T cell regulation via STAT3, leading eventually to insulin resistance and worsening diet-induced obesity (180). Moreover, as expected for IL-6 having a typical role as a pro-inflammatory cytokine, its deletion causes reversal of pro-inflammatory signaling in the obese state (179). In terms of browning activation, IL-6 is implicated in inducing inguinal WAT atrophy by accelerating WAT lipolysis and browning (181). In any case, these available contradictory data concerning the role of IL-6 are indicative of both pro- and anti-inflammatory actions. A schematic showing the actions of inflammatory mediators on brown and white adipocytes is presented in **Figure 1**.

INSULIN SENSITIVITY

Pro-inflammatory signaling can disrupt the insulin signaling cascade and impair the insulin sensitivity of BAT. Although, IL-1, TNF-α, MIF, and IL-6 have consistently been shown to

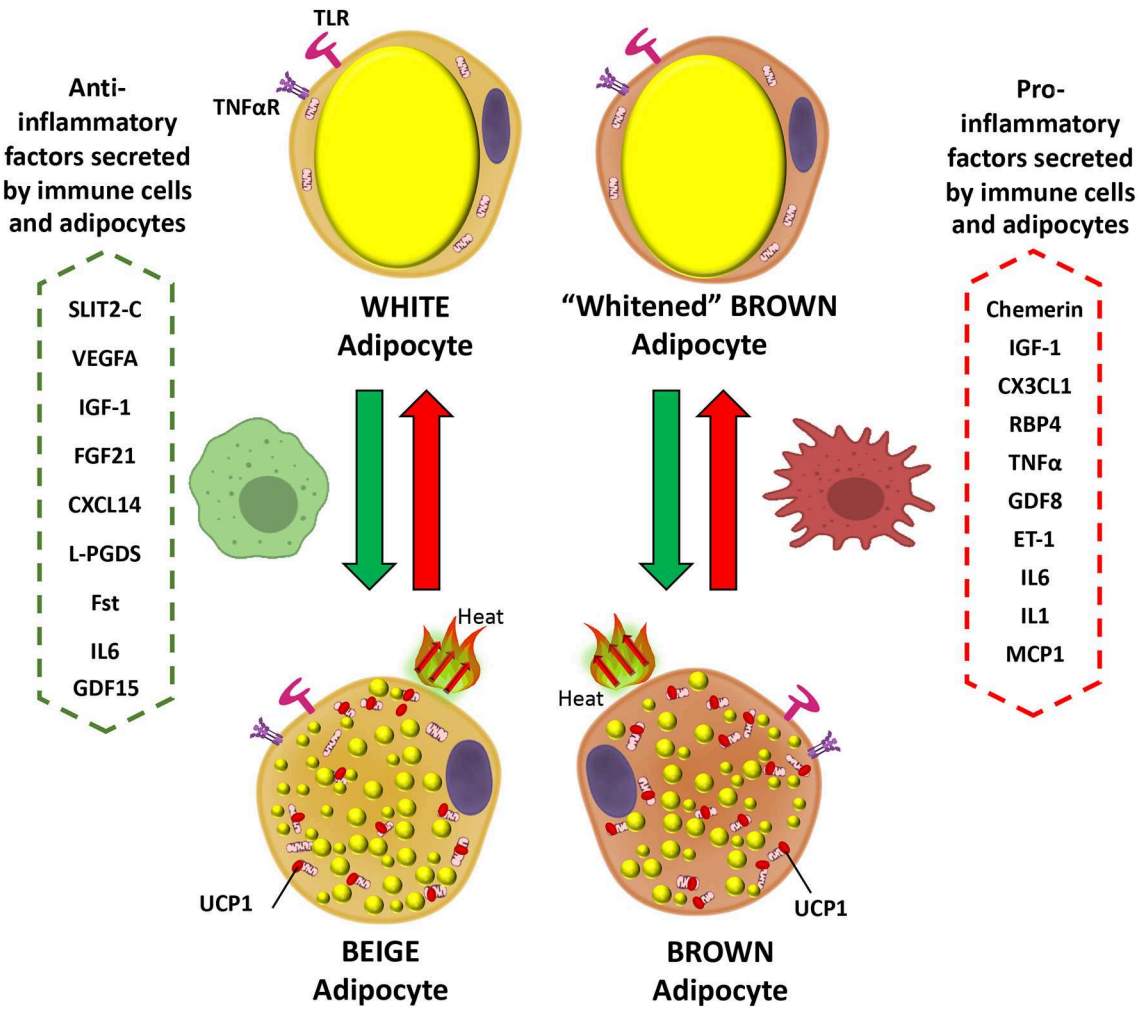

FIGURE 1 | Inflammatory mediator actions on white and brown adipocytes. Pro-inflammatory factors secreted by immune cells and brown/beige adipocytes prevent the expression of brown fat genes in adipocytes, including UCP1, the main thermogenic protein (red arrows). In contrast anti-inflammatory mediators promote the transition of white to beige adipocytes and could prevent expression of the "whitened" brown adipocyte phenotype in brown adipose tissue (green arrows). IGF-1, Insulin-Like Growth Factor-1; CX3CL1, Fractaline; RBP4, Retinol-Binding Protein 4; TNFα, Tumor necrosis factor a; GDF8, Growth differentiation factor 8; ET-1, Endothelin 1; IL6, Interleukin 6; IL1, Interleukin 1; MCP1, Monocyte Chemoattractant Protein-1; SLIT2-C, C-terminal fragment of SLIT2 protein; VEGFA, Vascular endothelial growth factor A; FGF21, Fibroblast growth factor 21; CXCL14, C-X-C motif chemokine ligand-14; L-PGDS, Lipocalin prostaglandin D synthase; Fst, Follistatin; UCP1, Uncoupling Protein 1; GDF15, Growth and differentiation factor 15.

cause insulin resistance in WAT (182, 183), their effects have not been extensively explored in BAT at the molecular level. Elevated inflammatory marker levels in the diet induced obesity state in mice are suggested to be responsible for BAT insulin resistance via AKT (protein kinase B) and ERK pathways (52). TNF-α appears to play an important role in impairing insulin sensitivity of BAT. The mechanism has been discussed in detail and it involves disturbances of both MAP- kinases activation and IRS-2 and AKT (5–7). Mammalian target of rapamycin complex 2 (mTORC2), which activates inflammation, sustains thermogenesis via Akt-induced glucose uptake and glycolysis in BAT. This highlights the significance of glucose metabolism in BAT in thermogenesis and indicates the importance of identifying how inflammation can affect mTORC2-activation in BAT (184, 185). Alleviating the inflammation state in obesity may restore insulin sensitivity as targeting inflammation in diet induced obesity in mice leads to a decrease in adipocyte area, macrophage infiltration, proinflammatory gene expression, along with JNK and NF-κB activation and increased insulin sensitivity via increased AKT phosphorylation (186, 187). In this context, sucrose non-fermenting related kinase (SNRK), a member of the AMPK-related kinase family, is found to suppress inflammation in WAT and is essential for maintaining UCP1 expression for BAT thermogenesis. Dysregulation of this anti-inflammatory kinase leads to induction of insulin resistance in BAT via impairment of the PP2A-Akt pathway (188, 189). As a result, inflammation is a modulator of insulin responses in BAT and is strongly linked to UCP1 expression and thermogenesis. It

is important to determine the role of each inflammatory cytokine in insulin resistance and thermogenesis in order to identify therapeutic targets.

MITOCHONDRIAL FUNCTION IS AFFECTED BY INFLAMMATORY PATHWAYS

Inflammation and mitochondrial dysfunction are closely linked with obesity and associated with alteration in mitochondrial function and mass (190, 191). These alterations are further demonstrated by downregulation of mitochondrial biogenesis, oxidative metabolic pathways, and oxidative phosphorylation proteins in WAT in obesity, and a negative correlation with pro-inflammatory cytokines (192). Evidence indicates that proinflammatory cytokines have a significant influence on modulating mitochondrial efficiency leading to effects on energy homeostasis in human white adipocytes. TNF-α most dramatically alters 3T3-L1 adipocyte mitochondrial functions, whereas IL-1β and IL-6 have more modest effects. Moreover, activation of the NLRP3 inflammasome in macrophages attenuates UCP1 induction and mitochondrial respiration in cultures of primary adipocytes possibly via IL-1, while the absence of NLRP3 is protective for UCP1 and adaptive thermogenesis capacity in adipocytes (111, 193, 194).

The activation of pattern recognition receptors in brown adipocytes and subsequent increased inflammation leads to mitochondrial dysfunction and suppression of mitochondrial respiration with reduced UCP1 expression levels and repressed white adipocyte browning capacity in response to adrenergic stimulation. Mechanistically, these effects are likely to involve inhibition of SIRT1 activity (53, 110, 111). Moreover, deletion of TLR4 protected mitochondrial function and thermogenesis in WAT (111). However, there is a suggestion that mitochondrial dysfunction in adipocytes is a primary cause of adipose tissue inflammation, adipocyte enlargement and insulin resistance. According to this hypothesis mitochondrial dysfunction and fatty acid oxidation in adipocytes leads to adipocyte enlargement because of triglyceride accumulation. Furthermore, adipocyte mitochondrial dysfunction leads to pseudo-hypoxia with greater accumulation of hypoxia-inducible factor 1α (HIF-1α), which elevates adipose tissue inflammation and fibrosis (195, 196). Similarly, alteration of mitochondrial capacity in BAT might be functionally associated with defective thermogenesis and energy expenditure in obesity and increased risk to develop obesity-induced insulin resistance.

Using a mouse model of chronic systemic inflammation, which exhibits increased circulating levels of inflammatory cytokines and abnormal regulation of both innate and adaptive immune responses, mitochondrial swelling is detected with severe damage of the cristae, in addition to reduced cold-induced thermogenic capacity and UCP1-dependent mitochondrial respiration (197). Furthermore, low grade inflammation in BAT in obesity is found as a contributor to excess reactive oxygen species (ROS) production and associated oxidative stress, which may cause mitochondrial dysfunction (198–202). Further investigations in BAT confirmed increased inflammation and ROS generation, but this was accompanied by the doubling of mitochondria respiration compared to lean subjects. It is possible that if the obesogenic conditions were maintained for longer, mitochondria would have eventually failed to deal with obesity stress and thermogenic capacity would be ultimately compromised (49). ROS production does not necessarily have negative consequences in BAT. Consistent with beneficial effects of increased ROS, activated BAT thermogenesis *in vivo* is defined by a substantial increase in mitochondrial ROS levels and pharmacological depletion of mitochondrial ROS leads to hypothermia upon cold exposure, and inhibits UCP1-dependent increases in whole body energy expenditure (203).

Mitochondrial dysfunction resulting from deletion of the mitochondrial transcription factor A (TFAM) leads to adipocyte death coincident with inflammation in WAT and a whitening of BAT with decreased energy expenditure. BAT whitening in these mice is mainly explained by impairment of mitochondrial electron transport chain function, reduced fatty acid oxidation, and increased circulating fatty acids, rather than a conversion of brown to white adipocytes (204). These findings highlight the link between mitochondrial function and inflammation and point to mitochondria dysfunction leading to increased inflammation which could ultimately lead to a vicious cycle.

ANTI-INFLAMMATORY PATHWAYS AND BAT FUNCTION

Strategies that target the inflammatory status may have the potential to reverse adipose tissue dysfunction and prevent progression of metabolic diseases. Suppression of inflammation using pharmacological agents, with reduction of pro-inflammatory cytokines and macrophage infiltration in WAT, improves AKT-phosphorylation in response to insulin along with improved body weight and fat mass (187, 205–207). Cytarabine, which has immunosuppressive actions, is associated with enhanced BAT activity via the AMPK pathway raising the possibility it could be developed for anti-obesity therapy (208). There is also evidence that dietary intervention can have anti-inflammation activity which leads to enhanced insulin sensitivity. Food extracts with a high content of either flavonoids, phenolic compounds, p-coumaric acid, quercetin, or resveratrol have been found to exert systemic anti-inflammatory actions via inhibition of TNF-α-triggered activation of MAPKs and NFκB in human white adipocytes which improve insulin sensitivity (186). Specifically, Curcumin intervention was found to reduce mouse WAT inflammation and increase BAT UCP1 expression via PPAR-dependent and -independent mechanisms. It reduces macrophage infiltration and proinflammation cytokine expression in both macrophages and adipocytes along with increased energy expenditure and body temperature in response to cold (209).

Fatty acids (FA) are another example of dietary constituents that act as inflammation modulators. Importantly, ω3-FAs (n-3 polyunsaturated fatty acids (n-3PUFAs) have anti-inflammatory effects and may significantly impact chronic inflammatory

diseases including obesity related disorders (210). An ω3-enriched diet, in non-obesogenic non-inflammatory conditions, leads to synthesis of oxylipins which have an anti-inflammatory response in both WAT and BAT with a macrophage modulation effect, but with no influence on inflammatory cytokine secretion (209). FFAs are active stimulators for members of the rhodopsin-like family of G protein-coupled receptors (GPCRs) including GPR40, GPR41, GPR43, GPR84, and GPR120 (211, 212). GPR120 is highly expressed in both BAT and WAT. and positively impacts metabolic health by stimulating mitochondrial respiration in brown fat via intracellular Ca^{2+} release which results in mitochondrial depolarization and fragmentation. This occurs along with mitochondrial UCP1 activation, which may act synergistically with mitochondrial fragmentation to increase respiration. GPR120 activation by the agonist TUG-891 upregulates fat combustion in BAT thereby reducing fat mass, while GPR120 deficiency diminishes expression of genes involved in nutrient metabolism (213). Moreover, GPR120 deficiency leads to obesity, glucose intolerance, and hepatic steatosis in mice fed a high-fat diet (214). Importantly, GPR120 mediates the anti-inflammatory and insulin sensitizing effects of ω3-FAs including inhibition of inflammatory pathways and cytokine secretion in adipocytes and macrophages (215, 216). A role for GPR120 in BAT activation and WAT browning in response to cold via FGF21 secretion has also been confirmed (217).

CONCLUSION

Immune responses pose a significant metabolic challenge for the host due a range of energetically expensive processes including inflammatory mediator production and cell migration and proliferation. There is a trade-off between the energetic demands of immunity and homeothermy that permits a hypometabolic-hypothermic state to favor the immune system. Peripheral insulin resistance provides a mechanism for reallocating metabolic fuels to immune cells due to decreased nutrient storage in fat, muscle, and liver. The precise role of BAT in the hypometabolic-hypothermic state is currently unclear. Although BAT is generally more resistant to inflammatory stimuli than WAT, the repression of thermogenesis by inflammation may be a key energy trade-off to allow sufficient resources for immune responses. Importantly, BAT-mediated thermogenesis reactivation seems to be required for the exit from the hypometabolic-hypothermic state (218).

Many immune and inflammatory cells actively participate in the regulation of BAT thermogenesis, WAT browning and ultimately have the capacity to participate in controlling energy balance, glycemia, and lipidemia. Pro-inflammatory mediators secreted by both immune cells and adipocytes inhibit thermogenesis activation in BAT and browning of WAT in contrast to anti-inflammatory factors that have a positive influence. Additional research is needed to demonstrate the effect of each one of these mediators on brown and beige adipose cells and fully explain the pathways involved at the molecular level that regulate immune cells and brown/beige adipocytes interactions. This could lead to new therapeutic strategies to improve metabolic health and combating obesity and associated metabolic diseases.

AUTHOR CONTRIBUTIONS

All authors listed have made a substantial, direct and intellectual contribution to the work, and approved it for publication.

FUNDING

This work was supported by The Graduate School, University of Warwick.

ACKNOWLEDGMENTS

The authors would like to acknowledge CARA, The Council for At-Risk Academics, Warwick Medical School.

REFERENCES

1. McNelis JC, Olefsky JM. Macrophages, immunity, and metabolic disease. *Immunity*. (2014) 41:36–48. doi: 10.1016/j.immuni.2014.05.010
2. Olefsky JM, Glass CK. Macrophages, inflammation, and insulin resistance. *Annu Rev Physiol.* (2010) 72:219–46. doi: 10.1146/annurev-physiol-021909-135846
3. Saltiel AR, Olefsky JM. Inflammatory linking obesity and metabolic disease and metabolic disease. *J Clin Invest*. (2017) 127:1–4. doi: 10.1172/JCI92035
4. Xiao L, Yang X, Lin Y, Li S, Jiang J, Qian S, et al. Large adipocytes function as antigen-presenting cells to activate CD4 + T cells via upregulating MHCII in obesity. *Int J Obes.* (2016) 40:112–20. doi: 10.1038/ijo.2015.145
5. Valverde AM, Teruel T, Navarro P, Benito M, Lorenzo M. Tumor necrosis factor-α causes insulin receptor substrate-2-mediated insulin resistance and inhibits insulin-induced adipogenesis in fetal brown adipocytes. *Endocrinology*. (1998) 139:1229–38. doi: 10.1210/endo.139.3.5854
6. Lorenzo M, Alvaro C De, E-e JAS, Ferna S. Insulin resistance induced by tumor necrosis factor-Alpha in myocytes and brown adipocytes. *J Anim Sci.* (2008) 86:94–104. doi: 10.2527/jas.2007-0462
7. Nieto-Vazquez I, Fernández-Veledo S, Krämer DK, Vila-Bedmar R, Garcia-Guerra L, Lorenzo M. Insulin resistance associated to obesity: the link TNF-alpha. *Arch Physiol Biochem.* (2008) 114:183–94. doi: 10.1080/13813450802181047
8. Sakamoto T, Takahashi N, Sawaragi Y, Naknukool S, Yu R, Goto T, et al. Inflammation induced by RAW macrophages suppresses UCP1 mRNA induction via ERK activation in 10T1/2 adipocytes. *Am J Physiol Physiol.* (2013) 304:C729–38. doi: 10.1152/ajpcell.00312.2012
9. Halberg N, Wernsted I, Scherer P. The adipocyte as an endcrine cell. *Endocrinol Metab Clin North Am.* (2009) 37:1–15. doi: 10.1016/j.ecl.2008.07.002
10. Lo KA, Sun L. Turning WAT into BAT: a review on regulators controlling the browning of white adipocytes. *Biosci Rep.* (2013) 33:711–9. doi: 10.1042/BSR20130046
11. Armani A, Mammi C, Marzolla V, Calanchini M, Antelmi A, Rosano GMC, et al. Cellular models for understanding adipogenesis, adipose dysfunction, and obesity. *J Cell Biochem*. (2010) 110:564–72. doi: 10.1002/jcb.22598
12. Berry DC, Stenesen D, Zeve D, Graff JM. The developmental origins of adipose tissue. *Development*. (2013) 140:3939–49. doi: 10.1242/dev.080549

13. Martinez-Santibañez, WonCho K, Lumeng CN. Imaging white adipose tissue with confocal microscopy. *Methods Enzym.* (2014) 537:17–30. doi: 10.1016/B978-0-12-411619-1.00002-1
14. Scherer PE. Adipose tissue: from lipid storage compartment to endocrine organ. *Diabetes.* (2006) 55:1537–45. doi: 10.2337/db06-0263
15. MacDougald OA, Burant CF. The rapidly expanding family of adipokines. *Cell Metab.* (2007) 6:159–61. doi: 10.1016/j.cmet.2007.08.010
16. Rega-Kaun G, Kaun C, Wojta J. More than a simple storage organ: adipose tissue as a source of adipokines involved in cardiovascular disease. *Thromb Haemost.* (2013) 110:641–50. doi: 10.1160/TH13-03-0212
17. Cinti S. The adipose organ at glance. *Dis Model Mech.* (2012) 5:588–94. doi: 10.1242/dmm.009662
18. Cannon B, Nedergaard J. Brown adipose tissue: function and physiological significance. *Physiol Rev.* (2004) 84:277–359. doi: 10.1152/physrev.00015.2003
19. Ronti T, Lupattelli G, Mannarino E. The endocrine function of adipose tissue: an update. *Clin Endocrinol.* (2006) 64:355–65. doi: 10.1111/j.1365-2265.2006.02474.x
20. Petrovic N, Walden TB, Shabalina IG, Timmons JA, Cannon B, Nedergaard J. Chronic peroxisome proliferator-activated receptor γ (PPARγ) activation of epididymally derived white adipocyte cultures reveals a population of thermogenically competent, UCP1-containing adipocytes molecularly distinct from classic brown adipocytes. *J Biol Chem.* (2010) 285:7153–64. doi: 10.1074/jbc.M109.053942
21. Wu J, Khandekar M, Nuutila P, Schaart G, Huang K, Tu H, et al. Beige adipocytes are a distinct type of thermogenic fat cell in mouse and human. *Cell.* (2012) 150:366–76. doi: 10.1016/j.cell.2012.05.016
22. Giralt M, Villarroya F. White, brown, beige/brite: different adipose cells for different functions? *Endocrinology.* (2013) 154:2992–3000. doi: 10.1210/en.2013-1403
23. Rosenwald M, Wolfrum C. The origin and definition of brite versus white and classical brown adipocytes. *Adipocyte.* (2014) 3:4–9. doi: 10.4161/adip.26232
24. Villarroya F, Cereijo R, Villarroya J, Giralt M. Brown adipose tissue as a secretory organ. *Nat Rev Endocrinol.* (2017) 13:26–35. doi: 10.1038/nrendo.2016.136
25. Leitner BP, Huang S, Brychta RJ, Duckworth CJ, Baskin AS, McGehee S, et al. Mapping of human brown adipose tissue in lean and obese young men. *Proc Natl Acad Sci USA.* (2017) 114:8649–54. doi: 10.1073/pnas.1705287114
26. Vijgen GHEJ, Bouvy ND, Teule GJJ, Brans B, Schrauwen P, van Marken Lichtenbelt WD. Brown adipose tissue in morbidly obese subjects. *PLoS ONE.* (2011) 6:2–7. doi: 10.1371/journal.pone.0017247
27. Matsushita M, Yoneshiro T, Aita S, Kameya T, Sugie H, Saito M. Impact of brown adipose tissue on body fatness and glucose metabolism in healthy humans. *Int J Obes.* (2014) 38:812–7. doi: 10.1038/ijo.2013.206
28. van Marken Lichtenbelt WD, Vanhommerig JW, Smulders NM, Drossaerts JMAFL, Kemerink GJ, Bouvy ND, et al. Cold-activated brown adipose tissue in healthy men. *N Engl J Med.* (2009) 360:1500–8. doi: 10.1056/NEJMoa0808718
29. Ferre P, Burnol AF, Leturque A, Terretaz J, Penicaud L, Jeanrenaud B, et al. Glucose utilization *in vivo* and insulin-sensitivity of rat brown adipose tissue in various physiological and pathological conditions. *Biochem J.* (1986) 233:249–52. doi: 10.1042/bj2330249
30. Liu X, Wang S, You Y, Meng M, Zheng Z, Liu L, et al. Brown adipose tissue transplantation reverses obesity in Ob/Ob mice. *Endocrinology.* (2015) 156:2461–9. doi: 10.1210/en.2014-1598
31. Gunawardana SC, Piston DW. Reversal of type 1 diabetes in mice by brown adipose tissue transplant. *Diabetes.* (2012) 61:674–82. doi: 10.2337/db11-0510
32. Shankar K, Kumar D, Gupta S, Varshney S, Rajan S, Srivastava A, et al. Role of brown adipose tissue in modulating adipose tissue in fl ammation and insulin resistance in high-fat diet fed mice. *Eur J Pharmacol.* (2019) 854:354–64. doi: 10.1016/j.ejphar.2019.02.044
33. Stanford KI, Middelbeek RJW, Townsend KL, An D, Nygaard EB, Hitchcox KM, et al. Brown adipose tissue regulates glucose homeostasis and insulin sensitivity. *J Clin Invest.* (2013) 123:215–23. doi: 10.1172/JCI62308
34. Xiaomeng L, Zongji Z, Xiaoming Z, Minghui M, Lan L, Yanyan S, et al. Brown adipose tissue transplantation improves whole-body energy metabolism. *Cell Res.* (2013) 23:851–4. doi: 10.1038/cr.2013.64
35. Berbeé JFP, Boon MR, Khedoe PPSJ, Bartelt A, Schlein C, Worthmann A, et al. Brown fat activation reduces hypercholesterolaemia and protects from atherosclerosis development. *Nat Commun.* (2015) 6:6356. doi: 10.1038/ncomms7356
36. Koksharova E, Ustyuzhanin D, Philippov Y, Mayorov A, Shestakova M, Shariya M, et al. The relationship between brown adipose tissue content in supraclavicular fat depots and insulin sensitivity in patients with type 2 diabetes mellitus and prediabetes. *Diabetes Technol Ther.* (2017) 19:96–102. doi: 10.1089/dia.2016.0360
37. Chondronikola M, Volpi E, Borsheim E, Porter C, Annamalai P, Enerback S, et al. Brown adipose tissue improves whole-body glucose homeostasis and insulin sensitivity in humans. *Diabetes.* (2014) 63:4089–99. doi: 10.2337/db14-0746
38. Wu C, Cheng W, Sun Y, Dang Y, Gong F, Zhu H, et al. Activating brown adipose tissue for weight loss and lowering of blood glucose levels: a microPET study using obese and diabetic model mice. *PLoS ONE.* (2014) 9:1–14. doi: 10.1371/journal.pone.0113742
39. Sakamoto T, Nitta T, Maruno K, Yeh YS, Kuwata H, Tomita K, et al. Macrophage infiltration into obese adipose tissues suppresses the induction of UCP1 level in mice. *Am J Physiol Endocrinol Metab.* (2016) 310:E676–87. doi: 10.1152/ajpendo.00028.2015
40. Rissanen A, Orava J, Nuutila P, Noponen T, Parkkola R, Viljanen T, et al. Blunted metabolic responses to cold and insulin stimulation in brown adipose tissue of obese humans. *Obes.* (2013) 21:2279–87. doi: 10.1002/oby.20456
41. Penicaud L, Ferre P, Terretaz J, Kinebanyan MF, Leturque A, Dore E, et al. Development of obesity in Zucker rats. Early insulin resistance in muscles but normal sensitivity in white adipose tissue. *Diabetes.* (1987) 36:626–31. doi: 10.2337/diabetes.36.5.626
42. Tran K Van, Gealekman O, Frontini A, Zingaretti MC, Morroni M, Giordano A, et al. The vascular endothelium of the adipose tissue gives rise to both white and brown fat cells. *Cell Metab.* (2012) 15:222–9. doi: 10.1016/j.cmet.2012.01.008
43. Wolf Y, Boura-Halfon S, Cortese N, Haimon Z, Sar Shalom H, Kuperman Y, et al. Brown-adipose-tissue macrophages control tissue innervation and homeostatic energy expenditure. *Nat Immunol.* (2017) 18:665–74. doi: 10.1038/ni.3746
44. Kooijman S, van den Heuvel JK, Rensen PCN. Neuronal control of brown fat activity. *Trends Endocrinol Metab.* (2015) 26:657–68. doi: 10.1016/j.tem.2015.09.008
45. Odegaard JI, Chawla A. Mechanisms of macrophage activation in obesity-induced insulin resistance. *Nat Clin Pract Endocrinol Metab.* (2008) 4:619–26. doi: 10.1038/ncpendmet0976
46. Tilg H, Moschen AR. Inflammatory mechanisms in the regulation of insulin resistance. *Mol Med.* (2008) 14:222–31. doi: 10.2119/2007-00119.Tilg
47. Chawla A, Nguyen KD, Goh YPS. Macrophage-mediated inflammation in metabolic disease. *Nat Rev Immunol.* (2011) 11:738–49. doi: 10.1038/nri3071
48. McGregor RA, Kwon EY, Shin SK, Jung UJ, Kim E, Park JHY, et al. Time-course microarrays reveal modulation of developmental, lipid metabolism and immune gene networks in intrascapular brown adipose tissue during the development of diet-induced obesity. *Int J Obes.* (2013) 37:1524–31. doi: 10.1038/ijo.2013.52
49. Alcalá M, Calderon-Dominguez M, Bustos E, Ramos P, Casals N, Serra D, et al. Increased inflammation, oxidative stress and mitochondrial respiration in brown adipose tissue from obese mice. *Sci Rep.* (2017) 7:1–12. doi: 10.1038/s41598-017-16463-6
50. Fitzgibbons TP, Kogan S, Aouadi M, Hendricks GM, Straubhaar J, Czech MP. Similarity of mouse perivascular and brown adipose tissues and their resistance to diet-induced inflammation. *Am J Physiol Hear Circ Physiol.* (2011) 301:H1425–37. doi: 10.1152/ajpheart.00376.2011
51. Dowal L, Parameswaran P, Phat S, Akella S, Majumdar ID, Ranjan J, et al. Intrinsic properties of brown and white adipocytes have differential effects on macrophage inflammatory responses. *Mediators Inflamm.* (2017) 2017:9067049. doi: 10.1155/2017/9067049

52. Roberts-Toler C, O'Neill BT, Cypess AM. Diet-induced obesity causes insulin resistance in mouse brown adipose tissue. *Obesity*. (2015) 23:1765–70. doi: 10.1002/oby.21134
53. Bae J, Ricciardi CJ, Esposito D, Komarnytsky S, Hu P, Curry BJ, et al. Activation of pattern recognition receptors in brown adipocytes induces inflammation and suppresses uncoupling protein 1 expression and mitochondrial respiration. *AJP Cell Physiol*. (2014) 306:C918–30. doi: 10.1152/ajpcell.00249.2013
54. Xu H, Barnes GT, Yang Q, Tan G, Yang D, Chou CJ, et al. Chronic inflammation in fat plays a crucial role in the development of obesity-related insulin resistance. *J Clin Invest*. (2003) 112:1821–30. doi: 10.1172/JCI200319451
55. Hansen IR, Jansson KM, Cannon B, Nedergaard J. Contrasting effects of cold acclimation versus obesogenic diets on chemerin gene expression in brown and brite adipose tissues. *Biochim Biophys Acta*. (2014) 1841:1691–9. doi: 10.1016/j.bbalip.2014.09.003
56. Klepac K, Kilić A, Gnad T, Brown LM, Herrmann B, Wilderman A, et al. The G q signalling pathway inhibits brown and beige adipose tissue. *Nat Commun*. (2016) 7:10895. doi: 10.1038/ncomms10895
57. Rosell M, Hondares E, Iwamoto S, Gonzalez FJ, Wabitsch M, Staels B, et al. Peroxisome proliferator-activated receptors-α and -γ and cAMP-mediated pathways, control retinol-binding protein-4 gene expression in brown adipose tissue. *Endocrinology*. (2012) 153:1162–73. doi: 10.1210/en.2011-1367
58. Steculorum SM, Ruud J, Karakasilioti I, Backes H, Engström Ruud L, Timper K, et al. AgRP neurons control systemic insulin sensitivity via myostatin expression in brown adipose tissue. *Cell*. (2016) 165:125–38. doi: 10.1016/j.cell.2016.02.044
59. Polyák Á, Winkler Z, Kuti D, Ferenczi S, Kovács KJ. Brown adipose tissue in obesity: fractalkine-receptor dependent immune cell recruitment affects metabolic-related gene expression. *Biochim Biophys Acta*. (2016) 1861:1614–22. doi: 10.1016/j.bbalip.2016.07.002
60. Yamashita H, Sato Y, Kizaki T, Oh-ishi S, Nagasawa J, Ohno H. Basic fibroblast growth factor (bFGF) contributes to the enlargement of brown adipose tissue during cold acclimation. *Pflügers Arch*. (1994) 428:352–6. doi: 10.1007/BF00724518
61. Lorenzo M, Valverde AM, Teruel T, Benito M. IGF-I is a mitogen involved in differentiation-related gene expression in fetal rat brown adipocytes. *J Cell Biol*. (1993) 123:1567–75. doi: 10.1083/jcb.123.6.1567
62. Burysek L, Houstek J. B-Adrenergic stimulation of interleukin-la and interleukin-6 expression in mouse brown adipocytes. *FEBS Lett*. (1997) 411:83–6. doi: 10.1016/S0014-5793(97)00671-6
63. Chartoumpekis DV, Habeos IG, Ziros PG, Psyrogiannis AI, Kyriazopoulou VE, Papavassiliou AG. Brown adipose tissue responds to cold and adrenergic stimulation by induction of FGF21. *Mol Med*. (2011) 17:736–40. doi: 10.2119/molmed.2011.00075
64. Hondares E, Iglesias R, Giralt A, Gonzalez FJ, Giralt M, Mampel T, et al. Thermogenic activation induces FGF21 expression and release in brown adipose tissue. *J Biol Chem*. (2011) 286:12983–90. doi: 10.1074/jbc.M110.215889
65. Braga M, Reddy ST, Vergnes L, Pervin S, Grijalva V, Stout D, et al. Follistatin promotes adipocyte differentiation, browning, and energy metabolism. *J Lipid Res*. (2014) 55:375–84. doi: 10.1194/jlr.M039719
66. Svensson KJ, Long JZ, Jedrychowski MP, Cohen P, Lo JC, Serag S, et al. A secreted Slit2 fragment regulates adipose tissue thermogenesis and metabolic function. *Cell Metab*. (2016) 23:454–66. doi: 10.1016/j.cmet.2016.01.008
67. Cereijo R, Gavaldà-Navarro A, Cairó M, Quesada-López T, Villarroya J, Morón-Ros S, et al. CXCL14, a brown adipokine that mediates brown-fat-to-macrophage communication in thermogenic adaptation. *Cell Metab*. (2018) 28:750–63.e6. doi: 10.1016/j.cmet.2018.07.015
68. Sun K, Kusminski CM, Luby-Phelps K, Spurgin SB, An YA, Wang QA, et al. Brown adipose tissue derived VEGF-A modulates cold tolerance and energy expenditure. *Mol Metab*. (2014) 3:474–83. doi: 10.1016/j.molmet.2014.03.010
69. Xue Y, Petrovic N, Cao R, Larsson O, Lim S, Chen S, et al. Hypoxia-independent angiogenesis in adipose tissues during cold acclimation. *Cell Metab*. (2009) 9:99–109. doi: 10.1016/j.cmet.2008.11.009
70. Virtue S, Feldmann H, Christian M, Tan CY, Masoodi M, Dale M, et al. A new role for lipocalin prostaglandin D synthase in the regulation of brown adipose tissue substrate utilization. *Diabetes*. (2012) 61:3139–47. doi: 10.2337/db12-0015
71. Campderrós L, Moure R, Cairó M, Gavaldà-Navarro A, Quesada-López T, Cereijo R, et al. Brown adipocytes secrete GDF15 in response to thermogenic activation. *Obesity*. (2019) 27:1606–16. doi: 10.1002/oby.22584
72. Kotzbeck P, Giordano A, Mondini E, Murano I, Severi I, Venema W, et al. Brown adipose tissue whitening leads to brown adipocyte death and adipose tissue inflammation. *J Lipid Res*. (2018) 59:784–94. doi: 10.1194/jlr.M079665
73. Müller TD, Lee SJ, Jastroch M, Kabra D, Stemmer K, Aichler M, et al. p62 Links β-adrenergic input to mitochondrial function and thermogenesis. *J Clin Invest*. (2013) 123:469–78. doi: 10.1172/JCI64209
74. Wynn TA, Chawla A, Pollard JW. Origins and hallmarks of macrophages: development, homeostasis, and disease. *Nature*. (2013) 496:445–55. doi: 10.1038/nature12034
75. Hui X, Gu P, Zhang J, Nie T, Pan Y, Wu D, et al. Adiponectin enhances cold-induced browning of subcutaneous adipose tissue via promoting M2 macrophage proliferation. *Cell Metab*. (2015) 22:279–90. doi: 10.1016/j.cmet.2015.06.004
76. Lv Y, Zhang SY, Liang X, Zhang H, Xu Z, Liu B, et al. Adrenomedullin 2 enhances beiging in white adipose tissue directly in an adipocyte-autonomous manner and indirectly through activation of M2 macrophages. *J Biol Chem*. (2016) 291:23390–402. doi: 10.1074/jbc.M116.735563
77. Rao RR, Long JZ, White JP, Svensson KJ, Lou J, Lokurkar I, et al. Meteorin-like is a hormone that regulates immune-adipose interactions to increase beige fat thermogenesis. *Cell*. (2014) 157:1279–91. doi: 10.1016/j.cell.2014.03.065
78. Reitman ML. How does fat transition from white to beige? *Cell Metab*. (2017) 26:14–6. doi: 10.1016/j.cmet.2017.06.011
79. Thomas D, Apovian C. Macrophage functions in lean and obese adipose tissue. *Metabolism*. (2017) 72:120–43. doi: 10.1016/j.metabol.2017.04.005
80. Qiu Y, Nguyen KD, Odegaard JI, Cui X, Tian X, Locksley RM, et al. Eosinophils and type 2 cytokine signaling in macrophages orchestrate development of functional beige fat. *Cell*. (2014) 157:1292–308. doi: 10.1016/j.cell.2014.03.066
81. Shan B, Wang X, Wu Y, Xu C, Xia Z, Dai J, et al. The metabolic ER stress sensor IRE1α suppresses alternative activation of macrophages and impairs energy expenditure in obesity. *Nat Immunol*. (2017) 18:519–29. doi: 10.1038/ni.3709
82. Nguyen KD, Qiu Y, Cui X, Goh YPS, Mwangi J, David T, et al. Alternatively activated macrophages produce catecholamines to sustain adaptive thermogenesis. *Nature*. (2011) 480:104–8. doi: 10.1038/nature10653
83. Fischer K, Ruiz HH, Jhun K, Finan B, Oberlin DJ, Van Der Heide V, et al. Alternatively activated macrophages do not synthesize catecholamines or contribute to adipose tissue adaptive thermogenesis. *Nat Med*. (2017) 23:623–30. doi: 10.1038/nm.4316
84. Camell CD, Sander J, Spadaro O, Lee A, Nguyen KY, Wing A, et al. Inflammasome-driven catecholamine catabolism in macrophages blunts lipolysis during ageing. *Nature*. (2017) 550:119–23. doi: 10.1038/nature24022
85. Pirzgalska RM, Seixas E, Seidman JS, Link VM, Sánchez NM, Mahú I, et al. Sympathetic neuron-associated macrophages contribute to obesity by importing and metabolizing norepinephrine. *Nat Med*. (2017) 23:1309–18. doi: 10.1038/nm.4422
86. Galli SJ, Nakae S, Tsai M. Mast cells in the development of adaptive immune responses. *Nat Immunol*. (2005) 6:135–42. doi: 10.1038/ni1158
87. Chaldakov GN, Tonchev AB, Tuncel N, Atanassova P, Aloe L. Chapter 12: Adipose tissue and mast cells: adipokines as Yin–Yang modulators of inflammation. In: Giamila Fantuzzi TM, editor. *Adipose Tissue and Adipokines in Health and Disease (Nutrition and Health)*. Totowa, NJ: Humana Press (2007). p. 151–9.
88. Liu J, Divoux A, Sun J, Zhang J, Clément K, Glickman JN, et al. Genetic deficiency and pharmacological stabilization of mast cells reduce diet-induced obesity and diabetes in mice. *Nat Med*. (2009) 15:940–5. doi: 10.1038/nm.1994
89. Desautels M, Wollin A, Halvorson I, Muralidhara DV, Thornhill J. Role of mast cell histamine in brown adipose tissue thermogenic response to

VMH stimulation. *Am J Physiol Regul Integr Comp Physiol.* (1994) 266:R831–7. doi: 10.1152/ajpregu.1994.266.3.R831
90. Finlin BS, Zhu B, Confides AL, Westgate PM, Harfmann BD, Dupont-Versteegden EE, et al. Mast cells promote seasonal white adipose beiging in humans. *Diabetes.* (2017) 66:1237–46. doi: 10.2337/db16-1057
91. Finlin BS, Confides AL, Zhu B, Boulanger MC, Memetimin H, Taylor KW, et al. Adipose tissue mast cells promote human adipose beiging in response to cold. *Sci Rep.* (2019) 9:1–10. doi: 10.1038/s41598-019-45136-9
92. Zhang X, Wang X, Yin H, Zhang L, Feng A, Zhang QX, et al. Functional inactivation of mast cells enhances subcutaneous adipose tissue browning in mice. *Cell Rep.* (2019) 28:792–803.e4. doi: 10.1016/j.celrep.2019.06.044
93. Chmelar J, Chatzigeorgiou A, Chung KJ, Prucnal M, Voehringer D, Roers A, et al. No role for mast cells in obesity-related metabolic dysregulation. *Front Immunol.* (2016) 7:1–8. doi: 10.3389/fimmu.2016.00524
94. Gutierrez DA, Muralidhar S, Feyerabend TB, Herzig S, Rodewald HR. Hematopoietic kit deficiency, rather than lack of mast cells, protects mice from obesity and insulin resistance. *Cell Metab.* (2015) 21:678–91. doi: 10.1016/j.cmet.2015.04.013
95. Sakaguchi S, Yamaguchi T, Nomura T, Ono M. Regulatory T cells and immune tolerance. *Cell.* (2008) 133:775–87. doi: 10.1016/j.cell.2008.05.009
96. Feuerer M, Herrero L, Cipolletta D, Naaz A, Wong J, Nayer A, et al. Fat Treg cells: a liaison between the immune and metabolic systems. *Nat Med.* (2009) 15:930–9. doi: 10.1038/nm.2002
97. Medrikova D, Sijmonsma TP, Sowodniok K, Richards DM, Delacher M, Sticht C, et al. Brown adipose tissue harbors a distinct sub-population of regulatory T cells. *PLoS ONE.* (2015) 10:e0118534. doi: 10.1371/journal.pone.0118534
98. Wood IS, Wang B, Trayhurn P. IL-33, a recently identified interleukin-1 gene family member, is expressed in human adipocytes. *Biochem Biophys Res Commun.* (2009) 384:105–9. doi: 10.1016/j.bbrc.2009.04.081
99. Zeyda M, Wernly B, Demyanets S, Kaun C, Hämmerle M, Hantusch B, et al. Severe obesity increases adipose tissue expression of interleukin-33 and its receptor ST2, both predominantly detectable in endothelial cells of human adipose tissue. *Int J Obes.* (2013) 37:658–65. doi: 10.1038/ijo.2012.118
100. Brestoff JR, Artis D. Immune regulation of metabolic homeostasis in health and disease. *Cell.* (2015) 161:146–60. doi: 10.1016/j.cell.2015.02.022
101. Brestoff JR, Kim BS, Saenz SA, Stine RR, Monticelli LA, Sonnenberg GF, et al. Group 2 innate lymphoid cells promote beiging of white adipose tissue and limit obesity. *Nature.* (2015) 519:242–6. doi: 10.1038/nature14115
102. Lee M, Odegaard JI, Mukundan L, Qiu Y, Molofsky AB, Nussbaum JC, et al. Activated type 2 innate lymphoid cells regulate beige fat biogenesis. *Cell.* (2015) 160:74–87. doi: 10.1016/j.cell.2014.12.011
103. Ding X, Luo Y, Zhang X, Zheng H, Yang X, Yang X, et al. IL-33-driven ILC2/eosinophil axis in fat is induced by sympathetic tone and suppressed by obesity. *J Endocrinol.* (2016) 231:35–48. doi: 10.1530/JOE-16-0229
104. Goto T, Naknukool S, Yoshitake R, Hanafusa Y, Tokiwa S, Li Y, et al. Proinflammatory cytokine interleukin-1β suppresses cold-induced thermogenesis in adipocytes. *Cytokine.* (2016) 77:107–14. doi: 10.1016/j.cyto.2015.11.001
105. Rebiger L, Lenzen S, Mehmeti I. Susceptibility of brown adipocytes to pro-inflammatory cytokine toxicity and reactive oxygen species. *Biosci Rep.* (2016) 36:1–11. doi: 10.1042/BSR20150193
106. García M del C, Pazos P, Lima L, Diéguez C. Regulation of energy expenditure and brown/beige thermogenic activity by interleukins: new roles for old actors. *Int J Mol Sci.* (2018) 19:2569. doi: 10.3390/ijms19092569
107. van den Berg SM, van Dam AD, Rensen PCN, de Winther MPJ, Lutgens E. Immune modulation of brown(ing) adipose tissue in obesity. *Endocr Rev.* (2017) 38:46–68. doi: 10.1210/er.2016-1066
108. Estève D, Boulet N, Volat F, Zakaroff-Girard A, Ledoux S, Coupaye M, et al. Human white and brite adipogenesis is supported by MSCA1 and is impaired by immune cells. *Stem Cells.* (2015) 33:1277–91. doi: 10.1002/stem.1916
109. Martins FF, Bargut TCL, Aguila MB, Mandarim-de-Lacerda CA. Thermogenesis, fatty acid synthesis with oxidation, and inflammation in the brown adipose tissue of ob/ob (–/–) mice. *Ann Anat.* (2017) 210:44–51. doi: 10.1016/j.aanat.2016.11.013
110. Nøhr MK, Bobba N, Richelsen B, Lund S, Pedersen SB. Inflammation downregulates UCP1 expression in brown adipocytes potentially via SIRT1 and DBC1 interaction. *Int J Mol Sci.* (2017) 18:1006. doi: 10.3390/ijms18051006
111. Okla M, Zaher W, Alfayez M, Chung S. Inhibitory effects of Toll-like receptor 4, NLRP3 inflammasome, and interleukin-1β on white adipocyte browning. *Inflammation.* (2018) 41:626–42. doi: 10.1007/s10753-017-0718-y
112. Lee SE, Kang SG, Choi MJ, Jung SB, Ryu MJ, Chung HK, et al. Growth differentiation factor 15 mediates systemic glucose regulatory action of T-helper type 2 cytokines. *Diabetes.* (2017) 66:2774–88. doi: 10.2337/db17-0333
113. Chung K-J, Chatzigeorgiou A, Economopoulou M, Garcia-Martin R, Alexaki VI, Mitroulis I, et al. A self-sustained loop of inflammation-driven inhibition of beige adipogenesis in obesity. *Nat Immunol.* (2017) 18:654–64. doi: 10.1038/ni.3728
114. Sanchez-Infantes D, White UA, Elks CM, Morrison RF, Gimble JM, Considine RV, et al. Oncostatin M is produced in adipose tissue and is regulated in conditions of obesity and type 2 diabetes. *J Clin Endocrinol Metab.* (2014) 99:1–9. doi: 10.1210/jc.2013-3555
115. Sánchez-Infantes D, Cereijo R, Peyrou M, Piquer-Garcia I, Stephens JM, Villarroya F. Oncostatin m impairs brown adipose tissue thermogenic function and the browning of subcutaneous white adipose tissue. *Obesity.* (2017) 25:85–93. doi: 10.1002/oby.21679
116. Guo T, Marmol P, Moliner A, Björnholm M, Zhang C, Shokat KM, et al. Adipocyte ALK7 links nutrient overload to catecholamine resistance in obesity. *Elife.* (2014) 3:e03245. doi: 10.7554/eLife.03245
117. Andersson O, Korach-Andre M, Reissmann E, Ibáñez CF, Bertolino P. Growth/differentiation factor 3 signals through ALK7 and regulates accumulation of adipose tissue and diet-induced obesity. *Proc Natl Acad Sci USA.* (2008) 105:7252–6. doi: 10.1073/pnas.0800272105
118. Valladares A, Roncero C, Benito M, Porras A. TNF-α inhibits UCP-1 expression in brown adipocytes via ERKs - opposite effect of p38MAPK. *FEBS Lett.* (2001) 493:6–11. doi: 10.1016/S0014-5793(01)02264-5
119. Suárez-Zamorano N, Fabbiano S, Chevalier C, Stojanović O, Colin DJ, Stevanović A, et al. Microbiota depletion promotes browning of white adipose tissue and reduces obesity. *Nat Med.* (2015) 21:1497–501. doi: 10.1038/nm.3994
120. Gavaldà-Navarro A, Moreno-Navarrete JM, Quesada-López T, Cairó M, Giralt M, Fernández-Real JM, et al. Lipopolysaccharide-binding protein is a negative regulator of adipose tissue browning in mice and humans. *Diabetologia.* (2016) 59:2208–18. doi: 10.1007/s00125-016-4028-y
121. Olefsky JM. IKKε: a bridge between obesity and inflammation. *Cell.* (2009) 138:834–6. doi: 10.1016/j.cell.2009.08.018
122. Kumari M, Wang X, Lantier L, Lyubetskaya A, Eguchi J, Kang S, et al. IRF3 promotes adipose inflammation and insulin resistance and represses browning. *J Clin Invest.* (2016) 126:2839–54. doi: 10.1172/JCI86080
123. Chiang S, Bazuine M, Lumeng CN, Geletka LM, White NM, Ma J, et al. The protein kinase IKKε regulates energy expenditure, insulin sensitivity and chronic inflammation in obese mice. *Cell.* (2010) 138:961–75. doi: 10.1016/j.cell.2009.06.046
124. Shahid M, Javed AA, Chandra D, Ramsey HE, Shah D, Khan MF, et al. IEX-1 deficiency induces browning of white adipose tissue and resists diet-induced obesity. *Sci Rep.* (2016) 6:1–14. doi: 10.1038/srep24135
125. Yang L, Calay ES, Fan J, Arduini A, Kunz RC, Gygi SP, et al. S-Nitrosylation links obesity-associated inflammation to endoplasmic reticulum dysfunction. *Science.* (2015) 349:500–6. doi: 10.1126/science.aaa0079
126. Otoda T, Takamura T, Misu H, Ota T, Murata S, Hayashi H, et al. Proteasome dysfunction mediates obesity-induced endoplasmic reticulum stress and insulin resistance in the liver. *Diabetes.* (2013) 62:811–24. doi: 10.2337/db11-1652
127. Wikstrom JD, Mahdaviani K, Liesa M, Sereda SB, Si Y, Las G, et al. Hormone-induced mitochondrial fission is utilized by brown adipocytes as an amplification pathway for energy expenditure. *EMBO J.* (2014) 33:418–36. doi: 10.1002/embj.201385014
128. Arruda AP, Pers BM, Parlakgül G, Güney E, Inouye K, Hotamisligil GS. Chronic enrichment of hepatic endoplasmic reticulum-mitochondria contact leads to mitochondrial dysfunction in obesity. *Nat Med.* (2014) 20:1427–35. doi: 10.1038/nm.3735
129. Gregor MF, Misch ES, Yang L, Hummasti S, Inouye KE, Lee AH, et al. The role of adipocyte XBP1 in metabolic regulation during lactation. *Cell Rep.* (2013) 3:1430–9. doi: 10.1016/j.celrep.2013.03.042

130. Bartelt A, Widenmaier SB, Schlein C, Johann K, Goncalves RLS, Eguchi K, et al. Brown adipose tissue thermogenic adaptation requires Nrf1-mediated proteasomal activity. *Nat Med*. (2018) 24:292–303. doi: 10.1038/nm.4481
131. Hou Y, Liu Z, Zuo Z, Gao T, Fu J, Wang H, et al. Adipocyte-specific deficiency of Nfe2l1 disrupts plasticity of white adipose tissues and metabolic homeostasis in mice. *Biochem Biophys Res Commun*. (2018) 503:264–70. doi: 10.1016/j.bbrc.2018.06.013
132. Lehrke M, Becker A, Greif M, Stark R, Laubender RP, Von Ziegler F, et al. Chemerin is associated with markers of inflammation and components of the metabolic syndrome but does not predict coronary atherosclerosis. *Eur J Endocrinol*. (2009) 161:339–44. doi: 10.1530/EJE-09-0380
133. Rourke JL, Muruganandan S, Dranse HJ, McMullen NM, Sinal CJ. Gpr1 is an active chemerin receptor influencing glucose homeostasis in obese mice. *J Endocrinol*. (2014) 222:201–15. doi: 10.1530/JOE-14-0069
134. Mattern A, Zellmann T, Beck-Sickinger AG. Processing, signaling, and physiological function of chemerin. *IUBMB Life*. (2014) 66:19–26. doi: 10.1002/iub.1242
135. Böhm F, Pernow J. The importance of endothelin-1 for vascular dysfunction in cardiovascular disease. *Cardiovasc Res*. (2007) 76:8–18. doi: 10.1016/j.cardiores.2007.06.004
136. Kowalczyk A, Kleniewska P, Kolodziejczyk M, Skibska B, Goraca A. The role of endothelin-1 and endothelin receptor antagonists in inflammatory response and sepsis. *Arch Immunol Ther Exp*. (2015) 63:41–52. doi: 10.1007/s00005-014-0310-1
137. Eriksson AKS, Van Harmelen V, Stenson BM, Åström G, Wåhlén K, Laurencikiene J, et al. Endothelin-1 stimulates human adipocyte lipolysis through the ET A receptor. *Int J Obes*. (2009) 33:67–74. doi: 10.1038/ijo.2008.212
138. Shimizu I, Maruyama S, Walsh K, Shimizu I, Aprahamian T, Kikuchi R, et al. Vascular rarefaction mediates whitening of brown fat in obesity Find the latest version: vascular rarefaction mediates whitening of brown fat in obesity. *J Clin Invest*. (2014) 124:2099–112. doi: 10.1172/JCI71643
139. Park J, Kim M, Sun K, An YA, Gu X, Scherer PE. VEGF-A - expressing adipose tissue shows rapid beiging and enhanced survival after transplantation and confers IL-4-independent metabolic improvements. *Diabetes*. (2017) 66:1479–90. doi: 10.2337/db16-1081
140. Farjo KM, Farjo RA, Halsey S, Moiseyev G, Ma J-x. Retinol-binding protein 4 induces inflammation in human endothelial cells by an NADPH oxidase- and nuclear factor Kappa B-dependent and retinol-independent mechanism. *Mol Cell Biol*. (2012) 32:5103–15. doi: 10.1128/MCB.00820-12
141. Kotnik P, Fischer-Posovszky P, Wabitsch M. RBP4: a controversial adipokine. *Eur J Endocrinol*. (2011) 165:703–11. doi: 10.1530/EJE-11-0431
142. Guo H, Foncea R, O'Byrne SM, Jiang H, Zhang Y, Deis JA, et al. Lipocalin 2, a regulator of retinoid homeostasis and retinoid-mediated thermogenic activation in adipose tissue. *J Biol Chem*. (2016) 291:11216–29. doi: 10.1074/jbc.M115.711556
143. Hondares E, Rosell M, Gonzalez FJ, Giralt M, Iglesias R, Villarroya F. Hepatic FGF21 expression is induced at birth via PPARα in response to milk intake and contributes to thermogenic activation of neonatal brown fat. *Cell Metab*. (2010) 11:206–12. doi: 10.1016/j.cmet.2010.02.001
144. Fisher FF, Kleiner S, Douris N, Fox EC, Mepani RJ, Verdeguer F, et al. FGF21 regulates PGC-1α and browning of white adipose tissues in adaptive thermogenesis. *Genes Dev*. (2012) 26:271–81. doi: 10.1101/gad.177857.111
145. Lynch L, Hogan AE, Duquette D, Lester C, Banks A, LeClair K, et al. iNKT cells induce FGF21 for thermogenesis and are required for maximal weight loss in GLP1 therapy. *Cell Metab*. (2016) 24:510–9. doi: 10.1016/j.cmet.2016.08.003
146. Giralt M, Gavaldà-Navarro A, Villarroya F. Fibroblast growth factor-21, energy balance and obesity. *Mol Cell Endocrinol*. (2015) 418:66–73. doi: 10.1016/j.mce.2015.09.018
147. Véniant MM, Sivits G, Helmering J, Komorowski R, Lee J, Fan W, et al. Pharmacologic effects of FGF21 are independent of the "browning" of white adipose tissue. *Cell Metab*. (2015) 21:731–8. doi: 10.1016/j.cmet.2015.04.019
148. Wang N, Zhao T-T, Li S-M, Sun X, Li Z-C, Li Y-H, et al. Fibroblast growth factor 21 exerts its anti-inflammatory effects on multiple cell types of adipose tissue in obesity. *Obesity*. (2019) 27:399–408. doi: 10.1002/oby.22376
149. Hara T, Tanegashima K. Pleiotropic functions of the CXC-type chemokine CXCL14 in mammals. *J Biochem*. (2012) 151:469–76. doi: 10.1093/jb/mvs030
150. Hara T, Nakayama Y. Chapter 5 CXCL14 and insulin action. *Vitam Horm*. (2009) 80:107–23. doi: 10.1016/S0083-6729(08)00605-5
151. Zhang S, Sun WY, Wu JJ, Wei W. TGF-β signaling pathway as a pharmacological target in liver diseases. *Pharmacol Res*. (2014) 85:15–22. doi: 10.1016/j.phrs.2014.05.005
152. Eckel J. Skeletal muscle: a novel secretory organ. In: *The Cellular Secretome and Organ Crosstalk*. London: Elsevier (2018). p. 65–90.
153. Choi SC, Han JK. Chapter Five: negativenegative regulation of activin signal transduction. 1st ed. Vol. 85. In: *Vitamins and Hormones*. London: Elsevier Inc. (2011). p. 79–104.
154. Seong HA, Manoharan R, Ha H. Smad proteins differentially regulate obesity-induced glucose and lipid abnormalities and inflammation via class-specific control of AMPK-related kinase MPK38/MELK activity. *Cell Death Dis*. (2018) 9:471. doi: 10.1038/s41419-018-0489-x
155. Yadav H, Quijano C, Kamaraju AK, Gavrilova O, Malek R, Chen W, et al. Protection from obesity and diabetes by blockade of TGF-β/Smad3 signaling. *Cell Metab*. (2011) 14:67–79. doi: 10.1016/j.cmet.2011.04.013
156. Koncarevic A, Kajimura S, Cornwall-Brady M, Andreucci A, Pullen A, Sako D, et al. A novel therapeutic approach to treating obesity through modulation of TGFβ signaling. *Endocrinology*. (2012) 153:3133–46. doi: 10.1210/en.2012-1016
157. Braga M, Pervin S, Norris K, Bhasin S, Singh R. Inhibition of *in vitro* and *in vivo* brown fat differentiation program by myostatin. *Obesity*. (2013) 21:1180–8. doi: 10.1002/oby.20117
158. Pervin S, Singh V, Tucker A, Collazo J, Singh R. Modulation of transforming growth factor-β/follistatin signaling and white adipose browning: therapeutic implications for obesity related disorders. *Horm Mol Biol Clin Investig*. (2017) 31:1868–91. doi: 10.1515/hmbci-2017-0036
159. Fournier B, Murray B, Gutzwiller S, Marcaletti S, Marcellin D, Bergling S, et al. Blockade of the activin receptor IIB activates functional brown adipogenesis and thermogenesis by inducing mitochondrial oxidative metabolism. *Mol Cell Biol*. (2012) 32:2871–9. doi: 10.1128/MCB.06575-11
160. Zhang C, McFarlane C, Lokireddy S, Masuda S, Ge X, Gluckman PD, et al. Inhibition of myostatin protects against diet-induced obesity by enhancing fatty acid oxidation and promoting a brown adipose phenotype in mice. *Diabetologia*. (2012) 55:183–93. doi: 10.1007/s00125-011-2304-4
161. Dong J, Dong Y, Dong Y, Chen F, Mitch WE, Zhang L. Inhibition of myostatin in mice improves insulin sensitivity via irisin-mediated cross talk between muscle and adipose tissues. *Int J Obes*. (2016) 40:434–42. doi: 10.1038/ijo.2015.200
162. Emmerson PJ, Duffin KL, Chintharlapalli S, Wu X. GDF15 and growth control. *Front Physiol*. (2018) 9:1712. doi: 10.3389/fphys.2018.01712
163. Macia L, Tsai VWW, Nguyen AD, Johnen H, Kuffner T, Shi YC, et al. Macrophage inhibitory cytokine 1 (MIC-1/GDF15) decreases food intake, body weight and improves glucose tolerance in mice on normal & obesogenic diets. *PLoS ONE*. (2012) 7:e34868. doi: 10.1371/journal.pone.0034868
164. Chrysovergis K, Wang X, Kosak J, Lee SH, Kim JS, Foley JF, et al. NAG-1/GDF-15 prevents obesity by increasing thermogenesis, lipolysis and oxidative metabolism. *Int J Obes*. (2014) 38:1555–64. doi: 10.1038/ijo.2014.27
165. Tong M, Jun T, Nie Y, Hao J, Fan D. The role of the Slit/Robo signaling pathway. *J Cancer*. (2019) 10:2694–705. doi: 10.7150/jca.31877
166. Ishii T. Close teamwork between Nrf2 and peroxiredoxins 1 and 6 for the regulation of prostaglandin D2 and E2 production in macrophages in acute inflammation. *Free Radic Biol Med*. (2015) 88(Part B):189–98. doi: 10.1016/j.freeradbiomed.2015.04.034
167. Lee M-WM, Lee M-WM, Oh K-J. Adipose tissue-derived signatures for obesity and type 2 diabetes: adipokines, batokines and MicroRNAs. *J Clin Med*. (2019) 8:854. doi: 10.3390/jcm8060854
168. Tanaka R, Miwa Y, Mou K, Tomikawa M, Eguchi N, Urade Y, et al. Knockout of the l-pgds gene aggravates obesity and atherosclerosis in mice. *Biochem Biophys Res Commun*. (2009) 378:851–6. doi: 10.1016/j.bbrc.2008.11.152
169. Duchamp C, Burton KA, Géloën A, Dauncey MJ. Transient upregulation of IGF-I gene expression in brown adipose tissue of cold-exposed rats. *Am J Physiol*. (1997) 272:453–60. doi: 10.1152/ajpendo.1997.272.3.E453

170. Spadaro O, Camell CD, Bosurgi L, Nguyen KY, Youm YH, Rothlin CV, et al. IGF1 shapes macrophage activation in response to immunometabolic challenge. *Cell Rep*. (2017) 19:225–34. doi: 10.1016/j.celrep.2017.03.046
171. Chang HR, Kim HJ, Xu X, Ferrante AW. Macrophage and adipocyte IGF1 maintain adipose tissue homeostasis during metabolic stresses. *Obesity*. (2016) 24:172–83. doi: 10.1002/oby.21354
172. Pellegrinelli V, Carobbio S, Vidal-Puig A. Adipose tissue plasticity: how fat depots respond differently to pathophysiological cues. *Diabetologia*. (2016) 59:1075–88. doi: 10.1007/s00125-016-3933-4
173. Gunawardana SC, Piston DW. Insulin-independent reversal of type 1 diabetes in nonobese diabetic mice with brown adipose tissue transplant. *Am J Physiol*. (2015) 308:E1043–55. doi: 10.1152/ajpendo.00570.2014
174. Egecioglu E, Anesten F, Schéle E, Palsdottir V. Interleukin-6 is important for regulation of core body temperature during long-term cold exposure in mice. *Biomed Rep*. (2018) 9:206–12. doi: 10.3892/br.2018.1118
175. Mauer J, Chaurasia B, Goldau J, Vogt MC, Ruud J, Nguyen KD, et al. Signaling by IL-6 promotes alternative activation of macrophages to limit endotoxemia and obesity-associated resistance to insulin. *Nat Immunol*. (2014) 15:423–30. doi: 10.1038/ni.2865
176. Kristóf E, Klusóczki Á, Veress R, Shaw A, Combi ZS, Varga K, et al. Interleukin-6 released from differentiating human beige adipocytes improves browning. *Exp Cell Res*. (2019) 377:47–55. doi: 10.1016/j.yexcr.2019.02.015
177. DeFuria J, Belkina AC, Jagannathan-Bogdan M, Snyder-Cappione J, Carr JD, Nersesova YR, et al. B cells promote inflammation in obesity and type 2 diabetes through regulation of T-cell function and an inflammatory cytokine profile. *Proc Natl Acad Sci USA*. (2013) 110:5133–8. doi: 10.1073/pnas.1215840110
178. Pal M, Febbraio MA, Whitham M. From cytokine to myokine: the emerging role of interleukin-6 in metabolic regulation. *Immunol Cell Biol*. (2014) 92:331–9. doi: 10.1038/icb.2014.16
179. Bastard JP, Jardel C, Bruckert E, Blondy P, Capeau J, Laville M, et al. Elevated levels of interleukin 6 are reduced in serum and subcutaneous adipose tissue of obese women after weight loss. *J Clin Endocrinol Metab*. (2000) 85:3338–42. doi: 10.1210/jcem.85.9.6839
180. Priceman SJ, Kujawski M, Shen S, Cherryholmes GA, Lee H, Zhang C, et al. Regulation of adipose tissue T cell subsets by Stat3 is crucial for diet-induced obesity and insulin resistance. *Proc Natl Acad Sci USA*. (2013) 110:13079–84. doi: 10.1073/pnas.1311557110
181. Han J, Meng Q, Shen L, Wu G. Interleukin-6 induces fat loss in cancer cachexia by promoting white adipose tissue lipolysis and browning. *Lipids Health Dis*. (2018) 17:1–8. doi: 10.1186/s12944-018-0657-0
182. McArdle MA, Finucane OM, Connaughton RM, McMorrow AM, Roche HM. Mechanisms of obesity-induced inflammation and insulin resistance: insights into the emerging role of nutritional strategies. *Front Endocrinol*. (2013) 4:52. doi: 10.3389/fendo.2013.00052
183. Kwon H, Pessin JE. Adipokines mediate inflammation and insulin resistance. *Front Endocrinol*. (2013) 4:71. doi: 10.3389/fendo.2013.00071
184. Albert V, Svensson K, Shimobayashi M, Colombi M, Muñoz S, Jimenez V, et al. mTORC 2 sustains thermogenesis via Akt-induced glucose uptake and glycolysis in brown adipose tissue. *EMBO Mol Med*. (2016) 8:232–46. doi: 10.15252/emmm.201505610
185. Martinez N, Cheng CY, Ketheesan N, Cullen A, Tang Y, Lum J, et al. mTORC2/Akt activation in adipocytes is required for adipose tissue inflammation in tuberculosis. *EBioMedicine*. (2019) 45:314–27. doi: 10.1016/j.ebiom.2019.06.052
186. Vazquez-Prieto MA, Bettaieb A, Haj FG, Fraga CG, Oteiza PI. (–)-Epicatechin prevents TNFα-induced activation of signaling cascades involved in inflammation and insulin sensitivity in 3T3-L1 adipocytes. *Arch Biochem Biophys*. (2012) 527:113–8. doi: 10.1016/j.abb.2012.02.019
187. Chen C, Zhang W, Shi H, Zhuo Y, Yang G, Zhang A, et al. A novel benzenediamine derivative FC98 reduces insulin resistance in high fat diet-induced obese mice by suppression of metaflammation. *Eur J Pharmacol*. (2015) 761:298–308. doi: 10.1016/j.ejphar.2015.06.021
188. Li J, An R, Liu S, Xu H. Deregulation of PP2A-Akt interaction contributes to sucrose non-fermenting related kinase (SNRK) deficiency induced insulin resistance in adipose tissue (P21-071-19). *Curr Dev Nutr*. (2019) 3(Supplement_1):26–35. doi: 10.1093/cdn/nzz041.P21-071-19
189. Li J, Feng B, Nie Y, Jiao P, Lin X, Huang M, et al. Sucrose nonfermenting-related kinase regulates both adipose inflammation and energy homeostasis in mice and humans. *Diabetes*. (2018) 67:400–11. doi: 10.2337/db17-0745
190. Putti R, Sica R, Migliaccio V, Lionetti L. Diet impact on mitochondrial bioenergetics and dynamics. *Front Physiol*. (2015) 6:109. doi: 10.3389/fphys.2015.00109
191. Zorzano A, Liesa M, Palacín M. Role of mitochondrial dynamics proteins in the pathophysiology of obesity and type 2 diabetes. *Int J Biochem Cell Biol*. (2009) 41:1846–54. doi: 10.1016/j.biocel.2009.02.004
192. Heinonen S, Buzkova J, Muniandy M, Kaksonen R, Ollikainen M, Ismail K, et al. Impaired mitochondrial biogenesis in adipose tissue in acquired obesity. *Diabetes*. (2015) 64:3135–45. doi: 10.2337/db14-1937
193. Keuper M, Sachs S, Walheim E, Berti L, Raedle B, Tews D, et al. Activated macrophages control human adipocyte mitochondrial bioenergetics via secreted factors. *Mol Metab*. (2017) 6:1226–39. doi: 10.1016/j.molmet.2017.07.008
194. Hahn WS, Kuzmicic J, Burrill JS, Donoghue MA, Foncea R, Jensen MD, et al. Proinflammatory cytokines differentially regulate adipocyte mitochondrial metabolism, oxidative stress, and dynamics. *Am J Physiol*. (2014) 306:1033–45. doi: 10.1152/ajpendo.00422.2013
195. Woo CY, Jang JE, Lee SE, Koh EH, Lee KU. Mitochondrial dysfunction in adipocytes as a primary cause of adipose tissue inflammation. *Diabetes Metab J*. (2019) 43:247–56. doi: 10.4093/dmj.2018.0221
196. Gurung P, Lukens JR, Kanneganti T-D. Mitochondria: diversity in the regulation of the NLRP3 inflammasome. *Trends Mol Med*. (2015) 21:193–201. doi: 10.1016/j.molmed.2014.11.008
197. de-Lima-Júnior JC, Souza GF, Moura-Assis A, Gaspar RS, Gaspar JM, Rocha AL, et al. Abnormal brown adipose tissue mitochondrial structure and function in IL10 deficiency. *EBioMedicine*. (2019) 39:436–47. doi: 10.1016/j.ebiom.2018.11.041
198. Frohnert BI, Bernlohr DA. Protein carbonylation, mitochondrial dysfunction, and insulin resistance. *Adv Nutr*. (2013) 4:157–63. doi: 10.3945/an.112.003319
199. Patti ME, Corvera S. The role of mitochondria in the pathogenesis of type 2 diabetes. *Endocr Rev*. (2010) 31:364–95. doi: 10.1210/er.2009-0027
200. Fernández-Sánchez A, Madrigal-Santillán E, Bautista M, Esquivel-Soto J, Morales-González Á, Esquivel-Chirino C, et al. Inflammation, oxidative stress, and obesity. *Int J Mol Sci*. (2011) 12:3117–32. doi: 10.3390/ijms12053117
201. Bondia-Pons I, Ryan L, Martinez JA. Oxidative stress and inflammation interactions in human obesity. *J Physiol Biochem*. (2012) 68:701–11. doi: 10.1007/s13105-012-0154-2
202. Matsuda M, Shimomura I. Increased oxidative stress in obesity: implications for metabolic syndrome, diabetes, hypertension, dyslipidemia, atherosclerosis, and cancer. *Obes Res Clin Pract*. (2013) 7:e330–41. doi: 10.1016/j.orcp.2013.05.004
203. Chouchani ET, Kazak L, Jedrychowski MP, Lu GZ, Erickson BK, Szpyt J, et al. Mitochondrial ROS regulate thermogenic energy expenditure and sulfenylation of UCP1. *Nature*. (2016) 532:112–6. doi: 10.1038/nature17399
204. Vernochet C, Damilano F, Mourier A, Bezy O, Mori MA, Smyth G, et al. Adipose tissue mitochondrial dysfunction triggers a lipodystrophic syndrome with insulin resistance, hepatosteatosis, and cardiovascular complications. *FASEB J*. (2014) 28:4408–19. doi: 10.1096/fj.14-253971
205. Yuan M, Konstantopoulos N, Lee J, Hansen L, Li ZW, Karin M, et al. Reversal of obesity- and diet-induced insulin resistance with salicylates or targeted disruption of Ikkβ. *Science*. (2001) 293:1673–7. doi: 10.1126/science.1061620
206. Larsen CM, Faulenbach M, Vaag A, Vølund A, Ehses JA, Seifert B, et al. Interleukin-1-receptor antagonist in type 2 diabetes mellitus. *N Engl J Med*. (2007) 356:1517–26. doi: 10.1056/NEJMoa065213
207. Sanchez-Zamora Y, Terrazas LI, Vilches-Flores A, Leal E, Juárez I, Whitacre C, et al. Macrophage migration inhibitory factor is a therapeutic target in treatment of non-insulin-dependent diabetes mellitus. *FASEB J*. (2010) 24:2583–90. doi: 10.1096/fj.09-147066
208. Brendle C, Stefan N, Stef I, Ripkens S, Soekler M, la Fougère C, et al. Impact of diverse chemotherapeutic agents and external factors on activation of brown adipose tissue in a large patient collective. *Sci Rep*. (2019) 9:1–8. doi: 10.1038/s41598-018-37924-6

209. Song Z, Revelo X, Shao W, Tian L, Zeng K, Lei H, et al. Dietary curcumin intervention targets mouse white adipose tissue inflammation and brown adipose tissue UCP1 expression. *Obesity*. (2018) 26:547–58. doi: 10.1002/oby.22110
210. Talukdar S, Olefsky JM, Osborn O. Targeting GPR120 and other fatty acid-sensing GPCRs ameliorates insulin resistance and inflammatory diseases. *Trends Pharmacol Sci*. (2011) 32:543–50. doi: 10.1016/j.tips.2011.04.004
211. Hirasawa A, Hara T, Katsuma S, Adachi T, Tsujimoto G. Free fatty acid receptors and drug discovery. *Biol Pharm Bull*. (2008) 31:1847–51. doi: 10.1248/bpb.31.1847
212. Yonezawa T, Kurata R, Yoshida K, Murayama MA, Cui X, Hasegawa A. Free fatty acids-sensing G protein-coupled receptors in drug targeting and therapeutics. *Curr Med Chem*. (2013) 20:3855–71. doi: 10.2174/09298673113209990168
213. Schilperoort M, Dam AD, Hoeke G, Shabalina IG, Okolo A, Hanyaloglu AC, et al. The GPR 120 agonist TUG−891 promotes metabolic health by stimulating mitochondrial respiration in brown fat. *EMBO Mol Med*. (2018) 10:1–18. doi: 10.15252/emmm.201708047
214. Caiazzo R, Van Hul W, Van Gaal L, Horber F, Balkau B, Pigeyre M, et al. Dysfunction of lipid sensor GPR120 leads to obesity in both mouse and human. *Nature*. (2012) 483:350–4. doi: 10.1038/nature 10798
215. Oh DY, Talukdar S, Bae EJ, Imamura T, Morinaga H, Fan W, et al. GPR120 is an omega-3 fatty acid receptor mediating potent anti-inflammatory and insulin-sensitizing effects. *Cell*. (2010) 142:687–98. doi: 10.1016/j.cell.2010.07.041
216. Oh DY, Walenta E, Akiyama TE, Lagakos WS, Lackey D, Pessentheiner AR, et al. A Gpr120-selective agonist improves insulin resistance and chronic inflammation in obese mice. *Nat Med*. (2014) 20:942–7. doi: 10.1038/nm.3614
217. Quesada-López T, Cereijo R, Turatsinze J, Planavila A, Cairó M, Gavaldà-Navarro A, et al. The lipid sensor GPR120 promotes brown fat activation and FGF21 release from adipocytes. *Nat Commun*. (2016) 7:13479. doi: 10.1038/ncomms13479
218. Ganeshan K, Nikkanen J, Man K, Leong YA, Sogawa Y, Maschek JA, et al. Energetic trade-offs and hypometabolic states promote disease tolerance. *Cell*. (2019) 177:399–413.e12. doi: 10.1016/j.cell.2019.01.050

Conflict of Interest: The authors declare that the research was conducted in the absence of any commercial or financial relationships that could be construed as a potential conflict of interest.

frontiers in Endocrinology

MINI REVIEW
published: 15 April 2020
doi: 10.3389/fendo.2020.00185

Combating Obesity With Thermogenic Fat: Current Challenges and Advancements

Ruping Pan[1], *Xiaohua Zhu*[1], *Pema Maretich*[2] *and Yong Chen*[3]*

[1] Department of Nuclear Medicine, Tongji Hospital, Tongji Medical College, Huazhong University of Science and Technology, Wuhan, China, [2] Department of Biology, Massachusetts Institute of Technology, Cambridge, MA, United States, [3] Department of Endocrinology, Internal Medicine, Tongji Hospital, Tongji Medical College, Huazhong University of Science and Technology, Wuhan, China

Brown fat and beige fat are known as thermogenic fat due to their contribution to non-shivering thermogenesis in mammals following cold stimulation. Beige fat is unique due to its origin and its development in white fat. Subsequently, both brown fat and beige fat have become viable targets to combat obesity. Over the last few decades, most therapeutic strategies have been focused on the canonical pathway of thermogenic fat activation via the β3-adrenergic receptor (AR). Notwithstanding, administering β3-AR agonists often leads to side effects including hypertension and particularly cardiovascular disease. It is thus imperative to search for alternative therapeutic approaches to combat obesity. In this review, we discuss the current challenges in the field with respect to stimulating brown/beige fat thermogenesis. Additionally, we include a summary of other newly discovered pathways, including non-AR signaling- and non-UCP1-dependent mechanisms, which could be potential targets for the treatment of obesity and its related metabolic diseases.

Keywords: obesity, brown fat, beige fat, thermogenesis, β-adrenergic signaling, UCP1, calcium cycling, glycolytic beige fat

OPEN ACCESS

Edited by:
Takeshi Yoneshiro, University of California, San Francisco, United States

Reviewed by:
Alessandra Feraco, San Raffaele Pisana (IRCCS), Italy
Kerry Loomes, The University of Auckland, New Zealand

***Correspondence:**
Yong Chen
tj.y.chen@vip.163.com

Specialty section:
This article was submitted to Obesity, a section of the journal Frontiers in Endocrinology

Received: *02 December 2019*
Accepted: *16 March 2020*
Published: *15 April 2020*

Citation:
Pan R, Zhu X, Maretich P and Chen Y (2020) Combating Obesity With Thermogenic Fat: Current Challenges and Advancements. Front. Endocrinol. 11:185. doi: 10.3389/fendo.2020.00185

INTRODUCTION

In recent years, obesity has become an ever-growing public health crisis. Its related diseases include type 2 diabetes, hypertension, cardiovascular disease, and cancer. The treatments for obesity have been shown to be minimally effective and often come with a slew of side effects. Generally, the production of heat is accompanied by a concomitant increase in the lipolysis of triglycerides and the oxidation of fatty acids (1). Thus, stimulating thermogenesis is a useful tool with which to combat obesity. In addition to shivering thermogenesis, non-shivering thermogenesis plays an important role in energy homeostasis. It was originally thought to occur only in newborn humans as a means to maintain their body temperatures as there exists abundant brown fat in their body. However, in 2007, brown fat was discovered in adult humans using 18^{F}-fluorodeoxyglucose positron emission tomography/computed tomography (18^{F}FDG-PET/CT)-based imaging (2). Importantly, the activity of brown fat in humans is negatively correlated to body mass index (BMI) and positively correlated to glucose tolerance as well as insulin sensitivity (3). Thus, non-shivering thermogenesis has become an area of interest as a means to promote more robust basal metabolism and consequently reduce the prevalence of diseases caused by a surplus of energy stores.

Canonically, the metabolic effect of brown fat is mediated by the activation of β-adrenergic signaling and the regulatory effect of uncoupling protein 1 (UCP1). The former is mediated by norepinephrine which is released from the sympathetic nerve terminals, and the latter contributes to the generation of heat through the mitochondria (4). As a result, most efforts to induce brown fat thermogenesis in mammals have focused on developing β3-adrenergic receptor (AR) agonists. However, β3-AR is not specific to adipose tissue, and its global activation oftentimes leads to deleterious side effects. For this reason, recent efforts in the field have focused on better understanding the mechanisms of brown fat activation that bypass ARs.

BROWN/BEIGE ADIPOSE TISSUE BIOLOGY

Brown/Beige Adipose Tissue

In a healthy adult human, as much as 20–35% of the body weight is composed of white adipose tissue (WAT) (5), located predominantly in the subcutaneous and the visceral regions of the body. However, during disease states such as obesity, BMI can be above 30 kg/m^2. WAT serves as the main energy store for the body, while brown adipose tissue (BAT) dissipates energy into heat via non-shivering thermogenesis (6–8).

In humans, BAT is located primarily in the cervical, supra-clavicular, supra-adrenal, and para-spinal regions (2). Morphologically, brown adipocytes are composed of multilocular small droplets and abundant mitochondria, which play a crucial role in non-shivering thermogenesis. BAT innervation by the sympathetic nervous system is important for its development and activation (9). Classically, following cold exposure, norepinephrine is released from the sympathetic nervous system. It then binds to the β3-AR in brown adipocytes, leading to an activation of adenylyl cyclase, an increase in cAMP levels, and the activation of protein kinase A (PKA). This, in turn, induces lipolysis in brown adipocytes. Moreover, UCP1, a mitochondrial membrane protein expressed primarily in BAT, has been shown to play a key role in the process of non-shivering thermogenesis. It uncouples the respiratory chain of oxidative phosphorylation within the mitochondria, leading to a production of transmembrane proton flow and generation of heat. Prolonged β3-adrenergic stimulation has been demonstrated to be necessary for sustained thermogenic activity (10).

Beige adipocytes were defined by the Spiegelman group in 2012 (11). However, brown-like adipocytes in mice was described as early as 1984 by Young et al. (12). The cells were found to be distributed in WAT after cold exposure or adrenergic stimulation. Furthermore, beige adipocytes appear morphologically similar to brown adipocytes, express UCP1, and also generate heat in the form of non-shivering thermogenesis (13, 14). They are innervated by the sympathetic nervous system as well (14). Indeed the density of noradrenergic fibers dramatically increases in murine WAT depot after cold stimulation or transgenic overexpression of protein PR domain containing 16 (PRDM16), which is a main regulator of brown adipogenesis (15). This indicates the importance of sympathetic stimulus in the development of beige adipocytes. The presence of beige adipocytes in humans is supported not only by ^{18}FFDG-PET/CT imaging but also by anatomical and transcriptome profiling, revealing that the supra-clavicular region of ^{18}FFDG-positive depots mainly consists of beige adipocytes (16), while the cervical region consists of classical brown adipocytes (17).

Targeting Brown/Beige Fat Thermogenesis

While skeletal muscle-mediated shivering thermogenesis consumes a great deal of energy in cold, non-shivering thermogenesis contributes to energy expenditure even at low levels of cold stimulation. It has been shown that both BAT and skeletal muscle play a role in non-shivering thermogenesis (18, 19). Under mild cold conditions, UCP1-based thermogenesis in BAT and sarcolipin-based thermogenesis in skeletal muscle work synergistically. When either thermogenic processes is impaired, the other is upregulated to maintain temperature homeostasis in mice (20). However, the mechanism of this functional crosstalk between BAT and skeletal muscle remains unclear. Furthermore, during prolonged cold exposure, muscle shivering intensity decreases while BAT activity increases (21). This suggests a pivotal role of BAT in thermogenesis under thermal stress. Therefore, increasing BAT mass and activity by stimulating its development and adrenergic response can be strategies to combat obesity in mammals.

Crucially, scientists have discovered that classical brown adipocytes share a common progenitor with skeletal myocytes (22). It has been shown that PRDM16, peroxisome proliferator-activated receptor γ (PPARγ), and CCAAT/enhancer-binding protein β (C/EBPβ) are master regulators of brown adipogenesis. PRDM16 has been shown to control the switch between skeletal myoblasts and brown adipocytes (22). Moreover, it binds directly to PPARγ to stimulate brown adipogenesis. C/EBPβ has been shown to play a crucial role in BAT development as well (23), binding to PRDM16 and initiating the switch from myoblast to BAT differentiation (24). Additionally, data indicate that PRDM16 binds to many other regulatory factors including peroxisome proliferator-activated receptor γ-coactivator 1α (PGC1α), PGC1β, euchromatic histone-lysine N-methyltransferase 1 (EHMT1), C-terminal-binding proteins (CtBPs), and early B cell factor-2 (EBF2). It likely forms a complex with these factors to regulate brown/beige adipocyte development (25–28). Although active BAT has been detected by ^{18}FFDG-PET/CT imaging in adult humans after cold stimulation, it has primarily been found in people who are young and lean, with a lower BMI (3). Numerous studies have indicated that BAT activity is inversely related to BMI (8, 29–31). This may also likely be attributed to the increase in cold insulation and the subsequent protection of heat loss associated with higher adiposity. This paradox presents a challenge in simply targeting BAT to treat obese patients.

Since beige fat in humans is gradually recognized (16), scientists have honed on inducing beige adipogenesis to combat a variety of metabolic disorders. Unlike white or classic brown adipocytes, the origin of beige adipocytes is extremely heterogenous. Beige adipocytes have been reported to be

TABLE 1 | Molecules promotional for brown and/or beige adipogenesis and their potential targets.

Molecules	Potential targets	References
Thiazolidinediones	SIRT1-PPARγ	(43) (41)
Melatonin	UCP1-PGC-1α	(49)
Berberine	AMPK-PGC-1α and PRDM16	(50) (51)
Green tea	AMPK	(52)
Menthol	UCP1	(53)
Irisin	p38 MAPK-ERK	(54) (55)
Ginsenoside	PPARγ and AMPK	(56) (57)
Retinoic acid	p38 MAPK	(58)
Resveratrol	AMPK	(59)
Fenofibrate	PPARα	(38)
Curcumin	β3-AR	(60) (61)
Capsaicin	SIRT1-PPARγ-PRDM16	(39)
Artepillin C	UCP1 and PRDM16	(62)
Bitter melon seed oil	Mitochondrial uncoupling	(63)
Omega-3 fatty acid	UCP1	(64) (65)
Butein	Prdm4	(66)
Catecholamines	β-AR and mTORC1	(67)
Eicosapentaenoic acid	AMPK, PGC-1α, PPARγ, PRDM16, and UCP1	(68)
Dietary luteolin	AMPK and PGC-1α	(69)
AICAR	AMPK	(70)
Farnesol	PPARγ, CEBPα, and AMPK	(71)
Cryptotanshinone	AMPK and p38 MAPK	(72)
Albiflorin	AMPK and PI3K/AKT	(73)
Trans-anethole	AMPK-SIRT1-PPARα-PGC-1α	(74)
Magnolol	AMPK, PPARγ, and PKA	(75)
Xanthohumol	AMPK	(76)
(-)-Epigallocatechin-3-gallate (EGCG)	AMPK	(77)
L-Rhamnose	β3 -AR, SIRT1, PKA, and p-38	(78)
Grape pomace extract	PKA, AMPK, p38, and ERK PGC-1α, PPARγ, PRDM16, and UCP1	(79)
Phytol	AMPK	(80)
Raspberry	AMPKα1	(81)
Nobiletin	AMPK and PKA	(82)
Medicarpin	AMPK	(83)
Olaparib	AMPK- SIRT1	(84)
Genistein	AMPK	(85)
Dietary sea buckthorn pomace	AMPK-PGC-1α-UCP1	(86)
Zeaxanthin	AMPKα1	(87)
Trans-cinnamic Acid	AMPK	(88)
Metformin	AMPK	(89)
6-Gingerol	AMPK	(90)
Dietary apple polyphenols	AMPKα	(91)

AMPK, AMP-activated protein kinase; AR, adrenergic receptor; C/EBP, CCAAT/enhancer-binding protein; MAPK, mitogen-activated protein kinase; ERK, extracellular signal-regulated protein kinase; mTORC1, mammalian target of rapamycin complex 1; PI3K/AKT, phosphatidylinositol3kinase/protein kinase B; PPAR, peroxisome proliferator-activated receptor; PGC-1α, PPARγ coactivator-1α; Prdm, transcription factor positive regulatory domain; SIRT1, sirtuin 1; UCP, uncoupling protein.

transdifferentiated from white adipocytes (32, 33) or directly differentiated from distinct progenitors including PDGFRα$^+$ (34), mural (35, 36), or MyoD$^+$ progenitors (37). Numerous studies indicate that UCP1, one of the main regulators of adaptive thermogenesis, contributes to beige fat development (38–40). Moreover, classical beige adipocytes are governed by PRDM16 as well (41, 42). Deacetylation of PRDM16 and PPARγ by sirtuin 1 (SIRT1) stabilizes the PRDM16/PPARγ complex, contributing to beige adipogenesis (39, 43). Alternatively, SIRT1 is activated and regulated by Ca^{2+}/calmodulin-dependent protein kinase β (CaMKKβ) and AMP-activated protein kinase (AMPK) (44–46), the latter of which plays a role in fatty acid oxidation. Other positive regulators of beige adipogenesis include bone morphogenetic proteins (47) and fibroblast growth factor 21 (48).

For years, targeting the β-adrenergic signaling pathway has been the therapeutic strategy to induce beige adipogenesis and thereby combat obesity. A variety of natural compounds and clinical medications used for treating metabolic diseases, shown in **Table 1**, have been shown to induce beige fat development. Of note, irisin and berberine are two molecules which show stimulatory effects on beige fat and brown fat in humans (51, 55).

POTENTIAL ANTI-OBESITY DRUGS AND THEIR SAFETY

Adrenergic Receptor Agonists

Adrenergic signaling, in particular β3-AR, is a well-established pathway for BAT activation and beige fat development in response to cold temperatures. Common selective β3-AR agonists and antagonists have been summarized in a 2011 review by Bhadada et al. (92). Several β3-AR agonists have been shown to induce thermogenesis (93, 94). However, β3-AR are distributed throughout the body, including in the central nervous system, myocardium, blood vessels, smooth gastrointestinal and skeletal muscles, gallbladder, urinary bladder, prostate, etc. (95). Potential binding of β3-AR agonists with receptors located elsewhere may cause unexpected side effects.

Currently, some β3-AR agonists including mirabegron, vibegron, ritobegron, and solabegron have been extensively investigated. Some have even been approved for clinical use to treat overactive bladders and urinary incontinence (96–98). Although mirabegron has been found to induce BAT activity as measured by ^{18F}FDG-PET/CT (99), increase non-esterified fatty

acids by up to 68%, and boost resting energy expenditure by up to 5.8% (100) in humans, no β3-AR agonists has been approved to treat metabolic disorders thus far. The most common off-target binding sites of β3-AR agonists are myocardium and blood vessels (92, 101–103). Notably, it has been indicated that β3-AR stimulation is related to heart failure because of the negative inotropic effect of β3-AR agonists (104, 105). Additionally, different agonists present inconsistent effects on blood vessels (92). Some cause vasodilation, which may give rise to tachycardia, while others promote vasoconstriction, which is associated with high blood pressure. These potentially fatal side effects make β3-AR agonists unsuitable stimulants for thermogenic activity in the clinic.

PPARγ Receptor Agonists

PPAR receptors also play a critical role in regulating whole-body energy homeostasis. These receptors are abundantly expressed in adipose tissue, liver, and skeletal muscle, in addition to immune and gastrointestinal systems, and are known to regulate brown adipogenesis as well as glucose uptake and lipid biosynthesis in WAT (106, 107). PPARγ receptor agonists, such as troglitazone, rosiglitazone, and pioglitazone, have been applied to treat metabolic disorders and type 2 diabetes due to their insulin-sensitizing effects (108). However, due to side effects such as hepatotoxicity, myocardial infarction, bladder cancer, and heart failure, PPARγ receptor agonists have largely been withdrawn from the market (109). Although some PPARγ receptor agonists, such as pioglitazone, have been shown to cause weight gain in humans (110, 111), studies have indicated that rosiglitazone may induce beige fat development in mice through the activation of the SIRT1–PRDM16 pathway (41, 43). This suggests that PPARγ receptor agonists may be leveraged to combat obesity. Yet due to the potentially fatal side effects mentioned above, their clinical use remains problematic. Currently, several dual-acting PPARγ agonists have been synthesized. Promising studies have shown that certain PPARγ agonists may be beneficial in treating metabolic disorders with minimal off-target effects (112).

NON-CANONICAL MECHANISMS INVOLVED IN NON-SHIVERING THERMOGENESIS

AR activation triggers the process of non-shivering thermogenesis in response to cold, as shown in **Figure 1**,

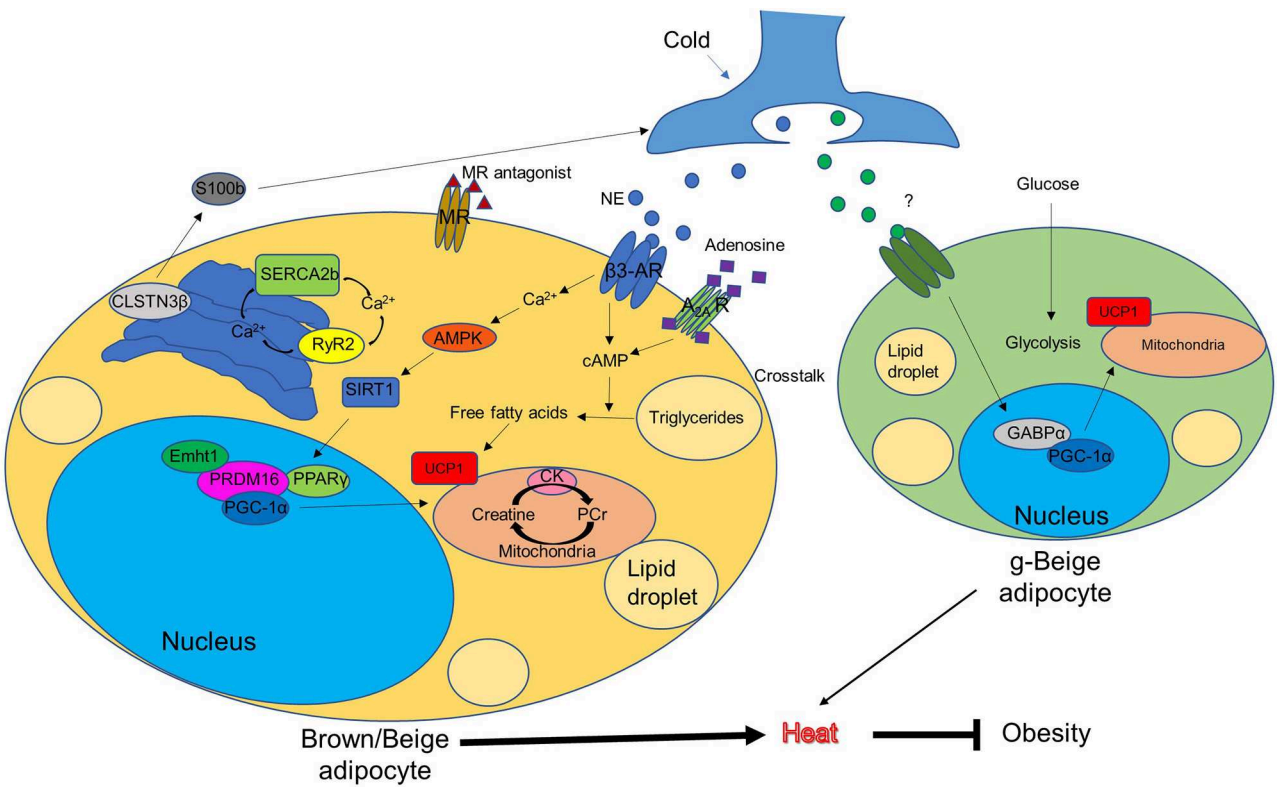

FIGURE 1 | Conventional and unconventional mechanisms of brown/beige thermogenesis (potential approaches to combat obesity). AMPK, AMP-activated protein kinase; AR, adrenergic receptor; CK, creatine kinase; CLSTN3β, calsyntenin3β; Ehmt1, euchromatic histone-lysine N-methyltransferase 1; GABPα, GA-binding protein α; g-beige adipocyte, glycolytic-beige adipocyte; MR, mineralocorticoid receptor; NE, norepinephrine; PCr, phosphocreatine; PPARγ, peroxisome proliferator-activated receptor gamma; PGC-1α, PPARγ coactivator-1α; PRDM16, protein PR domain containing 16; RyR2, ryanodine receptor 2; SERCA2b, sarco/endoplasmic reticulum Ca^{2+}-ATPase 2b; SIRT1, sirtuin 1; UCP1, uncoupling protein 1.

while mitochondrial membrane protein UCP1 is the key driver of heat production in BAT. The UCP1 levels in beige fat are lower than in BAT. This has previously led to the misconception that the contribution of beige fat in the regulation of whole-body energy balance is marginal (113). However, UCP1 knockout mice without functional BAT can gradually adapt to and survive cold temperatures by increasing their recruitment of beige fat (114, 115). This suggests that UCP1 may be dispensable for beige fat induction. This phenotype suggests that other UCP1-independent mechanisms are involved in beige fat-regulated energy homeostasis. Furthermore, several studies have identified other pathways which activate BAT or induce beige adipogenesis, independent of ARs signaling (37, 116, 117). Here we describe a few novel mechanisms that have recently been implicated in the thermogenic regulation of BAT and beige fat (**Figure 1**).

Adenosine–A_{2A} Receptor Signaling

A 2014 paper from the Pfeifer Lab describes adenosine–A_{2A} receptor signaling in response to sympathetic stimulation, which reduces levels of diet-induced obesity and improves glucose tolerance (116). After sympathetic stimulation by norepinephrine, brown adipocytes themselves release adenosine, which binds to A_{2A} receptors and contributes to energy expenditure. A_{2A} receptor knockout mice exhibit reduced thermogenesis and oxygen consumption in cold conditions compared to wild-type mice. Conversely, A_{2A} agonist treatment increases BAT activation and energy expenditure in mice. This highlights the important role of A_{2A} receptor in the regulation of energy expenditure in BAT. Furthermore, A2A stimulation by either its pharmacological activators or overexpression using lentiviral vector injections protects mice from diet-induced obesity while inducing beige fat development.

Mineralocorticoid Receptor Antagonism

In mice, mineralocorticoid receptor antagonists prevent high fat diet-induced decline in glucose tolerance and induce beige fat development in visceral and inguinal WAT as indicated by an upregulation of brown adipocyte-specific transcripts and increased levels of UCP1. These findings correspond to the results detected by 18^{F}FDG-PET/CT (117). Mineralocorticoid receptor antagonists reduce the autophagic rate in WAT depots. Moreover, when autophagy is repressed using its repressor bafilomycin A1, the effects mimic that of mineralocorticoid receptor antagonists. Furthermore, a more recent study in humans also indicates a positive correlation between mineralocorticoid receptor antagonism and BAT thermogenesis (118), suggesting the potential therapeutic benefit of mineralocorticoid receptor antagonism on obesity.

Calsyntenin3β-S100b Signaling

A recent study from Spiegelman's group has identified a thermogenic adipocyte-specific protein [calsyntenin3β (CLSTN3β)], which is primarily located on the endoplasmic reticulum. This protein promotes sympathetic innervation in adipose tissue in mice (119). Knockout or transgenic overexpression of CLSTN3β in mice impairs or enhances sympathetic innervation in BAT, respectively. CLSTN3β activation leads to the secretion of S100b, a trophic factor which stimulates neurite outgrowth, from the thermogenic adipocytes. S100b deficiency reduces sympathetic innervation in BAT, while the forced expression of S100b rescues the phenotype caused by CLSTN3β ablation. Therefore, selectively targeting CLSTN3β-S100b in thermogenic adipocytes may minimize the off-target side effects in other organs and provide a new therapeutic opportunity for promoting thermogenic anti-obesity effects.

Creatine-Driven Substrate Cycling

Another study from Spiegelman's group has identified arginine/creatine metabolism as a beige fat signature using quantitative mitochondrial proteomics (120). It contributes to beige fat-mediated energy expenditure and thermal homeostasis in mice. Cold exposure stimulates the activity of mitochondrial creatine kinase, which promotes creatine metabolism and in turn, increases ATP demand and induces ADP-dependent mitochondrial respiration in beige fat. Notably, in mice lacking UCP1, creatine metabolism compensatorily induces whole-body energy expenditure in response to cold. Furthermore, researchers identified phosphatase orphan 1 as a regulator of creatine-driven adipocyte respiration. It is concluded that creatine metabolism could be potentially targeted to increase basal energy expenditure.

Sarco/Endoplasmic Reticulum Ca^{2+}-ATPase 2b (SERCA2b)-Mediated Calcium Cycling

Another UCP1-independent signaling pathway in beige fat was described by our group. This novel mechanism involves sarco/endoplasmic reticulum Ca^{2+}-ATPase 2b (SERCA2b)-mediated calcium cycling, which ultimately regulates glucose metabolism (121). Unlike brown adipocytes, beige adipocytes display higher ATP synthesis capacity. In the absence of UCP1, they gain fuel from glucose through multiple metabolic ways including glycolysis, TCA metabolism, and the mitochondrial electron transport chain through the SERCA2b-ryanodine receptor 2 (RyR2) pathway. Of note, the transgenic overexpression of PRDM16 is still able to protect mice from diet-induced obesity in the absence of UCP1. The present study strongly suggests that UCP1 is dispensable in beige fat for non-shivering thermogenesis. SERCA2b-mediated calcium cycling represents an evolutionarily conserved mechanism for maintaining energy homeostasis.

Glycolytic Beige Fat

Our discovery of a distinct form of thermogenic cell was revolutionary in the field of fat biology. This cell, which was termed glycolytic beige adipocyte, exhibits adaptive thermogenesis and energy homeostasis in cold conditions in the absence of β-ARs signaling (37). These unique beige adipocytes are differentiated from $MyoD^{+}$ progenitors in inguinal WAT. The process is mediated by GA-binding protein α through a myogenic intermediate. To better understand the mechanism by which these cells improved glucose tolerance

and increased basal metabolism, we created a glycolytic beige fat-deficient mouse model. We found that glucose uptake, as detected by 18^{F}FDG-PET/CT, in the inguinal WAT of those mice is significantly reduced. Moreover, we noticed a decrease in oxygen consumption rate and extracellular acidification rate in isolated tissues. Glycolytic beige adipocytes are distinct from conventional beige adipocytes in their developmental origin, regulation, and enhanced glucose oxidation. This β-AR-independent pathway has opened up a new path for the treatment of obesity.

DISCUSSION AND PROSPECTS

In mammals, brown fat and beige fat play a crucial role in non-shivering thermogenesis and energy homeostasis. Inducing their development or activation is a viable approach to combat obesity. Classic brown fat and beige fat thermogenesis is mediated by β3-AR signaling and UCP1. Previous research has focused on the development of β3-AR agonists or PPARγ agonists to treat metabolic disorders including obesity. However, the clinical outcomes are unsatisfactory due to their deleterious side effects. The added stress from these agonists to the cardiovascular systems is particularly harmful (103, 104, 108).

Alternative pathways which bypass canonical thermogenic regulators are of great interest. Surprisingly, UCP1 knockout mice and β-AR knockout mice are able to acclimate to cold environments (114, 115). This suggests that other compensatory pathways, independent of UCP1 or β-AR, are involved in regulating whole-body thermogenesis and energy homeostasis. Pathways associated with this acclimation, shown in **Figure 1**, include: two non-AR-dependent pathways mediated by other thermogenic cell-expressing receptors, such as A_{2A} receptors and mineralocorticoid receptors, whose activation by adenosine or inhibition by its antagonists contribute to energy expenditure; the thermogenic adipocyte-specific CLSTN3β-S100b signaling pathway, which regulates thermogenesis through promoting the sympathetic innervation of the thermogenic adipose tissue; two distinct UCP1-independent pathways in beige fat, including creatine-driven substrate cycling and SERCA2b-RyR2 signaling, which compensate for the loss of UCP1 and contribute to energy expenditure; and a subtype of beige fat, originating from $MyoD^{+}$ progenitors, which is required for thermal regulation in the absence of β-ARs signaling.

It is important to note that these signaling pathways may only be a small part of the mechanisms involved in the regulation of BAT and beige fat on thermogenesis. Particularly, the role of beige fat in heat generation seems to be extremely multifaceted and, as such, is an active area of research. Notably, our group has identified glycolytic beige fat, marking for the first time that a subtype of beige fat has been described. We believe that multiple subtypes of beige fat with distinct origins and unique biological characterizations may exist. It is likely that there exists a robust crosstalk between different thermogenic cell types to maintain energy balance under different conditions. A better understanding of the plasticity of beige fat as well as of brown fat will likely provide new discoveries on metabolic adaptation and thus new therapeutic approaches to combat metabolic disorders including obesity.

AUTHOR CONTRIBUTIONS

RP and YC wrote the manuscript. RP, XZ, PM, and YC edited the manuscript.

FUNDING

This work was supported by a grant from Tongji Hospital in Huazhong University of Science and Technology (Grant No. 2201103295 to YC).

REFERENCES

1. Dawkins MJ, Scopes JW. Non-shivering thermogenesis and brown adipose tissue in the human new-born infant. *Nature.* (1965) 206:201–2. doi: 10.1038/206201b0
2. Nedergaard J, Bengtsson T, Cannon B. Unexpected evidence for active brown adipose tissue in adult humans. *Am J Physiol Endocrinol Metab.* (2007) 293:E444–52. doi: 10.1152/ajpendo.00691.2006
3. Matsushita M, Yoneshiro T, Aita S, Kameya T, Sugie H, Saito M. Impact of brown adipose tissue on body fatness and glucose metabolism in healthy humans. *Int J Obes.* (2014) 38:812–7. doi: 10.1038/ijo.2013.206
4. Rodriguez-Cuenca S, Pujol E, Justo R, Frontera M, Oliver J, Gianotti M, et al. Sex-dependent thermogenesis, differences in mitochondrial morphology and function, and adrenergic response in brown adipose tissue. *J Biol Chem.* (2002) 277:42958–63. doi: 10.1074/jbc.M207229200
5. Gallagher D, Visser M, Sepulveda D, Pierson RN, Harris T, Heymsfield SB. How useful is body mass index for comparison of body fatness across age, sex, and ethnic groups? *Am J Epidemiol.* (1996) 143:228–39. doi: 10.1093/oxfordjournals.aje.a008733
6. Rothwell NJ, Stock MJ. A role for brown adipose tissue in diet-induced thermogenesis. *Nature.* (1979) 281:31–5. doi: 10.1038/281031a0
7. Fischer AW, Schlein C, Cannon B, Heeren J, Nedergaard J. Intact innervation is essential for diet-induced recruitment of brown adipose tissue. *Am J Physiol Endocrinol Metab.* (2019) 316:E487–503. doi: 10.1152/ajpendo.00443.2018
8. Cypess AM, Lehman S, Williams G, Tal I, Rodman D, Goldfine AB, et al. Identification and importance of brown adipose tissue in adult humans. *N Engl J Med.* (2009) 360:1509–17. doi: 10.1056/NEJMoa0810780
9. Steiner G, Loveland M, Schonbaum E. Effect of denervation on brown adipose tissue metabolism. *Am J Physiol.* (1970) 218:566–70. doi: 10.1152/ajplegacy.1970.218.2.566
10. Young P, Wilson S, Arch JR. Prolonged beta-adrenoceptor stimulation increases the amount of GDP-binding protein in brown adipose tissue mitochondria. *Life Sci.* (1984) 34:1111–7. doi: 10.1016/0024-3205(84)90081-X
11. Wu J, Bostrom P, Sparks LM, Ye L, Choi JH, Giang AH, et al. Beige adipocytes are a distinct type of thermogenic fat cell in mouse and human. *Cell.* (2012) 150:366–76. doi: 10.1016/j.cell.2012.05.016
12. Young P, Arch JR, Ashwell M. Brown adipose tissue in the parametrial fat pad of the mouse. *FEBS Lett.* (1984) 167:10–4. doi: 10.1016/0014-5793(84)80822-4
13. Petrovic N, Walden TB, Shabalina IG, Timmons JA, Cannon B, Nedergaard J. Chronic peroxisome proliferator-activated receptor gamma (PPARgamma) activation of epididymally derived white adipocyte cultures reveals a population of thermogenically competent, UCP1-containing adipocytes

molecularly distinct from classic brown adipocytes. *J Biol Chem.* (2010) 285:7153–64. doi: 10.1074/jbc.M109.053942
14. Seale P, Conroe HM, Estall J, Kajimura S, Frontini A, Ishibashi J, et al. Prdm16 determines the thermogenic program of subcutaneous white adipose tissue in mice. *J Clin Invest.* (2011) 121:96–105. doi: 10.1172/JCI 44271
15. Murano I, Barbatelli G, Giordano A, Cinti S. Noradrenergic parenchymal nerve fiber branching after cold acclimatisation correlates with brown adipocyte density in mouse adipose organ. *J Anat.* (2009) 214:171–8. doi: 10.1111/j.1469-7580.2008.01001.x
16. Jespersen NZ, Larsen TJ, Peijs L, Daugaard S, Homoe P, Loft A, et al. A classical brown adipose tissue mRNA signature partly overlaps with brite in the supraclavicular region of adult humans. *Cell Metab.* (2013) 17:798–805. doi: 10.1016/j.cmet.2013.04.011
17. Cypess AM, White AP, Vernochet C, Schulz TJ, Xue R, Sass CA, et al. Anatomical localization, gene expression profiling and functional characterization of adult human neck brown fat. *Nat Med.* (2013) 19:635–9. doi: 10.1038/nm.3112
18. Aydin J, Shabalina IG, Place N, Reiken S, Zhang SJ, Bellinger AM, et al. Nonshivering thermogenesis protects against defective calcium handling in muscle. *FASEB J.* (2008) 22:3919–24. doi: 10.1096/fj.08-113712
19. Enerback S, Jacobsson A, Simpson EM, Guerra C, Yamashita H, Harper ME, et al. Mice lacking mitochondrial uncoupling protein are cold-sensitive but not obese. *Nature.* (1997) 387:90–4. doi: 10.1038/387090a0
20. Bal NC, Singh S, Reis FCG, Maurya SK, Pani S, Rowland LA, et al. Both brown adipose tissue and skeletal muscle thermogenesis processes are activated during mild to severe cold adaptation in mice. *J Biol Chem.* (2017) 292:16616–25. doi: 10.1074/jbc.M117.790451
21. Blondin DP, Daoud A, Taylor T, Tingelstad HC, Bezaire V, Richard D, et al. Four-week cold acclimation in adult humans shifts uncoupling thermogenesis from skeletal muscles to brown adipose tissue. *J Physiol.* (2017) 595:2099–113. doi: 10.1113/JP273395
22. Seale P, Bjork B, Yang W, Kajimura S, Chin S, Kuang S, et al. PRDM16 controls a brown fat/skeletal muscle switch. *Nature.* (2008) 454:961–7. doi: 10.1038/nature07182
23. Tanaka T, Yoshida N, Kishimoto T, Akira S. Defective adipocyte differentiation in mice lacking the C/EBPbeta and/or C/EBPdelta gene. *EMBO J.* (1997) 16:7432–43. doi: 10.1093/emboj/16.24.7432
24. Kajimura S, Seale P, Kubota K, Lunsford E, Frangioni JV, Gygi SP, et al. Initiation of myoblast to brown fat switch by a PRDM16-C/EBP-beta transcriptional complex. *Nature.* (2009) 460:1154–8. doi: 10.1038/nature08262
25. Seale P, Kajimura S, Yang W, Chin S, Rohas LM, Uldry M, et al. Transcriptional control of brown fat determination by PRDM16. *Cell Metab.* (2007) 6:38–54. doi: 10.1016/j.cmet.2007.06.001
26. Ohno H, Shinoda K, Ohyama K, Sharp LZ, Kajimura S. EHMT1 controls brown adipose cell fate and thermogenesis through the PRDM16 complex. *Nature.* (2013) 504:163–7. doi: 10.1038/nature12652
27. Kajimura S, Seale P, Tomaru T, Erdjument-Bromage H, Cooper MP, Ruas JL, et al. Regulation of the brown and white fat gene programs through a PRDM16/CtBP transcriptional complex. *Genes Dev.* (2008) 22:1397–409. doi: 10.1101/gad.1666108
28. Rajakumari S, Wu J, Ishibashi J, Lim HW, Giang AH, Won KJ, et al. EBF2 determines and maintains brown adipocyte identity. *Cell Metab.* (2013) 17:562–74. doi: 10.1016/j.cmet.2013.01.015
29. van Marken Lichtenbelt WD, Vanhommerig JW, Smulders NM, Drossaerts JM, Kemerink GJ, Bouvy ND, et al. Cold-activated brown adipose tissue in healthy men. *N Engl J Med.* (2009) 360:1500–8. doi: 10.1056/NEJMoa0808718
30. Saito M, Okamatsu-Ogura Y, Matsushita M, Watanabe K, Yoneshiro T, Nio-Kobayashi J, et al. High incidence of metabolically active brown adipose tissue in healthy adult humans: effects of cold exposure and adiposity. *Diabetes.* (2009) 58:1526–31. doi: 10.2337/db09-0530
31. Zingaretti MC, Crosta F, Vitali A, Guerrieri M, Frontini A, Cannon B, et al. The presence of UCP1 demonstrates that metabolically active adipose tissue in the neck of adult humans truly represents brown adipose tissue. *FASEB J.* (2009) 23:3113–20. doi: 10.1096/fj.09-133546
32. Barbatelli G, Murano I, Madsen L, Hao Q, Jimenez M, Kristiansen K, et al. The emergence of cold-induced brown adipocytes in mouse white fat depots is determined predominantly by white to brown adipocyte transdifferentiation. *Am J Physiol Endocrinol Metab.* (2010) 298:E1244–53. doi: 10.1152/ajpendo.00600.2009
33. Frontini A, Vitali A, Perugini J, Murano I, Romiti C, Ricquier D, et al. White-to-brown transdifferentiation of omental adipocytes in patients affected by pheochromocytoma. *Biochim Biophys Acta.* (2013) 1831:950–9. doi: 10.1016/j.bbalip.2013.02.005
34. Lee YH, Petkova AP, Granneman JG. Identification of an adipogenic niche for adipose tissue remodeling and restoration. *Cell Metab.* (2013) 18:355–67. doi: 10.1016/j.cmet.2013.08.003
35. Long JZ, Svensson KJ, Tsai L, Zeng X, Roh HC, Kong X, et al. A smooth muscle-like origin for beige adipocytes. *Cell Metab.* (2014) 19:810–20. doi: 10.1016/j.cmet.2014.03.025
36. Vishvanath L, MacPherson KA, Hepler C, Wang QA, Shao M, Spurgin SB, et al. Pdgfrbeta+ mural preadipocytes contribute to adipocyte hyperplasia induced by high-fat-diet feeding and prolonged cold exposure in adult mice. *Cell Metab.* (2016) 23:350–9. doi: 10.1016/j.cmet.2015.10.018
37. Chen Y, Ikeda K, Yoneshiro T, Scaramozza A, Tajima K, Wang Q, et al. Thermal stress induces glycolytic beige fat formation via a myogenic state. *Nature.* (2019) 565:180–5. doi: 10.1038/s41586-018-0801-z
38. Rachid TL, Penna-de-Carvalho A, Bringhenti I, Aguila MB, Mandarim-de-Lacerda CA, Souza-Mello V. Fenofibrate (PPARalpha agonist) induces beige cell formation in subcutaneous white adipose tissue from diet-induced male obese mice. *Mol Cell Endocrinol.* (2015) 402:86–94. doi: 10.1016/j.mce.2014.12.027
39. Baskaran P, Krishnan V, Ren J, Thyagarajan B. Capsaicin induces browning of white adipose tissue and counters obesity by activating TRPV1 channel-dependent mechanisms. *Br J Pharmacol.* (2016) 173:2369–89. doi: 10.1111/bph.13514
40. Bargut TCL, Souza-Mello V, Aguila MB, Mandarim-de-Lacerda CA. Browning of white adipose tissue: lessons from experimental models. *Horm Mol Biol Clin Investig.* (2017) 31. doi: 10.1515/hmbci-2016-0051
41. Ohno H, Shinoda K, Spiegelman BM, Kajimura S. PPARgamma agonists induce a white-to-brown fat conversion through stabilization of PRDM16 protein. *Cell Metab.* (2012) 15:395–404. doi: 10.1016/j.cmet.2012.01.019
42. Lo KA, Sun L. Turning WAT into BAT: a review on regulators controlling the browning of white adipocytes. *Biosci Rep.* (2013) 33:711–19. doi: 10.1042/BSR20130046
43. Qiang L, Wang L, Kon N, Zhao W, Lee S, Zhang Y, et al. Brown remodeling of white adipose tissue by SirT1-dependent deacetylation of PPARgamma. *Cell.* (2012) 150:620–32. doi: 10.1016/j.cell.2012.06.027
44. Passariello CL, Gottardi D, Cetrullo S, Zini M, Campana G, Tantini B, et al. Evidence that AMP-activated protein kinase can negatively modulate ornithine decarboxylase activity in cardiac myoblasts. *Biochim Biophys Acta.* (2012) 1823:800–7. doi: 10.1016/j.bbamcr.2011.12.013
45. Lau AW, Liu P, Inuzuka H, Gao D. SIRT1 phosphorylation by AMP-activated protein kinase regulates p53 acetylation. *Am J Cancer Res.* (2014) 4:245–55.
46. Peng Y, Rideout DA, Rakita SS, Gower WR Jr, You M, Murr MM, et al. Does LKB1 mediate activation of hepatic AMP-protein kinase (AMPK) and sirtuin1 (SIRT1) after Roux-en-Y gastric bypass in obese rats? *J Gastrointest Surg.* (2010) 14:221–8. doi: 10.1007/s11605-009-1102-5
47. Gustafson B, Hammarstedt A, Hedjazifar S, Hoffmann JM, Svensson PA, Grimsby J, et al. BMP4 and BMP antagonists regulate human white and beige adipogenesis. *Diabetes.* (2015) 64:1670–81. doi: 10.2337/db14-1127
48. Huang Z, Zhong L, Lee JTH, Zhang J, Wu D, Geng L, et al. The FGF21-CCL11 axis mediates beiging of white adipose tissues by coupling sympathetic nervous system to type 2 immunity. *Cell Metab.* (2017) 26:493–508.e4. doi: 10.1016/j.cmet.2017.08.003
49. Jimenez-Aranda A, Fernandez-Vazquez G, Campos D, Tassi M, Velasco-Perez L, Tan DX, et al. Melatonin induces browning of inguinal white adipose tissue in Zucker diabetic fatty rats. *J Pineal Res.* (2013) 55:416–23. doi: 10.1111/jpi.12089
50. Zhang Z, Zhang H, Li B, Meng X, Wang J, Zhang Y, et al. Berberine activates thermogenesis in white and brown adipose tissue. *Nat Commun.* (2014) 5:5493. doi: 10.1038/ncomms6493
51. Wu L, Xia M, Duan Y, Zhang L, Jiang H, Hu X, et al. Berberine promotes the recruitment and activation of brown adipose tissue in mice and humans. *Cell Death Dis.* (2019) 10:468. doi: 10.1038/s41419-019-1706-y
52. Yamashita Y, Wang L, Wang L, Tanaka Y, Zhang T, Ashida H. Oolong, black and pu-erh tea suppresses adiposity in mice via activation of AMP-activated protein kinase. *Food Funct.* (2014) 5:2420–9. doi: 10.1039/C4FO00095A

53. Rossato M, Granzotto M, Macchi V, Porzionato A, Petrelli L, Calcagno A, et al. Human white adipocytes express the cold receptor TRPM8 which activation induces UCP1 expression, mitochondrial activation and heat production. *Mol Cell Endocrinol.* (2014) 383:137–46. doi: 10.1016/j.mce.2013.12.005
54. Zhang Y, Li R, Meng Y, Li S, Donelan W, Zhao Y, et al. Irisin stimulates browning of white adipocytes through mitogen-activated protein kinase p38 MAP kinase and ERK MAP kinase signaling. *Diabetes.* (2014) 63:514–25. doi: 10.2337/db13-1106
55. Zhang Y, Xie C, Wang H, Foss RM, Clare M, George EV, et al. Irisin exerts dual effects on browning and adipogenesis of human white adipocytes. *Am J Physiol Endocrinol Metab.* (2016) 311:E530–41. doi: 10.1152/ajpendo.00094.2016
56. Mu Q, Fang X, Li X, Zhao D, Mo F, Jiang G, et al. Ginsenoside Rb1 promotes browning through regulation of PPARgamma in 3T3-L1 adipocytes. *Biochem Biophys Res Commun.* (2015) 466:530–5. doi: 10.1016/j.bbrc.2015.09.064
57. Kim K, Nam KH, Yi SA, Park JW, Han JW, Lee J. Ginsenoside Rg3 induces browning of 3T3-L1 adipocytes by activating AMPK signaling. *Nutrients.* (2020) 12. doi: 10.3390/nu12020427
58. Wang J, Sun GJ, Ding J, Zhang JX, Cui Y, Li HR, et al. WY14643 combined with all-trans retinoic acid acts via p38 MAPK to induce "browning" of white adipocytes in mice. *Genet Mol Res.* (2015) 14:6978–84. doi: 10.4238/2015.June.26.6
59. Wang S, Liang X, Yang Q, Fu X, Rogers CJ, Zhu M, et al. Resveratrol induces brown-like adipocyte formation in white fat through activation of AMP-activated protein kinase (AMPK) alpha1. *Int J Obes.* (2015) 39:967–76. doi: 10.1038/ijo.2015.23
60. Wang S, Wang X, Ye Z, Xu C, Zhang M, Ruan B, et al. Curcumin promotes browning of white adipose tissue in a norepinephrine-dependent way. *Biochem Biophys Res Commun.* (2015) 466:247–53. doi: 10.1016/j.bbrc.2015.09.018
61. Zhang X, Tian Y, Zhang H, Kavishwar A, Lynes M, Brownell AL, et al. Curcumin analogues as selective fluorescence imaging probes for brown adipose tissue and monitoring browning. *Sci Rep.* (2015) 5:13116. doi: 10.1038/srep13116
62. Nishikawa S, Aoyama H, Kamiya M, Higuchi J, Kato A, Soga M, et al. Artepillin C, a typical Brazilian propolis-derived component, induces brown-like adipocyte formation in C3H10T1/2 cells, primary inguinal white adipose tissue-derived adipocytes, and mice. *PLoS ONE.* (2016) 11:e0162512. doi: 10.1371/journal.pone.0162512
63. Chang YY, Su HM, Chen SH, Hsieh WT, Chyuan JH, Chao PM. Roles of peroxisome proliferator-activated receptor alpha in bitter melon seed oil-corrected lipid disorders and conversion of alpha-eleostearic acid into rumenic acid in C57BL/6J mice. *Nutrients.* (2016) 8:805. doi: 10.3390/nu8120805
64. Simopoulos A. The FTO gene, browning of adipose tissue and omega-3 fatty acids. *J Nutrigenet Nutrigenomics.* (2016) 9:123–6. doi: 10.1159/000448617
65. Simopoulos AP. An increase in the omega-6/omega-3 fatty acid ratio increases the risk for obesity. *Nutrients.* (2016) 8:128. doi: 10.3390/nu8030128
66. Song NJ, Choi S, Rajbhandari P, Chang SH, Kim S, Vergnes L, et al. Prdm4 induction by the small molecule butein promotes white adipose tissue browning. *Nat Chem Biol.* (2016) 12:479–81. doi: 10.1038/nchembio.2081
67. Liu D, Bordicchia M, Zhang C, Fang H, Wei W, Li JL, et al. Activation of mTORC1 is essential for beta-adrenergic stimulation of adipose browning. *J Clin Invest.* (2016) 126:1704–16. doi: 10.1172/JCI83532
68. Laiglesia LM, Lorente-Cebrian S, Prieto-Hontoria PL, Fernandez-Galilea M, Ribeiro SM, Sainz N, et al. Eicosapentaenoic acid promotes mitochondrial biogenesis and beige-like features in subcutaneous adipocytes from overweight subjects. *J Nutr Biochem.* (2016) 37:76–82. doi: 10.1016/j.jnutbio.2016.07.019
69. Zhang X, Zhang QX, Wang X, Zhang L, Qu W, Bao B, et al. Dietary luteolin activates browning and thermogenesis in mice through an AMPK/PGC1alpha pathway-mediated mechanism. *Int J Obes.* (2016) 40:1841–9. doi: 10.1038/ijo.2016.108
70. Abdul-Rahman O, Kristof E, Doan-Xuan QM, Vida A, Nagy L, Horvath A, et al. AMP-activated kinase (AMPK) activation by AICAR in human white adipocytes derived from pericardial white adipose tissue stem cells induces a partial beige-like phenotype. *PLoS ONE.* (2016) 11:e0157644. doi: 10.1371/journal.pone.0157644
71. Kim HL, Jung Y, Park J, Youn DH, Kang J, Lim S, et al. Farnesol has an anti-obesity effect in high-fat diet-induced obese mice and induces the development of beige adipocytes in human adipose tissue derived-mesenchymal stem cells. *Front Pharmacol.* (2017) 8:654. doi: 10.3389/fphar.2017.00654
72. Imran KM, Rahman N, Yoon D, Jeon M, Lee BT, Kim YS. Cryptotanshinone promotes commitment to the brown adipocyte lineage and mitochondrial biogenesis in C3H10T1/2 mesenchymal stem cells via AMPK and p38-MAPK signaling. *Biochim Biophys Acta Mol Cell Biol Lipids.* (2017) 1862:1110–20. doi: 10.1016/j.bbalip.2017.08.001
73. Jeong MY, Park J, Youn DH, Jung Y, Kang J, Lim S, et al. Albiflorin ameliorates obesity by inducing thermogenic genes via AMPK and PI3K/AKT *in vivo* and *in vitro*. *Metabolism.* (2017) 73:85–99. doi: 10.1016/j.metabol.2017.05.009
74. Kang NH, Mukherjee S, Min T, Kang SC, Yun JW. Trans-anethole ameliorates obesity via induction of browning in white adipocytes and activation of brown adipocytes. *Biochimie.* (2018) 151:1–13. doi: 10.1016/j.biochi.2018.05.009
75. Parray HA, Lone J, Park JP, Choi JW, Yun JW. Magnolol promotes thermogenesis and attenuates oxidative stress in 3T3-L1 adipocytes. *Nutrition.* (2018) 50:82–90. doi: 10.1016/j.nut.2018.01.017
76. Samuels JS, Shashidharamurthy R, Rayalam S. Novel anti-obesity effects of beer hops compound xanthohumol: role of AMPK signaling pathway. *Nutr Metab.* (2018) 15:42. doi: 10.1186/s12986-018-0277-8
77. Mi Y, Liu X, Tian H, Liu H, Li J, Qi G, et al. EGCG stimulates the recruitment of brite adipocytes, suppresses adipogenesis and counteracts TNF-alpha-triggered insulin resistance in adipocytes. *Food Funct.* (2018) 9:3374–86. doi: 10.1039/C8FO00167G
78. Choi M, Mukherjee S, Kang NH, Barkat JL, Parray HA, Yun JW. L-rhamnose induces browning in 3T3-L1 white adipocytes and activates HIB1B brown adipocytes. *IUBMB Life.* (2018) 70:563–73. doi: 10.1002/iub.1750
79. Rodriguez Lanzi C, Perdicaro DJ, Landa MS, Fontana A, Antoniolli A, Miatello RM, et al. Grape pomace extract induced beige cells in white adipose tissue from rats and in 3T3-L1 adipocytes. *J Nutr Biochem.* (2018) 56:224–33. doi: 10.1016/j.jnutbio.2018.03.001
80. Zhang F, Ai W, Hu X, Meng Y, Yuan C, Su H, et al. Phytol stimulates the browning of white adipocytes through the activation of AMP-activated protein kinase (AMPK) alpha in mice fed high-fat diet. *Food Funct.* (2018) 9:2043–50. doi: 10.1039/C7FO01817G
81. Zou T, Wang B, Yang Q, de Avila JM, Zhu MJ, You J, et al. Raspberry promotes brown and beige adipocyte development in mice fed high-fat diet through activation of AMP-activated protein kinase (AMPK) alpha1. *J Nutr Biochem.* (2018) 55:157–64. doi: 10.1016/j.jnutbio.2018.02.005
82. Lone J, Parray HA, Yun JW. Nobiletin induces brown adipocyte-like phenotype and ameliorates stress in 3T3-L1 adipocytes. *Biochimie.* (2018) 146:97–104. doi: 10.1016/j.biochi.2017.11.021
83. Imran KM, Yoon D, Kim YS. A pivotal role of AMPK signaling in medicarpin-mediated formation of brown and beige. *Biofactors.* (2018) 44:168–79. doi: 10.1002/biof.1392
84. Nagy L, Rauch B, Balla N, Ujlaki G, Kis G, Abdul-Rahman O, et al. Olaparib induces browning of *in vitro* cultures of human primary white adipocytes. *Biochem Pharmacol.* (2019) 167:76–85. doi: 10.1016/j.bcp.2019.06.022
85. Palacios-Gonzalez B, Vargas-Castillo A, Velazquez-Villegas LA, Vasquez-Reyes S, Lopez P, Noriega LG, et al. Genistein increases the thermogenic program of subcutaneous WAT and increases energy expenditure in mice. *J Nutr Biochem.* (2019) 68:59–68. doi: 10.1016/j.jnutbio.2019.03.012
86. Zhang T, Deng B, Zhang R, Qin X, Zhang J, Zhao J. Dietary sea buckthorn pomace induces beige adipocyte formation in inguinal white adipose tissue in lambs. *Animals.* (2019) 9:193. doi: 10.3390/ani9040193
87. Liu M, Zheng M, Cai D, Xie J, Jin Z, Liu H, et al. Zeaxanthin promotes mitochondrial biogenesis and adipocyte browning via AMPKalpha1 activation. *Food Funct.* (2019) 10:2221–33. doi: 10.1039/C8FO02527D
88. Kang NH, Mukherjee S, Yun JW. Trans-cinnamic acid stimulates white fat browning and activates brown adipocytes. *Nutrients.* (2019) 11:577. doi: 10.3390/nu11030577

89. Auger C, Knuth CM, Abdullahi A, Samadi O, Parousis A, Jeschke MG. Metformin prevents the pathological browning of subcutaneous white adipose tissue. *Mol Metab.* (2019) 29:12–23. doi: 10.1016/j.molmet.2019.08.011
90. Wang J, Zhang L, Dong L, Hu X, Feng F, and Chen F. 6-gingerol, a functional polyphenol of ginger, promotes browning through an AMPK-dependent pathway in 3T3-L1 adipocytes. *J Agric Food Chem.* (2019) 67:14056–65. doi: 10.1021/acs.jafc.9b05072
91. Zou T, Wang B, Li S, Liu Y, You J. Dietary apple polyphenols promote fat browning in high-fat diet-induced obese mice through activation of adenosine monophosphate-activated protein kinase alpha. *J Sci Food Agric.* (2020) 100:2389–98. doi: 10.1002/jsfa.10248
92. Bhadada SV, Patel BM, Mehta AA, Goyal RK. beta(3) receptors: role in cardoimetabolic disorders. *Ther Adv Endocrinol Metab.* (2011) 2:65–79. doi: 10.1177/2042018810390259
93. Gong DW, He Y, Karas M, Reitman M. Uncoupling protein-3 is a mediator of thermogenesis regulated by thyroid hormone, beta3-adrenergic agonists, and leptin. *J Biol Chem.* (1997) 272:24129–32. doi: 10.1074/jbc.272.39.24129
94. Nedergaard J, Cannon B. The 'novel' 'uncoupling' proteins UCP2 and UCP3: what do they really do? Pros and cons for suggested functions. *Exp Physiol.* (2003) 88:65–84. doi: 10.1113/eph8802502
95. Ursino MG, Vasina V, Raschi E, Crema F, De Ponti F. The beta3-adrenoceptor as a therapeutic target: current perspectives. *Pharmacol Res.* (2009) 59:221–34. doi: 10.1016/j.phrs.2009.01.002
96. Vonesh E, Gooch KL, Khangulov V, Schermer CR, Johnston KM, Szabo SM, et al. Cardoivascular risk profile in individuals initiating treatment for overactive bladder - challenges and learnings for comparative analysis using linked claims and electronic medical record databases. *PLoS ONE.* (2018) 13:e0205640. doi: 10.1371/journal.pone.0205640
97. Mitcheson HD, Samanta S, Muldowney K, Pinto CA, Rocha BA, Green S, et al. Vibegron (RVT-901/MK-4618/KRP-114V) administered once daily as monotherapy or concomitantly with tolterodine in patients with an overactive bladder: a multicenter, phase IIb, randomized, double-blind, controlled trial. *Eur Urol.* (2019) 75:274–82. doi: 10.1016/j.eururo.2018.10.006
98. Keam SJ. Vibegron: first global approval. *Drugs.* (2018) 78:1835–9. doi: 10.1007/s40265-018-1006-3
99. Cypess AM, Weiner LS, Roberts-Toler C, Franquet Elia E, Kessler SH, Kahn PA, et al. Activation of human brown adipose tissue by a beta3-adrenergic receptor agonist. *Cell Metab.* (2015) 21:33–8. doi: 10.1016/j.cmet.2014.12.009
100. Baskin AS, Linderman JD, Brychta RJ, McGehee S, Anflick-Chames E, Cero C, et al. Regulation of human adipose tissue activation, gallbladder size, and bile acid metabolism by a beta3-adrenergic receptor agonist. *Diabetes.* (2018) 67:2113–25. doi: 10.2337/db18-0462
101. Arch JR. Challenges in beta(3)-adrenoceptor agonist drug development. *Ther Adv Endocrinol Metab.* (2011) 2:59–64. doi: 10.1177/2042018811398517
102. Malik M, van Gelderen EM, Lee JH, Kowalski DL, Yen M, Goldwater R, et al. Proarrhythmic safety of repeat doses of mirabegron in healthy subjects: a randomized, double-blind, placebo-, and active-controlled thorough QT study. *Clin Pharmacol Ther.* (2012) 92:696–706. doi: 10.1038/clpt.2012.181
103. Loh RKC, Formosa MF, La Gerche A, Reutens AT, Kingwell BA, Carey AL. Acute metabolic and cardoivascular effects of mirabegron in healthy individuals. *Diabetes Obes Metab.* (2019) 21:276–84. doi: 10.1111/dom.13516
104. Cheng HJ, Zhang ZS, Onishi K, Ukai T, Sane DC, Cheng CP. Upregulation of functional beta(3)-adrenergic receptor in the failing canine myocardium. *Circ Res.* (2001) 89:599–606. doi: 10.1161/hh1901.098042
105. Zhang ZS, Cheng HJ, Onishi K, Ohte N, Wannenburg T, Cheng CP. Enhanced inhibition of L-type Ca^{2+} current by beta3-adrenergic stimulation in failing rat heart. *J Pharmacol Exp Ther.* (2005) 315:1203–11. doi: 10.1124/jpet.105.089672
106. Zhou T, Yan X, Wang G, Liu H, Gan X, Zhang T, et al. Evolutionary pattern and regulation analysis to support why diversity functions existed within PPAR gene family members. *Biomed Res Int.* (2015) 2015:613910. doi: 10.1155/2015/613910
107. Diamant M, Heine RJ. Thiazolidinedoines in type 2 diabetes mellitus: current clinical evidence. *Drugs.* (2003) 63:1373–405. doi: 10.2165/00003495-200363130-00004
108. Nanjan MJ, Mohammed M, Prashantha Kumar BR, Chandrasekar MJN. Thiazolidinedoines as antidiabetic agents: a critical review. *Bioorg Chem.* (2018) 77:548–67. doi: 10.1016/j.bioorg.2018.02.009
109. Kung J, Henry RR. Thiazolidinedione safety. *Expert Opin Drug Saf.* (2012) 11:565–79. doi: 10.1517/14740338.2012.691963
110. Berhanu P, Perez A, Yu S. Effect of pioglitazone in combination with insulin therapy on glycaemic control, insulin dose requirement and lipid profile in patients with type 2 diabetes previously poorly controlled with combination therapy. *Diabetes Obes Metab.* (2007) 9:512–20. doi: 10.1111/j.1463-1326.2006.00633.x
111. Mattoo V, Eckland D, Widel M, Duran S, Fajardo C, Strand J, et al. Metabolic effects of pioglitazone in combination with insulin in patients with type 2 diabetes mellitus whose disease is not adequately controlled with insulin therapy: results of a six-month, randomized, double-blind, prospective, multicenter, parallel-group study. *Clin Ther.* (2005) 27:554–67. doi: 10.1016/j.clinthera.2005.05.005
112. Ammazzalorso A, Maccallini C, Amoia P, Amoroso R. Multitarget PPARgamma agonists as innovative modulators of the metabolic syndrome. *Eur J Med Chem.* (2019) 173:261–73. doi: 10.1016/j.ejmech.2019.04.030
113. Nedergaard J, Cannon B. UCP1 mRNA does not produce heat. *Biochim Biophys Acta.* (2013) 1831:943–9. doi: 10.1016/j.bbalip.2013.01.009
114. Meyer CW, Willershauser M, Jastroch M, Rourke BC, Fromme T, Oelkrug R, et al. Adaptive thermogenesis and thermal conductance in wild-type and UCP1-KO mice. *Am J Physiol Regul Integr Comp Physiol.* (2010) 299:R1396–406. doi: 10.1152/ajpregu.00021.2009
115. Ukropec J, Anunciado RP, Ravussin Y, Hulver MW, Kozak LP. UCP1-independent thermogenesis in white adipose tissue of cold-acclimated Ucp1-/- mice. *J Biol Chem.* (2006) 281:31894–908. doi: 10.1074/jbc.M606114200
116. Gnad T, Scheibler S, von Kugelgen I, Scheele C, Kilic A, Glode A, et al. Adenosine activates brown adipose tissue and recruits beige adipocytes via A2A receptors. *Nature.* (2014) 516:395–9. doi: 10.1038/nature13816
117. Armani A, Cinti F, Marzolla V, Morgan J, Cranston GA, Antelmi A, et al. Mineralocorticoid receptor antagonism induces browning of white adipose tissue through impairment of autophagy and prevents adipocyte dysfunction in high-fat-diet-fed mice. *FASEB J.* (2014) 28:3745–57. doi: 10.1096/fj.13-245415
118. Thuzar M, Law WP, Dimeski G, Stowasser M, Ho KKY. Mineralocorticoid antagonism enhances brown adipose tissue function in humans: a randomized placebo-controlled cross-over study. *Diabetes Obes Metab.* (2019) 21:509–16. doi: 10.1111/dom.13539
119. Zeng X, Ye M, Resch JM, Jedrychowski MP, Hu B, Lowell BB, et al. Innervation of thermogenic adipose tissue via a calsyntenin 3beta-S100b axis. *Nature.* (2019) 569:229–35. doi: 10.1038/s41586-019-1156-9
120. Kazak L, Chouchani ET, Jedrychowski MP, Erickson BK, Shinoda K, Cohen P, et al. A creatine-driven substrate cycle enhances energy expenditure and thermogenesis in beige fat. *Cell.* (2015) 163:643–55. doi: 10.1016/j.cell.2015.09.035
121. Ikeda K, Kang Q, Yoneshiro T, Camporez JP, Maki H, Homma M, et al. UCP1-independent signaling involving SERCA2b-mediated calcium cycling regulates beige fat thermogenesis and systemic glucose homeostasis. *Nat Med.* (2017) 23:1454–65. doi: 10.1038/nm.4429

Conflict of Interest: The authors declare that the research was conducted in the absence of any commercial or financial relationships that could be construed as a potential conflict of interest.

The handling editor declared a past co-authorship with the authors YC.

frontiers in Endocrinology

REVIEW
published: 16 April 2020
doi: 10.3389/fendo.2020.00145

Role of Brown Adipose Tissue in Adiposity Associated With Narcolepsy Type 1

Maaike E. Straat[1,2]*, *Mink S. Schinkelshoek*[3,4], *Rolf Fronczek*[3,4], *Gerrit Jan Lammers*[3,4], *Patrick C. N. Rensen*[1,2] *and Mariëtte R. Boon*[1,2]

[1] Division of Endocrinology, Department of Medicine, Leiden University Medical Center, Leiden, Netherlands, [2] Einthoven Laboratory for Experimental Vascular Medicine, Leiden University Medical Center, Leiden, Netherlands, [3] Department of Neurology, Leiden University Medical Center, Leiden, Netherlands, [4] Sleep Wake Centre SEIN, Heemstede, Netherlands

Narcolepsy type 1 is a neurological sleep-wake disorder caused by the destruction of orexin (hypocretin)-producing neurons. These neurons are particularly located in the lateral hypothalamus and have widespread projections throughout the brain, where they are involved, e.g., in the regulation of the sleep-wake cycle and appetite. Interestingly, a higher prevalence of obesity has been reported in patients with narcolepsy type 1 compared to healthy controls, despite a normal to decreased food intake and comparable physical activity. This suggests the involvement of tissues implicated in total energy expenditure, including skeletal muscle, liver, white adipose tissue (WAT), and brown adipose tissue (BAT). Recent evidence from pre-clinical studies with orexin knock-out mice demonstrates a crucial role for the orexin system in the functionality of brown adipose tissue (BAT), probably through multiple pathways. Since BAT is a highly metabolically active organ that combusts fatty acids and glucose toward heat, thereby contributing to energy metabolism, this raises the question of whether BAT plays a role in the development of obesity and related metabolic diseases in narcolepsy type 1. BAT is densely innervated by the sympathetic nervous system that activates BAT, for instance, following cold exposure. The sympathetic outflow toward BAT is mainly mediated by the dorsomedial, ventromedial, arcuate, and paraventricular nuclei in the hypothalamus. This review focuses on the current knowledge on the role of the orexin system in the control of energy balance, with specific focus on BAT metabolism and adiposity in both preclinical and clinical studies.

Keywords: brown adipose tissue, energy metabolism, hypothalamus, narcolepsy type 1, obesity, orexin, sympathetic nervous system

OPEN ACCESS

Edited by:
Massimiliano Caprio, Università telematica San Raffaele, Italy

Reviewed by:
Carmelo Quarta, Institut National de la Santé et de la Recherche Médicale (INSERM), France
Thomas Alexander Lutz, University of Zurich, Switzerland

***Correspondence:**
Maaike E. Straat
m.e.straat@lumc.nl

Specialty section:
This article was submitted to Obesity, a section of the journal Frontiers in Endocrinology

Received: *01 December 2019*
Accepted: *02 March 2020*
Published: *16 April 2020*

Citation:
Straat ME, Schinkelshoek MS, Fronczek R, Lammers GJ, Rensen PCN and Boon MR (2020) Role of Brown Adipose Tissue in Adiposity Associated With Narcolepsy Type 1. Front. Endocrinol. 11:145. doi: 10.3389/fendo.2020.00145

INTRODUCTION

Narcolepsy type 1 is a sleep-wake disorder characterized by excessive daytime sleepiness and episodes of sudden muscle weakness, known as cataplexy. Narcolepsy type 1 is caused by the loss of more than 90% of orexin-producing neurons in the hypothalamus (1). For several decades, a higher prevalence of obesity has been reported in patients with narcolepsy type 1 compared to healthy controls, despite a normal to decreased food intake (2, 3). However, the mechanism underlying the increased adiposity in this patient population remains unclear and may involve tissues implicated in total energy expenditure including skeletal muscle, liver, white adipose tissue,

and brown adipose tissue (BAT). Indeed, results from preclinical studies suggest a role for BAT in the increased adiposity after disease onset. The purpose of this review is to give an overview of the current knowledge on the role of the orexin system in the control of energy balance including food intake and energy expenditure with special emphasis on BAT metabolism. The ultimate aim is to increase the knowledge on the pathophysiology of adiposity development in patients with narcolepsy type 1.

NARCOLEPSY TYPE 1: EPIDEMIOLOGY AND PATHOPHYSIOLOGY

Narcolepsy type 1 is a rare neurological disorder characterized by a dysregulated sleep-wake cycle. Age of onset peaks in adolescence and the disease affects around 15–50 per 100,000 individuals in the United States and Europe. Whether gender differences in the prevalence of narcolepsy type 1 exist is still unclear, since several epidemiological studies in Europe and the United States show inconsistent results (4–6). Narcolepsy type 1 is caused by the destruction of orexin-producing neurons in the hypothalamus. The exact pathophysiology remains unclear, but it is presumably caused by multiple triggers, eventually leading to an autoimmune-mediated destruction of these neurons (1). Projections of orexin-producing neurons extend throughout the brain, where they, amongst others, are involved in the regulation of wakefulness, metabolic circuits, and autonomic function (1, 7, 8). The main symptoms of narcolepsy type 1 include excessive daytime sleepiness and cataplexy (1). Cataplexy is the sudden bilateral loss of muscle tone evoked by an emotional trigger, frequently after laughter. Consciousness is typically preserved in these attacks, which are mostly of short duration (9). Other symptoms of narcolepsy type 1 comprise, amongst others, sleep paralysis, hypnagogic and hypnopompic hallucinations, and fragmented night sleep (1).

ADIPOSITY IN NARCOLEPSY TYPE 1

Interestingly, apart from symptoms associated with a dysregulated sleep-wake cycle, obesity, defined as a body mass index above 30 kg/m^2, is significantly more prevalent in patients with narcolepsy type 1 compared with the general population. Already in 1934, an increased prevalence of obesity amongst patients with narcolepsy type 1 was reported (2). In the following decades, the BMI of patients with narcolepsy type 1 was repeatedly confirmed to be higher compared to the general population (10–14). It is estimated that obesity affects around 30% of patients with narcolepsy type 1, without statistically proven differences between men and women (11–13). A study performed in France even reported rates over 50% in children with narcolepsy type 1 (14). In comparison, the prevalence of obesity in the European Union was 14.9% in 2017 (15). Studies comparing patients with narcolepsy type 1 with patients who are diagnosed with idiopathic hypersomnia, a neurologic disorder characterized by excessive daytime sleepiness but with normal orexin signaling, found that patients with narcolepsy type 1 have a significantly higher BMI and a larger waist circumference compared with patients with idiopathic hypersomnia (12, 16). Moreover, children diagnosed with narcolepsy type 1 rapidly gain weight shortly after disease onset (17). This suggests a direct pathogenic link between a decreased orexin signaling and higher BMI in narcolepsy type 1, rather than disease-related behavior leading to weight gain. In order to understand the pathophysiological link between orexin and obesity, a further understanding of the orexin system is needed.

THE OREXIN SYSTEM: AN OVERVIEW

Orexin A and orexin B, also known as hypocretin 1 and hypocretin 2, are neuropeptides discovered in 1998, by two independent research groups who both gave the peptides a different name (18, 19). The group who gave the neuropeptides the name "orexin," which is derived from the Greek word for "appetite,"ὄρεξις, recognized the orexin system as a regulator of the feeding system. This was due to the finding that the orexin-producing neurons are located in the lateral hypothalamic area (LHA), which was known as the main regulator of the feeding system (18, 20). The name "hypocretin" highlights both the hypothalamic origin and morphologic resemblance to incretin hormones (19). The neuropeptides are synthesized from a precursor peptide, prepro-orexin, and are produced by orexin-producing neurons mainly located in the LHA but also in the perifornical area, dorsomedial hypothalamic area (DMH), and posterior hypothalamus (21). Both orexin neuropeptides are able to bind to two G-protein coupled receptors, orexin receptor type 1 (OXR1), and orexin receptor type 2 (OXR2). Orexin A, compared to orexin B, has a 10 times higher affinity for OXR1, and both orexins have the same affinity for OXR2 (18). The two types of orexins and receptors appear to have a partly overlapping and partly distinct function (22). Besides orexins, the orexin-producing neurons also release other neuromodulators, such as glutamate, dynorphin, and neuronal activity-regulated pentraxin (NARP) (23–25).

The orexin-producing neurons have extended projections throughout the central nervous system, where they fulfill multiple functions (8). As mentioned above, the orexin system is now well-acknowledged to play a role in the regulation of sleep and wakefulness since orexin deficiency causes narcolepsy type 1 in humans and animals (7, 26). Furthermore, orexins play an important part in other motivational behaviors such as the regulation of body weight, autonomic function, the reward system, emotion, memory, and stress (18, 27). For these purposes, efferent signaling via monoamine neurons, such as the noradrenergic neurons of the locus coeruleus, the serotonergic neurons of the raphe nuclei, the histaminergic neurons of the posterior hypothalamus, and the dopaminergic neurons of the ventral tegmental area, appears to be particularly important (1, 28).

Afferent signaling toward the orexin-producing neurons provides information about the environmental state and originates from several distinct brain regions. During wakefulness, the cholinergic system of the basal forebrain

and emotional stimuli from the limbic system excite the orexin-producing neurons. During sleep, the GABAergic neurons of the preoptic area inhibit orexin-producing neurons. The serotonergic neurons of the raphe nuclei are involved in a negative feedback pathway, involved in both afferent and efferent signaling systems (29, 30). Furthermore, orexin-producing neurons receive information about energy homeostasis from the arcuate nucleus of the hypothalamus (ARC), which is particularly involved in food intake, and through several humeral factors and food-related cues, which will be discussed later in this review (31, 32).

In the following paragraphs, we will focus on the role of the orexin system in the regulation of body weight through modulation of energy intake and expenditure.

THE OREXIN SYSTEM AND FOOD INTAKE

The first study that described the existence of orexin neuropeptides, produced by neurons in the "feeding center" of the LHA, showed that centrally administered orexin stimulates food intake in rats. Furthermore, the study reported an increase of prepro-orexin mRNA in fasted rats (18). This indicates that orexin-producing neurons are able to register the food status in order to increase food intake in times of fasting and thereby maintain energy homeostasis (18). In line with this, OXR antagonists and orexin antibodies inhibit food intake after central administration, and orexin-deficient mice show decreased food intake (33–35). The latter supports the physiological function of orexin in the regulation of feeding behavior in addition to the pharmacological role of administered orexin. From an evolutionary point of view, feeding behavior has a close interplay with arousal, locomotor activity, and reward mechanisms. In response to food deprivation, arousal pathways are activated, resulting in the increased motor activity, and wakefulness necessary for food-seeking. The orexin system is proposed to play a role in this regulation by evoking a correct behavior in response to nutrient deprivation. In line with this, intracerebroventricular injection of orexin A increases food intake during the light inactive phase in rats but not in the dark phase when rodents are normally already awake (36). Furthermore, orexin signaling positively correlates with wakefulness, and centrally administrated orexin significantly correlates with an increase in vigilance and motor activity (37). Mice lacking orexin-producing neurons or the orexin gene do not show an increase in arousal or locomotor activity in response to fasting, which confirms the physiological role of orexin in the activation of arousal pathways (38). Interestingly, Gonzalez et al. (39) found that upregulated orexin levels in response to fasting drop directly after sensing food, even before digestion. This suggests that orexin is useful in case of food deprivation, but its function is terminated by the action of eating, regardless of nutritional value (39).

In addition to the increase of arousal and vigilance to promote food intake, the orexin-producing neurons also more directly, and independently from arousal pathways, increase food consumption. They do so by projecting to other hypothalamic regions. For instance, orexins are found to have an excitatory effect on melanin-concentrating hormone (MCH) neurons, which anatomically also have a close relationship to orexin-producing neurons in the LHA (40). Furthermore, the orexins modulate orexigenic and anorexigenic neuron populations in the arcuate nucleus of the hypothalamus (ARC). Pro-opiomelanocortin (POMC) neurons in the ARC produce α-melanocyte-stimulating hormone (α-MSH), which stimulates melanocortin receptors in the paraventricular nucleus of the hypothalamus (PVN) to reduce food intake. Orexin A suppresses POMC neurons, leading to lower levels of α-MSH in mice and thereby possibly to hyperphagia (41). The strong orexigenic neuropeptide-Y (NPY) is also produced in the ARC and is bidirectionally involved in orexin signaling. Orexin-induced food intake partially runs via NPY neurons in the ARC, but in turn, NPY neurons modulate the orexin-producing neurons in the LHA as well (31, 42, 43).

Various afferent modulating factors are known to stimulate orexin signaling (**Figure 1**). The stomach-derived hormone ghrelin, generally known to induce appetite in times of food restriction, activates orexin-producing neurons in the LHA (44). Correspondingly, glucose levels negatively influence orexin signaling, suggesting that low energy levels activate arousal pathways to provide energy homeostasis (38). In addition, the adipose tissue-derived hormone leptin, an appetite suppressor, attenuates orexin action, possibly through an indirect suppression via the adjacent neurotensin neurons (45, 46).

Thus, hypothalamic orexins are modulated by nutritional status to influence the regulation of food intake, doing so by the control of arousal and vigilance and by their effect on orexigenic and anti-orexigenic neuropeptides within the hypothalamus.

APPETITE IN NARCOLEPSY TYPE 1

In line with the appetite-increasing effects of orexin, patients with narcolepsy type 1 tend to have a lower food intake compared to controls. Several studies have investigated whether differences in appetite hormones are related to this. The role of the adipokine leptin has been studied in several clinical trials with conflicting results. Smaller clinical cohort studies indicate lower plasma leptin levels and a loss of circadian rhythmicity in patients with narcolepsy type 1 (47, 48). However, the most recent and bigger cohort studies did not show a difference in leptin levels in plasma or cerebrospinal fluid, nor in circadian secretion of the hormone (49–51). The appetite-inducing hormone ghrelin seems not to be different between patients with narcolepsy type 1 and controls. Nonetheless, one study reports that plasma levels of the hormone obestatin, which is transcribed from the same gene as ghrelin, are elevated in narcolepsy type 1 patients compared to healthy controls (50, 52). This coincided with a disturbed autonomous function. The authors speculate that disturbed cholinergic signaling leads to higher obestatin release, but thus far, clear evidence for this hypothesis is lacking (52).

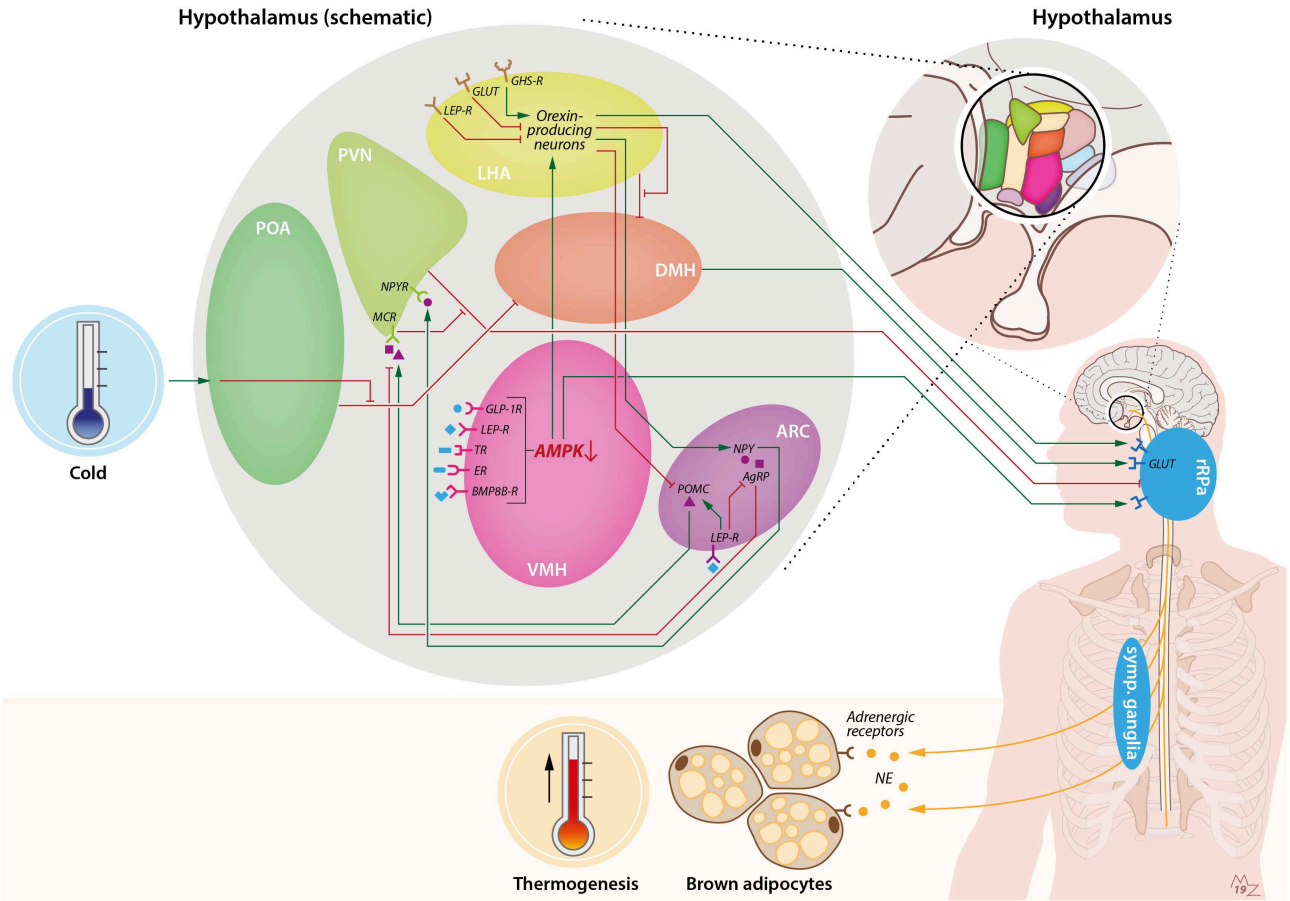

FIGURE 1 | Hypothalamic pathways involved in sympathetic activation of BAT by cold and orexin. Cold exposure activates BAT by stimulation of the preoptic area of the hypothalamus (POA). This leads to suppression of the inhibiting GABAergic tone toward the dorsomedial nucleus of the hypothalamus (DMH), resulting in stimulation of rostral raphe pallidus (rRPa) neurons that are located in the medulla oblongata. From the rRPa, the activity of sympathetic neurons that run toward brown adipocytes is subsequently activated to release noradrenalin (NE), which binds to adrenergic receptors on brown adipocytes to induce thermogenesis. Several other brain pathways converge onto BAT. For instance, the ventromedial nucleus of the hypothalamus (VMH) possesses several receptors for peripheral signals such as GLP-1, leptin, thyroid hormone, estradiol, and bone morphogenetic protein 8B (BMP8B), which lead to activation of BAT via inhibition of AMP-activated protein kinase (AMPK) and stimulation of the rRPa. In addition, the arcuate nucleus of the hypothalamus (ARC) is involved in the thermoregulatory responses by BAT via the anorexigenic POMC neurons and orexigenic agouti-related peptide (AgRP) and neuropeptide-Y (NPY) neurons. Activation of pro-opiomelanocortin (POMC) neurons leads to stimulation of melanocortin receptors (MCRs) in the paraventricular nucleus of the hypothalamus (PVN), which in turn inhibits the GABAergic tone toward the rRPa. On the contrary, stimulation of AgRP neurons in the ARC results in inhibition of the MCR. NPY neurons in the ARC stimulate the neuropeptide-Y receptor (NPYR) on the PVN, thereby suppressing BAT thermogenesis through the GABAergic tone from the PVN toward the rRPa. Within the ARC, leptin stimulates POMC neurons and inhibits AgRP neurons, thereby stimulating BAT thermogenesis. Orexin is connected to BAT via several pathways. First, orexin-producing neurons, predominantly present in the lateral hypothalamic area (LHA), are able to inhibit the GABAergic tone of neurons in the LHA toward neurons in the DMH, thereby stimulating rRPa neurons. Furthermore, there is a link between the VMH and LHA via AMPK inhibition. Inhibition of AMPK in the VMH leads to stimulation of orexin-producing neurons and, subsequently, stimulation of rRPa neurons, resulting in sympathetic activation of BAT. Orexin-producing neurons also project to the ARC, where they inhibit POMC neurons and stimulate NPY neurons. Several food-related cues are able to influence orexin signaling. Glucose levels are negatively correlated with orexin signaling. Leptin is able to attenuate orexin-neuron activity, while ghrelin enhances orexin-neuron activity. BMP8B-R, bone morphogenetic protein 8B receptor; ER, estradiol receptor; GABA-R, GABA receptor; GHS-R, growth hormone secretagogue receptor (e.g., ghrelin receptor); GLP-1R, glucagon-like-peptide-1 receptor; GLUT, glucose transporter; LEP-R, leptin receptor; TR, thyroid receptor.

ENERGY EXPENDITURE IN NARCOLEPSY TYPE 1

Despite a lower food intake, patients with narcolepsy type 1 tend to be overweight to obese (3, 10). Preclinical studies also reveal a higher fat accumulation in orexin-deficient rodents, despite a significantly lower calorie consumption (35). Obesity is the result of a disequilibrium between energy intake and energy expenditure. Therefore, orexins must also influence the other side of the energy balance, e.g., the regulation of energy expenditure. Orexin promotes food-seeking behavior, so it increases locomotor activity in rats (53). This would lead to the logical suggestion that in case of orexin deficiency, lower physical activity might contribute to the weight gain.

However, in patients with narcolepsy type 1, a decrease in locomotor activity does not fully explain the amount of weight gain after disease onset (3, 54, 55). A lower metabolic rate is therefore hypothesized to be causally related to the positive energy balance in patients with narcolepsy type 1. Several studies in adolescents and adults demonstrated that basal metabolic rate did not significantly differ between patients with narcolepsy type 1 and healthy controls (54, 56, 57). In contrast, Dahmen et al. (57) found a significantly lower energy expenditure and basal metabolic rate in non-obese patients with narcolepsy type 1 compared with controls. This difference was not found in obese patients with narcolepsy type 1. The authors speculated that these findings could be explained by a mechanism in which the development of narcolepsy type 1 leads to a higher individual BMI set point that, in turn, leads to a decrease in basal metabolic rate. Once this BMI set point is reached, the metabolic rate will return to a normal level (57). In line with this, Wang et al. (58) showed that the BMI increase is higher in children diagnosed with narcolepsy type 1 compared to controls of the same age and that this BMI increase is accompanied by a decrease in basal metabolic rate. Both the higher increase in BMI and lower basal metabolic rate return to values observed in healthy age-matched controls 3–4 years after diagnosis (58).

Several metabolic organs contribute substantially to energy metabolism, including WAT, liver, muscle, and energy-combusting BAT. One previous study showed that patients with narcolepsy type 1 tend to have lower plasma glycerol levels compared to healthy controls, which might indicate a lower rate of lipolysis in adipose tissue, resulting in more fat storage. This coincided with higher insulin-induced glucose uptake by skeletal muscles, pointing toward more glycogenesis. Hepatic insulin sensitivity appeared to be unaffected (59). Thus, narcolepsy type 1 might result in a more "anabolic" state of the body. However, in-depth research into the underlying mechanism is missing. The sympathetic nervous system has a crucial role in the regulation of energy metabolism (60). Patients with narcolepsy type 1 show autonomic abnormalities, with some studies reporting a decreased sympathetic activity, heart rate variability, and blood pressure during wakefulness (56, 61). In contrast, those parameters are shown to be normal to high during sleep (62–64). However, standardized measurement methods are lacking, and untreated patients have an inability to remain awake, which makes reliable autonomic measurements a challenge (65). Nonetheless, several preclinical studies have revealed that the orexin system influences the sympathetic outflow toward peripheral tissues. More specifically, centrally administered orexin in rodents induces a rise in blood pressure, heart rate, and plasma catecholamine levels and increases in energy expenditure and thermogenesis (66–68). The increase in thermogenesis might be due to an increase in sympathetic outflow toward energy-combusting BAT, on which we will focus in the next paragraph.

ACTIVATION OF BROWN ADIPOSE TISSUE

BAT is an organ that is particularly involved in non-shivering thermogenesis and is therewith known to significantly contribute to energy metabolism in rodents as well as in humans (69). After activation, BAT combusts triglyceride-derived fatty acids and glucose into heat due to the unique presence of uncoupling protein-1 (UCP-1) in the inner mitochondrial membrane. Morphologically, brown adipocytes contain numerous small lipid droplets and possess large numbers of mitochondria, resulting in the characteristic brownish color. Besides the classical brown adipocytes, which lie in depots around the cervical and supraclavicular area, brown-like adipocytes, so called "beige/brite" cells that are scattered within white adipose tissue, are also involved in the process of thermogenesis (70). In mice, prolonged activation of BAT through cold exposure or by directly targeting certain receptors present on BAT induces weight loss and reduces plasma triglycerides and cholesterol (71, 72). Consequently, this leads to a reduction of atherosclerosis development (71). In humans, activation of BAT by cold exposure increases energy metabolism and decreases fat mass, thereby being a promising target to combat adiposity (73). The current gold standard to visualize BAT in human is by measuring its glucose uptake with a [^{18}F]fluorodeoxyglucose ([^{18}F]FDG) positron emission tomography (PET)/computed tomography (CT) scan. This method uses the glucose analog [^{18}F]FDG as a tracer to visualize glucose uptake by metabolically active tissues (74, 75).

BAT is known to be strongly innervated by the sympathetic nervous system, which activates BAT following a variety of stimuli, of which cold exposure is the best known (76). Cold exposure results in activation of receptors from the transient receptor potential (TRP) family in the skin. Then, these receptors send a signal via the dorsal horn neurons toward the preoptic area of the hypothalamus (POA; **Figure 1**) (77–79). From here, the efferent signal runs through the dorsomedial nucleus of the hypothalamus (DMH). In thermoneutral conditions, the DMH is inhibited through a continuous GABAergic tone from neurons in the POA. However, stimulation of the POA by a cold stimulus provokes inhibition of this GABAergic tone toward the DMH, resulting in stimulation of glutamate receptors at the medullary rostral raphe pallidus (rRPa) neurons. Sympathetic premotor neurons at the rRPa generate sympathetic outflow toward BAT, resulting in activation of BAT and enhanced thermogenesis (78, 80–82). Several additional efferent routes involving different hypothalamic nuclei and pathways are involved in the control of thermogenesis in response to various other stimuli. In general, all of these pathways lead to the generation of sympathetic outflow from BAT sympathetic premotor neurons at the medullary rRPa (80). One of those nuclei is the ventromedial nucleus of the hypothalamus (VMH) (83, 84). Preclinical studies show that several hormones influencing energy homeostasis modulate BAT activity independently of cold through the VMH. These hormones, such as thyroid hormones, bone

morphogenetic protein 8B (BMP8B), glucagon-like-peptide-1, leptin, and estradiol, enhance the sympathetic outflow toward BAT via the rRPa after binding in the VMH. Multiple studies reveal that they do so by modulation of a pathway that involves inhibition of AMP-activated protein kinase (AMPK), which subsequently results in stimulation of sympathetic nerve fibers (80, 81, 85–90). Furthermore, neuron populations in the ARC play an important role in modulation of BAT activity (81, 91). Amongst those are the orexigenic NPY- and agouti-related peptide (AgRP)-expressing neurons and the anorexigenic POMC neurons (92). As mentioned before, the POMC neurons excrete α-MSH, which stimulates melanocortin receptors in the PVN. Apart from suppression of food intake, this also enhances sympathetic outflow toward BAT through inhibition of GABAergic projections to the rRPa, resulting in a negative energy balance (93). On the contrary, AgRP and NPY are thought to stimulate appetite and reduce sympathetic outflow toward BAT through inhibition of the melanocortin receptors and stimulation of the NPY receptors, respectively (80, 94). Leptin consecutively induces the POMC neurons, and thus α-MSH, to signal toward the melanocortin receptors in the PVN and thereby enhances thermogenesis through the same pathway. Simultaneously leptin inhibits the AgRP and NPY neurons (95).

In conclusion, BAT is a highly metabolically active organ with a function in thermoregulation. BAT is densely innervated by the sympathetic nervous system, and several hypothalamic nuclei and pathways are involved in the central stimulation of BAT. Interestingly, the neuronal areas and neuropeptides involved in the regulation of BAT partly overlap those involved in the orexin system. Both are acknowledged players in energy metabolism. Therefore, the following paragraph focuses on the interplay between the two systems.

ROLE OF THE OREXIN SYSTEM IN BROWN ADIPOSE TISSUE ACTIVATION

Compelling evidence points toward a role of the orexin system in the regulation of thermogenesis by BAT. Yet, uncertainty exists about the exact mechanism and pathways involved. In 1999, increased plasma norepinephrine levels were shown after central injection of a high dose of orexin A but not orexin B in mice (66). After that, multiple studies followed that investigated the pharmacological effect of intracerebroventricular administration of orexin A, and the majority showed an increase in thermogenesis (67, 96–99). However, the involvement of BAT remained controversial due to contrasting results found by different research groups. In 2003, centrally injected orexin A was shown to increase whole-body energy expenditure, colonic temperature, and heart rate in rats, but the involvement of BAT was not specifically studied (67). Monda et al. (96–99) incorporated BAT in their studies and showed an increase in sympathetic firing rate toward BAT and a rise in BAT temperature after injection of orexin A in rats. On the contrary, another research group suggested that the thermogenic response upon orexin A is not regulated by BAT but rather by skeletal muscle. They demonstrated an increase in *Ucp3* mRNA expression in skeletal muscle after central orexin A administration, but no changes in *Ucp1* on BAT (100). In line with this, Haynes et al. (36) did not find temperature changes in BAT after 8 days of orexin A infusion in rats. Furthermore, in obese mice, they show that an orexin 1 receptor antagonist reduces weight gain and BAT weight and upregulates *Ucp1* expression (101). In lean rats, orexin 1 receptor antagonism also leads to an upregulation of *Ucp1* expression together with an increase in BAT thermogenesis and a reduction in body weight (102).

The discrepancy in results points toward a more complex involvement of the orexin system in the regulation of thermogenesis by BAT. Besides the orexin neuropeptides, other co-existent neurotransmitters are released by the orexin-producing neurons such as glutamate and dynorphin (23, 24). To address the difference between involvement of the orexin neuropeptides and the orexin-producing neurons, Zhang et al. (103) investigated the effect of an orexin neuropeptide knockout model (OX-KO) vs. the complete ablation of the orexin-producing neurons (OX-AB) in mice. OX-KO mice have a translocation in the prepro-orexin gene and, therefore, do not produce orexin neuropeptides, whereas OX-AB mice have completely ablated orexin-producing neurons and hence also lack the co-existent modulators in addition to orexin. The study demonstrated that OX-AB mice showed lower BAT activity and *Ucp1* expression in response to stress, while OX-KO mice did not show a difference in BAT activity (103), pointing toward the involvement of the orexin-producing neurons instead of the orexin neuropeptides. Several years later, the same group showed that the thermogenic fever response upon prostaglandin E_2 (PGE_2) injection in the medial POA was attenuated in OX-AB mice but not in OX-KO mice. OX-AB mice were less tolerant to cold exposure, despite similar locomotor activity compared to OX-KO and wildtype mice. BAT morphology appeared to be normal in both mouse models. In addition, they showed that treatment with the glutamate receptor antagonist prior to PGE_2 injection or cold exposure inhibited a thermogenic response in wildtype mice (104). The involvement of the orexin-producing neurons in the thermogenic response by BAT has also been investigated in rats. In line with the aforementioned results, OX-AB rats compared to wild-type rats have a reduced thermogenic response to basic life events, such as light changes and food intake, and after specific stimuli, such as stress or cold (105, 106). These results indicate the involvement of the orexin-producing neurons in the thermogenic regulation by BAT, at least partly regulated by glutamate rather than the orexin neuropeptide itself.

Besides the effect of orexin-producing neurons on BAT activity, orexin-producing neurons are also thought to play a pivotal role in the development and differentiation of BAT early in life. In 2011, Sellayah et al. (107) used an orexin null mouse model, in which mice are orexin-deficient since birth. They observed more rapid weight gain on a high-fat diet and an impaired diet-induced thermogenesis compared to wild-type mice. Morphologically, BAT appeared to be less brown with

fewer mitochondria, lipid droplets, and intracellular triglycerides compared to in wild-type mice. White adipose tissue, on the contrary, appeared to be normal. This suggests that orexin influences the differentiation of BAT in the developmental stage. They also showed that restoring orexin during the prenatal stage of the orexin null pups resulted in recovery of BAT morphology in the newborn pups. The effect of orexin on the development and differentiation of BAT in the prenatal phase is suggested to be primarily mediated by OXR1 and not by OXR2 (108). Interestingly, orexin seems to be important not only in the prenatal development of BAT but also in the differentiation of BAT later in life. With increasing age, BAT function declines, and it appears morphologically to be more white (109, 110). Chronic injection (2 weeks) of orexin intraperitoneally in old (2-years-old) mice improved age-related decline in BAT morphology and function. In line with this, orexin-producing neuron ablation caused characteristics of aging in BAT (109). Thus, on top of the thermogenic function of BAT, orexin-producing neurons also appear to play a crucial role in the differentiation and development of BAT, not only in early life but also during aging.

NEUROENDOCRINE PATHWAYS INVOLVED IN OREXIGENIC THERMOREGULATION

Several research groups aimed to identify the neuroendocrine pathway involved in orexigenic thermoregulation (**Figure 1**). Inhibition of the GABAergic tone of neurons in the LHA was shown to increase sympathetic nervous signaling and BAT activity (111). When neurons in the DMH or RPa were inhibited, the effect was reversed. This suggests that at least one of the BAT stimulatory pathways runs via the disinhibition of LHA, which in turn excites the DMH and RPa. However, it remained unclear whether this effect is the result of orexin-producing neurons or other neurons in the LHA (111). In 2011, this pathway was further unraveled by using retrograde anatomical tracing from BAT toward the hypothalamus and the simultaneous immunohistochemical staining of orexin-producing neurons. The researchers demonstrated the existence of orexigenic connections between the perifornical lateral hypothalamus and the rRPa and dense orexin innervation on the rRPa, strongly pointing toward the involvement of orexin in the aforementioned thermogenic pathway (112). It remains to be elucidated what exact effect the orexin-producing neurons have on the rRPa. Proposed mechanisms include a presynaptic effect on glutamate receptors or a rather postsynaptic effect, either direct or by modulating GABA signaling (113). Additionally, other brain regions were shown to be important in thermoregulation by BAT. The cerebral cortex seems to be important in prostaglandin-induced hyperthermia, and an intact VMH appears to be necessary for the activation of thermogenesis (97, 99). Martins et al. (114) demonstrated how the VMH is involved in the orexigenic regulation of BAT thermogenesis. They showed a pathway in which BMP8B, via inhibition of AMPK in the VMH and glutaminergic signaling, results in stimulation of OXR1 in the LHA and subsequently activation of BAT thermogenesis. Interestingly, this pathway was dependent on estrogen and was thus exclusively observed in females (114). This result might be of interest because of the well-known gender differences in fat storage. Women generally exhibit more subcutaneous fat, which has higher potency for lipolysis and browning as compared to visceral fat, which is found to a higher extent in men (115). Gender differences in the presence and metabolic activity of supraclavicular BAT also seem to favor women (115, 116). However, as mentioned before, no gender differences in the prevalence of adiposity in patients with narcolepsy type 1 have been reported. The pathway involving inhibition of AMKP in the VMH connects nicely with the aforementioned reports from other research groups describing the involvement of the LHA in the sympathetic stimulation of BAT. Recently, another interesting pathway involving the brain dopamine system has been described. The dopamine receptor 2 on GABAergic neurons in the LHA and zona incerta appears to be able to upregulate *Ucp1*, BAT thermogenesis, and energy expenditure in mice. This pathway is dependent on orexin signaling (117). The fact that dopamine plays a role in the orexigenic thermogenesis was reported before, when ablating the dopamine neurons resulted in abolishment of the orexigenic increase in body temperature (98).

Altogether, the majority of rodent studies point toward a crucial role for orexin-producing neurons rather than the orexin neuropeptides in BAT functionality. On top of this, orexin neuropeptides appear to play a role in BAT development and differentiation.

HUMAN PERSPECTIVE

The emerging evidence that the orexin system is involved in BAT function in rodents leads to the hypothesis that impaired BAT functionality could be causally involved in the increased adiposity in patients with narcolepsy type 1. To the best of our knowledge, only two recent studies have investigated this issue. One study investigated BAT activity between patients with narcolepsy type 1 and healthy controls. In all subjects, [^{18}F]FDG uptake by BAT was measured after 2 h of mild cold exposure. No difference was found between the groups, indicating no difference in glucose uptake by BAT. However, there are several limitations imposed by the study design. This study was performed with a small sample size ($n = 7$ per group), and a fixed mild temperature was used as a cold stimulus to activate BAT. Possibly, this does not result in maximal activation of BAT for all individuals. Especially for patients with narcolepsy type 1, who are reported to have a higher distal skin temperature, probably due to vasodilatation, cold exposure could have evoked a larger stimulus on BAT, leading to overestimation of their BAT activity compared to the healthy controls (118). In addition, the use of [^{18}F]FDG-PET/CT scans to visualize human BAT is currently under debate, considering that BAT mainly combusts triglyceride-derived fatty acids, while [^{18}F]FDG-PET/CT scans only visualize glucose uptake. On top of that, glucose uptake is highly impaired in insulin-resistant conditions, which could

be an issue for measuring BAT in overweight and obese people (119). However, a valuable addition in this study was the use of [^{123}I]MIBG-SPECT/CT scanning, which visualizes sympathetic nervous stimulation. They showed intact adrenergic innervation in the BAT of patients with narcolepsy type 1, suggesting that at least the sympathetic outflow is maintained (120). In the same year, Drissi et al. (121) aimed to investigate adipose tissue distribution measured with MRI in a thermoneutral condition. They showed no differences in supraclavicular BAT between patients with narcolepsy type 1 and healthy controls. It is important to note that this is in line with preclinical studies showing that BAT in mice appeared to be morphologically normal in OX-AB mice. However, BAT functionality was attenuated in the absence of the orexin-producing neurons (104), and BAT functionality was not examined in the study of Drissi et al. (121).

The limitations of the available human studies illustrate the challenge of translating preclinical studies into human studies. Different animal models exist that mimic the phenotype of narcolepsy type 1. However, none of the currently existing models adequately and precisely reflect the human situation. As mentioned above, in patients with narcolepsy type 1, orexin-producing neurons are lost, resulting in the loss of orexin but also of the co-expressed glutamate, dynorphin, and NARP (25). Therefore, mouse models that mimic narcolepsy type 1 by means of inhibition of the OXR or a lack of prepro-orexin might not be fully adequate. Orexin-producing neuron ablation appears to come closer to the human phenotype (35). Nonetheless, patients with narcolepsy type 1 develop the disease during life following an autoimmune response, which hinders the development of escape pathways to substitute for the lost functions. Accordingly, a mouse model has been developed that uses a tetracycline-controlled transcriptional activation system and is able to time the orexin-producing neuron degeneration (122). This mouse model strongly resembles the human situation and could therefore provide more valuable information about metabolic changes that occur after the onset of narcolepsy type 1.

CONCLUSION AND FUTURE PERSPECTIVES

Patients with narcolepsy type 1 are at increased risk for obesity, despite a normal to reduced food intake. Results from preclinical studies strongly suggest that destruction of orexin-producing neurons leads to diminished BAT functionality and subsequently to impaired energy homeostasis. Preclinical studies revealed several neuroendocrine pathways involved in orexigenic thermoregulation. However, to date, convincing evidence from human studies about impaired BAT function in patients with narcolepsy type 1 is lacking. Currently, new techniques for visualization and quantification of BAT volume and activity are evolving at a high rate, including the use of magnetic resonance imaging to measure fat fraction and perfusion changes in BAT upon activation. This could be promising for patient populations in which detecting BAT activity by [^{18}F]FDG-PET/CT scan is hampered due to insulin resistance. A crucial influencing factor to take into account is a different temperature perception in patients with narcolepsy type 1, which can markedly influence the cold-induced measurements often used in BAT research. In addition, more insight is needed into the involvement of the orexin-producing neurons in neuroendocrine pathways involved in energy expenditure by BAT and whether these pathways are disturbed in narcolepsy type 1 patients. To further explore the contribution of skeletal muscle and white adipose tissue in the regulation of energy metabolism after orexin deficiency, tissue biopsies in combination with *ex vivo* mitochondrial respiration measurements and metabolomics could provide additional knowledge on metabolic processes within these tissues. Although no significant gender differences in obesity rates amongst patients with narcolepsy type 1 have yet been described, the involvement of gender hormones in the characteristics of both WAT and BAT and their central actions in the brain raise questions about whether sex hormones influence the development of adiposity after orexin-producing neuron destruction. Therefore, the influence of gender is a topic that requires further study.

More knowledge about the pathogenesis underlying the increased BMI in patients with narcolepsy type 1 could lead to the development of more effective treatment options to counter their increased adiposity and to improve their metabolic health. Therefore, additional studies are highly warranted to further investigate BAT functionality in this metabolically compromised patient population.

AUTHOR CONTRIBUTIONS

MES wrote and submitted the manuscript. MSS, RF, GL, PR, and MB critically reviewed the manuscript.

FUNDING

This work was supported by a Dutch Diabetes Research Foundation Fellowship to MB (grant 2015.81.1808) and the Netherlands CardioVascular Research Initiative: the Dutch Heart Foundation, Dutch Federation of University Medical Centers, the Netherlands Organization for Health Research and Development and the Royal Netherlands Academy of Sciences (CVON2017-20 GENIUS-II). PR is an Established Investigator of the Netherlands Heart Foundation (grant 2009T038).

ACKNOWLEDGMENTS

We thank Manon Zuurmond for providing the image in **Figure 1**.

REFERENCES

1. Bassetti CLA, Adamantidis A, Burdakov D, Han F, Gay S, Kallweit U, et al. Narcolepsy—clinical spectrum, aetiopathophysiology, diagnosis and treatment. *Nat Rev Neurol*. (2019) 15:519–39. doi: 10.1038/s41582-019-0226-9
2. Daniels L. Narcolepsy. *Medicine*. (1934) 13:1–122. doi: 10.1097/00005792-193413010-00001
3. Lammers GJ, Pijl H, Iestra J, Langius JA, Buunk G, Meinders AE. Spontaneous food choice in narcolepsy. *Sleep*. (1996) 19:75–6. doi: 10.1093/sleep/19.1.75
4. Ohayon MM, Priest RG, Zulley J, Smirne S, Paiva T. Prevalence of narcolepsy symptomatology and diagnosis in the European general population. *Neurology*. (2002) 58:1826–33. doi: 10.1212/WNL.58.12.1826
5. Silber MH, Krahn LE, Olson EJ, Pankratz VS. The epidemiology of narcolepsy in Olmsted County, Minnesota: a population-based study. *Sleep*. (2002) 25:197–202. doi: 10.1093/sleep/25.2.197
6. Scheer D, Schwartz SW, Parr M, Zgibor J, Sanchez-Anguiano A, Rajaram L. Prevalence and incidence of narcolepsy in a US health care claims database, 2008–2010. *Sleep*. (2019) 42:zsz091. doi: 10.1093/sleep/zsz091
7. Peyron C, Faraco J, Rogers W, Ripley B, Overeem S, Charnay Y, et al. A mutation in a case of early onset narcolepsy and a generalized absence of hypocretin peptides in human narcoleptic brains. *Nat Med*. (2000) 6:991–7. doi: 10.1038/79690
8. Peyron C, Tighe DK, van den Pol AN, de Lecea L, Heller HC, Sutcliffe JG, et al. Neurons containing hypocretin (orexin) project to multiple neuronal systems. *J Neurosci*. (1998) 18:9996–10015. doi: 10.1523/JNEUROSCI.18-23-09996.1998
9. Overeem S, van Nues SJ, van der Zande WL, Donjacour CE, van Mierlo P, Lammers GJ. The clinical features of cataplexy: a questionnaire study in narcolepsy patients with and without hypocretin-1 deficiency. *Sleep Med*. (2011) 12:12–8. doi: 10.1016/j.sleep.2010.05.010
10. Schuld A, Hebebrand J, Geller F, Pollmacher T. Increased body-mass index in patients with narcolepsy. *Lancet*. (2000) 355:1274–5. doi: 10.1016/S0140-6736(05)74704-8
11. Dahmen N, Bierbrauer J, Kasten M. Increased prevalence of obesity in narcoleptic patients and relatives. *Eur Arch Psychiatry Clin Neurosci*. (2001) 251:85–9. doi: 10.1007/s004060170057
12. Kok SW, Overeem S, Visscher TL, Lammers GJ, Seidell JC, Pijl H, et al. Hypocretin deficiency in narcoleptic humans is associated with abdominal obesity. *Obes Res*. (2003) 11:1147–54. doi: 10.1038/oby.2003.156
13. Won C, Mahmoudi M, Qin L, Purvis T, Mathur A, Mohsenin V. The impact of gender on timeliness of narcolepsy diagnosis. *J Clin Sleep Med*. (2014) 10:89–95. doi: 10.5664/jcsm.3370
14. Inocente CO, Lavault S, Lecendreux M, Dauvilliers Y, Reimao R, Gustin MP, et al. Impact of obesity in children with narcolepsy. *CNS Neurosci Ther*. (2013) 19:521–8. doi: 10.1111/cns.12105
15. Eurostat. *Obesity Rate by Body Mass Index (BMI)*. Available online at: https://ec.europa.eu/eurostat/databrowser/view/sdg_02_10/default/table?lang=en (accessed January 31, 2020).
16. Poli F, Plazzi G, Di DG, Ribichini D, Vicennati V, Pizza F, et al. Body mass index-independent metabolic alterations in narcolepsy with cataplexy. *Sleep*. (2009) 32:1491–7. doi: 10.1093/sleep/32.11.1491
17. Ponziani V, Gennari M, Pizza F, Balsamo A, Bernardi F, Plazzi G. Growing up with type 1 narcolepsy: its anthropometric and endocrine features. *J Clin Sleep Med*. (2016) 12:1649–57. doi: 10.5664/jcsm.6352
18. Sakurai T, Amemiya A, Ishii M, Matsuzaki I, Chemelli RM, Tanaka H, et al. Orexins and orexin receptors: a family of hypothalamic neuropeptides and G protein-coupled receptors that regulate feeding behavior. *Cell*. (1998) 92:573–85. doi: 10.1016/S0092-8674(00)80949-6
19. de Lecea L, Kilduff TS, Peyron C, Gao X, Foye PE, Danielson PE, et al. The hypocretins: hypothalamus-specific peptides with neuroexcitatory activity. *Proc Natl Acad Sci USA*. (1998) 95:322–7. doi: 10.1073/pnas.95.1.322
20. Stuber GD, Wise RA. Lateral hypothalamic circuits for feeding and reward. *Nat Neurosci*. (2016) 19:198–205. doi: 10.1038/nn.4220
21. Nambu T, Sakurai T, Mizukami K, Hosoya Y, Yanagisawa M, Goto K. Distribution of orexin neurons in the adult rat brain. *Brain Res*. (1999) 827:243–60. doi: 10.1016/S0006-8993(99)01336-0
22. Marcus JN, Aschkenasi CJ, Lee CE, Chemelli RM, Saper CB, Yanagisawa M, et al. Differential expression of orexin receptors 1 and 2 in the rat brain. *J Comp Neurol*. (2001) 435:6–25. doi: 10.1002/cne.1190
23. Abrahamson EE, Leak RK, Moore RY. The suprachiasmatic nucleus projects to posterior hypothalamic arousal systems. *Neuroreport*. (2001) 12:435–40. doi: 10.1097/00001756-200102120-00048
24. Chou TC, Lee CE, Lu J, Elmquist JK, Hara J, Willie JT, et al. Orexin (hypocretin) neurons contain dynorphin. *J Neurosci*. (2001) 21:Rc168. doi: 10.1523/JNEUROSCI.21-19-j0003.2001
25. Mahoney CE, Cogswell A, Koralnik IJ, Scammell TE. The neurobiological basis of narcolepsy. *Nat Rev Neurosci*. (2019) 20:83–93. doi: 10.1038/s41583-018-0097-x
26. Chemelli RM, Willie JT, Sinton CM, Elmquist JK, Scammell T, Lee C, et al. Narcolepsy in orexin knockout mice: molecular genetics of sleep regulation. *Cell*. (1999) 98:437–51. doi: 10.1016/S0092-8674(00)81973-X
27. Sakurai T. The role of orexin in motivated behaviours. *Nat Rev Neurosci*. (2014) 15:719–31. doi: 10.1038/nrn3837
28. Vittoz NM, Berridge CW. Hypocretin/orexin selectively increases dopamine efflux within the prefrontal cortex: involvement of the ventral tegmental area. *Neuropsychopharmacology*. (2006) 31:384–95. doi: 10.1038/sj.npp.1300807
29. Sakurai T, Nagata R, Yamanaka A, Kawamura H, Tsujino N, Muraki Y, et al. Input of orexin/hypocretin neurons revealed by a genetically encoded tracer in mice. *Neuron*. (2005) 46:297–308. doi: 10.1016/j.neuron.2005.03.010
30. Inutsuka A, Yamanaka A. The physiological role of orexin/hypocretin neurons in the regulation of sleep/wakefulness and neuroendocrine functions. *Front Endocrinol*. (2013) 4:18. doi: 10.3389/fendo.2013.00018
31. Fu L-Y, Acuna-Goycolea C, van den Pol AN. Neuropeptide Y inhibits hypocretin/orexin neurons by multiple presynaptic and postsynaptic mechanisms: tonic depression of the hypothalamic arousal system. *J Neurosci*. (2004) 24:8741–51. doi: 10.1523/JNEUROSCI.2268-04.2004
32. Campbell RE, Smith MS, Allen SE, Grayson BE, Ffrench-Mullen JMH, Grove KL. Orexin neurons express a functional pancreatic polypeptide Y4 receptor. *J Neurosci*. (2003) 23:1487–97. doi: 10.1523/JNEUROSCI.23-04-01487.2003
33. Haynes AC, Jackson B, Chapman H, Tadayyon M, Johns A, Porter RA, et al. A selective orexin-1 receptor antagonist reduces food consumption in male and female rats. *Regulat Peptides*. (2000) 96:45–51. doi: 10.1016/S0167-0115(00)00199-3
34. Yamada H, Okumura T, Motomura W, Kobayashi Y, Kohgo Y. Inhibition of food intake by central injection of anti-orexin antibody in fasted rats. *Biochem Biophys Res Commun*. (2000) 267:527–31. doi: 10.1006/bbrc.1999.1998
35. Hara J, Beuckmann CT, Nambu T, Willie JT, Chemelli RM, Sinton CM, et al. Genetic ablation of orexin neurons in mice results in narcolepsy, hypophagia, and obesity. *Neuron*. (2001) 30:345–54. doi: 10.1016/S0896-6273(01)00293-8
36. Haynes AC, Jackson B, Overend P, Buckingham RE, Wilson S, Tadayyon M, et al. Effects of single and chronic intracerebroventricular administration of the orexins on feeding in the rat. *Peptides*. (1999) 20:1099–105. doi: 10.1016/S0196-9781(99)00105-9
37. Estabrooke IV, McCarthy MT, Ko E, Chou TC, Chemelli RM, Yanagisawa M, et al. Fos expression in orexin neurons varies with behavioral state. *J Neurosci*. (2001) 21:1656–62. doi: 10.1523/JNEUROSCI.21-05-01656.2001
38. Yamanaka A, Beuckmann CT, Willie JT, Hara J, Tsujino N, Mieda M, et al. Hypothalamic orexin neurons regulate arousal according to energy balance in mice. *Neuron*. (2003) 38:701–13. doi: 10.1016/S0896-6273(03)00331-3
39. Gonzalez JA, Jensen LT, Iordanidou P, Strom M, Fugger L, Burdakov D. Inhibitory interplay between orexin neurons and eating. *Curr Biol*. (2016) 26:2486–91. doi: 10.1016/j.cub.2016.07.013
40. van den Pol AN, Acuna-Goycolea C, Clark KR, Ghosh PK. Physiological properties of hypothalamic MCH neurons identified with selective expression of reporter gene after recombinant virus infection. *Neuron*. (2004) 42:635–52. doi: 10.1016/S0896-6273(04)00251-X
41. Morello G, Imperatore R, Palomba L, Finelli C, Labruna G, Pasanisi F, et al. Orexin-A represses satiety-inducing POMC neurons and contributes to obesity via stimulation of endocannabinoid signaling. *Proc Natl Acad Sci USA*. (2016) 113:4759–64. doi: 10.1073/pnas.1521304113
42. Yamanaka A, Kunii K, Nambu T, Tsujino N, Sakai A, Matsuzaki I, et al. Orexin-induced food intake involves neuropeptide Y pathway. *Brain Res*. (2000) 859:404–9. doi: 10.1016/S0006-8993(00)02043-6

43. Niimi M, Sato M, Taminato T. Neuropeptide Y in central control of feeding and interactions with orexin and leptin. *Endocrine*. (2001) 14:269–73. doi: 10.1385/ENDO:14:2:269
44. Cone JJ, McCutcheon JE, Roitman MF. Ghrelin acts as an interface between physiological state and phasic dopamine signaling. *J Neurosci*. (2014) 34:4905–13. doi: 10.1523/JNEUROSCI.4404-13.2014
45. Goforth PB, Myers MG. Roles for orexin/hypocretin in the control of energy balance and metabolism. *Curr Top Behav Neurosci*. (2017) 33:137–56. doi: 10.1007/7854_2016_51
46. Goforth PB, Leinninger GM, Patterson CM, Satin LS, Myers MG Jr. Leptin acts via lateral hypothalamic area neurotensin neurons to inhibit orexin neurons by multiple GABA-independent mechanisms. *J Neurosci*. (2014) 34:11405–15. doi: 10.1523/JNEUROSCI.5167-13.2014
47. Schuld A, Blum WF, Uhr M, Haack M, Kraus T, Holsboer F, et al. Reduced leptin levels in human narcolepsy. *Neuroendocrinology*. (2000) 72:195–8. doi: 10.1159/000054587
48. Kok SW, Meinders AE, Overeem S, Lammers GJ, Roelfsema F, Frolich M, et al. Reduction of plasma leptin levels and loss of its circadian rhythmicity in hypocretin (orexin)-deficient narcoleptic humans. *J Clin Endocrinol Metab*. (2002) 87:805–9. doi: 10.1210/jcem.87.2.8246
49. Dahmen N, Engel A, Helfrich J, Manderscheid N, Lobig M, Forst T, et al. Peripheral leptin levels in narcoleptic patients. *Diabetes Technol Ther*. (2007) 9:348–53. doi: 10.1089/dia.2006.0037
50. Donjacour CE, Pardi D, Aziz NA, Frolich M, Roelfsema F, Overeem S, et al. Plasma total ghrelin and leptin levels in human narcolepsy and matched healthy controls: basal concentrations and response to sodium oxybate. *J Clin Sleep Med*. (2013) 9:797–803. doi: 10.5664/jcsm.2924
51. Arnulf I, Lin L, Zhang J, Russell IJ, Ripley B, Einen M, et al. CSF versus serum leptin in narcolepsy: is there an effect of hypocretin deficiency? *Sleep*. (2006) 29:1017–24. doi: 10.1093/sleep/29.8.1017
52. Huda MS, Mani H, Durham BH, Dovey TM, Halford JC, Aditya BS, et al. Plasma obestatin and autonomic function are altered in orexin-deficient narcolepsy, but ghrelin is unchanged. *Endocrine*. (2013) 43:696–704. doi: 10.1007/s12020-012-9838-1
53. Ida T, Nakahara K, Katayama T, Murakami N, Nakazato M. Effect of lateral cerebroventricular injection of the appetite-stimulating neuropeptide, orexin and neuropeptide Y, on the various behavioral activities of rats. *Brain Res*. (1999) 821:526–9. doi: 10.1016/S0006-8993(99)01131-2
54. Chabas D, Foulon C, Gonzalez J, Nasr M, Lyon-Caen O, Willer JC, et al. Eating disorder and metabolism in narcoleptic patients. *Sleep*. (2007) 30:1267–73. doi: 10.1093/sleep/30.10.1267
55. Middelkoop HA, Lammers GJ, Van Hilten BJ, Ruwhof C, Pijl H, Kamphuisen HA. Circadian distribution of motor activity and immobility in narcolepsy: assessment with continuous motor activity monitoring. *Psychophysiology*. (1995) 32:286–91. doi: 10.1111/j.1469-8986.1995.tb02957.x
56. Fronczek R, Overeem S, Reijntjes R, Lammers GJ, van Dijk JG, Pijl H. Increased heart rate variability but normal resting metabolic rate in hypocretin/orexin-deficient human narcolepsy. *J Clin Sleep Med*. (2008) 4:248–54. doi: 10.5664/jcsm.27188
57. Dahmen N, Tonn P, Messroghli L, Ghezel-Ahmadi D, Engel A. Basal metabolic rate in narcoleptic patients. *Sleep*. (2009) 32:962–4 doi: 10.1093/sleep/32.7.962
58. Wang Z, Wu H, Stone WS, Zhuang J, Qiu L, Xu X, et al. Body weight and basal metabolic rate in childhood narcolepsy: a longitudinal study. *Sleep Med*. (2016) 25:139–44. doi: 10.1016/j.sleep.2016.06.019
59. Donjacour CE, Aziz NA, Overeem S, Kalsbeek A, Pijl H, Lammers GJ. Glucose and fat metabolism in narcolepsy and the effect of sodium oxybate: a hyperinsulinemic-euglycemic clamp study. *Sleep*. (2014) 37:795–801. doi: 10.5665/sleep.3592
60. Peterson HR, Rothschild M, Weinberg CR, Fell RD, McLeish KR, Pfeifer MA. Body fat and the activity of the autonomic nervous system. *N Engl J Med*. (1988) 318:1077–83. doi: 10.1056/NEJM198804283181701
61. Donadio V, Liguori R, Vandi S, Pizza F, Dauvilliers Y, Leta V, et al. Lower wake resting sympathetic and cardiovascular activities in narcolepsy with cataplexy. *Neurology*. (2014) 83:1080–6. doi: 10.1212/WNL.0000000000000793
62. Donadio V, Liguori R, Vandi S, Giannoccaro MP, Pizza F, Leta V, et al. Sympathetic and cardiovascular changes during sleep in narcolepsy with cataplexy patients. *Sleep Med*. (2014) 15:315–21. doi: 10.1016/j.sleep.2013.12.005
63. Dauvilliers Y, Jaussent I, Krams B, Scholz S, Lado S, Levy P, et al. Non-dipping blood pressure profile in narcolepsy with cataplexy. *PLoS ONE*. (2012) 7:e38977. doi: 10.1371/journal.pone.0038977
64. van der Meijden WP, Fronczek R, Reijntjes RH, Corssmit EP, Biermasz NR, Lammers GJ, et al. Time- and state-dependent analysis of autonomic control in narcolepsy: higher heart rate with normal heart rate variability independent of sleep fragmentation. *J Sleep Res*. (2015) 24:206–14. doi: 10.1111/jsr.12253
65. Plazzi G, Moghadam KK, Maggi LS, Donadio V, Vetrugno R, Liguori R, et al. Autonomic disturbances in narcolepsy. *Sleep Med Rev*. (2011) 15:187–96. doi: 10.1016/j.smrv.2010.05.002
66. Shirasaka T, Nakazato M, Matsukura S, Takasaki M, Kannan H. Sympathetic and cardiovascular actions of orexins in conscious rats. *Am J Physiol*. (1999) 277:R1780–5. doi: 10.1152/ajpregu.1999.277.6.R1780
67. Wang J, Osaka T, Inoue S. Orexin-A-sensitive site for energy expenditure localized in the arcuate nucleus of the hypothalamus. *Brain Res*. (2003) 971:128–34. doi: 10.1016/S0006-8993(03)02437-5
68. Samson WK, Gosnell B, Chang JK, Resch ZT, Murphy TC. Cardiovascular regulatory actions of the hypocretins in brain. *Brain Res*. (1999) 831:248–53. doi: 10.1016/S0006-8993(99)01457-2
69. Ruiz JR, Martinez-Tellez B, Sanchez-Delgado G, Osuna-Prieto FJ, Rensen PCN, Boon MR. Role of human brown fat in obesity, metabolism and cardiovascular disease: strategies to turn up the heat. *Progr Cardiovasc Dis*. (2018) 61:232–45. doi: 10.1016/j.pcad.2018.07.002
70. Ikeda K, Maretich P, Kajimura S. The common and distinct features of brown and beige adipocytes. *Trends Endocrinol Metab*. (2018) 29:191–200. doi: 10.1016/j.tem.2018.01.001
71. Berbee JF, Boon MR, Khedoe PP, Bartelt A, Schlein C, Worthmann A, et al. Brown fat activation reduces hypercholesterolaemia and protects from atherosclerosis development. *Nat Commun*. (2015) 6:6356. doi: 10.1038/ncomms7356
72. Boon MR, Kooijman S, van Dam AD, Pelgrom LR, Berbee JF, Visseren CA, et al. Peripheral cannabinoid 1 receptor blockade activates brown adipose tissue and diminishes dyslipidemia and obesity. *FASEB J*. (2014) 28:5361–75. doi: 10.1096/fj.13-247643
73. Yoneshiro T, Aita S, Matsushita M, Kayahara T, Kameya T, Kawai Y, et al. Recruited brown adipose tissue as an antiobesity agent in humans. *J Clin Invest*. (2013) 123:3404–8. doi: 10.1172/JCI67803
74. van der Lans AA, Hoeks J, Brans B, Vijgen GH, Visser MG, Vosselman MJ, et al. Cold acclimation recruits human brown fat and increases non-shivering thermogenesis. *J Clin Invest*. (2013) 123:3395–403. doi: 10.1172/JCI68993
75. Nedergaard J, Bengtsson T, Cannon B. Unexpected evidence for active brown adipose tissue in adult humans. *Am J Physiol Endocrinol Metab*. (2007) 293:E444–52. doi: 10.1152/ajpendo.00691.2006
76. Bartness TJ, Vaughan CH, Song CK. Sympathetic and sensory innervation of brown adipose tissue. *Int J Obesity*. (2005). 34(Suppl.1):S36–42. doi: 10.1038/ijo.2010.182
77. Nakamura K, Morrison SF. Preoptic mechanism for cold-defensive responses to skin cooling. *J Physiol*. (2008) 586:2611–20. doi: 10.1113/jphysiol.2008.152686
78. Nakamura K. Central circuitries for body temperature regulation and fever. *Am J Physiol Regulat Integr Comp Physiol*. (2011) 301:R1207–28. doi: 10.1152/ajpregu.00109.2011
79. Nakamura K, Morrison SF. A thermosensory pathway that controls body temperature. *Nat Neurosci*. (2008) 11:62–71. doi: 10.1038/nn2027
80. Contreras C, Nogueiras R, Dieguez C, Rahmouni K, Lopez M. Traveling from the hypothalamus to the adipose tissue: the thermogenic pathway. *Redox Biol*. (2017) 12:854–63. doi: 10.1016/j.redox.2017.04.019
81. Labbe SM, Caron A, Lanfray D, Monge-Rofarello B, Bartness TJ, Richard D. Hypothalamic control of brown adipose tissue thermogenesis. *Front Syst Neurosci*. (2015) 9:150. doi: 10.3389/fnsys.2015.00150

82. Morrison SF, Madden CJ, Tupone D. Central control of brown adipose tissue thermogenesis. *Front Endocrinol*. (2012) 3:5. doi: 10.3389/fendo.2012.00005
83. Perkins MN, Rothwell NJ, Stock MJ, Stone TW. Activation of brown adipose tissue thermogenesis by the ventromedial hypothalamus. *Nature*. (1981) 289:401–2. doi: 10.1038/289401a0
84. Minokoshi Y, Saito M, Shimazu T. Sympathetic denervation impairs responses of brown adipose tissue to VMH stimulation. *Am J Physiol*. (1986) 251:R1005–8. doi: 10.1152/ajpregu.1986.251.5.R1005
85. Minokoshi Y, Haque MS, Shimazu T. Microinjection of leptin into the ventromedial hypothalamus increases glucose uptake in peripheral tissues in rats. *Diabetes*. (1999) 48:287–91. doi: 10.2337/diabetes.48.2.287
86. Toda C, Shiuchi T, Lee S, Yamato-Esaki M, Fujino Y, Suzuki A, et al. Distinct effects of leptin and a melanocortin receptor agonist injected into medial hypothalamic nuclei on glucose uptake in peripheral tissues. *Diabetes*. (2009) 58:2757–65. doi: 10.2337/db09-0638
87. Martinez de Morentin PB, Gonzalez-Garcia I, Martins L, Lage R, Fernandez-Mallo D, Martinez-Sanchez N, et al. Estradiol regulates brown adipose tissue thermogenesis via hypothalamic AMPK. *Cell Metab*. (2014) 20:41–53. doi: 10.1016/j.cmet.2014.03.031
88. Lopez M, Dieguez C, Nogueiras R. Hypothalamic GLP-1: the control of BAT thermogenesis and browning of white fat. *Adipocyte*. (2015) 4:141–5. doi: 10.4161/21623945.2014.983752
89. Whittle AJ, Carobbio S, Martins L, Slawik M, Hondares E, Vazquez MJ, et al. BMP8B increases brown adipose tissue thermogenesis through both central and peripheral actions. *Cell*. (2012) 149:871–85. doi: 10.1016/j.cell.2012.02.066
90. van Dam AD, Kooijman S, Schilperoort M, Rensen PC, Boon MR. Regulation of brown fat by AMP-activated protein kinase. *Trends Mol Med*. (2015) 21:571–9. doi: 10.1016/j.molmed.2015.07.003
91. Song CK, Vaughan CH, Keen-Rhinehart E, Harris RB, Richard D, Bartness TJ. Melanocortin-4 receptor mRNA expressed in sympathetic outflow neurons to brown adipose tissue: neuroanatomical and functional evidence. *Am J Physiol Regulat Integr Comp Physiol*. (2008) 295:R417–28. doi: 10.1152/ajpregu.00174.2008
92. Schwartz MW, Woods SC, Porte D Jr, Seeley RJ, Baskin DG. Central nervous system control of food intake. *Nature*. (2000) 404:661–71. doi: 10.1038/35007534
93. Madden CJ, Morrison SF. Neurons in the paraventricular nucleus of the hypothalamus inhibit sympathetic outflow to brown adipose tissue. *Am J Physiol Regulat Integr Comp Physiol*. (2009) 296:R831–43. doi: 10.1152/ajpregu.91007.2008
94. Geerling JJ, Boon MR, Kooijman S, Parlevliet ET, Havekes LM, Romijn JA, et al. Sympathetic nervous system control of triglyceride metabolism: novel concepts derived from recent studies. *J Lipid Res*. (2014) 55:180–9. doi: 10.1194/jlr.R045013
95. Butler AA, Cone RD. The melanocortin receptors: lessons from knockout models. *Neuropeptides*. (2002) 36:77–84. doi: 10.1054/npep.2002.0890
96. Monda M, Viggiano A, Mondola P, De Luca V. Inhibition of prostaglandin synthesis reduces hyperthermic reactions induced by hypocretin-1/orexin A. *Brain Res*. (2001) 909:68–74. doi: 10.1016/S0006-8993(01)02606-3
97. Monda M, Viggiano AN, Viggiano AL, Fuccio F, De Luca V. Cortical spreading depression blocks the hyperthermic reaction induced by orexin A. *Neuroscience*. (2004) 123:567–74. doi: 10.1016/j.neuroscience.2003.09.016
98. Monda M, Viggiano A, Viggiano A, Viggiano E, Messina G, Tafuri D, et al. Sympathetic and hyperthermic reactions by orexin A: role of cerebral catecholaminergic neurons. *Regulat Peptides*. (2007) 139:39–44. doi: 10.1016/j.regpep.2006.10.002
99. Monda M, Viggiano AN, Viggiano A, Viggiano E, Lanza A, De Luca V. Hyperthermic reactions induced by orexin A: role of the ventromedial hypothalamus. *Eur J Neurosci*. (2005) 22:1169–75. doi: 10.1111/j.1460-9568.2005.04309.x
100. Yoshimichi G, Yoshimatsu H, Masaki T, Sakata T. Orexin-A regulates body temperature in coordination with arousal status. *Exp Biol Med*. (2001) 226:468–76. doi: 10.1177/153537020122600513
101. Haynes AC, Chapman H, Taylor C, Moore GB, Cawthorne MA, Tadayyon M, et al. Anorectic, thermogenic and anti-obesity activity of a selective orexin-1 receptor antagonist in ob/ob mice. *Regulat Peptides*. (2002) 104:153–9. doi: 10.1016/S0167-0115(01)00358-5
102. Verty AN, Allen AM, Oldfield BJ. The endogenous actions of hypothalamic peptides on brown adipose tissue thermogenesis in the rat. *Endocrinology*. (2010) 151:4236–46. doi: 10.1210/en.2009-1235
103. Zhang W, Sunanaga J, Takahashi Y, Mori T, Sakurai T, Kanmura Y, et al. Orexin neurons are indispensable for stress-induced thermogenesis in mice. *J Physiol*. (2010) 588:4117–29. doi: 10.1113/jphysiol.2010.195099
104. Takahashi Y, Zhang W, Sameshima K, Kuroki C, Matsumoto A, Sunanaga J, et al. Orexin neurons are indispensable for prostaglandin E2-induced fever and defence against environmental cooling in mice. *J Physiol*. (2013) 591:5623–43. doi: 10.1113/jphysiol.2013.261271
105. Mohammed M, Ootsuka Y, Yanagisawa M, Blessing W. Reduced brown adipose tissue thermogenesis during environmental interactions in transgenic rats with ataxin-3-mediated ablation of hypothalamic orexin neurons. *Am J Physiol Regulat Integr Comp Physiol*. (2014) 307:R978–89. doi: 10.1152/ajpregu.00260.2014
106. Mohammed M, Yanagisawa M, Blessing W, Ootsuka Y. Attenuated cold defense responses in orexin neuron-ablated rats. *Temperature*. (2016) 3:465–75. doi: 10.1080/23328940.2016.1184366
107. Sellayah D, Bharaj P, Sikder D. Orexin is required for brown adipose tissue development, differentiation, and function. *Cell Metab*. (2011) 14:478–90. doi: 10.1016/j.cmet.2011.08.010
108. Sellayah D, Sikder D. Orexin receptor-1 mediates brown fat developmental differentiation. *Adipocyte*. (2012) 1:58–63. doi: 10.4161/adip.18965
109. Sellayah D, Sikder D. Orexin restores aging-related brown adipose tissue dysfunction in male mice. *Endocrinology*. (2014) 155:485–501. doi: 10.1210/en.2013-1629
110. Rogers NH, Landa A, Park S, Smith RG. Aging leads to a programmed loss of brown adipocytes in murine subcutaneous white adipose tissue. *Aging Cell*. (2012) 11:1074–83. doi: 10.1111/acel.12010
111. Cerri M, Morrison SF. Activation of lateral hypothalamic neurons stimulates brown adipose tissue thermogenesis. *Neuroscience*. (2005) 135:627–38. doi: 10.1016/j.neuroscience.2005.06.039
112. Tupone D, Madden CJ, Cano G, Morrison SF. An orexinergic projection from perifornical hypothalamus to raphe pallidus increases rat brown adipose tissue thermogenesis. *J Neurosci*. (2011) 31:15944–55. doi: 10.1523/JNEUROSCI.3909-11.2011
113. Morrison SF, Madden CJ, Tupone D. An orexinergic projection from perifornical hypothalamus to raphe pallidus increases rat brown adipose tissue thermogenesis. *Adipocyte*. (2012) 1:116–20. doi: 10.4161/adip.19736
114. Martins L, Seoane-Collazo P, Contreras C, Gonzalez-Garcia I, Martinez-Sanchez N, Gonzalez F, et al. A functional link between AMPK and Orexin mediates the effect of BMP8B on energy balance. *Cell Rep*. (2016) 16:2231–42. doi: 10.1016/j.celrep.2016.07.045
115. Palmer BF, Clegg DJ. The sexual dimorphism of obesity. *Mol Cell Endocrinol*. (2015) 402:113–9. doi: 10.1016/j.mce.2014.11.029
116. Cypess AM, Lehman S, Williams G, Tal I, Rodman D, Goldfine AB, et al. Identification and importance of brown adipose tissue in adult humans. *N Engl J Med*. (2009) 360:1509–17. doi: 10.1056/NEJMoa0810780
117. Folgueira C, Beiroa D, Porteiro B, Duquenne M, Puighermanal E, Fondevila MF, et al. Hypothalamic dopamine signaling regulates brown fat thermogenesis. *Nat Metab*. (2019) 1:811–29. doi: 10.1038/s42255-019-0099-7
118. Fronczek R, Overeem S, Lammers GJ, van Dijk JG, Van Someren EJ. Altered skin-temperature regulation in narcolepsy relates to sleep propensity. *Sleep*. (2006) 29:1444–9. doi: 10.1093/sleep/29.11.1444
119. Schilperoort M, Hoeke G, Kooijman S, Rensen PC. Relevance of lipid metabolism for brown fat visualization and quantification. *Curr Opin Lipidol*. (2016) 27:242–8. doi: 10.1097/MOL.0000000000000296

120. Enevoldsen LH, Tindborg M, Hovmand NL, Christoffersen C, Ellingsgaard H, Suetta C, et al. Functional brown adipose tissue and sympathetic activity after cold exposure in humans with type 1 narcolepsy. *Sleep*. (2018) 41:zsy092. doi: 10.1093/sleep/zsy092
121. Drissi NM, Romu T, Landtblom AM, Szakacs A, Hallbook T, Darin N, et al. Unexpected fat distribution in adolescents with narcolepsy. *Front Endocrinol*. (2018) 9:728. doi: 10.3389/fendo.2018.00728
122. Tabuchi S, Tsunematsu T, Black SW, Tominaga M, Maruyama M, Takagi K, et al. Conditional ablation of orexin/hypocretin neurons: a new mouse model for the study of narcolepsy and orexin system function. *J Neurosci*. (2014) 34:6495–509. doi: 10.1523/JNEUROSCI.0073-14.2014

Conflict of Interest: The authors declare that the research was conducted in the absence of any commercial or financial relationships that could be construed as a potential conflict of interest.

frontiers in Endocrinology

REVIEW
published: 21 April 2020
doi: 10.3389/fendo.2020.00222

Brown Adipose Tissue, Diet-Induced Thermogenesis, and Thermogenic Food Ingredients: From Mice to Men

Masayuki Saito[1]*, *Mami Matsushita*[2], *Takeshi Yoneshiro*[3] and *Yuko Okamatsu-Ogura*[1]

[1] Faculty of Veterinary Medicine, Hokkaido University, Sapporo, Japan, [2] Department of Nutrition, Tenshi College, Sapporo, Japan, [3] Division of Metabolic Medicine, Research Center for Advanced Science and Technology, The University of Tokyo, Tokyo, Japan

Since the recent rediscovery of brown adipose tissue (BAT) in adult humans, this thermogenic tissue has been attracting increasing interest. The inverse relationship between BAT activity and body fatness suggests that BAT, because of its energy dissipating activity, is protective against body fat accumulation. Cold exposure activates and recruits BAT, resulting in increased energy expenditure and decreased body fatness. The stimulatory effects of cold exposure are mediated through transient receptor potential (TRP) channels and the sympathetic nervous system (SNS). Most TRP members also function as chemesthetic receptors for various food ingredients, and indeed, agonists of TRP vanilloid 1 such as capsaicin and its analog capsinoids mimic the effects of cold exposure to decrease body fatness through the activation and recruitment of BAT. The antiobesity effect of other food ingredients including tea catechins may be attributable, at least in part, to the activation of the TRP–SNS–BAT axis. BAT is also involved in the facultative thermogenesis induced by meal intake, referred to as diet-induced thermogenesis (DIT), which is a significant component of the total energy expenditure in our daily lives. Emerging evidence suggests a crucial role for the SNS in BAT-associated DIT, particularly during the early phase, but several gut-derived humoral factors may also participate in meal-induced BAT activation. One intriguing factor is bile acids, which activate BAT directly through Takeda G-protein receptor 5 (TGR5) in brown adipocytes. Given the apparent beneficial effects of some TRP agonists and bile acids on whole-body substrate and energy metabolism, the TRP/TGR5–BAT axis represents a promising target for combating obesity and related metabolic disorders in humans.

Keywords: bile acids, brown adipose tissue, diet-induced thermogenesis, food ingredients, gut hormone, obesity, sympathetic nervous system, transient receptor potential channels

OPEN ACCESS

Edited by:
Massimiliano Caprio, Università telematica San Raffaele, Italy

Reviewed by:
Marco Infante, University of Miami, United States
Valeria Guglielmi, University of Rome Tor Vergata, Italy

***Correspondence:**
Masayuki Saito
saito@vetmed.hokudai.ac.jp

Specialty section:
This article was submitted to Obesity, a section of the journal Frontiers in Endocrinology

Received: *10 February 2020*
Accepted: *27 March 2020*
Published: *21 April 2020*

Citation:
Saito M, Matsushita M, Yoneshiro T and Okamatsu-Ogura Y (2020) Brown Adipose Tissue, Diet-Induced Thermogenesis, and Thermogenic Food Ingredients: From Mice to Men. Front. Endocrinol. 11:222. doi: 10.3389/fendo.2020.00222

INTRODUCTION

Brown adipose tissue (BAT) has long been recognized as the major site of non-shivering thermogenesis (NST) during cold exposure [cold-induced thermogenesis (CIT)] and arousal from hibernation in small rodents (1). Since the rediscovery of metabolically active BAT using fluorodeoxyglucose (FDG)-positron emission tomography (PET) and computed tomography (CT) in adult humans (2–5), subsequent experimental and clinical studies have dramatically increased our knowledge about the pathophysiological roles of BAT in the regulation of energy balance

and body fatness (6, 7). Human BAT, as in the case of rodent BAT, is activated by acute cold exposure (2, 5) or administration of β-adrenergic receptor (βAR) agonists (8), and contributes to increasing whole-body energy expenditure (EE) and fatty acid oxidation (9–12). The activity and prevalence of BAT substantially decrease in older and obese populations (2, 3, 13–16), and this age-related decline in BAT activity is closely associated with visceral fat accumulation (17). Prolonged exposure to cold recruits BAT, increases EE, and decreases body fat content (18–20). In addition, cold exposure improves glucose metabolism and insulin sensitivity (21–24). Thus, BAT could be a promising target to boost whole-body EE and prevent obesity and related metabolic disorders in humans (25–30).

Although cold exposure is undoubtedly the most physiological and effective regimen to activate and recruit BAT, it would be difficult and uncomfortable to increase human exposure to cold temperatures under well-controlled conditions with the presence of clothing and heating systems. Moreover, chronic cold exposure increases blood pressure (8) and may induce atherosclerosis (31). Thermogenesis observed after food intake [diet-induced thermogenesis (DIT)] is another component of NST. Although the involvement of BAT in DIT has been demonstrated in small rodents, only limited information is currently available in humans. The aim of this review article is to summarize and discuss the evidence for a role of BAT in DIT and thermogenesis induced by certain food ingredients in humans, considering that DIT is a significant component of whole-body EE in our usual daily life.

COLD-INDUCED BAT THERMOGENESIS

Although the mechanism of BAT-dependent CIT has mostly been investigated in small rodents, essentially the same mechanism is believed to work in humans. When animals are exposed to cold temperatures, cold is perceived by temperature sensors, transient receptor potential (TRP) channels, which are membrane proteins that transmit information about changes in the environment such as temperature, touch, pain, osmolarity, and naturally occurring substances (32). Cold-activated TRP on sensory neurons on the body surface transmit information to the brain and increase the activity of sympathetic nerves entering BAT (33). Noradrenaline (NA) released from sympathetic nerve endings stimulates brown adipocytes via the βAR and triggers cyclic adenosine monophosphate (cAMP)-activated intracellular events including hydrolysis of triglyceride, oxidation of resulting fatty acids, and activation of uncoupling protein 1 (UCP1), a key mitochondrial molecule for BAT thermogenesis. Sympathetic activation also results in increased fat mobilization in white adipose tissue, and released fatty acids are used in peripheral tissues including BAT. Although the principal substrate for BAT thermogenesis is fatty acids, glucose utilization is also enhanced in parallel with UCP1 activation, probably for a sufficient supply of oxaloacetate to enable the rapid oxidation of fatty acids and acetyl coenzyme A (CoA), and also for recovery of cellular adenosine triphosphate (ATP) levels by activating anaerobic glycolysis (34). Thus, UCP1-dependent glucose utilization could be a metabolic index of BAT thermogenesis, and has been applied in FDG-PET for assessing human BAT.

When animals are exposed to cold temperatures for a long time, they adapt to their surroundings by increasing the number of brown adipocytes and the amount of UCP1 through the proliferation of interstitial preadipocytes and matured adipocytes (35, 36). In addition to BAT hyperplasia, prolonged cold exposure gives rise to an apparent induction of UCP1-positive adipocytes in white adipose tissue. This type of adipocytes, termed "beige" or "brite" cells, is developmentally distinct from "classical" brown adipocytes, which derive from Myf5-positive myoblastic cells (6, 37). Thus, chronic cold exposure results in increased EE through the persistent activation and recruitment of classical brown adipocytes and beige cells, and the consequent "browning" of white adipose tissue and body fat reduction. As the FDG-PET/CT-detected and UCP1-positive human adipose depot consists of a mixture of brown and beige adipocytes (38–41), hereafter we shall refer to it collectively as BAT.

DIET-INDUCED ACTIVATION OF BAT

EE above the basal metabolic rate in response to meal intake is referred to as the "specific dynamic action of food," "thermic effects of food," or "DIT." The term DIT has often been used to describe the adaptive increase in EE observed after long-term overfeeding, which is also known as "luxury consumption" or "luxosconsumption." Since the publication of the report of Rothwell and Stock (42) in 1979, it has been demonstrated in small rodents that daily spontaneous feeding of high-calorie diets such as high-fat and cafeteria diets resulted in a lower energy efficiency with less weight gained than expected on the basis of on caloric intake, in parallel with an increased BAT activity and EE (43). The adaptive changes in response to overfeeding are not observed in animals without UCP1 (44). Thus, the role of BAT in adaptive increase in EE and maintaining energy balance seems to have been accepted, albeit not widely supported (45).

Thermogenesis after a single meal is expressed as the percentage of the energy content of the food ingested (∼10% for standard meals in humans). This is usually divided into two components: obligatory and facultative thermogenesis. Obligatory thermogenesis refers to the obligatory response including digestion, absorption, and storage of ingested nutrients, whereas facultative thermogenesis refers to the additional responses to obligatory thermogenesis and may be closely related to the adaptive increase in EE. In this work, we tentatively refer to facultative thermogenesis in response to single

Abbreviations: βAR, β-adrenergic receptor; BA, bile acids; BAT, brown adipose tissue; CCK, cholecystokinin; CIT, cold-induced thermogenesis; COMT, catechol-*O*-methyl transferase; CT, computed tomography; DIT, diet-induced thermogenesis; EE, energy expenditure; DHA, docosahexaenoic acid; EPA, eicosapentaenoic acid; FDG, fluorodeoxyglucose; GLP-1, glucagon-like peptide-1; GP, Grains of Paradise; NA, noradrenaline; NST, nonshivering metabolic thermogenesis; PET, positron emission tomography; SCTR, secretin receptor; SNS, sympathetic nervous system; TGR5, G-protein-coupled bile acid-activated receptor; TRP, transient receptor potential channel; TRPA1, TRP ankyrin subfamily member 1; TRPM8, TRP metastatin 8; TRPV1, TRP vanilloid 1; UCP1, uncoupling protein 1.

meals as DIT and discuss its mechanisms and pathophysiological relevance in the context with BAT.

Activation of BAT after a single meal was suggested in the 1980s by Glick et al. (46), who reported increased respiration rate of BAT in 2 h after food intake in rats. They also demonstrated a meal-induced increase in guanosine 5′-diphosphate (GDP) binding to mitochondria isolated from BAT, which was used as an index of UCP1 activation (47). Our team (48) found meal-induced metabolic activation of BAT in rats—that is, in 30 min after oral intake of a liquid meal, glucose utilization and fatty acid synthesis were increased in intact BAT, but to a much lower extent in surgically denervated BAT. The critical role of UCP1 in DIT was proved by simultaneous 24-h recording of food intake and oxygen consumption in UCP1-deficient mice maintained at a thermoneutral temperature of 30°C—that is, whole-body oxygen consumption in UCP1-deficient mice was lower than that in wild-type mice, particularly during the eating period (44).

DIET-INDUCED BAT THERMOGENESIS IN HUMANS

In humans, the possible contribution of BAT thermogenesis to DIT and regulation of energy balance have been suggested by studies on single nucleotide polymorphism in some BAT-related genes. For example, Trp64Arg mutation in the β3 adrenergic receptor (*β3AR*) gene and A3826G mutation in the *UCP1* gene are associated with higher body fatness, lower metabolic rate, and smaller weight loss via treatment with low-calorie diets (49–52). Nagai et al. (53) examined the effects of A-3826G mutation in the *UCP1* gene on DIT in boys, and found a reduced response 3 h after a high-fat meal in those carrying the G allele. They also found diminished CIT in the group with the GG allele compared with those carrying the AA + AG alleles (54).

Rediscovery of BAT in adult humans has prompted further studies to test whether BAT thermogenesis is activated after single meals. Vrieze et al. (55) measured BAT activity using FDG-PET/CT in healthy volunteers 90 min after meal intake, and unexpectedly found a reduction in FDG uptake into BAT compared with that after overnight fasting. Vosselman et al. (56) also reported that postprandial FDG uptake into BAT was much lower than cold-induced uptake, whereas whole-body EE was comparable. Although these results seem to be in conflict with the idea of postprandial activation of BAT thermogenesis, they can be explained by increased insulin-stimulated FDG uptake into skeletal muscle, which reduces FDG bioavailability for BAT, which in turn leads to underestimation of BAT activity. FDG uptake after a mild cold exposure is increased specifically in BAT, whereas that after food intake is increased in many insulin-sensitive tissues such as skeletal muscle, brown and white adipose tissue, and heart (10). Thus, although FDG uptake into BAT can be used as an index of BAT activity under certain restricted conditions, it is not always associated with BAT thermogenesis.

This limitation of FDG-PET/CT is overcome by measuring oxygen uptake using $^{15}O[O_2]$-PET and blood flow using $^{15}O[H_2O]$-PET, which are more descriptive indicators of thermogenesis and mitochondrial substrate oxidation. In fact, acute cold exposure evoked a marked increase in oxygen consumption and blood flow in parallel with increased whole-body EE (57). Moreover, Din et al. (58) demonstrated that oxygen consumption and blood flow in BAT rose immediately after meal intake to an extent comparable to those observed after cold exposure. To confirm the role of BAT in DIT, we measured whole-body EE continuously for 24 h in healthy humans using a human calorimeter (59). When the participants were divided into high BAT and low BAT groups according to the result of FDG-PET/CT examination, there was no significant difference in body composition and resting EE between the two groups. However, EE after meals was significantly higher in the high BAT group (9.7% of the total energy intake) than in the low BAT group (6.5%). Of note, the 24-h respiratory quotient was also apparently lower in the high BAT group, implying higher fat oxidation. Higher postprandial whole-body EE and substrate oxidation were also confirmed in participants with higher BAT activities (57). All these results indicate that BAT contributes to DIT, at least in part, in humans. This may also be indirectly supported by the finding that BAT recruitment by prolonged cold exposure is accompanied by enhanced DIT (21).

MECHANISMS OF DIT: THE SYMPATHETIC NERVOUS SYSTEM (SNS)

Based on the principal role of the SNS–βAR axis for CIT, it is conceivable that this axis is a key mechanism in diet-induced/postprandial BAT thermogenesis (**Figure 1**). In fact, in both experimental animals and humans, the plasma levels of NA and tissue NA turnover are low during fasting but increases immediately after food intake (60–63). Moreover, SNS activity in BAT estimated from tissue NA turnover is increased in mice chronically overfed with cafeteria and high-calorie diets (64, 65). Meanwhile, our team (48) found that in rats metabolic activation of BAT after intake of a liquid meal was diminished after surgical severing of sympathetic nerves entering BAT. These results are in line with the idea that diet-induced/postprandial BAT thermogenesis is mediated through sympathetic nerve activation. One interesting observation in our studies was that the meal-induced metabolic activation and NA turnover in BAT were reduced in rats given the same meal through a gastric tube. In the case of humans and dogs, LeBlanc et al. (66, 67) showed that responses in oxygen consumption, and plasma levels of NA and insulin shortly (1–2 h) after food intake were substantially reduced when food was administered through a stomach tube. They also reported lowered postprandial thermogenesis with a non-palatable meal in comparison with a highly palatable meal, despite using the same composition and amount in both meals (68). These results suggest that food palatability and oropharyngeal taste sensation play a significant role in diet-induced sympathetic activation and BAT thermogenesis. This may be consistent with the observation that the cafeteria feeding regimen with palatable foods is most efficient in producing a concomitant voluntary hyperphagia, elevated SNS activity, and BAT hyperplasia, thereby resulting in "luxusconsumption."

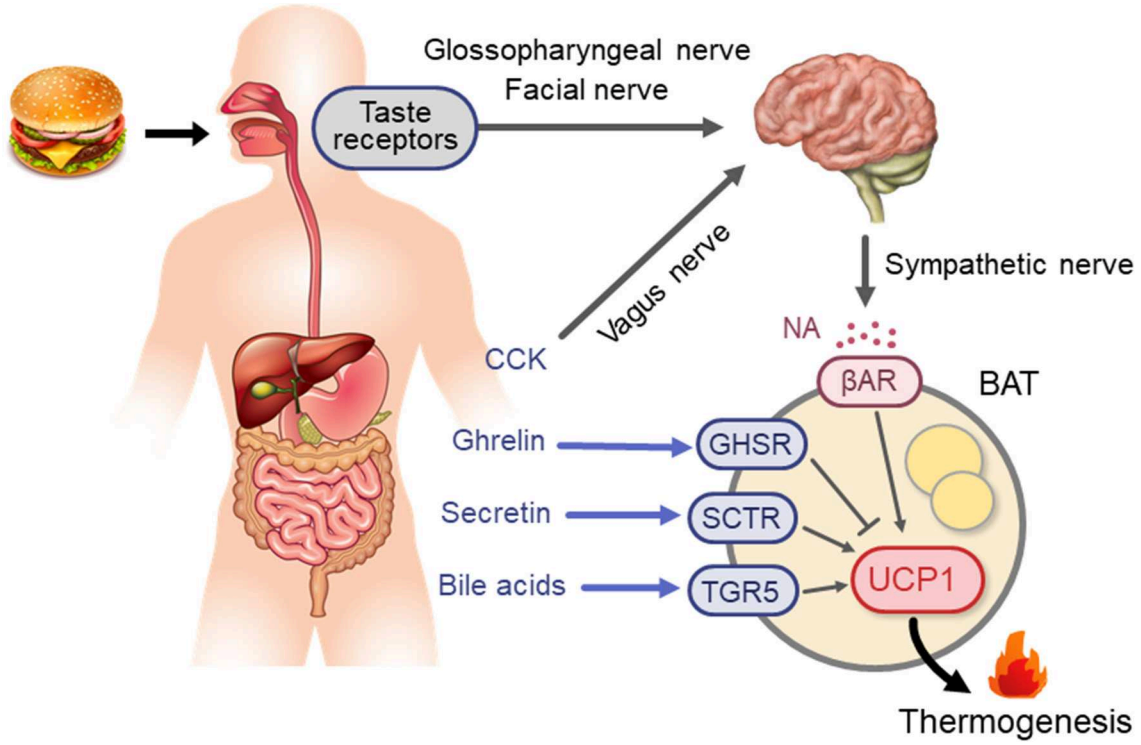

FIGURE 1 | Neural and endocrine mechanisms for BAT thermogenesis activated after meal intake. βAR, β-adrenergic receptor; BA, bile acids; BAT, brown adipose tissue; CCK, cholecystokinin; GHSR, ghrelin receptor; NA, noradrenaline; SCTR, secretin receptor; TGR5, G-protein-coupled bile acid-activated receptor; UCP1, uncoupling protein 1.

Thus, the SNS–BAT axis may be crucial for DIT, particularly during the early phase, in the same way as for CIT; however, this implication still seems controversial in humans. Wijers et al. (69) reported considerable interindividual variations in thermogenic responses to 84-h intervention by overfeeding and mild cold exposure in 13 male individuals, but a high correlation between the responses to the two interventions, suggesting a common regulation mechanism shared in DIT and CIT. However, there have been reports of an apparent dissociation of DIT with CIT in cold-adapted humans. For example, Peterson et al. (70) demonstrated that daily exposure of healthy men to cold temperatures for 4 weeks resulted in a 2-fold increase in CIT, in parallel with increased SNS activity, whereas it did not change the thermic effect of food. Lee et al. (21) also reported a dissociation between the effects of prolonged cold exposure on DIT and CIT. Moreover, blockade of βAR with propranolol was demonstrated to have only a small effect on the increase in whole-body EE after intake of carbohydrate-rich meals (71–73). All these results suggest that DIT in humans is regulated by some mechanisms different from, and/or in combination with, the SNS–βAR axis.

MECHANISMS OF DIT: GUT HORMONES AND BILE ACIDS

One of the likely factors involved in DIT may be gut hormones. Li et al. (74) found abundant expression of the secretin receptor (SCTR) in murine brown adipocytes, and demonstrated that secretin activates UCP1- and SCTR-dependent thermogenesis *in vitro* and *in vivo*. They also confirmed that the increment of plasma secretin levels induced by a single meal positively correlated with oxygen consumption and fatty acid uptake rates in BAT in humans. These observations collectively support the idea that meal-associated increase in circulating secretin activates BAT thermogenesis by binding to SCTR in brown adipocytes. Direct evidence for the thermogenic action of secretin on human BAT was obtained using FDG-PET/CT after secretin infusion, which significantly increased FDG uptake in supraclavicular BAT.

In addition to secretin, other gut hormones are also known to activate or suppress BAT thermogenesis in small rodents. Recently, Yamazaki et al. (75) reported that in rats, peripherally administered cholecystokinin (CCK) activates the SNS–BAT axis via the CCK receptor and vagal afferent nerves. Blouet and Shwartz (76) also demonstrated that in rats BAT thermogenesis induced by intraduodenal administration of lipids was abolished by administration of either the CCK receptor antagonist devazepide or the *N*-methyl-D-aspartate receptor blocker MK-801 directly into the caudomedial nucleus of the solitary tract. These results collectively indicate that CCK activates BAT thermogenesis via vagal afferent and sympathetic efferent nerves. In fact, Vijgen et al. (77) demonstrated that vagal afferents played a role in BAT thermogenesis in humans: vagus nerve

stimulation significantly increases whole-body EE in parallel with BAT activity assessed by FDG-PET/CT.

CCK is an anorexigenic hormone secreted from the duodenum after food intake, whereas ghrelin is an orexigenic hormone and its secretion from the stomach is reduced after food intake. Lin et al. (78) reported that ghrelin decreases UCP1 expression in brown adipocytes, and that during aging, plasma ghrelin and ghrelin receptor expression in BAT increases whereas BAT thermogenesis declines. It is thus possible that reduced secretion of ghrelin, together with increased secretion of CCK and secretin, contributes to BAT activation in response to food intake. This may be supported by an association of BAT with systemic concentrations of some gut hormones including ghrelin in humans (79). Thus, there are multiple factors/mechanisms for diet-induced/postprandial BAT thermogenesis, their actions being synergistic or independent of each other. However, the precise nature of their roles in DIT and whole-body EE in humans remain largely unexplained to date.

Another humoral factor may be bile acids (BA), which are secreted into the intestinal lumen in response to meal intake, modified by gut flora, and mostly returned to the liver. During enterohepatic circulation, BA is partially transferred into general circulation, resulting in a rapid postprandial increase in its plasma concentration (80, 81). BA are now recognized as a metabolic regulator, affecting multiple functions, in addition to lipid-digestive functions, to regulate energy metabolism, as well as glucose and lipid metabolism, through the activation of nuclear farnesoid X receptor and the G protein-coupled membrane receptor TGR5 (Takeda G-protein receptor 5) (82). In connection with the thermogenic and antiobesity effects of BA, Watanabe et al. (83) demonstrated that in mice BA activates TGR5 in brown adipocytes, leading to activation of type 2 deiodinase and increased thermogenic activity. Similar direct stimulatory effects of BA chenodeoxycholic acid on BAT were reported in humans using brown adipocytes *in vitro* and using FDG-PET/CT *in vivo* (84). BA also stimulates intestinal L-cell TGR5 to secrete glucagon-like peptide-1 (GLP-1). Although GLP-1 is known as an incretin to stimulate insulin secretion, it activates BAT thermogenesis and induces beige fat development through the action on its receptor in the hypothalamus (85) and the AMPK–SIRT-1–PGC1-α (AMP-activated protein kinase–sirtuin 1–peroxisome proliferator-activated receptor gamma coactivator 1-alpha) cell signaling pathway (86). Crucial roles of TGR5 were also demonstrated in browning of white adipose tissue under multiple environmental cues including cold exposure and prolonged high-fat diet feeding (87).

BAT THERMOGENESIS AND DIETARY FAT

Thermogenesis after a single meal is usually estimated to be 10% for standard meals; it varies depending on the composition of meals, being ∼3% for fat, 7% for carbohydrate, and 30% for protein. In contrast, sympathetic and BAT activation, and probably facultative thermogenesis (DIT), are low in animals fed on high-protein diets (88, 89). Accordingly, high-fat diets and/or cafeteria diets with high carbohydrate and fat contents have been widely used for activation and recruitment of BAT. In this context, what is interesting is that some types of dietary fat including fish oil help prevent cardiovascular and metabolic diseases, and visceral fat accumulation (90). Moreover, several studies conducted in human volunteers have reported that postprandial thermogenesis is greater after intake of a meal rich in polyunsaturated fatty acids compared to that rich in monosaturated and saturated fatty acids (91, 92). Earlier studies in rats have revealed that dietary fish oil and/or eicosapentaenoic acid (EPA) and docosahexaenoic acid (DHA) rich in fish oil enhance EE and prevent fat accumulation by inducing UCP1 in BAT (93, 94). Kim et al. (95) reported that UCP1 induction by dietary EPA and DHA is blocked by either subdiaphragmatic vagotomy or treatment with a βAR blocker. They also demonstrated that the thermogenic and antiobesity effects of EPA and DHA are abolished in mice lacking TRP vanilloid 1 (TRPV1), a member of the TRP family activated by vanilloid compounds. Considering that EPA and DHA have agonistic activity on TRPV1, it is likely that these polyunsaturated fatty acids stimulate the vagus nerve through TRPV1 in the gut, thereby activating the SNS–βAR axis and BAT thermogenesis (**Figure 2**).

In addition, direct action mechanisms of EPA in brown adipocytes have also been proposed. To cite an example, Kim et al. (96) reported that EPA is sensed by the membrane receptor free fatty acid receptor 4 in brown adipocytes, resulting in biogenesis of the microRNAs miR-30b and miR-378 and an increase of intracellular cAMP levels, both of which promote the transcriptional activation of brown adipogenesis, including UCP1 induction. The UCP1-inducing effects of EPA are also reported to be mediated via inhibition of production of ω6-derived oxygenated metabolites, such as oxylipins, that can impair UCP1 activation and induction (97). Despite the abundance of evidence in rodents, however, the thermogenic effect of EPA and DHA and its relation to BAT in humans remain to be investigated. In this context, one interesting development is a recent report by Leiria et al. (98), who observed that administration of a β3AR agonist induces a rapid increase in the plasma levels of 12- hydroxyeicosapentaenoic acid (12-HEPE) and 14-hydroxydocosahesanoic acids (14-HDHA), lipoxygenase products of EPA and DHA, in parallel with the BAT activity assessed by FDG-PET/CT, in humans. They also demonstrated in mice that activated brown adipocytes released 12-HEPE to promote glucose uptake into skeletal muscle and adipose tissues. Thus, it seems possible that 12-HEPE is a BAT-derived factor that improves insulin sensitivity and glucose metabolism (21–24).

BAT THERMOGENESIS INDUCED BY CAPSAICIN AND CAPSINOIDS

BAT thermogenesis is also induced by various non-caloric food ingredients and natural substances. One example of such ingredients is capsaicin, the major pungent component of chili peppers, which happens to be a potent activator of TRPV1. Capsaicin is the most consumed spice in the world, and its health beneficial effects, including thermogenic and antiobesity activities, have been known for centuries (99–101). However, because of its strong pungency, not everyone can consume capsaicin in large quantities. Capsinoids (capsiate,

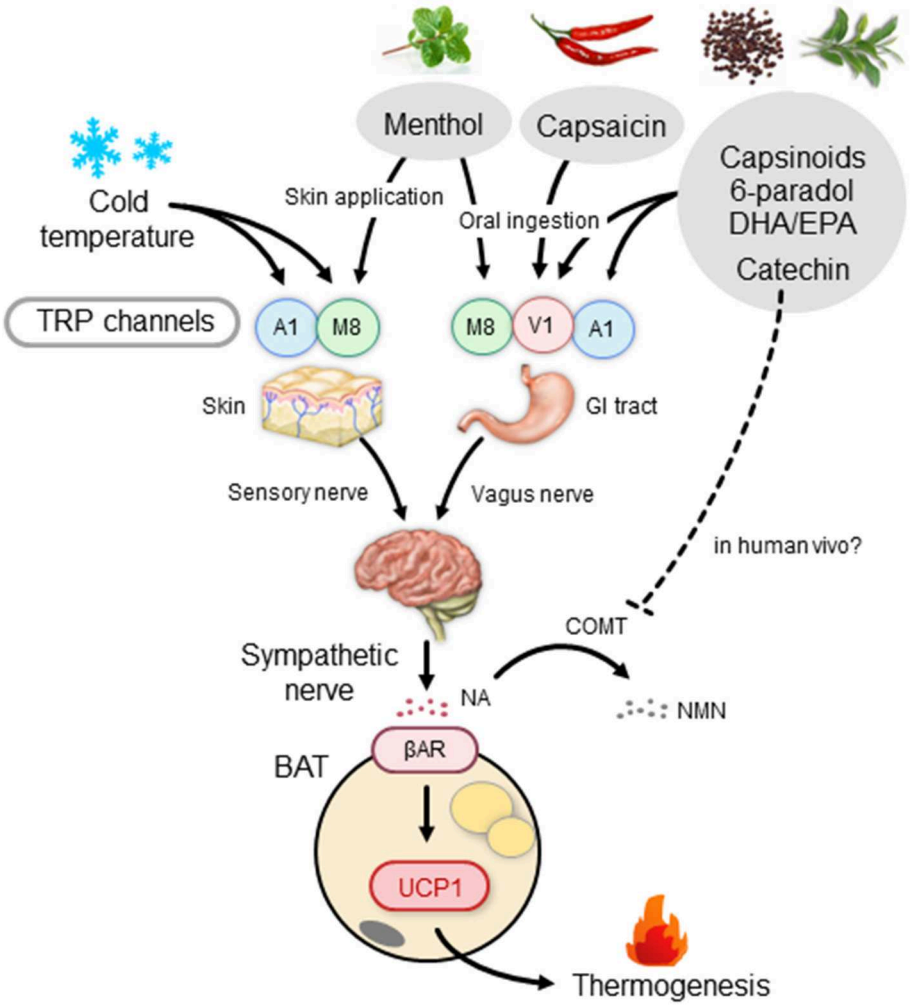

FIGURE 2 | BAT thermogenesis through the activation of the TRP–SNS axis by food ingredients. βAR, β-adrenergic receptor; BAT, brown adipose tissue; COMT, catechol-*O*-methyl transferase; DHA, docosahexaenoic acid; EPA, eicosapentaenoic acid; GI tract, gastrointestinal tract; NA, noradrenaline; NMN, normetanephrine; SNS, sympathetic nervous system; TRP, transient receptor potential channel; A1, TRP ankyrin subfamily member 1; M8, TRP metastatin 8; V1, TRP vanilloid 1; UCP1, uncoupling protein 1.

dihydrocapsiate, and nordihydrocapsiate) are capsaicin-like compounds found in a non-pungent type of red pepper, "CH-19 Sweet" (102). Capsaicin and capsinoids bind to TRPV1 with comparable affinities; however, pungency is much less defined in capsinoids (1/1,000). The low pungency exhibited by capsinoids may be attributable to the high lipophilicity of capsinoids, which render these molecules unable to access the termini of trigeminal nerves in the oral cavity, which is covered with epithelium (103).

Animal studies have demonstrated that oral administration of capsaicin and/or capsinoids can activate TRPV1 expressed in sensory nerves within the gastrointestinal tract and increase sympathetic nerve activity innervating BAT, inducing a rapid increase in BAT temperature, increasing whole-body EE, and decreasing body fat (104–106). These responses are blunted by the administration of β-adrenergic blockers (106) or through the denervation of vagal afferents and extrinsic nerves connected to the jejunum (104, 105). It was also reported that the thermogenic and fat-reducing effects of capsinoids are diminished in mice lacking either TRPV1 or UCP1 (105, 107, 108). Taken together, oral administration of either pungent capsaicin or non-pungent capsinoids increases whole-body EE and prevents obesity through the activation of the TRPV1–SNS–BAT axis in small rodents. It is possible that capsaicin also acts directly on TRPV1 expressed in BAT (109). By contrast, the direct action of capsinoids on TRPV1 in brown adipocytes is unlikely because orally ingested capsinoids are rapidly hydrolyzed in the small intestine and are usually undetectable in general circulation (110).

In humans, our team (111) found that a single oral ingestion of capsinoids increases EE in individuals with metabolically active BAT, but not in those without it. These findings indicate that the thermogenic effects of capsinoids are dependent on the presence of BAT—implying that capsinoids activate BAT and thereby increase EE. Furthermore, daily ingestion of capsinoids

for 6 weeks augments CIT in individuals with low BAT activities (18). Because interindividual (26) and intraindividual variations of CIT (112) are significantly related to BAT activity assessed by FDG-PET/CT, the capsinoid-induced increase in CIT reflects the recruitment of BAT. This was directly confirmed by using FDG-PET/CT (113, 114) and also through near-infrared time-resolved spectroscopy (NIRTRS) (114), a novel method for evaluating BAT density in a specific region of interest (115). Thus, capsinoids have the potential to activate and recruit human BAT, thereby contributing to their antiobesity effect. Indeed, after a 12-week oral ingestion of capsinoids, a slight but significant reduction of abdominal fat was observed in a group of obese individuals (116). Notably, the fat-reducing effect of capsinoids is attenuated in individuals who carry a mutated (Val585Ile) TRPV1 (116), consistent with the crucial role of TRPV1 in mice. As single and daily oral ingestions of capsinoids at doses of 30 (110) and 6–9 mg/day for 6–12 weeks (18, 114, 116), respectively, produced no serious adverse events, dietary supplementation with capsinoids appears to be safe and feasible for combating obesity.

Although the effects of capsinoids are similar to those of cold exposure, TRPV1 is not a cold sensor, but rather a sensor of noxious hot temperatures and low pH (117). It is therefore expected that human BAT is activated by nociceptive stimuli, including TRPV1 activation. In agreement with this concept, chronic adrenergic stress induced by burn trauma results in browning of white adipose tissue (118). Hence, it is conceivable that oral ingestion of capsinoids would lead to the activation of BAT thermogenesis through the TRPV1-mediated pathway in humans, whereas cold exposure would be more potent in inducing BAT activation than capsinoid ingestion (113). In light of a recent report claiming that capsinoid treatment in mice potentiates cold-induced browning of white fat (119), a combination of capsinoid supplementation and mild cold exposure may be an effective strategy for recruitment of BAT in humans.

ACTIVATION AND RECRUITMENT OF BAT BY TEA CAFFEINE AND CATECHINS

Other intriguing food ingredients that activate BAT thermogenesis are caffeine and catechins, which are abundantly found in green tea. Tea is made from the leaves of *Camellia sinensis* L., a species belonging to the Theaceae family. The manufacturing process produces various types of tea such as non-oxidized, non-fermented green tea, semifermented Oolong tea, and fermented black and red teas. These teas, particularly green tea, contain relatively large amounts of polyphenols, such as epicatechin and epigallocatechin gallate, which have various health benefits such as antiobesity, anticarcinogenic, and antibacterial properties (120, 121).

An apparent thermogenic effect of green tea extract in humans was reported first by Dulloo et al. (122). They demonstrated that ingestion of green tea extract containing catechins and caffeine elicited a 4% increase in 24-h EE coupled with an increase in fat oxidation. Ingestion of caffeine alone had only a very slight effect on EE, implying that the effects of green tea extract is mainly attributable to thermogenesis by catechins. Since then, the short-term thermogenic effects of green tea extract and/or catechins have been confirmed by several studies using various doses of the extract and duration (123–125). Their long-term effects on body fatness have also been repeatedly investigated. For example, Nagao et al. (126) reported a small (2–3%) but significant reduction of body fat content in a group of Japanese volunteers who underwent 12 weeks of treatment with green tea extract containing catechins. Similar fat-reducing effects of catechins were also confirmed in other studies (127–130), although there is also a report showing that there was no significant effect (131).

Although the possible involvement of BAT in the thermogenic and antiobesity effects of catechins has been suggested (132, 133), no evidence supporting this claim has been reported in humans. Recently, we found that an oral ingestion of catechin-rich tea produced a rapid increase in EE in individuals with higher BAT activities, but not in those with undetectable BAT activities (134). Moreover, a 5-week daily ingestion of catechin-rich tea resulted in a significant increase in CIT, an index of BAT activity. Although the active and placebo beverages contained a moderate amount of caffeine, the placebo ingestion did not produce any change in EE and CIT. The chronic effects of catechins on BAT were also confirmed using the NIRSTRS technique (135). Thus, it is highly likely that the observed thermogenesis is attributable to catechin, rather than caffeine. However, this does not rule out a possible synergistic action between catechins and caffeine (136, 137). Collectively, the thermogenic and fat-reducing effects of green tea extract rich in catechins would be attributable to the activation of BAT.

The thermogenic response to green tea extract has been proposed to be mediated through the direct stimulation of the NA–βAR cascade in BAT by inhibiting a catecholamine-degrading enzyme, catechol-*O*-methyl transferase (COMT), by catechins and a cAMP-degrading enzyme, phosphodiesterase, by caffeine (133). In support of this claim, Velickovic et al. (138) demonstrated a temperature increase in the supraclavicular region, which colocates to the main region of BAT, after intake of caffeine-rich coffee. However, COMT activity may not be impaired by oral catechin ingestion in humans (139), because of the much lower circulating levels of catechins after a single ingestion ($\sim$0.1 μM at maximum) (140) compared with the half-maximal inhibitory concentration for the COMT activity ($\sim$14 μM) (141). Thus, the role of COMT inhibition as a primary target of the catechin action on BAT thermogenesis remains controversial. To this end, it is interesting that Kurogi et al. (142, 143) reported that green tea epigallocatechin gallate and its auto-oxidation products activated TRPV1 and TRP ankyrin subfamily member 1 (TRPA1), another member of the TRP family, in intestinal enteroendocrine cells at concentrations comparable to those in the gastrointestinal tract after oral ingestion. It is thus possible that catechins activate and recruit BAT through the action on TRPV1/TRPA1 in sensory neurons in the gastrointestinal tract, in the same manner as capsinoids; however, further studies are necessary to confirm this theory.

THE TRP–BAT AXIS AS A TARGET OF ANTIOBESITY FOOD INGREDIENTS

In addition to capsaicin, capsinoids, and catechins, there are other food ingredients, particularly those in spicy foods, with agonistic activity to TRPV1 (144). For example, piperine is responsible for the pungency of black and white pepper; meanwhile, gingerols, shogaol, zingerone, and 6-paradol are found in ginger, some of which might be expected to activate BAT thermogenesis and reduce body fat. The seeds of Grains of Paradise [*Aframomumu melegueta* [Rosco] *K. Schum*.] (GP), which is also known as Guinea pepper or alligator pepper, are rich in 6-paradol and are commonly used as a spice for flavoring food; they also have a wide range of ethnobotanical uses (145). In humans, we found thermogenic responses to oral ingestion of an alcohol extract of GP in individuals with metabolically active BAT, but not in those without it (146), implying a BAT-dependent thermogenesis by GP extract. In line with the acute effects, in one study, daily ingestion of GP extract for 4 weeks resulted in a slight reduction in visceral fat (147). These results suggest that GP, like capsinoids and catechins, increases whole-body EE through the activation of BAT, thereby decreasing body fatness.

As noted above, TRPV1 is not a cold sensor, but a sensor of noxious hot temperatures higher than 43°C. Among the members of the TRP family, TRP metastatin 8 (TRPM8) and TRPA1 are the most likely receptor candidates to be sensitive to lower temperatures. As the mean activation temperatures of these two TRPs are lower than 17–25°C, chemical activation of these receptors is expected to mimic the effects of a mild cold exposure. A representative TRPM8 agonist is menthol, a cooling and flavor compound in mint. Application of menthol to the skin of whole trunk in mice was shown to induce autonomic and BAT responses, but at a much lower extent in TRPM8-deficient mice (148). A rapid increase in core and BAT temperatures was also observed after intragastric administration of menthol and 1,8-cineole, another TRPM8 agonist (149). Using mice lacking either TRPM8 or UCP1, Ma et al. (150) reported that a diet supplemented with menthol enhances UCP1-dependent thermogenesis and prevents high-fat diet-induced obesity in a TRPM8-dependent manner. In humans, a slight but significant elevation of metabolic rate after a single skin menthol administration was observed (151), although its relation to BAT was not investigated.

TRPA1 is activated by various pungent compounds, such as ally- and benzyl-isothiocyanates in mustard and wasabi (Japanese horseradish) and cinnamaldehyde in cinnamon or dried bark of cassia. These compounds are known to increase thermogenesis and UCP1 expression, and decrease body fat (149, 152, 153). In addition to these food ingredients, there are various natural compounds having agonistic activity for TRPM8 and TRPA1, some of which may also have the potential to activate BAT thermogenesis and reduce body fat. However, despite the evidence for BAT activation by these food ingredients in small rodents, their thermogenic and antiobesity effects, particularly those on BAT, have yet to be elucidated in humans.

CONCLUSION AND PERSPECTIVE

Since the rediscovery of metabolically active BAT in adult humans, BAT has been attracting increasing attention as a promising target for combating obesity and related diseases. In fact, several drugs targeting BAT have been tested for pharmacotherapy of obesity (154). In physiological terms, BAT thermogenesis is activated either by exposure to cold temperatures or after meal intake, but diet-induced BAT activation may contribute more significantly to whole-body EE in our usual daily life. As discussed above, BAT is activated by various postprandially secreted humoral factors such as BA and gut hormones, and by certain food ingredients acting on the TRP–SNS axis. Recent studies have shown that BAT is also involved in the regulation of systemic glucose and lipid homeostasis, directly by its intrinsic metabolic activity and probably through some BAT-derived humoral factors "batokines" (155). This may explain why some TRP agonists including capsinoids ameliorate insulin sensitivity and glucose homeostasis (156). Given the beneficial effects of various food ingredients and BA on substrate and energy metabolism, compounds activating the TRP/TGR5–BAT axis, by themselves and/or in combination with some drug, represent a promising option for combating obesity and related metabolic disorders.

In addition to the food ingredients discussed above, various food compounds such as curcumin, quercetin, thyme, allicin, retinoid acid, and resveratrols have been reported to activate and recruit BAT thermogenesis via multiple actions of mechanism that are either similar to or distinct from TRP-mediated processes (157, 158). Interestingly, the effects of some of these compounds including EPA are suggested to be mediated through the production of microRNAs (96, 159). However, most of these effects have been observed in studies using cells *in vitro* and mice/rats *in vivo*, whereas comparative evidence in humans is very limited. One of the reasons for this large gap may be related to the method used in assessing human BAT. To date, FDG-PET/CT is a standard tool used to measure human BAT (160); however, this option has serious limitations, including the enormous cost of the devices, radiation exposure, and acute cold exposure, which make repeated measurements difficult and an impediment in basic and clinical studies. There is therefore an urgent need to establish less invasive and simpler methods for quantitative assessment of human BAT. This would promote the development of practical, easy, and effective antiobesity regimens, particularly when searching for dietary factors/food ingredients that can activate and recruit BAT in humans.

AUTHOR CONTRIBUTIONS

MS wrote the first draft of the manuscript. TY reviewed the manuscript and drafted the figures. MM and YO-O critically reviewed the manuscript.

FUNDING

This study was supported by a Grant-in-Aid for Scientific Research from the Ministry of Education, Culture, Sports, Science, and Technology of Japan (Nos. 22590227, 24240092, 26860703, 16K15485, 18K11013).

REFERENCES

1. Cannon B, Nedergaard J. Brown adipose tissue: function and physiological significance. *Physiol Rev*. (2004) 84:277–359. doi: 10.1152/physrev.00015.2003
2. Saito M, Okamatsu-Ogura Y, Matsushita M, Watanabe K, Yoneshiro T, Nio-Kobayashi J, et al. High incidence of metabolically active brown adipose tissue in healthy adult humans: effects of cold exposure and adiposity. *Diabetes*. (2009) 58:1526–31. doi: 10.2337/db09-0530
3. van Marken Lichtenbelt WD, Vanhommerig JW, Smulders NM, Drossaerts JM, Kemerink GJ, Bouvy ND, et al. Cold-activated brown adipose tissue in healthy men. *N. Engl J Med*. (2009) 360:1500–8. doi: 10.1056/NEJMoa0808718
4. Cypess AM, Lehman S, Williams G, Tal I, Rodman D, Goldfine AB, et al. Identification and importance of brown adipose tissue in adult humans. *N Engl J Med*. (2009) 360:1509–17. doi: 10.1056/NEJMoa0810780
5. Virtanen KA, Lidell ME, Orava J, Heglind M, Westergren R, Niemi T, et al. Functional brown adipose tissue in healthy adults. *N Engl J Med*. (2009) 360:1518–25. doi: 10.1056/NEJMoa0808949
6. Kajimura S, Saito M. A new era in brown adipose tissue biology: molecular control of brown fat development and energy homeostasis. *Annu Rev Physiol*. (2014) 76:225–49. doi: 10.1146/annurev-physiol-021113-170252
7. Carpentier AC, Blondin DP, Virtanen KA, Richard D, Haman F, Turcotte EE. Brown adipose tissue energy metabolism in humans. *Front Endocrinol*. (2018) 9:447. doi: 10.3389/fendo.2018.00447
8. Cypess AM, Weiner LS, Roberts-Toler C, Franquet Elia E, Kessler SH, Kahn PA, et al. Activation of human brown adipose tissue by a β3-adrenergic receptor agonist. *Cell Metab*. (2015) 21:33–8. doi: 10.1016/j.cmet.2014.12.009
9. Yoneshiro T, Aita S, Matsushita M, Kameya T, Nakada K, Kawai Y, et al. Brown adipose tissue, whole-body energy expenditure, and thermogenesis in healthy adult men. *Obesity*. (2011) 19:13–6. doi: 10.1038/oby.2010.105
10. Orava J, Nuutila P, Lidell ME, Oikonen V, Noponen T, Viljanen T, et al. Different metabolic responses of human brown adipose tissue to activation by cold and insulin. *Cell Metab*. (2011) 14:272–9. doi: 10.1016/j.cmet.2011.06.012
11. Ouellet V, Labbe SM, Blondin DP, Phoenix S, Guerin B, Haman F, et al. Brown adipose tissue oxidative metabolism contributes to energy expenditure during acute cold exposure in humans. *J Clin Invest*. (2012) 122:545–52. doi: 10.1172/JCI60433
12. Chen KY, Brychta RJ, Linderman JD, Smith S, Courville A, Dieckmann W, et al. Brown fat activation mediates cold-induced thermogenesis in adult humans in response to a mild decrease in ambient temperature. *J Clin Endocrinol Metab*. (2013) 98:E1218–23. doi: 10.1210/jc.2012-4213
13. Pfannenberg C, Werner MK, Ripkens S, Stef I, Deckert A, Schmadl M, et al. Impact of age on the relationships of brown adipose tissue with sex and adiposity in humans. *Diabetes*. (2010) 59:1789–93. doi: 10.2337/db10-0004
14. Ouellet V, Routhier-Labadie A, Bellemare W, Lakhal-Chaieb L, Turcotte E, Carpentier AC, et al. Outdoor temperature, age, sex, body mass index, and diabetic status determine the prevalence, mass, and glucose-uptake activity of 18F-FDG-detected BAT in humans. *J Clin Endocrinol Metab*. (2011) 96:192–9. doi: 10.1210/jc.2010-0989
15. Persichetti A, Sciuto R, Rea S, Basciani S, Lubrano C, Mariani S, et al. Prevalence, mass, and glucose-uptake activity of (1)(8)F-FDG-detected brown adipose tissue in humans living in a temperate zone of Italy. *PLoS ONE*. (2013) 8:e63391. doi: 10.1371/journal.pone.0063391
16. Zhang Q, Ye H, Miao Q, Zhang Z, Wang Y, Zhu X, et al. Differences in the metabolic status of healthy adults with and without active brown adipose tissue. *Wien Klin Wochenschr*. (2013) 125:687–95. doi: 10.1007/s00508-013-0431-2
17. Yoneshiro T, Aita S, Matsushita M, Okamatsu-Ogura Y, Kameya T, Kawai Y, et al. Age-related decrease in cold-activated brown adipose tissue and accumulation of body fat in healthy humans. *Obesity*. (2011) 19:1755–60. doi: 10.1038/oby.2011.125
18. Yoneshiro T, Aita S, Matsushita M, Kayahara T, Kameya T, Kawai Y, et al. Recruited brown adipose tissue as an antiobesity agent in humans. *J Clin Invest*. (2013). 123:3404–8. doi: 10.1172/JCI 67803
19. van der Lans AA, Hoeks J, Brans B, Vijgen GH, Visser MG, Vosselman MJ, et al. Cold acclimation recruits human brown fat and increases nonshivering thermogenesis. *J Clin Invest*. (2013) 123:3395–403. doi: 10.1172/JCI68993
20. Blondin DP, Labbe SM, Tingelstad HC, Noll C, Kunach M, Phoenix S, et al. Increased brown adipose tissue oxidative capacity in cold-acclimated humans. *J Clin Endocrinol Metab*. (2014) 99:E438–46. doi: 10.1210/jc.2013-3901
21. Lee P, Smith S, Linderman J, Courville AB, Brychta RJ, Dieckmann W, et al. Temperature-acclimated brown adipose tissue modulates insulin sensitivity in humans. *Diabetes*. (2014) 63:3686–98. doi: 10.2337/db14-0513
22. Chondronikola M, Volpi E, Borsheim E, Porter C, Annamalai P, Enerback S, et al. Brown adipose tissue improves whole-body glucose homeostasis and insulin sensitivity in humans. *Diabetes*. (2014) 63:4089–99. doi: 10.2337/db14-0746
23. Matsushita M, Yoneshiro T, Aita S, Kameya T, Sugie H, Saito M. Impact of brown adipose tissue on body fatness and glucose metabolism in healthy humans. *Int J Obes*. (2014) 38:812–7. doi: 10.1038/ijo.2013.206
24. Hanssen MJ, Hoeks J, Brans B, van der Lans AA, Schaart G, van den Driessche JJ, et al. Short-term cold acclimation improves insulin sensitivity in patients with type 2 diabetes mellitus. *Nat Med*. (2015) 21:863–65. doi: 10.1038/nm.3891
25. Saito M. Brown adipose tissue as a regulator of energy expenditure and body fat in humans. *Diabetes Metab J*. (2013) 37:22–9. doi: 10.4093/dmj.2013.37.1.22
26. Yoneshiro T, Saito M. Activation and recruitment of brown adipose tissue as anti-obesity regimens in humans. *Ann Med*. (2015) 47:133–41. doi: 10.3109/07853890.2014.911595
27. Lidell ME, Betz MJ, Enerback S. Brown adipose tissue and its therapeutic potential. *J Intern Med*. (2014) 276:364–77. doi: 10.1111/joim.12255
28. Chechi K, Nedergaard J, Richard D. Brown adipose tissue as an anti-obesity tissue in humans. *Obes Rev*. (2014) 15:92–106. doi: 10.1111/obr.12116
29. Sidossis L, Kajimura S. Brown and beige fat in humans: thermogenic adipocytes that control energy and glucose homeostasis. *J Clin Invest*. (2015) 125:478–86. doi: 10.1172/JCI78362
30. Heeren J, Scheja L. Brown adipose tissue and lipid metabolism. *Curr Opin Lipidol*. (2018) 29:180–5. doi: 10.1097/MOL.0000000000000504
31. Dong M, Yang X, Lim S, Cao Z, Honek J, Lu H, et al. Cold exposure promotes atherosclerotic plaque growth and instability via UCP1-dependent lipolysis. *Cell Metab*. (2013) 18:118–29. doi: 10.1016/j.cmet.2013.06.003
32. Dhaka A, Viswanath V, Patapoutian A. Trp ion channels and temperature sensation. *Annu Rev Neurosci*. (2006) 29:135–61. doi: 10.1146/annurev.neuro.29.051605.112958
33. Nakamura K. Central circuitries for body temperature regulation and fever. *Am J Physiol Regul Integr Comp Physiol*. (2011) 301:R1207–28. doi: 10.1152/ajpregu.00109.2011
34. Inokuma K, Ogura-Okamatsu Y, Toda C, Kimura K, Yamashita H, Saito M. Uncoupling protein 1 is necessary for norepinephrine-induced glucose utilization in brown adipose tissue. *Diabetes*. (2005) 54:1385–91. doi: 10.2337/diabetes.54.5.1385
35. Bukowiecki LJ, Geloen A, Collet AJ. Proliferation and differentiation of brown adipocytes from interstitial cells during cold acclimation. *Am J Physiol*. (1986) 250:C880–7. doi: 10.1152/ajpcell.1986.250.6.C880
36. Okamatsu-Ogura Y, Fukano, K, Tsubota A, Nio-Kobayashi, Y, Nakamura K, Morimatsu M, et al. Cell-cycle arrest in mature adipocytes impairs BAT development but not WAT browning, and reduces adaptive thermogenesis in mice. *Sci Rep*. (2017) 7:6648. doi: 10.1038/s41598-017-07206-8
37. Harms M, Seale P. Brown and beige fat: development, function and therapeutic potential. *Nat Med*. (2013) 19:1252–63. doi: 10.1038/nm.3361
38. Finlin BS, Memetimin H, Confides AL, Kasza I, Zhu B, Vekaria HJ, et al. Human adipose beiging in response to cold and mirabegron. *JCI Insight*. (2018) 3:e121510. doi: 10.1172/jci.insight.121510
39. Sharp LZ, Shinoda K, Ohno H, Scheel DW, Tomoda E, Ruiz L, et al. Human BAT possesses molecular signatures that resemble beige/brite cells. *PLoS ONE*. (2012) 7:e49452. doi: 10.1371/journal.pone.0049452
40. Lidell ME, Betz MJ, Dahlqvist Leinhard O, Heglind M, Elander L, Slawik M, et al. Evidence for two types of brown adipose tissue in humans. *Nat Med*. (2013) 19:631–4. doi: 10.1038/nm.3017

41. Cypess AM, White AP, Vernochet C, Schulz TJ, Xue R, Sass CA, et al. Anatomical localization, gene expression profiling and functional characterization of adult human neck brown fat. *Nat Med*. (2013) 19:635–9. doi: 10.1038/nm.3112
42. Rothwell NJ, Stock MJ. A role for brown adipose tissue in diet-induced thermogenesis. *Nature*. (1979) 281:31–5. doi: 10.1038/281031a0
43. Fromme T, Klingenspor M. Uncoupling protein 1 expression and high-fat diets. *Am J Physiol Regul Integr Comp Physiol*. (2011) 300:R1–8. doi: 10.1152/ajpregu.00411.2010
44. von Essen G, Lindsund E, Cannon B, Nedergaard J. Adaptive facultative diet-induced thermogenesis in wild-type but not in UCP1-ablated mice. *Am J Physiol Endocrinol Metab*. (2017) 313:E515–27. doi: 10.1152/ajpendo.00097.2017
45. Kozak LP. Brown fat and the myth of diet-induced thermogenesis. *Cell Metab*. (2010) 11:263–7. doi: 10.1016/j.cmet.2010.03.009
46. Glick Z, Teague RJ, Bray GA. Brown adipose tissue: thermic response increased by a single low protein, high carbohydrate meal. *Science*. (1981) 213:1125–7. doi: 10.1126/science.7268419
47. Lupien JR, Glick Z, Saito M, Bray GA. Guanosine diphosphate binding to brown adipose tissue mitochondria is increased after single meal. *Am J Physiol*. (1985) 249:R694–8. doi: 10.1152/ajpregu.1985.249.6.R694
48. Saito M, Minokoshi Y, Shimazu T. Metabolic and sympathetic nerve activities of brown adipose tissue in tube-fed rats. *Am J Physiol*. (1989) 257:E374–8. doi: 10.1152/ajpendo.1989.257.3.E374
49. Oppert JM, Vohl MC, Chagnon M, Dionne FT, Cassard-Doulcier AM, Ricquier D, et al. DNA polymorphism in the uncoupling protein (UCP) gene and human body fat. *Int J Obes Relat Metab Disord*. (1994) 18:526–31.
50. Valve R, Heikkinen S, Rissanen A, Laakso M, Uusitupa M. Synergistic effect of polymorphisms in uncoupling protein 1 and beta3-adrenergic receptor genes on basal metabolic rate in obese Finns. *Diabetologia*. (1998) 41:357–61. doi: 10.1007/s001250050915
51. Kogure A, Yoshida T, Sakane N, Umekawa T, Takakura Y, Kondo M. Synergic effect of polymorphisms in uncoupling protein 1 and beta3-adrenergic receptor genes on weight loss in obese Japanese. *Diabetologia*. (1998) 41:1399. doi: 10.1007/s001250051084
52. Yoneshiro T, Ogawa T, Okamoto N, Matsushita M, Aita S, Kameya T, et al. Impact of UCP1 and β3AR gene polymorphisms on age-related changes in brown adipose tissue and adiposity in humans. *Int J Obes*. (2013) 37:993–8. doi: 10.1038/ijo.2012.161
53. Nagai N, Sakane N, Ueno LM, Hamada T, Moritani T. The−3826 A−>G variant of the uncoupling protein-1 gene diminishes postprandial thermogenesis after a high fat meal in healthy boys. *J Clin Endocrinol Metab*. (2003) 88:5661–7. doi: 10.1210/jc.2003-030672
54. Nagai N, Sakane N, Fujishita A, Fujiwara R, Kimura T, Kotani K, et al. The−3826 A −> G variant of the uncoupling protein-1 gene diminishes thermogenesis during acute cold exposure in healthy children. *Obes Res Clin Pract*. (2007) 1:99–107. doi: 10.1016/j.orcp.2007.02.001
55. Vrieze A, Schopman JE, Admiraal WM, Soeters MR, Nieuwdorp M, Verberne HJ, et al. Fasting and postprandial activity of brown adipose tissue in healthy men. *J Nucl Med*. (2012) 53:1407–10. doi: 10.2967/jnumed.111.100701
56. Vosselman MJ, Brans B, van der Lans AA, Wierts R, van Baak MA, Mottaghy FM, et al. Brown adipose tissue activity after a high-calorie meal in humans. *Am J Clin Nutr*. (2013) 98:57–64. doi: 10.3945/ajcn.113.059022
57. Muzik O, Mangner TJ, Leonard WR, Kumar A, Janisse J, Granneman JG. 15O PET measurement of blood flow and oxygen consumption in cold-activated human brown fat. *J Nucl Med*. (2013) 54:523–31. doi: 10.2967/jnumed.112.111336
58. Din MU, Saari T, Raiko J, Kudomi N, Maurer SF, Lahesmaa M, et al. Postprandial oxidative metabolism of human brown fat indicates thermogenesis. *Cell Metab*. (2018) 28:207–16. doi: 10.1016/j.cmet.2018.05.020
59. Hibi M, Oishi S, Matsushita M, Yoneshiro T, Yamaguchi T, Usui C, et al. Brown adipose tissue is involved in diet-induced thermogenesis and whole-body fat utilization in healthy humans. *Int J Obes*. (2016) 40:1655–61. doi: 10.1038/ijo.2016.124
60. Glick Z, Raum WJ. Norepinephrine turnover in brown adipose tissue is stimulated by a single meal. *Am J Physiol*. (1986) 251:R13–7. doi: 10.1152/ajpregu.1986.251.1.R13
61. Schwartz RS, Jaeger LF, Silberstein S, Veith RC. Sympathetic nervous system activity and the thermic effect of feeding in man. *Int J Obes*. (1987) 11:141–9.
62. Welle S, Lilavivat U, Campbell RG. Thermic effect of feeding in man: increased plasma norepinephrine levels following glucose but not protein or fat consumption. *Metabolism*. (1981) 30:953–8. doi: 10.1016/0026-0495(81)90092-5
63. van Baak MA. Meal-induced activation of the sympathetic nervous system and its cardiovascular and themogenic effects in man. *Physiol Behav*. (2008) 94:178–86. doi: 10.1016/j.physbeh.2007.12.020
64. Young JB, Saville E, Rothwell NJ, Stock MJ, Landsberg L. Effect of diet and cold exposure on norepinephrine turnover in brown adipose tissue of the rat. *J Clin Invest*. (1982) 69:1061–71. doi: 10.1172/JCI110541
65. Yoshida T, Fisler JS, Fukushima M, Bray GA, Schemmel RA. Diet, lighting, and food intake affect norepinephrine turnover in dietary obesity. *Am J Physiol*. (1987) 252:R402–8. doi: 10.1152/ajpregu.1987.252.2.R402
66. LeBlanc J, Cabanac M, Samson P. Reduced postprandial heat production with gavage as compared with meal feeding in human subjects. *Am J Physiol*. (1984) 246:E95–101. doi: 10.1152/ajpendo.1984.246.1.E95
67. Diamond P, Brondel L, LeBlanc J. Palatability and postprandial thermogenesis in dogs. *Am J Physiol*. (1985) 248:E75–9. doi: 10.1152/ajpendo.1985.248.1.E75
68. LeBlanc J, Brondel L. Role of palatability on meal-induced thermogenesis in human subjects. *Am J Physiol*. (1985) 248:E333–6. doi: 10.1152/ajpendo.1985.248.3.E333
69. Wijers SL, Saris WH, van Marken Lichtenbelt WD. Individual thermogenic responses to mild cold and overfeeding are closely related. *J Clin Endocrinol Metab*. (2007) 92:4299–305. doi: 10.1210/jc.2007-1065
70. Peterson CM, Lecoultre V, Frost EA, Simmons J, Redman LM, Ravussin E. The thermogenic responses to overfeeding and cold are differentially regulated. *Obesity*. (2016) 24:96–101. doi: 10.1002/oby.21233
71. Zwillich C, Martin B, Hofeldt F, Charles A, Subryan V, Burman K. Lack of effects of beta sympathetic blockade on the metabolic and respiratory responses to carbohydrate feeding. *Metabolism*. (1981) 30:451–6. doi: 10.1016/0026-0495(81)90179-7
72. Welle S, Campbell RG. Stimulation of thermogenesis by carbohydrate overfeeding. Evidence against sympathetic nervous system mediation. *J Clin Invest*. (1983) 71:916–25. doi: 10.1172/JCI110846
73. Thorne A, Wahren J. Beta-adrenergic blockade does not influence the thermogenic response to a mixed meal in man. *Clin Physiol*. (1989) 9:321–32. doi: 10.1111/j.1475-097X.1989.tb00986.x
74. Li Y, Schnabl K, Gabler SM, Willershauser M, Reber J, Karlas A, et al. Secretin-activated brown fat mediates prandial thermogenesis to induce satiation. *Cell*. (2018) 175:1561–74. doi: 10.1016/j.cell.2018.10.016
75. Yamazaki T, Morimoto-Kobayashi Y, Koizumi K, Takahashi C, Nakajima S, Kitao S, et al. Secretion of a gastrointestinal hormone, cholecystokinin, by hop-derived bitter components activates sympathetic nerves in brown adipose tissue. *J Nutr Biochem*. (2019) 64:80–7. doi: 10.1016/j.jnutbio.2018.10.009
76. Blouet C, Schwartz GJ. Duodenal lipid sensing activates vagal afferents to regulate non-shivering brown fat thermogenesis in rats. *PLoS ONE*. (2012) 7:e51898. doi: 10.1371/journal.pone.0051898
77. Vijgen GH, Bouvy ND, Leenen L, Rijkers K, Cornips E, Majoie M, et al. Vagus nerve stimulation increases energy expenditure: relation to brown adipose tissue activity. *PLoS ONE*. (2013) 8:e77221. doi: 10.1371/journal.pone.0077221
78. Lin L, Lee JH, Bongmba OY, Ma X, Zhu X, Sheikh-Hamad D, et al. The suppression of ghrelin signaling mitigates age-associated thermogenic impairment. *Aging*. (2014) 6:1019–32. doi: 10.18632/aging.100706
79. Chondronikola M, Porter C, Malagaris I, Nella AA, Sidossis LS. Brown adipose tissue is associated with systemic concentrations of peptides secreted from the gastrointestinal system and involved in appetite regulation. *Eur J Endocrinol*. (2017) 177:33–40. doi: 10.1530/EJE-16-0958
80. Haeusler RA, Camastra S, Nannipieri M, Astiarraga B, Castro-Perez J, Xie D, et al. Increased bile acid synthesis and impaired bile acid

transport in human obesity. *J Clin Endocrinol Metab.* (2016) 101, 935–44. doi: 10.1210/jc.2015-2583
81. Sonne DP, van Nierop FS, Kulik W, Soeters MR, Vilsbøll T, Knop FK, et al. Postprandial plasma concentrations of individual bile acids and FGF-19 in patients with type 2 diabetes. *J Clin Endocrinol Metab.* (2016) 101:3002–9. doi: 10.1210/jc.2016-1607
82. Vítek L, Haluzík M. The role of bile acids in metabolic regulation. *J Endocrinol.* (2016) 228:R85–96. doi: 10.1530/JOE-15-0469
83. Watanabe M, Houten SM, Mataki C, Christoffolete MA, Kim BW, Sato H, et al. Bile acids induce energy expenditure by promoting intracellular thyroid hormone activation. *Nature.* (2006) 439:484–9. doi: 10.1038/nature04330
84. Broeders EPM, Nascimento EBM, Bas Havekes B, Brans B, Roumans KHM, Tailleux A, et al. The bile acid chenodeoxycholic acid increases human brown adipose tissue activity. *Cell Metabolism.* (2015) 22:418–26. doi: 10.1016/j.cmet.2015.07.002
85. Beiroa D, Imbernon M, Gallego R, Senra A, Herranz D, Villarroya F, et al. GLP-1 agonism stimulates brown adipose tissue thermogenesis and browning through hypothalamic AMPK. *Diabetes.* (2014) 63:3346−−58. doi: 10.2337/db14-0302
86. Zhou J, Poudel A, Chandramani-Shivalingappa P, Biao Xu B, Ryan Welchko R, Li L. Liraglutide induces beige fat development and promotes mitochondrial function in diet induced obesity mice partially through AMPK-SIRT-1-PGC1-α cell signaling pathway. *Endocrine.* (2019) 64:271–83. doi: 10.1007/s12020-018-1826-7
87. Velazquez-Villegas LA, Perino A, Vera Lemos V, Zietak M, Nomura M, Willem T, et al. TGR5 signalling promotes mitochondrial fission and beige remodelling of white adipose tissue. *Nat Commun.* (2018) 9:245. doi: 10.1038/s41467-017-02068-0
88. Vander Tuig JG, Romsos DR. Effects of dietary carbohydrate, fat, and protein on norepinephrine turnover in rats. *Metabolism.* (1984) 33:26–33. doi: 10.1016/0026-0495(84)90158-6
89. Johnston JL, Balachandran AV. Effects of dietary protein, energy and tyrosine on central and peripheral norepinephrine turnover in mice. *J Nutr.* (1987) 117:2046–53. doi: 10.1093/jn/117.12.2046
90. Bender N, Portmann M, Heg Z, Hofmann K, Zwahlen M, Egger M. Fish or n3-PUFA intake and body composition: a systematic review and meta-analysis. *Obes Rev.* (2014) 15:657–65. doi: 10.1111/obr.12189
91. Clevenger HC, Kozimor AL, Paton CM, Cooper JA. Acute effect of dietary fatty acid composition on postprandial metabolism in women. *Exp Physiol.* (2014) 99:1182–90. doi: 10.1113/expphysiol.2013.077222
92. Cisneros LCV, Moreno AGM, Lopez-Espinoza A, Espinoza-Gallardo AC. Effect of the fatty acid composition of meals on postprandial energy expenditure: a systematic review. *Rev Assoc Med Bras.* (1992) 65:1022–31. doi: 10.1590/1806-9282.65.7.1022
93. Oudart H, Groscolas R, Calgari C, Nibbelink M, Leray C, Le Maho Y, et al. Brown fat thermogenesis in rats fed high-fat diets enriched with n-3 polyunsaturated fatty acids. *Int J Obes Relat Metab Disord.* (1997) 21:955–62. doi: 10.1038/sj.ijo.0800500
94. Kawada T, Kayahashi S, Hida Y, Koga K, Nadachi Y, Fushiki T. Fish (bonito) oil supplementation enhances the expression of uncoupling protein in brown adipose tissue of rat. *J Agric Food Chem.* (1998) 46:1225–7. doi: 10.1021/jf9711000
95. Kim M, Goto T, Yu R, Uchida K, Tominaga M, Kano Y, et al. Fish oil intake induces UCP1 upregulation in brown and white adipose tissue via the sympathetic nervous system. *Sci Rep.* (2015) 5:18013. doi: 10.1038/srep18013
96. Kim J, Okla M, Erickson A, Carr T, Natarajan SK, Chung S. Eicosapentaenoic acid potentiates brown thermogenesis through FFAR4-dependent up-regulation of miR-30b and miR-378. *J Biol Chem.* (2016) 291:20551–62. doi: 10.1074/jbc.M116.721480
97. Ghandour RA, Colson C, Giroud M, Maurer S, Rekima S, Ailhaud G, et al. Impact of dietary omega3 polyunsaturated fatty acid supplementation on brown and brite adipocyte function. *J Lipid Res.* (2018) 59:452–61. doi: 10.1194/jlr.M081091
98. Leiria LO, Wang CH, Lynes MD, Yang K, Shamsi F, Sato M, et al. 12-Lipoxygenase regulates cold adaptation and glucose metabolism by producing the omega-3 lipid 12-HEPE from brown fat. *Cell Metab.* (2019) 30:768–83. doi: 10.1016/j.cmet.2019.07.001
99. Lv J, Qi L, Yu C, Yang L, Guo Y, Chen Y, et al. Consumption of spicy foods and total and cause specific mortality: population based cohort study. *BMJ.* (2015). 351:h3942. doi: 10.1136/bmj.h3942
100. Ludy MJ, Moore GE, Mattes RD. The effects of capsaicin and capsiate on energy balance: critical review and meta-analyses of studies in humans. *Chem Senses.* (2012) 37:103–21. doi: 10.1093/chemse/bjr100
101. Tremblay A, Arguin H, Panahi S. Capsaicinoids: a spicy solution to the management of obesity? *Int J Obes.* (2016) 40:1198–204. doi: 10.1038/ijo.2015.253
102. Watanabe T, Ohnuki K, Kobata K. Studies on the metabolism and toxicology of emerging capsinoids. *Expert Opin Drug Metab Toxicol.* (2011) 7:533–42. doi: 10.1517/17425255.2011.562193
103. Uchida K, Dezaki K, Yoneshiro T, Watanabe T, Yamazaki J, Saito M, et al. Involvement of thermosensitive TRP channels in energy metabolism. *J Physiol Sci.* (2017) 67:549–60. doi: 10.1007/s12576-017-0552-x
104. Ono K, Tsukamoto-Yasui M, Hara-Kimura Y, Inoue N, Nogusa Y, Okabe Y, et al. Intragastric administration of capsiate, a transient receptor potential channel agonist, triggers thermogenic sympathetic responses. *J Appl Physiol.* (1985) 110:789–98. doi: 10.1152/japplphysiol.00128.2010
105. Kawabata F, Inoue N, Masamoto Y, Matsumura S, Kimura W, Kadowaki M, et al. Non-pungent capsaicin analogs (capsinoids) increase metabolic rate and enhance thermogenesis via gastrointestinal TRPV1 in mice. *Biosci Biotechnol Biochem.* (2009) 73:2690–97. doi: 10.1271/bbb.90555
106. Kawada T, Watanabe T, Takaishi T, Tanaka T, Iwai K. Capsaicin-induced beta-adrenergic action on energy metabolism in rats: influence of capsaicin on oxygen consumption, the respiratory quotient, and substrate utilization. *Proc Soc Exp Biol Med.* (1986) 183:250–6. doi: 10.3181/00379727-183-42414
107. Baskaran P, Krishnan V, Ren J, Thyagarajan B. Capsaicin induces browning of white adipose tissue and counters obesity by activating TRPV1 channel-dependent mechanisms. *Br J Pharmacol.* (2016) 173:2369–89. doi: 10.1111/bph.13514
108. Okamatsu-Ogura Y, Tsubota A, Ohygma K, Nogusa Y, Saito M, Kimura K. Capsinoids suppress diet-induced obesity through uncoupling protein 1-dependent mechanism in mice. *J Funct Foods.* (2015) 19:1–9. doi: 10.1016/j.jff.2015.09.005
109. Baskaran P, Krishnan V, Fettel K, Gao P, Zhu Z, Ren J, et al. TRPV1 activation counters diet-induced obesity through sirtuin-1 activation and PRDM-16 deacetylation in brown adipose tissue. *Int J Obes.* (2017) 41:739–49. doi: 10.1038/ijo.2017.16
110. Bernard BK, Tsubuku S, Kayahara T, Maeda K, Hamada M, Nakamura T, et al. Studies of the toxicological potential of capsihnoids: X. safety assessment and pharmacokinetics of capsioids in healthy male volunteers after a single oral ingestion of CH-19 sweet extract. *Int J Toxicol.* (2008) 27(Suppl. 3):137–47. doi: 10.1080/10915810802514476
111. Yoneshiro T, Aita S, Kawai Y, Iwanaga T, Saito M. Nonpungent capsaicin analogs (capsinoids) increase energy expenditure through the activation of brown adipose tissue in humans. *Am J Clin Nutr.* (2012) 95:845–50. doi: 10.3945/ajcn.111.018606
112. Yoneshiro T, Matsushita M, Nakae S, Kameya T, Sugie H, Tanaka S, et al. Brown adipose tissue is involved in the seasonal variation of cold-induced thermogenesis in humans. *Am J Physiol Regul Integr Comp Physiol.* (2016) 310:R999–1009. doi: 10.1152/ajpregu.00057.2015
113. Sun L, Camps SG, Goh HJ, Govindharajulu P, Schaefferkoetter JD, Townsend DW, et al. Capsinoids activate brown adipose tissue (BAT) with increased energy expenditure associated with subthreshold 18-fluorine fluorodeoxyglucose uptake in BAT-positive humans confirmed by positron emission tomography scan. *Am J Clin Nutr.* (2018) 107:62–70. doi: 10.1093/ajcn/nqx025
114. Nirengi S, Homma T, Inoue N, Sato H, Yoneshiro T, Matsushita M, et al. Assessment of human brown adipose tissue density during daily ingestion of thermogenic capsinoids using near-infrared time-resolved spectroscopy. *J Biomed Opt.* (2016) 21:091305. doi: 10.1117/1.JBO.21.9.091305
115. Nirengi S, Yoneshiro T, Sugie H, Saito M, Hamaoka T. Human brown adipose tissue assessed by simple, noninvasive near-infrared time-resolved spectroscopy. *Obesity.* (2015) 23:973–80. doi: 10.1002/oby.21012
116. Snitker S, Fujishima Y, Shen H, Ott S, Pi-Sunyer X, Furuhata Y, et al. Effects of novel capsinoid treatment on fatness and energy metabolism in humans:

possible pharmacogenetic implications. *Am J Clin Nutr.* (2009) 89:45–50. doi: 10.3945/ajcn.2008.26561
117. Tominaga M. Nociception and TRP channels. *Handb Exp Pharmacol.* (2007) 179:489–505. doi: 10.1007/978-3-540-34891-7_29
118. Sidossis LS, Porter C, Saraf MK, Borsheim E, Radhakrishnan RS, Chao T, et al. Browning of subcutaneous white adipose tissue in humans after severe adrenergic stress. *Cell Metab.* (2015) 22:219–27. doi: 10.1016/j.cmet.2015.06.022
119. Ohyama K, Nogusa Y, Shinoda K, Suzuki K, Bannai M, Kajimura S. A synergistic antiobesity effect by a combination of capsinoids and cold temperature through promoting beige adipocyte biogenesis. *Diabetes.* (2016) 65:1410–23. doi: 10.2337/db15-0662
120. Cabrera C, Artacho R, Gimenez R. Beneficial effects of green tea–a review. *J Am Coll Nutr.* (2006) 25:79–99. doi: 10.1080/07315724.2006.10719518
121. Thavanesan N. The putative effects of green tea on body fat: an evaluation of the evidence and a review of the potential mechanisms. *Br J Nutr.* (2011) 106:1297–309. doi: 10.1017/S0007114511003849
122. Dulloo AG, Duret C, Rohrer D, Girardier L, Mensi N, Fathi M, et al. Efficacy of a green tea extract rich in catechin polyphenols and caffeine in increasing 24-h energy expenditure and fat oxidation in humans. *Am J Clin Nutr.* (1999) 70:1040–5. doi: 10.1093/ajcn/70.6.1040
123. Berube-Parent S, Pelletier C, Dore J, Tremblay A. Effects of encapsulated green tea and Guarana extracts containing a mixture of epigallocatechin-3-gallate and caffeine on 24 h energy expenditure and fat oxidation in men. *Br J Nutr.* (2005) 94:432–6. doi: 10.1079/BJN20051502
124. Venables MC, Hulston CJ, Cox HR, Jeukendrup AE. Green tea extract ingestion, fat oxidation, and glucose tolerance in healthy humans. *Am J Clin Nutr.* (2008) 87:778–84. doi: 10.1093/ajcn/87.3.778
125. Hursel R, Viechtbauer W, Dulloo AG, Tremblay A, Tappy L, Rumpler W, et al. The effects of catechin rich teas and caffeine on energy expenditure and fat oxidation: a meta-analysis. *Obes Rev.* (2011) 12:e573–81. doi: 10.1111/j.1467-789X.2011.00862.x
126. Nagao T, Hase T, Tokimitsu I. A green tea extract high in catechins reduces body fat and cardiovascular risks in humans. *Obesity.* (2007) 15:1473–83. doi: 10.1038/oby.2007.176
127. Hursel R, Viechtbauer W, Westerterp-Plantenga MS. The effects of green tea on weight loss and weight maintenance: a meta-analysis. *Int J Obes.* (2009) 33:956–61. doi: 10.1038/ijo.2009.135
128. Westerterp-Plantenga MS, Lejeune MP, Kovacs EM. Body weight loss and weight maintenance in relation to habitual caffeine intake and green tea supplementation. *Obes Res.* (2005) 13:1195–204. doi: 10.1038/oby.2005.142
129. Wang H, Wen Y, Du Y, Yan X, Guo H, Rycroft JA, et al. Effects of catechin enriched green tea on body composition. *Obesity.* (2010) 18:773–9. doi: 10.1038/oby.2009.256
130. Hibi M, Takase H, Iwasaki M, Osaki N, Katsuragi K. Efficacy of tea catechin-rich beverages to reduce abdominal adiposity and metabolic syndrome risks in obese and overweight subjects: a pooled analysis of 6 human trials. *Nutr Res.* (2018) 55:1–10. doi: 10.1016/j.nutres.2018.03.012
131. Dostal AM, Arikawa A, Espejo L, Kurzer MS. Long-term supplementation of green tea extract does not modify adiposity or bone mineral density in a randomized trial of overweight and obese postmenopausal women. *J Nutr.* (2016) 146:256–64. doi: 10.3945/jn.115.219238
132. Nomura S, Ichinose T, Jinde M, Kawashima Y, Tachiyashiki K, Imaizumi K. Tea catechins enhance the mRNA expression of uncoupling protein 1 in rat brown adipose tissue. *J Nutr Biochem.* (2008) 19:840–7. doi: 10.1016/j.jnutbio.2007.11.005
133. Dulloo AG. The search for compounds that stimulate thermogenesis in obesity management: from pharmaceuticals to functional food ingredients. *Obes Rev.* (2011) 12:866–83. doi: 10.1111/j.1467-789X.2011.00909.x
134. Yoneshiro T, Matsushita M, Hibi M, Tone H, Takeshita M, Yasunaga K, et al. Tea catechin and caffeine activate brown adipose tissue and increase cold-induced thermogenic capacity in humans. *Am J Clin Nutr.* (2017) 105:873–81. doi: 10.3945/ajcn.116.144972
135. Nirengi S, Amagasa S, Homma T, Yoneshiro T, Matsumiya S, Kurosawa Y, et al. Daily ingestion of catechin-rich beverage increases brown adipose tissue density and decreases extramyocellular lipids in healthy young women. *Springerplus.* (2016) 5:1363. doi: 10.1186/s40064-016-3029-0
136. Westerterp-Plantenga MS. Green tea catechins, caffeine and body-weight regulation. *Physiol Behav.* (2010) 100:42–6. doi: 10.1016/j.physbeh.2010.02.005
137. Ferreira MA, Silva DM, de Morais AC Jr, Mota JF, Botelho PB. Therapeutic potential of green tea on risk factors for type 2 diabetes in obese adults - a review. *Obes Rev.* (2016) 17:1316–28. doi: 10.1111/obr.12452
138. Velickovic K, Wayne D, Leija HAL, Bloor I, Morris DE, Law J, et al. Caffeine exposure induces browning features in adipose tissue *in vitro* and *in vivo*. *Sci Rep.* (2019) 9:9104. doi: 10.1038/s41598-019-45540-1
139. Lorenz M, Paul F, Moobed M, Baumann G, Zimmermann BF, Stangl K, et al. The activity of catechol-O-methyltransferase (COMT) is not impaired by high doses of epigallocatechin-3-gallate (EGCG) *in vivo*. *Eur J Pharmacol.* (2014) 740:645–51. doi: 10.1016/j.ejphar.2014.06.014
140. Takahashi M, Miyashita M, Suzuki K, Bae SR, Kim HK, Wakisaka T, et al. Acute ingestion of catechin-rich green tea improves postprandial glucose status and increases serum thioredoxin concentrations in postmenopausal women. *Br J Nutr.* (2014) 112:1542–50. doi: 10.1017/S0007114514002530
141. Kadowaki M, Ootani E, Sugihara N, Furuno K. Inhibitory effects of catechin gallates on o-methyltranslation of protocatechuic acid in rat liver cytosolic preparations and cultured hepatocytes. *Biol Pharm Bull.* (2005) 28:1509–13. doi: 10.1248/bpb.28.1509
142. Kurogi M, Miyashita M, Emoto Y, Kubo Y, Saitoh O. Green tea polyphenol epigallocatechin gallate activates TRPA1 in an intestinal enteroendocrine cell line, STC-1. *Chem Senses.* (2012) 37:167–77. doi: 10.1093/chemse/bjr087
143. Kurogi M, Kawai Y, Nagatomo K, Tateyama M, Kubo Y, Saitoh O. Auto-oxidation products of epigallocatechin gallate activate TRPA1 and TRPV1 in sensory neurons. *Chem Senses.* (2015) 40:27–46. doi: 10.1093/chemse/bju057
144. Vriens J, Nilius B, Vennekens R. Herbal compounds and toxins modulating TRP channels. *Curr Neuropharmacol.* (2008) 6:79–96. doi: 10.2174/157015908783769644
145. Akendengue B, Louis AM. Medicinal plants used by the Masango people in Gabon. *J Ethnopharmacol.* (1994) 41:193-200. doi: 10.1016/0378-8741(94)90032-9
146. Sugita J, Yoneshiro T, Hatano T, Aita S, Ikemoto T, Uchiwa H, et al. Grains of paradise (Aframomum melegueta) extract activates brown adipose tissue and increases whole-body energy expenditure in men. *Br J Nutr.* (2013) 110:733–8. doi: 10.1017/S0007114512005715
147. Sugita J, Yoneshiro T, Sugishima Y, Ikemoto T, Uchiwa H, Suzuki I, et al. Daily ingestion of grains of paradise (Aframomum melegueta) extract increases whole-body energy expenditure and decreases visceral fat in humans. *J Nutr Sci Vitaminol.* (2014) 60:22–7. doi: 10.3177/jnsv.60.22
148. Tajino K, Matsumura K, Kosada K, Shibakusa T, Inoue K, Fushiki T, et al. Application of menthol to the skin of whole trunk in mice induces autonomic and behavioral heat-gain responses. *Am J Physiol Regul Integr Comp Physiol.* (2007) 293:R2128–35. doi: 10.1152/ajpregu.00377.2007
149. Masamoto Y, Kawabata F, Fushiki T. Intragastric administration of TRPV1, TRPV3, TRPM8, and TRPA1 agonists modulates autonomic thermoregulation in different manners in mice. *Biosci Biotechnol Biochem.* (2009) 73:1021–7. doi: 10.1271/bbb.80796
150. Ma S, Yu H, Zhao Z, Luo Z, Chen J, Ni Y, et al. Activation of the cold-sensing TRPM8 channel triggers UCP1-dependent thermogenesis and prevents obesity. *J Mol Cell Biol.* (2012) 4:88–96. doi: 10.1093/jmcb/mjs001
151. Valente A, Carrillo AE, Tzatzarakis MN, Vakonaki E, Tsatsakis AM, Kenny GP, et al. The absorption and metabolism of a single L-menthol oral versus skin administration: Effects on thermogenesis and metabolic rate. *Food Chem Toxicol.* (2015) 86:262–73. doi: 10.1016/j.fct.2015.09.018
152. Tamura Y, Iwasaki Y, Narukawa M, Watanabe T. Ingestion of cinnamaldehyde, a TRPA1 agonist, reduces visceral fats in mice fed a high-fat and high-sucrose diet. *J Nutr Sci Vitaminol.* (2012) 58:9–13. doi: 10.3177/jnsv.58.9
153. Zuo J, Zhao D, Yu N, Fang X, Mu Q, Ma Y, et al. Cinnamaldehyde ameliorates iiet-Induced obesity in mice by inducing browning of white adipose tissue. *Cell Physiol Biochem.* (2017) 42:1514–25. doi: 10.1159/000479268
154. Giordano A, Frontini A, Cinti S. Convertible visceral fat as a therapeutic target to curb obesity. *Nat Rev Drug Dis.* (2016) 15:405–24. doi: 10.1038/nrd.2016.31

155. Villarroya F, Cereijo R, Villarroya J, Giralt M. Brown adipose tissue as a secretory organ. *Nat Rev Endocrinol.* (2017) 13:26–35. doi: 10.1038/nrendo.2016.136
156. Kwon DY, Kim YS, Ryu SY, Cha MR, Yon GH, Yang HJ, et al. Capsiate improves glucose metabolism by improving insulin sensitivity better than capsaicin in diabetic rats. *J Nutr Biochem.* (2013) 24:1078–85. doi: 10.1016/j.jnutbio.2012.08.006
157. Okla M, Kim J, Koehler K, Chung S. Dietary factors promoting brown and beige fat development and thermogenesis. *Adv Nutr.* (2017) 8:473–83. doi: 10.3945/an.116.014332
158. Yoneshiro T, Matsushita M, Saito M. Translational aspects of brown fat activation by food-derived stimulants. *Handb Exp Pharmacol.* (2019) 251:359–79. doi: 10.1007/164_2018_159
159. Lorente-Cebrián S, Herrera K, Milagro FI, Sánchez J, Garza AL, Castro H. miRNAs and novel food compounds related to the browning process. *Int J Mol Sci.* (2019) 20:5998. doi: 10.3390/ijms20235998
160. Cypess AM, Haft CR, Laughlin MR, Hu HH. Brown fat in humans: consensus points and experimental guidelines. *Cell Metab.* (2014) 20:408–15. doi: 10.1016/j.cmet.2014.07.025

Conflict of Interest: The authors declare that the research was conducted in the absence of any commercial or financial relationships that could be construed as a potential conflict of interest.

frontiers in Endocrinology

REVIEW
published: 29 April 2020
doi: 10.3389/fendo.2020.00270

Exercise-Induced Adaptations to Adipose Tissue Thermogenesis

*Pablo Vidal and Kristin I. Stanford**

Department of Physiology and Cell Biology, Dorothy M. Davis Heart and Lung Research Institute, The Ohio State University Wexner Medical Center, Columbus, OH, United States

Exercise training results in beneficial adaptations to numerous tissues and offers protection against metabolic disorders including obesity and type 2 diabetes. Multiple studies have indicated that both white (WAT) and brown (BAT) adipose tissue may play an important role to mediate the beneficial effects of exercise. Studies from both rodents and humans have identified exercise-induced changes in WAT including increased mitochondrial activity and glucose uptake, an altered endocrine profile, and in rodents, a beiging of the WAT. Studies investigating the effects of exercise on BAT have resulted in conflicting data in terms of mitochondrial activity, glucose uptake, and thermogenic activity in rodents and humans, and remain an important area of investigation. This review discusses the exercise-induced adaptations to white and brown adipose tissue, distinguishing important differences between rodents and humans and highlighting the latest studies in the field and their implications.

Keywords: exercise, obesity, white adipose tissue (WAT), brown adipose tissue (BAT), thermogenesis

OPEN ACCESS

Edited by:
Takeshi Yoneshiro, University of California, San Francisco, United States

Reviewed by:
Alexander Bartelt, Ludwig Maximilian University of Munich, Germany
Maria Chondronikola, University of California, Davis, United States
Florian Kiefer, Medical University of Vienna, Austria

****Correspondence:***
Kristin I. Stanford
kristin.stanford@osumc.edu

Specialty section:
This article was submitted to Obesity, a section of the journal Frontiers in Endocrinology

Received: *10 February 2020*
Accepted: *14 April 2020*
Published: *29 April 2020*

Citation:
Vidal P and Stanford KI (2020) Exercise-Induced Adaptations to Adipose Tissue Thermogenesis. Front. Endocrinol. 11:270. doi: 10.3389/fendo.2020.00270

INTRODUCTION

Exercise training is an important non-pharmacological strategy to prevent and treat metabolic diseases, including obesity and type 2 diabetes. Exercise results in adaptations to almost all tissues in the body that contribute to the beneficial effects of exercise to improve whole-body metabolic health. A single bout of moderate intensity exercise has dramatic effects on glucose metabolism, lowering circulating insulin concentrations and improving skeletal muscle insulin sensitivity (1). Exercise training, defined as repeated bouts of exercise over a period of weeks, months, or years can decrease insulin concentrations and improve glucose tolerance (1, 2).

While it is well-established that exercise induces adaptations to skeletal muscle (2) and the cardiovascular system (3), several studies have now determined that exercise also results in adaptations to adipose tissue that improve whole-body metabolic health (4–15). These exercise-induced adaptations to adipose tissue include increased mitochondrial activity (5, 10), decreased cell size and lipid content (11), reduced inflammation (12, 13), and, in rodents, increased presence of thermogenic brown-like adipocytes or "beige" cells (6, 10, 15). Exercise also alters the endocrine profile of adipose tissue, inducing the release of adipokines and lipokines that mediate tissue-to-tissue communication and contribute to the improved metabolic homeostasis seen with exercise (9, 14, 16). Here, we will discuss studies investigating the exercise-induced adaptations to white and brown adipose tissue in humans and rodents, with a particular focus on the adaptations that contribute to thermogenesis.

ADIPOSE TISSUE

Adipose tissue is a type of connective tissue consisting primarily of mature adipocytes (∼ 65–90% in volume) (17, 18), a cell type whose defining characteristic is accumulation of internal fat droplets (19). In addition to the mature adipocytes, adipose tissue consists of a stromal vascular fraction (SVF). The SVF is immensely heterogeneous, containing pre-adipocytes, mesenchymal stem cells, endothelial cells, and a variety of immune cells, including macrophages and natural killer T cells (20). The SVF is very dynamic and can respond and adapt to stimulus such as β-adrenergic stimulation (20) and exercise (8).

Adipose tissue can be broadly classified into two different types, white adipose tissue and brown adipose tissue (21). Certain stimuli such as cold, sympathetic activation (22), exercise (6, 23) or an enriched environment (24) can give rise to a third type of adipocytes, beige adipocytes, within the WAT.

White Adipose Tissue

White adipose tissue (WAT) is composed of white adipocytes and its primary function is energy storage. Energy is stored by mature adipocytes in the form of triglycerides as one unilocular lipid droplet which occupies most of the cell volume and can vary in size (25). Adipose tissue is very dynamic, it can expand in size via hyperplasia or hypertrophy of the adipocytes (26, 27). WAT can be further subdivided into two different depots with distinct functions based on anatomical location, subcutaneous and visceral WAT (28).

Subcutaneous WAT

Subcutaneous WAT (scWAT) is located beneath the skin. In mice, scWAT is located in the inguinal, anterior axillary and interscapular regions (28–30). In humans, scWAT locations can be divided into lower-body, comprising gluteal and leg depots, and upper-body, in the anterior abdominal wall region (28). These distinct locations of scWAT adapt differently to the same stimulus (26, 31). Under obesogenic conditions, lower-body adipocytes tend to expand via hyperplasia, which has been associated with improved metabolic adaptations (32), while upper-body adipocytes expand via hypertrophy (26). Increases in upper-body scWAT are correlated with decreased insulin sensitivity and impaired glucose tolerance (31).

Visceral WAT

Visceral WAT (vWAT) surrounds internal organs. In mice, vWAT is found in the perigonadal, mesenteric, perirenal, retroperitoneal, cardiac, and triceps-associated regions (8, 28–30). In humans, vWAT is located in the intraabdominal (omental and mesenteric) as well as in the cardiac region (28). In lean individuals, vWAT accounts for 10–20% of the total fat mass in males and 5–8% in females (33).

There are distinct differences between scWAT and vWAT. These two adipose tissue depots behave and adapt differently to the same stimuli (26, 28, 34). Adipocytes in scWAT are smaller, have higher avidity for free fatty acid and triglyceride uptake, and are more sensitive to insulin compared to adipocytes from the vWAT (33, 35). Subcutaneous WAT has elevated expression of genes involved in glucose and lipid metabolism, and insulin signaling, compared to vWAT (36). Conversely, increases in vWAT are correlated with impaired glucose tolerance and increased insulin resistance (31) while increases in scWAT are correlated with improved metabolism (37).

Brown Adipose Tissue

Brown adipose tissue (BAT) is a metabolically active tissue that burns carbohydrates and lipids to generate heat (38–40). Brown adipocytes are characterized by multilocular lipid droplets, a central nucleus and a high density of mitochondria (41, 42). The most distinctive feature of brown adipocytes is the high expression of the thermogenic protein uncoupling protein 1 (UCP1) (43). UCP1 is located in the inner membrane of mitochondria and uncouples the proton gradient potential generated by the electron transport chain. Release of this chemical gradient results in the dissipation of energy in the form of heat. In rodents, BAT is found in the interscapular, mediastinal, perirenal, axillary, and cervical regions (29, 30, 44). BAT is a mammal-specific tissue and in humans, it was long thought to be present only in infants. In 2009, multiple studies demonstrated that BAT is also present in adult individuals (45–48). In humans, BAT is found in the cervical, supraclavicular, axillary, and paravertebral regions (45, 49), as well as in the perirenal region in infants (50). Perirenal BAT consists mainly of dormant brown adipocytes that can be stimulated to give rise to active brown adipocytes (51). Brown adipose tissue mass is negatively correlated with BMI and age in humans (45). Given this, and the functional role of BAT, targeting BAT as a therapeutic to combat obesity and metabolic disorders has become increasingly important.

Beige Adipocytes

Beige or brite (brown in white) adipocytes are a particular type of adipocytes within scWAT. Over 100 different stimuli are known to induce beiging, and most of them act through activation of the sympathetic nervous system (SNS) (52). Beige adipocytes have multilocular lipid droplets, a central nucleus, and a high density of mitochondria, similar to brown adipocytes. However, while brown adipocytes arise from *Pax7* and *Myf5* positive cells (53, 54), beige adipocytes arise from *Myf5* negative adipogenic stem cells within the adipose tissue (55, 56). White adipocyte tissue that has undergone beiging can be distinguished by the specific beiging markers *CD137*, *TBX1*, and *TMEM26* (30). Beige adipocytes function similarly to brown adipocytes in that they directly generate energy in the form of heat, contributing to thermogenesis. Beige adipocytes deviate from brown adipocytes in that they have a high degree of plasticity. In the absence of beiging stimuli, UCP1 expression, and mitochondrial content of beige adipocytes decrease and beige adipocytes transition to a white adipocyte phenotype (49). Increasing beige adipocytes has significant potential to combat obesity and type 2 diabetes.

EXERCISE-INDUCED ADAPTATIONS TO WAT

Exercise is an important therapeutic to prevent and treat metabolic diseases, including obesity and type 2 diabetes. Exercise results in adaptations to almost all tissues in the body, including adipose tissue. Exercise increases whole-body energy expenditure as chemical energy is converted into kinetic energy. During acute exercise, WAT has an important role in supplying this additional energy requirement from the triglyceride stores within the mature adipocytes (57). Independent from its role during acute exercise, chronic exercise leads to several metabolic adaptations in WAT (**Figure 1**). In this section, we will be reviewing the different metabolic adaptations that occur in WAT with exercise in both rodents and humans, including thermogenesis, mitochondrial adaptations, glucose metabolism, lipid metabolism, and endocrine adaptations.

Thermogenic Adaptations to WAT

An important exercise-induced adaptation to scWAT in rodents is the beiging of scWAT. Exercise induces an upregulation of thermogenic genes such as *Prdm16* and *Ucp1* in inguinal scWAT (6, 15, 58, 59) and an increased presence of adipocytes with multilocular lipid droplets (6, 60). The appearance of beige adipocytes does not occur homogeneously, as some regions of the inguinal scWAT are more prone to beiging than others (58, 61). This exercise-induced beiging is specific to scWAT, in particular the inguinal scWAT (8), and does not occur in vWAT (23, 60, 62). Beiging of scWAT is the molecular mechanism that leads to increased thermogenesis in WAT with exercise, as beige adipocytes increase non-shivering thermogenesis.

While beiging is an important adaptation to exercise, it is unclear why exercise induces a beiging of scWAT. Beiging of scWAT by non-exercise stimuli, including through cold-exposure, environmental factors or pharmaceuticals, is thought to be induced through a heat compensatory mechanism in which adrenergic stimulation compensates for heat loss with the upregulation of *UCP1* (44, 63–65). This explanation does not make sense in the context of exercise-induced beiging, because exercise itself increases heat production (66, 67). Several hypotheses have been proposed as the underlying mechanism, one of which is an increase in sympathetic innervation, which occurs in scWAT during exercise (52, 68) Other hypotheses have indicated that beiging occurs in response to the exercise-induced release of myokines, such as irisin (23), myostatin (69), meteorin-like 1 (Metrnl) (70), lactate (71), and β-aminoisobutyric acid (BAIBA) (72), or other secreted factors released during exercise, including brain-derived neurotrophic factor (BDNF) (24). More investigation is needed to fully understand this complex mechanism. These hypotheses are all important and plausible, but the most likely explanation is that the exercise-induced beiging of scWAT occurs because exercise decreases the adipocyte size and lipid content in scWAT, decreasing insulation of the body and necessitating heat production, which results in the beiging of scWAT (52, 73). The fact that mice are commonly housed at 20–22°C, the habitual indoor temperatures for humans, which itself contributes to mice being under chronic cold stress (74), provides further support for this explanation.

To address the hypothesis that beiging occurs in response to a loss of fat mass in a cold stress environment, multiple studies have investigated the effects of exercise at thermoneutrality (30°C) (14, 75, 76). Interestingly, when mice are housed at thermoneutral conditions, the exercise-induced increase of thermogenic gene expression and appearance of multilocular adipocytes exercise is blunted in male and female mice (75, 76), and this occurred independent of changes in body mass, fat mass, or running

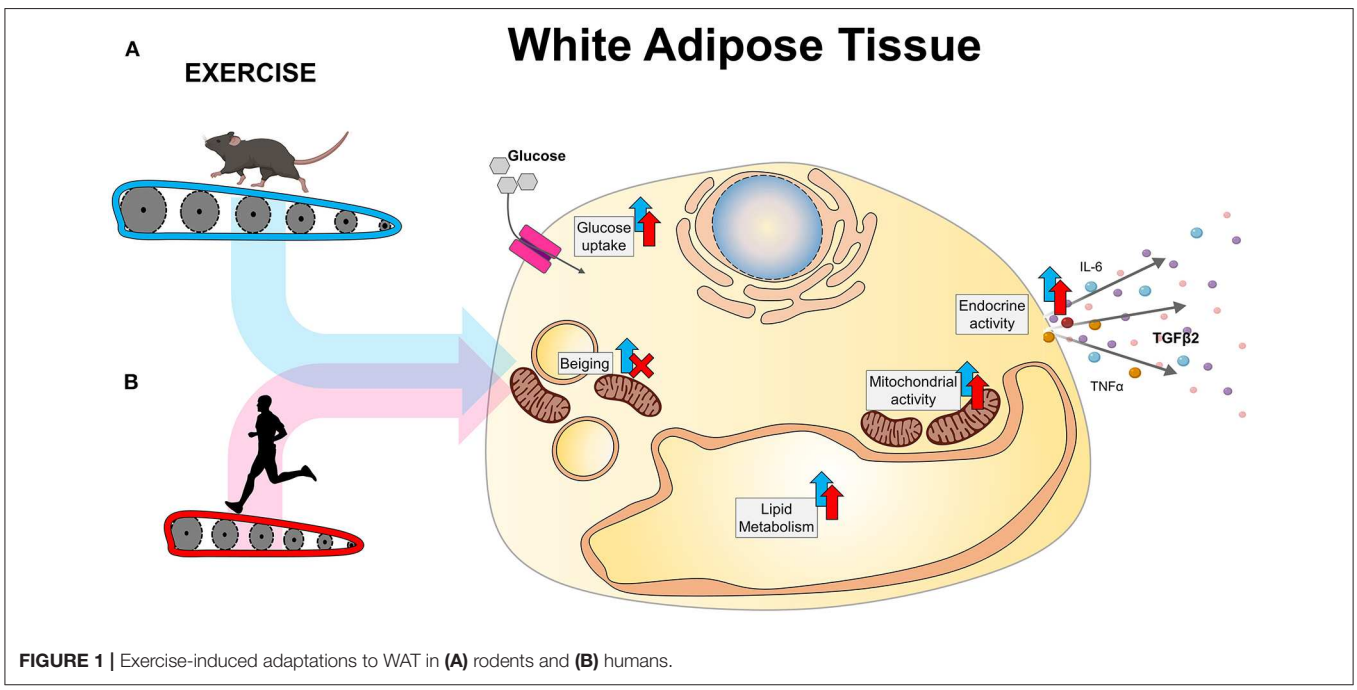

FIGURE 1 | Exercise-induced adaptations to WAT in **(A)** rodents and **(B)** humans.

distance. Interestingly, one of these studies investigated female mice and determined that total running distance was lower at thermoneutrality (∼40%) (76) and observed no differences in body weight or adiposity compared to sedentary mice, while another study determined that running distance was increased at thermoneutrality in male mice (∼50%) compared to mice at room temperature (75). These mice also had lower body mass compared to sedentary mice and mice housed at room temperature. While these discrepancies make some of the nuances between these studies difficult to interpret, each study determined that exercise-induced increase in thermogenic genes was blunted at thermoneutrality. These data suggest that the exercise-induced beiging is not a direct consequence of exercise, it is indirectly induced through other stimuli such as increased cold stress due to loss of WAT mass.

Several human studies have determined that exercise in humans does not induce beiging of scWAT (77–80). In lean or obese individuals, 10–16 weeks of endurance training did not change the expression of thermogenic genes including *UCP1*, *PRDM16*, and *PGC1A* in scWAT in males and females (77, 80–82). Studies conducted in highly exercise-trained populations and individuals with a more active lifestyle have also not observed any differences in *UCP1* expression in scWAT compared to sedentary controls (83, 84). These results collectively indicate that exercise does not induce beiging in humans.

The mechanistic reason as to why rodents and humans have opposite thermogenic adaptations in WAT is currently unknown. Similar to what has been discussed earlier, it is likely a result of cold stress; since rodents are smaller, they have a higher surface to volume ratio that makes them more susceptible to cold stress. Exercise decreases WAT accumulation, increasing cold stress, and thermogenic adaptations are increased to counter this effect. This would not be the case in humans, so the loss of WAT may not induce the same thermogenic response. However, most human studies investigating the effects of exercise on WAT have been conducted indoors in controlled environments. Investigating human subjects who exercise in the cold (i.e., skiers, open water swimmers) might result in a thermogenic response to human WAT.

Mitochondrial Adaptations to WAT

Exercise increases mitochondrial activity and density in scWAT and vWAT in rodents (5–8, 10, 58, 60, 85–87). Eleven days of voluntary wheel cage running increases the oxygen consumption rate of scWAT (6) and upregulates mitochondrial genes in both scWAT (6, 86) and vWAT (7, 8, 10, 58, 85). Importantly, exercise at thermoneutrality also results in upregulation of electron transport chain proteins (76), indicating that the increase in mitochondrial activity after exercise is independent of the beiging of WAT. *In vitro* studies indicate that exercise increases basal oxygen consumption rate of adipocytes differentiated from the SVF of scWAT (inguinal) or vWAT (perigonadal) of exercised mice (8), however maximal respiratory capacity only increased in adipocytes derived from scWAT (8). These data indicate that mitochondrial adaptations with exercise occur in both scWAT and vWAT in rodents, independent of beiging.

Exercise induces mitochondrial adaptations in human scWAT in lean male subjects (83, 88, 89) or young obese female subjects (77). Six weeks of high-intensity interval training (HIIT) increased mitochondrial respiration of scWAT (88). Ten to eighteen sessions of alternating continuous moderate-intensity training and HIIT did not change expression of genes involved in oxidative phosphorylation such as *PGC1A* or *COXIV* (78, 83, 90), but long term aerobic exercise-training increased expression of several genes involved in oxidative phosphorylation (89) and mitochondrial biogenesis (83). Exercise induced mitochondrial adaptations in vWAT have not been investigated in humans. Together these data indicate that exercise or increased physical activity increases mitochondrial activity in mouse and human WAT.

Adaptations to Glucose Metabolism in WAT

Exercise improves whole-body glucose homeostasis in rodents (91) and humans (1). Exercise increases glucose uptake and insulin sensitivity of scWAT (6, 15) and induces upregulation of genes and proteins involved in glucose metabolism in scWAT and vWAT (7, 8). These data indicate that exercise improves glucose metabolism in WAT in rodents. Here, we will focus on the effects of exercise in glucose homeostasis in WAT.

Recent studies have investigated the effects of exercise at thermoneutrality on glucose metabolism, with conflicting results. One study found that exercise still resulted in improvements in whole-body glucose tolerance (75), whereas another found no effect of exercise on whole-body glucose homeostasis at thermoneutrality (76). Interestingly, the latter found that there was an increase in *in vivo* insulin-stimulated ^{3}H-2DG uptake in vWAT at thermoneutrality, but no changes were found in scWAT (76). In the latter study, the lack of exercise-induced changes to glucose metabolism can likely be attributed to the fact that mice at thermoneutrality ran ∼40% less than mice at room temperature (76). As the results from these two studies are conflicting, the effects of exercise on glucose metabolism at thermoneutrality are unclear. Further research is essential to elucidate the effects of exercise at thermoneutrality on glucose metabolism and determine which adaptations arise at a systemic level and which are specific to the WAT.

Studies investigating exercise-induced adaptations to glucose homeostasis in human WAT are less comprehensive. One study determined that 6 months of exercise upregulated genes involved in glucose metabolism in lower-body scWAT (89). Two weeks of exercise increased insulin-stimulated glucose uptake in lower-body scWAT, but not upper-body scWAT or vWAT (92). These data indicate that scWAT and vWAT, and even upper-body and lower-body scWAT, have distinct adaptations to glucose metabolism with exercise. This is of particular interest to human physiology as humans with a higher proportion of upper-body WAT have been correlated with impaired glucose tolerance, while humans with a higher proportion of lower-body WAT are associated with improved glucose levels (32). These data indicate the lower scWAT has a prominent role on the effect on whole-body glucose homeostasis and is more susceptible to exercise.

Adaptations to Lipid Metabolism in WAT

Exercise effects lipid metabolism in WAT during exercise. Moderate exercise (40–65% VO_2 max) acutely increases whole-body lipolysis two to three times over basal rates after exercising for 30 min, and increases lipolysis up to 5-fold over basal after 4 h of exercise (93). Here, we will focus on the chronic adaptations of exercise to WAT with regard to lipid metabolism.

In rodents, exercise induces several adaptations that affect lipid metabolism including changes in gene expression (6, 8, 94), post-translational modifications (7) and an altered lipidomic profile (94). Two to three weeks of voluntary wheel cage running upregulates genes involved in fatty acid oxidation in scWAT and vWAT (6, 8), and genes involved in phospholipid metabolism in scWAT (94). Twelve days of voluntary wheel cage exercise increases phosphorylation of hormone sensitive lipase (HSL) (86), and exercise over a longer duration (6 weeks) increases phosphorylation of adipose triglyceride lipase (ATGL) (7). These post-translational modifications result in increased lipolytic activity of ATGL and HSL (95–97). Another study demonstrated that chronic treadmill training (8 weeks) did not increase the rate of lipolysis in isolated adipocytes under basal conditions, but when these adipocytes were stimulated by a β-adrenergic agonist, lipolysis was significantly increased in adipocytes isolated from exercised mice compared to adipocytes isolated from sedentary mice (98). Together, these results suggest that exercise induces adaptations that increase lipolysis.

Exercise also induces extensive adaptations to the lipidomic profile of scWAT in rodents. Previous work in our laboratory demonstrated that 3 weeks of exercise dramatically alters the lipidome of scWAT. Exercise significantly decreased the overall abundance of triacylglycerol (TAG), phosphatidylserines (PS) lysophosphatidylglycerols and lysophosphatidylinositols (LPI) (94). In addition to the changes in overall lipid classes, there were also decreases in several specific molecular species of phosphatidic acid, phosphatidylethanolamines (PE), and PS. These changes corresponded with a significant upregulation of several genes involved in phospholipid metabolism. These data suggest molecular species-specific remodeling of phospholipids and TAGs in scWAT in response to exercise (66, 94). The functional consequence of the exercise-induced changes to the lipidome of scWAT have not been identified, but that will be the focus of future investigation.

Research on the effects of chronic exercise on lipid metabolism in humans has not been thoroughly investigated. Studies have shown that active individuals (self-reported exercise >3x per week) have increased levels of *CPT1B*, the rate-limiting enzyme in fatty acid oxidation, in scWAT compared to sedentary individuals (83), and 6 months of exercise upregulates several genes involved in lipid metabolism (89). These data indicate that long-term exercise increases fatty acid oxidation in human WAT. However, shorter duration exercise interventions do not alter adaptations to lipid metabolism in WAT (82, 83). Three weeks of exercise in sedentary individuals did not change *CPT1B* levels (83), and 12 weeks of exercise in obese subjects did not change expression levels of *ATGL*, *HSL*, or other lipolytic enzymes (82). Taken together, these data indicate that exercise upregulates lipid metabolism in WAT of both rodents and humans.

Endocrine Adaptations to WAT

Exercise induces considerable adaptations to the secretory profile of several tissues, including adipose tissue (13, 99). Secretory factors released from adipose tissue have been labeled as adipokines. Four or more weeks of exercise in rodents decreases leptin and adiponectin mRNA levels in scWAT (100) and circulation (87, 100, 101) in rodents and humans. Exercise also increases expression of other factors such as TNF-α and IL-6 in both WAT depots and in circulation (85, 100).

Recent work in our laboratory determined that transplantation of scWAT from exercised donor mice into sedentary recipient mice resulted in improved whole-body glucose tolerance. Glucose uptake was also increased in BAT, soleus and tibialis anterior, indicating that an endocrine factor is released from exercise-trained scWAT to mediate these effects (6). TGF-β2 was recently identified as the adipokine responsible for these beneficial effects on glucose metabolism (14). TGF-β2 is an adipokine secreted in response to exercise in both rodents and humans from WAT. In rodents, acute treatment with TGF-β2 increased glucose uptake in soleus, heart and BAT, and increased fatty acid uptake in skeletal muscle. Notably, adipose tissue specific TGF-β2 knockout mice did not have exercise-induced improvements in systemic glucose uptake (14).

Exercise can also induce adaptations in WAT through myokines such as myostatin and BAIBA. Myostatin is a well-known factor that inhibits skeletal muscle growth (102). Exercise decreases myostatin levels in skeletal muscle and serum (103). Reduced levels of myostatin promote beiging of the scWAT in rodents (104) and are correlated with improved insulin sensitivity in humans (103). During exercise, increase in PGC1α triggers the secretion of β-aminoisobutyric acid (BAIBA) in both rodents and humans. BAIBA promotes beiging of scWAT in rodents while it is inversely correlated with serum glucose and insulin levels in humans (72). These data indicate that exercise stimulates release of secretory factors, from WAT as well as other tissues like skeletal muscle, that result in positive metabolic systemic and WAT specific adaptations.

Effects of Endurance vs. Resistance Exercise on WAT

Exercise can be broadly divided into endurance (aerobic) and resistance (strength) training (2). There have been several studies investigating the different adaptations of endurance and resistance training in skeletal muscle (2, 105), but this is not the case with adipose tissue. Most studies have investigated the effects of endurance training on adipose tissue, using treadmill or voluntary wheel cage running in rodents, and running or cycling for human studies. Some studies have compared the effects of different intensities, moderate (MIT) or high-intensity (HIT) endurance training on adipose tissue and found that MIT and HIT had similar effects on WAT in rodents (106, 107) and humans (92, 108). Meta-analysis comparing the effect of MIT or HIT on adiposity in humans found HIT resulted in a greater decrease in total fat mass (109). A few human studies have mixed endurance and resistance training in their exercise protocols, without finding any striking differences when compared to just

endurance training (14, 77, 79, 82). However, to our knowledge, the direct effect of resistance compared to endurance exercise in adipose tissue has not been investigated.

EXERCISE-INDUCED ADAPTATIONS TO BAT

BAT accounts for a small percentage of total fat mass than WAT, but it is a much more metabolically active tissue than WAT (110). Exercise increases energy expenditure, thus indirectly increasing in thermogenesis (111). BAT and WAT functions are different, and so are their exercise-induced adaptations. Here, we will discuss the different metabolic adaptations that occur in BAT with exercise in both rodents and humans (**Figure 2**).

Thermogenic Adaptations to BAT

The thermogenic effects of exercise on BAT in rodents have been thoroughly investigated, with conflicting results. Eleven weeks of swimming (6 days/week; 2 h per day) increased blood flow and oxygen consumption in response to acute injection with norepinephrine (NE) (112, 113), indicating that exercise may increase sensitivity to adrenergic stimulation in BAT. These data are difficult to interpret because swimming as an exercise modality indirectly results in cold stress. Interestingly, these studies found that when the water temperature is 32, 36, or 38°C, acute injection of NE had the same response to increase blood flow and oxygen consumption, but BAT mass was only increased when the water temperature was 32°C (112). Other studies investigated the effects of exercise on BAT using 6 weeks of treadmill training as the exercise protocol (114). Interestingly, there was no effect of treadmill exercise to affect oxygen consumption or blood flow at rest or after NE injection (114, 115). Furthermore, BAT mass and protein content were decreased with 6 weeks of treadmill training (115, 116), regardless of the ambient temperature of the exercise (room temperature or 4°C) (116). In female rats, 6 weeks of treadmill exercise increased BAT mass and total protein content (117), but 9 weeks of treadmill training reduced BAT mass and decreased *UCP1* expression (118). The reason for this is unclear, but it is possible that the discrepancies between these two studies could be explained by differences in the rat strain studied, as the first study used Sprague-Dawley while the latter used F-344 NNia. These data indicate that different exercise modalities, or different animal strains, could result in different adaptations to BAT.

More recent studies have indicated that exercise does not affect, or even decreases, BAT activity (58, 86, 119). Twelve days of voluntary wheel cage running in mice did not alter BAT mass (86), and 6 weeks of treadmill training in rats did not affect BAT mass, brown adipocyte size or *Ucp1* expression (58, 119). Oxidation of palmitate was also reduced in BAT *ex vivo* after 6 weeks of treadmill training, indicating exercise decreases fatty acid oxidation in BAT (58). Exercise at thermoneutrality also reduced BAT mass and did not alter markers of thermogenesis (75). These data indicate that exercise does not increase thermogenic activity in BAT in rodents in the absence of a cold stress (i.e., swimming).

There is currently a paucity of data that has investigated the thermogenic adaptations of BAT with exercise in humans. Studies have determined that endurance trained athletes subjected to cold exposure have decreased glucose uptake in BAT compared to sedentary subjects (84, 120). It is important to note that the current gold standard to measure BAT activity in humans is ^{18}FDG-PET/CT (121), and humans studies have only determined BAT mass and activity in the context of its ability to take up

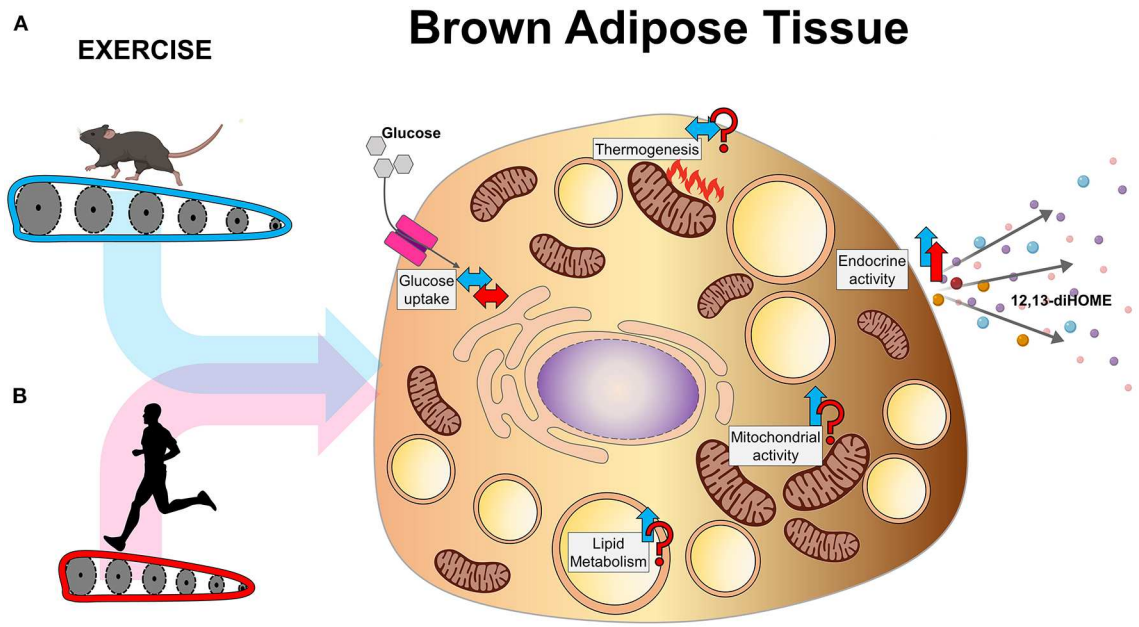

FIGURE 2 | Exercise-induced adaptations to BAT in **(A)** rodents and **(B)** humans.

glucose. Moreover, cold exposure is frequently needed to activate BAT for detection by ^{18}FDG-PET/CT scans. Other methods like infrared thermography (122) and T2 mapping (123) have been developed to evaluate BAT presence, but they have not yet been used to assess differences in BAT activity with exercise. Fat T2 relaxation time mapping is based on BAT having higher water content than WAT. This technique measures BAT activity and does not require cold exposure for detection (123). The use of these new techniques will be important to truly ascertain the effects of exercise on BAT in humans *in vivo.*

Mitochondrial Adaptations to BAT

The effects of exercise on mitochondrial activity in BAT have also been investigated. In rodents, 2–8 weeks of exercise did not change or decreased expression of mitochondrial genes (8, 58, 75, 76). Recent work in our laboratory determined that 11 days of voluntary wheel cage running (VWR) in male mice decreased basal oxygen consumption rate (OCR) in brown adipocytes differentiated from the SVF of BAT (8), but cells from both sedentary and exercise-trained BAT were able to respond to pharmacological stimulation to a similar extent. Eleven days of VWR decreased NADH autofluorescence, an indirect marker of metabolism, compared to the sedentary controls (8). In contrast, 6–8 weeks of treadmill training in rats significantly increased expression of proteins involved in mitochondrial biogenesis, such as *PGC1α*, *NRF1,* or *TFAM* (119, 124). The reason for the discrepancies in these studies are unclear, although duration, exercise modality, or species investigated (rat or mouse), could contribute to these different responses to exercise.

Studies on the effect of exercise in BAT mitochondria in humans are limited. One study found no differences on *PGC1α* expression in BAT between endurance athletes and sedentary males (84). Overall, exercise appears to decrease mitochondrial activity in BAT in mice, but more human studies are needed to elucidate the effects of exercise on mitochondrial activity in BAT.

Adaptations to Glucose Metabolism in BAT

The effects of exercise on glucose uptake in BAT in rodents are conflicting. On one hand, some studies have shown that 2–8 weeks of exercise upregulates expression of genes involved in insulin signaling, glucose and fatty acid oxidation in BAT (8, 124, 125). However, 2 weeks of exercise decreased basal glucose uptake in brown adipocytes differentiated from SVF (8). Another study indicated that 6 weeks of exercise did not effect *in vivo* glucose uptake in BAT at room temperature or thermoneutrality, measured by *in vivo* insulin-stimulated ^{3}H-2DG uptake (76). These data reveal that, although exercise results in an upregulation of genes involved in glucose metabolism, *in vivo* data in rodents indicates that exercise does not increase glucose uptake in BAT.

Several studies have indicated that exercise does not alter glucose uptake in BAT in humans. As little as 6 sessions of HIIT or moderate-intensity exercise-training in a 2 week period decreased insulin-stimulated glucose uptake in BAT (92), and 6 weeks of moderate-intensity continuous training did not affect cold-stimulated glucose uptake measured by ^{18}FDG-PET/CT (126). In addition, endurance athletes have reduced glucose uptake in BAT when subjected to cold stimulation compared to sedentary subjects (measured by ^{18}FDG-PET/CT) (84). Another study determined that there was no association of BAT mass or activity to physical activity in a cohort of 130 healthy, sedentary subjects (127). These data indicate that exercise or increased physical activity does not increase glucose metabolism in human BAT.

Adaptations to Lipid Metabolism in BAT

The effects of exercise on lipid metabolism in BAT has not been thoroughly investigated. Eleven days of exercise increased expression of genes involved in fatty acid oxidation (8), but decreased expression of genes involved in fatty acid biosynthesis (94), phospholipid metabolism (94) and lipolysis (8, 75). Oxidation of palmitate was also reduced in BAT *ex vivo* after 6 weeks of treadmill training (58).

Exercise affects the lipidomic profile of BAT by increasing total abundance of TAGs phosphatidylcholines (PC) and cholesterol esters, while decreasing cardiolipins and lysophosphatidylglycerols (94). Exercise also significantly increased several specific molecular species of PC and PE in BAT. These data show that exercise decreases lipid metabolism in BAT. To our knowledge, there are currently no studies analyzing the effect of exercise on lipid metabolism in human BAT. While it is clear that BAT lipid metabolism changes with exercise, the role of the exercise-induced decrease in lipolysis or changes in BAT lipidome have not been identified and will be the topic of future investigations.

Endocrine Adaptations to BAT

It is important to note that in most cases, particularly in human studies, BAT activity, and mass are measured by glucose uptake. This is important in most settings, however, since exercise is a thermogenic activity it is unlikely that exercise would increase glucose uptake in BAT. This has led several groups to hypothesize that exercise may alter the endocrine activity of BAT. In fact, multiple studies have identified an endocrine role for BAT in response to exercise (13, 16, 128). Recent work in our laboratory identified the lipokine, 12,13-diHOME, to be released from BAT in response to exercise in mice and humans (9) Upregulation of 12,13-diHOME activates fatty acid uptake and oxidation in skeletal muscle without affecting glucose homeostasis (9). This data shows a direct role of BAT to improve metabolic health with exercise. These are the first data to identify a secreted factor from BAT with exercise to mediate skeletal muscle metabolic adaptations.

FUTURE DIRECTIONS AND CONCLUSIONS

Exercise results in positive metabolic adaptations in both white and brown adipose tissue. Exercise increases mitochondrial activity, glucose metabolism, and endocrine activity in WAT in both rodents and humans. Notably, beiging of WAT only occurs with exercise in rodents, but both humans and rodents have increased mitochondrial activity independent of beiging of WAT. Exercise increases endocrine activity of BAT but does not affect

glucose uptake in rodents and humans. Additionally, exercise does not affect thermogenesis and decreases mitochondrial activity in BAT in rodents.

An important point of investigation has been the effects of exercise-induced beiging in WAT. While this adaptation has been clearly identified in rodents, studies in humans have not identified the same effects. More recent studies have begun to investigate the effects of exercise at thermoneutrality to parse apart the direct effects of exercise on beiging, and have demonstrated that exercise at thermoneutrality blunts the effects of exercise on thermogenic gene expression (75, 76). Expanding these studies will provide greater insight and translational relevance for determining the effects of exercise on WAT (and potentially BAT).

Most of the studies discussed in this review have been conducted in either males or females. This is of particular importance as there are clear sex differences in adipose tissue depots among males and females, with females having a higher percentage of WAT (27) and higher BAT activity at rest (45). Another important issue in the field of BAT thermogenesis, especially in human studies, is the measurement of BAT activity. ^{18}FDG-PET/CT is the gold standard for measurement of BAT mass and activity in humans, however, this analysis is solely based on the ability of BAT to uptake glucose to use it as a substrate. This highlights the importance of new techniques to accurately measure BAT activity and establish *in vivo* measurements of BAT thermogenic capacity, including in the context of exercise. Newer techniques such as infrared thermography and T2 mapping are potential mechanisms to elucidate the adaptations of BAT to exercise.

There is a need for the comprehensive understanding of the mechanisms underlying the chronic adaptations of adipose tissue with exercise. A single session of exercise leads to acute changes in expression of several genes (129). Successive bouts of exercise most lead to a cumulative effect of these acute changes resulting in chronic adaptations, which contribute to changes in glucose metabolism, fatty acid metabolism, and mitochondrial activity. Post-translational modifications such as protein phosphorylation regulate protein activity (130), and chronic exercise increases overall phosphorylation of proteins such as HSL and ATGL, which result in increased lipolytic activity (7, 75). Epigenetic modifications may also be underlying drivers of exercise-induce adaptations to exercise; studies have shown that exercise results in changes to the genome-wide DNA methylation pattern of human WAT (131, 132). These studies indicate that epigenetic modifications could oversee the chronic adaptations to adipose tissue with exercise by promoting or inhibiting expression of metabolic genes. Understanding factors that trigger exercise-induced adaptations remains an open field that will be an important for future investigations.

Together these studies highlight the importance of exercise to alter function of WAT and BAT that could provide important targets to improve metabolic health and reduce obesity. Future studies will investigate other mechanisms by which exercise exerts metabolic adaptations on adipose tissue such as increased mitochondrial function, improved glucose homeostasis or endocrine function, providing important translational relevance for exercise as a therapeutic tool.

AUTHOR CONTRIBUTIONS

PV and KS designed, wrote, and edited the manuscript.

FUNDING

This work was supported by National Institutes of Health Grants R01-HL138738 to KS, R01-AG060542 to KS.

REFERENCES

1. Goodyear LJ, Kahn BB. Exercise, glucose transport, and insulin sensitivity. *Annu Rev Med.* (1998) 49:235–61. doi: 10.1146/annurev.med.49.1.235
2. Egan B, Zierath JR. Exercise metabolism and the molecular regulation of skeletal muscle adaptation. *Cell Metab.* (2013) 17:162–84. doi: 10.1016/j.cmet.2012.12.012
3. Hellsten Y, Nyberg M. Cardiovascular adaptations to exercise training. *Compr Physiol.* (2015) 6:1–32. doi: 10.1002/cphy.c140080
4. Blond MB, Rosenkilde M, Gram AS, Tindborg M, Christensen AN, Quist JS, et al. How does 6 months of active bike commuting or leisure-time exercise affect insulin sensitivity, cardiorespiratory fitness and intra-abdominal fat? A randomised controlled trial in individuals with overweight and obesity. *Br J Sports Med.* (2019) 53:1183–92. doi: 10.1136/bjsports-2018-100036
5. Stallknecht B, Vinten J, Ploug T, Galbo H. Increased activities of mitochondrial enzymes in white adipose tissue in trained rats. *Am J Physiol.* (1991) 261(3 Pt 1):E410–4. doi: 10.1152/ajpendo.1991.261.3.E410
6. Stanford KI, Middelbeek RJ, Townsend KL, Lee MY, Takahashi H, So K, et al. A novel role for subcutaneous adipose tissue in exercise-induced improvements in glucose homeostasis. *Diabetes.* (2015) 64:2002–14. doi: 10.2337/db14-0704
7. Stephenson EJ, Lessard SJ, Rivas DA, Watt MJ, Yaspelkis BB III, Koch LG, et al. Exercise training enhances white adipose tissue metabolism in rats selectively bred for low- or high-endurance running capacity. *Am J Physiol Endocrinol Metab.* (2013) 305:E429–38. doi: 10.1152/ajpendo.00544.2012
8. Lehnig AC, Dewal RS, Baer LA, Kitching KM, Munoz VR, Arts PJ, et al. Exercise training induces depot-specific adaptations to white and brown adipose tissue. *iScience.* (2019) 11:425–39. doi: 10.1016/j.isci.2018.12.033
9. Stanford KI, Lynes MD, Takahashi H, Baer LA, Arts PJ, May FJ, et al. 12,13-diHOME: an exercise-induced lipokine that increases skeletal muscle fatty acid uptake. *Cell Metab.* (2018) 27:1111–20.e3. doi: 10.1016/j.cmet.2018.04.023
10. Sutherland LN, Bomhof MR, Capozzi LC, Basaraba SA, Wright DC. Exercise and adrenaline increase PGC-1{alpha} mRNA expression in rat adipose tissue. *J Physiol.* (2009) 587(Pt 7):1607–17. doi: 10.1113/jphysiol.2008.165464
11. Craig BW, Hammons GT, Garthwaite SM, Jarett L, Holloszy JO. Adaptation of fat cells to exercise: response of glucose uptake and oxidation to insulin. *J Appl Physiol Respir Environ Exerc Physiol.* (1981) 51:1500–6. doi: 10.1152/jappl.1981.51.6.1500
12. Geng L, Liao B, Jin L, Huang Z, Triggle CR, Ding H, et al. Exercise alleviates obesity-induced metabolic dysfunction via enhancing FGF21 sensitivity in adipose tissues. *Cell Rep.* (2019) 26:2738–52.e4. doi: 10.1016/j.celrep.2019.02.014
13. Lee S, Norheim F, Langleite TM, Gulseth HL, Birkeland KI, Drevon CA. Effects of long-term exercise on plasma adipokine levels and inflammation-related gene expression in subcutaneous adipose tissue in sedentary dysglycaemic, overweight men and sedentary

normoglycaemic men of healthy weight. *Diabetologia.* (2019) 62:1048–64. doi: 10.1007/s00125-019-4866-5
14. Takahashi H, Alves CRR, Stanford KI, Middelbeek RJW, Pasquale N, Ryan RE, et al. TGF-β2 is an exercise-induced adipokine that regulates glucose and fatty acid metabolism. *Nat Metab.* (2019) 1:291–303. doi: 10.1038/s42255-018-0030-7
15. Trevellin E, Scorzeto M, Olivieri M, Granzotto M, Valerio A, Tedesco L, et al. Exercise training induces mitochondrial biogenesis and glucose uptake in subcutaneous adipose tissue through eNOS-dependent mechanisms. *Diabetes.* (2014) 63:2800–11. doi: 10.2337/db13-1234
16. Rodriguez A, Becerril S, Ezquerro S, Mendez-Gimenez L, Fruhbeck G. Crosstalk between adipokines and myokines in fat browning. *Acta Physiol.* (2017) 219:362–81. doi: 10.1111/apha.12686
17. Garrow JS. New approaches to body composition. *Am J Clin Nutr.* (1982) 35(Suppl. 5):1152–8. doi: 10.1093/ajcn/35.5.1152
18. Goglia F, Geloen A, Lanni A, Minaire Y, Bukowiecki LJ. Morphometric-stereologic analysis of brown adipocyte differentiation in adult mice. *Am J Physiol.* (1992) 262(4 Pt 1):C1018–23. doi: 10.1152/ajpcell.1992.262.4.C1018
19. Ali AT, Hochfeld WE, Myburgh R, Pepper MS. Adipocyte and adipogenesis. *Eur J Cell Biol.* (2013) 92:229–36. doi: 10.1016/j.ejcb.2013.06.001
20. Burl RB, Ramseyer VD, Rondini EA, Pique-Regi R, Lee YH, Granneman JG. Deconstructing adipogenesis induced by β3-adrenergic receptor activation with single-cell expression profiling. *Cell Metab.* (2018) 28:300–9.e4. doi: 10.1016/j.cmet.2018.05.025
21. Fawcett DW. Differences in physiological activity in brown and white fat as revealed by histochemical reactions. *Science.* (1947) 105:123–5. doi: 10.1126/science.105.2718.123
22. Labbé SM, Caron A, Chechi K, Laplante M, Lecomte R, Richard D. Metabolic activity of brown, "beige," and white adipose tissues in response to chronic adrenergic stimulation in male mice. *Am J Physiol Endocrinol Metab.* (2016) 311:E260–8. doi: 10.1152/ajpendo.00545.2015
23. Bostrom P, Wu J, Jedrychowski MP, Korde A, Ye L, Lo JC, et al. A PGC1-α-dependent myokine that drives brown-fat-like development of white fat and thermogenesis. *Nature.* (2012) 481:463–8. doi: 10.1038/nature10777
24. Cao L, Choi EY, Liu X, Martin A, Wang C, Xu X, et al. White to brown fat phenotypic switch induced by genetic and environmental activation of a hypothalamic-adipocyte axis. *Cell Metab.* (2011) 14:324–38. doi: 10.1016/j.cmet.2011.06.020
25. Roncari DA, Hamilton BS. Cellular and molecular factors in adipose tissue growth and obesity. *Adv Exp Med Biol.* (1993) 334:269–77. doi: 10.1007/978-1-4615-2910-1_20
26. Tchoukalova YD, Votruba SB, Tchkonia T, Giorgadze N, Kirkland JL, Jensen MD. Regional differences in cellular mechanisms of adipose tissue gain with overfeeding. *Proc Natl Acad Sci USA.* (2010) 107:18226–31. doi: 10.1073/pnas.1005259107
27. Tchoukalova YD, Koutsari C, Karpyak MV, Votruba SB, Wendland E, Jensen MD. Subcutaneous adipocyte size and body fat distribution. *Am J Clin Nutr.* (2008) 87:56–63. doi: 10.1093/ajcn/87.1.56
28. Tchkonia T, Thomou T, Zhu Y, Karagiannides I, Pothoulakis C, Jensen MD, et al. Mechanisms and metabolic implications of regional differences among fat depots. *Cell Metab.* (2013) 17:644–56. doi: 10.1016/j.cmet.2013.03.008
29. Cinti S. The adipose organ. *Prostaglandins Leukot Essent Fatty Acids.* (2005) 73:9–15. doi: 10.1016/j.plefa.2005.04.010
30. de Jong JM, Larsson O, Cannon B, Nedergaard J. A stringent validation of mouse adipose tissue identity markers. *Am J Physiol Endocrinol Metab.* (2015) 308:E1085–105. doi: 10.1152/ajpendo.00023.2015
31. Kissebah AH, Krakower GR. Regional adiposity and morbidity. *Physiol Rev.* (1994) 74:761–811. doi: 10.1152/physrev.1994.74.4.761
32. Karpe F, Pinnick KE. Biology of upper-body and lower-body adipose tissue–link to whole-body phenotypes. *Nat Rev Endocrinol.* (2015) 11:90–100. doi: 10.1038/nrendo.2014.185
33. Wajchenberg BL. Subcutaneous and visceral adipose tissue: their relation to the metabolic syndrome. *Endocr Rev.* (2000) 21:697–738. doi: 10.1210/edrv.21.6.0415
34. Zuriaga MA, Fuster JJ, Gokce N, Walsh K. Humans and mice display opposing patterns of "Browning" gene expression in visceral and subcutaneous white adipose tissue depots. *Front Cardiovasc Med.* (2017) 4:27. doi: 10.3389/fcvm.2017.00027
35. Ibrahim MM. Subcutaneous and visceral adipose tissue: structural and functional differences. *Obes Rev.* (2010) 11:11–8. doi: 10.1111/j.1467-789X.2009.00623.x
36. Atzmon G, Yang XM, Muzumdar R, Ma XH, Gabriely I, Barzilai N. Differential gene expression between visceral and subcutaneous fat depots. *Horm Metab Res.* (2002) 34:622–8. doi: 10.1055/s-2002-38250
37. Pinnick KE, Nicholson G, Manolopoulos KN, McQuaid SE, Valet P, Frayn KN, et al. Distinct developmental profile of lower-body adipose tissue defines resistance against obesity-associated metabolic complications. *Diabetes.* (2014) 63:3785–97. doi: 10.2337/db14-0385
38. Himms-Hagen J. Brown adipose tissue thermogenesis, energy balance, and obesity. *Can J Biochem Cell Biol.* (1984) 62:610–7. doi: 10.1139/o84-081
39. Bartelt A, Bruns OT, Reimer R, Hohenberg H, Ittrich H, Peldschus K, et al. Brown adipose tissue activity controls triglyceride clearance. *Nat Med.* (2011) 17:200–5. doi: 10.1038/nm.2297
40. Lowell BB, Spiegelman BM. Towards a molecular understanding of adaptive thermogenesis. *Nature.* (2000) 404:652–60. doi: 10.1038/35007527
41. Chu M, Sampath H, Cahana DY, Kahl CA, Somwar R, Cornea A, et al. Spatiotemporal dynamics of triglyceride storage in unilocular adipocytes. *Mol Biol Cell.* (2014) 25:4096–105. doi: 10.1091/mbc.e14-06-1085
42. Cohen P, Spiegelman BM. Cell biology of fat storage. *Mol Biol Cell.* (2016) 27:2523–7. doi: 10.1091/mbc.e15-10-0749
43. Golozoubova V, Hohtola E, Matthias A, Jacobsson A, Cannon B, Nedergaard J. Only UCP1 can mediate adaptive nonshivering thermogenesis in the cold. *FASEB J.* (2001) 15:2048–50. doi: 10.1096/fj.00-0536fje
44. Cannon B, Nedergaard J. Brown adipose tissue: function and physiological significance. *Physiol Rev.* (2004) 84:277–359. doi: 10.1152/physrev.00015.2003
45. Cypess AM, Lehman S, Williams G, Tal I, Rodman D, Goldfine AB, et al. Identification and importance of brown adipose tissue in adult humans. *N Engl J Med.* (2009) 360:1509–17. doi: 10.1056/NEJMoa0810780
46. Saito M, Okamatsu-Ogura Y, Matsushita M, Watanabe K, Yoneshiro T, Nio-Kobayashi J, et al. High incidence of metabolically active brown adipose tissue in healthy adult humans: effects of cold exposure and adiposity. *Diabetes.* (2009) 58:1526–31. doi: 10.2337/db09-0530
47. van Marken Lichtenbelt WD, Vanhommerig JW, Smulders NM, Drossaerts JM, Kemerink GJ, Bouvy ND, et al. Cold-activated brown adipose tissue in healthy men. *N Engl J Med.* (2009) 360:1500–8. doi: 10.1056/NEJMoa0808718
48. Virtanen KA, Lidell ME, Orava J, Heglind M, Westergren R, Niemi T, et al. Functional brown adipose tissue in healthy adults. *N Engl J Med.* (2009) 360:1518–25. doi: 10.1056/NEJMoa0808949
49. Ikeda K, Maretich P, Kajimura S. The common and distinct features of brown and beige adipocytes. *Trends Endocrinol Metab.* (2018) 29:191–200. doi: 10.1016/j.tem.2018.01.001
50. Lean ME, James WP, Jennings G, Trayhurn P. Brown adipose tissue uncoupling protein content in human infants, children and adults. *Clin Sci.* (1986) 71:291–7. doi: 10.1042/cs0710291
51. Jespersen NZ, Feizi A, Andersen ES, Heywood S, Hattel HB, Daugaard S, et al. Heterogeneity in the perirenal region of humans suggests presence of dormant brown adipose tissue that contains brown fat precursor cells. *Mol Metab.* (2019) 24:30–43. doi: 10.1016/j.molmet.2019.03.005
52. Nedergaard J, Cannon B. The browning of white adipose tissue: some burning issues. *Cell Metab.* (2014) 20:396–407. doi: 10.1016/j.cmet.2014.07.005
53. Seale P, Bjork B, Yang W, Kajimura S, Chin S, Kuang S, et al. PRDM16 controls a brown fat/skeletal muscle switch. *Nature.* (2008) 454:961–7. doi: 10.1038/nature07182
54. Lepper C, Fan CM. Inducible lineage tracing of Pax7-descendant cells reveals embryonic origin of adult satellite cells. *Genesis.* (2010) 48:424–36. doi: 10.1002/dvg.20630
55. Berry DC, Jiang Y, Graff JM. Mouse strains to study cold-inducible beige progenitors and beige adipocyte formation and function. *Nat Commun.* (2016) 7:10184. doi: 10.1038/ncomms10184
56. Wu J, Bostrom P, Sparks LM, Ye L, Choi JH, Giang AH, et al. Beige adipocytes are a distinct type of thermogenic fat cell in mouse and human. *Cell.* (2012) 150:366–76. doi: 10.1016/j.cell.2012.05.016

57. Jones NL, Heigenhauser GJ, Kuksis A, Matsos CG, Sutton JR, Toews CJ. Fat metabolism in heavy exercise. *Clin Sci.* (1980) 59:469–78. doi: 10.1042/cs0590469
58. Wu MV, Bikopoulos G, Hung S, Ceddia RB. Thermogenic capacity is antagonistically regulated in classical brown and white subcutaneous fat depots by high fat diet and endurance training in rats: impact on whole-body energy expenditure. *J Biol Chem.* (2014) 289:34129–40. doi: 10.1074/jbc.M114.591008
59. Knudsen JG, Murholm M, Carey AL, Bienso RS, Basse AL, Allen TL, et al. Role of IL-6 in exercise training- and cold-induced UCP1 expression in subcutaneous white adipose tissue. *PLoS ONE.* (2014) 9:e84910. doi: 10.1371/journal.pone.0084910
60. Xu X, Ying Z, Cai M, Xu Z, Li Y, Jiang SY, et al. Exercise ameliorates high-fat diet-induced metabolic and vascular dysfunction, and increases adipocyte progenitor cell population in brown adipose tissue. *Am J Physiol Regul Integr Comp Physiol.* (2011) 300:R1115–25. doi: 10.1152/ajpregu.00806.2010
61. Chi J, Wu Z, Choi CHJ, Nguyen L, Tegegne S, Ackerman SE, et al. Three-dimensional adipose tissue imaging reveals regional variation in beige fat biogenesis and PRDM16-dependent sympathetic neurite density. *Cell Metab.* (2018) 27:226–36.e3. doi: 10.1016/j.cmet.2017.12.011
62. Seale P, Conroe HM, Estall J, Kajimura S, Frontini A, Ishibashi J, et al. Prdm16 determines the thermogenic program of subcutaneous white adipose tissue in mice. *J Clin Invest.* (2011) 121:96–105. doi: 10.1172/JCI44271
63. Ghorbani M, Claus TH, Himms-Hagen J. Hypertrophy of brown adipocytes in brown and white adipose tissues and reversal of diet-induced obesity in rats treated with a beta3-adrenoceptor agonist. *Biochem Pharmacol.* (1997) 54:121–31. doi: 10.1016/S0006-2952(97)00162-7
64. Ghorbani M, Himms-Hagen J. Appearance of brown adipocytes in white adipose tissue during CL 316,243-induced reversal of obesity and diabetes in Zucker fa/fa rats. *Int J Obes Relat Metab Disord.* (1997) 21:465–75. doi: 10.1038/sj.ijo.0800432
65. Cousin B, Cinti S, Morroni M, Raimbault S, Ricquier D, Penicaud L, et al. Occurrence of brown adipocytes in rat white adipose tissue: molecular and morphological characterization. *J Cell Sci.* (1992) 103(Pt 4):931–42.
66. Lehnig AC, Stanford KI. Exercise-induced adaptations to white and brown adipose tissue. *J Exp Biol.* (2018) 221(Pt Suppl. 1):jeb161570. doi: 10.1242/jeb.161570
67. Saugen E, Vollestad NK. Nonlinear relationship between heat production and force during voluntary contractions in humans. *J Appl Physiol.* (1995) 79:2043–9. doi: 10.1152/jappl.1995.79.6.2043
68. Ranallo RF, Rhodes EC. Lipid metabolism during exercise. *Sports Med.* (1998) 26:29–42. doi: 10.2165/00007256-199826010-00003
69. Feldman BJ, Streeper RS, Farese RV Jr, Yamamoto KR. Myostatin modulates adipogenesis to generate adipocytes with favorable metabolic effects. *Proc Natl Acad Sci USA.* (2006) 103:15675–80. doi: 10.1073/pnas.0607501103
70. Rao RR, Long JZ, White JP, Svensson KJ, Lou J, Lokurkar I, et al. Meteorin-like is a hormone that regulates immune-adipose interactions to increase beige fat thermogenesis. *Cell.* (2014) 157:1279–91. doi: 10.1016/j.cell.2014.03.065
71. Carriere A, Jeanson Y, Berger-Muller S, Andre M, Chenouard V, Arnaud E, et al. Browning of white adipose cells by intermediate metabolites: an adaptive mechanism to alleviate redox pressure. *Diabetes.* (2014) 63:3253–65. doi: 10.2337/db13-1885
72. Roberts LD, Bostrom P, O'Sullivan JF, Schinzel RT, Lewis GD, Dejam A, et al. beta-Aminoisobutyric acid induces browning of white fat and hepatic beta-oxidation and is inversely correlated with cardiometabolic risk factors. *Cell Metab.* (2014) 19:96–108. doi: 10.1016/j.cmet.2013.12.003
73. Stanford KI, Goodyear LJ. Exercise regulation of adipose tissue. *Adipocyte.* (2016) 5:153–62. doi: 10.1080/21623945.2016.1191307
74. Fischer AW, Cannon B, Nedergaard J. Optimal housing temperatures for mice to mimic the thermal environment of humans: an experimental study. *Mol Metab.* (2018) 7:161–70. doi: 10.1016/j.molmet.2017.10.009
75. McKie GL, Medak KD, Knuth CM, Shamshoum H, Townsend LK, Peppler WT, et al. Housing temperature affects the acute and chronic metabolic adaptations to exercise in mice. *J Physiol.* (2019) 597:4581–600. doi: 10.1113/JP278221
76. Raun SH, Henriquez-Olguín C, Karavaeva I, Ali M, Møller LLV, Kot W, et al. Housing temperature influences exercise training adaptations in mice. *Nat Commun.* (2020) 11:1560. doi: 10.1038/s41467-020-15311-y
77. Brandao CFC, de Carvalho FG, Souza AO, Junqueira-Franco MVM, Batitucci G, Couto-Lima CA, et al. Physical training, UCP1 expression, mitochondrial density, and coupling in adipose tissue from women with obesity. *Scand J Med Sci Sports.* (2019) 29:1699–706. doi: 10.1111/sms.13514
78. Camera DM, Anderson MJ, Hawley JA, Carey AL. Short-term endurance training does not alter the oxidative capacity of human subcutaneous adipose tissue. *Eur J Appl Physiol.* (2010) 109:307–16. doi: 10.1007/s00421-010-1356-3
79. Norheim F, Langleite TM, Hjorth M, Holen T, Kielland A, Stadheim HK, et al. The effects of acute and chronic exercise on PGC-1α, irisin and browning of subcutaneous adipose tissue in humans. *FEBS J.* (2014) 281:739–49. doi: 10.1111/febs.12619
80. Tsiloulis T, Carey AL, Bayliss J, Canny B, Meex RCR, Watt MJ. No evidence of white adipocyte browning after endurance exercise training in obese men. *Int J Obes (Lond).* (2018) 42:721–7. doi: 10.1038/ijo.2017.295
81. Nakhuda A, Josse AR, Gburcik V, Crossland H, Raymond F, Metairon S, et al. Biomarkers of browning of white adipose tissue and their regulation during exercise- and diet-induced weight loss. *Am J Clin Nutr.* (2016) 104:557–65. doi: 10.3945/ajcn.116.132563
82. Stinkens R, Brouwers B, Jocken JW, Blaak EE, Teunissen-Beekman KF, Hesselink MK, et al. Exercise training-induced effects on the abdominal subcutaneous adipose tissue phenotype in humans with obesity. *J Appl Physiol.* (2018) 125:1585–93. doi: 10.1152/japplphysiol.00496.2018
83. Pino MF, Parsons SA, Smith SR, Sparks LM. Active individuals have high mitochondrial content and oxidative markers in their abdominal subcutaneous adipose tissue. *Obesity.* (2016) 24:2467–70. doi: 10.1002/oby.21669
84. Vosselman MJ, Hoeks J, Brans B, Pallubinsky H, Nascimento EB, van der Lans AA, et al. Low brown adipose tissue activity in endurance-trained compared with lean sedentary men. *Int J Obes.* (2015) 39:1696–702. doi: 10.1038/ijo.2015.130
85. Castellani L, Root-Mccaig J, Frendo-Cumbo S, Beaudoin MS, Wright DC. Exercise training protects against an acute inflammatory insult in mouse epididymal adipose tissue. *J Appl Physiol.* (2014) 116:1272–80. doi: 10.1152/japplphysiol.00074.2014
86. Knuth CM, Peppler WT, Townsend LK, Miotto PM, Gudiksen A, Wright DC. Prior exercise training improves cold tolerance independent of indices associated with non-shivering thermogenesis. *J Physiol.* (2018) 596:4375–91. doi: 10.1113/JP276228
87. Laye MJ, Rector RS, Warner SO, Naples SP, Perretta AL, Uptergrove GM, et al. Changes in visceral adipose tissue mitochondrial content with type 2 diabetes and daily voluntary wheel running in OLETF rats. *J Physiol.* (2009) 587(Pt 14):3729–39. doi: 10.1113/jphysiol.2009.172601
88. Dohlmann TL, Hindso M, Dela F, Helge JW, Larsen S. High-intensity interval training changes mitochondrial respiratory capacity differently in adipose tissue and skeletal muscle. *Physiol Rep.* (2018) 6:e13857. doi: 10.14814/phy2.13857
89. Ronn T, Volkov P, Tornberg A, Elgzyri T, Hansson O, Eriksson KF, et al. Extensive changes in the transcriptional profile of human adipose tissue including genes involved in oxidative phosphorylation after a 6-month exercise intervention. *Acta Physiol.* (2014) 211:188–200. doi: 10.1111/apha.12247
90. Flores-Opazo M, Boland E, Garnham A, Murphy RM, McGee SL, Hargreaves M. Exercise and GLUT4 in human subcutaneous adipose tissue. *Physiol Rep.* (2018) 6:e13918. doi: 10.14814/phy2.13918
91. Ikemoto S, Thompson KS, Itakura H, Lane MD, Ezaki O. Expression of an insulin-responsive glucose transporter (GLUT4) minigene in transgenic mice: effect of exercise and role in glucose homeostasis. *Proc Natl Acad Sci USA.* (1995) 92:865–9. doi: 10.1073/pnas.92.3.865
92. Motiani P, Virtanen KA, Motiani KK, Eskelinen JJ, Middelbeek RJ, Goodyear LJ, et al. Decreased insulin-stimulated brown adipose tissue

glucose uptake after short-term exercise training in healthy middle-aged men. *Diabetes Obes Metab.* (2017) 19:1379–88. doi: 10.1111/dom.12947
93. Wolfe RR. Fat metabolism in exercise. *Adv Exp Med Biol.* (1998) 441:147–56. doi: 10.1007/978-1-4899-1928-1_14
94. May FJ, Baer LA, Lehnig AC, So K, Chen EY, Gao F, et al. Lipidomic adaptations in white and brown adipose tissue in response to exercise demonstrate molecular species-specific remodeling. *Cell Rep.* (2017) 18:1558–72. doi: 10.1016/j.celrep.2017.01.038
95. Bartz R, Zehmer JK, Zhu M, Chen Y, Serrero G, Zhao Y, et al. Dynamic activity of lipid droplets: protein phosphorylation and GTP-mediated protein translocation. *J Proteome Res.* (2007) 6:3256–65. doi: 10.1021/pr070158j
96. Zimmermann R, Strauss JG, Haemmerle G, Schoiswohl G, Birner-Gruenberger R, Riederer M, et al. Fat mobilization in adipose tissue is promoted by adipose triglyceride lipase. *Science.* (2004) 306:1383–6. doi: 10.1126/science.1100747
97. Steinberg D. Interconvertible enzymes in adipose tissue regulated by cyclic AMP-dependent protein kinase. *Adv Cyclic Nucleotide Res.* (1976) 7:157–98.
98. Higa TS, Spinola AV, Fonseca-Alaniz MH, Evangelista FS. Remodeling of white adipose tissue metabolism by physical training prevents insulin resistance. *Life Sci.* (2014) 103:41–8. doi: 10.1016/j.lfs.2014.02.039
99. Hackney AC, Lane AR. Exercise and the regulation of endocrine hormones. *Prog Mol Biol Transl Sci.* (2015) 135:293–311. doi: 10.1016/bs.pmbts.2015.07.001
100. Gollisch KS, Brandauer J, Jessen N, Toyoda T, Nayer A, Hirshman MF, et al. Effects of exercise training on subcutaneous and visceral adipose tissue in normal- and high-fat diet-fed rats. *Am J Physiol Endocrinol Metab.* (2009) 297:E495–504. doi: 10.1152/ajpendo.90424.2008
101. Bradley RL, Jeon JY, Liu FF, Maratos-Flier E. Voluntary exercise improves insulin sensitivity and adipose tissue inflammation in diet-induced obese mice. *Am J Physiol Endocrinol Metab.* (2008) 295:E586–94. doi: 10.1152/ajpendo.00309.2007
102. McPherron AC, Lawler AM, Lee SJ. Regulation of skeletal muscle mass in mice by a new TGF-beta superfamily member. *Nature.* (1997) 387:83–90. doi: 10.1038/387083a0
103. Hittel DS, Axelson M, Sarna N, Shearer J, Huffman KM, Kraus WE. Myostatin decreases with aerobic exercise and associates with insulin resistance. *Med Sci Sports Exerc.* (2010) 42:2023–9. doi: 10.1249/MSS.0b013e3181e0b9a8
104. Shan T, Liang X, Bi P, Kuang S. Myostatin knockout drives browning of white adipose tissue through activating the AMPK-PGC1α-Fndc5 pathway in muscle. *FASEB J.* (2013) 27:1981–9. doi: 10.1096/fj.12-225755
105. Pillon NJ, Gabriel BM, Dollet L, Smith JAB, Sardon Puig L, Botella J, et al. Transcriptomic profiling of skeletal muscle adaptations to exercise and inactivity. *Nat Commun.* (2020) 11:470. doi: 10.1038/s41467-019-13869-w
106. Martinez-Huenchullan SF, Ban LA, Olaya-Agudo LF, Maharjan BR, Williams PF, Tam CS, et al. Constant-Moderate and high-intensity interval training have differential benefits on insulin sensitive tissues in high-fat fed mice. *Front Physiol.* (2019) 10:459. doi: 10.3389/fphys.2019.00459
107. Groussard C, Maillard F, Vazeille E, Barnich N, Sirvent P, Otero YF, et al. Tissue-Specific oxidative stress modulation by exercise: a comparison between MICT and HIIT in an obese rat model. *Oxid Med Cell Longev.* (2019) 2019:1965364. doi: 10.1155/2019/1965364
108. Lunt H, Draper N, Marshall HC, Logan FJ, Hamlin MJ, Shearman JP, et al. High intensity interval training in a real world setting: a randomized controlled feasibility study in overweight inactive adults, measuring change in maximal oxygen uptake. *PLoS ONE.* (2014) 9:e83256. doi: 10.1371/journal.pone.0083256
109. Viana RB, Naves JPA, Coswig VS, de Lira CAB, Steele J, Fisher JP, et al. Is interval training the magic bullet for fat loss? A systematic review and meta-analysis comparing moderate-intensity continuous training with high-intensity interval training (HIIT). *Br J Sports Med.* (2019) 53:655–64. doi: 10.1136/bjsports-2018-099928
110. Bartelt A, Heeren J. Adipose tissue browning and metabolic health. *Nat Rev Endocrinol.* (2014) 10:24–36. doi: 10.1038/nrendo.2013.204
111. Richard D, Rivest S. The role of exercise in thermogenesis and energy balance. *Can J Physiol Pharmacol.* (1989) 67:402–9. doi: 10.1139/y89-064
112. Hirata K. Blood flow to brown adipose tissue and norepinephrine- induced calorigenesis in physically trained rats. *Jpn J Physiol.* (1982) 32:279–91. doi: 10.2170/jjphysiol.32.279
113. Hirata K. Enhanced calorigenesis in brown adipose tissue in physically trained rats. *Jpn J Physiol.* (1982) 32:647–53. doi: 10.2170/jjphysiol.32.647
114. Wickler SJ, Stern JS, Glick Z, Horwitz BA. Thermogenic capacity and brown fat in rats exercise-trained by running. *Metabolism.* (1987) 36:76–81. doi: 10.1016/0026-0495(87)90067-9
115. Moriya K, Leblanc J, Arnold J. Effects of exercise and intermittent cold exposure on shivering and nonshivering thermogenesis in rats. *Jpn J Physiol.* (1987) 37:715–27. doi: 10.2170/jjphysiol.37.715
116. Richard D, Arnold J, Leblanc J. Energy balance in exercise-trained rats acclimated at two environmental temperatures. *J Appl Physiol.* (1986) 60:1054–9. doi: 10.1152/jappl.1986.60.3.1054
117. Yoshioka K, Yoshida T, Wakabayashi Y, Nishioka H, Kondo M. Effects of exercise training on brown adipose tissue thermogenesis in ovariectomized obese rats. *Endocrinol Jpn.* (1989) 36:403–8. doi: 10.1507/endocrj1954.36.403
118. Scarpace PJ, Yenice S, Tumer N. Influence of exercise training and age on uncoupling protein mRNA expression in brown adipose tissue. *Pharmacol Biochem Behav.* (1994) 49:1057–9. doi: 10.1016/0091-3057(94)90264-X
119. De Matteis R, Lucertini F, Guescini M, Polidori E, Zeppa S, Stocchi V, et al. Exercise as a new physiological stimulus for brown adipose tissue activity. *Nutr Metab Cardiovasc Dis.* (2013) 23:582–90. doi: 10.1016/j.numecd.2012.01.013
120. Singhal V, Maffazioli GD, Ackerman KE, Lee H, Elia EF, Woolley R, et al. Effect of chronic athletic activity on brown fat in young women. *PLoS ONE.* (2016) 11:e0156353. doi: 10.1371/journal.pone.0156353
121. Carpentier AC, Blondin DP, Virtanen KA, Richard D, Haman F, Turcotte EE. Brown adipose tissue energy metabolism in humans. *Front Endocrinol.* (2018) 9:447. doi: 10.3389/fendo.2018.00447
122. Nirengi S, Wakabayashi H, Matsushita M, Domichi M, Suzuki S, Sukino S, et al. An optimal condition for the evaluation of human brown adipose tissue by infrared thermography. *PLoS ONE.* (2019) 14:e0220574. doi: 10.1371/journal.pone.0220574
123. Holstila M, Pesola M, Saari T, Koskensalo K, Raiko J, Borra RJ, et al. MR signal-fat-fraction analysis and T2* weighted imaging measure BAT reliably on humans without cold exposure. *Metabolism.* (2017) 70:23–30. doi: 10.1016/j.metabol.2017.02.001
124. de Las Heras N, Klett-Mingo M, Ballesteros S, Martin-Fernandez B, Escribano O, Blanco-Rivero J, et al. Chronic exercise improves mitochondrial function and insulin sensitivity in brown adipose tissue. *Front Physiol.* (2018) 9:1122. doi: 10.3389/fphys.2018.01122
125. Barbosa MA, Guerra-Sa R, De Castro UGM, de Lima WG, Dos Santos RAS, Campagnole-Santos MJ, et al. Physical training improves thermogenesis and insulin pathway, and induces remodeling in white and brown adipose tissues. *J Physiol Biochem.* (2018) 74:441–54. doi: 10.1007/s13105-018-0637-x
126. Motiani P, Teuho J, Saari T, Virtanen KA, Honkala SM, Middelbeek RJ, et al. Exercise training alters lipoprotein particles independent of brown adipose tissue metabolic activity. *Obes Sci Pract.* (2019) 5:258–72. doi: 10.1002/osp4.330
127. Acosta FM, Martinez-Tellez B, Sanchez-Delgado G, Migueles JH, Contreras-Gomez MA, Martinez-Avila WD, et al. Association of objectively measured physical activity with brown adipose tissue volume and activity in young adults. *J Clin Endocrinol Metab.* (2019) 104:223–33. doi: 10.1210/jc.2018-01312
128. Stanford KI, Goodyear LJ. Muscle-Adipose tissue cross talk. *Cold Spring Harb Perspect Med.* (2018) 8:a029801. doi: 10.1101/cshperspect.a029801
129. Shen Y, Zhou H, Jin W, Lee HJ. Acute exercise regulates adipogenic gene expression in white adipose tissue. *Biol Sport.* (2016) 33:381–91. doi: 10.5604/20831862.1224395

130. Krebs EG. Historical perspectives on protein phosphorylation and a classification system for protein kinases. *Philos Trans R Soc Lond B Biol Sci.* (1983) 302:3–11. doi: 10.1098/rstb.1983.0033
131. Ronn T, Volkov P, Davegardh C, Dayeh T, Hall E, Olsson AH, et al. A six months exercise intervention influences the genome-wide DNA methylation pattern in human adipose tissue. *PLoS Genet.* (2013) 9:e1003572. doi: 10.1371/journal.pgen.1003572
132. Fabre O, Ingerslev LR, Garde C, Donkin I, Simar D, Barres R. Exercise training alters the genomic response to acute exercise in human adipose tissue. *Epigenomics.* (2018) 10:1033–50. doi: 10.2217/epi-2018-0039

Conflict of Interest: The authors declare that the research was conducted in the absence of any commercial or financial relationships that could be construed as a potential conflict of interest.

frontiers in Endocrinology

REVIEW
published: 19 May 2020
doi: 10.3389/fendo.2020.00261

Near-Infrared Time-Resolved Spectroscopy for Assessing Brown Adipose Tissue Density in Humans: A Review

Takafumi Hamaoka[1], Shinsuke Nirengi[2,3], Sayuri Fuse[1], Shiho Amagasa[4], Ryotaro Kime[1], Miyuki Kuroiwa[1], Tasuki Endo[1], Naoki Sakane[2], Mami Matsushita[5], Masayuki Saito[6], Takeshi Yoneshiro[7] and Yuko Kurosawa[1]*

[1] Department of Sports Medicine for Health Promotion, Tokyo Medical University, Tokyo, Japan, [2] Division of Preventive Medicine, National Hospital Organization Kyoto Medical Center, Clinical Research Institute, Kyoto, Japan, [3] Dorothy M. Davis Heart and Lung Research Institute, Wexner Medical Center, Columbus, OH, United States, [4] Department of Preventive Medicine and Public Health, Tokyo Medical University, Tokyo, Japan, [5] Department of Nutrition, Tenshi College, Sapporo, Japan, [6] Faculty of Veterinary Medicine, Hokkaido University, Sapporo, Japan, [7] Diabetes Center, University of California San Francisco, San Francisco, CA, United States

OPEN ACCESS

Edited by:
Jennifer L. Miles-Chan, University of Auckland, New Zealand

Reviewed by:
Francisco Miguel Acosta Manzano, Ministry of Economy and Competitiveness, Spain
Valentina Hartwig, Italian National Research Council, Italy

****Correspondence:***
Takafumi Hamaoka
kyp02504@nifty.com

Specialty section:
This article was submitted to Obesity, a section of the journal Frontiers in Endocrinology

Received: *04 February 2020*
Accepted: *08 April 2020*
Published: *19 May 2020*

Citation:
Hamaoka T, Nirengi S, Fuse S, Amagasa S, Kime R, Kuroiwa M, Endo T, Sakane N, Matsushita M, Saito M, Yoneshiro T and Kurosawa Y (2020) Near-Infrared Time-Resolved Spectroscopy for Assessing Brown Adipose Tissue Density in Humans: A Review. Front. Endocrinol. 11:261. doi: 10.3389/fendo.2020.00261

Brown adipose tissue (BAT) mediates adaptive thermogenesis upon food intake and cold exposure, thus potentially contributing to the prevention of lifestyle-related diseases. ^{18}F-fluorodeoxyglucose (FDG)–positron emission tomography (PET) with computed tomography (CT) (^{18}FDG–PET/CT) is a standard method for assessing BAT activity and volume in humans. ^{18}FDG–PET/CT has several limitations, including high device cost and ionizing radiation and acute cold exposure necessary to maximally stimulate BAT activity. In contrast, near-infrared spectroscopy (NIRS) has been used for measuring changes in O_2-dependent light absorption in the tissue in a non-invasive manner, without using radiation. Among NIRS, time-resolved NIRS (NIR_{TRS}) can quantify the concentrations of oxygenated and deoxygenated hemoglobin ([oxy-Hb] and [deoxy-Hb], respectively) by emitting ultrashort (100 ps) light pulses and counts photons, which are scattered and absorbed in the tissue. The basis for assessing BAT density (BAT-d) using NIR_{TRS} is that the vascular density in the supraclavicular region, as estimated using Hb concentration, is higher in BAT than in white adipose tissue. In contrast, relatively low-cost continuous wavelength NIRS (NIR_{CWS}) is employed for measuring relative changes in oxygenation in tissues. In this review, we provide evidence for the validity of NIR_{TRS} and NIR_{CWS} in estimating human BAT characteristics. The indicators (Ind_{NIRS}) examined were $[oxy\text{-}Hb]_{sup}$, $[deoxy\text{-}Hb]_{sup}$, total hemoglobin $[total\text{-}Hb]_{sup}$, Hb O_2 saturation (StO_{2sup}), and reduced scattering coefficient ($\mu_s'_{sup}$) in the supraclavicular region, as determined by NIR_{TRS}, and relative changes in corresponding parameters, as determined by NIR_{CWS}. The evidence comprises the relationships between the Ind_{NIRS} investigated and those determined by ^{18}FDG–PET/CT; the correlation between the Ind_{NIRS} and cold-induced thermogenesis; the relationship of the Ind_{NIRS} to parameters measured by ^{18}FDG–PET/CT, which responded to seasonal temperature fluctuations; the relationship of the Ind_{NIRS} and plasma lipid metabolites; the analogy of the Ind_{NIRS} to chronological and anthropometric data; and changes in the Ind_{NIRS} following thermogenic food supplementation. The $[total\text{-}Hb]_{sup}$ and $[oxy\text{-}Hb]_{sup}$ determined by NIR_{TRS}, but not

parameters determined by NIR_{CWS}, exhibited significant correlations with cold-induced thermogenesis parameters and plasma androgens in men in winter or analogies to ^{18}FDG–PET. We conclude that NIR_{TRS} can provide useful information for assessing BAT-d in a simple, rapid, non-invasive way, although further validation study is still needed.

Keywords: brown adipose tissue, adaptive thermogenesis, thermogenic food ingredients, androgens, lipid metabolites, seasonal temperature changes, non-invasive, ^{18}F-fluorodeoxyglucose–positron emission tomography

INTRODUCTION

Human adipose tissues are of a variety of types, such as white (WAT) and brown adipose tissue (BAT) (1). WAT is capable of depositing extra-energy as triglyceride droplets under conditions where energy intake is greater than its expenditure. In contrast, BAT promotes non-shivering thermogenesis to respond to decreases in core body temperature and, in contrast to WAT, is characterized by an abundance of mitochondria and vasculature. BAT has been extensively investigated in animals, and it has been determined that BAT-specific uncoupling protein (UCP)-1, mainly stimulated upon β_3-adrenergic activation by cold and/or dietary intervention, enables BAT to dissipate free energy to heat by proton discharge through the inner mitochondrial membrane (2, 3). BAT has drawn renewed attention since 2009, with several papers being published that report the existence of BAT deposits in adult humans (4–7), which had previously been thought to be lost during the process of maturation. Human BAT is reported to be related to lower adiposity [body mass index (BMI), the percentage of whole body fat (%BF), and visceral fat area (VFA)] (6–9) and increased glucose sensitivity (10). In experimental studies, repeated exposure to cold environment enhanced the BAT activity and improved glucose tolerance in obese counterparts (11) and patients with type 2 diabetes mellitus (12) as well as in healthy individuals (9, 13, 14). Thus, increasing BAT activity or volume may aid in combatting obesity and chronic diseases, such as type 2 diabetes mellitus.

It is well-known in humans that BAT can be evaluated by ^{18}F-fluorodeoxyglucose (FDG)–positron emission tomography (PET) with computed tomography (CT) (^{18}FDG–PET/CT) under cold-stimulated environments (3, 4, 6, 15). However, ^{18}FDG–PET/CT has several limitations, including the enormous cost of the device and ionizing radiation exposure, and acute cold exposure—necessary to maximally stimulate BAT activity (16), which make a longitudinal ^{18}FDG–PET/CT study difficult and disrupt interventional research, specifically longitudinal ones in humans. Cold exposure is primarily required in ^{18}FDG–PET/CT studies to activate human BAT, and various protocols have been applied in the past. While standardized guidelines have recently been proposed, differences between protocols remain a significant obstacle to the comparison of observations from different studies (17).

Other non-invasive technologies have been utilized for evaluating BAT characteristics in humans, such as magnetic resonance imaging (MRI) (18, 19), local skin thermal measurements (19), infrared thermography (20), and contrast ultrasound (21). A recent review on the detection of BAT using these non-invasive technologies can be found elsewhere (22). Regarding MRI technologies, proton-density fat fraction (PDFF) values are widely used to distinguish BAT from WAT (23, 24). However, the PDFF range in the supraclavicular region widely varies among individuals, which makes the differentiation of BAT from WAT difficult, although several new technologies, such as the measurement of T2* relaxation and diffusion-weighted imaging are under investigation (22). The local skin thermal measurements have been used for monitoring cold-induced temperature changes in the supraclavicular skin with infrared thermography (25, 26). However, heat measurements could be influenced by the tissue conductive properties and thickness of the subcutaneous adipose tissue (27), and the individual vasomotor response (28); these evaluation obstacles should be solved in the future.

In addition, near-infrared spectroscopy (NIRS) is a relatively newly introduced methodology to monitor BAT properties (29). The basis for the application of NIRS to evaluate BAT properties is that the microvascular bed, as evaluated by total hemoglobin (Hb) concentration $[\text{total-Hb}]_{sup}$ in the supraclavicular region, is more abundant in BAT than in WAT (30). Furthermore, NIR time-resolved spectroscopy (NIR_{TRS}) may be used to assess the density of the microvasculature as well as mitochondrial content in BAT by measuring the reduced scattering coefficient (μ_s'), which reflects the *in vitro* mitochondrial content (31). BAT is a highly innervated tissue and is also highly perfused when exposed to cold (32). As the concentrations of oxygenated and deoxygenated Hb in the supraclavicular region ($[\text{oxy-Hb}]_{sup}$ and $[\text{deoxy-Hb}]_{sup}$, respectively) are likely to change (especially $[\text{total-Hb}]_{sup}$, which reflects blood volume), it could be a valid measure of BAT vasculature.

The purpose of this article is to provide evidence concerning the ability of NIRS to evaluate BAT characteristics in humans. In

Abbreviations: $adjStO_2$, adjusted supraclavicular StO_2; AR, β3-adrenergic receptor; BAT, brown adipose tissue; BAT-d, vascular or mitochondrial density in BAT; BMI, body mass index; CIT, cold-induced thermogenesis; CT, computed tomography; deoxy-Hb, deoxygenated Hb; FDG, ^{18}F-fluorodeoxyglucose; Hb, hemoglobin; NE, norepinephrine; NIRS, near-infrared spectroscopy; NIR_{CWS}, NIR continuous-wave spectroscopy; NIR_{TRS}, NIR time-resolved spectroscopy; oxy-Hb, oxygenated Hb; StO_2, Hb O_2 saturation; PET, positron emission tomography; ROC, receiver operating characteristic; total-Hb, total hemoglobin; TRP, transient receptor potential channels; SUV_{max}, maximal standardized uptake value; SUV_{mean}, mean standardized uptake value; WAT, white adipose tissue; μ_a, absorption coefficient; μ_s', reduced scattering coefficient.

this review, we included studies examining BAT characteristics using NIRS in humans: most studies used NIR_{TRS} (29, 33–39), a technology to quantify both absolute tissue absorption and scattering characteristics, while some utilized NIR continuous wave spectroscopy (NIR_{CWS}), an inexpensive technology that only provides relative values of tissue oxygenation (32, 40). First, we present how NIRS functions to evaluate tissue oxygenation and blood volume. Then, we provide data indicating whether BAT characteristics can be evaluated using NIR_{CWS}. The main body of the paper presents a series of evidence for NIR_{TRS} to assess BAT characteristics. The evidence tested comprises (1) the relationship between parameters determined using NIRS and those measured by ^{18}FDG–PET/CT, (2) correlations between the NIRS parameters and cold-induced thermogenesis (CIT), (3) correspondence of the NIRS parameters to those reported using ^{18}FDG–PET/CT regarding chronological and anthropometric data, (4) the correspondence between NIRS parameters and those reported with ^{18}FDG–PET/CT in response to ambient temperature fluctuations, (5) the relationship between parameters determined using NIRS and plasma lipid metabolites, and (6) changes in NIRS parameters induced by supplementation with evidence-based thermogenic functional ingredients.

HOW NIRS FUNCTIONS AS EVALUATING TISSUE OXYGENATION AND BLOOD VOLUME

NIRS provides non-invasive monitoring of tissue oxygen and Hb dynamics *in vivo* (41–45). NIRS is able to monitor changes in O_2-dependent light absorption in the heme in the red blood cells circulating in biological tissues (46). There are mainly three types of NIRS devices: NIR_{CWS}, NIR_{TRS}, phase modulation NIR spectroscopy (NIR_{PMS}), etc. (46–48). The most popular NIRS devices use NIR_{CWS} that outputs only the qualitative tissue oxygenation. To calculate the changes in [oxy-Hb], [deoxy-Hb], [total-Hb], and Hb O_2 saturation (StO_2) using NIR_{CWS}, a combination of multiple-wavelengths can be adopted in accordance with the Beer–Lambert law. The main reason why quantitative data cannot be provided as continuous NIR light path traveled through tissues is unknown (42–45). However, spatially resolved NIRS (a type of NIR_{CWS}) is able to provide quantitative values considering several assumptions, although it is still unable to provide the tissue absorption and scattering properties.

On the other hand, NIR_{TRS} and NIR_{PMS} are more accurate, as they can quantify both tissue absorption and scattering characteristics. NIR_{TRS} emits ultrafast (100 ps) light pulses from the skin surface and measures the photon distributions across the biological tissue with a 2- to 4-cm distance from the light emission. NIR_{TRS} is able to quantitatively measure the absorption coefficient (μ_a), μ_s', and then calculates light path length, tissue [oxy-Hb], [deoxy-Hb], [total-Hb], and StO_2 (44, 45, 48). The validity of the signal obtained by NIR_{CWS} and NIR_{TRS} has been confirmed in an *in vitro* experiment using highly scattering Intralipid^{TM} (43, 44). Using this system, μ_a in the NIR range was found to be strongly correlated with [total-Hb] (43, 48). Furthermore, the study found a significant relationship between μ_s' at 780 nm and the homogenized tissue mitochondrial concentration (31).

STUDIES USING NIR_{CWS}

Prior to the NIR_{TRS} study on human BAT, one study attempted to correlate oxygen dynamics using NIR_{CWS} and BAT parameters (32). In this cross-sectional study, adult human subjects (25 subjects; 15 women and 10 men; mean age ± SD, 30 ± 7 years) were assigned into high- (BMI, 22.1 ± 3.1) and low-BAT groups (BMI, 24.7 ± 3.9) based on the levels of ^{18}F-FDG uptake in the cervical–supraclavicular region. It employed triple-oxygen PET scans ($H_2^{15}O$, $C^{15}O$, and $^{15}O_2$) and daily energy expenditure measurements under resting and mild cold (15.5°C) room conditions for 60 min using indirect calorimetry (32). They used a NIR_{CWS} parameter, adjusted supraclavicular StO_2 ($adjStO_2$), a balance between oxygen supply and uptake. In the high-BAT group, there was a significant negative correlation between oxygen consumption determined by PET scans and $adjStO_2$ ($p = 0.02$, $r^2 = 0.46$) in the supraclavicular region at rest and after the exposure to cold, indicating increased oxygen uptake in highly active BAT (32). However, it detected a limited effect on the difference in $adjStO_2$ between the two groups (32). It should be noted that the study presented several limitations to consider when interpreting its results: (1) a non-individualized cooling protocol was used; (2) only one NIR_{CWS} parameter, $adjStO_2$, was used in the analysis; and (3) no kinetics data determined by the NIR_{CWS} were provided.

Recently, in young healthy women, a study using the standardized cold exposure aimed to investigate the association between NIR_{CWS} parameters in the supraclavicular and forearm regions and BAT capacity assessed by ^{18}FDG–PET/CT (40). Briefly, the subjects arrived at the laboratory (a room temperature of 19.5–20°C) and wore a temperature-controlled water circulation cooling vest for 60 min, and the individual temperature to be exposed was determined, namely at ∼4°C above the threshold of shivering, 48–72 h prior to the ^{18}FDG–PET/CT measurements. No association was found between any NIR_{CWS} indicators and maximal standardized uptake value (SUV_{max}) and mean standardized uptake value (SUV_{mean}) of the radioactivity both under thermoneutral and cold conditions. Thus, NIR_{CWS} would not be an appropriate technology to evaluate BAT capacity in this demographic. The lack of significant association between NIR_{CWS} parameters is mainly due to differences in the instrumentation to that used in NIR_{TRS}, which provides absolute values for tissue hemodynamics. Furthermore, NIR_{CWS} permits an ∼15 mm depth of light penetration at a 30 mm input-output setups (44). However, the mean photon penetration would be deeper (∼20 mm at the 30-mm input–output setups) and wider when NIR_{TRS} is used (49), which influences the differences in sensitivity between NIR_{CWS} and NIR_{TRS} with respect to BAT detection. **Table 1** shows the relationship between $[oxy\text{-}Hb]_{sup}$, $[deoxy\text{-}Hb]_{sup}$,

TABLE 1 | Parameters obtained by continuous-wave near-infrared spectroscopy (NIR_{CWS}) for evaluating brown adipose tissue characteristics in the supraclavicular and control muscle regions.

					Correlation (r^2)								
					Supraclavicular region					Deltoid (forearm) region			
Ref. no.	Instrument	*n*	Study design	Parameters	μ_s'	Oxy-Hb	Deoxy-Hb	Total-Hb	StO_2	adjStO_2	μ_s'	Oxy-Hb	Deoxy-Hb	Total-Hb	StO_2
Muzik et al. (32)	NIR_{CWS}	25	Cross-sectional	VO_{2BAT}[#]	ND	ND	ND	ND	NM	**0.46***	ND	ND	ND	ND	NM
Acosta et al. (40)	NIR_{CWS}	18	Cross-sectional	SUV_{mean}	ND	−0.24	−0.06	−0.24	−0.20	NM	ND	0.01	0.08	0.04	−0.01
				SUV_{peak}	ND	−0.06	−0.22	−0.07	−0.04	NM	ND	0.11	**0.19***	0.15	0.05
				BAT volume	ND	0.00	−0.06	−0.02	−0.02	NM	ND	−0.01	0.12	0.03	−0.06

The correlation coefficients of parameters determined by NIR_{CWS} and the uptake of ^{18}F-fluorodeoxy glucose (FDG) are presented under cold-exposed condition.

μ_s', reduced scattering coefficient determined by NIR_{TRS}; oxy-Hb, oxygenated hemoglobin (Hb); deoxy-Hb, deoxygenated Hb; total-Hb, total Hb; StO_2, tissue hemoglobin oxygen saturation; adjStO_2, adjusted StO_2 in the supraclavicular region relative to the deltoid muscle; VO_{2BAT}, oxygen consumption in BAT; SUV_{mean}, the mean standardized uptake value of the radioactivity (SUV) assessed by ^{18}FDG–PET/CT; SUV_{max}, the maximal SUV assessed by ^{18}FDG–PET/CT; BAT volume, evaluated by summating all voxel volume with SUV >2.0 assessed by ^{18}FDG–PET/CT; Ref. no., reference numbers are obtained from the list of references in this paper; NM, not mentioned; ND, could not be determined.

[#]*Data obtained under thermoneutral conditions.*

*$P < 0.05$.

[total-Hb]$_{sup}$, StO_{2sup}, and adjStO_{2sup} determined by NIR_{CWS} and ^{18}FDG–PET/CT parameters (SUV_{max} and SUV_{mean}), which have been documented in previous studies (32, 40). The only NIR_{CWS} parameter found to be significantly correlated with a ^{18}FDG–PET/CT parameter, cold-induced oxygen uptake by BAT, is adjStO_2, and only in the high-BAT group.

Taken together, the studies using NIR_{CWS} (32, 40) present potential limitations beyond the fact that it cannot evaluate the absorption and scattering properties of the tissue, including that it is more sensitive to changes in the skin blood flow than NIR_{TRS} (32, 40). Therefore, NIR_{CWS} does not seem to be a valid measure for BAT function although emphasis should be placed in the need for further research examining this type of NIRS.

STUDIES USING NIR_{TRS}

Correlation Between Parameters Determined by NIR_{TRS} and ^{18}FDG–PET/CT Parameters

It is speculated that, as BAT exhibits higher microvascular density and mitochondrial contents compared to WAT, NIR_{TRS} can be used for assessing the density of microvascular or mitochondrial content in BAT (BAT-d) by measuring [total-Hb]$_{sup}$ and μ_s' in the supraclavicular region ($\mu_s'_{sup}$), which reflects the *in vitro* mitochondrial content (31). It may be expected that BAT would exhibit higher values for [total-Hb]$_{sup}$ and $\mu_s'_{sup}$ than those exhibited by WAT. As NIR_{TRS} measures the average tissue hemoglobin concentration in a volume of 4 cm^3 with a 3-cm optode separation (50), the ^{18}FDG–PET/CT-determined SUV_{mean} is the most appropriate indicators for comparison to those determined using NIR_{TRS}. Although the use of other radiotracer techniques, such as triple-oxygen scans ($H_2^{15}O$, $C^{15}O$, and $^{15}O_2$) would be more appropriate to reflect BAT activity, ^{18}FDG–PET/CT has been mostly used for determination of BAT activity owing to routine availability in a clinical science setup. First, 18 healthy male subjects (20.3 ± 1.8 years and BMI of 23.9 ± 3.1 kg/m^2) were recruited to examine changes in NIR_{TRS} parameters under acute cold environment. The [oxy-Hb]$_{sup}$, [deoxy-Hb]$_{sup}$, [total-Hb]$_{sup}$, StO_{2sup}, and $\mu_s'_{sup}$ were compared between a room temperature under thermoneutral conditions and cold conditions (19°C) for 2 h. As there was no change in the [total-Hb]$_{sup}$ and $\mu_s'_{sup}$ at 19°C compared to baseline conditions measured at 27°C, NIR_{TRS} can be used without the necessity of cold exposure (29). Second, to test this hypothesis, [total-Hb]$_{sup}$ and $\mu_s'_{sup}$ were compared to the SUV_{mean} assessed by ^{18}FDG–PET/CT (29) in a cross-sectional design. Twenty-nine healthy male subjects (23.3 ± 2.2 years and BMI of 21.6 ± 1.8 kg/m^2) were recruited to evaluate the relationship between SUV_{mean} and NIR_{TRS} parameters. The results demonstrated that [total-Hb]$_{sup}$ and $\mu_s'_{sup}$ under warm environment is significantly correlated with the SUV_{mean} under cold environment but only in the supraclavicular fossa, a region of BAT located (29). Other parameters, except adjStO_2 specifically in the supraclavicular region, also showed significant correlation with SUV_{max} and SUV_{mean} under cold environment (**Table 2**). Collectively, the

TABLE 2 | Parameters for evaluating brown adipose tissue characteristics using near-infrared time-resolved spectroscopy (NIR_{TRS}) in the supraclavicular and control muscle regions.

					Correlation (r^2)									
					Supraclavicular region					Deltoid (forearm) region				
Ref. no.	Instrument	*n*	Study design	Parameters	μ_s'	Oxy-Hb	Deoxy-Hb	Total-Hb	StO_2	$AdjStO_2$	μ_s'	Oxy-Hb	Deoxy-Hb	Total-Hb	StO_2
Nirengi et al. (29)	NIR_{TRS}	18	Cross-sectional	SUV_{mean}	**0.41***	**0.52***	**0.48***	**0.53***	**0.14***	0.07	0.08	0.25	0.21	0.20	0.08
				SUV_{max}	**0.44***	**0.52***	**0.49***	**0.53***	**0.18***	0.08	0.04	0.27	0.23	0.12	0.05

The correlation coefficients of tissue-oxygenated hemoglobin (oxy-Hb), deoxygenated Hb (deoxy-Hb), total Hb (total-Hb), tissue Hb oxygen saturation (StO_2,), and optical scattering parameters as determined by NIR_{TRS} under thermoneutral conditions and the uptake of ^{18}F-fluorodeoxy glucose (FDG) or cold-induced thermogenesis are presented.

μ_s', reduced scattering coefficient determined by NIR_{TRS}; adjusted StO_2 in the supraclavicular region relative to the deltoid muscle; SUV_{mean}, the mean standardized uptake value of the radioactivity (SUV) assessed by ^{18}FDG–PET/CT; SUV_{max}, the maximal SUV assessed by ^{18}FDG–PET/CT; BAT volume, evaluated by summating all voxel volume with SUV >2.0 assessed by ^{18}FDG–PET/CT; Ref. no., reference number is obtained from the list of references in this paper.

*$^*P < 0.05$.

$[total\text{-}Hb]_{sup}$, $[oxy\text{-}Hb]_{sup}$, and $[deoxy\text{-}Hb]_{sup}$ show significant correlations to BAT activity determined by ^{18}FDG–PET/CT. StO_{2sup}, however, proved to be inferior, and $adjStO_2$ was completely insensitive to changes in BAT activity (**Table 2**).

A 2-h cold exposure doubles the BAT blood flow (32), which appeared to be inconsistent with our observations. In an attempt to interpret this apparent discrepancy, we speculated that NIR_{TRS} parameters are susceptible to the change in the volume but less sensitive to the change in the flow. The blood flow can be calculated by multiplying the blood flow velocity by the cross-sectional area of the vessel (the volume). There is presently a lack of NIR_{TRS}-derived data concerning blood flow in BAT. Alternatively, while muscle blood flow increases by some 10-fold during peak exercise (51, 52), [total-Hb], an indicator of blood volume, monitored by NIR_{TRS} elevates only 1.1-fold (43). Thus, the change in blood volume measurable by NIR_{TRS} is marginal compared to increases in blood flow velocity during metabolic activation. Collectively, both $\mu_s'_{sup}$ and $[total\text{-}Hb]_{sup}$ were evaluated using the NIR_{TRS} technique can be applied to assess BAT-d in humans and are equivalent to the active BAT intensity or the BAT volume, as measured by ^{18}FDG–PET/CT under cold environment (29). Usually, to assign participants into high-BAT (BAT [+]) and low-BAT (BAT [−]) groups, a cutoff value of 2.0 for SUV_{mean} is applied. The accuracy of $[total\text{-}Hb]_{sup}$ or $\mu_s'_{sup}$ in representing BAT activity was analyzed. Accordingly, the area under the receiver operating characteristic (ROC) curve was determined by SUV_{mean} of 2.0 nearest to (0, 1) for $\mu_s'_{sup}$ and $[total\text{-}Hb]_{sup}$ (29). When 74.0 μM or 6.8 cm^{-1} was selected as the cutoff value, meaning that $[total\text{-}Hb]_{sup}$ or $\mu_s'_{sup}$ larger than 74.0 μM or 6.8 cm^{-1}, respectively, are regarded as BAT [+], ROC analysis yields results that are very good when compared to SUV_{mean} (29).

Correlation Between Parameters Determined by NIR_{TRS} and CIT

It is well-documented in rodents that the upregulation of the UCP-1 in brown adipocytes upon cold increases whole body oxygen consumption, termed as CIT. Although several authors have shown that CIT does not always reflect BAT activity (53), that the contribution of BAT thermogenesis to CIT is marginal (∼10 kcal/day when maximally activated) (54), and no correlation is found between BAT and CIT (55), the magnitude of CIT is related to the amount of BAT activity and/or volume (9, 56–59). Thus, having already observed a significant correlation between NIR_{TRS} parameters and SUV_{mean} assessed by ^{18}FDG–PET/CT (29) in humans, the validity of NIR_{TRS} parameters were further examined by comparing $[total\text{-}Hb]_{sup}$ and $\mu_s'_{sup}$ to CIT in healthy individuals [age of 20.0 (median), 19.0 (the first quartile), and 21.0 (the third quartile) year; BMI of 24.2 (21.6, 25.7) kg/m^2] with $[total\text{-}Hb]_{sup}$ of 50–125 μM in a cross-sectional study (37). The participants sat for 20 min at 27°C with a light clothing, and NIR_{TRS} measurements were conducted for 5 min after fasting for 6–12 h. Then, the participants were tested at room temperature of

TABLE 3 | Relationship between parameters determined by near-infrared time-resolved spectroscopy (NIR_{TRS}) under thermoneutral or cold condition and pulmonary oxygen uptake during cold exposure.

					Correlation (r^2)									
					Supraclavicular region					Deltoid (forearm) region				
Ref. no.	Instrument	*n*	Study design	Parameters	μ_s'	Oxy-Hb	Deoxy-Hb	Total-Hb	StO_2	μ_s'	Oxy-Hb	Deoxy-Hb	Total-Hb	StO_2
Nirengi et al. (37)	NIR_{TRS}	18	Cross-sectional	CIT 27°C	0.00	**0.38***	**0.49***	**0.41***	0.14	0.09	0.06	0.04	0.06	0.04
				CIT 19°C	0.08	**0.24***	0.16	**0.23***	0.01	0.15	0.02	0.09	0.04	0.06

Results of NIR_{TRS} parameters [tissue-oxygenated hemoglobin (oxy-Hb), deoxygenated Hb (deoxy-Hb), total Hb (total-Hb), tissue Hb oxygen saturation (StO_2,), and optical scattering parameters] and cold-induced thermogenesis (CIT) for healthy men under thermoneutral (27°C) or cold condition (19°C) are presented.
μ_s', reduced scattering coefficient determined by NIR_{TRS}.
$^*P < 0.05$.

19°C for 2 h with their feet intermittently placed on a cloth-wrapped ice for ∼4 min every 5 min (9). A significant correlation was found between $[total\text{-}Hb]_{sup}$, $[oxy\text{-}Hb]_{sup}$, or $[deoxy\text{-}Hb]_{sup}$ only under thermoneutral conditions and CIT, but not between $adjStO_2$ or ${\mu_s'}_{sup}$ and CIT (37). In contrast, previous studies reported a significant correlation in the supraclavicular region between the $adjStO_2$ and oxygen consumption by BAT under cold environment and between ${\mu_s'}_{sup}$ and SUV_{max} and SUV_{mean} (29, 32). It is noted that a personalized cooling protocol may be a better procedure to induce a CIT response personalized to each individual (60). Collectively, although the $[total\text{-}Hb]_{sup}$, $[oxy\text{-}Hb]_{sup}$, and $[deoxy\text{-}Hb]_{sup}$ are markers for BAT activity as evaluated by CIT, the $adjStO_2$ and ${\mu_s'}_{sup}$ become less sensitive to CIT (**Table 3**).

Relationship Between NIR_{TRS} Parameters in the Supraclavicular Region and Chronological and Anthropometric Data

^{18}FDG–PET/CT studies have revealed that a significant relationship exists between BAT activity and chronological and anthropometrical parameters (4, 5, 29, 56). Cold-stimulated ^{18}FDG–PET/CT studies have shown that BAT activity negatively associated with age, sex, BMI, %BF mass, and VFA, and also that BAT was a significant independent determinant of glucose and HbA1c levels, after adjustment for age, sex, and body adiposity (10, 56).

A cross-sectional study using NIR_{TRS} demonstrated that $[total\text{-}Hb]_{sup}$ under warm environment was negatively associated with age and body adiposity in 413 Japanese individuals [a median age of 43.0 (33.0–58.0, interquartile range) years, BMI of 22.5 (20.7–24.5) kg/m^2, and %BF of 26.8% (20.6–32.3%)] in winter (33) (**Figure 1**). With the exception of participants in their 20s, there were no sex-related differences in $[total\text{-}Hb]_{sup}$ among the groups tested (**Figure 1**). Multivariate analyses revealed that the %BF and VFA were significantly negatively correlated with $[total\text{-}Hb]_{sup}$ (33). The observation of the study was analogous to data acquired using ^{18}FDG–PET/CT, indicating the usefulness of the parameter $[total\text{-}Hb]_{sup}$. In contrast, μ_s' was found to be significantly negatively correlated with some of the anthropometrical parameters. Together, the $[oxy\text{-}Hb]_{sup}$ and $[deoxy\text{-}Hb]_{sup}$ displayed similar accuracy to the $[total\text{-}Hb]_{sup}$ for detecting relationships with chronological and anthropometric data (**Table 4**).

Changes in NIR_{TRS} Parameters in the Supraclavicular Region in Response to Ambient Temperature Fluctuations

BAT increases in winter according to ^{18}FDG–PET/CT studies (4, 56–59). However, one study reported that early winter showed higher BAT activity than late winter or early spring (61). A cross-sectional study (35) reported that $[total\text{-}Hb]_{sup}$ was higher in winter than in summer. It has also been reported that a lower average ambient temperature during the 4–6 weeks before the measurement day increases $[total\text{-}Hb]_{sup}$ (33). This finding is consistent with previous findings reporting that, while BAT activity rose during the winter, a few months are needed for the increase in BAT activity after a decrease in the air temperature (58). A longitudinal study using the same healthy subjects (men/women, 35/23; mean age, 37.4 years; mean BMI, 22.5 kg/m^2; BAT positive rate, 48%) in summer and winter under thermoneutral conditions revealed a significant increase in $[total\text{-}Hb]_{sup}$, but not in the reference region or in the μ_s' from any regions (37). It is unclear why ${\mu_s'}_{sup}$ region did not change between summer and winter. However, it is speculated that if triglyceride droplet in the supraclavicular area decreases in winter owing to the increase in BAT (or beiging), the μ_s' should decrease because WAT (triglyceride droplet) obtains high scattering characteristics (62). Thus, even increasing the mitochondria content (the increase in μ_s') would offset the decrease in WAT (the decrease in μ_s'), indicating that $[total\text{-}Hb]_{sup}$ may be a better indicator of BAT activity than ${\mu_s'}_{sup}$. We demonstrated seasonal changes in other NIR_{TRS} parameters, which supplement previously published findings in **Table 5** (35, 37). The $[oxy\text{-}Hb]_{sup}$ and the $[total\text{-}Hb]_{sup}$ obtain similar tendency for monitoring seasonal fluctuations in BAT-d. In winter, the decrease in the deltoid [deoxy-Hb] demonstrated that muscle metabolism blunted in winter and that this is less reliable than $[oxy\text{-}Hb]_{sup}$ or $[total\text{-}Hb]_{sup}$ (**Table 5**).

Collectively, the $[oxy\text{-}Hb]_{sup}$, $[total\text{-}Hb]_{sup}$, StO_{2sup}, and $adjStO_2$ can detect seasonal fluctuations of BAT-d, which is

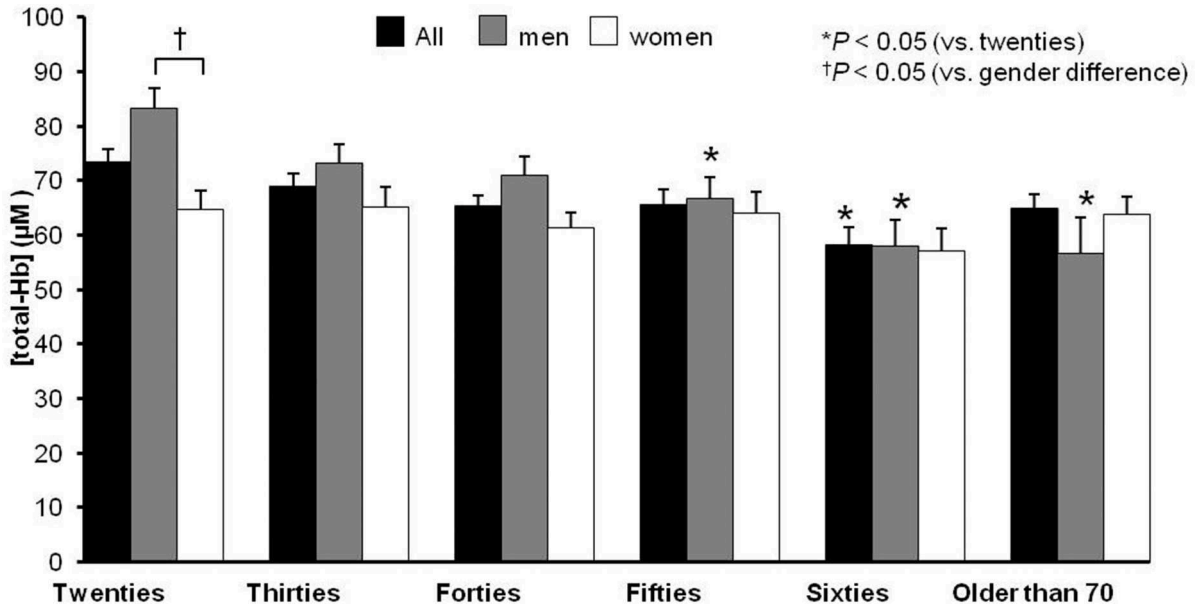

FIGURE 1 | Chronological and sex differences in terms of the concentration of the supraclavicular total hemoglobin [total-Hb], an indicator of brown adipose tissue (BAT). The supraclavicular [total-Hb] potentially containing BAT. The BAT-positive rate ($SUV_{max} > 2.0$) is indicated in the bottom of the figure based on previous studies (29, 33). The values are presented as means ± standard error (SE), adjusting for body mass index, body fat ratio, and visceral fat area. ©SPIE. Reproduced by permission of the publisher. Adopted from reference (33).

TABLE 4 | Relationship between parameters in the supraclavicular region obtained by near-infrared time-resolved spectroscopy (NIR_{TRS}) and anthropometric and body composition parameters.

					Correlation (r^2)					
					Supraclavicular region					
Ref. no.	Instrument	*n*	Study design	Parameters	μ_s'	Oxy-Hb	Deoxy-Hb	Total-Hb	StO_2	$AdjStO_2$
Fuse et al. (33)	NIR_{TRS}	413	Cross-sectional	Age	0.00	**0.07***	**0.04***	**0.06***	**0.02***	NM
				BMI	**0.02***	**0.11***	**0.12***	**0.12***	0.00	NM
				%body fat	0.00	**0.16***	**0.10***	**0.15***	**0.02***	NM
				Visceral fat area	**0.01***	**0.13***	**0.12***	**0.14***	0.00	NM

The correlation coefficients of brown adipose tissue (BAT)-related parameters [tissue oxygenated hemoglobin (oxy-Hb), deoxygenated Hb (deoxy-Hb), total Hb (total-Hb), tissue Hb oxygen saturation (StO_2,), and optical scattering parameters] as determined by NIR_{TRS} and body composition and anthropometric parameters are presented.
μ_s', reduced scattering coefficient determined by NIR_{TRS}; $adjStO_2$, adjusted StO_2 in the supraclavicular region relative to the deltoid muscle; BMI, body mass index; Ref. no., reference number is obtained from the list of references in this paper; NM, not mentioned.
*$P < 0.05$.

consistent with the findings of previous ^{18}FDG–PET/CT studies (4, 56–59).

Correlation Between NIRS Parameters in the Supraclavicular Region and Lipid Metabolites

Finding blood biomolecules correlated with BAT characteristics would permit us to advance human BAT studies because PET/CT studies may be difficult owing to ionizing radiation and cold exposures. Studies on lipidomic profiles have clarified BAT and WAT characteristics according to muscle contractions or cold environment (11, 12, 14, 16). BAT characteristics are related to unique profiles of lipid metabolites, such as the concentration of lysophosphatidylcholine-acyl (LysoPC-acyl) C16:0 in humans (63), and the concentration of phosphatidylethanolamine (PE) in the BAT and WAT was decreased in high-fat diet-fed mice (14). The relationships have been examined in the winter and summer between $[total\text{-}Hb]_{sup}$, a parameter for evaluating BAT-d, measured using NIR_{TRS} and plasma lipids in humans (38). Healthy volunteers with $[total\text{-}Hb]_{sup}$ values over 74.0 μM (high BAT-d) were studied ($n = 23$) and control volunteers with lower $[total\text{-}Hb]_{sup}$ values <70.0 μM (low BAT-d) ($n = 23$) were tested. Ninety-two plasma samples were examined (23 men and 23 women, aged 21–55; BMI, 21.9 ± 3.0 kg/m^2,

TABLE 5 | Changes in parameters obtained by near-infrared time-resolved spectroscopy (NIR_{TRS}) by seasonal temperature changes.

				Change by supplementation or season (%)									
				Supraclavicular region					Deltoid region				
Ref. no.	Instrument	*n*	Study design	Modulation	μ_s'	Oxy-Hb	Deoxy-Hb	Total-Hb	StO_2	$AdjStO_2$	μ_s'	Oxy-Hb	Deoxy-Hb	Total-Hb	StO_2
Nirengi et al. (35)	NIR_{TRS}	40	Cross-sectional	Season	10.0	**31.0***	9.2	**23.7***	**5.9***	**5.1***	7.2	28.7	23.7	27.2	0.5
Nirengi et al. (37)	NIR_{TRS}	58	Longitudinal	Season	−4.1	**16.5***	5.7	**12.9***	**2.8***	**1.5***	−0.3	−0.5	**−4.5***	−3.0	**1.3***

The percentage changes in the NIR_{TRS} parameters [tissue oxygenated hemoglobin (oxy-Hb), deoxygenated Hb (deoxy-Hb), total Hb (total-Hb), tissue Hb oxygen saturation (StO_2),, and optical scattering parameters] are presented due to seasonal temperature fluctuations.

μ_s', reduced scattering coefficient determined by NIR_{TRS}; $adjStO_2$, adjusted StO_2 in the supraclavicular region relative to the deltoid muscle; NIR_{CWS}, NIR continuous-wave spectroscopy; Ref. no., reference numbers are obtained from the list of references in this paper.

$^*P < 0.05$.

%BF 23.3 ± 8.0%), in summer and winter. Using liquid chromatography-time-of-flight-mass spectrometry, plasma lipid profiles were determined. The $[total\text{-}Hb]_{sup}$ was determined as a parameter of BAT-d using NIR_{TRS} under thermoneutral conditions. Body composition parameters, such as %BF and VFA, were examined. Univariate and multivariate regression analyses were used to determine factors affecting $[total\text{-}Hb]_{sup}$. In men, there were 37 metabolites showing positive correlations and 20 metabolites showing negative correlations ($P < 0.05$) with $[total\text{-}Hb]_{sup}$, respectively. After the Q values were obtained by correcting false discovery rate, only androgens (testosterone, androstanedione, dehydroandrosterone, dehydroepiandrosterone, or epitestosterone) showed a significant ($Q < 0.05$) positive correlation with $[total\text{-}Hb]_{sup}$ in men in winter. Multivariate regression analysis revealed that $[total\text{-}Hb]_{sup}$ showed a significant correlation with androgens in men and VFA in women in winter. Notably, the $[total\text{-}Hb]_{sup}$ showed a significant relationship with androgens in winter in men but did not with any body-composition characteristics, such as whole body and visceral adiposity, which are generally associated with $[total\text{-}Hb]_{sup}$. Although androgens deteriorated the BAT capacity *in vitro* (64), testosterone induced a preferable effect on BAT activity, body adiposity, and energy expenditure in animal models (65–67). Thus, BAT characteristics might be predicted by measuring plasma androgens as a biomarker in men in the winter. However, further detailed research is needed to discover biomarkers that predict BAT in women.

Changes in NIRS Parameters in the Supraclavicular Region by Thermogenic Functional Ingredients

Recent studies have demonstrated that BAT can improve health status and has a protective effect on lifestyle-related diseases (4–11, 13, 14). Consequently, research has been focused on finding methods for effectively enhancing BAT activity and/or mass (9, 11–14). Developed strategies include cold acclimation (9, 11–14) and acute treatment of β_3-adrenergic receptor (AR) agonists in humans (68). However, cold exposure intervention would not be easy to apply to daily life (9), and β3-AR agonists may elicit unpreferable influence, including a risk for hypertension and increased susceptibility to arterial sclerosis (68). Recent investigations have revealed the mechanisms underlying the effects of thermogenic food ingredients. Pathways involved include the transient receptor potential channels (TRP)-BAT axis, a site of adaptive thermogenesis evoked by β-adrenoceptor activation (69). The TRP-BAT axis comprises the activation of cold-sensitive TRP channels located in peripheral tissues, such as the skin and intestines. The activation of TRP channels results in the signal delivery through the afferent nerve to the hypothalamus, which then evokes sympathetic nerve activation within BAT. This causes norepinephrine (NE) release, initiating β-adrenergic tracts to brown adipocytes and eliciting UCP1 upregulation and adaptive thermogenesis (69). In contrast to cold exposure intervention, functional food ingredients may be easily incorporated into daily life. This has been confirmed in animals and humans and includes capsinoids as TRP vanilloid

1 agonists, catechins as TRPA1/V1 agonists, and so on (70). Furthermore, they have the benefit of having no apparent side effects (9, 34, 36, 69, 70).

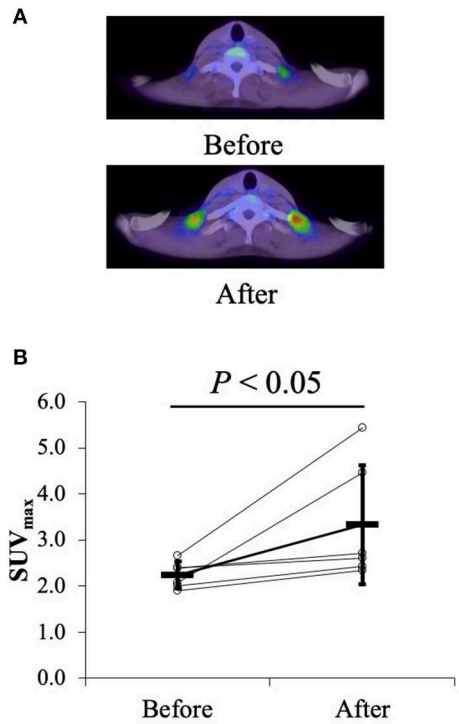

FIGURE 2 | (A) Typical images of the uptake of ^{18}F-fluorodeoxy glucose (FDG) (mean standardized uptake value) before and after the 6-weeks capsiate supplementation in the supraclavicular region. **(B)** Maximal standardized uptake value (SUV_{max}) pre- and post-supplementation. ©SPIE. Reproduced by permission of the publisher. Adopted from reference (34).

Among thermogenic food ingredients, substances, such as capsiate are known to increase BAT activity (9, 70). Previously, the effect of capsiate on $[total\text{-}Hb]_{sup}$, determined by the NIR_{TRS}, was examined (34). Twenty healthy individuals [capsiate group (n = 10) vs. placebo group (n = 10), 20.7 ± 1.2 years vs. 20.9 ± 0.9 years; BMI, 21.4 ± 1.8 vs. 21.9 ± 1.0 kg/m^2; %BF, 21.3 ± 7.6% vs. 22.9 ± 8.7%] were supplemented either with capsiate (9 mg/day) daily for 8 weeks or a placebo in a paralleled, double-blind manner, and $[total\text{-}Hb]_{sup}$ was measured during the treatment period, and for an 8-weeks follow-up period under thermoneutral conditions (34). The study also measured BAT activity with ^{18}FDG–PET/CT under cold-exposure conditions as previously reported (29). This was only done twice (not every 2 weeks), pre- and post-supplementation, to reduce participant exposure to ionizing radiation. The study demonstrated a parallel change in BAT-d (+46.4%, $P < 0.05$) pre- and post-supplementation, evaluated as $[total\text{-}Hb]_{sup}$, or as BAT activity (+48.8%, $P < 0.05$) evaluated as the SUV_{max}, a parameter of the BAT capacity, by ^{18}FDG–PET/CT, after the supplementation of thermogenic capsiate (**Figures 2**, **3**). During the 8-weeks follow-up period, the $[total\text{-}Hb]_{sup}$ decreased both in the capsiate and placebo groups; the decrease was greater in the capsiate group (albeit not significantly, P = 0.07) compared to that of the placebo group.

Previous studies examined whether a catechins-rich green tea extract increases energy consumption in humans (71–74). Animal studies have shown that catechin intake increases BAT, the effects of which were abolished when the β-blocker was administrated (75, 76). Thus, we used NIR_{TRS} under thermoneutral conditions to test the effect of sustained catechin-rich ingredient (540 mg/day) intake on $[total\text{-}Hb]_{sup}$ and investigated potential associations between changes in $[total\text{-}Hb]_{sup}$ and body adiposity in 22 healthy women college students [catechin group (n = 10) vs. placebo group (n = 11), 21.1

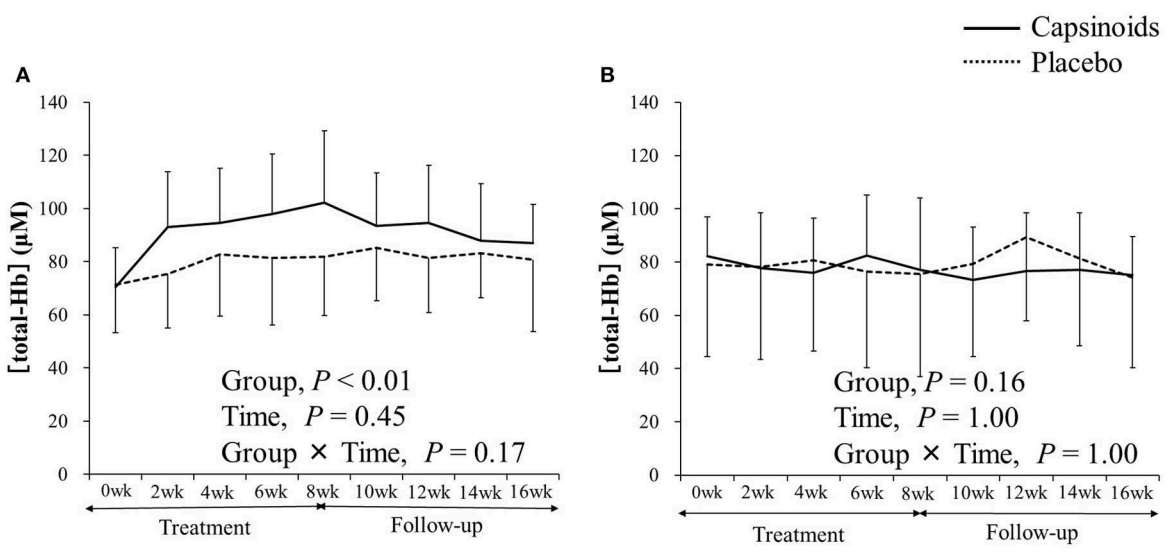

FIGURE 3 | The concentration of total hemoglobin [total-Hb], an indicator of brown adipose tissue (BAT) in **(A)** the supraclavicular fossa potentially containing BAT and **(B)** the deltoid, a control region. Adopted from Nirengi et al. (34). ©SPIE. Reproduced by permission of the publisher.

TABLE 6 | Changes in parameters obtained by near-infrared time-resolved spectroscopy (NIR_{TRS}) for evaluating changes in brown adipose tissue characteristics by the supplementation with thermogenic ingredients.

					Change by supplementation or season (%)									
					Supraclavicular region					Deltoid region				
Ref. no.	Instrument	*n*	Study design	Modulation	μ_s'	Oxy-Hb	Deoxy-Hb	Total-Hb	StO_2	AdjStO$_2$	μ_s'	Oxy-Hb	Deoxy-Hb	Total-Hb	StO_2
Nirengi et al. (34)	NIR_{TRS}	20	Capsinoid	8 weeks on	9.3	**49.5***	**41.0***	**46.4***	1.80	0.80	**9.7***	−6.0	−7.5	−6.7	1.1
				8 weeks washout	11.1	**−16.4***	−2.5	**−12.5***	**−4.8***	**−4.2***	0.6	−2.1	1.3	−1.4	−0.7
Nirengi et al. (36)	NIR_{TRS}	22	Catechins	12 weeks on	1.8	**15.6***	**35.1***	**21.5***	**−4.8***	**−10.3***	−9.3	12.4	−8.5	4.0	7.3

The percentage changes in the NIR_{TRS} parameters [tissue oxygenated hemoglobin (oxy-Hb), deoxygenated Hb (deoxy-Hb), total Hb (total-Hb), tissue Hb oxygen saturation (StO_2,), and optical scattering parameters] are presented due to the supplementation with thermogenic ingredients.

μ_s', reduced scattering coefficient determined by NIR_{TRS}; adjStO_2, adjusted StO_2 in the supraclavicular region relative to the deltoid muscle; NIR_{CWS}, NIR continuous-wave spectroscopy; Ref. no., reference numbers are obtained from the list of references in this paper.

*$^*P < 0.05$.

± 2.0 years vs. 20.5 ± 2.1 years; BMI, 21.1 ± 1.3 vs. 20.9 ± 1.6 kg/m^2; %BF, 24.0 ± 3.5% vs. 25.8 ± 7.6%] (36). That study revealed that the [total-Hb]$_{sup}$ was elevated by 19% in the catechin group only after 12 weeks (36). As for the μ_s', which was not documented in the previous study, it did not change during catechin ingestion. There was a significant negative relationship between the enhancement in [total-Hb]$_{sup}$ and the decrease in extramyocellular lipids, an indicator for possible insulin insensitivity (77), in the vastus lateralis muscle determined by proton-magnetic resonance spectroscopy ($r = -0.66$, $P < 0.05$).

After further analysis, some of which has not been documented in the previous study (34), capsiate supplementation was shown to cause a significant increase in [total-Hb]$_{sup}$, [oxy-Hb]$_{sup}$, and [deoxy-Hb]$_{sup}$ and, upon its withdrawal, a decrease in [total-Hb]$_{sup}$, [oxy-Hb]$_{sup}$, StO_{2sup}, and adjStO_2 (**Table 6**). Similarly, by the catechins intervention, the [oxy-Hb]$_{sup}$, [deoxy-Hb]$_{sup}$, StO_{2sup}, and adjStO_2 obtain the same result as the [total-Hb]$_{sup}$ for assessing increases in BAT-d (36). Collectively, studies into functional ingredient supplementation using NIR_{TRS} suggest that [oxy-Hb]$_{sup}$ and [total-Hb]$_{sup}$ are particularly suitable for the evaluation of BAT-d in intervention studies where the use of ^{18}FDG–PET/CT is not applicable (**Table 6**).

Limitations and Perspectives

The studies using NIRS contain several limitations. Several optical issues should be considered, as the multilayer, inhomogeneous tissue property created by skin, adipose tissue, and muscle may affect *in vivo* tissue scattering and absorption characteristics and modulation of optical path. In a study (39), the optical characteristics in the deltoid, abdominal, and supraclavicular regions were tested using NIR_{TRS}. The results indicate that there are unique region-specific relationships between [total-Hb] and μ_s', suggesting that examining the [total-Hb]–μ_s' relationship is a practical way to distinguish BAT from other tissues. It could be noted that due to the nature of optical measurements, the placement of the optodes for the NIR_{TRS} must be always secure and in the same area, especially during longitudinal studies. Although NIR_{TRS} is able to quantify tissue oxygen dynamics, the values are affected by optical characteristics underlying subcutaneous adipose tissue in the supraclavicular region, which varies depending on the body composition of subjects, thereby influencing NIR_{TRS} measurements. The reason is that the values obtained is diluted by the lower [Hb] in the subcutaneous adipose tissue (78). The [total-Hb]$_{sup}$ values can be recalculated by considering the thickness of the adipose layer (79).

As no change in the [total-Hb]$_{sup}$ and $\mu_s'_{sup}$ was observed during 2-h conditions at 19°C compared to baseline conditions at 27°C (29), NIR_{TRS} cannot detect changes in BAT characteristics responding to an acute cold exposure in nature because NIR_{TRS} is insensitive to changes in the blood flow (33, 35–37). However, a newly developed NIR_{TRS} system contains six wavelengths (760, 800, 830, 908, 936, and 976 nm), of which the latter three wavelengths are adopted to detect optical characteristics of lipids and water (80). This system could provide information on the changes in tissue water and lipid content in response to acute interventions, such as experimental cold exposure, which cannot

be obtained using the conventional three-wavelength NIR_{TRS} system. The new six-wavelength NIR_{TRS} system could contribute further insight on the chronic as well as acute responsiveness of BAT metabolism in humans.

Finally, future studies should obtain further evidence to validate BAT evaluation using NIR_{TRS} because ^{18}FDG–PET/CT measurements include several limitations. BAT mainly consumes intracellular lipids, as well as plasma non-esterified fatty acids and those derived from lipoproteins—whereas ^{18}FDG–PET/CT measures a glucose analog. The lack of standardization when quantifying BAT by ^{18}FDG–PET/CT is also a problem. Thus, additional experiments to reach this conclusion are required, such as (1) examining whether NIR_{TRS} parameters actually represent the *in vivo* mitochondrial density of BAT, or are related to molecules implicated in the vascularization and thermogenesis of BAT [e.g., vascular endothelial-cell growth factor (VEGF), UCP-1, peroxisome proliferator-activated receptor γ coactivator 1-α (PGC1-α)]. This could be carried out by taking human biopsies from the supraclavicular area and examining the relationship between NIR_{TRS} parameters and the molecular signature of this tissue; (2) using other radiotracers beyond ^{18}F-FDG, such as ^{15}O, $H_2^{15}O$, $C^{15}O$, or ^{11}C-acetate, which will allow to measure the real oxygen consumption, tissue perfusion, and metabolic activity of human BAT and which are more likely to represent the thermogenic nature or activity of this tissue than ^{18}F-FDG; (3) carrying out studies where the kinetics of NIR_{TRS} are related to the kinetics of the metabolic activity of BAT (dynamic PET/CT); (4) using different cooling protocols, aiming to standardize the cooling stress to which individuals are submitted (avoiding potential biases in individual BAT activation); and (5) performing reliability studies to examine whether NIR_{TRS} measures can be replicated in the short and long term.

CONCLUSION

Correlation coefficients are presented for parameters determined by NIRS and ^{18}FDG–PET/CT, CIT, or anthropometric and body composition parameters. Significant correlations were found between $[total\text{-}Hb]_{sup}$, $[oxy\text{-}Hb]_{sup}$, $[deoxy\text{-}Hb]_{sup}$, $\mu_s'_{sup}$, $StO2_{sup}$, or $adjStO_2$ and ^{18}FDG–PET/CT indicators; between $[total\text{-}Hb]_{sup}$, $[oxy\text{-}Hb]_{sup}$, or $[deoxy\text{-}Hb]_{sup}$ and CIT; and between $[total\text{-}Hb]_{sup}$, $[oxy\text{-}Hb]_{sup}$, or $[deoxy\text{-}Hb]_{sup}$ and anthropometric and body composition indicators. The percentage changes in NIR_{TRS} parameters as a consequence of either seasonal temperature fluctuations or dietary supplementation with thermogenic ingredients are presented. Seasonal temperature fluctuations influenced $[total\text{-}Hb]_{sup}$, $[oxy\text{-}Hb]_{sup}$, $StO2_{sup}$, and $adjStO_2$. Studies on thermogenic capsinoid or catechin supplementation revealed a significant increase in $[total\text{-}Hb]_{sup}$, $[oxy\text{-}Hb]_{sup}$, and $[deoxy\text{-}Hb]_{sup}$. Upon withdrawal of these supplements, a decrease in $[total\text{-}Hb]_{sup}$, $[oxy\text{-}Hb]_{sup}$, $StO2_{sup}$, and $adjStO_2$ was seen. Recently, androgens were found to show a significant positive correlation with $[total\text{-}Hb]_{sup}$ only in men in winter. Thus, BAT characteristics might be predicted by measuring plasma androgens as a biomarker in men in the winter.

We conclude that NIR_{TRS} would be a useful non-invasive technology for assessing BAT-d, although further validation is still needed. Among the parameters evaluated by NIR_{TRS}, the $[oxy\text{-}Hb]_{sup}$ as well as $[total\text{-}Hb]_{sup}$ would be applicable to assessing BAT characteristics in both cross-sectional and interventional studies.

AUTHOR CONTRIBUTIONS

TH, SN, SF, and YK collected the relevant literature and wrote the manuscript. SA, RK, MK, and TE assisted in illustrations, formatting, and collection of literature. NS, MM, MS, and TY coordinated and edited the relevant discussion on PET/CT measurements and BAT.

FUNDING

We have been granted by Japan Society for the Promotion of Science (15H03100 and 19H04061), which is an independent administrative institution, established by way of a national law for the purpose of contributing to the advancement of science in all fields of the natural and social sciences and the humanities.

ACKNOWLEDGMENTS

This work was supported by JSPS KAKENHI (15H03100 and 19H04061).

REFERENCES

1. Chondronikola M, Sidossis LS. Brown and beige fat: from molecules to physiology. *Biochim Biophys Acta*. (2019) 1864:91–103. doi: 10.1016/j.bbalip.2018.05.014
2. Davis TRA, Johnston DR, Bell FC, Cremer BJ. Regulation of shivering and nonshivering heat production during acclimation of rats. *Am J Physiol Legacy Content*. (1960) 198:471–5. doi: 10.1152/ajplegacy.1960.198.3.471
3. Rothwell NJ, Stock MJ. A role for brown adipose tissue in diet-induced thermogenesis. *Nature*. (1979) 281:31–5. doi: 10.1038/281031a0
4. Saito M, Okamatsu-Ogura Y, Matsushita M, Watanabe K, Yoneshiro T, Nio-Kobayashi J, et al. High incidence of metabolically active brown adipose tissue in healthy adult humans: effects of cold exposure and adiposity. *Diabetes*. (2009) 58:1526–31. doi: 10.2337/db09-0530
5. Cypess AM, Lehman S, Williams G, Tal I, Rodman D, Goldfine AB, et al. Identification and importance of brown adipose tissue in adult humans. *N Engl J Med*. (2009) 360:1509–17. doi: 10.1056/NEJMoa0810780
6. van Marken Lichtenbelt WD, Vanhommerig JW, Smulders NM, Drossaerts JMAFL, Kemerink GJ, Bouvy ND, et al. Cold-activated brown adipose tissue in healthy men. *N Engl J Med*. (2009) 360:1500–8. doi: 10.1056/NEJMoa0808718
7. Virtanen KA, Lidell ME, Orava J, Heglind M, Westergren R, Niemi T, et al. Functional brown adipose tissue in healthy adults. *N Engl J Med*. (2009) 360:1518–25. doi: 10.1056/NEJMoa0808949
8. Pfannenberg C, Werner MK, Ripkens S, Stef I, Deckert A, Schmadl M, et al. Impact of age on the relationships of brown adipose tissue with sex and adiposity in humans. *Diabetes*. (2010) 59:1789–93. doi: 10.2337/db10-0004

9. Yoneshiro T, Aita S, Matsushita M, Kayahara T, Kameya T, Kawai Y, et al. Recruited brown adipose tissue as an antiobesity agent in humans. *J Clin Invest*. (2013) 123:3404–8. doi: 10.1172/JCI67803
10. Matsushita M, Yoneshiro T, Aita S, Kameya T, Sugie H, Saito M. Impact of brown adipose tissue on body fatness and glucose metabolism in healthy humans. *Int J Obes*. (2014) 38:812–7. doi: 10.1038/ijo.2013.206
11. Hanssen MJW, van der Lans AAJJ, Brans B, Hoeks J, Jardon KMC, Schaart G, et al. Short-term cold acclimation recruits brown adipose tissue in obese humans. *Diabetes*. (2016) 65:1179–89. doi: 10.2337/db15-1372
12. Hanssen MJW, Hoeks J, Brans B, van der Lans AAJJ, Schaart G, van den Driessche JJ, et al. Short-term cold acclimation improves insulin sensitivity in patients with type 2 diabetes mellitus. *Nat Med*. (2015) 21:863–5. doi: 10.1038/nm.3891
13. Blondin DP, Labbé SM, Tingelstad HC, Noll C, Kunach M, Phoenix S, et al. Increased brown adipose tissue oxidative capacity in cold-acclimated humans. *J Clin Endocrinol Metab*. (2014) 99:E438–46. doi: 10.1210/jc.2013-3901
14. van der Lans AAJJ, Hoeks J, Brans B, Vijgen GHEJ, Visser MGW, Vosselman MJ, et al. Cold acclimation recruits human brown fat and increases nonshivering thermogenesis. *J Clin Invest*. (2013) 123:3395–403. doi: 10.1172/JCI68993
15. Cypess AM, Lehman S, Williams G, Tal I, Rodman D, Goldfine AB, et al. Identification and importance of brown adipose tissue in adult humans. *N Engl J Med*. (2009) 360:1509–17. doi: 10.3201/eid1910.130203
16. Borga M, Virtanen KA, Romu T, Leinhard OD, Persson A, Nuutila P, et al. Brown adipose tissue in humans: detection and functional analysis using PET (positron emission tomography), MRI (magnetic resonance imaging), and DECT (dual energy computed tomography). *Methods Enzymol*. (2014) 537:141–59. doi: 10.1016/B978-0-12-411619-1.00008-2
17. Chen KY, Cypess AM, Laughlin MR, Haft CR, Hu HH, Bredella MA, et al. Brown adipose reporting criteria in imaging STudies (BARCIST 1.0): recommendations for standardized FDG-PET/CT experiments in humans. *Cell Metab*. (2016) 24:210–22. doi: 10.1016/j.cmet.2016.07.014
18. Koskensalo K, Raiko J, Saari T, Saunavaara V, Eskola O, Nuutila P, et al. Human brown adipose tissue temperature and fat fraction are related to its metabolic activity. *J Clin Endocrinol Metab*. (2017) 102:1200–7. doi: 10.1210/jc.2016-3086
19. Sun L, Verma S, Michael N, Chan SP, Yan J, Sadananthan SA, et al. Brown adipose tissue: multimodality evaluation by PET, MRI, infrared thermography, and whole-body calorimetry (tactical-ii). *Obesity*. (2019) 27:1434–42. doi: 10.1002/oby.22560
20. Thuzar M, Law WP, Dimeski G, Stowasser M, Ho KKY. Mineralocorticoid antagonism enhances brown adipose tissue function in humans: a randomized placebo-controlled cross-over study. *Diabetes Obes Metab*. (2018) 21:509–16. doi: 10.1111/dom.13539
21. Baron DM, Clerte M, Brouckaert P, Raher MJ, Flynn AW, Zhang H, et al. *In vivo* noninvasive characterization of brown adipose tissue blood flow by contrast ultrasound in mice. *Circ Cardiovasc Imaging*. (2012) 5:652–9. doi: 10.1161/CIRCIMAGING.112.975607
22. Ong FJ, Ahmed BA, Oreskovich SM, Blondin DP, Haq T, Konyer NB, et al. Recent advances in the detection of brown adipose tissue in adult humans: a review. *Clin Sci*. (2018) 32:1039–54. doi: 10.1042/CS20170276
23. Franz D, Weidlich D, Freitag F, Holzapfel C, Drabsch T, Baum T, et al. Association of proton density fat fraction in adipose tissue with imaging-based and anthropometric obesity markers in adults. *Int J Obes*. (2018) 42:175–82. doi: 10.1038/ijo.2017.194
24. Gifford A, Towse TF, Walker RC, Avison MJ, Welch EB. Characterizing active and inactive brown adipose tissue in adult humans using PET-CT and MR imaging. *Am J Physiol Endocrinol Metab*. (2016) 311:E95–104. doi: 10.1152/ajpendo.00482.2015
25. Law JM, Morris DE, Astle V, Finn E, Muros JJ, Robinson LJ, et al. Brown adipose tissue response to cold stimulation is reduced in girls with autoimmune hypothyroidism. *J Endocr Soc*. (2019) 3:2411–26. doi: 10.1210/js.2019-00342
26. El Hadi H, Frascati A, Granzotto M, Silvestrin V, Ferlini E, Vettor R, et al. Infrared thermography for indirect assessment of activation of brown adipose tissue in lean and obese male subjects. *Physiol Meas*. (2016) 37:N118–28. doi: 10.1088/0967-3334/37/12/N118
27. Cypess AM, Haft CR, Laughlin MR, Hu HH. Brown fat in humans: consensus points and experimental guidelines. *Cell Metab*. (2014) 20:408–15. doi: 10.1016/j.cmet.2014.07.025
28. Kamiya A, Michikami D, Iwase S, Mano T. Decoding rule from vasoconstrictor skin sympathetic nerve activity to nonglabrous skin blood flow in humans at normothermic rest. *Neurosci Lett*. (2008) 439:13–7. doi: 10.1016/j.neulet.2008.04.018
29. Nirengi S, Yoneshiro T, Sugie H, Saito M, Hamaoka T. Human brown adipose tissue assessed by simple, noninvasive near-infrared time-resolved spectroscopy. *Obesity*. (2015) 23:973–80. doi: 10.1002/oby.21012
30. Cinti S. Transdifferentiation properties of adipocytes in the adipose organ. *Am J Phys Endocrinol Metab*. (2009) 297:E977–86. doi: 10.1152/ajpendo.00183.2009
31. Beauvoit B, Chance B. Time-resolved spectroscopy of mitochondria, cells and tissues under normal and pathological conditions. *Mol Cell Biochem*. (1998) 184:445–55.
32. Muzik O, Mangner TJ, Leonard WR, Kumar A, Janisse J, Granneman JG. 15O PET measurement of blood flow and oxygen consumption in cold-activated human brown fat. *J Nuclear Med*. (2013) 54:523–31. doi: 10.2967/jnumed.112.111336
33. Fuse S, Nirengi S, Amagasa S, Homma T, Kime R, Endo T, et al. Brown adipose tissue density measured by near-infrared time-resolved spectroscopy in Japanese, across a wide age range. *J Biomed Opt*. (2018) 23:1–9. doi: 10.1117/1.JBO.23.6.065002
34. Nirengi S, Homma T, Inoue N, Sato H, Yoneshiro T, Matsushita M, et al. Assessment of human brown adipose tissue density during daily ingestion of thermogenic capsinoids using near-infrared time-resolved spectroscopy. *J Biomed Opt*. (2016) 21:091305. doi: 10.1117/1.JBO.21.9.091305
35. Nirengi S, Sakane N, Amagasa S, Wakui S, Homma T, Kurosawa Y, et al. Seasonal differences in brown adipose tissue density and pulse rate variability in a thermoneutral environment. *J Physiol Anthropol*. (2018) 37:6. doi: 10.1186/s40101-018-0166-x
36. Nirengi S, Amagasa S, Homma T, Yoneshiro T, Matsumiya S, Kurosawa Y, et al. Daily ingestion of catechin-rich beverage increases brown adipose tissue density and decreases extramyocellular lipids in healthy young women. *SpringerPlus*. (2016) 5:1363. doi: 10.1186/s40064-016-3029-0
37. Nirengi S, Fuse S, Amagasa S, Homma T, Kime R, Kuroiwa M, et al. applicability of supraclavicular oxygenated and total hemoglobin evaluated by near-infrared time-resolved spectroscopy as indicators of brown adipose tissue density in humans. *Int J Mol Sci*. (2019) 20:2214. doi: 10.3390/ijms20092214
38. Fuse S, Sugimoto M, Kurosawa Y, Kuroiwa M, Aita Y, Tomita A, et al. Relationships between plasma lipidomic profiles and brown adipose tissue density in humans. *Int J Obes*. (2020). doi: 10.1038/s41366-020-0558-y. [Epub ahead of print].
39. Fuse S, Hamaoka T, Kuroiwa M, Kime R, Endo T, Tanaka R, et al. Identification of human brown/beige adipose tissue using near-infrared time-resolved spectroscopy. In: *Biophotonics in Exercise Science, Sports Medicine, Health Monitoring Technologies, and Wearables* (2020). doi: 10.1117/12.2545273
40. Acosta FM, Berchem J, Martinez-Tellez B, Sanchez-Delgado G, Alcantara JMA, Ortiz-Alvarez L, et al. Near-infrared spatially resolved spectroscopy as an indirect technique to assess brown adipose tissue in young women. *Mol Imaging Biol*. (2019) 21:328–338. doi: 10.1007/s11307-018-1244-5
41. Jöbsis FF. Noninvasive, infrared monitoring of cerebral and myocardial oxygen sufficiency and circulatory parameters. *Science*. (1977) 198:1264–7. doi: 10.1126/science.929199
42. Delpy DT, Cope M. Quantification in tissue near–infrared spectroscopy. *Philos Trans R Soc Lond B Biol Sci*. (1997) 352:649–59. doi: 10.1098/rstb.1997.0046
43. Ferrari M, Mottola L, Quaresima V. Principles, techniques, and limitations of near infrared spectroscopy. Can *J Appl Physiol*. (2004) 29:463–87. doi: 10.1139/h04-031
44. Chance B, Dait MT, Zhang C, Hamaoka T, Hagerman F. Recovery from exercise-induced desaturation in the quadriceps muscles of elite competitive rowers. *Am J Phys Cell Physiol*. (1992) 262:C766–75. doi: 10.1152/ajpcell.1992.262.3.C766
45. Chance B, Nioka S, Kent J, McCully K, Fountain M, Greenfeld R, et al. Time-resolved spectroscopy of hemoglobin and myoglobin in resting and ischemic muscle. *Anal. Biochem*. (1988) 174:698–707. doi: 10.1016/0003-2697(88)90076-0
46. Hamaoka T, McCully KK. Review of early development of near-infrared spectroscopy and recent advancement of studies on muscle

oxygenation and oxidative metabolism. *J Physiol Sci*. (2019) 69:799–811. doi: 10.1007/s12576-019-00697-2
47. Hamaoka T, Katsumura T, Murase N, Nishio S, Osada T, Sako T, et al. Quantification of ischemic muscle deoxygenation by near infrared time-resolved spectroscopy. *J Biomed Opt*. (2000) 5:102–5. doi: 10.1117/1.429975
48. Hamaoka T, McCully KK, Quaresima V, Yamamoto K, Chance B. Near-infrared spectroscopy/imaging for monitoring muscle oxygenation and oxidative metabolism in healthy and diseased humans. *J Biomed Opt*. (2007) 12:062105. doi: 10.1117/1.2805437
49. Gunadi S, Leung TS, Elwell CE, Tachtsidis I. Spatial sensitivity and penetration depth of three cerebral oxygenation monitors. *Biomed Opt Express*. (2014) 5:2896–912. doi: 10.1364/BOE.5.002896
50. Chance B, Leigh JS, Miyake H, Smith DS, Nioka S, Greenfeld R, et al. Comparison of time-resolved and -unresolved measurements of deoxyhemoglobin in brain. *Proc Natl Acad Sci USA*. (1988) 85:4971–5. doi: 10.1073/pnas.85.14.4971
51. Stebbings GK, Morse CI, McMahon GE, Onambele GL. Resting arterial diameter and blood flow changes with resistance training and detraining in healthy young individuals. *J Athl Train*. (2013) 48:209–19. doi: 10.4085/1062-6050-48.1.17
52. Ferreira LF, Hueber DM, Barstow TJ. Effects of assuming constant optical scattering on measurements of muscle oxygenation by near-infrared spectroscopy during exercise. *J Appl Phys*. (2007) 102:358–67. doi: 10.1152/japplphysiol.00920.2005
53. Blondin DP, Labbé SM, Phoenix S, Guérin B, Turcotte ÉE, Richard D, et al. Contributions of white and brown adipose tissues and skeletal muscles to acute cold-induced metabolic responses in healthy men. *J Phys*. (2015) 593:701–14. doi: 10.1113/jphysiol.2014.283598
54. u Din M, Raiko J, Saari T, Kudomi N, Tolvanen T, Oikonen V, et al. Human brown adipose tissue [15O]O_2 PET imaging in the presence and absence of cold stimulus. *Eur J Nucl Med Mol Imaging*. (2016) 43:1878–86. doi: 10.1007/s00259-016-3364-y
55. Sanchez-Delgado G, Martinez-Tellez B, Garcia-Rivero Y, Alcantara JMA, Acosta FM, Amaro-Gahete FJ, et al. Brown adipose tissue and skeletal muscle ^{18}F-FDG activity after a personalized cold exposure is not associated with cold-induced thermogenesis and nutrient oxidation rates in young healthy adults. *Front Physiol*. (2018) 9:1577. doi: 10.3389/fphys.2018.01577
56. Yoneshiro T, Aita S, Matsushita M, Kameya T, Nakada K, Kawai Y, et al. Brown adipose tissue, whole-body energy expenditure, and thermogenesis in healthy adult men. *Obesity*. (2011) 19:13–6. doi: 10.1038/oby.2010.105
57. Cohade C, Mourtzikos KA, Wahl RL. "USA-Fat": prevalence is related to ambient outdoor temperature-evaluation with 18F-FDG PET/CT. *J Nuclear Med*. (2003) 44:1267–70.
58. Au-Yong ITH, Thorn N, Ganatra R, Perkins AC, Symonds ME. Brown adipose tissue and seasonal variation in humans. *Diabetes*. (2009) 58:2583–87. doi: 10.2337/db09-0833
59. Yoneshiro T, Matsushita M, Nakae S, Kameya T, Sugie H, Tanaka S, et al. Brown adipose tissue is involved in the seasonal variation of cold-induced thermogenesis in humans. *Am J Physiol Regul Integr Comp Physiol*. (2016) 310:R999–1009. doi: 10.1152/ajpregu.00057.2015
60. Martinez-Tellez B, Sanchez-Delgado G, Garcia-Rivero Y, Alcantara JMA, Martinez-Avila WD, Muñoz-Hernandez M V., et al. A new personalized cooling protocol to activate brown adipose tissue in young adults. *Front Physiol*. (2017) 8:863. doi: 10.3389/fphys.2017.00863
61. Kim S, Krynyckyi BR, Machac J, Kim CK. Temporal relation between temperature change and FDG uptake in brown adipose tissue. *Eur J Nucl Med Mol Imaging*. (2008) 35:984–9. doi: 10.1007/s00259-007-0670-4
62. Yang Y, Soyemi OO, Landry MR, Soller BR. Influence of a fat layer on the near infrared spectra of human muscle: quantitative analysis based on two-layered monte carlo simulations and phantom experiments. *Opt Express*. (2005) 13:1570–9. doi: 10.1364/opex.13.001570
63. Boon MR, Bakker LEH, Prehn C, Adamski J, Vosselman MJ, Jazet IM, et al. LysoPC-acyl C16:0 is associated with brown adipose tissue activity in men. *Metabolomics*. (2017) 13:48. doi: 10.1007/s11306-017-1185-z
64. Varlamov O, White AE, Carroll JM, Bethea CL, Reddy A, Slayden O, et al. Androgen effects on adipose tissue architecture and function in nonhuman primates. *Endocrinology*. (2012) 153:3100–10. doi: 10.1210/en.2011-2111
65. Cannon B, Nedergaard J. Brown adipose tissue: function and physiological significance. *Physiol Rev*. (2004) 84:277–359. doi: 10.1152/physrev.00015.2003
66. Law J, Bloor I, Budge H, Symonds ME. The influence of sex steroids on adipose tissue growth and function. *Horm Mol Biol Clin Investig*. (2014) 19:13–24. doi: 10.1515/hmbci-2014-0015
67. Yanase T, Fan WQ, Kyoya K, Min L, Takayanagi R, Kato S, et al. Androgens and metabolic syndrome: Lessons from androgen receptor knock out (ARKO) mice. *J Steroid Biochem Mol Biol*. (2008) 109:254–7. doi: 10.1016/j.jsbmb.2008.03.017
68. Cypess AM, Weiner LS, Roberts-Toler C, Elía EF, Kessler SH, Kahn PA, et al. Activation of human brown adipose tissue by a β3-adrenergic receptor agonist. *Cell Metab*. (2015) 21:33–8. doi: 10.1016/j.cmet.2014.12.009
69. Cannon B, Nedergaard J. Nonshivering thermogenesis and its adequate measurement in metabolic studies. *J Exp Biol*. (2011) 214:242–53. doi: 10.1242/jeb.050989
70. Saito M, Yoneshiro T. Capsinoids and related food ingredients activating brown fat thermogenesis and reducing body fat in humans. *Curr Opin Lipidol*. (2013) 24:71–7. doi: 10.1097/MOL.0b013e32835a4f40
71. Yoneshiro T, Matsushita M, Hibi M, Tone H, Takeshita M, Yasunaga K, et al. Tea catechin and caffeine activate brown adipose tissue and increase cold-induced thermogenic capacity in humans. *Am J Clin Nutr*. (2017) 105:873–81. doi: 10.3945/ajcn.116.144972
72. Dulloo AG, Seydoux J, Girardier L, Chantre P, Vandermander J. Green tea and thermogenesis: interactions between catechin-polyphenols, caffeine and sympathetic activity. *Int J Obes Relat Metab Disord*. (2000) 24:252–8. doi: 10.1038/sj.ijo.0801101
73. Gosselin C, Haman F. Effects of green tea extracts on non-shivering thermogenesis during mild cold exposure in young men. *Br J Nutr*. (2013) 110:282–8. doi: 10.1017/S0007114512005089
74. Hursel R, Westerterp-Plantenga MS. Catechin- and caffeine-rich teas for control of body weight in humans. *Am J Clin Nutr*. (2013) 98:1682S−93S. doi: 10.3945/ajcn.113.058396
75. Nomura S, Ichinose T, Jinde M, Kawashima Y, Tachiyashiki K, Imaizumi K. Tea catechins enhance the mRNA expression of uncoupling protein 1 in rat brown adipose tissue. *J Nutr Biochem*. (2008) 19:840–7. doi: 10.1016/j.jnutbio.2007.11.005
76. Choo JJ. Green tea reduces body fat accretion caused by high-fat diet in rats through beta-adrenoceptor activation of thermogenesis in brown adipose tissue. *J Nutr Biochem*. (2003) 14:671–6. doi: 10.1016/j.jnutbio.2003.08.005
77. Hausman GJ, Basu U, Du M, Fernyhough-Culver M, Dodson M V. Intermuscular and intramuscular adipose tissues: bad vs. good adipose tissues. *Adipocyte*. (2014) 3:242–55. doi: 10.4161/adip.28546
78. McCully KK, Hamaoka T. Near-infrared spectroscopy: what can it tell us about oxygen saturation in skeletal muscle? *Exerc Sport Sci Rev*. (2000) 28:123–7.
79. Yamamoto K, Niwayama M, Kohata D, Kudo N, Hamaoka T, Kime R, et al. Functional imaging of muscle oxygenation using a 200-channel cw NIRS system. In: *BiOS 2001 The International Symposium on Biomedical Optics*, San Jose, CA (2001). p. 142–52.
80. Suzuki H, Ohmae E, Yoshimoto K, Wada H, Homma S, Suzuki N, et al. Water and lipid contents measured at various parts of the human body with a six-wavelength time-resolved spectroscopy system. *Opt Tomogr Spectrosc Tissue XIII*. (2019) 10874:108740A. doi: 10.1117/12.2507429

Conflict of Interest: The authors declare that the research was conducted in the absence of any commercial or financial relationships that could be construed as a potential conflict of interest.

The reviewer FA declared a past co-authorship with one of the authors TH to the handling editor.

frontiers in Endocrinology

ORIGINAL RESEARCH
published: 12 June 2020
doi: 10.3389/fendo.2020.00387

ESRRG and PERM1 Govern Mitochondrial Conversion in Brite/Beige Adipocyte Formation

Sebastian Müller[1,2,3], Aliki Perdikari[1], Dianne H. Dapito[1], Wenfei Sun[1], Bernd Wollscheid[2], Miroslav Balaz[1] and Christian Wolfrum[1]**

[1] Institute of Food, Nutrition and Health, Department of Health Sciences and Technology (D-HEST), ETH Zürich, Zurich, Switzerland, [2] Institute of Translational Medicine, Department of Health Sciences and Technology (D-HEST), ETH Zürich, Zurich, Switzerland, [3] Life Science Zurich Graduate School, Molecular Life Sciences Program, Zurich, Switzerland

When exposed to cold temperatures, mice increase their thermogenic capacity by an expansion of brown adipose tissue mass and the formation of brite/beige adipocytes in white adipose tissue depots. However, the process of the transcriptional changes underlying the conversion of a phenotypic white to brite/beige adipocytes is only poorly understood. By analyzing transcriptome profiles of inguinal adipocytes during cold exposure and in mouse models with a different propensity to form brite/beige adipocytes, we identified ESRRG and PERM1 as modulators of this process. The production of heat by mitochondrial uncoupled respiration is a key feature of brite/beige compared to white adipocytes and we show here that both candidates are involved in PGC1α transcriptional network to positively regulate mitochondrial capacity. Moreover, we show that an increased expression of ESRRG or PERM1 supports the formation of brown or brite/beige adipocytes *in vitro* and *in vivo*. These results reveal that ESRRG and PERM1 are early induced in and important regulators of brite/beige adipocyte formation.

Keywords: beige adipocytes, brown adipocyte, adipogenesis, estrogen receptor, adipose tissue

OPEN ACCESS

Edited by:
Patrick C. N. Rensen, Leiden University Medical Center, Netherlands

Reviewed by:
Didier F. Pisani, Centre National de la Recherche Scientifique (CNRS), France
Vincenzo Marzolla, San Raffaele Pisana (IRCCS), Italy

****Correspondence:***
Christian Wolfrum
christian-wolfrum@ethz.ch
Miroslav Balaz
miroslav-balaz@ethz.ch

Specialty section:
This article was submitted to Obesity, a section of the journal Frontiers in Endocrinology

Received: *14 February 2020*
Accepted: *15 May 2020*
Published: *12 June 2020*

Citation:
Müller S, Perdikari A, Dapito DH, Sun W, Wollscheid B, Balaz M and Wolfrum C (2020) ESRRG and PERM1 Govern Mitochondrial Conversion in Brite/Beige Adipocyte Formation. Front. Endocrinol. 11:387. doi: 10.3389/fendo.2020.00387

INTRODUCTION

White and brown adipose tissue have divergent functions. White adipocytes store chemical energy within a single lipid droplet to release it back to the body when needed. In contrast, brown adipocytes primarily convert chemical energy into heat through the action of uncoupling protein 1 (UCP1) (1, 2). It is known that brown adipocytes do not only reside in a distinct fat pad in the interscapular region in rodents, but are also found interspersed between white adipocytes in other anatomical locations (3, 4). The latter have been termed brite ("brown-in-white") or beige adipocytes and are identified by their multilocular appearance and the expression of UCP1 (5). Their formation can be induced through a plethora of stimuli, most prominently through exposure of the animals to a cold environment, by beta-adrenergic stimulation (6) and other endocrine factors (7, 8). Experimental evidence suggests that the arising brite/beige adipocytes can derive from *de novo* differentiation of stem cells (9, 10) as well as by direct interconversion of mature adipocytes (11–13).

The orphan nuclear estrogen related receptor gamma (ESRRG) is highly expressed in energy dependent tissues such as brain, heart, skeletal muscle, kidney and BAT and is responsible for cell-type specific function in the majority of those tissues (14). Studies have shown that ESRRG is not important for brown preadipocyte differentiation but for brown adipocyte function, acting in a complementary way together with other ESRR members in mitochondrial biogenesis and oxidative

function (15). In fact, it was shown that ESRR members mediate the adaptive response of BAT to adrenergic stimulation (16). Moreover, ESRRG is necessary for the induction of UCP1 in *in vitro* differentiating cells (17) and for the maintenance of BAT thermogenic activity *in vivo* (18). ESRRG was shown to interact with GADD45γ to regulate UCP1 levels during cold adaption of brown adipose tissue (19). In regards to browning of white adipose tissue, the 1-benzyl-4-phenyl-1H-1,2,3-triazole derivative is shown to enhance the function of ESRRG and increase browning *in vitro* and *in vivo* (20). The potential transcription factor PGC1 and ESRR-induced regulator in muscle 1 (PERM1) has not been described in the context of adipose tissue so far, but was recently reported to regulate OXPHOS proteins in muscle *in vitro* and *in vivo* (21, 22). As ESRRG, PERM1 acts downstream of PGC1α, a master-regulator of mitochondrial capacity (23).

We aimed to study the latter process and showed that as early as 24 h after a cold stimulus, several known browning markers are significantly upregulated in the white adipocyte fraction. Importantly, we identified ESRRG and PERM1 as novel transcriptional regulators of brite/beige adipocyte formation.

RESULTS

Upregulation of Esrrg and Perm1 Expression in the Inguinal White Adipose Tissue Mature Adipocyte Fraction of 129/SV Mice Upon 24 h of Cold Exposure

To study the transcriptional events underlying the appearance of brite/beige adipocytes we housed 129/SV mice at 8°C for 24 h, 7 days or kept them at room temperature. In order to identify transcriptional changes induced by acute and prolonged cold exposure, we performed transcriptomic analysis of the mature inguinal white adipocyte (ingWA) fraction using RNA microarray. We excluded from further analysis two out of five individual mice housed at room temperature which already expressed high levels of *Ucp1* (**Figure S1**), a phenomenon previously described in literature (24). Intriguingly, on the transcriptome level, the browning program was fully activated already after 24 h of cold exposure, as demonstrated by the upregulation of common browning makers *Dio2, Fabp3, Cpt1b, Perilipin 5, Cox7a1,* and *Ucp1* (**Figure 1A**). Even though there is a clear difference in the multilocular adipocyte content (**Figure S1B**), the transcriptomic changes between 24 h and 7 days of cold exposure were only marginal (**Figure 1B**), indicating that the transcriptional program for brite/beige adipocyte formation is kept constant after the initial activation. A key feature in the appearance of brite/beige adipocytes is the increase in mitochondrial capacity (25, 26). We found specific nuclear encoded mitochondrial genes upregulated already after 24 h of cold exposure, indicating mitochondrial remodeling. On the other hand, mitochondrial encoded genes were only regulated after 7 days of cold exposure, which likely reflects the bulk increase in mitochondrial mass (**Figure 1C**). Analysis of early transcriptional changes revealed two genes, *Esrrg* and *Perm1*, to be significantly upregulated after 24 h of cold exposure (**Figure 1A**). We confirmed the expression of *Esrrg* and *Perm1* by qRT-PCR in ingWA fraction 24 h after cold exposure in an independent cohort of mice (**Figure 1D**). We further validated the *Esrrg* and *Perm1* expression in pure populations of mature adipocyte isolated by fluorescent activated cell sorting (FACS, **Figure S1C**). We used transgenic mice in the C57BL/6 background expressing green-fluorescent protein (GFP) under the control of the *Ucp1* promoter housed at 8°C for 7 days. RNA expression analysis revealed *Perm1* exclusive expression in the brite/beige adipocyte fraction, while *Esrrg* expression was enriched in the brite/beige compared to the white adipocytes (**Figure 1E**).

Transcriptome Analysis Shows That Esrrg and Perm1 Expression Positively Correlates With Browning Markers

The 129/SV mouse strain has a higher propensity of browning in the ingWA compared to C57BL/6 (27, 28). Therefore, we analyzed if this phenotypic difference can be recapitulated through whole transcriptome analysis. The adipocyte fractions of the ingWA, epididymal white (epiWA) and interscapular brown adipose tissue (iBA) were isolated from both strains housed at room temperature and analyzed by next-generation RNA sequencing. Classical browning markers *Ucp1*, *Cox7a1,* and *Cidea* were nearly absent in epiWA of C57BL/6 with very low expression in the 129/SV mouse model (**Figure 2A**), while they were expressed higher in the ingWA of 129/SV mice, indicating the presence of few brite/beige cells already at room temperature. Interestingly, we detected browning markers at higher levels in the iBA of C57BL/6 in comparison to 129/SV, potentially indicating a compensatory mechanism, to keep the total brown/brite/beige capacity constant. The expression levels of *Esrrg* and *Perm1* accurately correlated with browning markers in the two mouse models (**Figure 2B**), suggesting a possible role in brite/beige and brown adipocytes. To validate that changes on the transcript level also result in increased protein abundance, we cold-exposed 129/SV mice for 3 and 7 days, respectively. We could show that PERM1 is not detectable at room temperature but is expressed after cold stimulation in ingWA (**Figure 2C**). Due to the unavailability of ESRRG specific antibodies, we could not confirm protein expression of ESRRG.

Perm1 mRNA and Protein Is Expressed in High Energy Demanding Tissues

To characterize further the candidate genes *Esrrg* and *Perm1*, we analyzed the expression pattern in a tissue panel of C57BL/6 mice housed at room temperature. Interestingly, while we detected broad expression of *Pgc1α* and *Esrrg*, *Perm1* expression was confined to tissues with a high energy demand, in particular iBAT, skeletal muscle and heart (**Figure 3A**), confirmed also on protein level (**Figure 3B**). The importance of ESRRG and PERM1 in energy metabolism is evident in global ESRRG knockout mice, which die shortly after birth, due to a heart-defect, as the organ cannot sustain its function despite an increase in mitochondrial number (29). In this study, *Perm1* is considerably

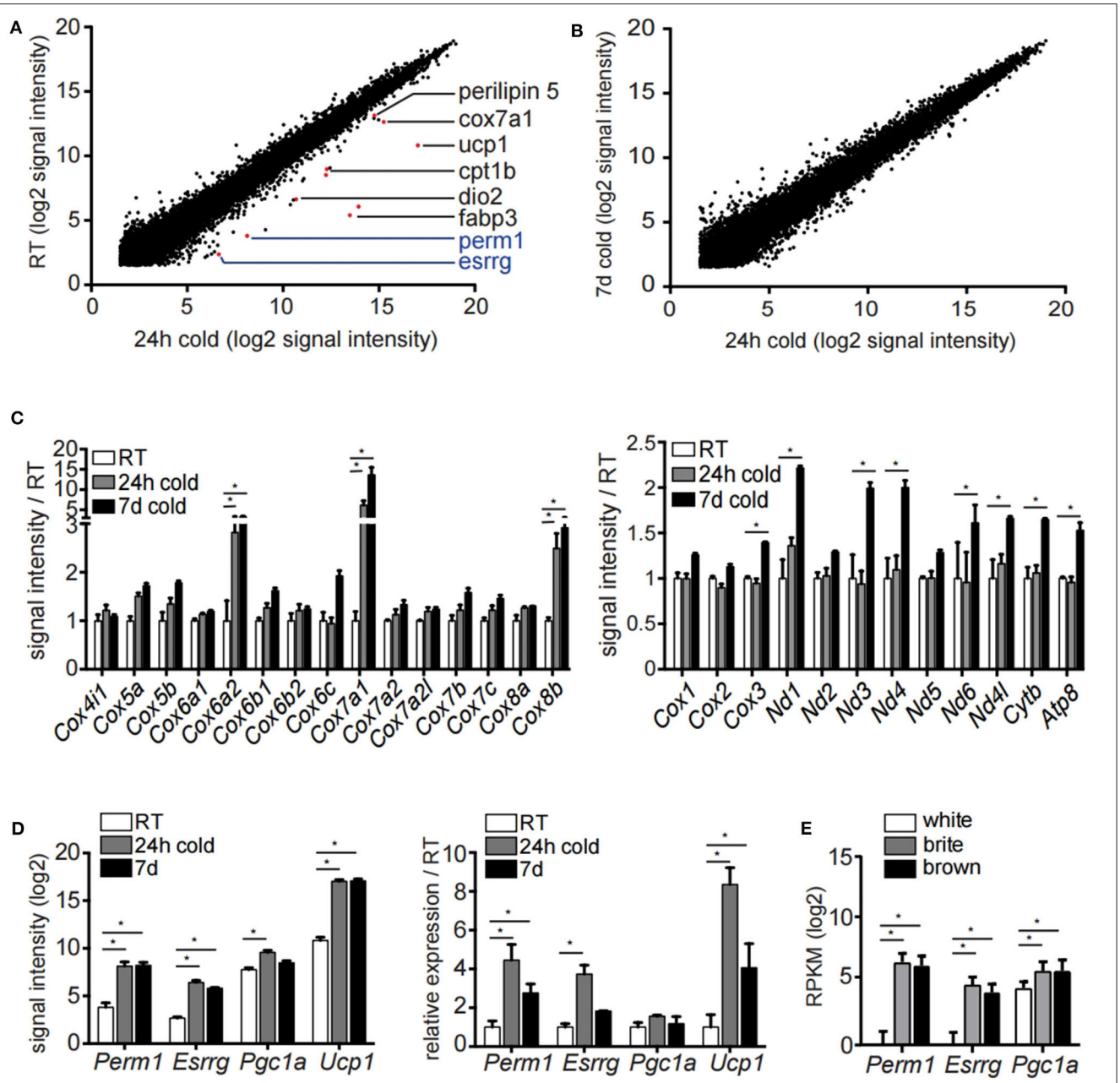

FIGURE 1 | Microarray analysis of inguinal white adipocytes during cold exposure. **(A,B)** Signal intensities (log2) of all probes measured of the extracted RNA of the adipocyte fraction of ingWA comparing 24 h cold exposure and room temperature **(A)** or 24 h and 7 days cold exposure **(B)**. Depicted in red are browning markers upregulated after cold treatment. **(C)** Signal intensity of specific nuclear encoded mitochondrial genes for OXPHOS complex IV (left) and all mitochondrial encoded genes (right) in room temperature, after 24 h and 7 days of cold exposure. Data are presented as microarray signal intensities relative to room temperature as mean with SEM ($n = 3$–5). **(D)** Expression of target genes *Perm1*, *Esrrg*, *Pgc1α,* and *Ucp1* in room temperature, after 24 h and 7 days of cold exposure shown in the microarray (left) and in an independent cohort of mice via qRT-PCR (right). Data are presented as signal intensities (log2) or relative expression (ddCt) compared to room temperature, respectively, as mean with SEM ($n = 3$-5 per cohort). **(E)** Expression of target genes *Perm1*, *Esrrg,* and *Pgc1α* in FACS sorted mature adipocytes according to GFP expression under control of the *Ucp1* promoter. Data are presented as mean RPKM (log2) with SD ($n = 10$ per cell type). Statistical testing (*t*-test) was performed between room temperature condition and cold housing for 24 h or 7 days, respectively, or between sorted white adipocytes and brite or brown adipocytes. A statistically significant result, meaning *p*-value < 0.05, is indicated with an asterisk (*).

downregulated, in heart tissue of the *Esrrg* knockout mice (**Figure 3C**). Moreover, a recent study by Harms and colleagues describes a whitening of brown adipose tissue upon knockout of *Prdm16*, a master regulator of the brown adipocyte program (30), in mature brown adipocytes (31). Consistently, in the publicly available dataset, *Perm1* is also among the highest

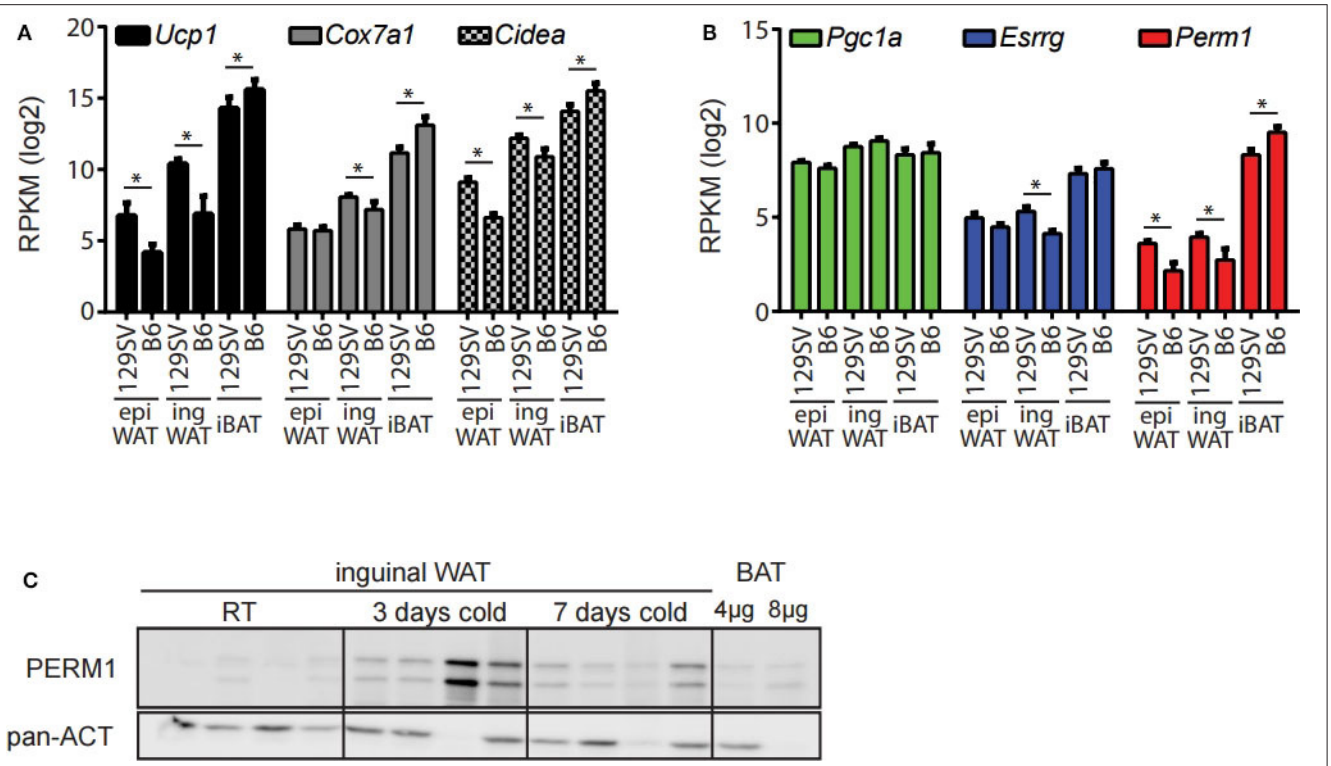

FIGURE 2 | *Esrrg* and *Perm1* mirror thermogenic capacity in adipocyte fractions of 129/SV and C57BL/6 mouse models. **(A)** Expression of common browning markers *Ucp1*, *Cox7a1,* and *Cidea* in the adipocyte fractions of epiWA, ingWA, and iBA in 129/SV or C57BL/6 mice housed at room temperature. Data are presented as mean RPKM with SEM ($n = 4$). **(B)** Expression of *Pgc1α, Esrrg, and Perm1* in the adipocyte fractions of epiWA, ingWA and iBA in 129/SV or C57BL/6 mice housed at room temperature. Data are presented as mean RPKM with SEM ($n = 4$). **(C)** PERM1 and UCP1 protein levels in ingWAT of 129/SV mice at room temperature and after 3 and 7 days of cold exposure. BAT at 1/10 and 1/5 of protein loaded shown for comparison. Each lane represents a single mouse ($n = 4$). Statistical testing (*t*-test) was performed between the mouse strains (129SV & B6) in each of the different tissue derived adipocyte fractions. A statistically significant result, meaning p-value < 0.05, is indicated with an asterisk (*).

downregulated proteins in the whitened BAT of these mice (**Figure 3D**).

Esrrg and Perm1 Show Low Expression in *in vitro* Differentiated Adipocytes and Abundance Was Increased Upon Adenoviral Overexpression of Pgc1a

In order to establish an *in vitro* model to characterize the function and the role of PERM1 and ESRRG in brite/beige adipocyte formation, we isolated stromal-vascular fraction (SVF) of the epiWA, ingWA and iBA depots of 129/SV mice and subjected them to *in vitro* brite/beige adipocyte differentiation (10). To assess the dynamics of *Perm1* and *Esrrg* expression during the differentiation of SVF cells into adipocytes, we harvested cells every 2 days starting from induction (day 0). *Pparγ*, as a general adipocyte marker, indicated adipocyte differentiation of cells derived from all three tissues, while browning markers *Ucp1* and *Cox7a1* were only detected in ingWA-derived SVF cells and were strongly induced in iBA-derived SVF cells during the differentiation time course (**Figure 4A**). While *Pgc1α* expression levels resembled these observations, *Esrrg* and *Perm1* could not be detected in ingWA-derived differentiating cells and were induced at very low levels in the iBA derived differentiating SVF cells, indicating that these cells are not a suitable model to study PERM1 and ESRRG function. In conclusion, while *Esrrg* and *Perm1* are strong indicators of browning capacity *in vivo*, their expression *in vitro* is limited.

To functionally characterize our candidate proteins, we used immortalized brown pre-adipocytes, which can be differentiated to mature adipocytes *in vitro* (32). *Esrrg* and *Perm1* were silenced in proliferating preadipocytes (day−2) or in mature adipocytes (day 5), to study their role in regulation of brown/beige adipocyte formation and thermogenic activity, respectively. SiRNA mediated knockdown of *Esrrg* in mature brown adipocytes at day 5 of differentiation led to a significant reduction in *Ucp1* and *Cox7a1*, while *Pgc1α* was not affected (**Figure 4B**), indicating that ESRRG drives brown adipocyte thermogenic activity. Moreover, siRNA mediated repression of *Esrrg* in preadipocytes prior to the induction of differentiation (siRNA treatment at day−2) resulted in significantly reduced expression of *Ucp1*, *Cox7a1,* and *Pgc1α* as well as *Esrrg* in mature adipocytes, indicating a role of *Esrrg* during the early phase

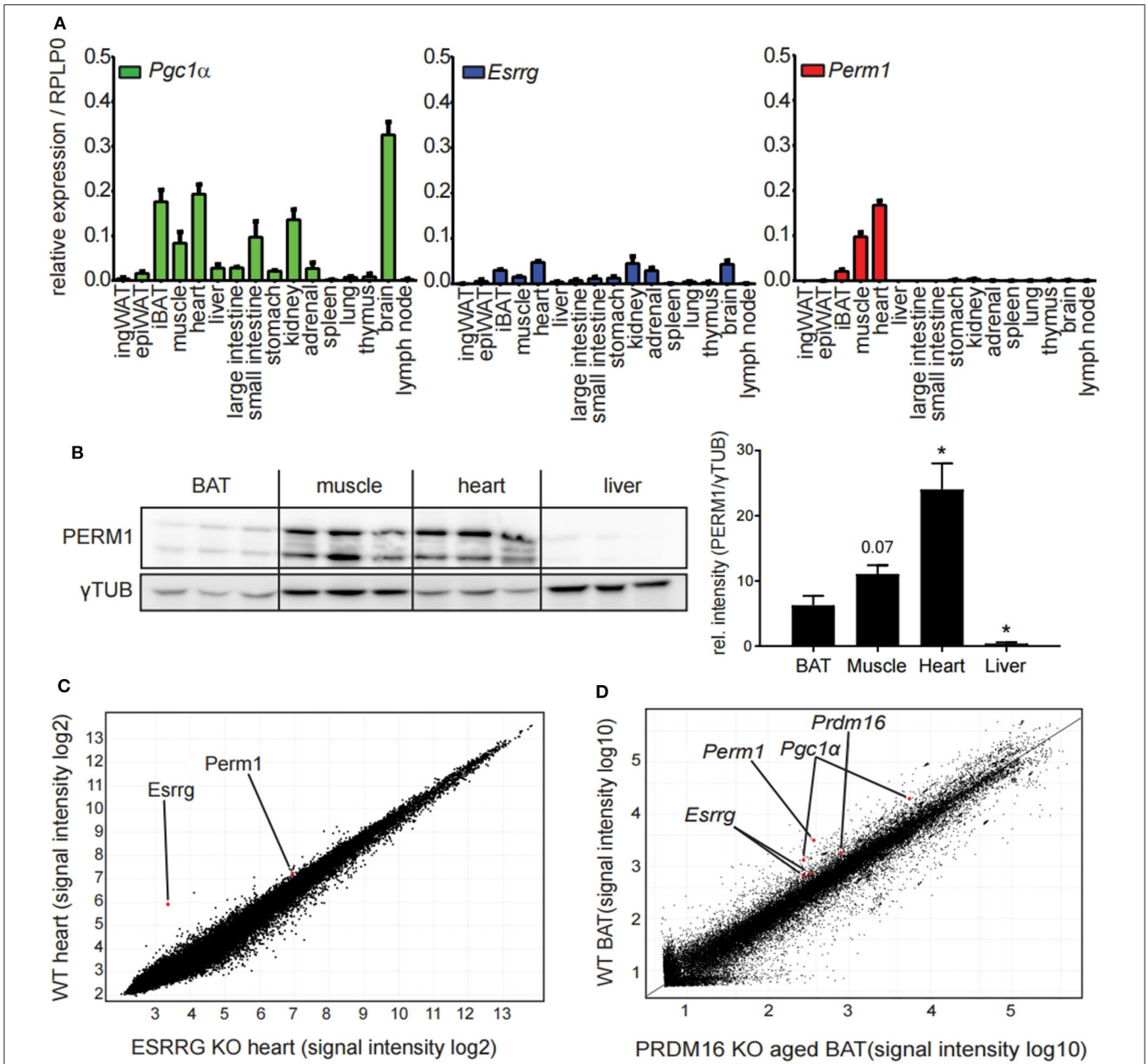

FIGURE 3 | PERM1 expression is confined to tissues with a high energy demand and with ESRRG involved in energy metabolism. **(A)** Expression of *Perm1*, *Esrrg,* and *Pgc1α* in a panel of 16 tissues derived from C57BL/6 mice housed at room temperature. Data are shown as relative expression to reference gene RPLP0 with SEM ($n = 5$). **(B)** Representative western blot and quantification of PERM1 in BAT, muscle, heart, and liver. Each lane represents a single mouse ($n = 3$). **(C)** Microarray analysis of RNA extracted from heart tissue of ESRRG knockout mice as described in (29). Data were retrieved from GSE8199, plotted are all transcripts as log2 signal intensities ($n = 3$). **(D)** Representative microarray analysis of RNA extracted from BAT of aged mice, where PRDM16 is knocked out under the control of MYF5 promoter, leading to a whitening of BAT, as described in (31). Data were retrieved from GSE55080, depicted is one representative microarray with all probes as signal intensities (total $n = 4$). A statistically significant result, meaning p-value < 0.05, is indicated with an asterisk (*).

of adipogenic differentiation (**Figure 4C**). Altogether, these data indicate that ESRRG controls both formation as well as the thermogenic activity of brown/beige adipocytes. We were unable to achieve knockdown of *Perm1* with siRNA treatment; hence, no change in expression of other genes was observed (**Figure S2A**). As the expression levels of *Esrrg* and *Perm1 in vitro* are low, we aimed to increase their levels and analyze the concurrent functional implications. We employed an adenoviral system to overexpress either PGC1α or green fluorescent protein (GFP) as a control [kindly provided by Prof. Christoph Handschin (33)], as PGC1α was shown to increase *Perm1* and *Esrrg* abundance in muscle studies (21). We demonstrated that *Perm1*

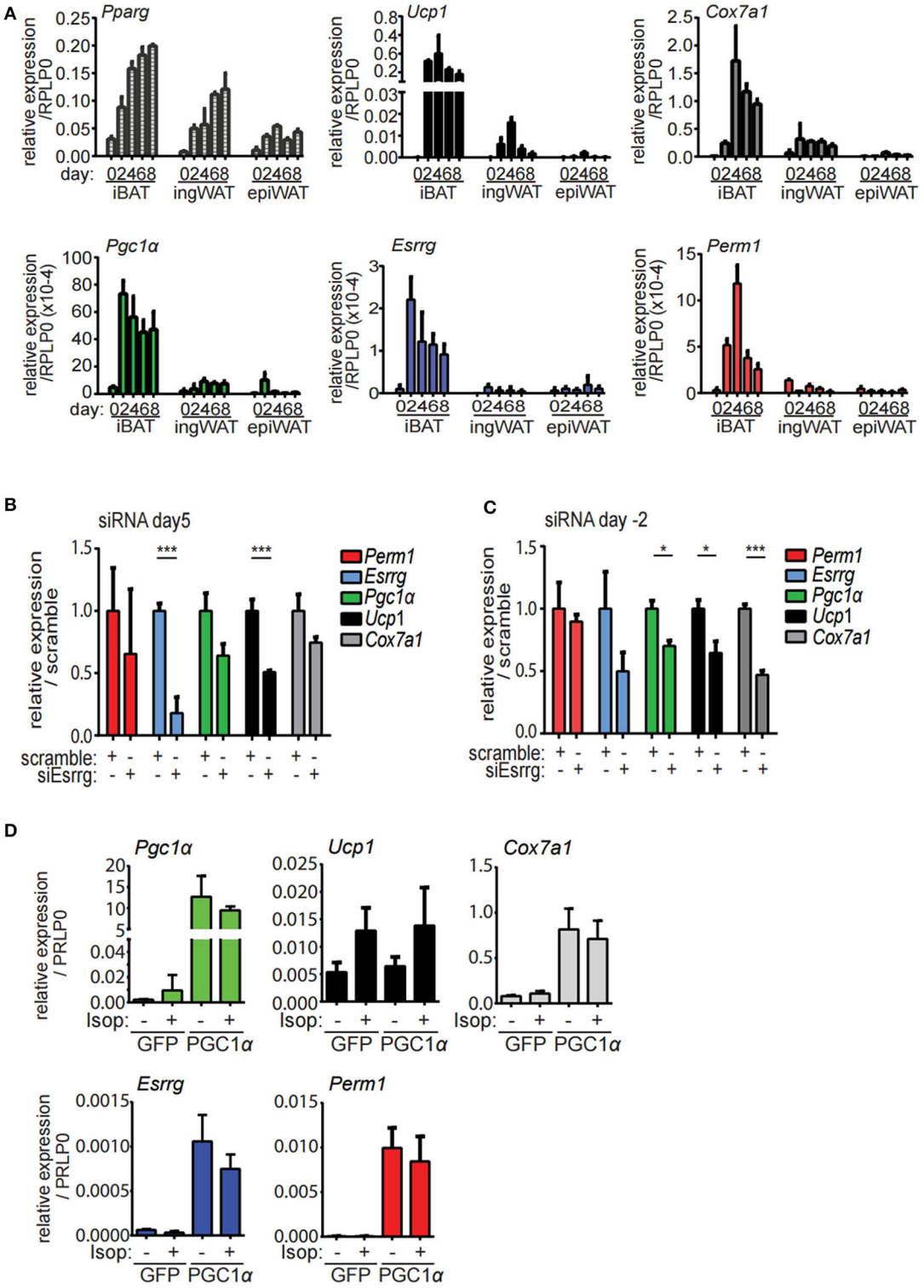

FIGURE 4 | *Esrrg* and *Perm1* have low expression levels *in vitro* but can be induced in a PGC1α dependent manner. **(A)** Time course of *in vitro* brite/beige adipocyte differentiation of SVF derived from iBA, ingWA or epiWA of 129/SV mice. *Pparg* (all isoforms) is shown as general adipocyte marker, *Ucp1,* and *Cox7a1* as markers for brown adipocytes. Data are presented as relative expression to reference gene RPLP0 with SEM ($n = 3$). **(B)** Gene expression in immortalized brown mature

(Continued)

FIGURE 4 | adipocytes *in vitro* differentiated and treated with siRNAs targeting *Esrrg* at day 5 of differentiation. Data are presented as relative expression (ddCt) relative to non-targeting siRNA as mean with SD ($n = 3$). **(C)** Gene expression in immortalized brown pre-adipocytes treated with siRNAs targeting *Esrrg 2* days prior to induction of differentiation. RNA was extracted on day 8 after induction and data are presented as expression (ddCt) relative to non-targeting siRNA as mean with SD ($n = 3$). **(D)** Gene expression in immortalized brown mature adipocytes *in vitro* differentiated and infected with adenovirus to overexpress PGC1α or GFP at day 5 after induction. Data are presented as relative expression to reference gene RPLP0 with SD ($n = 3$). A statistically significant result, meaning p-value < 0.05 and < 0.001, is indicated with an asterisk (*) and (***), respectively.

and *Esrrg* could be upregulated in a *Pgc1α* dependent manner in *in vitro* differentiated mature brown adipocytes (**Figure 4D**). Interestingly, *Cox7a1* was co-regulated, while *Ucp1* levels were unaffected. The latter can be explained by *Ucp1* expression being already affected by control adenovirus treatment compared to untreated cells (**Figure S2C**). Moreover, the combination of adenoviral and siRNA treatment resulted in non-differentiating cells (data not shown). Notably, adenoviral overexpression of PGC1α in immortalized pre-adipocytes already lead to the expression of known target genes *Esrra* and *Cox7a1* in a *Pgc1α*-dependent manner, but not *Esrrg* or *Perm1* (**Figure S2D**).

Expression of Perm1 in a Doxycycline Induced Stable Cell Line Leads to Increased OXPHOS Protein Expression

Since endogenous expression of *Esrrg* and *Perm1* is low *in vitro*, we set out to establish a model system, which does not rely on adenoviral transduction and allows for targeted expression of either *Esrrg* or *Perm1*. Therefore, we used the lentiviral pInducer21 system (34) to express *Esrrg* or *Perm1* under the control of doxycycline, including GFP as a positive selection marker for transduced cells. Immortalized brown preadipocytes were infected and FACS sorted according to their GFP signals, to polyclonally generate six cell lines having negative, low or high GFP expression, corresponding to their ability to express either ESRRG or PERM1 upon doxycycline treatment. As a next step, we differentiated the pInducer_Esrrg cell lines (**Figure 5A**) in the presence of doxycycline during the last 3 days of differentiation. Indeed, we could show the effective induction of *Esrrg*, which inversely correlated with *Ucp1* mRNA expression (**Figure 5B**). On the protein level, UCP1 was increased in an *Esrrg*-dependent manner, while the representative proteins of the oxidative phosphorylation chain (OXPHOS) were not affected (**Figure 5C**). Similar experiments with the pInducer_Perm1 cell lines demonstrated an efficient induction of PERM1 on transcript and protein level, while UCP1 remained unaffected (**Figures 5D,E**). Interestingly, components of the OXPHOS showed a trend to be positively affected by PERM1 expression. To corroborate this finding, we repeated the experiment with a prolonged doxycycline treatment (last 4 days of differentiation) of the pInducer_Perm1 cell lines. The omission of doxycycline during the 6-h isoproterenol stimulation led to a significant decrease in induced *Perm1* mRNA (**Figure S3A**) and protein levels. Moreover we observed the recently described adverse effects of doxycycline on mitochondrial stability, by inhibiting the mitochondrial ribosome (35). Despite these confounding effects, we demonstrated an increase in representative OXPHOS proteins in a PERM1 dependent manner (**Figures 5F,G**). Moreover, these experiments did not reveal a direct regulation of *Perm1* by *Esrrg* or vice versa (**Figure S3B**).

In vivo Overexpression of PERM1 Correlates With Increase in Levels of Selective OXPHOS Components

Since ESRRG and PERM1 can positively regulate brown adipocyte function *in vitro*, we aimed to investigate whether their overexpression also supports browning of white adipose tissue *in vivo*. Therefore, we directly injected adenoviruses into the right ingWA fat-pad of 129/SV mice, which led to the overexpression of either *Esrrg* or *Perm1*, and control virus for LacZ expression into the left ingWA fat pad of the same mouse (**Figure 6A**). Two days after injection, our target proteins were only expressed locally, and we could not detect a spread to liver on transcript (**Figure S4**) and protein level (**Figure 6B**). Two days after the injections, we exposed the animals to 8°C for 7 days to induce browning of ingWA. Intriguingly, despite varying degrees of browning in the individual animals, we observed an asymmetric browning between the fat pads injected with virus overexpressing *Esrrg* and the control virus, supporting that *Esrrg* overexpression lead to increased levels of UCP1 *in vivo* (**Figure 6C**). *Perm1* overexpression on the other hand, led to a selective increase in Complex 1, 3, and 5 of the OXPHOS, while UCP1 levels remained rather constant (**Figures 6D,E**). In summary, based on our data we propose that ESRRG and PERM1 support browning *in vitro* and *in vivo*. While ESRRG regulates UCP1 abundance, PERM1 controls the amount of the OXPHOS components.

DISCUSSION

During cold exposure, mice must increase their thermogenic capacity to maintain their body temperature by increasing brown adipose tissue mass and forming brite/beige adipocytes within white adipose tissue depots (36, 37). Experimental evidence demonstrates that brite/beige adipocytes can arise from *de novo* differentiated stem cells (9, 10) or by conversion of mature adipocytes in the ingWA (12, 13). In this study, we solely analyzed the floating adipocyte fraction after cold exposure, thereby excluding cold induced transcriptional changes in stromal cells, as is described in whole tissue analyses (38). We could show that common browning factors are already fully upregulated on a transcriptional level after 24 h of cold stimulation, while morphological and UCP1 protein expressing brite/beige adipocytes are only detectable after several days of cold exposure, depending on the mouse model used (9, 12, 25).

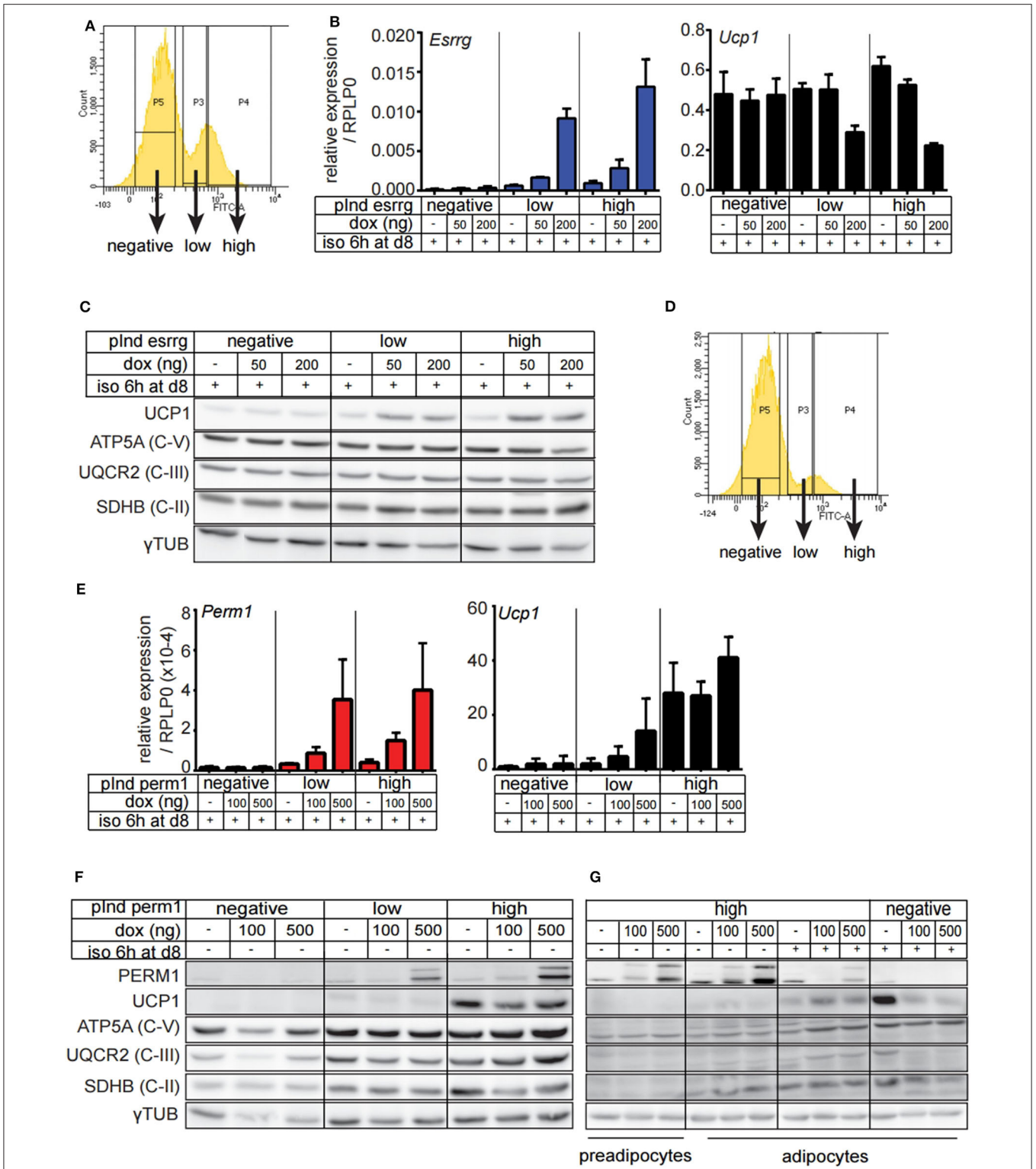

FIGURE 5 | Generation and characterization of brown adipocyte cell lines expressing either ESRRG or PERM1 in a doxycycline dependent manner. **(A)** Representative FACS plots from immortalized brown pre-adipocytes transduced with lentiviral particles containing pInd21_ESRRG to polyclonally generate new cell lines where ESRRG is not expressed or is lowly or highly induced by doxycycline treatment, respectively. **(B)** *Esrrg* and *Ucp1* expression in *in vitro* differentiated

(Continued)

FIGURE 5 | pInducer_ESRRG cell lines, treated with doxycycline from day 5 to 8. Data are presented as relative expression to reference gene *RPLP0* with SD ($n = 3$). **(C)** UCP1, ATP5A, UQCR2, and SDHB expression in *in vitro* differentiated pInducer_ESRRG cell lines, treated with doxycycline from day 5 to 8. Gray dotted line indicates removal of the marker lane from the digital blot image. **(D)** Representative FACS plots from immortalized brown pre-adipocytes transduced with lentiviral particles containing pInd21_PERM2 to polyclonally generate new cell lines where PERM1 is not expressed or is lowly or highly induced by doxycycline treatment, respectively. **(E)** *Perm1* and *Ucp1* expression in *in vitro* differentiated pInducer_PERM1 cell lines treated with doxycycline from day 5 to 8. Data are presented as relative expression to reference gene *RPLP0* with SD ($n = 3$). **(F)** UCP1, ATP5A, UQCR2, and SDHB protein levels in *in vitro* differentiated pInducer_PERM1 cell lines, treated with doxycycline from day 5 to 8. Gray dotted line indicates removal of the marker lane from the digital blot image. **(G)** UCP1, ATP5A, UQCR2, and SDHB expression in pInducer_PERM1 cell lines treated in preadipocyte state with doxycycline for 96 h or *in vitro* differentiated and treated with doxycycline from day 4 to 8. Gray dotted lines indicate removal of the marker lane from the digital blot image.

Mitochondria are the main functional organelles for non-shivering thermogenesis (26). Based on our transcriptomic profile, we detected a selective upregulation of specific OXPHOS components after 24 h of cold exposure, indicating remodeling concurrent with expansion of mitochondria, during the conversion of a phenotypic white to a phenotypic brite/beige cell. Similar observations have been made in ultra-structural analyses of mitochondria during cold adaption in inguinal white adipocytes (39). On a proteomic level, it has been shown, that brown fat mitochondria rather resemble those of muscle than of white adipose tissue (40). Intriguingly, ESRRG and PERM1, the candidates we propose to govern this phenotypic conversion, are important regulators of mitochondrial capacity in muscle tissues (22, 41).

The orphan nuclear receptor ESRRG has already been shown to be necessary for the induction of UCP1 in *in vitro* differentiating cells (17) as well as for maintaining BAT thermogenic activity *in vivo* (16, 18). We corroborated these results by showing that knockdown of *Esrrg* in brown preadipocytes or in mature brown adipocyte *in vitro* leads to a decrease in UCP1 expression. This data is consistent with the phenotype of adipocyte-specific *Esrrg* knockout mice, which display marked downregulation of BAT-selective genes, pronounced whitening of BAT and cold intolerance (18). Moreover, it has recently been shown that ESRRG interacts with GADD45γ to regulate UCP1 levels during cold adaption of brown adipose tissue (19). According to our data, ESRRG exerts a similar function in regulating UCP1 induction during the formation of brite/beige adipocytes. Cold exposure of 129/SV mice for 24 h showed increased levels of *Esrrg* and *Ucp1* in the mature adipocyte fraction of the ingWAT.

The potential transcription factor PERM1 has not been described in the context of adipose tissue so far, but was recently reported to regulate OXPHOS proteins in muscle *in vitro* and *in vivo* (21, 22). We observed very low expression levels of PERM1 in brown adipocytes *in vitro* similar to a study comparing *in vitro* differentiated C2C12 cells to primary murine muscle, where PERM1 was more than 100-fold less abundant in C2C12 cells (42).

ESRRG and PERM1 act downstream of PGC1α, a master-regulator of mitochondrial capacity (23). Since PGC1α is highly regulated post-transcriptionally (43, 44), the transcript level alone is of limited informational value. When we analyzed the transcriptional profiles of the adipocyte fractions of different adipose tissue depots in 129/SV and C57BL/6 mice, we found that although *Pgc1a* expression is similar between the two strains and different depots, *Esrrg* and *Perm1* expression accurately mirrors the increased thermogenic capacity of 129/SV mice. Moreover, we gathered further evidence that total thermogenic capacity is kept rather constant (45, 46) by demonstrating that C57BL/6 mice have higher expression of classical browning marker genes in interscapular brown adipocytes, while in 129/SV mice, expression of browning markers is distributed between interscapular brown and inguinal white adipocyte fractions. *In vivo*, we could show that overexpression of PERM1, although does not increase UCP1 expression, correlates with OXPHOS components regulation, suggesting an important role of PERM1 in mitochondrial function. Multiple reports indicate that regulating brite adipocyte formation is sufficient to elicit a metabolic phenotype (24, 47–49). Therefore, molecules inducing brown/beige adipocyte formation and activity such as irisin, BMP7, FGF21, natriuretic peptides and mineralocorticoid receptor antagonists have attracted a lot of attention in recent years (44, 50–54). Here, we show that ESRRG and PERM1 govern the phenotypic conversion of white to brite/beige adipocytes. However, future studies are needed to validate the therapeutic potential of these two transcriptional regulators in animal models of obesity.

By analyzing the transcriptome of adipocytes of different mouse models and inguinal adipocytes during cold exposure, we identified ESRRG and PERM1 as regulators of brite/beige adipocyte formation. Both ESRRG and PERM1 are under the control of the PGC1α transcriptional network and upon cold exposure, their expression is increased in ingWA. While ESRRG controls UCP1 levels, PERM1 is regulating the components of the oxidative phosphorylation chain and both processes together are key events in the phenotypic conversion of a white to a brite/beige adipocyte.

LIMITATIONS OF STUDY

Our paper lacks the exact molecular mechanism through which PERM1 and ESRRG modulate the browning process. We show descriptive evidence from several angles, but in the scope of this study lack the appropriate *in vivo* models, to show a mechanistic link to certain physiological functions. Future studies are needed to validate the metabolic impact of

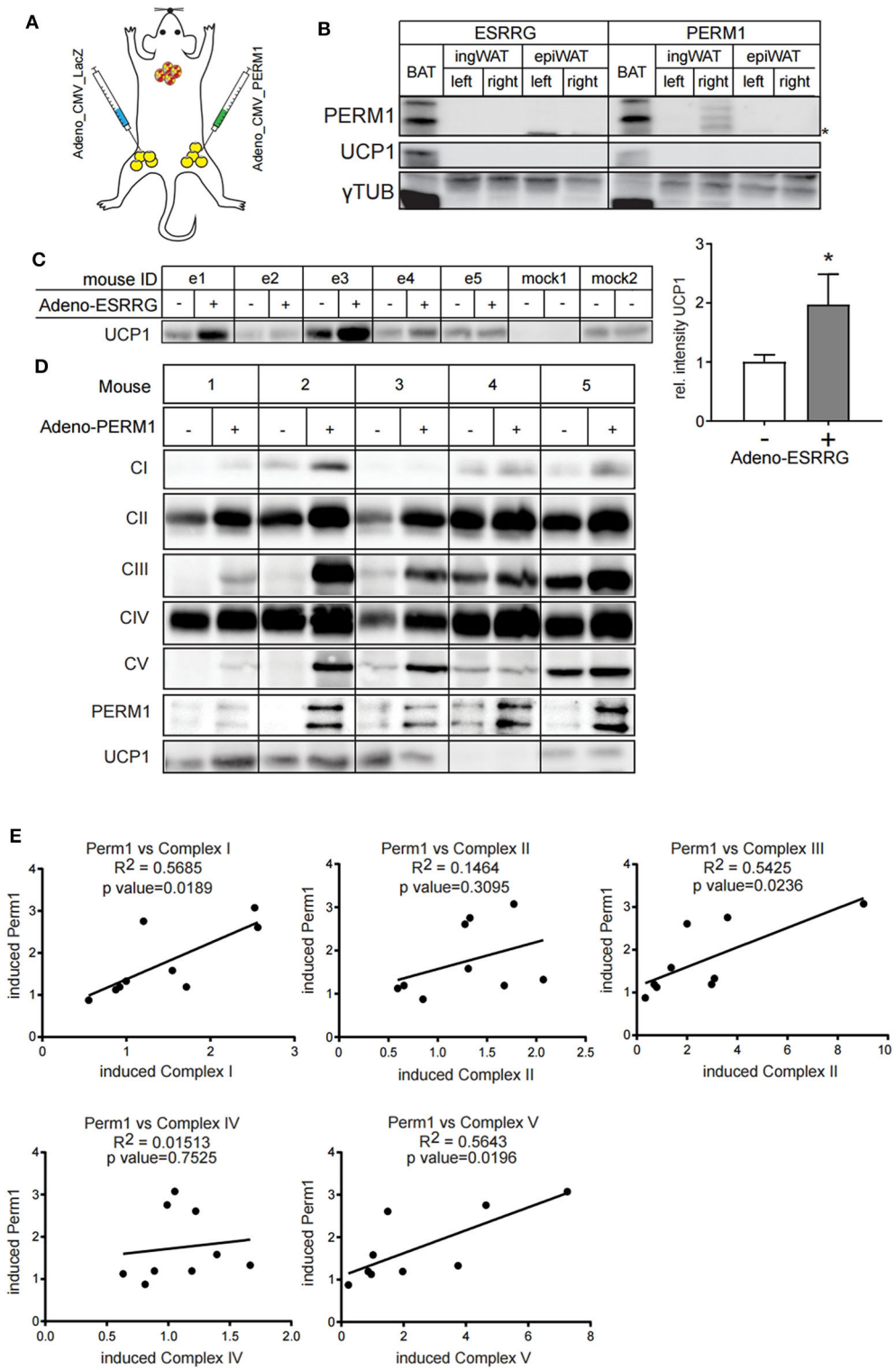

FIGURE 6 | ESRRG and PERM1 positively regulate browning of ingWAT *in vivo*. **(A)** Schematic illustration of the direct injection of adenoviral particles leading to the overexpression of LacZ (left ingWA fat pad) and PERM1 (right ingWA fat pad) in the same mouse. **(B)** PERM1 detection in the ingWA fat pad injected with the adenoviral particles for PERM1 overexpression. **(C)** Representative western blot and quantification of UCP1 in the ingWA fat pad injected with adenoviral particles for ESRRG overexpression (+). **(D)** Representative blots for OXPHOS complex subunits, UCP1 and PERM1 expression in ingWA fat pad injected with the adenoviral particles of PERM1 overexpression. **(E)** Correlation of PERM1 expression with different OXPHOS subunits as shown by protein expression in nine mice injected in one ingWA fat pad with adenoviral particles for PERM1 overexpression. A statistically significant result, meaning p-value < 0.05, is indicated with an asterisk (*).

PERM1 and ESRRG on mitochondrial function and brown/beige adipocyte thermogenic activity.

EXPERIMENTAL PROCEDURES

Chemicals and Reagents

All chemicals and reagents were obtained from Sigma-Aldrich, unless specified otherwise.

Cloning and Virus Production

Cloning

Coding transcript sequences for *Esrrg* and *Perm1* were retrieved from Ensembl and synthesized (GenScript) in sequence verified puc57 carrier plasmids flanked by NruI and XhoI restriction sites (Perm1: 2455 residues; Esrrg: 1408 residues). Both constructs were cloned into pENTR1A_dual_selection (Invitrogen) entry vectors for further use.

Adenovirus Production

Adenoviral particles carrying overexpression constructs under control of the CMV promotor to express either GFP or PGC1α were a kind gift by Prof. Handschin and described elsewhere (55). Plasmids to produce adenoviral particles to overexpress ESRRG or PERM1 were generated with the pAd/CMV/V5-DEST Gateway Vector Kit (Invitrogen) by gateway cloning through a one-step LR-clonase (Invitrogen) reaction. Directing of insertion and nucleotide sequence of the insert was verified by sequencing analysis (Microsynth). Viruses were produced and passaged in HEK 293A cells (Invitrogen), purified with the Adenovirus Standard Purification ViraKit (Virapur) according to manufacturer's instructions and titrated by FACS analysis (GFP, PGC1α) or plague assays (ESRRG, PERM1, LacZ).

Lentivirus Production

The destination vector pINDUCER21 (ORF-EG) for lentivirus production was a gift from Stephen Elledge & Thomas Westbrook (Addgene plasmid # 46948) (34). ESRRG and PERM1 sequences were inserted into the pINDUCER21 plasmid by gateway cloning through a one-step LR-clonase (Invitrogen) reaction. Directing of insertion and nucleotide sequence of the insert was verified by sequencing analysis (Microsynth). Lentiviral particles were produced in HEK 293T cells (Thermo Fischer) by co-transfection of psPAX2 (a gift from Didier Trono; Addgene plasmid # 12260), pMD2.g (a gift from Didier Trono; Addgene plasmid # 12259) and pINDUCER21 plasmid in a 9:1:10 ratio using Lipofectamine 2000 (Thermo Fisher). Cells were incubated with DMEM supplemented with 10 % FBS, 1.1 % BSA and 5 mM sodium butyrate for 36 h. Supernatant was harvested, centrifuged for 5 min at 200 g to pellet cellular debris and filtered (0.45 μm). Before freezing the crude virus preparation, 5 μg/ml polybrene was added.

Experimental Models

Mouse Work

129S2/SvPasCrl wild-type mice for all experiments were acquired from Charles-River at 4 weeks of age. C57BL/6N wild-type mice were bred in-house. *Ucp1-GFP* mice were previously described (12). All experiments were performed with young adult (12 weeks old) male mice kept on an inverted 12 h dark/light cycle and fed chow diet *ad libitum*. Cold stimulation was performed in temperature and humidity-controlled climate chambers (Memmert) with 4-5 animals housed in type II cages at an air-temperature of 8° C. All animal procedures were approved by the Veterinary office of the Canton of Zürich.

Virus Injection

Purified adenoviral particles were pre-incubated for 2 h at room temperature with 1.2 % poly-lysine. Animals were anesthetized by intra-peritoneal injection of 50 μl of a 1:1 mixture of Xylosine (1:5 in PBS) and Ketamine (1:2.5 in PBS). Adenoviruses (50 μl, 5.0 x 10^9 PFU/ml per fat pad) were directly injected into the ingWAT fat pad through the skin.

Tissue Sampling

For tissue sampling, animals were euthanized in carbon dioxide atmosphere. Popliteal lymph nodes were carefully removed, and adipose tissue depots were dissected and snap frozen in liquid nitrogen. For tissue sampling after adenoviral injections, euthanized animals were perfused utilizing a peristaltic pump with PBS containing 5 mM EDTA.

Adipocyte and SVF Isolation

Dissected adipose tissues were minced and incubated in 5 ml collagenase buffer (25 mM $KHCO_3$, 12 mM KH_2PO_4, 1.2 mM $MgSO_4$, 4.8 mM KCl, 120 mM NaCl, 1.2 mM $CaCl_2$, 5 mM glucose, 2.5% BSA, 2 mg/ml collagenase type II (clostridium histolyticum); sterile filtered (0.2 μm) for 60 min at 37 °C on a shaker and repeatedly re-suspended. The reaction was stopped by addition of 5 ml DMEM (Gibco) supplemented with 10 % FBS (Gibco) and 1 % Pen/Strep (Gibco) and centrifugation for 5 min at 200 g. The floating adipocyte fraction was carefully removed and filtered through 100 μm cell strainer (BD bioscience). Before further processing, the adipocyte fraction was washed three times by careful resuspension in separate tubes with 1 ml PBS (Gibco) followed by centrifugation for 2 min at 200 g. The SVF pellet was filtered through a 40 μm cell strainer (BD bioscience) and incubated in 1 ml erythrocyte lysis buffer (154 mM NH_4lC, 10 mM $KHCO_3$ and 0.1 m M EDTA) for 5 min at 24°C. After centrifugation for 5 min at 200 g, the SVF cells were re-suspended in DMEM supplemented with 10 % FBS and 1 % Pen/Strep.

Cell Sorting of Adipocyte Populations

FACS sorting of adipocytes according to their GFP expression was described previously (56). Briefly, cell sorting of adipocytes was performed using an Aria III high-speed sorter (BD Bioscience). A nozzle of 130 mm diameter, sheath pressure of 10 psi and a standard 4-way purity mask as described in the sorter manual was used during all sorts. Transgenic *Ucp1-eGFP* mice, expressing the eGFP protein under the control of *Ucp1* promoter, were cold acclimated at 8°C for 7 days and the mature adipocyte fractions from iBAT and iWAT were separated by FACS using eGFP. The adipocyte population was first defined in the forward and side scatter by size and internal complexity characteristics. The GFP^+ population was defined in the respective gate and the mature brown adipocytes were

isolated from the mature fraction of iBAT. The same strategy was applied for the mature adipocyte fraction of iWAT to isolate the GFP^+ population, which constitutes brite adipocytes, and the adjacent GFP^- population that constitutes white adipocytes. For each sample, 3 or 6 same gender mice were pooled per sample and 500–3,000 cells were collected directly in RNA Lysis Buffer (Qiagen) and kept on ice until frozen and stored at −80°C.

Cell Culture Work

All cells were routinely passaged in complete DMEM (Gibco) supplemented with 10 % FBS (Gibco) and 1 % Pen/Strep (Gibco), unless stated otherwise. Isolated SVF cells were plated confluent at a density of 100 000 per well in a 96-well plate (day−2). Brown adipogenesis was induced (day 0) by addition of 5 mM dexamethasone, 0.5 mg/ml insulin, 0.5 mM isobutyl methylxanthine, 1 μM rosiglitazone and 1 nM T3 in complete DMEM. Two days after induction the medium was switched to complete DMEM supplemented with 0.5 mg/ml insulin and 1 nM T3, the medium was refreshed every other day until the cells were harvested (day 8). Immortalized brown pre-adipocytes as well as derived pINDUCER21_ESRRG and pINDUCER21_PERM1 cell lines were grown to confluence. Differentiation was induced the next day by addition of complete DMEM supplemented with 20 nM insulin, 0.5 mM isobutyl methylxanthine, 125 μM indomethacin, 1 μM dexamethasone, 1 nM T3 and 1 μM rosiglitazone. Two days after induction the medium was switched to complete DMEM supplemented with 20 nM insulin and 1 nM T3, consecutively the medium was refreshed every other day until the cells were harvested (day 8). Isoproterenol (1 μM) and doxycycline treatments of the pINDUCER cell lines were performed in addition, at the indicated time-points. To knockdown candidate proteins, 15 nmol siRNA smart-pools (4 siRNAs per gene, Dharmacon) were reverse-transfected into pre-adipocytes (day−2) or mature adipocytes (day 5) using Lipofectamine RNAiMAX (Invitrogen).

Adenoviral Infection

Adenoviral infections were performed at day 5 of differentiation. Purified viral particles were pre-incubated in complete DMEM supplemented with 1.2 % poly-lysine (vol/vol) for 2 h at room temperature, before being added to the culture at MOI of 10, if not indicated otherwise.

Lentiviral Infection and Cell Line Generation

For lentiviral infection of immortalized brown pre-adipocytes, crude virus preparation was added to sub-confluent cells and the culture plate centrifuged at 200 g for 10 min. After 1-h incubation at 37°C the crude virus was diluted 1:1 with complete DMEM. After 24 h the medium was changed to complete DMEM. The infected cells were passaged for 2 weeks and the integration of the pINDUCER construct verified by visible GFP expression through microscopy. Polyclonal FACS sorting was performed at the ETHZ Flow Cytometry Core Facility on a FACS Aria III (BD Biosciences) flow cytometer.

Sample Preparation and Molecular Analyses

RNA Extraction

RNA extraction of adipocyte fractions from single mice for microarray analysis was performed using the RNeasy Mini Kit (Qiagen). For NGS analysis, adipocytes fractions of three mice were pooled and lysed in Trizol reagent (Life Technologies). Samples were centrifuged at 14,000 x g for 15 min and the interphase transferred to a new tube. After addition of chloroform, RNA in the colorless upper phase was purified with the RNeasy Mini Kit (Qiagen). From whole tissues and *in vitro* differentiated adipocytes, RNA was extracted with the Trizol reagent according to the manufacturer's instructions followed by DNase digestion (Invitrogen) and purification through NaOAc precipitation. RNA quantity and purity were controlled with a Nanodrop-2000 spectrophotometer. Of *in vitro* differentiated SVF cells and pInducer cell lines RNA extraction, DNase digestion and direct on-column cDNA synthesis was performed using the MultiMACS system (Miltenyi Biotec) according to the manufacturer's instructions.

cDNA Synthesis and Quantitative Real-Time PCR

Reverse transcription was performed using the High Capacity cDNA Reverse transcription kit (Applied Biosystems) with 1 μg RNA per reaction or the MultiMACS system (Miltenyi Biotec). QRT-PCR was performed with Fast Sybr Green Master Mix (Life Technologies) in 10 μl reactions in 96-well format on StepOnePlus (Applied Biosystems) or in 384-well on ViiA7 (Applied Biosystems) systems. All primers used are listed in **Supplemental Table 1**.

Microarray Analysis

RNA probe labeling, purification, hybridization to the microarray and scanning was performed by the Functional Genomics Center Zurich (FGCZ) utilizing the Mouse Gene Expression v2 4 × 44K, G4846A Microarray Kit (Agilent). Raw data extraction was performed by the FGCZ, in brief, the raw probe intensities were extracted with Agilent's Feature Extraction software (v9.5.3.1). Log2-transformation and normalization using the quantile normalization method were performed with R (v3.1). To find genes with significant expression changes between groups, empirical Bayes statistics were applied to the data by moderating the standard errors of the estimated values using the limma-package (v3.18) (57). *P*-values were obtained from the moderated t-statistic and corrected for multiple testing with the Benjamini–Hochberg method.

Next-Generation Sequencing Analysis

RNA sequencing was performed utilizing the HiSeq 2000 (Illumina) platform as previously described (56). Raw data was analyzed at the FGCZ. In brief, sequences were aligned to the Mus musculus reference genome (build GRCm38) and quantification of gene level expression was carried out using RSEM (Version 1.2.12) (58, 59). RNAseq data of pure murine white, brite/beige and brown

adipocytes was previously published (56) and is available in the European Nucleotide Archive under accession number PRJEB20634.

Protein Extraction and Western Blotting

In vitro differentiated adipocytes were scraped off the culture plates in RIPA buffer [50 mM Tris pH 7.4, 150 mM NaCl, 5 mM EDTA, 1 % NP40, protease inhibitor cocktail (Roche)]. Muscle and heart tissues were powdered on dry ice using a mortar and pestle prior to re-suspension in RIPA. Lysates were further processed with a TissueLyser LT (Qiagen; 5 min at 50 Hz) and sonicated in an ice-cooled branson-type sonication bath for 30 min before being cleared of debris by centrifugation at 14,000 g for 15 min at 4°C. For adipose tissues, RIPA buffer was supplemented with 0.5 % sodium deoxycholate, 1 % Triton-X and 10 % glycerol and additionally centrifuged at 14,000 g for 15 min at 23°C to remove the liquid fat layer prior to clearing of debris. Protein concentration of the supernatants was determined either by DC Protein Assay (Bio-Rad) or Pierce BCA assay (Thermo Scientific). Equal amounts of proteins were separated on SDS-polyacrylamide gels in a Mini-Protean tetra (Bio-Rad) apparatus, before transfer to a nitrocellulose membrane (PerkinElmer). Antibodies used for probing were UCP1 (1:1000, ab10983, Abcam), PERM1 (C1orf170, 1:1000, HPA031711, Atlas Antibodies), total OXPHOS (1:500, ab110413, Abcam), pan-Actin (D18C11, 1:1000, CS#8456, Cell Signaling) and γ-tubulin (1:6000, T6557, Sigma-Aldrich). Chemiluminescent signals of the HRP-conjugated secondary antibodies (Calbiochem) were visualized by a LAS 4000 mini ImageQuant system (GE Healthcare Life Sciences).

Quantification and Statistical Analysis

For *in vivo* studies, littermates were randomly assigned to the groups. Sample sizes were determined on the basis of previous experiments using similar methodologies. The animal numbers used for all experiments are indicated in the corresponding figure legends. All cell culture experiments were performed with 2–3 technical replicates for RNA and protein analysis, and independently reproduced 2–4 times. Results are reported as mean ± SEM or SD, as indicated in the figure legends. Two-tailed unpaired Student's *T*-test was applied on comparison of two groups. In case of non-normal data distribution, a non-parametric Wilcoxon test was performed. ANOVA was applied on comparisons of multiple groups. Pearson's correlation coefficient was calculated, and all statistical analyses were performed using GraphPad Prism 6 and R version 3.4.4. Statistical differences are indicated as *for $P < 0.05$, **for $P < 0.01$ and ***for $P < 0.001$.

DATA AVAILABILITY STATEMENT

All datasets generated for this study are included in the article/**Supplementary Material**.

ETHICS STATEMENT

The animal study was reviewed and approved by Kantonales Vetamt Zürich.

AUTHOR CONTRIBUTIONS

SM and CW designed the study. BW and CW supervised the experiments. SM, AP, DD, and WS performed the experiments. SM and BW performed the proteome analysis. SM, AP, WS, and MB performed the transcriptome analysis. SM, MB, and CW wrote the paper. All authors reviewed and edited the manuscript. All authors contributed to the article and approved the submitted version.

SUPPLEMENTARY MATERIAL

The Supplementary Material for this article can be found online at: https://www.frontiersin.org/articles/10.3389/fendo.2020.00387/full#supplementary-material

Figure S1 | *Ucp1* expression in ingWA of individual mice during cold exposure. **(A)** *Ucp1* expression levels in the adipocyte fraction of ingWA of individual mice house at room temperature or cold exposed for 24 h or 7 days, respectively. Dotted line separates groups at room temperature with low or high *Ucp1* expression. Data is presented as log2 microarray signal intensity. **(B)** Representative immunohistochemical images of inguinal WAT (H&E stained) from a different cohort of mice housed at room temperature (RT), 24 h or 7 days at 8°C. Major morphological changes are visible after 7 days of cold exposure, only minor changes after 24 h. Micrographs were taken at 10x magnification. **(C)** Representative FACS plots from interscapular BAT (iBAT) and inguinal WAT (iWAT), and gating strategy for GFP^+ brown adipocytes, GFP^+ brite and GFP^- white adipocytes.

Figure S2 | *In vitro* characterization of ESRRG and PERM1. **(A)** Gene expression in immortalized brown mature adipocytes *in vitro* differentiated and treated with siRNAs targeting *Perm1* at day 5 of differentiation. Data are presented as relative expression (ddCt) relative to non-targeting siRNA as mean with SD ($n = 3$). **(B)** Gene expression in immortalized brown mature adipocytes *in vitro* differentiated and treated with siRNAs targeting *Perm1* 2 days prior to differentiation. Data are presented as relative expression (ddCt) relative to non-targeting siRNA as mean with SD ($n = 3$). **(C)** *Ucp1* expression in immortalized brown mature adipocytes *in vitro* differentiated and infected either with mock or with adenovirus to overexpress PGC1α or GFP at day 5 after induction. Data are presented as relative expression to reference gene RPLP0 with SD ($n = 3$). **(D)** Gene expression in immortalized brown mature adipocytes infected with different concentrations of adenoviral particles for PGC1α overexpression. Data are presented as relative expression to the lowest virus concentration (1/32 dilution; $n = 1$ per condition).

Figure S3 | *Esrrg* and *Perm1* do not induce each other in *in vitro* differentiated brown adipocytes **(A)** *Perm1* expression after doxycycline is omitted during 6-h isoproterenol stimulation. Data are presented as relative expression to reference gene *RPLP0* as mean with SD ($n = 3$). **(B)** *Perm1* and *Esrrg* expression in in *in vitro* differentiated pInducer_ESRRG and pInducer_PERM1 cell lines, respectively, treated with doxycycline from day 5 to 8. Data are presented as relative expression to reference gene *RPLP0* as mean with SD ($n = 3$).

Figure S4 | Overexpression of PERM1 or ESRRG by direct adenoviral injection is confined to the fat pad injected. **(A)** *Esrrg* or *Perm1* expression in the fat pad injected with the respective adenovirus. Data are presented as relative expression to reference gene *RPLP0* ($n = 1$ mouse per virus).

REFERENCES

1. Cannon B, Nedergaard J. Brown adipose tissue: function and physiological significance. *Physiol Rev.* (2004) 84:277–359. doi: 10.1152/physrev.00015.2003
2. Cinti S. The adipose organ. *Prostaglandins Leukot Essent Fatty Acids.* (2005) 73:9–15. doi: 10.1016/j.plefa.2005.04.010
3. Young P, Arch JR, Ashwell M. Brown adipose tissue in the parametrial fat pad of the mouse. *FEBS Lett.* (1984) 167:10–4. doi: 10.1016/0014-5793848 0822-4
4. Cousin B, Cinti S, Morroni M, Raimbault S, Ricquier D, Penicaud L, et al. Occurrence of brown adipocytes in rat white adipose tissue: molecular and morphological characterization. *J Cell Sci.* (1992) 103(Pt 4):931–42.
5. Rosenwald M, Wolfrum C. The origin and definition of brite versus white and classical brown adipocytes. *Adipocyte.* (2014) 3:4–9. doi: 10.4161/adip.26232
6. Himms-Hagen J, Cui J, Danforth E, Jr., Taatjes DJ, Lang SS, Waters BL, et al. Effect of CL-316,243, a thermogenic beta 3-agonist, on energy balance and brown and white adipose tissues in rats. *Am J Physiol.* (1994) 266:R1371–82. doi: 10.1152/ajpregu.1994.266.4.R1371
7. Bartelt A, Heeren J. Adipose tissue browning and metabolic health. *Nat Rev Endocrinol.* (2014) 10:24–36. doi: 10.1038/nrendo.2013.204
8. Frontini A, Vitali A, Perugini J, Murano I, Romiti C, Ricquier D, et al. White-to-brown transdifferentiation of omental adipocytes in patients affected by pheochromocytoma. *Biochim Biophys Acta.* (2013) 1831:950–9. doi: 10.1016/j.bbalip.2013.02.005
9. Wang QA, Tao C, Gupta RK, Scherer PE. Tracking adipogenesis during white adipose tissue development, expansion and regeneration. *Nat Med.* (2013) 19:1338–44. doi: 10.1038/nm.3324
10. Wu J, Bostrom P, Sparks LM, Ye L, Choi JH, Giang AH, et al. Beige adipocytes are a distinct type of thermogenic fat cell in mouse and human. *Cell.* (2012) 150:366–76. doi: 10.1016/j.cell.2012.05.016
11. Cinti S. Transdifferentiation properties of adipocytes in the adipose organ. *Am J Physiol Endocrinol Metab.* (2009) 297:E977–86. doi: 10.1152/ajpendo.00183.2009
12. Rosenwald M, Perdikari A, Rulicke T, Wolfrum C. Bi-directional interconversion of brite and white adipocytes. *Nat Cell Biol.* (2013) 15:659–67. doi: 10.1038/ncb2740
13. Lee YH, Petkova AP, Konkar AA, Granneman JG. Cellular origins of cold-induced brown adipocytes in adult mice. *FASEB J.* (2015) 29:286–99. doi: 10.1096/fj.14-263038
14. Alaynick WA, Way JM, Wilson SA, Benson WG, Pei L, Downes M, et al. ERRγ regulates cardiac, gastric, and renal potassium homeostasis. *Mol. Endocrinol.* (2010) 24:299–309. doi: 10.1210/me.2009-0114
15. Gantner ML, Hazen BC, Eury E, Brown EL, Kralli A. Complementary roles of estrogen-related receptors in brown adipocyte thermogenic function. *Endocrinology.* (2016) 157:4770–81. doi: 10.1210/en.2016-1767
16. Brown EL, Hazen BC, Eury E, Wattez JS, Gantner ML, Albert V, et al. Estrogen-related receptors mediate the adaptive response of brown adipose tissue to adrenergic stimulation. *iScience.* (2018) 2:221–37. doi: 10.1016/j.isci.2018.03.005
17. Dixen K, Basse AL, Murholm M, Isidor MS, Hansen LH, Petersen MC, et al. ERRgamma enhances UCP1 expression and fatty acid oxidation in brown adipocytes. *Obesity.* (2013) 21:516–24. doi: 10.1002/oby.20067
18. Ahmadian M, Liu S, Reilly SM, Hah N, Fan W, Yoshihara E, et al. ERRgamma preserves brown fat innate thermogenic activity. *Cell Rep.* (2018) 22:2849–59. doi: 10.1016/j.celrep.2018.02.061
19. Gantner ML, Hazen BC, Conkright J, Kralli A. GADD45γ regulates the thermogenic capacity of brown adipose tissue. *Proc Natl Acad Sci USA.* (2014) 111:11870–5. doi: 10.1073/pnas.1406638111
20. Xu S, Mao L, Ding P, Zhuang X, Zhou Y, Yu L, et al. 1-Benzyl-4-phenyl-1H-1,2,3-triazoles improve the transcriptional functions of estrogen-related receptor γ and promote the browning of white adipose. *Bioorg Med Chem.* (2015) 23:3751–60. doi: 10.1016/j.bmc.2015.03.082
21. Cho Y, Hazen BC, Russell AP, Kralli A. Peroxisome proliferator-activated receptor gamma coactivator 1 (PGC-1)- and estrogen-related receptor (ERR)-induced regulator in muscle 1 (Perm1) is a tissue-specific regulator of oxidative capacity in skeletal muscle cells. *J Biol Chem.* (2013) 288:25207–18. doi: 10.1074/jbc.M113.489674
22. Cho Y, Hazen BC, Gandra PG, Ward SR, Schenk S, Russell AP, et al. Perm1 enhances mitochondrial biogenesis, oxidative capacity, and fatigue resistance in adult skeletal muscle. *FASEB J.* (2016) 30:674–87. doi: 10.1096/fj.15-276360
23. Puigserver P, Wu Z, Park CW, Graves R, Wright M, Spiegelman BM. A cold-inducible coactivator of nuclear receptors linked to adaptive thermogenesis. *Cell.* (1998) 92:829–39. doi: 10.1016/S0092-8674(00)81410-5
24. Cohen P, Levy JD, Zhang Y, Frontini A, Kolodin DP, Svensson KJ, et al. Ablation of PRDM16 and beige adipose causes metabolic dysfunction and a subcutaneous to visceral fat switch. *Cell.* (2014) 156:304–16. doi: 10.1016/j.cell.2013.12.021
25. Gospodarska E, Nowialis P, Kozak LP. Mitochondrial turnover: a phenotype distinguishing brown adipocytes from interscapular brown adipose tissue and white adipose tissue. *J Biol Chem.* (2015) 290:8243–55. doi: 10.1074/jbc.M115.637785
26. Shabalina IG, Petrovic N, de Jong JM, Kalinovich AV, Cannon B, Nedergaard J. UCP1 in brite/beige adipose tissue mitochondria is functionally thermogenic. *Cell Rep.* (2013) 5:1196–203. doi: 10.1016/j.celrep.2013.10.044
27. Kozak LP. The genetics of brown adipocyte induction in white fat depots. *Front Endocrinol (Lausanne).* (2011) 2:64. doi: 10.3389/fendo.2011.00064
28. Li Y, Bolze F, Fromme T, Klingenspor M. Intrinsic differences in BRITE adipogenesis of primary adipocytes from two different mouse strains. *Biochim Biophys Acta.* (2014) 1841:1345–52. doi: 10.1016/j.bbalip.2014.06.003
29. Alaynick WA, Kondo RP, Xie W, He W, Dufour CR, Downes M, et al. ERRgamma directs and maintains the transition to oxidative metabolism in the postnatal heart. *Cell Metab.* (2007) 6:13–24. doi: 10.1016/j.cmet.2007.06.007
30. Seale P, Kajimura S, Yang W, Chin S, Rohas LM, Uldry M, et al. Transcriptional control of brown fat determination by PRDM16. *Cell Metab.* (2007) 6:38–54. doi: 10.1016/j.cmet.2007.06.001
31. Harms MJ, Ishibashi J, Wang W, Lim HW, Goyama S, Sato T, et al. Prdm16 is required for the maintenance of brown adipocyte identity and function in adult mice. *Cell Metab.* (2014) 19:593–604. doi: 10.1016/j.cmet.2014.03.007
32. Klein J, Fasshauer M, Klein HH, Benito M, Kahn CR. Novel adipocyte lines from brown fat: a model system for the study of differentiation, energy metabolism, and insulin action. *Bioessays.* (2002) 24:382–8. doi: 10.1002/bies.10058
33. Handschin C, Lin J, Rhee J, Peyer AK, Chin S, Wu PH, et al. Nutritional regulation of hepatic heme biosynthesis and porphyria through PGC-1alpha. *Cell.* (2005) 122:505–15. doi: 10.1016/j.cell.2005.06.040
34. Meerbrey KL, Hu G, Kessler JD, Roarty K, Li MZ, Fang JE, et al. The pINDUCER lentiviral toolkit for inducible RNA interference *in vitro* and *in vivo*. *Proc Natl Acad Sci USA.* (2011) 108:3665–70. doi: 10.1073/pnas.1019736108
35. Moullan N, Mouchiroud L, Wang X, Ryu D, Williams EG, Mottis A, et al. Tetracyclines disturb mitochondrial function across eukaryotic models: a call for caution in biomedical research. *Cell Rep.* (2015) 10:1681–91. doi: 10.1016/j.celrep.2015.02.034
36. Lowell BB, Hamann A, Lawitts JA, Himms-Hagen J, Boyer BB, Kozak LP, et al. Development of obesity in transgenic mice after genetic ablation of brown adipose tissue. *Nature.* (1993) 366:740–2. doi: 10.1038/366740a0
37. Enerback S, Jacobsson A, Simpson EM, Guerra C, Yamashita H, Harper ME, et al. Mice lacking mitochondrial uncoupling protein are cold-sensitive but not obese. *Nature.* (1997) 387:90–4. doi: 10.1038/387090a0
38. Rosell M, Kaforou M, Frontini A, Okolo A, Chan YW, Nikolopoulou E, et al. Brown and white adipose tissues: intrinsic differences in gene expression and response to cold exposure in mice. *Am J Physiol Endocrinol Metab.* 306:E945–64. doi: 10.1152/ajpendo.00473.2013
39. Loncar D. Convertible adipose tissue in mice. *Cell Tissue Res.* (1991) 266:149–61. doi: 10.1007/BF00678721
40. Forner F, Kumar C, Luber CA, Fromme T, Klingenspor M, Mann M. Proteome differences between brown and white fat mitochondria reveal specialized metabolic functions. *Cell Metab.* (2009) 10:324–35. doi: 10.1016/j.cmet.2009.08.014
41. Rangwala SM, Wang X, Calvo JA, Lindsley L, Zhang Y, Deyneko G, et al. Estrogen-related receptor gamma is a key regulator of muscle mitochondrial activity and oxidative capacity. *J Biol Chem.* (2010) 285:22619–29. doi: 10.1074/jbc.M110.125401

42. Deshmukh AS, Murgia M, Nagaraj N, Treebak JT, Cox J, Mann M. Deep proteomics of mouse skeletal muscle enables quantitation of protein isoforms, metabolic pathways, and transcription factors. *Mol Cell Proteomics.* (2015) 14:841–53. doi: 10.1074/mcp.M114.044222
43. Fernandez-Marcos PJ, Auwerx J. Regulation of PGC-1alpha, a nodal regulator of mitochondrial biogenesis. *Am J Clin Nutr.* (2011) 93:884S−90. doi: 10.3945/ajcn.110.001917
44. Fisher FM, Kleiner S, Douris N, Fox EC, Mepani RJ, Verdeguer F, et al. FGF21 regulates PGC-1α and browning of white adipose tissues in adaptive thermogenesis. *Genes Dev.* (2012) 26:271–81. doi: 10.1101/gad.177857.111
45. Schulz TJ, Huang P, Huang TL, Xue R, McDougall LE, Townsend KL, et al. Brown-fat paucity due to impaired BMP signalling induces compensatory browning of white fat. *Nature.* (2013) 495:379–83. doi: 10.1038/nature11943
46. Nedergaard J, Cannon B. The browning of white adipose tissue: some burning issues. *Cell Metab.* (2014) 20:396–407. doi: 10.1016/j.cmet.2014.07.005
47. Kazak L, Chouchani ET, Jedrychowski MP, Erickson BK, Shinoda K, Cohen P, et al. A creatine-driven substrate cycle enhances energy expenditure and thermogenesis in beige fat. *Cell.* (2015) 163:643–55. doi: 10.1016/j.cell.2015.09.035
48. Qiang L, Wang L, Kon N, Zhao W, Lee S, Zhang Y, et al. Brown remodeling of white adipose tissue by SirT1-dependent deacetylation of Ppargamma. *Cell.* (2012) 150:620–32. doi: 10.1016/j.cell.2012.06.027
49. Shinoda K, Ohyama K, Hasegawa Y, Chang HY, Ogura M, Sato A, et al. Phosphoproteomics identifies CK2 as a negative regulator of beige adipocyte thermogenesis and energy expenditure. *Cell Metab.* (2015) 22:997–1008. doi: 10.1016/j.cmet.2015.09.029
50. Armani A, Cinti F, Marzolla V, Morgan J, Cranston GA, Antelmi A, et al. Mineralocorticoid receptor antagonism induces browning of white adipose tissue through impairment of autophagy and prevents adipocyte dysfunction in high-fat-diet-fed mice. *FASEB J.* (2014) 28:3745–57. doi: 10.1096/fj.13-245415
51. Bostrom P, Wu J, Jedrychowski MP, Korde A, Ye L, Lo JC, et al. A PGC1-alpha-dependent myokine that drives brown-fat-like development of white fat and thermogenesis. *Nature.* (2012) 81:463–8. doi: 10.1038/nature10777
52. Tseng YH, Kokkotou E, Schulz TJ, Huang TL, Winnay JN, Taniguchi CM, et al. New role of bone morphogenetic protein 7 in brown adipogenesis and energy expenditure. *Nature.* (2008) 454:1000–4. doi: 10.1038/nature07221
53. Liu D, Ceddia RP, Collins S. Cardiac natriuretic peptides promote adipose 'browning' through mTOR complex-1. *Mol Metab.* (2018) 9:192–8. doi: 10.1016/j.molmet.2017.12.017
54. Bordicchia M, Liu D, Amri EZ, Ailhaud G, Dessi-Fulgheri P, Zhang C, et al. Cardiac natriuretic peptides act via p38 MAPK to induce the brown fat thermogenic program in mouse and human adipocytes. *J Clin Invest.* (2012) 122:1022–36. doi: 10.1172/JCI59701
55. Lehman JJ, Barger PM, Kovacs A, Saffitz JE, Medeiros DM, Kelly DP. Peroxisome proliferator-activated receptor gamma coactivator-1 promotes cardiac mitochondrial biogenesis. *J Clin Invest.* (2000) 106:847–56. doi: 10.1172/JCI10268
56. Perdikari A, Leparc GG, Balaz M, Pires ND, Lidell ME, Sun W, et al. BATLAS: deconvoluting brown adipose tissue. *Cell Rep.* (2018) 25:784–97. doi: 10.1016/j.celrep.2018.09.044
57. Ritchie ME, Phipson B, Wu D, Hu Y, Law CW, Shi W, et al. limma powers differential expression analyses for RNA-sequencing and microarray studies. *Nucleic Acids Res.* (2015) 43:e47. doi: 10.1093/nar/gkv007
58. Bolger AM, Lohse M, Usadel B. Trimmomatic: a flexible trimmer for Illumina sequence data. *Bioinformatics.* (2014) 30:2114–20. doi: 10.1093/bioinformatics/btu170
59. Li B, Dewey CN. RSEM: accurate transcript quantification from RNA-Seq data with or without a reference genome. *BMC Bioinformatics.* (2011) 12:323. doi: 10.1186/1471-2105-12-323

Conflict of Interest: The authors declare that the research was conducted in the absence of any commercial or financial relationships that could be construed as a potential conflict of interest.

frontiers in Endocrinology

MINI REVIEW
published: 28 July 2020
doi: 10.3389/fendo.2020.00498

UCP1 Dependent and Independent Thermogenesis in Brown and Beige Adipocytes

Kenji Ikeda and Tetsuya Yamada*

Department of Molecular Endocrinology and Metabolism, Tokyo Medical and Dental University, Bunkyo, Japan

Mammals have two types of thermogenic adipocytes: brown adipocytes and beige adipocytes. Thermogenic adipocytes express high levels of uncoupling protein 1 (UCP1) to dissipates energy in the form of heat by uncoupling the mitochondrial proton gradient from mitochondrial respiration. There is much evidence that UCP1 is the center of BAT thermogenesis and systemic energy homeostasis. Recently, UCP1 independent thermogenic pathway identified in thermogenic adipocytes. Importantly, the thermogenic pathways are different in brown and beige adipocytes. Ca^{2+}-ATPase 2b calcium cycling mechanism is selective to beige adipocytes. It remains unknown how the multiple thermogenic mechanisms are coordinately regulated. The discovery of UCP1-independent thermogenic mechanisms potential offer new opportunities for improving obesity and type 2 diabetes particularly in groups such as elderly and obese populations who do not possess UCP1 positive adipocytes.

Keywords: thermogenic fat, brown adipocyte, beige adipocyte, adipogenesis, uncoupling protein 1

OPEN ACCESS

Edited by:
Matthias Johannes Betz, University Hospital of Basel, Switzerland

Reviewed by:
Vibha Singhal, Massachusetts General Hospital, United States
Marco Infante, University of Miami, United States

****Correspondence:***
Kenji Ikeda
kikeda.mem@tmd.ac.jp

Specialty section:
This article was submitted to Obesity, a section of the journal Frontiers in Endocrinology

Received: *20 March 2020*
Accepted: *23 June 2020*
Published: *28 July 2020*

Citation:
Ikeda K and Yamada T (2020) UCP1 Dependent and Independent Thermogenesis in Brown and Beige Adipocytes. Front. Endocrinol. 11:498. doi: 10.3389/fendo.2020.00498

THERMOGENIC FAT: BROWN AND BEIGE ADIPOCYTES

Mammals have brown and beige thermogenic adipocytes, which are both rich in mitochondria and express uncoupling protein 1 (UCP1). However, brown and beige adipocytes play distinct developmental and anatomical roles in rodents and humans. Brown adipocytes are located in the interscapular and perirenal regions of rodents and infants. By contrast, beige adipocytes (or brite adipocytes) are induced thermogenic adipocytes found sporadically within the white adipose tissue (WAT). The development of beige adipocytes is called "browning" or "beiging." Beige adipocytes are induced by environmental stimuli, such as chronic cold, β3-adrenergic receptor agonists, peroxisome proliferator-activated receptor gamma (PPARγ) agonists, exercise (1), and cachexia (2). Since the emergence of evidence that adult humans have brown adipose tissue (BAT) (3–7), the debate over whether adult humans have beige adipocytes has been crucial to the metabolic field.

The function of BAT is to regulate the systemic energy balance through non-shivering thermogenesis (NST). Transcriptional analysis of adult human BAT revealed expression of molecular markers specific for murine beige adipocytes (8–10). By contrast, the deep neck region in adult humans possesses thermogenic fat that is similar to the brown fat of mice (11). Of note, clonal analysis of adipose tissue from adult humans revealed evidence that humans have beige adipocytes (12). Even adults who do not exhibit brown fat by ^{18}F-labeled fluorodeoxyglucose positron emission tomography/computerized tomography (^{18}F-FDG-PET/CT) develop thermogenic fat upon prolonged cold stimulation (13–15).

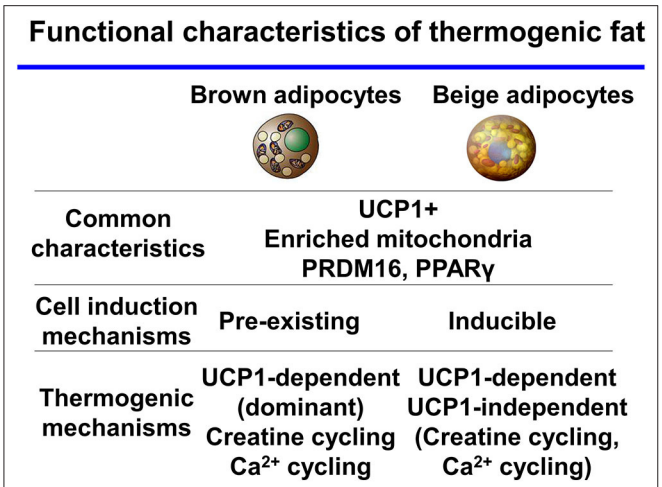

FIGURE 1 | Functional characteristics of thermogenic fat brown and beige adipocytes share many characteristics. In contrast, thermogenic mechanisms are discrete between the two cell types.

Many studies have reported that the amount of cold-induced thermogenic fat positively correlates with the degree of NST and improvements in insulin sensitivity in humans (13–16). Recently, a study showed a much wider distribution of BAT, including in the abdominal subcutaneous regions, in adult humans by refined ^{18}F-FDG-PET/CT imaging (17). These results support the existence of thermogenic adipocytes in adult humans. Thermogenic adipocytes have the characteristics of the beige-like inducible adipocytes that contribute to whole-body energy homeostasis. Based on these findings, researchers have hypothesized that beige fat may be a promising new therapeutic target to increase energy expenditure and treat obesity and type 2 diabetes. Future studies will determine the function and distinct, essential characteristics of beige fat in humans. While brown and beige adipocytes share many characteristics such as express UCP1, enriched mitochondria, and differentiation mechanisms-transcriptional factor PR domain-containing protein 16 (PRDM16), PPARγ. In contrast to this, recent studies, mainly in mice, suggest discrete thermogenic mechanisms in the two cell types (**Figure 1**). In this review, we discuss thermogenic mechanisms and pathways in thermogenic fat.

UCP1-DEPENDENT THERMOGENESIS IN THERMOGENIC FAT: BROWN AND BEIGE ADIPOCYTES

UCP1 localizes to the mitochondrial inner membrane. It generates heat by dissipating the energy proton gradient from the electron transport chain in mitochondrial respiration. There is considerable evidence that UCP1 is at the center of BAT thermogenesis and systemic energy homeostasis. Many studies have investigated if UCP1 is essential to thermogenesis in thermogenic adipocytes. Ucp1 knockout (KO) mice are unable to maintain their body temperature and develop hypothermia upon acute cold challenge (18). In addition, BAT-deficient mice created by transgenic expression of diphtheria toxin showed diabetic and obese phenotypes in room-temperature environments (19).

The re-synthesis of triacylglycerols after lipolysis is a thermogenic process that is dependent on the amount of ATP needed for triacylglycerol synthesis. Fatty acid synthesis and oxidation are both stimulated and tightly regulated by adrenergic activation (20). Upon adrenergic stimulation, brown adipocyte lipolysis and mitochondrial respiration are activated in a UCP1-dependent manner (21).

However, recent studies in mice with BAT-specific deficiencies in the lipolysis enzyme adipose triglyceride lipase (ATGL) or the ATGL-activating protein comparative gene identification-58 (CGI-58) revealed that the absence of lipolysis in BAT does not change NST (22, 23). These results suggest the existence of compensatory pathways that require further investigation.

UCP1 IS DISPENSABLE FOR THERMOGENESIS IN THERMOGENIC FAT

UCP1, often called thermogenin, had been thought to be the only thermogenic protein responsible for NST in thermogenic fat (24, 25). However, the Kozak group demonstrated that mixed strain F1 *Ucp1* KO mice were able to adapt to cold exposure with gradual acclimation (26–30). Recently, our study revealed that, in an increased beige fat-enriched mouse model, fatty acid-binding protein (aP2)-promoter *Prdm16* transgenic mice (aP2-PRDM16) transgenic × *Ucp1* KO mice could maintain their temperature in a cold environment although mice totally lacking Ucp1 could not (31). This finding suggests the existence of physiologically relevant UCP1-independent thermogenesis in adipocytes.

Intriguingly, *Ucp1* KO mice fed a high-fat diet (HFD) were resistant to the development of obesity at room temperature, suggesting the activation of a UCP1-independent thermogenic pathway (18, 32). Skeletal muscle has mainly been thought to contribute to UCP1-independent thermogenesis via increased capacity for shivering thermogenesis caused by chronic contractile activity (24). However, the findings of the studies on skeletal muscle UCP1-independent thermogenesis are inconsistent and the mechanism requires further investigation (24, 30, 33–36).

UCP1-INDEPENDENT THERMOGENIC MECHANISMS IN THERMOGENIC FAT

UCP1 has been thought to be responsible for regulating the energy expenditure and glucose homeostasis of brown and beige fat. The beige fat-deficient adipocyte-specific *Prdm16* KO and adipocyte-specific euchromatic histone-lysine *N*-methyltransferase 1 (EHMT1) KO mice have obese and diabetic phenotypes at room temperature due to insulin resistance (37, 38). However, *Ucp1* KO mice do not have a diabetic phenotype and only develop an obese phenotype under thermoneutral conditions (18, 39). This discrepancy in the metabolic phenotypes of *Ucp1* KO and beige fat-deficient mice

suggests that brown and beige fat have UCP1-independent metabolic mechanisms that contribute to systemic energy and glucose homeostasis.

Many observations support the existence of UCP1-independent metabolic mechanisms. The inguinal WAT of *Ucp1* KO mice maintained in a chronic cold environment showed greater respiration than that of *Ucp1* KO mice maintained under thermoneutrality (30). In addition, chronic β3 adrenergic agonist treatment increased oxygen consumption in the epididymal WAT of *Ucp1* KO mice (20). Recently, creatine-substrate cycling (28, 40, 41) and Ca^{2+} cycling have been identified as UCP1-independent thermogenic pathways.

Creatine-Substrate Cycling

A decline in creatine levels has been linked to the inhibition of thermal responses through unknown mechanisms in rodent models (42, 43). Kazak et al. recently found that creatine substrate cycling stimulates mitochondrial respiration and serves as a thermogenic pathway in thermogenic adipocytes (28, 41). This pathway was discovered in the mitochondria of murine beige fat. Recently, the creatine thermogenic pathway has been suggested to exist in other adipocytes because fat-specific deletion of the creatine synthesis rate-limiting enzyme glycine amidinotransferase (Gatm) reduced creatine levels in BAT and conferred mild cold intolerance (40). Global creatine transporter (*Slc6a8*) KO mice had similar levels of creatine reduction as the adipocyte-specific *Gatm* KO mice, and had an obese phenotype compared to controls (44). Similarly, creatine enzyme *Ckmt1* and *Ckb* double KO mice showed cold intolerance and reduced norepinephrine responses to activate thermogenic respiration (45). These data support the role of the creatine substrate cycling pathway as an adaptive thermogenesis pathway *in vivo*.

UCP1-Independent Thermogenesis: Ca^{2+}-Dependent ATP Hydrolysis in Brown Adipocytes and Muscle

Calcium transport contributes to NST in both BAT and muscle through sarco-endoplasmic reticulum ATPase (SERCA) activity (46–48). In muscle, Ca^{2+} cycling pathways involving SERCA drive thermogenesis such as malignant hyperthermia. Ca^{2+} cycling in the extraocular heater muscle cells of fish suggests the process may be evolutionarily conserved (49, 50).

Sarcolipin (SLN) is a direct peptide-binding SERCA that localizes to the sarcoplasmic reticulum of skeletal muscle. SLN regulates SERCA-mediated ATP turnover in muscle via Ca^{2+} cycling without affecting ATPase activity (51). SLN may function as an uncoupler of calcium transport from ATP hydrolysis via SERCA, which would be elevated in NST (52). The physiological role of SLN in NST is supported by several mouse studies. *Sln* KO animals are mildly cold-intolerant (53). In a mouse model of surgical intrascapular BAT ablation, the removal of BAT was tolerated in the setting of acute cold exposure. By contrast, intrascapular BAT ablation in *Sln* KO mice resulted in cold intolerance, despite the maintenance of skeletal muscle shivering (53). Moreover, *Sln* KO mice fed a HFD had an obese phenotype, whereas mice with muscle-specific transgenic expression of *Sln* fed a HFD had an obesity-resistant phenotype (54, 55). These data support the role of SLN in regulating systemic energy expenditure via calcium uncoupling (53).

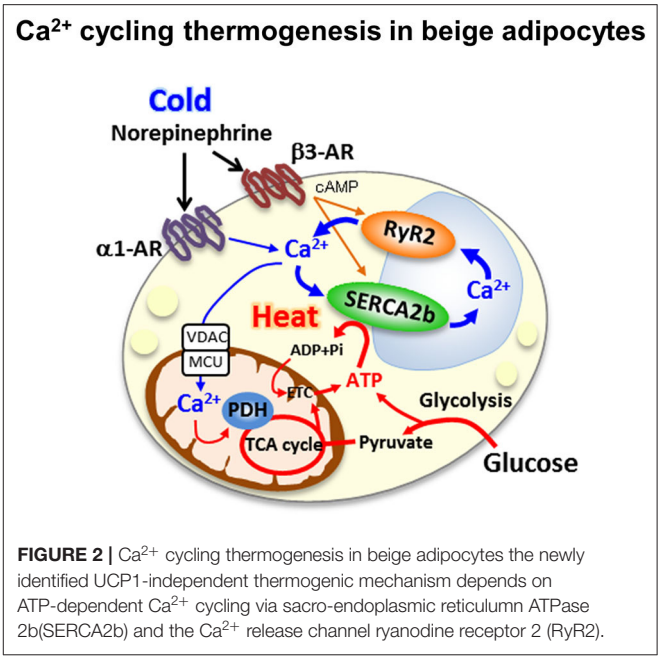

FIGURE 2 | Ca^{2+} cycling thermogenesis in beige adipocytes the newly identified UCP1-independent thermogenic mechanism depends on ATP-dependent Ca^{2+} cycling via sacro-endoplasmic reticulumn ATPase 2b(SERCA2b) and the Ca^{2+} release channel ryanodine receptor 2 (RyR2).

UCP1-Independent Calcium Cycling Thermogenic Mechanisms in Beige Adipocytes

Our recent study revealed a new thermogenic mechanism in beige adipocytes. The newly identified UCP1-independent thermogenic mechanism depends on ATP-dependent Ca^{2+} cycling via SERCA2b and the Ca^{2+} release channel ryanodine receptor 2 (RyR2) (**Figure 2**) (31). Adipocyte-specific *Serca2* KO mice have impaired beige adipocyte thermogenesis. Intriguingly, the SERCA2b-mediated Ca^{2+} cycling thermogenic mechanism is necessary for beige adipocyte thermogenesis, but dispensable in brown adipocytes. The selectivity of this pathway for beige fat relate to the ability of beige adipocytes to produce ATP due to their high expression of ATP synthase. Thus, beige adipocytes can generate heat in an ATP-dependent manner through SERCA2b-mediated Ca^{2+} cycling even in the absence of UCP1. Brown adipocytes express low levels of ATP synthase and cannot produce ATP due to their low ATP synthesis capacity (56).

Furthermore, our study showed that beige fat dramatically contributes to whole-body energy and glucose homeostasis via UCP1-independent metabolic mechanisms. Mice with beige fat-specific overexpression of Prdm16 driven by the aP2 promoter were protected from diet-induced obesity compared to littermate control mice (57). Furthermore, aP2-*Prdm16* transgenic × *Ucp1* KO mice fed a HFD were resistant to obesity, even in the absence of UCP1 (31). Importantly, both aP2-*Prdm16* transgenic mice and aP2-*Prdm16* transgenic × *Ucp1* KO mice showed dramatically better glucose homeostasis on a HFD than mice

with normal *Prdm16* expression. These data strongly support the existence of a UCP1-independent metabolic mechanism in beige fat that contributes to systemic energy and glucose homeostasis. Therefore, Ca^{2+} cycling mediated by SERCA2–RyR2 signaling in beige adipocytes may be a potential therapeutic target for obesity and type 2 diabetes. For example, S107, a pharmacological RyR2 stabilizer that minimizes Ca^{2+} leak from RyR2 and increases Ca^{2+} loading from the endoplasmic reticulum (58), enhances Ca^{2+} cycling thermogenesis. S107 treatment of *Ucp1* KO mice induced resistance to hypothermia upon cold exposure by activating UCP1-independent thermogenesis (31).

Nevertheless, there is concern that activation of Ca^{2+} cycling *in vivo* may have potentially harmful effects on skeletal muscle and the heart. *Ryr1* mutation causes malignant hyperthermia (50), and human *RYR2* gene mutations cause arrhythmogenic right ventricular cardiomyopathy type 2 and lethal arrhythmia due to catecholaminergic polymorphic ventricular tachycardia (59, 60). Given that activating systemic Ca^{2+} cycling may be harmful, it may be promising to activate Ca^{2+} cycling selectively in beige fat to treat obesity and type 2 diabetes while avoiding harmful effects on the muscle and heart.

BEYOND THERMOGENESIS IN THERMOGENIC ADIPOCYTES

Recently, some studies shed light on the physiological function of beige fat to repress adipose tissue fibrosis; these findings are likely to extend beyond thermogenesis (61). Chronic cold-acclimated mice or mice with adipocyte-specific *Prdm16* overexpression markedly repress adipose tissue fibrosis. Of note, this repressive effect was independent of UCP1 and independent of body weight reduction (62). The repression of adipose tissue fibrosis caused notable improvements in systemic glucose homeostasis via a UCP1-independent mechanism (62). Although the findings need to be supported by further work, it appears that beige fat can repress adipose tissue fibrosis and control whole-body glucose homeostasis. Brown and beige fat release several physiological agents, known as "batokines," to control systemic glucose homeostasis (63–66). These data suggest that thermogenic fat has an important physiological function beyond thermogenesis.

DISCUSSION

As thermogenic adipocytes exert multiple thermogenic mechanisms, it will be critical to determine how the regulation of the multiple mechanisms is orchestrated. SLN, a crucial calcium uncoupler, is not expressed in beige adipocytes (31); beige adipocytes must utilize an unknown regulator of the calcium system. Further work is needed to determine the regulator of SERCA2B activity and calcium uncoupler in beige adipocytes.

Brown adipocytes and beige adipocytes have common characteristics, but recent evidence indicates that they have distinct thermogenic mechanisms and functions. Of note, UCP1 is still the main regulator of thermogenesis in BAT, as revealed by numerous studies. However, emerging evidence suggests that beige fat uses UCP1-independent thermogenic pathways, which substantially contribute to systemic energy homeostasis. It will be essential to determine the coordination and contribution of the canonical (UCP1-dependent) and non-canonical (UCP1-independent) thermogenic mechanisms in adipose tissue to whole-body energy homeostasis. In particular, the newly identified UCP1-independent thermogenic pathways creatine substrate cycling and Ca^{2+} cycling should be evaluated as non-canonical mechanisms of thermogenesis.

Intriguingly, Ca^{2+} cycling-related thermogenesis seems to be evolutionarily conserved in humans and mice, and even in species that lack functional UCP1, such as pigs (31). These data suggest that UCP1-independent Ca^{2+} cycling thermogenesis may be the fundamental thermogenic system. Importantly, fibroblast growth factor 21 (FGF21) signaling increases intracellular Ca^{2+} levels in adipocytes (67) and induces browning (68). Recent evidence indicates that the anti-obesity and anti-diabetic activities of FGF21 are UCP1-independent (69, 70). Furthermore, FGF21 and UCP1 are not required for cold environment acclimation in mice (71). These findings suggest that at least some of the metabolic actions of FGF21 are mediated via UCP1-independent thermogenesis in adipose tissue.

It is of high clinical importance to determine the regulator of UCP1-independent thermogenesis because understanding the mechanism may lead to the development of new treatments for obesity and type 2 diabetes. This may be promising for treating obese and elderly populations who do not possess UCP1-positive adipocytes. The current literature suggests that it may be possible to selectively activate UCP1-independent thermogenesis, such as that mediated by Ca^{2+} cycling, to treat patients who lack UCP1-positive adipocytes. New tools such as "designer receptors exclusively activated by designer drugs" (DREADD) and the optogenetic tool channel rhodopsin 2 (ChR2) (72) may modulate intracellular calcium signaling pathways in adipocytes and lead to novel treatments for obesity and type 2 diabetes.

AUTHOR CONTRIBUTIONS

KI and TY wrote the manuscript and edited the manuscript. All authors contributed to the article and approved the submitted version.

FUNDING

This work was supported by AMED under Grant Number JP19gm6210011, *JSPS KAKENHI Gra*nt Number 19K23745 and to KI. KI was supported Boehringer/Lilly Diabetes Research Grant in Japan Diabetes Foundation, The 2020 Inamori Research Grant Program, Kanae Foundation for the Promotion of Medical Science, the Naito Foundation, Ono Medical Research Foundation, Novartis Foundation(Japan) for the Promotion of Science, The Uehara Memorial Foundation, MSD Life Science Foundation, Public Interest Incorporated Foundation, research grant of Astellas Foundation for Research on Metabolic Disorders, Mochida Memorial Foundation for Medical and Pharmaceutical Research, The Ichiro Kanehara Foundation.

REFERENCES

1. Stanford KI, Middelbeek RJ, Goodyear LJ. Exercise effects on white adipose tissue: beiging and metabolic adaptations. *Diabetes.* (2015) 64:2361–8. doi: 10.2337/db15-0227
2. Petruzzelli M, Schweiger M, Schreiber R, Campos-Olivas R, Tsoli M, Allen J, et al. A switch from white to brown fat increases energy expenditure in cancer-associated cachexia. *Cell Metab.* (2014) 20:433–47. doi: 10.1016/j.cmet.2014.06.011
3. van Marken Lichtenbelt WD, Vanhommerig JW, Smulders NM, Drossaerts JM, Kemerink GJ, Bouvy ND, et al. Cold-activated brown adipose tissue in healthy men. *N Engl J Med.* (2009) 360:1500–8. doi: 10.1056/NEJMoa0808718
4. Saito M, Okamatsu-Ogura Y, Matsushita M, Watanabe K, Yoneshiro T, Nio-Kobayashi J, et al. High incidence of metabolically active brown adipose tissue in healthy adult humans: effects of cold exposure and adiposity. *Diabetes.* (2009) 58:1526–31. doi: 10.2337/db09-0530
5. Cypess AM, Lehman S, Williams G, Tal I, Rodman D, Goldfine AB, et al. Identification and importance of brown adipose tissue in adult humans. *N Engl J Med.* (2009) 360:1509–17. doi: 10.1056/NEJMoa0810780
6. Virtanen KA, Lidell ME, Orava J, Heglind M, Westergren R, Niemi T, et al. Functional brown adipose tissue in healthy adults. *N Engl J Med.* (2009) 360:1518–25. doi: 10.1056/NEJMoa0808949
7. Nedergaard J, Bengtsson T, Cannon B. Unexpected evidence for active brown adipose tissue in adult humans. *Am J Phys Endocrinol Metab.* (2007) 293:E444–52. doi: 10.1152/ajpendo.00691.2006
8. Lidell ME, Betz MJ, Dahlqvist Leinhard O, Heglind M, Elander L, Slawik M, et al. Evidence for two types of brown adipose tissue in humans. *Nat Med.* (2013) 19:631–4. doi: 10.1038/nm.3017
9. Wu J, Bostrom P, Sparks LM, Ye L, Choi JH, Giang AH, et al. Beige adipocytes are a distinct type of thermogenic fat cell in mouse and human. *Cell.* (2012) 150:366–76. doi: 10.1016/j.cell.2012.05.016
10. Sharp LZ, Shinoda K, Ohno H, Scheel DW, Tomoda E, Ruiz L, et al. Human BAT possesses molecular signatures that resemble beige/brite cells. *PLoS ONE.* (2012) 7:e49452. doi: 10.1371/journal.pone.0049452
11. Cypess AM, White AP, Vernochet C, Schulz TJ, Xue R, Sass CA, et al. Anatomical localization, gene expression profiling and functional characterization of adult human neck brown fat. *Nat Med.* (2013) 19:635–9. doi: 10.1038/nm.3112
12. Shinoda K, Luijten IH, Hasegawa Y, Hong H, Sonne SB, Kim M, et al. Genetic and functional characterization of clonally derived adult human brown adipocytes. *Nat Med.* (2015) 21:389–94. doi: 10.1038/nm.3819
13. Lee P, Smith S, Linderman J, Courville AB, Brychta RJ, Dieckmann W, et al. Temperature-acclimated brown adipose tissue modulates insulin sensitivity in humans. *Diabetes.* (2014) 63:3686–98. doi: 10.2337/db14-0513
14. van der Lans AA, Hoeks J, Brans B, Vijgen GH, Visser MG, Vosselman MJ, et al. Cold acclimation recruits human brown fat and increases nonshivering thermogenesis. *J Clin Invest.* (2013) 123:3395–403. doi: 10.1172/JCI68993
15. Yoneshiro T, Aita S, Matsushita M, Kayahara T, Kameya T, Kawai Y, et al. Recruited brown adipose tissue as an antiobesity agent in humans. *J Clin Invest.* (2013) 123:3404–8. doi: 10.1172/JCI67803
16. Hanssen MJ, Hoeks J, Brans B, van der Lans AA, Schaart G, van den Driessche JJ, et al. Short-term cold acclimation improves insulin sensitivity in patients with type 2 diabetes mellitus. *Nat Med.* (2015) 21:863–5. doi: 10.1038/nm.3891
17. Leitner BP, Huang S, Brychta RJ, Duckworth CJ, Baskin AS, McGehee S, et al. Mapping of human brown adipose tissue in lean and obese young men. *Proc Natl Acad Sci USA.* (2017) 114:8649–54. doi: 10.1073/pnas.1705287114
18. Enerback S, Jacobsson A, Simpson EM, Guerra C, Yamashita H, Harper ME, et al. Mice lacking mitochondrial uncoupling protein are cold-sensitive but not obese. *Nature.* (1997) 387:90–4. doi: 10.1038/387090a0
19. Lowell BB, V SS, Hamann A, Lawitts JA, Himms-Hagen J, Boyer BB, et al. Development of obesity in transgenic mice after genetic ablation of brown adipose tissue. *Nature.* (1993) 366:740–2. doi: 10.1038/366740a0
20. Granneman JG, Burnazi M, Zhu Z, Schwamb LA. White adipose tissue contributes to UCP1-independent thermogenesis. *Am J Physiol Endocrinol Metab.* (2003) 285:E1230–6. doi: 10.1152/ajpendo.00197.2003
21. Li Y, Fromme T, Schweizer S, Schottl T, Klingenspor M. Taking control over intracellular fatty acid levels is essential for the analysis of thermogenic function in cultured primary brown and brite/beige adipocytes. *EMBO Rep.* (2014) 15:1069–76. doi: 10.15252/embr.201438775
22. Schreiber R, Diwoky C, Schoiswohl G, Feiler U, Wongsiriroj N, Abdellatif M, et al. Cold-induced thermogenesis depends on ATGL-mediated lipolysis in cardiac muscle, but not brown adipose tissue. *Cell Metab.* (2017) 26:753–63 e7. doi: 10.1016/j.cmet.2017.09.004
23. Shin H, Ma Y, Chanturiya T, Cao Q, Wang Y, Kadegowda AKG, et al. Lipolysis in brown adipocytes is not essential for cold-induced thermogenesis in mice. *Cell Metab.* (2017) 26:764–77 e5. doi: 10.1016/j.cmet.2017.09.002
24. Golozoubova V, Hohtola E, Matthias A, Jacobsson A, Cannon B, Nedergaard J. Only UCP1 can mediate adaptive nonshivering thermogenesis in the cold. *FASEB J.* (2001) 15:2048–50. doi: 10.1096/fj.00-0536fje
25. Nedergaard J, Golozoubova V, Matthias A, Asadi A, Jacobsson A, Cannon B. UCP1: the only protein able to mediate adaptive non-shivering thermogenesis and metabolic inefficiency. *Biochim Biophys Acta.* (2001) 1504:82–106. doi: 10.1016/S0005-2728(00)00247-4
26. Hofmann WE, Liu X, Bearden CM, Harper ME, Kozak LP. Effects of genetic background on thermoregulation and fatty acid-induced uncoupling of mitochondria in UCP1-deficient mice. *J Biol Chem.* (2001) 276:12460–5. doi: 10.1074/jbc.M100466200
27. Golozoubova V, Cannon B, Nedergaard J. UCP1 is essential for adaptive adrenergic nonshivering thermogenesis. *Am J Physiol Endocrinol Metab.* (2006) 291:E350–7. doi: 10.1152/ajpendo.00387.2005
28. Kazak L, Chouchani ET, Jedrychowski MP, Erickson BK, Shinoda K, Cohen P, et al. A creatine-driven substrate cycle enhances energy expenditure and thermogenesis in beige fat. *Cell.* (2015) 163:643–55. doi: 10.1016/j.cell.2015.09.035
29. Keipert S, Kutschke M, Lamp D, Brachthauser L, Neff F, Meyer CW, et al. Genetic disruption of uncoupling protein 1 in mice renders brown adipose tissue a significant source of FGF21 secretion. *Mol Metab.* (2015) 4:537–42. doi: 10.1016/j.molmet.2015.04.006
30. Ukropec J, Anunciado RP, Ravussin Y, Hulver MW, Kozak LP. UCP1-independent thermogenesis in white adipose tissue of cold-acclimated Ucp1-/- mice. *J Biol Chem.* (2006) 281:31894–908. doi: 10.1074/jbc.M606114200
31. Ikeda K, Kang Q, Yoneshiro T, Camporez JP, Maki H, Homma M, et al. UCP1-independent signaling involving SERCA2b-mediated calcium cycling regulates beige fat thermogenesis and systemic glucose homeostasis. *Nat Med.* (2017) 23:1454–65. doi: 10.1038/nm.4429
32. Liu X, Rossmeisl M, McClaine J, Riachi M, Harper ME, Kozak LP. Paradoxical resistance to diet-induced obesity in UCP1-deficient mice. *J Clin Invest.* (2003) 111:399–407. doi: 10.1172/JCI200315737
33. Meyer CW, Willershauser M, Jastroch M, Rourke BC, Fromme T, Oelkrug R, et al. Adaptive thermogenesis and thermal conductance in wild-type and UCP1-KO mice. *Am J Physiol Regul Integr Comp Physiol.* (2010) 299:R1396–406. doi: 10.1152/ajpregu.00021.2009
34. Mineo PM, Cassell EA, Roberts ME, Schaeffer PJ. Chronic cold acclimation increases thermogenic capacity, non-shivering thermogenesis and muscle citrate synthase activity in both wild-type and brown adipose tissue deficient mice. *Comp Biochem Physiol A, Mol Integr Physiol.* (2012) 161:395–400. doi: 10.1016/j.cbpa.2011.12.012
35. Monemdjou S, Hofmann WE, Kozak LP, Harper ME. Increased mitochondrial proton leak in skeletal muscle mitochondria of UCP1-deficient mice. *Am J Physiol Endocrinol Metab.* (2000) 279:E941–6. doi: 10.1152/ajpendo.2000.279.4.E941
36. Shabalina IG, Hoeks J, Kramarova TV, Schrauwen P, Cannon B, Nedergaard J. Cold tolerance of UCP1-ablated mice: a skeletal muscle mitochondria switch toward lipid oxidation with marked UCP3 up-regulation not associated with increased basal, fatty acid- or ROS-induced uncoupling or enhanced GDP effects. *Biochim Biophys Acta.* (2010) 1797:968–80. doi: 10.1016/j.bbabio.2010.02.033
37. Ohno H, Shinoda K, Ohyama K, Sharp LZ, Kajimura S. EHMT1 controls brown adipose cell fate and thermogenesis through the PRDM16 complex. *Nature.* (2013) 504:163–7. doi: 10.1038/nature12652
38. Cohen P, Levy JD, Zhang Y, Frontini A, Kolodin DP, Svensson KJ, et al. Ablation of PRDM16 and beige adipose causes metabolic dysfunction and a subcutaneous to visceral fat switch. *Cell.* (2014) 156:304–16. doi: 10.1016/j.cell.2013.12.021

39. Feldmann HM, Golozoubova V, Cannon B, Nedergaard J. UCP1 ablation induces obesity and abolishes diet-induced thermogenesis in mice exempt from thermal stress by living at thermoneutrality. *Cell Metab.* (2009) 9:203–9. doi: 10.1016/j.cmet.2008.12.014
40. Kazak L, Chouchani ET, Lu GZ, Jedrychowski MP, Bare CJ, Mina AI, et al. Genetic depletion of adipocyte creatine metabolism inhibits diet-induced thermogenesis and drives obesity. *Cell Metab.* (2017) 26:693. doi: 10.1016/j.cmet.2017.09.007
41. Bertholet AM, Kazak L, Chouchani ET, Bogaczynska MG, Paranjpe I, Wainwright GL, et al. Mitochondrial patch clamp of beige adipocytes reveals UCP1-positive and UCP1-negative cells both exhibiting futile creatine cycling. *Cell Metab.* (2017) 25:811–22.e4. doi: 10.1016/j.cmet.2017.03.002
42. Wakatsuki T, Hirata F, Ohno H, Yamamoto M, Sato Y, Ohira Y. Thermogenic responses to high-energy phosphate contents and/or hindlimb suspension in rats. *Japan J Physiol.* (1996) 46:171–5. doi: 10.2170/jjphysiol.46.171
43. Yamashita H, Ohira Y, Wakatsuki T, Yamamoto M, Kizaki T, Oh-ishi S, et al. Increased growth of brown adipose tissue but its reduced thermogenic activity in creatine-depleted rats fed beta-guanidinopropionic acid. *Biochim Biophys Acta.* (1995) 1230:69–73. doi: 10.1016/0005-2728(95)00067-S
44. Perna MK, Kokenge AN, Miles KN, Udobi KC, Clark JF, Pyne-Geithman GJ, et al. Creatine transporter deficiency leads to increased whole body and cellular metabolism. *Amino acids.* (2016) 48:2057–65. doi: 10.1007/s00726-016-2291-3
45. Streijger F, Pluk H, Oerlemans F, Beckers G, Bianco AC, Ribeiro MO, et al. Mice lacking brain-type creatine kinase activity show defective thermoregulation. *Physiol Behav.* (2009) 97:76–86. doi: 10.1016/j.physbeh.2009.02.003
46. de Meis L. Brown adipose tissue Ca2+-ATPase: uncoupled ATP hydrolysis and thermogenic activity. *J Biol Chem.* (2003) 278:41856–61. doi: 10.1074/jbc.M308280200
47. de Meis L, Arruda AP, da Costa RM, Benchimol M. Identification of a Ca2+-ATPase in brown adipose tissue mitochondria: regulation of thermogenesis by ATP and Ca2+. *J Biol Chem.* (2006) 281:16384–90. doi: 10.1074/jbc.M600678200
48. Periasamy M, Maurya SK, Sahoo SK, Singh S, Sahoo SK, Reis FCG, et al. Role of SERCA pump in muscle thermogenesis and metabolism. *Compreh Physiol.* (2017) 7:879–90. doi: 10.1002/cphy.c160030
49. Block BA. Thermogenesis in muscle. *Annu Rev Physiol.* (1994) 56:535–77. doi: 10.1146/annurev.ph.56.030194.002535
50. Rosenberg H, Pollock N, Schiemann A, Bulger T, Stowell K. Malignant hyperthermia: a review. *Orphanet J Rare Dis.* (2015) 10:93. doi: 10.1186/s13023-015-0310-1
51. Smith WS, Broadbridge R, East JM, Lee AG. Sarcolipin uncouples hydrolysis of ATP from accumulation of Ca2+ by the Ca2+-ATPase of skeletal-muscle sarcoplasmic reticulum. *Biochem J.* (2002) 361(Pt 2):277–86. doi: 10.1042/bj3610277
52. Sahoo SK, Shaikh SA, Sopariwala DH, Bal NC, Periasamy M. Sarcolipin protein interaction with sarco(endo)plasmic reticulum Ca2+ ATPase (SERCA) is distinct from phospholamban protein, and only sarcolipin can promote uncoupling of the SERCA pump. *J Biol Chem.* (2013) 288:6881–9. doi: 10.1074/jbc.M112.436915
53. Bal NC, Maurya SK, Sopariwala DH, Sahoo SK, Gupta SC, Shaikh SA, et al. Sarcolipin is a newly identified regulator of muscle-based thermogenesis in mammals. *Nat Med.* (2012) 18:1575–9. doi: 10.1038/nm.2897
54. Rowland LA, Maurya SK, Bal NC, Kozak L, Periasamy M. Sarcolipin and uncoupling protein 1 play distinct roles in diet-induced thermogenesis and do not compensate for one another. *Obesity (Silver Spring).* (2016) 24:1430–3. doi: 10.1002/oby.21542
55. Maurya SK, Bal NC, Sopariwala DH, Pant M, Rowland LA, Shaikh SA, et al. Sarcolipin is a key determinant of the basal metabolic rate, and its overexpression enhances energy expenditure and resistance against diet-induced obesity. *J Biol Chem.* (2015) 290:10840–9. doi: 10.1074/jbc.M115.636878
56. Kramarova TV, Shabalina IG, Andersson U, Westerberg R, Carlberg I, Houstek J, et al. Mitochondrial ATP synthase levels in brown adipose tissue are governed by the c-Fo subunit P1 isoform. *FASEB J.* (2008) 22:55–63. doi: 10.1096/fj.07-8581com
57. Seale P, Conroe HM, Estall J, Kajimura S, Frontini A, Ishibashi J, et al. Prdm16 determines the thermogenic program of subcutaneous white adipose tissue in mice. *J Clin Invest.* (2011) 121:96–105. doi: 10.1172/JCI44271
58. Andersson DC, Marks AR. Fixing ryanodine receptor Ca leak - a novel therapeutic strategy for contractile failure in heart and skeletal muscle. *Drug Disc Today Dis Mech.* (2010) 7:e151–e7. doi: 10.1016/j.ddmec.2010.09.009
59. Tiso N, Stephan DA, Nava A, Bagattin A, Devaney JM, Stanchi F, et al. Identification of mutations in the cardiac ryanodine receptor gene in families affected with arrhythmogenic right ventricular cardiomyopathy type 2 (ARVD2). *Hum Mol Genet.* (2001) 10:189–94. doi: 10.1093/hmg/10.3.189
60. Marks AR, Priori S, Memmi M, Kontula K, Laitinen PJ. Involvement of the cardiac ryanodine receptor/calcium release channel in catecholaminergic polymorphic ventricular tachycardia. *J Cell Physiol.* (2002) 190:1–6. doi: 10.1002/jcp.10031
61. Kajimura S, Spiegelman BM, Seale P. Brown and beige fat: physiological roles beyond heat generation. *Cell Metab.* (2015) 22:546–59. doi: 10.1016/j.cmet.2015.09.007
62. Hasegawa Y, Ikeda K, Chen Y, Alba DL, Stifler D, Shinoda K, et al. Repression of adipose tissue fibrosis through a PRDM16-GTF2IRD1 complex improves systemic glucose homeostasis. *Cell Metab.* (2018) 27:180–94 e6. doi: 10.1016/j.cmet.2017.12.005
63. Svensson KJ, Long JZ, Jedrychowski MP, Cohen P, Lo JC, Serag S, et al. A secreted Slit2 fragment regulates adipose tissue thermogenesis and metabolic function. *Cell Metab.* (2016) 23:454–66. doi: 10.1016/j.cmet.2016.01.008
64. Long JZ, Svensson KJ, Bateman LA, Lin H, Kamenecka T, Lokurkar IA, et al. The secreted enzyme PM20D1 regulates lipidated amino acid uncouplers of Mitochondria. *Cell.* (2016) 166:424–35. doi: 10.1016/j.cell.2016.05.071
65. Wang GX, Zhao XY, Meng ZX, Kern M, Dietrich A, Chen Z, et al. The brown fat-enriched secreted factor Nrg4 preserves metabolic homeostasis through attenuation of hepatic lipogenesis. *Nat Med.* (2014) 20:1436–43. doi: 10.1038/nm.3713
66. Leiria LO, Wang CH, Lynes MD, Yang K, Shamsi F, Sato M, et al. 12-lipoxygenase regulates cold adaptation and glucose metabolism by producing the omega-3 lipid 12-HEPE from brown fat. *Cell Metab.* (2019). 30:768–83 e7. doi: 10.1016/j.cmet.2019.07.001
67. Moyers JS, Shiyanova TL, Mehrbod F, Dunbar JD, Noblitt TW, Otto KA, et al. Molecular determinants of FGF-21 activity-synergy and cross-talk with PPARgamma signaling. *J Cell Physiol.* (2007) 210:1–6. doi: 10.1002/jcp.20847
68. Fisher FM, Kleiner S, Douris N, Fox EC, Mepani RJ, Verdeguer F, et al. FGF21 regulates PGC-1alpha and browning of white adipose tissues in adaptive thermogenesis. *Genes Dev.* (2012) 26:271–81. doi: 10.1101/gad.177857.111
69. Veniant MM, Sivits G, Helmering J, Komorowski R, Lee J, Fan W, et al. Pharmacologic effects of FGF21 are independent of the "browning" of white adipose tissue. *Cell Metab.* (2015) 21:731–8. doi: 10.1016/j.cmet.2015.04.019
70. Samms RJ, Smith DP, Cheng CC, Antonellis PP, Perfield JW, 2nd, Kharitonenkov A, et al. Discrete aspects of FGF21 in vivo pharmacology do not require UCP1. *Cell Rep.* (2015) 11:991–9. doi: 10.1016/j.celrep.2015.04.046
71. Keipert S, Kutschke M, Ost M, Schwarzmayr T, van Schothorst EM, Lamp D, et al. Long-term cold adaptation does not require FGF21 or UCP1. *Cell Metab.* (2017) 26:437–46.e5. doi: 10.1016/j.cmet.2017.07.016
72. Tajima K, Ikeda K, Tanabe Y, Thomson EA, Yoneshiro T, Oguri Y, et al. Wireless optogenetics protects against obesity via stimulation of non-canonical fat thermogenesis. *Nat Commun.* (2020) 11:1730. doi: 10.1038/s41467-020-15589-y

Conflict of Interest: The authors declare that the research was conducted in the absence of any commercial or financial relationships that could be construed as a potential conflict of interest.

frontiers in Endocrinology

REVIEW
published: 07 August 2020
doi: 10.3389/fendo.2020.00421

Magnetic Resonance Imaging Techniques for Brown Adipose Tissue Detection

Mingming Wu[1], Daniela Junker[1], Rosa Tamara Branca[2†] and Dimitrios C. Karampinos[1†]*

[1] Department of Diagnostic and Interventional Radiology, School of Medicine, Technical University of Munich, Munich, Germany, [2] Department of Physics and Astronomy, University of North Carolina at Chapel Hill, Chapel Hill, NC, United States

Magnetic resonance imaging (MRI) and magnetic resonance spectroscopy (MRS) methods can non-invasively assess brown adipose tissue (BAT) structure and function. Recently, MRI and MRS have been proposed as a means to differentiate BAT from white adipose tissue (WAT) and to extract morphological and functional information on BAT inaccessible by other means. Specifically, proton MR (^{1}H) techniques, such as proton density fat fraction mapping, diffusion imaging, and intermolecular multiple quantum coherence imaging, have been employed to access BAT microstructure; MR thermometry, relaxometry, and MRI and MRS with ^{31}P, ^{2}H, ^{13}C, and ^{129}Xe have shown to provide complementary information on BAT function. The purpose of the present review is to provide a comprehensive overview of MR imaging and spectroscopy techniques used to detect BAT in rodents and in humans. The present work discusses common challenges of current methods and provides an outlook on possible future directions of using MRI and MRS in BAT studies.

Keywords: brown adipose tissue (BAT), white adipose tissue (WAT), magnetic resonance imaging, magnetic resonance spectroscopy, morphology, activation, thermogenesis

OPEN ACCESS

Edited by:
Takeshi Yoneshiro, The University of Tokyo, Japan

Reviewed by:
Takafumi Hamaoka, Tokyo Medical University, Japan
Valeria Guglielmi, University of Rome Tor Vergata, Italy

****Correspondence:***
Mingming Wu
mingming.wu@tum.de

† These authors share senior authorship

Specialty section:
This article was submitted to Obesity, a section of the journal Frontiers in Endocrinology

Received: *05 March 2020*
Accepted: *27 May 2020*
Published: *07 August 2020*

Citation:
Wu M, Junker D, Branca RT and Karampinos DC (2020) Magnetic Resonance Imaging Techniques for Brown Adipose Tissue Detection. Front. Endocrinol. 11:421. doi: 10.3389/fendo.2020.00421

INTRODUCTION

Role of Biomedical Imaging in BAT Research

Even though the presence of brown adipose tissue (BAT) in human adults had been reported back in 1972 (1), its relevance in adult humans has largely been neglected by the scientific and medical community until 2009.

In vivo detection of BAT activity in fluorine-18 fluorodeoxyglucose (^{18}F-FDG) positron emission tomography (PET) scans dates back to 1996 (2). However, only in 2002 co-registered PET and computed tomography (CT) images allowed to recognize that the increased symmetrical ^{18}F-FDG uptake seen in the cervical and thoracic spine region of cancer patients, initially attributed to muscular uptake, was due to activated BAT (3). Initially seen as nuisance, the detection of active BAT in adult humans sparked a scientific curiosity only after 2009, when three simultaneous publications in the *New England Journal of Medicine* (4–6) reported that the glucose-avid adipose tissue detected in adult humans on PET/CT scans had been confirmed to be BAT by adipose tissue biopsies and molecular biology analyses (4–6).

In the last 10 years, a variety of imaging techniques have been deployed to detect and understand the role of BAT in humans. While for ethical reasons biopsies of human BAT have been limited to mostly cadavers or tissues excised as part of oncological procedures (7), biomedical imaging techniques have enabled us to study the morphology and function of this tissue *in vivo*.

Tomographic imaging techniques such as PET, CT, and magnetic resonance imaging (MRI) have enabled the detection of BAT in both rodents and humans, while providing spatially resolved information on its morphology and functional properties. The large amount of ongoing studies and recent publications involving biomedical imaging of BAT speaks both for the vast interest in BAT research and for the importance of high-quality non-invasive imaging.

The present review introduces briefly the main imaging modalities used to research BAT in rodents and humans. Then, it focuses on current MR methods that have shown to provide both morphological and functional information on BAT. The underlying properties and limitations of MR techniques applied in BAT research are also discussed in a comprehensive way. Finally, an outlook on possible future directions is provided.

Biomedical Imaging Modalities for BAT Research

An overview of the different imaging modalities in BAT research is given in **Table 1**.

Since 2009, most BAT imaging studies have used ^{18}F-FDG-PET to identify activated BAT in humans (8), despite its many known limitations (9): First, the exposure to ionizing radiation is a major concern when applying PET for studying BAT, especially for longitudinal studies in healthy, young, or pediatric populations. Second, fatty acids hydrolyzed from intracellular triglycerides, not glucose, are the main substrates for BAT oxidative metabolism (10). Because in BAT, glucose is used mainly for *de novo* lipogenesis, which is highly dependent on intracellular lipid content, glucose uptake in BAT may not always reflect its thermogenic activity (11). Therefore, the underlying assumption that glucose uptake reflects the thermogenic activity of the tissue has recently been questioned (12, 13). While fatty acid tracers would be a better probe of BAT thermogenesis, competition between exogenous fatty acid tracers and intracellular fatty acids released from intracellular triglycerides practically leads to little contrast between BAT and white adipose tissue (WAT) (14). Finally, while some radiotracers may not rely on BAT activation (15) for BAT detection, the most commonly used radiotracer, ^{18}F-FDG, does rely on BAT activation. Specifically, inactive BAT will not be identified in ^{18}F-FDG PET scans, while different degrees of BAT activation, coupled with the poor test–retest reliability of FDG PET/CT in measuring BAT glucose metabolism (16), is expected to lead to a great variation in estimates of BAT volumes, from as low as 10 ml (17) to as much as 650 ml (18).

Because of its low anatomical spatial resolution, PET is usually combined with either CT (PET/CT) or MRI (PET/MRI). In PET/CT, metabolically active BAT is identified as a tissue with a radiodensity between −100 and −30 Hounsfield units (HU) on the CT images (19). During activation, a further increase in tissue radiodensity of about 10 HU can be observed in supraclavicular regions known to contain BAT (20). However, due to the broad overlap of HU values between BAT and WAT, it remains nearly impossible to differentiate BAT from WAT solely based on a single CT measurement. Dual-energy CT (DECT) offers the possibility to measure tissue attenuation at two different energies, and it has been suggested as a way to differentiate BAT from the less hydrated WAT (21). However, radiation exposure associated with CT examinations makes longitudinal CT examinations in healthy volunteers unfeasible.

Small studies in mice and humans have also investigated the use of contrast-enhanced ultrasound (CEUS) for BAT detection (22, 23). During adrenergic stimulation in mice and cold activation in humans, an increase in BAT blood flow was detected by CEUS. The low cost of US is attractive for the investigation of BAT activation, especially when searching for BAT-targeted therapies. However, in obese subjects, tissue hypertrophy leads to a reduction in tissue vascular density as well as to a reduction in tissue blood flow (24). Since BAT detection and differentiation from WAT with CEUS is based on the higher vascular density of BAT and on the increase in tissue blood flow during stimulation, it is expected to be less effective in animal models of obesity or in obese subjects.

Optical techniques are an emerging tool for BAT imaging, especially in rodents. It has been shown that Cerenkov luminescence imaging (CLI) with ^{18}F-FDG can be used to optically image BAT in small animals (25). Even though cheaper and faster than PET, CLI again comes with the need for radiotracer injection. Near-infrared time-resolved spectroscopy (NIR_{TRS}) has also been used in humans to provide separate independent information on tissue absorption and scattering of BAT. Specifically, a significant correlation was found between ^{18}F-FDG-PET standardized uptake values (SUV) of BAT activity and tissue scattering properties in the supraclavicular region, potentially related to oxy- and deoxy-hemoglobin concentration in the tissue (26). However, these measurements reflect tissue distribution and content in the entire region of interest, including skin, muscle, and subcutaneous WAT that can be present in the region, making the interpretation of the results a challenge. NIR fluorescence imaging allows quantitation of BAT perfusion and thus provides an indirect measurement of BAT activity. The requirement of a fluorescent dye, however, precludes its use in humans (27). Real-time sensing of hemoglobin by multispectral optoacoustic tomography (MSOT) was recently described as a label-free non-invasive imaging tool of BAT activation that enables longitudinal measurements in individual subjects (28).

Abbreviations: ADC, apparent diffusion coefficient; ASL, arterial spin labeling; BAT, brown adipose tissue; BOLD, blood oxygenation level dependent; CEUS, contrast-enhanced ultrasound; CLI, Cerenkov luminescence imaging; CT, computed tomography; DCE-MRI, dynamic contrast-enhanced magnetic resonance imaging; DECT, dual-energy CT; DMI, deuterium metabolic imaging; DWI, diffusion-weighted imaging; DW-MRS, diffusion-weighted magnetic resonance spectroscopy; ^{18}F-FDG, fluorine-18 fluorodeoxyglucose; fMRI, functional magnetic resonance imaging; HP, hyperpolarized; HU, Hounsfield units; iBAT, interscapular BAT; iMQC, intermolecular multiple quantum coherence; iZQC, intermolecular zero quantum coherence; MION, monocrystalline iron oxide nanoparticles; MRI, magnetic resonance imaging; MRS, magnetic resonance spectroscopy; MSOT, multispectral optoacoustic tomography; NIR_{TRS}, near-infrared time-resolved spectroscopy; PDFF, proton density fat fraction; PET, positron emission tomography; PRFS, proton resonance frequency shift; QSM, quantitative susceptibility mapping; SNR, signal-to-noise ratio; SPION, superparamagnetic iron oxide nanoparticles; SUV, standardized uptake values; TE, echo time; TR, repetition time; TRL-^{59}FE-SPIO, triglyceride-rich lipoprotein-^{59}FE-SPIOs; UCP-1, uncoupling protein-1; WAT, white adipose tissue; ZSI, Z-spectrum imaging.

TABLE 1 | Comparison of the different imaging modalities (including strengths and weaknesses).

	Free of ionizing radiation	Free of injections	Independence on current BAT- activity	Quantitative imaging possible	Spatial resolution	3D possible	Penetration depth	Required scan time	Costs for hardware
PET✦	✗	✗	(✗, ✓) radiotracer dependent	(✓)	Low >1 mm^3	✓	Unlimited	Long	High
CT✦	✗	✓	✓ HU is hydration-dependent	✓	Medium <1 mm^3	✓	Unlimited	Short (seconds)	Medium
CEUS✦	✓	✗	✗	(✓)	Medium <1 mm^3	✗	Limited	Short	Low (~10.000 USD)
Optical techniques	✓	(✗)	(✗)	✓	High <<1 mm^3	✗	Low	Short	Low
MRI✦	✓	(✓, ✗)	✓	✓	Medium ~1 mm^3	✓	Unlimited	Long (minutes)	High (~1 Mio USD per Tesla)

Techniques that the co-authors have experience with are marked with a✦. ✗ means no and ✓ stands for yes. The parentheses indicate that the statement is true only under certain circumstances.

However, MSOT only renders cross-sectional images. Thus, volumetric quantification of BAT mass can become challenging. Furthermore, by using light as a probe, MSOT as any other optical imaging technique has a limited penetration depth (2–5 cm), which can be a challenge for its adoption in humans or for the detection of BAT in overweight and obese individuals.

MRI for BAT Research

MRI provides superior tissue contrast and adequate spatial resolution when compared to other tomographic imaging techniques. Contrast in MR images is determined by the chemical composition and microstructure of the tissue of interest, which directly affect frequency, density, diffusion, and relaxation properties of the detected nuclear spins. By careful design of the MR pulse sequence, one property can be emphasized over another. Therefore, one could imagine to leverage on the MR-detectable endogenous differences between WAT and BAT to differentiate these two tissues. By virtue of being radiation-free, MR can be safely used in longitudinal studies in human subjects of all age groups, aiming at understanding how BAT evolves over the course of a lifetime.

MR methodologies for studying BAT and applications of MRI techniques for probing BAT in health and disease have been previously summarized in publications reviewing the use of different imaging modalities in BAT research (9, 21, 29–36). Some of the MRI techniques used to detect BAT have also been reviewed as part of techniques used for the non-invasive assessment of different fat and adipose tissue depots (37, 38). However, only two review papers have focused entirely on MRI techniques used to detect BAT in the research setting (39, 40). The present work aims at a more comprehensive and updated review of the state-of-the-art MR techniques and applications for BAT research.

An electronic search in PubMed (http://www.ncbi.nlm.nih.gov/pubmed) was performed without a starting date up to February 2020 using as search terms "brown adipose tissue" and one of the following terms: "Magnetic Resonance Imaging" or "Magnetic Resonance Spectroscopy." The search results included investigations in rodents and/or in humans. The reference lists of relevant articles were also screened.

The following sections include a critical assessment of current MR techniques used to detect BAT, most of which have been used by the co-authors of the present review.

Overview of MR Contrast Mechanisms for BAT Detection

MR can differentiate BAT from WAT based on morphological (**Figure 1A**) and functional (**Figure 1B**) differences between these two tissues. Differentiation based on morphological differences is advantageous because it does not require stimulation and activation of the tissue. Morphologically, the presence of multiple, smaller lipid droplets in BAT adipocytes makes this tissue more hydrated than WAT. Differences in tissue hydration can be measured by fat fraction mapping techniques. Furthermore, BAT is highly vascularized and brown adipocytes have numerous iron-rich mitochondria (**Figures 2**, **3**), which are responsible for the brown color of the tissue under natural light. Both the presence of iron at the inner mitochondria membrane and magnetic susceptibility gradients generated at the many water–fat interfaces lead to a rapid signal dephasing. This effect is clearly visible in T_2*-weighted as well as T_2-weighted images, in which BAT appears darker than WAT. Microstructural differences between white and brown adipocytes translate in differences in diffusion properties of both water and fat spins in these two tissues. Because the inner mitochondrial membrane is not permeable to water, water diffusion inside and outside the mitochondria wall is greatly restricted. Restricted water diffusion is reflected in a smaller apparent diffusion coefficient (ADC) that can be measured by diffusion-weighted MRI. Similarly, because lipids are confined in smaller lipid droplets in BAT, diffusion of lipid molecules in BAT is also more restricted. A smaller fat ADC can be measured in BAT compared to WAT by diffusion-weighted MRI/MRS.

BAT activation leads to a change of many MR tissue properties (**Figure 1B**). After cold exposure or food intake, thermogenic

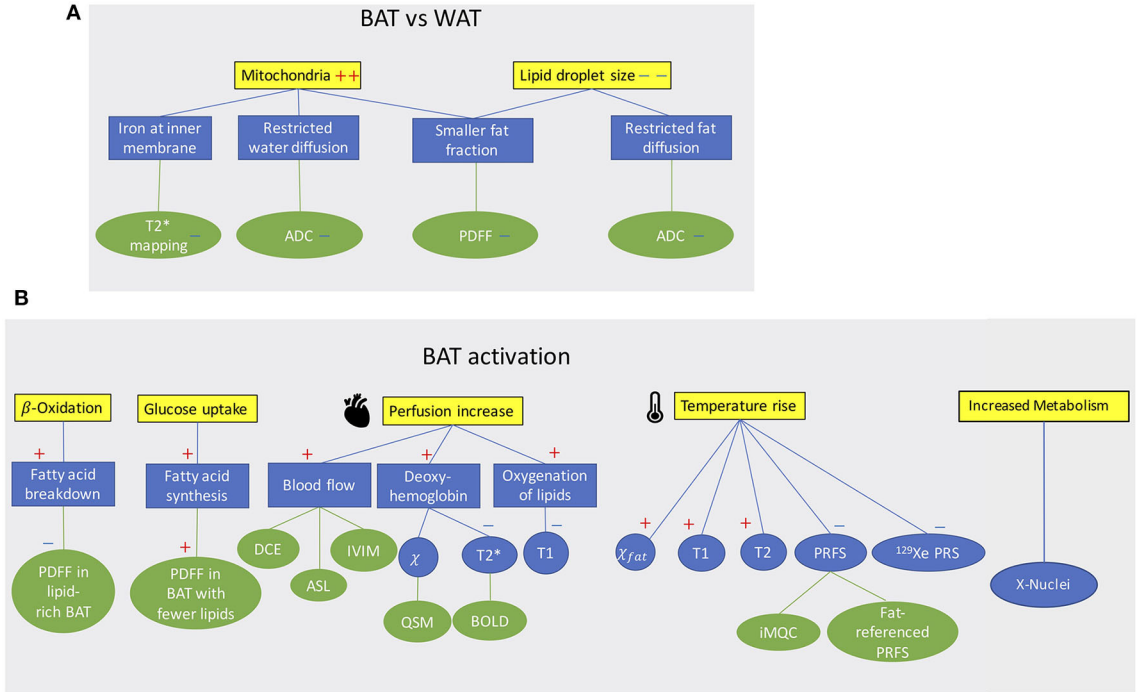

FIGURE 1 | (A) Conceptual schematic highlighting morphological differences between BAT and WAT detectable with MR contrast. **(B)** Conceptual schematic of MR contrast mechanisms for detecting BAT function. A "+" sign indicates an increase a "–" sign indicates a decrease.

FIGURE 2 | Schematic showing morphological differences between BAT and WAT cells. BAT is composed of adipocytes much smaller in size than white adipocytes, and with a cytoplasm occupied by multiple small lipid droplets (multilocular adipocytes), often of less than few micrometers in diameter, distributed uniformly throughout the entire depot. As a result, compared to classical white adipose tissue, where a single fat droplet occupies most of the cell cytoplasm, brown adipocytes appear much more hydrated, with a water content typically ranging between 50 and 70%. The presence of numerous mitochondria inside the BAT cell with UCP1 in the mitochondrial membrane (**Figure 3**) allows for its vivid metabolism.

activity in BAT is mediated by the sympathetic nervous system. Metabolic activity propels hydrolysis of local triglycerides and fatty acid consumption via β-oxidation. Depletion of triglycerides in BAT can be detected as a decrease in tissue fat content. At the same time, increased glucose uptake during BAT activation (glucose is expected to be used for de novo lipogenesis as well as to sustain the cell's ATP demand) and the metabolic fate of glucose could be traced by using HP ^{13}C-pyruvate or ^{2}H-glucose MRI.

The increased oxygen demand in BAT is met by an increase in tissue perfusion. Changes in BAT perfusion and oxygenation can be detected by several MR techniques, such as T2*-weighted techniques, dynamic contrast enhanced MRI, dynamic susceptibility contrast ^{1}H MRI, and HP ^{129}Xe MRI.

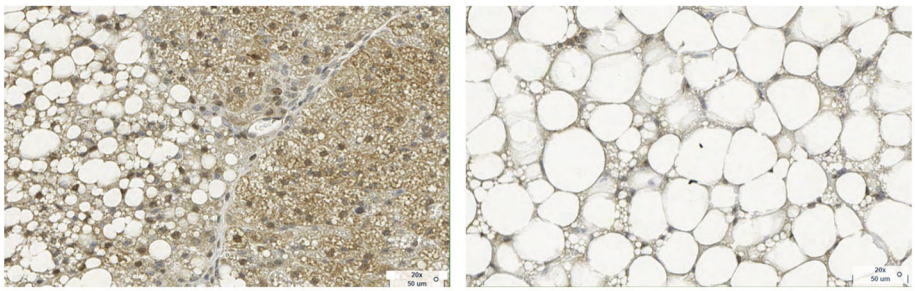

FIGURE 3 | Histology images with UCP1 staining for C57BL/6 and obese phenotype mouse. This figure is original and based on data from (41).

Since heat production is the main function of BAT, an increase in BAT temperature can be detected and quantified by measuring temperature-sensitive MR parameters such as the water resonance frequency, T_1 and T_2 relaxation times of ^{1}H, as well as the frequency of other temperature-sensitive nuclei such as ^{129}Xe.

In the following description, MR techniques are described using the following three labels: "widely used techniques" for techniques used in multiple published studies, and "technique of limited use" indicating a method that has not become established because of certain limitations.

Considerations for Application of Quantitative MR Techniques to BAT

Most of the previously mentioned ^{1}H-based MR techniques (fat fraction, T_1, T_2, T_2^*, and diffusion-weighted) primarily measure properties of water components in tissue. However, the same techniques can be used to probe fat components. In humans and in rodents, BAT contains both water and fat spin components, something that needs to be considered when applying quantitative MRI in BAT-containing depots. Specifically, quantitative imaging techniques that take into account the presence of both water and spin components need to be adopted. Possible approaches include either the suppression of the unwanted tissue component (e.g., fat suppression) or modeling the presence of both water and fat components. As an example, BAT water and fat components are characterized by different T_1 and T_2 relaxation times and diffusion properties: the water component in BAT has typically shorter T_2, longer T_1, and a lower diffusion constant than the corresponding fat component.

ANATOMY OF BAT DEPOTS IN RODENTS AND HUMANS

Adipocyte Types

Both in rodents and in humans, different types of adipocytes can be found: white, classical brown, and beige (brown-like-in-white, brite, inducible brown) adipocytes, with the latter having an intermediate morphology between white and brown adipocytes. Brown adipocytes share a common origin with skeletal muscle cells, while white adipocytes have distinct progenitor cells (42, 43). Beige adipocytes can transdifferentiate from white adipocytes and differentiate *de novo* from progenitor cells (44). To date, different lineage markers have been found for beige adipocytes, supporting the idea that beige adipocytes might exist in multiple subtypes, depending on external stimuli (45).

Morphologically, white adipocytes exhibit a single large intracellular lipid droplet and only few mitochondria, whereas brown adipocytes have multiple small cytoplasmic lipid droplets, often of less than few micrometers in diameter, and numerous mitochondria (**Figure 3**). Beige adipocytes are multilocular, like brown adipocytes, but are much bigger in size. Regarding functionality, white adipocytes store excess lipids in the form of triglycerides, while brown adipocytes can either store energy in the form of fat or dissipate energy as heat. This is accomplished thanks to a protein called the uncoupling protein-1 (UCP-1), which is present in the mitochondria of brown adipocytes at high concentration and is considered a marker of brown adipocytes. Beige adipocytes are also capable of storing fat or producing heat but, compared to classical brown adipocytes, have a remarkably reduced thermogenic potential. S100 calcium-binding protein B and leptin, adipokines relevant in the regulation of physiological functions, can be found on white and beige adipocytes, but not in brown adipocytes (44).

Rodents

In rodents, BAT is found primarily in the interscapular region and axillae, with the interscapular BAT depot (iBAT) being the largest one (11, 46) (**Figure 4A**). Other small depots, often only few millimeters in size, but still visible upon dissection, are often found in the supraclavicular, cervical, supraspinal, and perirenal areas. Because of their smaller size, these depots are harder to identify and differentiate from WAT. Other BAT depots are also found, upon dissection, in the anterior subcutaneous and suprascapular region, as well as in the inguinal region. These depots contain unilocular brown adipocytes with morphology and function that more closely resemble that of classical white adipocytes.

Humans

BAT in humans is usually present in mixed depots of white, brite, and classical brown adipocytes (47, 48). Human BAT is predominantly found in the cervical, supraclavicular, axillary, mediastinal, paravertebral, and perirenal (49) regions (**Figure 4B**). Exposure to cold can lead to an increase in BAT volume of activity as detected by FDG-PET (50).

Due to great cellular heterogeneity of supraclavicular fat, efforts have been made to find cell-surface markers to characterize different types of cells in the region. Recently, different cell-surface markers have been identified to distinguish between brown, beige, and white adipocytes in human biopsies (51, 52). For example, BAT in human infants appears similar to classical rodent BAT (48), while beige marker proteins can be found as well (53). Since no imaging methods are capable of differentiating classical brown adipocytes from beige adipocytes yet, the described mixture of different cell types will hereinafter be referred to as "BAT."

CHARACTERIZING BAT WATER–FAT COMPOSITION

The MR protocol most commonly used to assess BAT morphology and to differentiate BAT from WAT is based on the quantification of water and fat content in the tissue. Because, compared to WAT, BAT has a reduced fat content (**Figures 2**, **3**), quantification of water–fat composition in tissues can be used to differentiate BAT from WAT. Single-voxel proton MRS or chemical shift encoding-based water–fat MRI are the two main approaches used to quantify water–fat composition in tissues with MR (54).

Single-Voxel Proton MR Spectroscopy [Technique of Limited Use]

Single-voxel proton MRS can be used to quantify water and fat content within a small 3D volume. MRS can spectrally resolve the different fat peaks and thus measure adipose tissue fatty acid composition (55). If single-voxel MRS is performed with variable T_1- and T_2-weightings, it can also be used to extract relaxation properties of water and fat components in BAT (55). However, when applied to the heterogeneous fat tissue in the human supraclavicular fossa, single-voxel MRS measurements can be challenging. Breathing motion and magnetic susceptibility gradients between water and fat compartments significantly broaden the spectral lines, making it difficult to correctly quantify water and fat spin components. A reduction of the voxel size rarely helps, as magnetic susceptibility gradients between water and fat compartments are quite strong, both at a macroscopic and microscopic level. In addition, breathing motion further complicates shimming procedures and leads to voxel mis-registration across averages, which can become particularly severe when small voxels are employed. Finally, to extract the proton density fat fraction (PDFF), MRS acquisitions need to employ a long repetition time (TR), to minimize T_1 weighting effects, and an acquisition with multiple echo times (TE) to correct for T_2 weighting effects. Long acquisition times, coupled with voxel mis-registration due to physiological motion, cause severe spectral line broadening, hampering correct quantification of water and fat spin components in the region.

Chemical-Shift-Encoded MRI [Widely Used Technique]

While early MR-based BAT fat fraction measurements were based on frequency selective excitation methods to collect a signal-weighted fat fraction image (56, 57), recently chemical shift encoding methods have become widely used for BAT detection. These methods are able to quantify the PDFF, defined as the proportion of mobile proton density in tissue attributable to fat, which is nowadays considered a standardized imaging biomarker of tissue fat content (58). PDFF has shown excellent linearity, accuracy, and precision across different field strengths and scanner manufacturers for liver applications (59) and is thus used to assess fat infiltration in liver, abdominal organs (54), and bone marrow (60). Chemical shift encoding-based water–fat imaging combines a (2D or 3D) multi-echo gradient echo acquisition with a water–fat separation reconstruction to extract spatially resolved fat fraction maps. The water and fat contribution to the signal within one voxel is determined after accounting for known confounding factors, including the presence of multiple fat peaks, T_2^* decay, T_1 bias, and phase error effects, as already shown in the liver (54) and bone marrow (60). However, there is no systematic analysis on the effect of confounding factors for BAT PDFF estimations using chemical shift encoding-based water–fat imaging. Thus, the methodologies already available for PDFF estimation in other tissues should be adopted to obtain confounder-free BAT PDFF estimation, such as using an average adipose tissue fat spectrum (61, 62), using small flip angles for reducing T_1 bias effects (63, 64), and addressing phase errors depending on the employed imaging methodology (65, 66). If phase errors can be corrected, complex-based methods should be preferred over magnitude-based methods, thanks to the reduced sensitivity of complex-based methods to signal model mismatches (67, 68). If magnitude-based methods are employed, magnetic susceptibility-induced fat resonance shifts can affect PDFF quantification especially in the borders of the supraclavicular fossa (69). Finally, T_2^* decay effects should be considered since BAT has shorter T_2^* than WAT.

Just like MRS, chemical shift encoding-based water–fat imaging of the human supraclavicular fossa is challenged by strong macroscopic magnetic field inhomogeneities, which are particularly strong in the supraclavicular region, located right above the lungs, by variations in macroscopic field inhomogeneities due to respiratory motion, which make the magnetic field gradient time-dependent, as well as by microscopic magnetic susceptibility gradients. The presence of time-dependent magnetic field gradients can result in an incorrect field map estimation and produce the infamous water–fat swaps in the water–fat separation reconstruction. There is a plethora of field mapping techniques addressing such field map errors by imposing a smoothness constraint on the field map estimation (70) or by demodulating an a priori known magnetic field inhomogeneity contributions (71, 72).

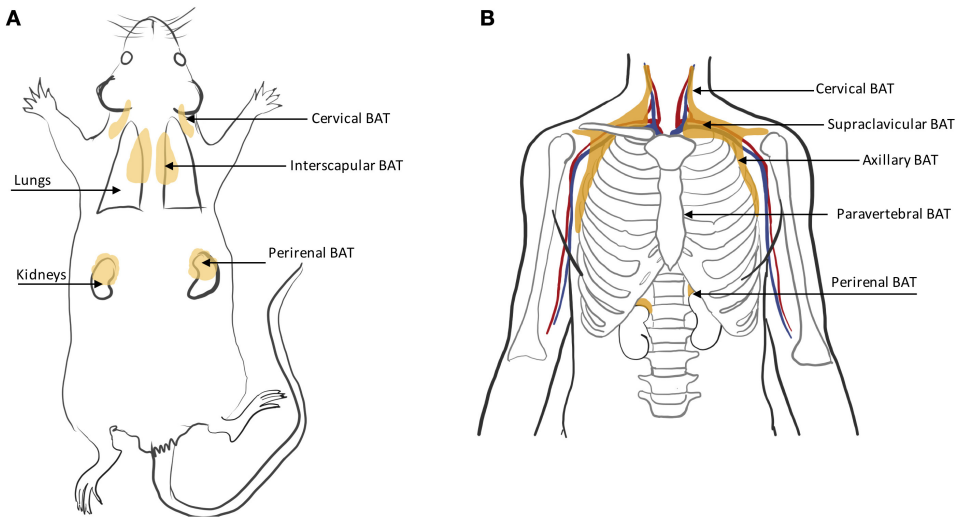

FIGURE 4 | Schematic displaying major BAT depots in **(A)** rodent and **(B)** human anatomy.

Z-Spectrum Imaging [Recently Proposed Technique]

An alternative method to chemical shift encoding-based water–fat imaging, named Z-spectrum imaging (ZSI), was recently proposed to measure tissue fat content. The method consists in sweeping a saturation pulse across a spectral region that includes water and fat frequencies. Signal intensity as a function of saturation frequency is then used to obtain a Z-spectrum from which water and fat signal components can be extracted, on a voxel-by-voxel basis. This method was initially tested in excised BAT samples and *in vivo* in humans (73), and later implemented to measure temperature in a water–fat emulsion phantom (74). With this method, the phase of the MR signal is completely ignored, so there are no phase distortions, and no assumption is made on the relative water–fat frequency, which is known to be greatly affected by microscopic field inhomogeneities in supraclavicular fat (69). Compared to PDFF, this approach is time consuming, as reconstruction of a Z-spectrum requires the acquisition of multiple images (one for each saturation frequency). Also, subject motion during the acquisition of multiple images, required for the Z-spectrum, may result in voxel misregistration and thus hamper the water–fat quantification.

BAT Water–Fat Composition in Rodents

In chow-fed mice and rats living below thermoneutrality (i.e., standard laboratory living conditions), BAT is composed of multilocular adipocytes that are much smaller in size than white adipocytes. Brown adipocytes appear much more hydrated than classical WAT, with a water content typically ranging between 50 and 70%. In obese mice or humanized mice (mice living at thermoneutral conditions and fed a Western diet), the structure of BAT resembles much more that of adult humans, with UCP1-rich adipocytes surrounded by lipid-filled unilocular adipocytes, with much bigger cell sizes and with enlarged lipid droplets that often merge together into a single large lipid droplet (**Figure 3**) (75).

Detection of BAT water–fat composition in rodents by MRI dates back to 1989 (76), when chemical shift imaging was used in rats to identify not only the large iBAT depot, clearly visible in T_2-weighted and T_2*-weighted images, but also the much smaller BAT depots found in the supraclavicular, cervical, and axillary regions. In rodents housed under standard laboratory living conditions, which lead to chronic thermal stress in mice, these depots maintain the unique ∼50/50 −30/70 water–fat composition characteristic of BAT (77), and therefore are easily identifiable on fat fraction maps. More interestingly, selective detection of water and fat signals enables not just a more accurate identification of these smaller BAT depots than T_2-weighted and T_2*-weighted images, but also the detection of changes in tissue fat content produced by cold acclimation or drug treatment. In this case, both MRS and chemical shift encoding-based water–fat imaging can be used as a valuable tool for monitoring lipid loss in BAT (due to both lipid oxidation and lipid export) during stimulation of non-shivering thermogenesis (78).

While selective detection and mapping of water and fat proton density can be time-consuming, chemical shift encoding techniques have the major advantage of being much faster (79), enabling mapping of water–fat tissue content in the entire body of small rodents in just a few minutes and with very high resolution, which is key for the reduction of partial volume effects and for the detection of other small BAT depots, whose size is often smaller than a few mm^3 (57).

BAT Water–Fat Composition in Humans: Studies at Thermoneutrality

Histological analyses performed on both human cadavers (1, 7) and biopsies (4, 6, 46) have shown that the amount and

microscopic appearance of BAT in humans vary widely. In newborn humans, who rely on BAT thermogenesis to maintain their core body temperature, BAT is much more hydrated than in adult humans, with BAT areas made predominantly of typical multilocular BAT cells (80). In adult humans, BAT is more heterogeneous: brown adipocytes comprise both unilocular and multilocular fat cells, mostly found dispersed among white adipocytes. This heterogeneity found in adult humans, which is not recapitulated in infants or in rodents, leads to a wide variation in tissue water–fat composition.

In humans, BAT water–fat composition is predominantly measured by using chemical shift encoding-based water–fat imaging techniques. These techniques are widely available in clinical MR scanners and have shown great reproducibility and repeatability, independently of BAT metabolic activity (81–83). To detect and characterize BAT, chemical-shift encoding-based water–fat imaging techniques have been used on the supraclavicular adipose tissue in humans across all ages. Studies in infants (48, 84, 85), children (79), adolescents (86), and adults (81, 87–94) have demonstrated the feasibility of this technique in humans. A favored method to measure BAT fat fraction is the measurement of the PDFF, which has been used in several studies for human BAT on grounds of its robustness and standardization (81, 88, 92, 94). Histological verification of MRI results was only performed in small post-mortem studies (48, 84) and in a single case of a living human adult (95).

BAT Water–Fat Composition in Humans: Studies During Cold Exposure

Cold activation induces lipid consumption in BAT. Several recent studies have tracked water–fat composition of supraclavicular fat in adult humans during cold activation. While some studies reported a decrease in supraclavicular fat fraction after cold-induced non-shivering thermogenesis, thus pointing to evidence of BAT lipid consumption in the region (90, 96–101), other studies did not find a consistent or significant change in fat content (34, 101).

The presence of two BAT cell populations, one with a higher lipid content that is predominantly consuming fat for thermogenesis, and one with a lower lipid content that is refueling its lipid stores from glucose and fatty acid uptake, could in part explain the contradictory results found in the literature (102). In support of this hypothesis, a recent study, which grouped the pixels into ranges of percentage decades and followed their changes over time (99), found a significant cold-induced decrease in lipid-rich voxels of the supraclavicular depot and a concomitant significant increase of PDFF in voxels with lower PDFF. Similarly, another study, which analyzed fat fraction on a voxel-by-voxel basis (102), found the largest cold-induced changes occurring in the fat fraction range of 70–100% at thermoneutrality (102). As the presence of two cell populations has never been reported in rodents, additional studies are needed to support this hypothesis.

Furthermore, while some studies have reported a correlation between glucose uptake in PET examinations and MRI fat fraction found after cold activation of BAT (98, 103, 104), other studies have found no correlation (34, 92, 101). In particular, by using combined PET/MR scans, McCallister et al. tried to find a difference in fat fraction between glucose avid and non-glucose avid regions within the supraclavicular fat depot. Despite some areas of very high glucose uptake appeared to display lower fat fractions in a couple of their study subjects (92), this was not the case in all of the subjects examined. Also, PET-based glucose uptake was shown to correlate with changes in MRI fat fraction in some, but not in all subjects (92). We believe that the greater BAT heterogeneity found in adult humans, which is not recapitulated in rodents that live under constant thermal stress, thus have well-defined and confined BAT depots, is the main reason for the conflicting results found in adult humans.

MRI of BAT Water–Fat Composition in Metabolic Dysfunction

BAT has been shown to be involved in body weight regulation, glucose, and lipid homeostasis in mice (105–107). In humans, an increase in BAT activity, measured by PET/CT, has shown to be correlated with increased energy expenditure (104, 108, 109). Furthermore, an inverse correlation was found between BAT volume of activity and body mass index (BMI), as well as body adiposity (110, 111). These correlations are of interest regarding potential therapeutic targets for obesity. More interestingly, it has been shown that activation of BAT increases glucose and triglyceride clearance in humans, potentially decreasing the risk of developing diabetes and other obesity comorbidities (4, 86, 108, 112, 113). In human adults with obesity, effects of cold and insulin on BAT activity were reported to be restricted (114–116). MRI studies of BAT influencing metabolic dysfunction and secondary diseases have been performed more recently. A correlation between the supraclavicular PDFF, as a surrogate marker for BAT presence, and anthropometric as well as MRI-based obesity markers was shown (88). In adult patients with clinically manifest cardiovascular disease, an assumed presence of BAT, determined by MRI fat fraction in supraclavicular adipose tissue, correlated with a more favorable metabolic profile and less obesity (81). Male human subjects with obesity showed higher MRI-based fat fraction and fat fraction changes under thermal challenges correlated with hypermetabolic BAT volume and with BAT activity, as measured by PET/CT in this study (98).

Limitations of Water–Fat MR Based Techniques

A clear identification of BAT only based on MRI fat fraction measurements remains challenging for several reasons. First, in rodents and humans, BAT lipid content is modulated by acute and chronic exposure to cold or adrenergic stimulation; thus, it varies widely with age, BMI, thermal living conditions, and diet (1, 7, 46, 75, 107, 117). Consequently, the water–fat composition of BAT can be a moving target, which alone can be limited in indicating the presence/absence of BAT.

Second, adult humans lack relatively large and homogeneous BAT depots such as the iBAT depot present in rodents. In humans, most BAT is localized in the supraclavicular fossa, which histologically is known to be a heterogeneous

mixture of BAT and WAT. This heterogeneity is reflected in a heterogeneity in fat–water content in the region (6). In principle, one could think of increasing spatial resolution to reduce partial volume effect and become more "sensitive" to the cellular structure. In practice, however, a twofold reduction in the linear voxel dimension will require an increase in scan time of 64-fold, to maintain the same signal-to-noise ratio (SNR) (118). More importantly, fat fraction mapping techniques assume that each voxel encompasses the exact same anatomical region during spatial encoding, an assumption that can be easily violated when small voxels are employed in a region like the supraclavicular region, which is highly susceptible to motion.

Third, as adult humans are rarely under constant thermal stress, human BAT hydration is considerably reduced with respect to rodent BAT and presents a much higher intra- and inter-subject heterogeneity that can explain the different contrasting results reported in the literature. Specifically, while some measurements of PDFF in supraclavicular fat have shown a strong correlation between BMI and tissue fat content in the region (88), other studies trying to determine a fat fraction threshold to differentiate BAT from WAT within the supraclavicular fat region have reported that no universal fat fraction cutoff could be identified to reliably differentiate BAT from WAT (119). Another study using combined PET/MRI showed that, within the supraclavicular fat depot, glucose avid BAT regions had similar water–fat composition of glucose negative region, indicating that a subject-dependent fat fraction cutoff does not exist either (92).

Adipose tissue hydration has been reported to vary significantly, not only in regions containing BAT, but also in WAT (88, 120). Specifically, human subcutaneous adipose tissue PDFF has been shown to be positively correlated with anthropometric obesity markers (88). Although the exact explanation for the above association remains unclear, the variability of WAT hydration further complicates the use of PDFF for studying BAT in humans.

Even though many recent studies have been employing PDFF measurements addressing known confounding factors, there is a significant amount of literature reporting signal-weighted fat fraction values, which challenges the direct comparison of human supraclavicular fat fraction results across imaging studies. Therefore, standardization of fat fraction measurements in the human supraclavicular fossa would be beneficial.

Within the last 7 years of MRI studies using fat fraction techniques, it seems that fat fraction within the human supraclavicular fossa is not specific enough to identify pockets of BAT mixed with WAT within the supraclavicular fat in adult humans. While PDFF is a specific quantitative biomarker of hepatic steatosis, PDFF is not a specific biomarker of BAT. Nonetheless, measurements of changes in tissue fat fraction upon activation could increase PDFF specificity to BAT (38–40). In this context, it is important to point out that functional measurements including changes in tissue fat fraction or glucose uptake using PET may increase PDFF specificity. However, such functional measurements may not add any additional information in subjects in which BAT has a reduced fat-burning capacity or glucose uptake capacity at the time of measurement.

MR Image Analysis Aspects

The main interscapular BAT depot is most commonly used for BAT characterization in rodents. Because of its homogenous and unique microstructure, this region can be easily segmented from muscle and subcutaneous fat. Previous efforts to automatize the segmentation procedure of interscapular BAT by MRI have been using neural network techniques applied on fat fraction and T_2 measurements, as well as on fat fraction and T_2 and T_2^* measurements (121, 122).

Image analysis and segmentation of the human BAT are more challenging. As in rodents, the analysis is often restricted to areas where BAT is most commonly found, and which comprises the cervical, supraclavicular, and axillar region, where this tissue is found between muscles and surrounding major blood vessels. Segmentation of human BAT is challenging because:

1) There is no clear or consistent tissue boundary toward the cranial, caudal, or lateral direction.
2) Partial volume effects occur, even with an image resolution of 1 mm^3:
   a. Histological analysis of human supraclavicular fat has shown that the area contains only small clusters of multilocular brown adipocytes, mixed with WAT (1, 4, 75). At the typical resolution used in MRI, one should expect partial volume effects.
   b. The pocket is rich in larger and smaller blood vessels containing blood that contribute to partial volume effects.
3) There is no consensus on the lower and upper fat fraction threshold needed to segment this tissue. In many human fat fraction studies, the entire supraclavicular fat, with a fat fraction ranging from 30 to 80%, is often labeled as BAT, with the lower boundary only needed to exclude muscle and blood vessels. Others have included all voxels with a PDFF greater than a chosen lower threshold.

The most commonly seen approach for BAT segmentation involves a crude manual segmentation in the supraclavicular fossa, followed by applying a threshold and an erosion step to prevent partial volume effects from neighboring tissues such as muscle.

Nonetheless, a semi-automated segmentation for processing BAT in the cervical–supraclavicular depot was suggested using an atlas-based approach (123). The atlas was generated based on previously manually segmented data and aimed at including adipose tissue located between the clavicle and the scapula. A manually pre-segmented data set was then registered onto the atlas to generate the final mask. However, not all of the adipose tissue between the bones was included and the lateral borders of the mask did not follow a clear anatomical structure. A different study, that had both cold-activated PET/CT data and MRI data available in over 20 subjects used information from all three image modalities to generate a common mask. A rigid image co-registration was done to overlay the MR data with the PET/CT

data scans (89). In any case, special care is needed not to include neighboring bone tissue signal that also has fat fraction values similar to adipose tissue.

When PDFF techniques are used to characterize differences in fat fraction in supraclavicular fat over time, or after acute stimulation of BAT thermogenesis, co-registration of pre- and post-PDFF maps also needs to be addressed (102).

CHARACTERIZING BAT MICROSTRUCTURE

T_2* and R_2* Mapping at Rest [Widely Used Technique]

T_2* mapping quantifies the presence of microscopic field inhomogeneities and can be sensitive to microstructural components with different magnetic susceptibility. T_2* mapping is a popular imaging technique for measuring endogenous iron concentration in different organs (i.e., brain, liver) or the concentration of exogenous paramagnetic contrast agents. T_2* mapping is typically performed using a multi-echo gradient echo acquisition and it can be combined with a single T_2* decay signal model in tissues containing just water, and with the water–fat signal model in tissues containing both water and fat. BAT T_2* mapping has been therefore previously performed in combination with fat fraction mapping using a chemical shift encoding-based water–fat imaging method. Multiple previous works have shown that BAT has shorter T_2* and thus greater R_2* (defined as the inverse of T2*) than WAT, both in mice (124) and in humans (79, 90, 96, 98, 125–127). The shorter T_2* of BAT is attributed to the abundance of iron-rich mitochondria, which confer to this tissue its characteristic brown color.

Despite numerous publications on the accuracy and precision of T_2* mapping in water-dominant tissues, little is known about the accuracy and precision of T_2* mapping in fat-dominant tissues. A recent study showed a markedly decreased range of T_2* value and standard deviation of supraclavicular and gluteal adipose tissue when using a 20-multiecho gradient echo acquisition vs. a 6-multiecho gradient echo acquisition (125). One factor that contributes to the overestimation of T2* in case of considering fewer echoes is that the exponential decay, caused by T2*, is not well-depicted when only considering the shorter echo times in the signal fitting routine. A higher number of sampled echoes at a constant echo time step (optimal for water–fat separation) has been therefore recommended in order to improve adipose tissue T_2* precision and to decrease the sensitivity of adipose tissue T_2* results on the underlying fatty acid composition (125) (**Figure 5**).

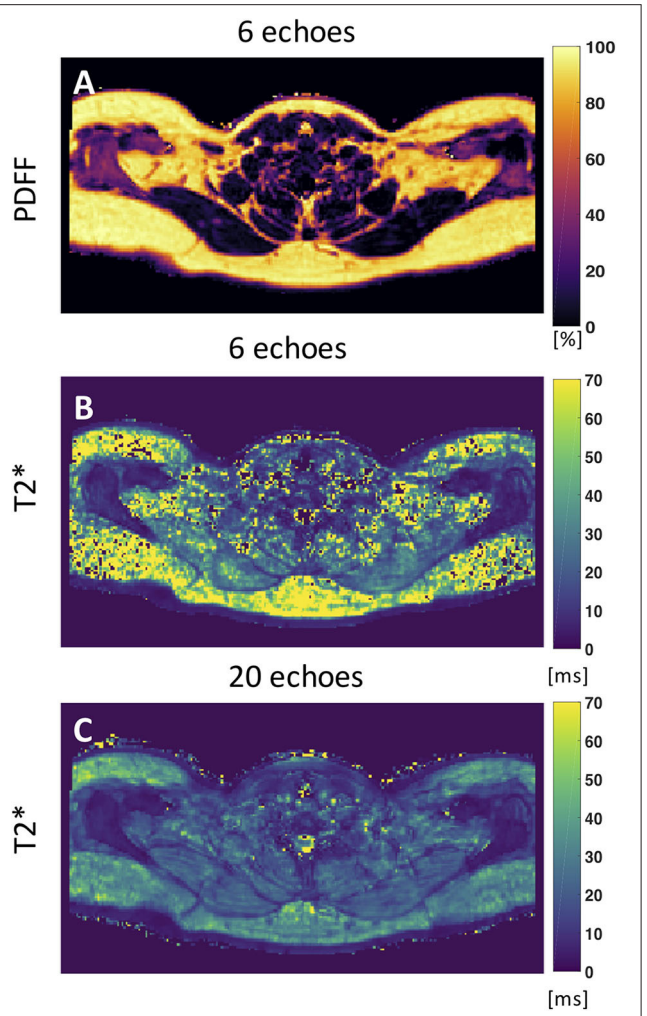

FIGURE 5 | Axial PDFF and T_2^* maps of human supraclavicular fat. **(A)** PDFF map calculated using 6 echoes. **(B)** The T_2^* map estimated from the 6-echo data set is noisy and includes severely overestimated values in both the subcutaneous region and the supraclavicular fossa. **(C)** The T2* map estimated by using 20 echoes yields a more robust and smooth fitting result. This figure is original and based on data from (125).

Probing Microstructure With Intermolecular Multiple Quantum Coherences [Recently Proposed Technique]

Non-linear MR signals, such as those originating from intermolecular multiple quantum coherences (iMQCs) between water and fat spins, have been used to detect BAT. iMQCs between ^{1}H spins residing in water and fat molecules can be made observable by using a clever combination of RF pulses and magnetic field gradients that modulate the longitudinal magnetization, break its spatial isotropy, and reintroduce the effect of long-range dipolar field interaction between the correlated spins (128, 129). Under the effect of the long-range dipolar field, antiphase magnetization originating from iMQCs can evolve in an observable signal. Modulation of the longitudinal magnetization on a cellular size scale can be used for amplifying the iMQC signal between water and fat spins that are only a few micrometers apart, while suppressing the iMQC signal between water and fat spins that are far from each and that possibly reside in different tissues. Therefore, these signals can provide a better way to probe water–fat composition at the cellular level, a scale that is currently inaccessible by clinical MR techniques.

The ability to select water–fat iMQC signal from BAT, and suppress water–fat iMQC signal from mixtures of fat and muscle, was first demonstrated in 2011 (130). Later, the same technique was applied *in vivo* to map BAT distribution in mice (118) and rats (131).

Applications in humans, however, have been limited by the poor SNR achievable with clinical scanners. The iMQC signal intensity scales as the square of magnetization density and thus as the square of the magnetic field strength. This means that at 3 T, the signal is only 20% of the signal obtainable at 7 T, at which mouse studies have been performed (118), and <4% of the signal obtainable at 9.4 T, at which rat studies have been performed (131). Also at 3 T, the dipolar demagnetization time (i.e., the time needed to the dipolar field to refocus the signal originating from iMQCs) is several hundreds of milliseconds—much longer than the characteristic T_2 and T_2^* of BAT, thus further limiting the detectable signal. Finally, the water–fat iMQC signal intensity is maximized for homogeneous equal emulsions of water and fat spins, on which these techniques are typically tested (132, 133). Thus, while at 3 T the low signal intensity may still enable low-resolution background free maps of BAT in humans, the relative scarcity and heterogeneity of BAT depots in humans, coupled with its less favorable water–fat composition, may preclude collection of high-resolution 3D maps needed for accurate quantification of BAT.

Probing Microstructure via Diffusion Contrast

Diffusion-Weighted MR Measurements

Diffusion-weighted imaging (DWI) can probe water diffusion at the microscopic level. In DWI, magnetic field gradients are applied to encode and decode nuclear spin positions at the microscopic level, along a specific direction. In the presence of molecular diffusion between the encoding and decoding gradients, the spins acquire an additional phase that prevents their complete refocusing during acquisition, leading to a signal reduction. As the signal reduction is directly proportional to spin diffusion, the images will acquire a contrast that is diffusion-weighted.

In addition to a qualitative assessment of water diffusion, that is for instance sufficient to detect an acute ischemic stroke, quantitative mapping of diffusion properties can be done to quantify water diffusion that directly reflects the microstructural properties of tissue. For this task, an ADC map is generated by acquiring images at different diffusion gradients strengths/timing (*b*-values) before fitting a mono-exponential signal decay on a voxel-by-voxel basis. By probing the diffusion behavior of both water and fat components, DWI and DW-MRS techniques can leverage the difference in cellular structure between BAT and WAT to differentiate these two tissues.

DWI of Water [Recently Proposed Technique]

A study on 28 subjects comprising normal-weight and obese children compared the average ADC value of the water signal between the two cohorts using a multi-shot turbo-spin-echo-based sequence (134). In this study, no fat suppression was used and only two *b*-values were used for ADC calculation. No significant difference was found between the two groups before adjusting for pubertal status and gender. The slight tendency of a more restricted water diffusion behavior in the BAT of the obese cohort was explained with a reduced extracellular space due to the presence of large adipocytes. However, it is important to note that to selectively probe diffusion properties of water in BAT, suppression of all lipid signals is required, as previously done in bone marrow (135).

DW-MRS of Fat and Water [Recently Proposed Technique]

DW-MRS enables one to assess the diffusion properties of both water and lipid signals, without the need for signal suppression. The measured diffusion-weighted signal depends on the lipid diffusion properties, and on the shape, dimensions, and orientation of the restricted geometry in which fat molecules diffuse. These are known to be very different in BAT compared to WAT. In BAT, triglycerides form multiple small fat droplets, whereas in WAT, they form a single, large, unilocular fat droplet. Because fat diffuses 100 times slower than water, to probe lipid diffusion properties, strong diffusion encoding gradients are required, which may not be available in a clinical scanner. By applying high *b*-value gradients at variable diffusion times, one can detect differences in cell size using DW-MRS (136, 137). This idea has been applied *in vitro* on *ex vivo* BAT samples excited from the interscapular region using a preclinical MR scanner: a lower ADC was found in the WAT samples of rats on a high-fat diet compared to those on a normal chow diet. The lower ADC in WAT of mice with a high fat diet has been linked to lower diffusion coefficients in the presence of longer fatty acid chain lengths and more saturated fatty acids in the triglycerides. Assuming fat droplets of a spherical shape, fitting the MR signal for different *b*-values to analytical signal expressions can provide an estimation of the droplet sizes in BAT (138). In rodents, smaller radii were found for BAT of chow diet rats, which agreed with histological findings.

In vivo, lipid droplet size measurements in non-moving organs (e.g., leg bone marrow) have been demonstrated (137). However, motion-induced intra-voxel spin dephasing will yield additional signal attenuation, which in turn leads to an overestimation of fat diffusion properties. This includes scanner table vibrations (139) but also physiological motion, including respiratory motion and tissue deformation due to vessel pulsation. A flow-compensated, cardiac-triggered and respiratory navigator-gated DW-MRS sequence has been proposed to compensate for motion other than diffusion (140) when scanning the supraclavicular fossa in humans. However, the fact that a signal decay of the fat peaks already at low *b*-values was detected, where we would not expect diffusion effects of fat, indicates residual motion effects on the measured DW fat signals—even when using flow-compensated diffusion waveforms.

The diffusion behavior of the water peak in the human supraclavicular fossa has been investigated as well (141). The acquisition was respiratory- and cardiac-triggered. The water signal was referenced to the fat peaks before fitting the ADC value to mitigate any residual impact of motion on the fitted

ADC (**Figure 6**). This prevented an overestimation of ADC due to motion-induced intra-voxel dephasing. In this preliminary study, a more restricted diffusion behavior of the water signal in people with known brown fat was found (142), which stands in contrast to the findings of the study using DWI (134). A possible explanation for the more restricted water diffusion would be that a part of the measured water spins originates from inside the mitochondria of BAT, thus experiencing a more restricted environment compared to the cytoplasm or extracellular space in WAT. However, how cytoplasmic and extracellular water of BAT contribute to the DW-MRS signal is not clear. A complex mixture of hindered (by fat droplets and mitochondria) diffusion and restricted diffusion (by the cell membrane and the inner mitochondrial membrane) could be thought of for cytoplasmic water. Further measurements coupled with histological assessment of the tissue are required for a better modeling of the DW-MRS signal in BAT.

CHARACTERIZING BAT FUNCTION

Beyond the commonly used ^{18}F-FDG PET for measuring BAT function, MRI offers versatile contrast mechanisms to assess BAT function. The MR contrast mechanisms proposed to characterize BAT function and their application in differentiating BAT from WAT are reviewed in the next sections.

Multi-Modal Imaging (PET-MRI) [Widely Used Technique]

While most of the human BAT studies are performed on PET/CT platforms, more and more studies are performed using PET/MRI. Major advantages of PET/MRI over PET/CT include a lower radiation burden (as MRI replaces CT for attenuation correction and anatomical information), and the possibility to better characterize glucose avid BAT regions in terms of iron content and tissue perfusion by MRI. When compared to MRI alone, the combined use of PET/MRI increases the accuracy of MRI BAT detection, at least in those subjects that exhibit metabolically active BAT in ^{18}F-FDG-PET scans (**Figure 7**).

While several studies have shown that fat fraction in supraclavicular fat is significantly different than fat fraction of subcutaneous white fat (82, 119, 143), PET/CT and PET/MRI images of human BAT, as well as histology examinations of human BAT, have clearly shown that not the entire supraclavicular/cervical fat depot, but only a fraction of it contains BAT. Therefore, one logical question is whether fat fraction mapping techniques can help identify BAT within the much larger supraclavicular fat depot. To answer this question, PET/CT studies in combination with MRI studies (119, 126, 143) or combined PET/MRI studies (92) have been performed in the last 10 years. In these studies, it was clearly shown that significant differences exist in T_2 and T_2* relaxation times, as well as in fat fraction values between subcutaneous and supraclavicular fat, but that the fat distribution of the supraclavicular/cervical fat compartments does not correlate with the FDG uptake. In other words, a specific fat fraction threshold could not be found *in vivo* in adult humans to differentiate areas with or without BAT within the supraclavicular fat depot. This finding should not be surprising given the large difference in BAT morphology and hydration between humans and rodents (75), in which most of the fat fraction methods have been validated.

Indirect evidence of the improved accuracy provided by combined PET/MRI technique is the ability to detect small changes in BAT fat fraction during prolonged cold exposure, at least in some subjects. MRI studies assessing the change in fat fraction and T2* values of the supraclavicular fat depot upon activation have shown contrasting results on the correlation of these values with glucose uptake (126). However, a much higher correlation was found when the analysis was focused on selected regions within the supraclavicular fat. Although the degree of glucose uptake in each subject cannot be taken as a surrogate measure of the degree of BAT thermogenic activity, an increased glucose uptake is still expected to be present in functional BAT. Therefore, hybrid PET/MRI might represent the ideal multi-modal imaging tool for BAT evaluation.

Metabolic Imaging With X-Nuclei

^{31}P, ^{13}C, and ^{2}H MR Measurements [Recently Proposed Techniques]

With ^{31}P NMR spectroscopy, one can typically probe phosphate metabolism, which permits the phosphorylation of ADP, converting it into ATP. In ^{31}P spectra, resonance frequency lines from free phosphate, phosphocreatine, as well as the α-, β-, and γ-ATP (where the Greek letter corresponds to the position of the phosphate within the ATP molecule) can be easily identified, while the concentration of ADP, under physiological conditions, is too low to be detected, and is typically calculated indirectly using the other ^{31}P peaks. When evaluating ^{31}P NMR spectra, a reduction in the phosphocreatine peak or in the PCr/ATP ratio is typically associated with an increase in cell energy demand, while the rate of PCr recovery is considered an indicator of mitochondrial oxidative capacity, thus providing a way to evaluate mitochondrial function *in vivo*. Interestingly, in a study investigating brown fat tissue dynamics by ^{31}P NMR, no changes were observed in the PCr/ATP ratio (calculated as PCr/γ-ATP ratio), or in the ATP/ADP ratio (calculated as β-ATP/α-ATP ratio) (78), neither in wild type nor in UCP1-KO mice, and independently of previous cold or 30°C acclimation. This finding was interpreted as ATP still being generated at a sufficient rate during BAT activation to cover the cellular needs for enzyme activation and biosynthesis. When data of wild type and UCP1-KO mice before NA injection were pooled, the authors found a significantly lower PCr/ATP ratio in cold-acclimated mice compared to warm-acclimated mice, indicating a higher ATP concentration in BAT under chronic stimulation.

Although ^{31}P-MRS has been used to study tissue metabolism *in vivo*, this technique is challenged by the low MR sensitivity to the ^{31}P nucleus and the low *in vivo* concentrations of phosphate metabolites. Taken together, these two effects greatly limit spatial resolution and introduce confounding factors in the interpretation of the spectra from partial volume effect.

^{13}C is a stable isotope of carbon. Unlike ^{12}C, the most abundant stable isotope of carbon with a zero nuclear spin, ^{13}C has a nuclear spin of ½ and is therefore MR-visible. Because

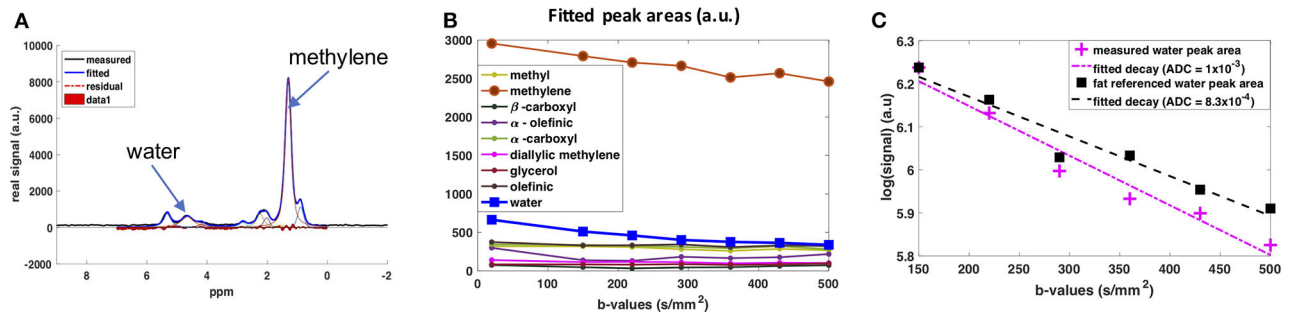

FIGURE 6 | DW-MRS of water component in human supraclavicular fat using a both respiratory and cardiac triggered acquisition scheme. **(A)** Example of spectral fitting results for a voxel within the supraclavicular fossa. **(B)** Fitted spectral peak areas for eight fat peaks and water peak for a range of different *b*-values. **(C)** ADC fitting results for the water peak. In pink: Data points and fitted mono-exponential decay without fat referencing. In blue: Data points and fitted mono-exponential decay after referencing to the fat peaks, under the assumption that the decay in fat is due only to motion effects at these low *b*-values. This figure is original and based on data from (141).

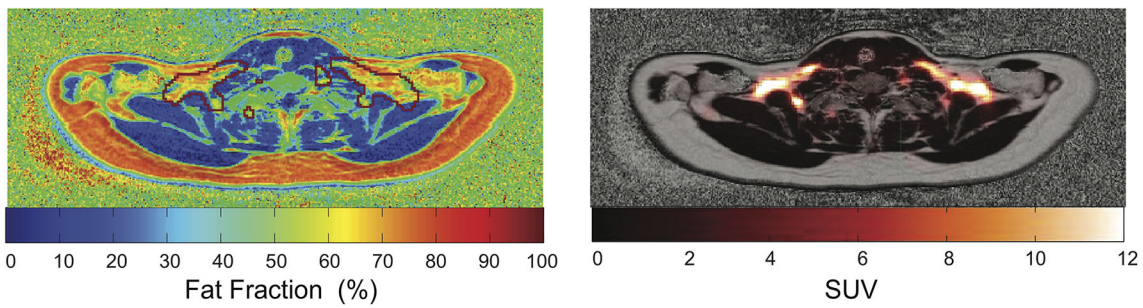

FIGURE 7 | Overlay of PET images and MR-based PDFF maps. The red mark indicates regions with SUV > 2.5. This figure is original and based on data from (92).

of the low natural abundance of this isotope, *in vivo* ^{13}C MRS is technically and experimentally challenging and typically requires infusion of ^{13}C-labeled molecules. Hyperpolarization increases the MR sensitivity to the ^{13}C-labeled molecules by four orders of magnitude, such that one can detect these molecules *in vivo* at micromolar concentrations and track their metabolic conversion into their downstream metabolites. Among the different hyperpolarized (HP) ^{13}C tracers, [1-^{13}C]-pyruvate is most widely used because it is easy to polarize and it has a relatively long longitudinal relaxation time ($T_1 \approx 60$ s), which enables the detection of this molecule and its downstream products before the nuclear spin polarization decays back to thermal equilibrium. In tissues, conversion of HP [1-^{13}C]-pyruvate into [1-^{13}C]-lactate, [1-^{13}C]-alanine, and [^{13}C]-bicarbonate can be observed by ^{13}C NMR spectroscopy and imaging right after infusion of HP [1-^{13}C]-pyruvate. The ratio between bicarbonate and lactate can be used as a marker of aerobic versus anaerobic metabolism (**Figure 8**), thus providing additional metabolic information on the fate of glucose that ^{18}F-FDG-PET cannot provide.

While HP [1-^{13}C]-pyruvate has been mainly used for preclinical and clinical cancer studies, two preclinical studies have shown applications of HP [1-^{13}C]-pyruvate for BAT detection in mice and rats. In a study on cold-exposed mice (144), an increase in pyruvate tissue uptake and a non-statistically significant increase in the lactate/bicarbonate ratio was observed in cold-acclimatized mice compared to warm-acclimatized mice, suggesting a tendency toward increased anaerobic metabolism during cold exposure, contrary to what one would expect in BAT. Furthermore, it was found that the [1-^{13}C]-bicarbonate/[1-^{13}C]-pyruvate ratio increased by 13-fold after cold exposure, compared to the thermo-neutral condition. Yet, no differences in pyruvate metabolism were observed during acute noradrenergic stimulation of BAT, in marked contrast to an early study that had shown increased conversion of pre-polarized [1-^{13}C] pyruvate into ^{13}C-bicarbonate and [1-^{13}C]-lactate in rats (145). This discrepancy between the two studies, however, should come as no surprise. While in the earlier study, rats were anesthetized with ketamine, in the second study, mice were anesthetized with isoflurane, an anesthetic known to suppress BAT thermogenesis and blunt BAT response to noradrenergic stimulation.

Also, one should keep in mind that quantification of anaerobic/aerobic metabolism with [1-^{13}C] pyruvate in BAT is challenging, as this requires mapping of [1-^{13}C] pyruvate and its downstream products at a relatively high spatial (to avoid partial volume effects) and temporal resolution, to enable kinetic analyses. Clearly, the reduced intensity of the bicarbonate peak (~2 orders of magnitude smaller than pyruvate), coupled with the limited spatial/temporal resolution with which dynamic metabolites data can be acquired, makes quantification of aerobic/anaerobic metabolism in BAT a challenge.

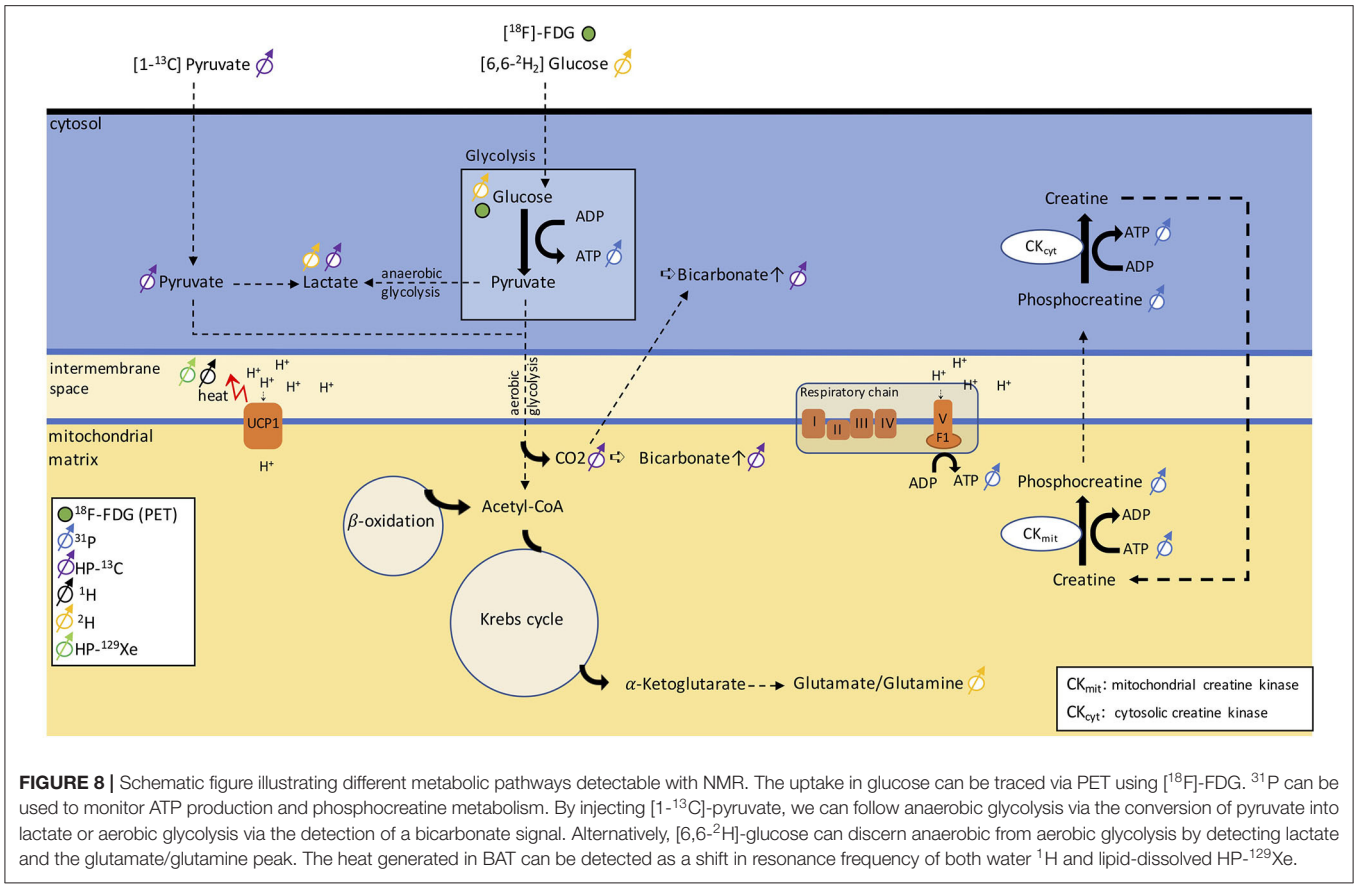

FIGURE 8 | Schematic figure illustrating different metabolic pathways detectable with NMR. The uptake in glucose can be traced via PET using [^{18}F]-FDG. ^{31}P can be used to monitor ATP production and phosphocreatine metabolism. By injecting [1-^{13}C]-pyruvate, we can follow anaerobic glycolysis via the conversion of pyruvate into lactate or aerobic glycolysis via the detection of a bicarbonate signal. Alternatively, [6,6-^{2}H]-glucose can discern anaerobic from aerobic glycolysis by detecting lactate and the glutamate/glutamine peak. The heat generated in BAT can be detected as a shift in resonance frequency of both water ^{1}H and lipid-dissolved HP-^{129}Xe.

Deuterium, ^{2}H, is a stable isotope of hydrogen with a very low natural abundance (<2%) and with a nuclear spin of 1. The short longitudinal relaxation time of this quadrupolar nucleus enables rapid signal averaging and the acquisition of a deuterium spectrum from natural abundant deuterium in a matter of several minutes, at high magnetic field strengths. The deuterium chemical shift range is comparable to that of ^{1}H. Therefore, without injection of a ^{2}H-labeled tracer, deuterium spectra of tissues closely resemble ^{1}H spectra. Because of the low natural isotopic abundance of ^{2}H, ^{2}H-NMR spectroscopy is often performed in combination with oral intake or intravenous infusion of non-radioactive ^{2}H-labeled glucose, often used to assess tumor metabolism. Injection of [6,6-$^{2}H_2$]-glucose at mM concentrations leads to the appearance in the ^{2}H spectra of a glucose peak whose intensity is comparable to that of natural abundance ^{2}H water. After several minutes, conversion of ^{2}H-labeled glucose into downstream metabolites such as glutamine and glutamate, as well as lactate (**Figure 8**), has been observed *in vivo* in ^{2}H spectra of the brain and liver. Thus, this technique, named deuterium metabolic imaging (DMI), as ^{13}C, can reveal glucose metabolism beyond mere uptake.

Recently, a study demonstrated the application of DMI to study BAT in rats at 9.4 T. In this study, a rapid increase followed by a rapid decrease of the injected ^{2}H-glucose signal was observed in cold-acclimated rats but not in warm-acclimated rats, whereas the lactate/glucose ratio was not significantly different between the two groups. When looking at the spectra, however, spectral resolution and SNR seem to be a major issue for quantification. While in the brain, good field homogeneity and the lack of a lipid signal are a prerequisite for robust quantification of glutamate/glutamine and lactate, in lipid-rich BAT, the presence of a relatively large lipid signal at about 1.3 ppm from natural abundant ^{2}H lipids (which is typically much larger than the lactate signal originating from injected ^{2}H-labeled glucose) is expected to make quantification of ^{2}H-labeled lactate at 1.33 ppm a challenge. Surprisingly, no lipid peak contaminations were reported in the DMI BAT study by Riis-Vestergaard et al. (146), despite the high fat content typically present in the BAT of rats. Aside from the lipid contamination, which can be a major confounding factor in the interpretation of DMI spectra of fat tissues, it is important to note that ^{2}H SNR scales as the square of the magnetic field strength; thus, high magnetic field strengths will be paramount for human translation of this technique.

Measuring BAT Perfusion

While in general tissue perfusion does not always match tissue metabolism (147, 148), in both rodents and humans, sympathic nervous system stimulation of BAT typically results in an increase in tissue perfusion (17, 149–152).

During stimulation of thermogenesis in BAT, local vessels and capillary beds are dilated to increase BAT perfusion, while arterial–arterial shunts are used to divert blood from WAT

to BAT (153). However, because the adrenergically stimulated increase in BAT blood flow is qualitatively and quantitatively independent of thermogenesis (148) [increase blood flow to BAT is observed in mice regardless of the degree of their thermogenic response (41, 154)], one should keep in mind that measurements of changes in BAT perfusion represent a promising way to probe BAT stimulation but not thermogenic response in BAT.

Contrast-Enhanced MRI [Recently Proposed Techniques]

The standard procedure in routine clinical MRI for assessing tissue perfusion relies on observing the local signal enhancement after intravenous injection of a contrast agent, such as a gadolinium compound, which shortens T_1 relaxation. Therefore, T_1-weighted sequences are employed for assessing perfusion using dynamic contrast-enhanced MRI (DCE-MRI). By tracking the MR signal dynamics during the time after contrast agent injection, the time-to-peak or the mean transit time can be calculated for a given anatomical region.

Sbarbati et al. (155) studied the interscapular BAT of rats after BAT activation with adrenaline and compared the spin echo-based DCE-MRI signal to the same signal from a control group. In contrast to the skeletal muscle of the anterior limb, the signal enhancement in the iBAT region was found to be significantly higher for the stimulated group compared to the non-stimulated group. Similarly, another study in rats used DCE-MRI in a cold-exposed and a thermoneutral control group (156). The uptake of contrast agent was three times higher in the iBAT of the activated group compared to the control group, while no significant difference was found in the interscapular WAT. More recently, a more quantitative study of the uptake kinetics using DCE-MRI, correlated with fat fraction maps, was performed in rats (157). The volume transfer constant from blood plasma into the extracellular-extravascular spaces and the concentration of the contrast agent were calculated. The iBAT depot was studied after cold activation and compared to a thermoneutral group. Activation of the iBAT depot was also induced by injection of a β_3-agonist and compared to a control group injected with saline. Moreover, the effect of beiging of inguinal WAT after chronic injection of a β_3-agonist was demonstrated. The study showed a decrease in fat fraction, and an increase in tissue perfusion in both iBAT and inguinal beige fat after activation.

Because of the risks associated with gadolinium injection (nephrogenic systemic fibrosis and the yet unknown consequences of long-term gadolinium depositions in tissues such as the brain), DCE-MRI has not yet been used in humans to study BAT. However, a rich blood perfusion of human BAT was reported as an incidental finding during MR angiography in newborn children and shown in previous review publications (39, 40).

An alternative to T_1-shortening gadolinium-based contrast agents are superparamagnetic iron oxide nanoparticles (SPIONs), that shorten T_1, T_2, and T_2^*. Monocrystalline iron oxide nanoparticles (MIONs) belong to the group of SPIONs that have a long blood pool half-life and are already clinically used for liver imaging and angiography. MIONs have been used to study BAT perfusion in rats after injection of a β_3-adrenergic receptor agonist (158). Blood perfusion was estimated based on the signal intensity change in T_2-weighted fast spin-echo images. However, a low accuracy was reported for this method.

Radioactively labeled superparamagnetic iron oxide nanoparticles [Triglyceride-Rich Lipoprotein (TRL)-^{59}FE-SPIOs] have been embedded into a lipoprotein layer to study the uptake of the nanoparticles by different organs, such as the liver, blood, muscle, and BAT after either intravenous or intraperitoneal injection (159). Cold-exposed mice showed a significant decrease of T_2^* in BAT while this was not observed in the control group. Irrespective of the BAT activation, the TRL-^{59}FE-SPIOs led to a decrease of T_2^* in the liver, and no significant uptake was detected in the muscle. Radioactivity measurements revealed quantitative distributions of the lipoproteins in the respective organs.

Arterial Spin Labeling [Recently Proposed Technique]

Arterial spin labeling (ASL), also known as arterial spin tagging, has been extensively used to study brain perfusion without the need for contrast agent injection. In ASL, nuclear spins in an artery are first tagged by using either an inversion pulse or saturation pulse. When the tagged blood reaches the perfused capillaries further downstream, the contrast in the now acquired image changes depending on the rate of perfusion. A small human study conducted by Dai et al. found an increased perfusion of 86 ± 32% in BAT after cold exposure in a cohort of 10 young volunteers, but claim that this evaluation is challenging due to the proximity to large vessels, which leads to an overestimation of the perfusion (160).

Hyperpolarized Xenon MRI [Recently Proposed Technique]

Hyperpolarized xenon gas-enhanced MRI, a technique widely used to detect lung ventilation function in humans, has also been used to detect BAT, both in rodents (41, 154) and in humans (161). Xenon gas has a relatively high solubility in tissue (162, 163). This means that, once inhaled, the inert gas slowly diffuses into tissue and blood. Because of the high solubility of xenon in lipids (162), circulating xenon preferentially accumulates in fat-rich tissues, like BAT, at a rate that is directly proportional to tissue perfusion and blood flow. As a result, upon xenon inhalation, changes in BAT blood flow can be detected easily in xenon MR spectra and in images as an increase in the lipid peak originating from xenon dissolved in the lipid compartments of BAT (41). Because the degree of xenon uptake in BAT depends not only on tissue blood flow, but also on xenon solubility in the tissue (i.e., tissue fat content), similar signal enhancements are typically observed in BAT of obese mice, in which vascular rarefaction (BAT adipocytes are in general much larger than in lean mice) and the consequent reduction in tissue blood flow is overcompensated by the increase in xenon solubility in the tissue.

By having a radiodensity similar to that of iodine, the same selective uptake of xenon into BAT during stimulation of BAT thermogenesis can be detected in CT images (153) with a spatial resolution greater than what is currently achievable with hyperpolarized xenon gas MRI (**Figure 9**). This was recently

demonstrated both in rodents and in non-human primates, in which BAT microstructure and distribution more closely resembles that in humans (153).

While the specific and strong increase in xenon uptake in BAT can lead to background-free detection of BAT in HP ^{129}Xe MR images, spatial resolution is not enough for accurate quantification of its mass, which in turn could be quantified by high-resolution xenon-enhanced CT (153). However, the strong temperature sensitivity of the chemical shift of xenon dissolved in the lipids of BAT can be used to directly probe tissue thermogenic function.

Measuring BAT Oxygenation

T_1 Relaxation [Recently Proposed Technique]

One recent work has suggested a combined chemical shift T_1 mapping sequence that simultaneously maps T_1 of fat and water in voxels containing both species to directly measure BAT oxygenation *in vivo* (164). For this study, a saturation recovery sampling scheme was implemented in combination with a phase-modulated readout. By using this approach, T_1 values of water/fat emulsions equilibrated with different gas mixtures were measured along with the T_1 of lipids in BAT *in vivo,* in anesthetized rats, under a carbogen (95% O_2-5% CO_2) challenge. In both cases, a decrease in lipid T_1 was found with increased tissue oxygenation. In the analysis, a signal model consisting of a single fat peak was used, while in a similar work, a peak-resolved T_1 estimation using an inversion recovery-prepared MRS sequence was employed to estimate the effect of oxygenation on T_1 of the methylene peak of WAT and lard (165). Unfortunately, these two studies do not allow us to draw any conclusion on the T_1 behavior of lipids in BAT during normal BAT activation for two reasons: First, it is not clear whether, under normal breathing conditions and during BAT activation, lipid oxygenation in BAT will increase or decrease. This is because, during BAT activation, while blood flow increases, oxygen consumption increases even more. Indeed, at least in mice, activation leads to a complete deoxygenation of venous blood, and to an overall increase in tissue R_2* and magnetic susceptibility (166, 167). Second, as temperature is also known to have a strong effect on the T_1 of lipids (lipid T_1 increases with temperature) (168), application of this technique to BAT would require simultaneous and independent measurements of both temperature and tissue oxygenation.

Measuring Hemoglobin Dynamics in BAT

In contrast to the diamagnetic properties of water and fat, oxyhemoglobin is only weakly diamagnetic, while deoxyhemoglobin is strongly paramagnetic. Activation of BAT is expected to lead to changes in tissue perfusion as well as to changes in oxy and deoxyhemoglobin concentration in blood that can be observed as changes in T_2* as well as changes in magnetic susceptibility.

T_2*-Weighted Imaging [Widely Used Technique]

Functional magnetic resonance imaging (fMRI) is based on the blood oxygenation level-dependent (BOLD) contrast (169). In activated areas of the brain, the increase in oxygen consumption and thus the increase in oxygen demand are overcompensated by an increase in tissue perfusion, which locally leads to a surplus of oxyhemoglobin in comparison to the strongly paramagnetic deoxyhemoglobin (170, 171). This leads to a reduction of the local susceptibility gradients, to a longer T2*, and thus to an increase in the MR signal intensity (172).

Conversely in BAT, activation leads to a *decrease* in blood oxygenation level and thus to a drop in T_2*, and to a consequent reduction in MR signal intensity that can be clearly observed in rodents near the Sulzer's vein during noradrenergic stimulation of the tissue (166, 167). In humans, whether the MR signal increases or decreases upon activation is still unclear. While some studies have found an increase in the MR signal intensity in glucose-avid regions of the supraclavicular fat depot during cold exposure (158), other studies have found glucose-avid regions in which the signal increases along with regions in which the signal decreases (143). This is not surprising, as even in the brain, variations in the subject's heart rate and breathing pattern are known to result in significant MR signal changes that can be easily misinterpreted as the result of hemodynamic changes due to a local increase in metabolic activity (173).

Quantitative Susceptibility Mapping (QSM) [Recently Proposed Technique]

QSM aims at finding the underlying magnetic volume susceptibility values for each pixel based on the measured field map, which represents the off-resonance frequency with regard to the excitation RF frequency. Due to the iron-rich mitochondria in BAT, QSM could be a promising method to discern BAT from WAT. However, so far, only studies measuring the increase in BAT perfusion, and the relative change in magnetic susceptibility, during BAT activation have been reported (167). Specifically, a strong shift toward higher magnetic susceptibility values was detected during BAT activation in a mouse model after injection of a β_3-agonist (167), in agreement with previous BOLD studies showing an increase in tissue deoxy-hemoglobin content and a consequent decrease in the MR signal intensity during BAT activation in mice (166, 167).

Measuring BAT Temperature

1H-Based MR Thermometry [Recently Proposed Technique]

BAT temperature measurements represent the most direct and accurate way to detect BAT metabolic activity as, when active, this tissue oxidizes fatty acids to generate heat (11). Yet, up to recently, non-invasive monitoring of thermogenic activity in rodents has been assessed only indirectly, by either measurements of resting energy expenditure with indirect calorimetry, by rectal temperature measurements, or by estimating the ability of the animal to defend its core body temperature when exposed to cold. The interpretation of these results is not obvious, as these measurements cannot differentiate the contribution of cold-induced non-shivering thermogenesis generated from BAT from that of cold-induced shivering thermogenesis generated from skeletal muscle. In humans, surface skin temperature measurements and whole body core temperature measurements have been performed (97),

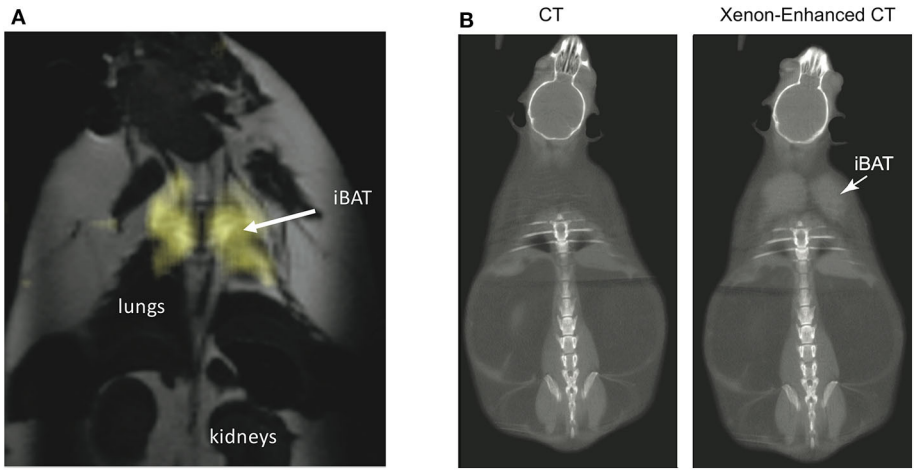

FIGURE 9 | Xenon uptake in BAT of an ob/ob mouse detected by hyperpolarized ^{129}Xe MRI and xenon-enhanced CT. **(A)** 2D HP ^{129}Xe MRI (yellow) overlaid onto an anatomical ^{1}H image. The HP ^{129}Xe image shows background free maps of iBAT in an ob/ob mouse. This figure is original and based on data from (41). **(B)** (Non-enhanced) and (xenon-enhanced) coronal CT image of a different ob/ob mouse. Selective xenon uptake in iBAT leads to a remarkable change in tissue radiodensity. This figure is original and based on data from (153).

which present the same limitations found in rodents. Skin temperature measurements by infrared thermography are often used outside the MR scanner to detect BAT activation (104, 174). However, these measurements are not very specific as they are strongly influenced by other physiological responses such as vasoconstriction and consequent reduction in local tissue blood flow, as well as by the subcutaneous fat layer thickness, which makes these measurements even less reliable in overweight and obese subjects (175). MRI could play a pivotal role in assessing BAT thermogenesis. MRI has long been used for non-invasive temperature measurements of tissues as almost all MR parameters [T_1 (176), T_2 (177), proton density (178), diffusion (179), and water resonance frequency (179)] are temperature sensitive and have been used as tissue temperature sensors. In practice, in most preclinical and clinical applications, the temperature-induced proton resonance frequency shift (PRFS) of water is the preferred temperature probe for three main reasons: First, the temperature dependence of the water chemical shift is tissue-independent (−0.01 ppm/°C), removing the need of a pre-calibration scan in the tissue of interest; Second, the temperature dependence of water chemical shift is linear, further simplifying the conversion of frequency shifts into temperature changes; Third, this method is very fast as the water resonance frequency shift can be directly deduced from a phase change of the MR signal.

Unfortunately, the need of two images to extract frequency changes and the relatively small effect of temperature on the water resonance frequency make these measurements highly susceptible to motion; this encompasses tissue displacement of the ROI as well as field changes due to motion outside the ROI.

On a standard 3-T MRI system, the temperature-induced shift of the water resonance frequency is only about 1 Hz/°C, compared to the much stronger shift of 10–50 Hz induced by magnetic susceptibility gradients, field drift, and respiratory motion. While in tissues containing fat, the almost temperature-insensitive resonance frequency of lipid protons could, in principle, be used to correct for macroscopic field inhomogeneity and motion (180), in practice, this is not possible without incurring in temperature errors of a few degrees Celsius (181, 182). At the macroscopic and microscopic level, water and fat spins reside in different tissue compartments with different magnetic susceptibilities. Therefore, the local magnetic field experienced by water protons is not the same as the one experienced by fat protons. The difference in the local field experienced by the two chemically different spins, which depends on the specific intra-voxel distribution of water and fat spins and on the orientation of the distribution with respect to the main magnetic field, can be on the order of a few tenths of ppm (181–183). These microscopic susceptibility gradients preclude the possibility of a pre-calibration of water-fat frequency shift as a function of temperature *in vitro*, in samples that do not necessarily reflect the specific intra-voxel water-fat distribution and orientation found *in vivo*. In addition, the magnetic susceptibility of fat increases with temperature by 0.008 ppm/°C, leading to a change in the local magnetic field distribution that is typically observed as a broadening of the water resonance frequency peak, and to a non-linear and nonlocal relation between temperature and water resonance frequency (183). As already stated, the relative water–fat frequency separation strongly depends on the specific intra-voxel water–fat distribution. Therefore, *in vitro* calibration on water–fat mixtures cannot be used to estimate absolute tissue temperature *in vivo*, as it has been done in some studies (91). Also *in vivo*, voxel misregistration due to breathing motion can undermine measurements of temperature change in the tissue (184). While these effects due to the presence of fat have not precluded the use of PRFS for temperature monitoring during thermal ablation treatments of

tumors, where the temperature is raised by tens of degrees Celsius to cause tissue necrosis (185), or in rodents, where BAT temperature can increase by more than 5°C (186), it can be a limiting factor in the measurement of the small temperature increase (1–2°C) expected in human BAT during cold exposure.

In principle, one could think of using iMQC to remove the effect of magnetic field inhomogeneity and motion at the microscopic level. One particular type of iMQC signal, the intermolecular zero quantum coherence (iZQC), evolves at the difference in frequency between water and methylene protons, resulting in removal of some inhomogeneous broadening at the microscopic level, and possibly enabling absolute temperature measurements in the tissue (132). In practice, this is precluded by the much higher sensitivity of the water–fat iZQC frequency to the specific water–fat distribution at the microscopic level (187).

129Xe-Based MR Thermometry [Recently Proposed Technique]

Recently, the use of hyperpolarized ^{129}Xe gas for MR thermometry measurements in fat-containing tissues was demonstrated (188). This method relies on the much higher temperature sensitivity (−0.2 ppm/°C) of the chemical shift of xenon dissolved in fat, the major resonance frequency detected in ^{129}Xe spectra acquired in BAT. This methodology was demonstrated in both rodents (41, 154, 183) and humans (189). More recently, the ability to directly measure absolute temperature in fat tissues was demonstrated (154). This is accomplished by using the lipid protons, in which xenon dissolves, as an internal resonance frequency reference to remove the effect of magnetic susceptibility gradients and to make the measurement insensitive to changes in the local magnetic susceptibility caused by possible changes in tissue oxygenation levels (**Figure 10**). Absolute temperature measurements would be particularly advantageous in humans, where a single measurement of absolute temperature could be used to tell apart active from inactive BAT.

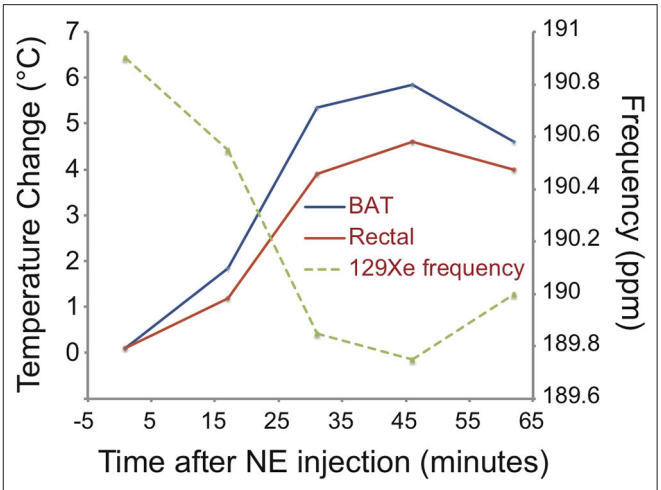

FIGURE 10 | Temperature change in iBAT as detected by hyperpolarized ^{129}Xe MR thermometry in a C57BL/6 mouse during norepinephrine stimulation of BAT thermogenesis. Right after the injection of norepinephrine, an up-field drift of the temperature-sensitive resonance frequency of xenon dissolved in the lipid droplets of BAT is observed. The frequency drift reflects a change in iBAT temperature of almost 6°C . The change in rectal temperature follows, with some delay, the change in BAT temperature, indicating that BAT is the main driver for the increase in body temperature. This figure is original and based on data from (41).

DISCUSSION

MRI measurements of tissue fat fraction have gained much attention as a radiation-free alternative to ^{18}F-FDG-PET/CT. **Table 2** summarizes a critical assessment of existing MR methods in BAT research. These techniques have been proposed to differentiate the more hydrated BAT from WAT independently of BAT thermogenic activity and were the first to be used in humans. One reason is that MR fat fraction measurements are widely available on clinical scanners, where they are typically employed for estimating fat fraction in organs such as the liver, skeletal muscle, and bone marrow. However, as discussed in the 2019 ISMRM Workshop on MRI of Obesity and Metabolic Disorders (191), there is no consensus on the specificity of these techniques for BAT detection, or on the specific protocol needed for quantitative measurement of fat fraction and fat fraction changes in human supraclavicular fat.

Another issue faced by current biomedical imaging research of BAT is the lack of a good animal model. Most of the techniques have been validated in mice or rats that are young, fed on a low-calorie diet, and living under constant thermal stress, i.e., under thermal and nutritional conditions that are very far from human conditions. Thus, their BAT morphology (tissue fat content, average cell size, mitochondria content, and vascularization) and thermogenic capacity (UCP1 content) are different from that of adult humans. It should therefore come as no surprise if human translations of these techniques do not turn out as expected. As animal models have been extremely valuable for developing novel MR methodologies, the choice of the appropriate animal model should be carefully considered before human translation of these technologies. For example, humanized mice, i.e., mice fed with a Western diet and kept at a thermoneutral condition, whose BAT better resembles that of adult humans, could be a better choice than chow fed mice kept at a standard laboratory temperature.

MR Experimental Challenges

Because of its location, right above the chest cavity, BAT is highly susceptible to motion, which can lead to tissue displacement and consequent field variations during image acquisition (**Supplementary Material 1**). In addition, organized around major vessels, which supply the upper extremities and the head with blood, the tissue is also extremely sensitive to pulsation artifacts (**Supplementary Material 2**). If no triggering or other motion control is done, motion can significantly blur any tissue maps and introduce errors in the quantitative measurements. Ghosting artifacts originating from periodic respiratory motion can be reduced either by avoiding the phase encoding direction along the axis of motion (most severe in feet/head direction) or by a respiratory-triggered acquisition. The sensitivity to any motion becomes especially evident when several images are required to generate one quantitative map,

TABLE 2 | Comparison of advantages and weaknesses of existing MR methods for BAT research.

	Differentiating BAT/WAT at rest	BAT activation detection	How quantitative at the moment	Availability	Motion robustness	Temporal resolution	Spatial resolution	Specificity for BAT	Other physiological confounders	Contrast agent-free
BAT Morphology										
PDFF✦	−	+	++	(+)	+	−	++	−		✓
T2* mapping✦	+	(−)	−	(+)	+	−	++	(+)	Perfusion	✓
DW-MRS of fat✦	++	−	+	+	−−	−	−−	+		✓
DW-MRS of water✦	+	−	−	+	−	−	−−	(+)		✓
BAT Perfusion + Oxygenation										
DCE✦	+	++	−	+	+	++	+	+		✗
ASL✦	+	++	−	+	−	+	+	+		✓
BOLD✦	−	+	−	+	−−	+	++	(+)	Microstructure	✓
Xenon✦ (Perfusion rodents with respiratoy trigger)	+	++	++	−	++	+	−	+		✗
Xenon✦ (Perfusion Humans)	+	++	+	−	++	++	−−	+		✗
BAT Thermometry										
PRFS✦	−−	(+)	(−)	+	−−	−	+	(+)	Many (190)	✓
Xenon✦ (Thermometry)	−	++	++	−	++	++	−	++		✗
iMQC✦	+	+	(+)	(+)	++	−−	−−	(+)	Fat susceptibility	✓
BAT Metabolism										
^{31}P	−	(−)	(+)	(+)	+	−−	−−	+	Partial volume	✓
^{13}C	−	+	(+)	−−	++	++	−−	+	Fast metabolic dynamics	✗
^{2}H✦ (^{2}H-glucose)	−	+	−	−	−	−−	−−	−	Fat peak contaminates metabolites	✗

Grades were given ranging from "−−" for very bad performance to "++" for very good performance. The parentheses indicate that the statement holds true only under certain circumstances. Techniques that the co-authors have experience with to study BAT are marked with a✦.

including DWI, MR fat fraction maps, T_2* mapping, etc. In case of diffusion contrast, physiological motion may be misinterpreted as diffusion, causing an overestimation of the diffusion parameter. In case of phase-sensitive acquisitions such as fat fraction and T_2* mapping, the periodic field variations may hamper accurate estimation of these parameters. How respiratory motion-induced tissue displacement and main magnetic field fluctuations influence the estimated fat fraction remains a critical unanswered question and needs to be addressed in future studies (192).

FUTURE PERSPECTIVES

MRI offers the possibility to perform larger and longitudinal studies in healthy cohorts as it does not use ionizing radiation and, usually, does not need injections of contrast material. Longitudinal studies could help in assessing the efficacy of BAT targeting therapies, as well as understanding the role of BAT within the complex human physiology.

However, cost, long scan times, and the need to use specific sequences limit the application of MRI in large cohorts, so most MRI studies published so far are reported on smaller numbers of participants ($n < 100$).

BAT imaging is challenging because of its temporal heterogeneity: Because BAT can be regarded as a highly active organ, its presence, morphology, and activity strongly depend on a range of environmental (weather, season) and hormonal (for instance postprandial, menstrual cycle) conditions. While future imaging study designs should pay more attention to these factors, these factors may also open many doors for potential interesting investigations. Certainly, when doing activation studies, MR methods will need to improve in temporal resolution.

BAT imaging is also challenging because of its spatial heterogeneity: Because BAT is highly vascularized, and interweaved with WAT, MR methods for characterizing BAT will highly profit from a higher spatial resolution, avoiding partial volume effects. This could be realized by translation to higher magnetic fields, the use of superconducting RF receive coils (193, 194), more advanced acquisition and reconstruction techniques involving parallel imaging (195) and compressed sensing (196), and better signal modeling (197) in case of quantitative MR parameter fitting.

BAT imaging is also challenging because of motion influences from both breathing and vessel pulsation. Instead of simply translating quantitative parameter mapping methods established in examinations of other more rigid body parts, such as the brain or the musculoskeletal system, more inspiration could be found from cardiac MR.

So far, the implemented MR methods have been more reliable in detecting activated BAT vs. non-activated BAT compared to differentiating non-activated BAT from WAT (99, 102). One striking reason for this is the fact that the allegedly quantitative methods were in fact rather qualitative, providing only a contrast between the activated and the non-activated state. Good news is that the development of quantitative MR methods is not for a long time yet exhausted. There is a lot of promising work left to do in the entire pipeline from clever sequence design, over parameter modeling and image analysis.

For making MR research of BAT a success story, emphasis must be placed on the continuous development of robust and reproducible quantitative methods.

CONCLUSION

MRI and MRS provide a wide range of tools for assessing various aspects of both BAT morphometry and function. They are very attractive because they have no limitation in imaging penetration depth, do not deliver any mutagenic radiation, and work with spins residing naturally in the body as well as with a range of MR-sensitive tracers. MR methods to assess BAT microstructure include fat fraction mapping, T2* mapping, diffusion imaging, and iMQC imaging. BAT metabolic activity can be examined directly with ^{31}P, ^{2}H, and hyperpolarized ^{13}C MRI and MRS, and indirectly via perfusion sensitive sequences including DCE, QSM, T2*, and ^{129}Xe. MR thermometry was successfully used to observe thermogenesis of BAT using PRFS in rodents and ^{129}Xe in humans. Despite the prosperous reports of MR studies of BAT, the wider adoption of many of these MR techniques requires further validation, including fat fraction mapping. Even though it is currently the most widely used technique, special care is required due to the here discussed limitations in quantifying the BAT fraction in the human supraclavicular fossa. Nonetheless, the versatility of possible MRI contrast mechanisms and the non-invasive character of MRI remain significant advocates for supporting continuous technical developments for MRI methods in the analysis of BAT morphometry and function.

AUTHOR CONTRIBUTIONS

DK devised the outline of the manuscript. All authors contributed to drafting a first version. RB and MW created the figures for the manuscript. RB, DK, and MW worked on continuous revision of the manuscript. Everyone read and approved the submitted version.

FUNDING

The present work was supported by the European Research Council (grant agreement no. 677661, ProFatMRI, and grant agreement no. 875488, FatVirtualBiopsy), the German Research Foundation (DFG-SFB824/A9), and the United States National Institute of Diabetes and Digestive and Kidney Diseases (R01DK108231).

SUPPLEMENTARY MATERIAL

The Supplementary Material for this article can be found online at: https://www.frontiersin.org/articles/10.3389/fendo.2020.00421/full#supplementary-material

Supplementary Material 1 | Illustration of respiratory motion induced effects on quantitative maps in the supraclavicular region by breath hold scans at full inspiration and full expiration using a 6-echo data set. **(A)** PDFF maps of the same slice show anatomical variations comparing the scan from inspiration and expiration state. **(B)** The corresponding calculated field maps from the different respiration states show a large field variation within one image due to the complex geometry in that region including the proximity to the lungs. **(C)** The large difference of the field maps between inspiration and expiration indicates large respiratory-induced field fluctuations that may cause quantification errors when not accounted for.

Supplementary Material 2 | The video shows the pulsation effect of the large vessels within the supraclavicular fossa causing severe tissue deformation in the neighboring tissue. This is challenging in the context of diffusion-weighted acquisitions and quite similar to the motion problem faced during cardiac imaging.

REFERENCES

1. Heaton JM. The distribution of brown adipose tissue in the human. *J Anat.* (1972) 112(Pt 1):35–9.
2. Barrington SF, Maisey MN. Skeletal muscle uptake of fluorine-18-FDG: effect of oral diazepam. *J Nucl Med.* (1996) 37:1127–9.
3. Hany TF, Gharehpapagh E, Kamel EM, Buck A, Himms-Hagen J, von Schulthess GK. Brown adipose tissue: a factor to consider in symmetrical tracer uptake in the neck and upper chest region. *Eur J Nucl Med Mol Imaging.* (2002) 29:1393–8. doi: 10.1007/s00259-002-0902-6
4. Cypess AM, Lehman S, Williams G, Tal I, Rodman D, Goldfine AB, et al. Identification and importance of brown adipose tissue in adult humans. *N Engl J Med.* (2009) 360:1509–17. doi: 10.1056/NEJMoa0810780
5. van Marken Lichtenbelt WD, Vanhommerig JW, Smulders NM, Drossaerts JM, Kemerink GJ, Bouvy ND, et al. Cold-activated brown adipose tissue in healthy men. *N Engl J Med.* (2009) 360:1500–8. doi: 10.1056/NEJMoa0808718
6. Virtanen KA, Lidell ME, Orava J, Heglind M, Westergren R, Niemi T, et al. Functional brown adipose tissue in healthy adults. *N Engl J Med.* (2009) 360:1518–25. doi: 10.1056/NEJMoa0808949
7. Cinti S. The adipose organ. In: Fantuzzi G, Mazzone T, editors. *Adipose Tissue and Adipokines in Health and Disease*. Totowa, NJ: Humana Press (2007). p. 3–19. doi: 10.1007/978-1-59745-370-7_1
8. Chen KY, Cypess AM, Laughlin MR, Haft CR, Hu HH, Bredella MA, et al. Brown Adipose Reporting Criteria in Imaging Studies (BARCIST 1.0): recommendations for standardized FDG-PET/CT experiments in humans. *Cell Metab.* (2016) 24:210–22. doi: 10.1016/j.cmet.2016.07.014
9. Sampath SC, Sampath SC, Bredella MA, Cypess AM, Torriani M. Imaging of brown adipose tissue: state of the art. *Radiology.* (2016) 280:4–19. doi: 10.1148/radiol.2016150390

10. Ma SW, Foster DO. Uptake of glucose and release of fatty acids and glycerol by rat brown adipose tissue *in vivo*. *Can J Physiol Pharmacol.* (1986) 64:609–14. doi: 10.1139/y86-101
11. Cannon B, Nedergaard J. Brown adipose tissue: function and physiological significance. *Physiol Rev.* (2004) 84:277–359. doi: 10.1152/physrev.00015.2003
12. Blondin DP, Labbe SM, Noll C, Kunach M, Phoenix S, Guerin B, et al. Selective impairment of glucose but not fatty acid or oxidative metabolism in brown adipose tissue of subjects with type 2 diabetes. *Diabetes.* (2015) 64:2388–97. doi: 10.2337/db14-1651
13. Olsen JM, Csikasz RI, Dehvari N, Lu L, Sandström A, Öberg AI, et al. β3-Adrenergically induced glucose uptake in brown adipose tissue is independent of UCP1 presence or activity: Mediation through the mTOR pathway. *Mol Metab*. (2017) 6:611–9. doi: 10.1016/j.molmet.2017.02.006
14. Ouellet V, Labbe SM, Blondin DP, Phoenix S, Guerin B, Haman F, et al. Brown adipose tissue oxidative metabolism contributes to energy expenditure during acute cold exposure in humans. *J Clin Invest.* (2012) 122:545–52. doi: 10.1172/JCI60433
15. Hwang JJ, Yeckel CW, Gallezot JD, Aguiar RB, Ersahin D, Gao H, et al. Imaging human brown adipose tissue under room temperature conditions with (11)C-MRB, a selective norepinephrine transporter PET ligand. *Metabolism.* (2015) 64:747–55. doi: 10.1016/j.metabol.2015.03.001
16. Crandall JP, Gajwani P, Joo OH, Mawhinney DD, Sterzer F, Wahl RL. Repeatability of brown adipose tissue measurements on FDG PET/CT following a simple cooling procedure for BAT activation. *PLoS ONE.* (2019) 14:e0214765. doi: 10.1371/journal.pone.0214765
17. Muzik O, Mangner TJ, Leonard WR, Kumar A, Janisse J, Granneman JG. 15O PET measurement of blood flow and oxygen consumption in cold-activated human brown fat. *J Nucl Med*. (2013) 54:523–31. doi: 10.2967/jnumed.112.111336
18. Leitner BP, Huang S, Brychta RJ, Duckworth CJ, Baskin AS, McGehee S, et al. Mapping of human brown adipose tissue in lean and obese young men. *Proc Natl Acad Sci USA*. (2017) 114:8649–54. doi: 10.1073/pnas.1705287114
19. Hu HH, Chung SA, Nayak KS, Jackson HA, Gilsanz V. Differential computed tomographic attenuation of metabolically active and inactive adipose tissues: preliminary findings. *J Comput Assist Tomogr.* (2011) 35:65–71. doi: 10.1097/RCT.0b013e3181fc2150
20. Baba S, Jacene HA, Engles JM, Honda H, Wahl RL. CT Hounsfield units of brown adipose tissue increase with activation: preclinical and clinical studies. *J Nucl Med.* (2010) 51:246–50. doi: 10.2967/jnumed.109.068775
21. Borga M, Virtanen KA, Romu T, Leinhard OD, Persson A, Nuutila P, et al. Brown adipose tissue in humans: detection and functional analysis using PET (positron emission tomography), MRI (magnetic resonance imaging), and DECT (dual energy computed tomography). *Methods Enzymol.* (2014) 537:141–59. doi: 10.1016/B978-0-12-411619-1.00008-2
22. Flynn A, Li Q, Panagia M, Abdelbaky A, MacNabb M, Samir A, et al. Contrast-enhanced ultrasound: a novel noninvasive. Nonionizing method for the detection of brown adipose tissue in humans. *J Am Soc Echocardiogr.* (2015) 28:1247–54. doi: 10.1016/j.echo.2015.06.014
23. Baron DM, Clerte M, Brouckaert P, Raher MJ, Flynn AW, Zhang H, et al. *In vivo* noninvasive characterization of brown adipose tissue blood flow by contrast ultrasound in mice. *Circ Cardiovasc Imaging.* (2012) 5:652–9. doi: 10.1161/CIRCIMAGING.112.975607
24. Clerte M, Baron DM, Brouckaert P, Ernande L, Raher MJ, Flynn AW, et al. Brown adipose tissue blood flow and mass in obesity: a contrast ultrasound study in mice. *J Am Soc Echocardiogr*. (2013) 26:1465–73. doi: 10.1016/j.echo.2013.07.015
25. Zhang X, Kuo C, Moore A, Ran C. Cerenkov luminescence imaging of interscapular brown adipose tissue. *J Vis Exp*. (2014) 2014:e51790. doi: 10.3791/51790
26. Nirengi S, Yoneshiro T, Sugie H, Saito M, Hamaoka T. Human brown adipose tissue assessed by simple, noninvasive near-infrared time-resolved spectroscopy. *Obesity*. (2015) 23:973–80. doi: 10.1002/oby.21012
27. Nakayama A, Bianco AC, Zhang CY, Lowell BB, Frangioni JV. Quantitation of brown adipose tissue perfusion in transgenic mice using near-infrared fluorescence imaging. *Mol Imaging.* (2003) 2:37–49. doi: 10.1162/153535003765276273
28. Reber J, Willershauser M, Karlas A, Paul-Yuan K, Diot G, Franz D, et al. Non-invasive measurement of brown fat metabolism based on optoacoustic imaging of hemoglobin gradients. *Cell Metab.* (2018) 27:689–701 e4. doi: 10.1016/j.cmet.2018.02.002
29. Bauwens M, Wierts R, van Royen B, Bucerius J, Backes W, Mottaghy F, et al. Molecular imaging of brown adipose tissue in health and disease. *Eur J Nucl Med Mol Imaging.* (2014) 41:776–91. doi: 10.1007/s00259-013-2611-8
30. Chondronikola M, Beeman SC, Wahl RL. Non-invasive methods for the assessment of brown adipose tissue in humans. *J Physiol.* (2018) 596:363–78. doi: 10.1113/JP274255
31. Frankl J, Sherwood A, Clegg DJ, Scherer PE, Oz OK. Imaging metabolically active fat: a literature review and mechanistic insights. *Int J Mol Sci.* (2019) 20:5509. doi: 10.3390/ijms20215509
32. Marzola P, Boschi F, Moneta F, Sbarbati A, Zancanaro C. Preclinical *in vivo* imaging for fat tissue identification, quantification, and functional characterization. *Front Pharmacol.* (2016) 7:336. doi: 10.3389/fphar.2016.00336
33. Ntziachristos V, Pleitez MA, Aime S, Brindle KM. Emerging technologies to image tissue metabolism. *Cell Metab.* (2019) 29:518–38. doi: 10.1016/j.cmet.2018.09.004
34. Ong FJ, Ahmed BA, Oreskovich SM, Blondin DP, Haq T, Konyer NB, et al. Recent advances in the detection of brown adipose tissue in adult humans: a review. *Clin Sci.* (2018) 132:1039–54. doi: 10.1042/CS20170276
35. Sun L, Yan J, Sun L, Velan SS, Leow MKS. A synopsis of brown adipose tissue imaging modalities for clinical research. *Diabetes Metab.* (2017) 43:401–10. doi: 10.1016/j.diabet.2017.03.008
36. van der Lans AA, Wierts R, Vosselman MJ, Schrauwen P, Brans B, van Marken Lichtenbelt WD. Cold-activated brown adipose tissue in human adults: methodological issues. *Am J Physiol Regul Integr Comp Physiol.* (2014) 307:R103–13. doi: 10.1152/ajpregu.00021.2014
37. Franz D, Syvari J, Weidlich D, Baum T, Rummeny EJ, Karampinos DC. Magnetic resonance imaging of adipose tissue in metabolic dysfunction. *Rofo.* (2018) 190:1121–30. doi: 10.1055/a-0612-8006
38. Hu HH, Kan HE. Quantitative proton MR techniques for measuring fat. *NMR Biomed.* (2013) 26:1609–29. doi: 10.1002/nbm.3025
39. Hu HH. Magnetic resonance of brown adipose tissue: a review of current techniques. *Crit Rev Biomed Eng.* (2015) 43:161–81. doi: 10.1615/CritRevBiomedEng.2015014377
40. Karampinos DC, Weidlich D, Wu M, Hu HH, Franz D. Techniques and applications of magnetic resonance imaging for studying brown adipose tissue morphometry and function. *Handb Exp Pharmacol.* (2019) 251:299–324. doi: 10.1007/164_2018_158
41. Branca RT, He T, Zhang L, Floyd CS, Freeman M, White C, et al. Detection of brown adipose tissue and thermogenic activity in mice by hyperpolarized xenon MRI. *Proc Natl Acad Sci USA*. (2014) 111:18001–6. doi: 10.1073/pnas.1403697111
42. Petrovic N, Walden TB, Shabalina IG, Timmons JA, Cannon B, Nedergaard J. Chronic peroxisome proliferator-activated receptor gamma (PPARgamma) activation of epididymally derived white adipocyte cultures reveals a population of thermogenically competent, UCP1-containing adipocytes molecularly distinct from classic brown adipocytes. *J Biol Chem.* (2010) 285:7153–64. doi: 10.1074/jbc.M109.053942
43. Wu J, Bostrom P, Sparks LM, Ye L, Choi JH, Giang AH, et al. Beige adipocytes are a distinct type of thermogenic fat cell in mouse and human. *Cell.* (2012) 150:366–76. doi: 10.1016/j.cell.2012.05.016
44. Zoico E, Rubele S, De Caro A, Nori N, Mazzali G, Fantin F, et al. Brown and beige adipose tissue and aging. *Front Endocrinol.* (2019) 10:368. doi: 10.3389/fendo.2019.00368
45. Ikeda K, Maretich P, Kajimura S. The common and distinct features of brown and beige adipocytes. *Trends Endocrinol Metab.* (2018) 29:191–200. doi: 10.1016/j.tem.2018.01.001
46. Frontini A, Cinti S. Distribution and development of brown adipocytes in the murine and human adipose organ. *Cell Metab.* (2010) 11:253–6. doi: 10.1016/j.cmet.2010.03.004
47. Jespersen NZ, Larsen TJ, Peijs L, Daugaard S, Homoe P, Loft A, et al. A classical brown adipose tissue mRNA signature partly overlaps with brite in the supraclavicular region of adult humans. *Cell Metab.* (2013) 17:798–805. doi: 10.1016/j.cmet.2013.04.011

48. Lidell ME, Betz MJ, Dahlqvist Leinhard O, Heglind M, Elander L, Slawik M, et al. Evidence for two types of brown adipose tissue in humans. *Nat Med.* (2013) 19:631–4. doi: 10.1038/nm.3017
49. Jespersen NZ, Feizi A, Andersen ES, Heywood S, Hattel HB, Daugaard S, et al. Heterogeneity in the perirenal region of humans suggests presence of dormant brown adipose tissue that contains brown fat precursor cells. *Mol Metab.* (2019) 24:30–43. doi: 10.1016/j.molmet.2019.03.005
50. Blondin DP, Labbe SM, Tingelstad HC, Noll C, Kunach M, Phoenix S, et al. Increased brown adipose tissue oxidative capacity in cold-acclimated humans. *J Clin Endocrinol Metab.* (2014) 99:E438–46. doi: 10.1210/jc.2013-3901
51. Ussar S, Lee KY, Dankel SN, Boucher J, Haering MF, Kleinridders A, et al. ASC-1, PAT2, and P2RX5 are cell surface markers for white, beige, and brown adipocytes. *Sci Transl Med.* (2014) 6:247ra103. doi: 10.1126/scitranslmed.3008490
52. Perdikari A, Leparc GG, Balaz M, Pires ND, Lidell ME, Sun W, et al. BATLAS: deconvoluting brown adipose tissue. *Cell Rep.* (2018) 25:784–97.e4. doi: 10.1016/j.celrep.2018.09.044
53. Sharp LZ, Shinoda K, Ohno H, Scheel DW, Tomoda E, Ruiz L, et al. Human BAT possesses molecular signatures that resemble beige/brite cells. *PLoS ONE.* (2012) 7:e49452. doi: 10.1371/journal.pone.0049452
54. Reeder SB, Cruite I, Hamilton G, Sirlin CB. Quantitative assessment of liver fat with magnetic resonance imaging and spectroscopy. *J Magn Reson Imaging.* (2011) 34:729–49. doi: 10.1002/jmri.22580
55. Hamilton G, Smith DL, Jr., Bydder M, Nayak KS, Hu HH. MR properties of brown and white adipose tissues. *J Magn Reson Imaging.* (2011) 34:468–73. doi: 10.1002/jmri.22623
56. Lunati E, Marzola P, Nicolato E, Fedrigo M, Villa M, Sbarbati A. *In vivo* quantitative lipidic map of brown adipose tissue by chemical shift imaging at 4.7 Tesla. *J Lipid Res.* (1999) 40:1395–400.
57. Sbarbati A, Guerrini U, Marzola P, Asperio R, Osculati F. Chemical shift imaging at 4.7 tesla of brown adipose tissue. *J Lipid Res.* (1997) 38:343–7.
58. Reeder SB, Hu HH, Sirlin CB. Proton density fat-fraction: a standardized MR-based biomarker of tissue fat concentration. *J Magn Reson Imaging.* (2012) 36:1011–4. doi: 10.1002/jmri.23741
59. Yokoo T, Serai SD, Pirasteh A, Bashir MR, Hamilton G, Hernando D, et al. Linearity, bias, and precision of hepatic proton density fat fraction measurements by using MR imaging: a meta-analysis. *Radiology.* (2018) 286:486–98. doi: 10.1148/radiol.2017170550
60. Karampinos DC, Ruschke S, Dieckmeyer M, Diefenbach M, Franz D, Gersing AS, et al. Quantitative MRI and spectroscopy of bone marrow. *J Magn Reson Imaging.* (2018) 47:332–53. doi: 10.1002/jmri.25769
61. Hamilton G, Schlein AN, Middleton MS, Hooker CA, Wolfson T, Gamst AC, et al. *In vivo* triglyceride composition of abdominal adipose tissue measured by (1) H MRS at 3T. *J Magn Reson Imaging.* (2017) 45:1455–63. doi: 10.1002/jmri.25453
62. Ren J, Dimitrov I, Sherry AD, Malloy CR. Composition of adipose tissue and marrow fat in humans by 1H NMR at 7 Tesla. *J Lipid Res.* (2008) 49:2055–62. doi: 10.1194/jlr.D800010-JLR200
63. Karampinos DC, Yu H, Shimakawa A, Link TM, Majumdar S. T(1)-corrected fat quantification using chemical shift-based water/fat separation: application to skeletal muscle. *Magn Reson Med.* (2011) 66:1312–26. doi: 10.1002/mrm.22925
64. Liu CY, McKenzie CA, Yu H, Brittain JH, Reeder SB. Fat quantification with IDEAL gradient echo imaging: correction of bias from T(1) and noise. *Magn Reson Med.* (2007) 58:354–64. doi: 10.1002/mrm.21301
65. Ruschke S, Eggers H, Kooijman H, Diefenbach MN, Baum T, Haase A, et al. Correction of phase errors in quantitative water-fat imaging using a monopolar time-interleaved multi-echo gradient echo sequence. *Magn Reson Med.* (2017) 78:984–96. doi: 10.1002/mrm.26485
66. Yu H, Shimakawa A, McKenzie CA, Lu W, Reeder SB, Hinks RS, et al. Phase and amplitude correction for multi-echo water-fat separation with bipolar acquisitions. *J Magn Reson Imaging.* (2010) 31:1264–71. doi: 10.1002/jmri.22111
67. Wang X, Hernando D, Reeder SB. Sensitivity of chemical shift-encoded fat quantification to calibration of fat MR spectrum. *Magn Reson Med.* (2016) 75:845–51. doi: 10.1002/mrm.25681
68. Hernando D, Sharma SD, Kramer H, Reeder SB. On the confounding effect of temperature on chemical shift-encoded fat quantification. *Magn Reson Med.* (2014) 72:464–70. doi: 10.1002/mrm.24951
69. McCallister D, Zhang L, Burant A, Katz L, Branca RT. Effect of microscopic susceptibility gradients on chemical-shift-based fat fraction quantification in supraclavicular fat. *J Magn Reson Imaging.* (2019) 49:141–51. doi: 10.1002/jmri.26219
70. Hernando D, Kellman P, Haldar JP, Liang ZP. Robust water/fat separation in the presence of large field inhomogeneities using a graph cut algorithm. *Magn Reson Med.* (2010) 63:79–90. doi: 10.1002/mrm.22177
71. Diefenbach MN, Ruschke S, Eggers H, Meineke J, Rummeny EJ, Karampinos DC. Improving chemical shift encoding-based water-fat separation based on a detailed consideration of magnetic field contributions. *Magn Reson Med.* (2018) 80:990–1004. doi: 10.1002/mrm.27097
72. Sharma SD, Artz NS, Hernando D, Horng DE, Reeder SB. Improving chemical shift encoded water-fat separation using object-based information of the magnetic field inhomogeneity. *Magn Reson Med.* (2015) 73:597–604. doi: 10.1002/mrm.25163
73. Scotti A, Tain RW, Li W, Gil V, Liew CW, Cai K. Mapping brown adipose tissue based on fat water fraction provided by Z-spectral imaging. *J Magn Reson Imaging.* (2017) 47:1527–33. doi: 10.1002/jmri.25890
74. Scotti A, Li L, Damen F, Li W, Gil V, Zhu W, et al., Thermal measurement in fatty tissues with Z-Spectrum Imaging. In: *Proceedings of 27th Int Society for Magnetic Resonance in Medicine*. Montréal, QC (2019).
75. de Jong JMA, Sun W, Pires ND, Frontini A, Balaz M, Jespersen NZ, et al. Human brown adipose tissue is phenocopied by classical brown adipose tissue in physiologically humanized mice. *Nat Metab.* (2019) 1:830–43. doi: 10.1038/s42255-019-0101-4
76. Osculati F, Leclercq F, Sbarbati A, Zancanaro C, Cinti S, Antonakis K. Morphological identification of brown adipose tissue by magnetic resonance imaging in the rat. *Eur J Radiol.* (1989) 9:112–4.
77. Ito T, Tanuma Y, Yamada M, Yamamoto M. Morphological studies on brown adipose tissue in the bat and in humans of various ages. *Arch Histol Cytol.* (1991) 54:1–39. doi: 10.1679/aohc.54.1
78. Grimpo K, Volker MN, Heppe EN, Braun S, Heverhagen JT, Heldmaier G. Brown adipose tissue dynamics in wild-type and UCP1-knockout mice: *in vivo* insights with magnetic resonance. *J Lipid Res.* (2014) 55:398–409. doi: 10.1194/jlr.M042895
79. Hu HH, Yin L, Aggabao PC, Perkins TG, Chia JM, Gilsanz V. Comparison of brown and white adipose tissues in infants and children with chemical-shift-encoded water-fat MRI. *J Magn Reson Imaging.* (2013) 38:885–96. doi: 10.1002/jmri.24053
80. Kortelainen ML, Pelletier G, Ricquier D, Bukowiecki LJ. Immunohistochemical detection of human brown adipose tissue uncoupling protein in an autopsy series. *J Histochem Cytochem.* (1993) 41:759–64. doi: 10.1177/41.5.8468458
81. Franssens BT, Hoogduin H, Leiner T, van der Graaf Y, Visseren FLJ. Relation between brown adipose tissue and measures of obesity and metabolic dysfunction in patients with cardiovascular disease. *J Magn Reson Imaging.* (2017) 46:497–504. doi: 10.1002/jmri.25594
82. Franz D, Karampinos DC, Rummeny EJ, Souvatzoglou M, Beer AJ, Nekolla SG, et al. Discrimination between brown and white adipose tissue using a 2-point dixon water-fat separation method in simultaneous PET/MRI. *J Nucl Med.* (2015) 56:1742–7. doi: 10.2967/jnumed.115.160770
83. Holstila M, Virtanen KA, Gronroos TJ, Laine J, Lepomaki V, Saunavaara J, et al. Measurement of brown adipose tissue mass using a novel dual-echo magnetic resonance imaging approach: a validation study. *Metabolism.* (2013) 62:1189–98. doi: 10.1016/j.metabol.2013.03.002
84. Hu HH, Tovar JP, Pavlova Z, Smith ML, Gilsanz V. Unequivocal identification of brown adipose tissue in a human infant. *J Magn Reson Imaging.* (2012) 35:938–42. doi: 10.1002/jmri.23531
85. Hu HH, Wu TW, Yin L, Kim MS, Chia JM, Perkins TG, et al. MRI detection of brown adipose tissue with low fat content in newborns with hypothermia. *Magn Reson Imaging.* (2014) 32:107–17. doi: 10.1016/j.mri.2013.10.003
86. Lundstrom E, Ljungberg J, Andersson J, Manell H, Strand R, Forslund A, et al. Brown adipose tissue estimated with the magnetic resonance imaging fat fraction is associated with glucose metabolism in adolescents. *Pediatr Obes.* (2019) 14:e12531. doi: 10.1111/ijpo.12531
87. Chen YC, Cypess AM, Chen YC, Palmer M, Kolodny G, Kahn CR, et al. Measurement of human brown adipose tissue volume and activity using anatomic MR imaging and functional MR imaging. *J Nucl Med.* (2013) 54:1584–7. doi: 10.2967/jnumed.112.117275

88. Franz D, Weidlich D, Freitag F, Holzapfel C, Drabsch T, Baum T, et al. Association of proton density fat fraction in adipose tissue with imaging-based and anthropometric obesity markers in adults. *Int J Obes.* (2018) 42:175–82. doi: 10.1038/ijo.2017.194
89. Gifford A, Towse TF, Walker RC, Avison MJ, Welch EB. Human brown adipose tissue depots automatically segmented by positron emission tomography/computed tomography and registered magnetic resonance images. *J Vis Exp*. (2015) 96:52415. doi: 10.3791/52415
90. Gifford A, Towse TF, Walker RC, Avison MJ, Welch EB. Characterizing active and inactive brown adipose tissue in adult humans using PET-CT and MR imaging. *Am J Physiol Endocrinol Metab.* (2016) 311:E95–104. doi: 10.1152/ajpendo.00482.2015
91. Koskensalo K, Raiko J, Saari T, Saunavaara V, Eskola O, Nuutila P, et al. Human brown adipose tissue temperature and fat fraction are related to its metabolic activity. *J Clin Endocrinol Metab.* (2017) 102:1200–7. doi: 10.1210/jc.2016-3086
92. McCallister A, Zhang L, Burant A, Katz L, Branca RT. A pilot study on the correlation between fat fraction values and glucose uptake values in supraclavicular fat by simultaneous PET/MRI. *Magn Reson Med.* (2017) 78:1922–32. doi: 10.1002/mrm.26589
93. Romu T, Vavruch C, Dahlqvist-Leinhard O, Tallberg J, Dahlstrom N, Persson A, et al. A randomized trial of cold-exposure on energy expenditure and supraclavicular brown adipose tissue volume in humans. *Metabolism.* (2016) 65:926–34. doi: 10.1016/j.metabol.2016.03.012
94. Franssens BT, Eikendal AL, Leiner T, van der Graaf Y, Visseren FL, Hoogduin JM. Reliability and agreement of adipose tissue fat fraction measurements with water-fat MRI in patients with manifest cardiovascular disease. *NMR Biomed.* (2016) 29:48–56. doi: 10.1002/nbm.3444
95. Reddy NL, Jones TA, Wayte SC, Adesanya O, Sankar S, Yeo YC, et al. Identification of brown adipose tissue using MR imaging in a human adult with histological and immunohistochemical confirmation. *J Clin Endocrinol Metab.* (2014) 99:E117–21. doi: 10.1210/jc.2013-2036
96. Lundstrom E, Strand R, Johansson L, Bergsten P, Ahlstrom H, Kullberg J. Magnetic resonance imaging cooling-reheating protocol indicates decreased fat fraction via lipid consumption in suspected brown adipose tissue. *PLoS ONE.* (2015) 10:e0126705. doi: 10.1371/journal.pone.0126705
97. Stahl V, Maier F, Freitag MT, Floca RO, Berger MC, Umathum R, et al. *In vivo* assessment of cold stimulation effects on the fat fraction of brown adipose tissue using DIXON MRI. *J Magn Reson Imaging.* (2017) 45:369–80. doi: 10.1002/jmri.25364
98. Deng J, Neff LM, Rubert NC, Zhang B, Shore RM, Samet JD, et al. MRI characterization of brown adipose tissue under thermal challenges in normal weight, overweight, and obese young men. *J Magn Reson Imaging.* (2018) 47:936–47. doi: 10.1002/jmri.25836
99. Coolbaugh CL, Damon BM, Bush EC, Welch EB, Towse TF. Cold exposure induces dynamic, heterogeneous alterations in human brown adipose tissue lipid content. *Sci Rep.* (2019) 9:13600. doi: 10.1038/s41598-019-49936-x
100. Oreskovich SM, Ong FJ, Ahmed BA, Konyer NB, Blondin DP, Gunn E, et al. MRI reveals human brown adipose tissue is rapidly activated in response to cold. *J Endocr Soc.* (2019) 3:2374–84. doi: 10.1210/js.2019-00309
101. Gashi G, Madoerin P, Maushart CI, Michel R, Senn JR, Bieri O, et al. MRI characteristics of supraclavicular brown adipose tissue in relation to cold-induced thermogenesis in healthy human adults. *J Magn Reson Imaging.* (2019) 50:1160–8. doi: 10.1002/jmri.26733
102. Abreu-Vieira G, Sardjoe Mishre ASD, Burakiewicz J, Janssen LGM, Nahon KJ, van der Eijk JA, et al. Human brown adipose tissue estimated with magnetic resonance imaging undergoes changes in composition after cold exposure: an *in vivo* MRI study in healthy volunteers. *Front Endocrinol.* (2019) 10:898. doi: 10.3389/fendo.2019.00898
103. Andersson J, Lundstrom E, Engstrom M, Lubberink M, Ahlstrom H, Kullberg J. Estimating the cold-induced brown adipose tissue glucose uptake rate measured by (18)F-FDG PET using infrared thermography and water-fat separated MRI. *Sci Rep.* (2019) 9:12358. doi: 10.1038/s41598-019-48879-7
104. Sun L, Verma S, Michael N, Chan SP, Yan J, Sadananthan SA, et al. Brown adipose tissue: multimodality evaluation by PET, MRI, infrared thermography, and whole-body calorimetry (TACTICAL-II). *Obesity.* (2019) 27:1434–42. doi: 10.1002/oby.22560
105. Bartelt A, Bruns OT, Reimer R, Hohenberg H, Ittrich H, Peldschus K, et al. Brown adipose tissue activity controls triglyceride clearance. *Nat Med.* (2011) 17:200–5. doi: 10.1038/nm.2297
106. Stanford KI, Middelbeek RJ, Townsend KL, An D, Nygaard EB, Hitchcox KM, et al. Brown adipose tissue regulates glucose homeostasis and insulin sensitivity. *J Clin Invest.* (2013) 123:215–23. doi: 10.1172/JCI62308
107. Feldmann HM, Golozoubova V, Cannon B, Nedergaard J. UCP1 ablation induces obesity and abolishes diet-induced thermogenesis in mice exempt from thermal stress by living at thermoneutrality. *Cell Metab.* (2009) 9:203–9. doi: 10.1016/j.cmet.2008.12.014
108. Chondronikola M, Volpi E, Borsheim E, Porter C, Annamalai P, Enerback S, et al. Brown adipose tissue improves whole-body glucose homeostasis and insulin sensitivity in humans. *Diabetes.* (2014) 63:4089–99. doi: 10.2337/db14-0746
109. Yoneshiro T, Aita S, Matsushita M, Kayahara T, Kameya T, Kawai Y, et al. Recruited brown adipose tissue as an antiobesity agent in humans. *J Clin Invest.* (2013) 123:3404–8. doi: 10.1172/JCI67803
110. Saito M, Okamatsu-Ogura Y, Matsushita M, Watanabe K, Yoneshiro T, Nio-Kobayashi J, et al. High incidence of metabolically active brown adipose tissue in healthy adult humans: effects of cold exposure and adiposity. *Diabetes.* (2009) 58:1526–31. doi: 10.2337/db09-0530
111. Green AL, Bagci U, Hussein S, Kelly PV, Muzaffar R, Neuschwander-Tetri BA, et al. Brown adipose tissue detected by PET/CT imaging is associated with less central obesity. *Nucl Med Commun.* (2017) 38:629–35. doi: 10.1097/MNM.0000000000000691
112. Iwen KA, Backhaus J, Cassens M, Waltl M, Hedesan OC, Merkel M, et al. Cold-induced brown adipose tissue activity alters plasma fatty acids and improves glucose metabolism in men. *J Clin Endocrinol Metab.* (2017) 102:4226–34. doi: 10.1210/jc.2017-01250
113. Matsushita M, Yoneshiro T, Aita S, Kameya T, Sugie H, Saito M. Impact of brown adipose tissue on body fatness and glucose metabolism in healthy humans. *Int J Obes.* (2014) 38:812–7. doi: 10.1038/ijo.2013.206
114. Orava J, Nuutila P, Noponen T, Parkkola R, Viljanen T, Enerback S, et al. Blunted metabolic responses to cold and insulin stimulation in brown adipose tissue of obese humans. *Obesity.* (2013) 21:2279–87. doi: 10.1002/oby.20456
115. Hanssen MJ, Hoeks J, Brans B, van der Lans AA, Schaart G, van den Driessche JJ, et al. Short-term cold acclimation improves insulin sensitivity in patients with type 2 diabetes mellitus. *Nat Med.* (2015) 21:863–5. doi: 10.1038/nm.3891
116. Hanssen MJ, van der Lans AA, Brans B, Hoeks J, Jardon KM, Schaart G, et al. Short-term cold acclimation recruits brown adipose tissue in obese humans. *Diabetes.* (2016) 65:1179–89. doi: 10.2337/db15-1372
117. Cinti S. The adipose organ at a glance. *Dis Model Mech.* (2012) 5:588–94. doi: 10.1242/dmm.009662
118. Branca RT, Zhang L, Warren WS, Auerbach E, Khanna A, Degan S, et al. *In vivo* noninvasive detection of brown adipose tissue through intermolecular zero-quantum MRI. *PLoS ONE.* (2013) 8:e74206. doi: 10.1371/journal.pone.0074206
119. Jones TA, Wayte SC, Reddy NL, Adesanya O, Dimitriadis GK, Barber TM, et al. Identification of an optimal threshold for detecting human brown adipose tissue using receiver operating characteristic analysis of IDEAL MRI fat fraction maps. *Magn Reson Imaging.* (2018) 51:61–8. doi: 10.1016/j.mri.2018.04.013
120. Lemoine AY, Ledoux S, Quéguiner I, Caldérari S, Mechler C, Msika S, et al. Link between adipose tissue angiogenesis and fat accumulation in severely obese subjects. *J Clin Endocrinol Metab.* (2012) 97:E775–80. doi: 10.1210/jc.2011-2649
121. Bhanu Prakash KN, Srour H, Velan SS, Chuang KH. A method for the automatic segmentation of brown adipose tissue. *MAGMA.* (2016) 29:287–99. doi: 10.1007/s10334-015-0517-0
122. Bhanu Prakash KN, Verma SK, Yaligar J, Goggi J, Gopalan V, Lee SS, et al. Segmentation and characterization of interscapular brown adipose tissue in rats by multi-parametric magnetic resonance imaging. *MAGMA.* (2016) 29:277–86. doi: 10.1007/s10334-015-0514-3
123. Lundstrom E, Strand R, Forslund A, Bergsten P, Weghuber D, Ahlstrom H, et al. Automated segmentation of human cervical-supraclavicular adipose tissue in magnetic resonance images. *Sci Rep.* (2017) 7:3064. doi: 10.1038/s41598-017-01586-7
124. Hu HH, Hines CD, Smith DL, Jr., Reeder SB. Variations in T(2)* and fat content of murine brown and white adipose tissues by chemical-shift MRI. *Magn Reson Imaging.* (2012) 30:323–9. doi: 10.1016/j.mri.2011.12.004

125. Franz D, Diefenbach MN, Treibel F, Weidlich D, Syvari J, Ruschke S, et al. Differentiating supraclavicular from gluteal adipose tissue based on simultaneous PDFF and T2 * mapping using a 20-echo gradient-echo acquisition. *J Magn Reson Imaging.* (2019) 50:424–34. doi: 10.1002/jmri.26661
126. Holstila M, Pesola M, Saari T, Koskensalo K, Raiko J, Borra RJ, et al. MR signal-fat-fraction analysis and T2* weighted imaging measure BAT reliably on humans without cold exposure. *Metabolism.* (2017) 70:23–30. doi: 10.1016/j.metabol.2017.02.001
127. Hui SCN, Ko JKL, Zhang T, Shi L, Yeung DKW, Wang D, et al. Quantification of brown and white adipose tissue based on Gaussian mixture model using water-fat and T2* MRI in adolescents. *J Magn Reson Imaging.* (2017) 46:758–68. doi: 10.1002/jmri.25632
128. Warren WS, Lee S, Richter W, Vathyam S. Correcting the classical dipolar demagnetizing field in solution NMR. *Chem Phys Lett.* (1995) 247:207–14. doi: 10.1016/0009-2614(95)01184-5
129. Levitt MH. Demagnetization field effects in two-dimensional solution NMR. *Concept Magn Reson.* (1996) 8:77–103. doi: 10.1002/(SICI)1099-0534(1996)8:2<77::AID-CMR1>3.0.CO;2-L
130. Branca RT, Warren WS. *In vivo* brown adipose tissue detection and characterization using water-lipid intermolecular zero-quantum coherences. *Magn Reson Med.* (2011) 65:313–9. doi: 10.1002/mrm.22622
131. Bao J, Cui X, Cai S, Zhong J, Cai C, Chen Z. Brown adipose tissue mapping in rats with combined intermolecular double-quantum coherence and Dixon water-fat MRI. *NMR Biomed.* (2013) 26:1663–71. doi: 10.1002/nbm.3000
132. Galiana G, Branca RT, Jenista ER, Warren WS. Accurate temperature imaging based on intermolecular coherences in magnetic resonance. *Science.* (2008) 322:421–4. doi: 10.1126/science.1163242
133. Jenista ER, Galiana G, Branca RT, Yarmolenko PS, Stokes AM, Dewhirst MW, et al. Application of mixed spin iMQCs for temperature and chemical-selective imaging. *J Magn Reson.* (2010) 204:208–18. doi: 10.1016/j.jmr.2010.02.021
134. Deng J, Schoeneman SE, Zhang H, Kwon S, Rigsby CK, Shore RM, et al. MRI characterization of brown adipose tissue in obese and normal-weight children. *Pediatr Radiol.* (2015) 45:1682–9. doi: 10.1007/s00247-015-3391-z
135. Dieckmeyer M, Ruschke S, Eggers H, Kooijman H, Rummeny EJ, Kirschke JS, et al. ADC quantification of the vertebral bone marrow water component: removing the confounding effect of residual fat. *Magn Reson Med.* (2017) 78:1432–41. doi: 10.1002/mrm.26550
136. Verma SK, Nagashima K, Yaligar J, Michael N, Lee SS, Xianfeng T, et al. Differentiating brown and white adipose tissues by high-resolution diffusion NMR spectroscopy. *J Lipid Res.* (2017) 58:289–98. doi: 10.1194/jlr.D072298
137. Weidlich D, Honecker J, Gmach O, Wu M, Burgkart R, Ruschke S, et al. Measuring large lipid droplet sizes by probing restricted lipid diffusion effects with diffusion-weighted MRS at 3T. *Magn Reson Med.* (2019) 81:3427–39. doi: 10.1002/mrm.27651
138. Murday JS, Cotts RM. Self-diffusion coefficient of liquid lithium. *J Chem Phys.* (1968) 48:4938–45. doi: 10.1063/1.1668160
139. Weidlich D, Zamskiy M, Maeder M, Ruschke S, Marburg S, Karampinos DC. Reduction of vibration-induced signal loss by matching mechanical vibrational states: application in high b-value diffusion-weighted MRS. *Magn Reson Med*. (2019) 84:39–51. doi: 10.1002/mrm.28128
140. Weidlich D, Hock A, Ruschke S, Franz D, Hauner H, Rummeny EJ, et al., Improving the quality of DW spectra in the supraclavicular fossa with a navigator-gated and cardiac-triggered flow-compensated diffusion-weighted STEAM MRS acquisition. In: *Proceedings of 25th Int Society for Magnetic Resonance in Medicine*. Honolulu, HI (2017).
141. Wu M, Weidlich D, Ruschke S, Franz D, Karampinos DC. On the technical challenges of diffusion-weighted mr spectroscopy for water ADC quantification in human supraclavicular fat. In: *Proceedings of the 27th Int Society for Magnetic Resonance in Medicine.* Montréal, QC (2019).
142. Wu M, Held C, Patzelt L, Weidlich D, Ruschke S, Mengel L, et al. Brown adipose tissue water ADC quantification with Diffusion-Weighted MR Spectroscopy in the human supraclavicular fat. In: *ISMRM Workshop on MRI of Obesity & Metabolic Disorders*. Singapore (2019).
143. van Rooijen BD, van der Lans AA, Brans B, Wildberger JE, Mottaghy FM, Schrauwen P, et al. Imaging cold-activated brown adipose tissue using dynamic T2*-weighted magnetic resonance imaging and 2-deoxy-2-[18F]fluoro-D-glucose positron emission tomography. *Invest Radiol.* (2013) 48:708–14. doi: 10.1097/RLI.0b013e31829363b8
144. Riis-Vestergaard MJ, Breining P, Pedersen SB, Laustsen C, Stodkilde-Jorgensen H, Borghammer P, et al. Evaluation of active brown adipose tissue by the use of hyperpolarized [1-(13)C]pyruvate MRI in Mice. *Int J Mol Sci.* (2018) 19:2597. doi: 10.3390/ijms19092597
145. Lau AZ, Chen AP, Gu Y, Ladouceur-Wodzak M, Nayak KS, Cunningham CH. Noninvasive identification and assessment of functional brown adipose tissue in rodents using hyperpolarized (1)(3)C imaging. *Int J Obes.* (2014) 38:126–31. doi: 10.1038/ijo.2013.58
146. Riis-Vestergaard MJ, Laustsen C, Mariager CØ, Schulte RF, Pedersen SB, Richelsen B. Glucose metabolism in brown adipose tissue determined by deuterium metabolic imaging in rats. *Int J Obesity*. (2020) 44:1–11. doi: 10.1038/s41366-020-0533-7
147. Ernande L, Stanford KI, Thoonen R, Zhang H, Clerte M, Hirshman MF, et al. Relationship of brown adipose tissue perfusion and function: a study through beta2-adrenoreceptor stimulation. *J Appl Physiol.* (2016). 120:825–32. doi: 10.1152/japplphysiol.00634.2015
148. Abreu-Vieira G, Hagberg CE, Spalding KL, Cannon B, Nedergaard J. Adrenergically stimulated blood flow in brown adipose tissue is not dependent on thermogenesis. *Am J Physiol Endocrinol Metab.* (2015) 308:E822–9. doi: 10.1152/ajpendo.00494.2014
149. u Din M, Raiko J, Saari T, Kudomi N, Tolvanen T, Oikonen V, et al. Human brown adipose tissue [15O]O2 PET imaging in the presence and absence of cold stimulus. *Eur J Nuclear Med Mol Imaging.* (2016) 43:1878–86. doi: 10.1007/s00259-016-3364-y
150. Foster DO, Frydman ML. Nonshivering thermogenesis in the rat. II. measurements of blood flow with microspheres point to brown adipose tissue as the dominant site of the calorigenesis induced by noradrenaline. *Can J Physiol Pharmacol.* (1978) 56:110–22. doi: 10.1139/y78-015
151. Wickler SJ, Horwitz BA, Stern JS. Blood flow to brown fat in lean and obese adrenalectomized Zucker rats. *Am J Physiol.* (1986) 251(5 Pt 2):R851–8. doi: 10.1152/ajpregu.1986.251.5.R851
152. Muzik O, Mangner TJ, Granneman JG. Assessment of oxidative metabolism in brown fat using PET imaging. *Front Endocrinol.* (2012) 3:15. doi: 10.3389/fendo.2012.00015
153. Branca RT, McCallister A, Yuan H, Aghajanian A, Faber JE, Weimer N, et al. Accurate quantification of brown adipose tissue mass by xenon-enhanced computed tomography. *Proc Natl Acad Sci USA.* (2018) 115:174–9. doi: 10.1073/pnas.1714431115
154. Antonacci MA, McHugh C, Kelley M, McCallister A, Degan S, Branca RT. Direct detection of brown adipose tissue thermogenesis in UCP1–/– mice by hyperpolarized 129Xe MR thermometry. *Sci Rep.* (2019) 9:14865. doi: 10.1038/s41598-019-51483-4
155. Sbarbati A, Cavallini I, Marzola P, Nicolato E, Osculati F. Contrast-enhanced MRI of brown adipose tissue after pharmacological stimulation. *Magn Reson Med.* (2006) 55:715–8. doi: 10.1002/mrm.20851
156. Yaligar J, Verma SK, Gopalan V, Rengaraj A, Xianfeng T, Velan SS, editors. Evaluation of the vascular perfusion in activated brown adipose tissue by dynamic contrast enhanced MR imaging. In: *Proceedings of 25th Int Society for Magnetic Resonance in Medicine*. Honolulu, HI (2017).
157. Yaligar J, Verma SK, Gopalan V, Anantharaj R, Thu Le GT, Kaur K, et al. Dynamic contrast-enhanced MRI of brown and beige adipose tissues. *Magn Reson Med*. (2019) 84:384–95. doi: 10.1002/mrm.28118
158. Chen YI, Cypess AM, Sass CA, Brownell AL, Jokivarsi KT, Kahn CR, et al. Anatomical and functional assessment of brown adipose tissue by magnetic resonance imaging. *Obesity (Silver Spring).* (2012) 20:1519–26. doi: 10.1038/oby.2012.22
159. Jung CS, Heine M, Freund B, Reimer R, Koziolek EJ, Kaul MG, et al. Quantitative activity measurements of brown adipose tissue at 7 T magnetic resonance imaging after application of triglyceride-rich lipoprotein 59Fe-superparamagnetic iron oxide nanoparticle: intravenous versus intraperitoneal approach. *Invest Radiol.* (2016) 51:194–202. doi: 10.1097/RLI.0000000000000235
160. Dai W, Weines L, Alsop D, Cypess A, editors. Feasibility repeatability of brown adipose tissue volume perfusion activity using MRI. In: *Proceedings of 23rd Int Society for Magnetic Resonance in Medicine*. Toronto, ON (2015).
161. Branca RT, Zhang L, Burant A, Katz L, McCallister A, editors. Detection of human brown adipose tissue by MRI with hyperpolarized Xe-129 gas

validation by FDG-PET/MRI. In: *Proceedings of the 24th Int Society for Magnetic Resonance in Medicine*. Singapore (2016).
162. Bülow J, Jelnes R, Astrup A, Madsen J, Vilmann P. Tissue/blood partition coefficients for xenon in various adipose tissue depots in man. *Scand J Clin Lab Invest.* (1987) 47:1–3. doi: 10.1080/00365518709168861
163. Steward A, Allott PR, Cowles AL, Mapleson WW. Solubility coefficients for inhaled anaesthetics for water, oil and biological media. *Br J Anaesth.* (1973) 45:282–93. doi: 10.1093/bja/45.3.282
164. Franconi F, Lemaire L, Saint-Jalmes H, Saulnier P. Tissue oxygenation mapping by combined chemical shift and T1 magnetic resonance imaging. *Magn Reson Med.* (2018) 79:1981–91. doi: 10.1002/mrm.26857
165. Morozov D, Quirk JD, Beeman SC. Toward noninvasive quantification of adipose tissue oxygenation with MRI. *Int J Obes.* (2020). doi: 10.1038/s41366-020-0567-x. [Epub ahead of print].
166. Khanna A, Branca RT. Detecting brown adipose tissue activity with BOLD MRI in mice. *Magn Reson Med.* (2012) 68:1285–90. doi: 10.1002/mrm.24118
167. Simchick G, Yin A, Yin H, Zhao Q, editors. Dynamic monitoring of brown adipose tissue activation and white adipose tissue beiging. In: *Proceedings of 25th Int Society for Magnetic Resonance in Medicine*. Honolulu, HI (2017).
168. Baron P, Deckers R, Knuttel FM, Bartels LW. T1 and T2 temperature dependence of female human breast adipose tissue at 1.5 T: groundwork for monitoring thermal therapies in the breast. *NMR Biomed.* (2015) 28:1463–70. doi: 10.1002/nbm.3410
169. Ogawa S, Lee TM, Kay AR, Tank DW. Brain magnetic resonance imaging with contrast dependent on blood oxygenation. *Proc Natl Acad Sci USA.* (1990) 87:9868–72. doi: 10.1073/pnas.87.24.9868
170. Bren KL, Eisenberg R, Gray HB. Discovery of the magnetic behavior of hemoglobin: A beginning of bioinorganic chemistry. *Proc Natl Acad Sci USA.* (2015) 112:13123–7. doi: 10.1073/pnas.1515704112
171. Pauling L, Coryell CD. The magnetic properties and structure of hemoglobin. oxyhemoglobin and carbonmonoxyhemoglobin. *Proc Natl Acad Sci USA.* (1936) 22:210–6. doi: 10.1073/pnas.22.4.210
172. Kim SG, Ogawa S. Biophysical and physiological origins of blood oxygenation level-dependent fMRI signals. *J Cereb Blood Flow Metab.* (2012) 32:1188–206. doi: 10.1038/jcbfm.2012.23
173. Birn RM, Murphy K, Handwerker DA, Bandettini PA. fMRI in the presence of task-correlated breathing variations. *Neuroimage.* (2009) 47:1092–104. doi: 10.1016/j.neuroimage.2009.05.030
174. Law J, Chalmers J, Morris DE, Robinson L, Budge H, Symonds ME. The use of infrared thermography in the measurement and characterization of brown adipose tissue activation. *Temperature (Austin).* (2018) 5:147–61. doi: 10.1080/23328940.2017.1397085
175. Gatidis S, Schmidt H, Pfannenberg CA, Nikolaou K, Schick F, Schwenzer NF. Is it possible to detect activated brown adipose tissue in humans using single-time-point infrared thermography under thermoneutral conditions? impact of BMI and subcutaneous adipose tissue thickness. *PLoS ONE.* (2016) 11:e0151152. doi: 10.1371/journal.pone.0151152
176. Hynynen K, McDannold N, Mulkern RV, Jolesz FA. Temperature monitoring in fat with MRI. *Magn Reson Med.* (2000) 43:901–4. doi: 10.1002/1522-2594(200006)43:6<901::AID-MRM18>3.0.CO;2-A
177. Nelson TR, Tung SM. Temperature dependence of proton relaxation times *in vitro*. *Magn Reson Imaging.* (1987) 5:189–99. doi: 10.1016/0730-725X(87)90020-8
178. Chen J, Daniel BL, Pauly KB. Investigation of proton density for measuring tissue temperature. *J Magn Reson Imaging.* (2006) 23:430–4. doi: 10.1002/jmri.20516
179. Le Bihan D, Delannoy J, Levin RL. Temperature mapping with MR imaging of molecular diffusion: application to hyperthermia. *Radiology.* (1989) 171:853–7. doi: 10.1148/radiology.171.3.2717764
180. Soher BJ, Wyatt C, Reeder SB, MacFall JR. Noninvasive temperature mapping with MRI using chemical shift water-fat separation. *Magn Reson Med.* (2010) 63:1238–46. doi: 10.1002/mrm.22310
181. Sprinkhuizen SM, Konings MK, van der Bom MJ, Viergever MA, Bakker CJ, Bartels LW. Temperature-induced tissue susceptibility changes lead to significant temperature errors in PRFS-based MR thermometry during thermal interventions. *Magn Reson Med.* (2010) 64:1360–72. doi: 10.1002/mrm.22531
182. Baron P, Deckers R, Bouwman JG, Bakker CJG, de Greef M, Viergever MA, et al. Influence of water and fat heterogeneity on fat-referenced MR thermometry. *Magn Reson Med.* (2016) 75:1187–97. doi: 10.1002/mrm.25727
183. Zhang L, Burant A, McCallister A, Zhao V, Koshlap KM, Degan S, et al. Accurate MR thermometry by hyperpolarized (129) Xe. *Magn Reson Med.* (2017) 78:1070–9. doi: 10.1002/mrm.26506
184. Paulus A, van Ewijk PA, Nascimento EBM, De Saint-Hubert M, Hendrikx G, Vogg A, et al. Characterization of BAT activity in rats using invasive and non-invasive techniques. *PLoS ONE.* (2019) 14:e0215852. doi: 10.1371/journal.pone.0215852
185. Zhu M, Sun Z, Ng CK. Image-guided thermal ablation with MR-based thermometry. *Quant Imaging Med Surg.* (2017) 7:356–68. doi: 10.21037/qims.2017.06.06
186. Cheng C, Zou C, Wan Q, Qiao Y, Tie C, Pan M, et al. Magnetic resonance temperature imaging in activated brown adipose tissue of rat. In: *Proceedings of 27th Int Society for Magnetic Resonance in Medicine*. Montréal, QC (2019).
187. Zhang L, McCallister A, Koshlap KM, Branca RT. Correlation distance dependence of the resonance frequency of intermolecular zero quantum coherences and its implication for MR thermometry. *Magn Reson Med.* (2018) 79:1429–38. doi: 10.1002/mrm.26801
188. Antonacci MA, Zhang L, Degan S, Erdmann D, Branca RT. Calibration of methylene-referenced lipid-dissolved xenon frequency for absolute MR temperature measurements. *Magn Reson Med.* (2019) 81:765–72. doi: 10.1002/mrm.27441
189. Branca RT, Zhang L, Burant A, Antonacci M, McCallister A, Katz L, editors. Measurements of human brown adipose tissue temperature during cold exposure by hyperpolarized xenon MR thermometry. In: *Proceedings of the 26th Int Society for Magnetic Resonance in Medicine*. Paris (2018).
190. Winter L, Oberacker E, Paul K, Ji Y, Oezerdem C, Ghadjar P, et al. Magnetic resonance thermometry: Methodology, pitfalls and practical solutions. *Int J Hyperthermia.* (2016) 32:63–75. doi: 10.3109/02656736.2015.1108462
191. Hu HH, Branca RT, Hernando D, Karampinos DC, Machann J, McKenzie CA, et al. Magnetic resonance imaging of obesity and metabolic disorders: Summary from the 2019. ISMRM workshop. *Magn Reson Med.* (2020) 83:1565–76. doi: 10.1002/mrm.28103
192. Meineke J, Nielsen T. Data consistency-driven determination of B 0 - fluctuations in gradient-echo MRI. *Magn Reson Med.* (2019) 81:3046–55. doi: 10.1002/mrm.27630
193. van Heteren JG, James TW, Bourne LC. Thin film high temperature superconducting RF coils for low field MRI. *Magn Reson Med.* (1994) 32:396–400. doi: 10.1002/mrm.1910320315
194. In-Tsang L, Chang-Wei H, Li-Wei K, Hong-Chang Y, Ching Y, Wei-Hao C, et al. editors. Implementation of high-temperature superconducting tapes RF coils for 3T MRI system, 2005. In: *IEEE Engineering in Medicine and Biology 27th Annual Conference*. Shanghai (2005).
195. Pruessmann KP. Encoding and reconstruction in parallel MRI. *NMR Biomed.* (2006) 19:288–99. doi: 10.1002/nbm.1042
196. Lustig M, Donoho D, Pauly JM. Sparse MRI: the application of compressed sensing for rapid MR imaging. *Magn Reson Med.* (2007) 58:1182–95. doi: 10.1002/mrm.21391
197. Diefenbach MN, Liu C, Karampinos DC. Generalized parameter estimation in multi-echo gradient-echo-based chemical species separation. *Quant Imaging Med Surg.* (2020) 10:554–67. doi: 10.21037/qims.2020.02.07

Conflict of Interest: The authors declare that the research was conducted in the absence of any commercial or financial relationships that could be construed as a potential conflict of interest.

frontiers in Endocrinology

MINI REVIEW
published: 18 September 2020
doi: 10.3389/fendo.2020.00608

The Transcriptional Role of Vitamin A and the Retinoid Axis in Brown Fat Function

*Carsten T. Herz and Florian W. Kiefer**

Clinical Division of Endocrinology and Metabolism, Department of Medicine III, Medical University of Vienna, Vienna, Austria

In recent years, brown adipose tissue (BAT) has gained significance as a metabolic organ dissipating energy through heat production. Promotion of a thermogenic program in fat holds great promise as potential therapeutic tool to counteract weight gain and related sequelae. Current research efforts are aimed at identifying novel pathways regulating brown fat function and the transformation of white adipocytes into BAT-like cells, a process called "browning." Besides numerous genetic factors some circulating molecules can act as mediators of adipose tissue thermogenesis. Vitamin A metabolites, the retinoids, are potent regulators of gene transcription through nuclear receptor signaling and are thus involved in a plethora of metabolic processes. Accumulating evidence links retinoid action to brown fat function and browning of WAT mainly via orchestrating a transcriptional BAT program in adipocytes including expression of key thermogenic genes such as uncoupling protein 1. Here we summarize the current understanding how retinoids play a role in adipose tissue thermogenesis through transcriptional control of thermogenic gene cassettes and potential non-genomic mechanisms.

Keywords: vitamin A, retinoid, obesity, brown fat, adipose tissue browning, thermogenesis

OPEN ACCESS

Edited by:
Takeshi Yoneshiro,
The University of Tokyo, Japan

Reviewed by:
William S. Blaner,
Columbia University, United States
Shigeki Sugii,
*Institute of Bioengineering and Nanotechnology (A*STAR), Singapore*
Tsuyoshi Goto,
Kyoto University, Japan

***Correspondence:**
Florian W. Kiefer
florian.kiefer@meduniwien.ac.at

Specialty section:
This article was submitted to Obesity, a section of the journal Frontiers in Endocrinology

Received: *21 April 2020*
Accepted: *27 July 2020*
Published: *18 September 2020*

Citation:
Herz CT and Kiefer FW (2020) The Transcriptional Role of Vitamin A and the Retinoid Axis in Brown Fat Function. Front. Endocrinol. 11:608. doi: 10.3389/fendo.2020.00608

BROWN ADIPOSE TISSUE AND BROWNING OF WHITE FAT

Brown adipose tissue (BAT) is an adipose organ specialized in producing heat to maintain body temperature. Brown adipocytes, in contrast to white adipocytes, are rich in mitochondria and are characterized by a large number of small multilocular lipid droplets as compared to unilocular lipid droplets in white adipocytes (1). The mitochondria of brown adipocytes express uncoupling protein 1 (UCP1) in the inner mitochondrial membrane which, when activated, uncouples the proton motive forced generated by mitochondrial oxidative metabolism from ATP synthesis and thereby dissipates chemical energy as heat (1). Promotion of brown fat thermogenesis counteracts obesity and related complications in numerous animal models and has therefore evolved as a promising novel therapeutic concept in the fight against the human obesity epidemic (2). Classical BAT depots, as most comprehensively described in rodents, embody mainly interscapular, axillar, cervical, femoral, and perirenal depots (1). However, brown-like or so-called beige adipocytes can also be found in white adipose tissue (WAT) depots, predominantly in subcutaneous fat and to a lesser extent in visceral fat (3). Stimulation of BAT thermogenesis classically occurs through hypothalamic noradrenergic signaling via the β3-adrenergic pathway in response to cold (1). This results in activation of protein kinase A (PKA) which promotes

intracellular lipolysis and acts through the p38 MAPK as well as the CREB pathway which increases the expression of genes essential for the maintenance of thermogenic function such as UCP1, DIO2, and PGC1α (4). The emergence of beige adipocytes in WAT, coined "browning," can occur in response to various stimuli including a number of genetic factors, hormones and chronic cold exposure. Beige cells can possess characteristics of both, classic white and brown adipocytes. When activated, beige fat cells express significant amounts of UCP1 and contribute toward thermogenesis and energy expenditure (4). It remains a matter of debate whether these newly formed beige adipocytes stem from mature white adipocytes undergoing conversion to UCP1-expressing cells following thermogenic stimuli or if a pool of distinct precursor cells gives rise to beige adipocytes. Elegant lineage tracing studies in mice provided evidence for both theories (5, 6).

Whereas, the salutary metabolic effects of brown fat have been unequivocally demonstrated in rodents, the impact of BAT physiology on human energy metabolism and its relevance for metabolic disease is less well-understood. Currently, the gold standard for the detection and quantification of active BAT in humans is ^{18}F-fluorodeoxyglucose positron emission tomography/computed tomography (^{18}F-FDG PET/CT) (7). The most potent physiologic stimulus for BAT activation is cold exposure that results in significant uptake of ^{18}F-FDG in thermogenically active BAT depots and correlates in many studies with increased energy expenditure (8–11). The inverse relationships between active BAT and the degree of obesity and age also supports a potential protective role of BAT in metabolic disorders in humans (8, 12–14). Cold-induced BAT activity is mainly found in deep cervical, supraclavicular, para-aortal, and some renal fat depots in human adults (15). However, BAT in humans is not an organ as easily delineated from WAT as *bona fide* murine BAT since it comprises a mixture of brown and white adipocytes (16). The emergence of unilocular adipocytes in brown fat depots, called BAT whitening, has been demonstrated in animal models of aging and obesity (17, 18) and can be experimentally induced by high ambient temperature and defective β-adrenergic signaling, resulting in brown adipocyte death and inflammation (19). In contrast, clinical studies have found that repeated cold exposure over the course of 2 to 6 weeks, successfully increased the amount of active BAT as evidenced by ^{18}F-FDG-PET/CT imaging in lean and overweight individuals as well as patients with diabetes, respectively (9, 20–23). The observed changes in BAT mass were accompanied by reductions in body fatness and improvements in insulin sensitivity (9, 21, 23). These findings not only suggest that thermogenically active BAT can be recruited in humans but emphasize the potential for therapies targeted at BAT with the aim to re-establish relevant amounts in BAT-depleted states such as obesity or older age and thus reverse associated metabolic aberrations.

VITAMIN A AND RETINOID METABOLISM

Besides their functions in cell differentiation, embryonic development, reproduction, retinal function and immunity, vitamin A and its metabolites, the retinoids, have been recognized as important regulators of energy metabolism (24). Vitamin A must be obtained from the diet by intake of either preformed retinol or provitamin A (carotenoids) which can be converted to retinol by beta-carotene monooxygenase. After absorption, the majority (∼90%) is stored in the liver, while a smaller part (∼10%) is stored in adipocytes (25, 26). In the liver, vitamin A is primarily stored in the form of retinyl esters in cytoplasmic lipid droplets of hepatic stellate cells (80–90%) and hepatocytes (10–20%) (25). Mobilization occurs via hydrolysis and binding to retinol binding protein (RBP) which transports retinol to the target tissues (25). In adipocytes, RBP-bound retinol is taken up by the multi-transmembrane cell surface receptor STRA6 (27). Intracellularly, retinol is then either re-esterified or converted to retinoic acid via two oxidative reactions: In the first step, retinol is reversibly oxidized to retinaldehyde (Rald) by alcohol– and retinol dehydrogenases (ADHs, RDHs) followed by irreversible oxidation to retinoic acid. The enzyme class of retinaldehyde dehydrogenases (RALDHs) has been identified to catalyze this rate-limiting step of retinoid metabolism. Intracellular retinoic acid availability and nuclear transport is facilitated by cellular retinoic acid-binding proteins and fatty acid binding protein 4 (28–30). Retinoic acid signals predominantly through the nuclear receptors retinoic acid receptors (RAR), retinoid X receptors (RXR) and peroxisome proliferator-activated receptors (PPAR) (24, 31) and is thus a potent regulator or gene transcription (**Figure 1**). While 9-cis retinoic acid has been found to be a potent ligand for RXR, its physiological relevance is under debate (32, 33). Quantification of 9-cis retinoic acid failed in most tissues of mice, rats and humans (34, 35). Despite a questionable physiological role, endogenous 9-cis retinoic acids or synthetic analogs might still be promising candidates for the activation of a thermogenic program in adipocytes through RXR, as discussed in the following section.

RETINOIDS AND TRANSCRIPTIONAL CONTROL OF THE THERMOGENIC PROGRAM

Accumulating evidence suggests that retinoids are involved in a number of metabolic processes including glucose and lipid metabolism, adipocyte differentiation and thermogenic programming of fat cells. Retinoid actions on metabolic pathways mainly depend on the regulation of gene expression through the nuclear receptor RAR and RXR which can also form RAR/RXR heterodimers. In addition, RXR works in concert with PPARγ, another key nuclear receptor controlling energy pathways and particularly adipocyte function (**Figure 1**). In 3T3-L1 cells, a murine model for white adipocytes, the effects of retinoic acid can vary dependent upon the stage of adipogenesis and expression of the transcription factors RAR, RXR, and PPARγ. Early in adipogenesis, retinoic acid inhibits whereas after 48 h of differentiation it promotes fat cell formation (36). The silencing mediator of retinoid and thyroid hormone receptors (SMRT) serves as a corepressor for nuclear receptors and regulates adipocyte differentiation, adipose tissue accumulation

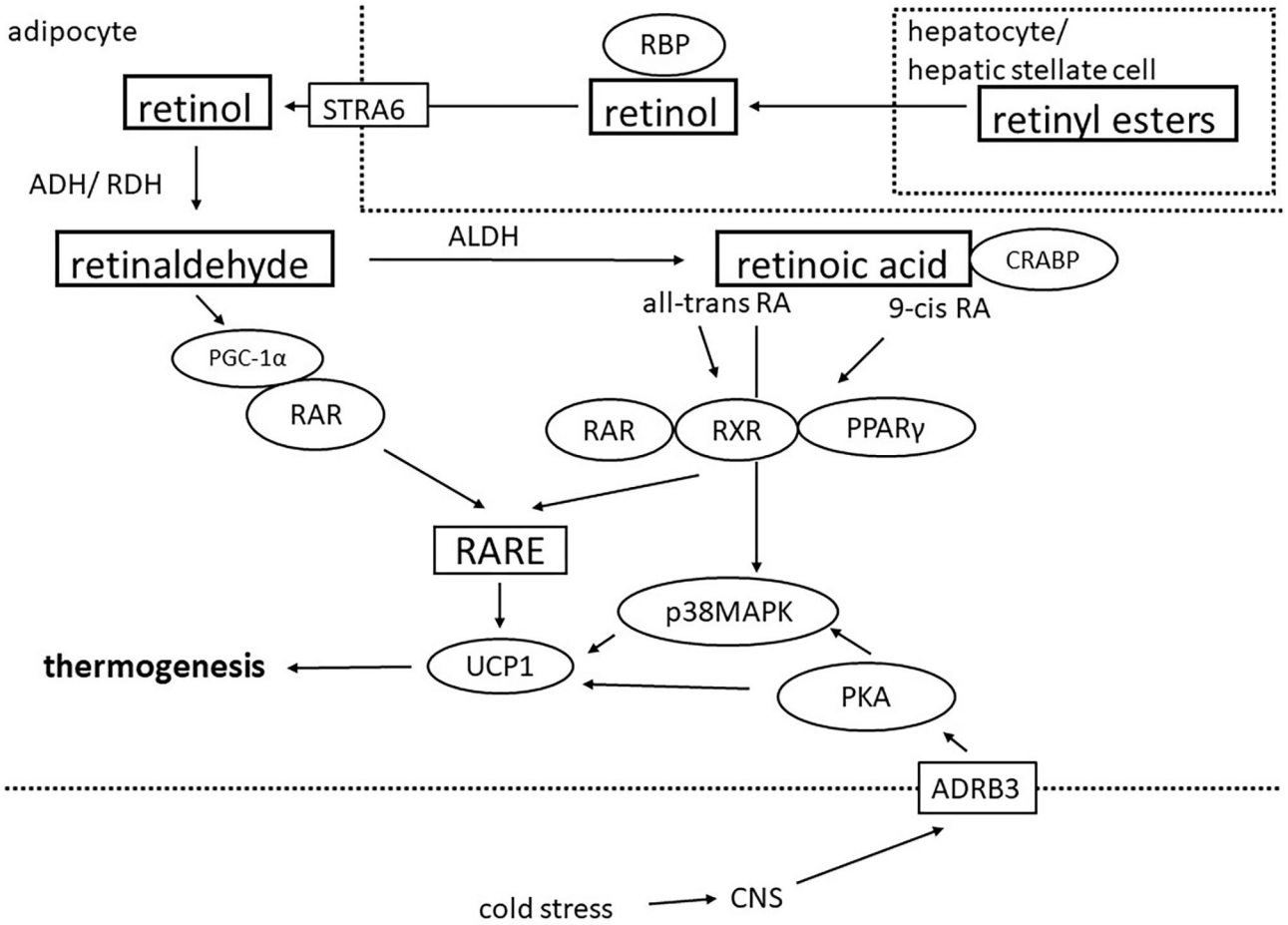

FIGURE 1 | Schematic showing how retinoids regulate thermogenic gene expression in adipocytes. Retinoids are mainly stored as retinyl esters stored in hepatic stellate cells or hepatocytes and can be transported as retinol bound to retinol-binding protein (RBP) to peripheral tissues including adipose tissue. After uptake via the multi-transmembrane cell surface receptor STRA6, retinol is oxidized by alcohol- and retinol dehydrogenases (ADH/ RDH) to retinaldehyde which in the next step gets converted to retinoic acid (RA) by aldehyde dehydrogenases (ALDH). In the cytosol, retinoic acid is bound to cellular retinoic acid binding proteins (CRABP). Retinaldehyde and all-trans RA can activate the nuclear retinoic acid receptor (RAR) while 9-cis RA activates both RAR and retinoid X receptor (RXR). RXR also forms heterodimers with peroxisome proliferator-activated receptor gamma (PPARγ). RAR and RXR bind as homo- or heterodimers to genomic retinoic acid response elements (RARE) which can be found in the promoter region of the UCP1 gene and thereby regulate thermogenic gene expression. In addition, cold stress is the canonical activator of the thermogenic program in adipocytes via stimulation of the central nervous system (CNS). Efferent sympathetic neurons activate membrane-bound β3-adrenergic receptors (ADRB3) which leads to activation of the protein kinase A (PKA)-p38 mitogen-activated protein kinase (p38MAPK) pathway resulting in the transcription of UCP-1 and other thermogenic genes.

and insulin sensitivity. SMRT knockout mice have higher body weight on high-fat diet but increased insulin-mediated glucose disposal possibly due to a combination mechanisms involving an increased number of smaller subcutaneous adipocytes as well as decreased leptin expression, resulting in greater caloric intake (37). Some evidence suggests that retinoids can also act through non-genomic mechanisms such as protein retinoylation, a posttranslational modification shown to mediate cell differentiation, cell growth and possibly steroidogenesis (38). In recent years retinoids have been repeatedly linked to the transcriptional control of a brown fat program. Already in 1995, it was first reported that all-trans retinoic acid induced Ucp1 expression in murine brown adipocytes independent of differentiation status. Retinoic acid-response elements were found in the upstream region of the rat Ucp1 gene and RARα was identified as a mediator of the UCP1 responsiveness to retinoic acid (39–41) (**Figure 1**). However, studies showing that the RXR ligand 9-cis-retinioc acid also promoted Ucp1 expression in brown adipocytes to a similar extent as noradrenaline suggested that RXR may also be involved in inducing a BAT transcriptional program. Indeed, co-transfection of murine expression vectors for the different RAR and RXR subtypes indicated that RARα, RARβ, and RXRα are the major retinoid-receptor subtypes mediating the transcriptional response of Ucp1 to retinoids (42). PPARδ is another nuclear receptor regulated by all-trans retinoic acid with the potential to regulate BAT activity (43).

In murine adipocyte cell lines, the effect of all-trans retinoic acid on thermogenic gene expression has however been shown to be independent of PPARδ (44). Retinoic acid may also alter the thermogenic capacity of brown adipocytes by non-genomic effects via induction of p38/MAPK phosphorylation (45). *In vivo*, the administration of both all-trans retinoic acid and 9-cis-retinioc acid markedly increased Ucp1 expression in brown fat depots in mice. 9-cis-retinoic acid even prevented BAT whitening through cold de-acclimation (46). In accordance, dietary supplementation of vitamin A in the form of retinyl acetate for 8-weeks significantly augmented Ucp1 expression in BAT of rats while decreasing the WAT marker leptin. Whole body adiposity was modestly reduced whereas feeding mice a retinol-deficient diet had the opposite effects (47, 48). Besides promoting thermogenic activity in *bona fide* brown adipocyte, retinoids also induce the emergence of brown-like thermogenic adipocytes in white adipose tissue depots: A four day subcutaneous treatment with all-trans retinoic acid in mice kept at thermoneutrality (30°C) which precludes sympathetic outflow to BAT and WAT due to cold stress resulted in higher expression levels of thermogenic genes as well as the appearance of multilocular adipocytes in the inguinal WAT depot (49). More recently, retinoic acid treatment in mice was shown to induce WAT browning by increasing adipose vascularity and promoting beige adipogenesis of platelet-derived growth factor receptor α positive adipose progenitors (50).

Besides retinoic acid, the precursor Rald has been identified as a signaling molecule in fat. Rald is essential in molecular vision processes, however a biological function outside the eye had long remained unknown. Work by Jorge Plutzky's group found that Rald is present in rodent WAT. *In vitro* stimulation with Rald inhibited white adipogenic differentiation in 3T3-L1 cells but markedly enhanced thermogenic gene expression in differentiated mesenchymal stem cells and primary human white adipocytes (51, 52). Rald treatment in murine adipocytes resulted in recruitment of the transcriptional co-activator Pgc1 to RAR present at the Ucp1 promoter. These transcriptional effects of Rald on thermogenesis were RAR-dependent. Mice deficient in Adh1a1, the enzyme converting Rald to retinoic acid, had elevated Rald levels in fat and were protected from diet-induced obesity due to increased energy dissipation. Mechanistically, Aldh1a1 deficiency promoted a thermogenic program in subcutaneous and even more so in visceral fat which rendered Aldh1a1$^{-/-}$ mice cold resistant. This thermogenic phenotype was reversible when Aldh1a1 deficient mice were treated with an RAR antagonist. WAT-selective knockdown of Aldh1a1 by antisense oligonucleotides conferred a similar thermogenic program as in Aldh1a1$^{-/-}$ mice, prevented diet-induced weight gain and improved glucose metabolism in mice suggesting that targeting Aldh1a1 in fat could be a potential therapeutic approach counteracting metabolic disease. Notably, Aldh1a1 is abundantly expressed in human visceral adipose tissue and increases with obesity (51, 52). In contrast, ablation of retinol dehydrogenase 1 (Rdh1) seems to have opposite effects. Rdh1 deficiency suppressed adiposity by promoting brown adipose adaptation to fasting and re-feeding. It has been shown that BAT activity is suppressed during fasting to preserve energy but it also contributes to diet induced-thermogenesis after food intake (10, 53, 54). Rdh1-null mice had lower body temperatures and a lower expression of Ucp1 in BAT. Mechanistically, Rdh1-deficiency resulted in decreased all-trans retinoic acid levels in BAT levels after refeeding which impaired lipolysis that is crucial for proper BAT function (55).

Whereas, all these data suggest that retinoids control thermogenic gene expression and BAT function, the retinoid pathways may also be regulated by cold exposure and adrenergic stimulation. The retinol transport protein RBP is induced by norepinephrine, cAMP and activators of PPARγ and PPARα in brown adipocytes. This effect requires the action of PPARγ-coactivator-1α and is absent in PPARα deficient adipocytes, suggesting that PPAR signaling is required of adrenergic induction of RBP in brown adipocytes (56).

All these reports show promise that retinoid pathways could serve as therapeutic targets to enhance energy expenditure and counteract obesity. Even though most reports stem from animal experiments, some *in vitro* studies in primary human adipocytes suggest that retinoids may also modulate thermogenic pathways in human fat (52). However, clinical studies on the association between retinoids and brown fat activity are lacking. Hence, validation of the previous preclinical findings in humans is warranted.

CONCLUSION

Retinoids are vitamin A derivatives that are tightly regulated by a network of converting enzymes. Retinoic acid has been established as potent transcriptional regulator of thermogenic gene expression in adipose tissue, both, *in vitro* and *in vivo*. However, recent evidence suggest that retinoic acid is not the only biologically active vitamin A metabolite regulating thermogenic processes in adipocytes. Also the precursors, retinol and retinaldehyde may have independent biological functions in adipose thermogenesis. Targeting the retinoid pathway e.g., by interfering with retinoid converting enzymes that alter retinoid concentrations in selective tissues may offer novel therapeutic avenues to harness the energy dissipating qualities of BAT and beige fat for counteracting obesity and associated metabolic complications.

AUTHOR CONTRIBUTIONS

All authors listed have made a substantial, direct and intellectual contribution to the work, and approved it for publication.

FUNDING

This work was supported by the Vienna Science and Technology Fund (WWTF) LS12-059 and the Austrian Science Fund (FWF) P 27391-B26 (both to FWK).

REFERENCES

1. Cannon B, Nedergaard J. Brown adipose tissue: function and physiological significance. *Physiol Rev.* (2004) 84:277–359. doi: 10.1152/physrev.00015.2003
2. Herz CT, Kiefer FW. Adipose tissue browning in mice and humans. *J Endocrinol.* (2019) 241:R97–109. doi: 10.1530/JOE-18-0598
3. Cousin B, Cinti S, Morroni M, Raimbault S, Ricquier D, Pénicaud L, et al. Occurrence of brown adipocytes in rat white adipose tissue: molecular and morphological characterization. *J Cell Sci.* (1992) 103:931–42.
4. Cinti S. Adipose organ development and remodeling. *Compr Physiol.* (2018) 8:1357–431. doi: 10.1002/cphy.c170042
5. Barbatelli G, Murano I, Madsen L, Hao Q, Jimenez M, Kristiansen K, et al. The emergence of cold-induced brown adipocytes in mouse white fat depots is determined predominantly by white to brown adipocyte transdifferentiation. *Am J Physiol Endocrinol Metab.* (2010) 298:E1244–53. doi: 10.1152/ajpendo.00600.2009
6. Wang QA, Tao C, Gupta RK, Scherer PE. Tracking adipogenesis during white adipose tissue development, expansion and regeneration. *Nat Med.* (2013) 19:1338–44. doi: 10.1038/nm.3324
7. Chen KY, Cypess AM, Laughlin MR, Haft CR, Hu HH, Bredella MA, et al. Brown Adipose Reporting Criteria in Imaging STudies (BARCIST 1.0): recommendations for standardized FDG-PET/CT experiments in humans. *Cell Metab.* (2016) 24:210–22. doi: 10.1016/j.cmet.2016.07.014
8. van Marken Lichtenbelt WD, Vanhommerig JW, Smulders NM, Drossaerts JMAFL, Kemerink GJ, Bouvy ND, et al. Cold-activated brown adipose tissue in healthy men. *N Engl J Med.* (2009) 360:1500–8. doi: 10.1056/NEJMoa0808718
9. Yoneshiro T, Aita S, Matsushita M, Kayahara T, Kameya T, Kawai Y, et al. Recruited brown adipose tissue as an antiobesity agent in humans. *J Clin Invest.* (2013) 123:3404–8. doi: 10.1172/JCI67803
10. Hibi M, Oishi S, Matsushita M, Yoneshiro T, Yamaguchi T, Usui C, et al. Brown adipose tissue is involved in diet-induced thermogenesis and whole-body fat utilization in healthy humans. *Int J Obes.* (2016) 40:1655–61. doi: 10.1038/ijo.2016.124
11. Yoneshiro T, Aita S, Matsushita M, Kameya T, Nakada K, Kawai Y, et al. Brown adipose tissue, whole-body energy expenditure, and thermogenesis in healthy adult men. *Obesity.* (2011) 19:13–6. doi: 10.1038/oby.2010.105
12. Virtanen KA, Lidell ME, Orava J, Heglind M, Westergren R, Niemi T, et al. Functional brown adipose tissue in healthy adults. *N Engl J Med.* (2009) 360:1518–25. doi: 10.1056/NEJMoa0808949
13. Saito M, Okamatsu-Ogura Y, Matsushita M, Watanabe K, Yoneshiro T, Nio-Kobayashi J, et al. High incidence of metabolically active brown adipose tissue in healthy adult humans: effects of cold exposure and adiposity. *Diabetes.* (2009) 58:1526–31. doi: 10.2337/db09-0530
14. Yoneshiro T, Aita S, Matsushita M, Okamatsu-Ogura Y, Kameya T, Kawai Y, et al. Age-related decrease in cold-activated brown adipose tissue and accumulation of body fat in healthy humans. *Obesity.* (2011) 19:1755–60. doi: 10.1038/oby.2011.125
15. Leitner BP, Huang S, Brychta RJ, Duckworth CJ, Baskin AS, McGehee S, et al. Mapping of human brown adipose tissue in lean and obese young men. *Proc Natl Acad Sci USA.* (2017) 114:8649–54. doi: 10.1073/pnas.1705287114
16. Zingaretti MC, Crosta F, Vitali A, Guerrieri M, Frontini A, Cannon B, et al. The presence of UCP1 demonstrates that metabolically active adipose tissue in the neck of adult humans truly represents brown adipose tissue. *FASEB J.* (2009) 23:3113–20. doi: 10.1096/fj.09-133546
17. Cinti S, Frederich RC, Zingaretti MC, De Matteis R, Flier JS, Lowell BB. Immunohistochemical localization of leptin and uncoupling protein in white and brown adipose tissue. *Endocrinology.* (1997) 138:797–804. doi: 10.1210/endo.138.2.4908
18. Sbarbati A, Morroni M, Zancanaro C, Cinti S. Rat interscapular brown adipose tissue at different ages: a morphometric study. *Int J Obes.* (1991) 15:581–7.
19. Kotzbeck P, Giordano A, Mondini E, Murano I, Severi I, Venema W, et al. Brown adipose tissue whitening leads to brown adipocyte death and adipose tissue inflammation. *J Lipid Res.* (2018) 59:784–94. doi: 10.1194/jlr.M079665
20. Hanssen MJW, van der Lans AAJJ, Brans B, Hoeks J, Jardon KMC, Schaart G, et al. Short-term cold acclimation recruits brown adipose tissue in obese humans. *Diabetes.* (2016) 65:1179–89. doi: 10.2337/db15-1372
21. Hanssen MJW, Hoeks J, Brans B, van der Lans AAJJ, Schaart G, van den Driessche JJ, et al. Short-term cold acclimation improves insulin sensitivity in patients with type 2 diabetes mellitus. *Nat Med.* (2015) 21:863–5. doi: 10.1038/nm.3891
22. van der Lans AAJJ, Hoeks J, Brans B, Vijgen GHEJ, Visser MGW, Vosselman MJ, et al. Cold acclimation recruits human brown fat and increases nonshivering thermogenesis. *J Clin Invest.* (2013) 123:3395–403. doi: 10.1172/JCI68993
23. Lee P, Smith S, Linderman J, Courville AB, Brychta RJ, Dieckmann W, et al. Temperature-acclimated brown adipose tissue modulates insulin sensitivity in humans. *Diabetes.* (2014) 63:3686–98. doi: 10.2337/db14-0513
24. Blaner WS. Vitamin A signaling and homeostasis in obesity, diabetes, and metabolic disorders. *Pharmacol Ther.* (2019) 197:153–78. doi: 10.1016/j.pharmthera.2019.01.006
25. Blaner WS, Li Y, Brun PJ, Yuen JJ, Lee SA, Clugston RD. Vitamin A absorption, storage and mobilization. *Subcell Biochem.* (2016) 81:95–125. doi: 10.1007/978-94-024-0945-1_4
26. Perumal J, Sriram S, Lim HQ, Olivo M, Sugii S. Retinoic acid is abundantly detected in different depots of adipose tissue by SERS. *Adipocyte.* (2016) 5:378–83. doi: 10.1080/21623945.2016.1245817
27. Kawaguchi R, Zhong M, Kassai M, Ter-Stepanian M, Sun H. Vitamin A transport mechanism of the multitransmembrane cell-surface receptor STRA6. *Membranes.* (2015) 5:425–53. doi: 10.3390/membranes5030425
28. Dong D, Ruuska SE, Levinthal DJ, Noy N. Distinct roles for cellular retinoic acid-binding proteins I and II in regulating signaling by retinoic acid. *J Biol Chem.* (1999) 274:23695–8. doi: 10.1074/jbc.274.34.23695
29. Sessler RJ, Noy N. A ligand-activated nuclear localization signal in cellular retinoic acid binding protein-II. *Mol Cell.* (2005) 18:343–53. doi: 10.1016/j.molcel.2005.03.026
30. Tan N-S, Shaw NS, Vinckenbosch N, Liu P, Yasmin R, Desvergne B, et al. Selective cooperation between fatty acid binding proteins and peroxisome proliferator-activated receptors in regulating transcription. *Mol Cell Biol.* (2002) 22:5114–27. doi: 10.1128/MCB.22.14.5114-5127.2002
31. Ziouzenkova O, Plutzky J. Retinoid metabolism and nuclear receptor responses: new insights into coordinated regulation of the PPAR-RXR complex. *FEBS Lett.* (2008) 582:32–8. doi: 10.1016/j.febslet.2007.11.081
32. Heyman RA, Mangelsdorf DJ, Dyck JA, Stein RB, Eichele G, Evans RM, Thaller C. 9-cis retinoic acid is a high affinity ligand for the retinoid X receptor. *Cell.* (1992) 68:397–406. doi: 10.1016/0092-8674(92)90479-V
33. Wolf G. Is 9-cis-retinoic acid the endogenous ligand for the retinoic acid-X receptor? *Nutr Rev.* (2006) 64:532–8. doi: 10.1111/j.1753-4887.2006.tb00186.x
34. Schmidt CK, Brouwer A, Nau H. Chromatographic analysis of endogenous retinoids in tissues and serum. *Anal Biochem.* (2003) 315:36–48. doi: 10.1016/S0003-2697(02)00662-0
35. Yamakoshi Y, Fukasawa H, Yamauchi T, Waki H, Kadowaki T, Shudo K, et al. Determination of endogenous levels of retinoic acid isomers in type II diabetes mellitus patients. Possible correlation with HbA1c values. *Biol Pharm Bull.* (2002) 25:1268–71. doi: 10.1248/bpb.25.1268
36. Xue JC, Schwarz EJ, Chawla A, Lazar MA. Distinct stages in adipogenesis revealed by retinoid inhibition of differentiation after induction of PPARgamma. *Mol Cell Biol.* (1996) 16:1567–75. doi: 10.1128/MCB.16.4.1567
37. Sutanto MM, Ferguson KK, Sakuma H, Ye H, Brady MJ, Cohen RN. The silencing mediator of retinoid and thyroid hormone receptors (SMRT) regulates adipose tissue accumulation and adipocyte insulin sensitivity in vivo. *J Biol Chem.* (2010) 285:18485–95. doi: 10.1074/jbc.M110.107680
38. Brun PJ, Yang KJZ, Lee SA, Yuen JJ, Blaner WS. Retinoids: potent regulators of metabolism. *Biofactors.* (2013) 39:151–63. doi: 10.1002/biof.1056
39. Alvarez R, de Andrés J, Yubero P, Viñas O, Mampel T, Iglesias R, et al. A novel regulatory pathway of brown fat thermogenesis. Retinoic acid is a transcriptional activator of the mitochondrial uncoupling protein gene. *J Biol Chem.* (1995) 270:5666–73. doi: 10.1074/jbc.270.10.5666

40. Rabelo R, Reyes C, Schifman A, Silva JE. A complex retinoic acid response element in the uncoupling protein gene defines a novel role for retinoids in thermogenesis. *Endocrinology.* (1996) 137:3488–96. doi: 10.1210/endo.137.8.8754778
41. Bonet ML, Puigserver P, Serra F, Ribot J, Vázquez F, Pico C, et al. Retinoic acid modulates retinoid X receptor alpha and retinoic acid receptor alpha levels of cultured brown adipocytes. *FEBS Lett.* (1997) 406:196–200. doi: 10.1016/S0014-5793(97)00274-3
42. Alvarez R, Checa M, Brun S, Viñas O, Mampel T, Iglesias R, et al. Both retinoic-acid-receptor- and retinoid-X-receptor-dependent signalling pathways mediate the induction of the brown-adipose-tissue-uncoupling-protein-1 gene by retinoids. *Biochem J.* (2000) 345:91–7. doi: 10.1042/bj3450091
43. Shaw N, Elholm M, Noy N. Retinoic acid is a high affinity selective ligand for the peroxisome proliferator-activated receptor beta/delta. *J Biol Chem.* (2003) 278:41589–92. doi: 10.1074/jbc.C300368200
44. Murholm M, Isidor MS, Basse AL, Winther S, Sørensen C, Skovgaard-Petersen J, et al. Retinoic acid has different effects on UCP1 expression in mouse and human adipocytes. *BMC Cell Biol.* (2013) 14:41. doi: 10.1186/1471-2121-14-41
45. Teruel T, Hernandez R, Benito M, Lorenzo M. Rosiglitazone and retinoic acid induce uncoupling protein-1 (UCP-1) in a p38 mitogen-activated protein kinase-dependent manner in fetal primary brown adipocytes. *J Biol Chem.* (2003) 278:263–9. doi: 10.1074/jbc.M207200200
46. Puigserver P, Vázquez F, Bonet ML, Picó C, Palou A. *In vitro* and *in vivo* induction of brown adipocyte uncoupling protein (thermogenin) by retinoic acid. *Biochem J.* (1996) 317 (Pt3):827–33. doi: 10.1042/bj3170827
47. Kumar MV, Sunvold GD, Scarpace PJ. Dietary vitamin A supplementation in rats: suppression of leptin and induction of UCP1 mRNA. *J Lipid Res.* (1999) 40:824–9.
48. Bonet ML, Oliver J, Picó C, Felipe F, Ribot J, Cinti S, et al. Opposite effects of feeding a vitamin A-deficient diet and retinoic acid treatment on brown adipose tissue uncoupling protein 1 (UCP1), UCP2 and leptin expression. *J Endocrinol.* (2000) 166:511–7. doi: 10.1677/joe.0.1660511
49. Mercader J, Ribot J, Murano I, Felipe F, Cinti S, Bonet ML, et al. Remodeling of white adipose tissue after retinoic acid administration in mice. *Endocrinology.* (2006) 147:5325–32. doi: 10.1210/en.2006-0760
50. Wang B, Fu X, Liang X, Deavila JM, Wang Z, Zhao L, et al. Retinoic acid induces white adipose tissue browning by increasing adipose vascularity and inducing beige adipogenesis of PDGFRα+ adipose progenitors. *Cell Discov.* (2017) 3:17036. doi: 10.1038/celldisc.2017.36
51. Ziouzenkova O, Orasanu G, Sharlach M, Akiyama TE, Berger JP, Viereck J, et al. Retinaldehyde represses adipogenesis and diet-induced obesity. *Nat Med.* (2007) 13:695–702. doi: 10.1038/nm1587
52. Kiefer FW, Vernochet C, O'Brien P, Spoerl S, Brown JD, Nallamshetty S, et al. Retinaldehyde dehydrogenase 1 regulates a thermogenic program in white adipose tissue. *Nat Med.* (2012) 18:918–25. doi: 10.1038/nm.2757
53. Hanssen MJW, Wierts R, Hoeks J, Gemmink A, Brans B, Mottaghy FM, et al. Glucose uptake in human brown adipose tissue is impaired upon fasting-induced insulin resistance. *Diabetologia.* (2015) 58:586–95. doi: 10.1007/s00125-014-3465-8
54. U Din M, Saari T, Raiko J, Kudomi N, Maurer SF, Lahesmaa M, et al. Postprandial oxidative metabolism of human brown fat indicates thermogenesis. *Cell Metab.* (2018) 28:207–16.e3. doi: 10.1016/j.cmet.2018.05.020
55. Krois CR, Vuckovic MG, Huang P, Zaversnik C, Liu CS, Gibson CE, et al. RDH1 suppresses adiposity by promoting brown adipose adaptation to fasting and re-feeding. *Cell Mol Life Sci.* (2019) 76:2425–47. doi: 10.1007/s00018-019-03046-z
56. Rosell M, Hondares E, Iwamoto S, Gonzalez FJ, Wabitsch M, Staels B, et al. Peroxisome proliferator-activated receptors-α and -γ, and cAMP-mediated pathways, control retinol-binding protein-4 gene expression in brown adipose tissue. *Endocrinology.* (2012) 153:1162–73. doi: 10.1210/en.2011-1367

Conflict of Interest: The authors declare that the research was conducted in the absence of any commercial or financial relationships that could be construed as a potential conflict of interest.

Advantages of publishing in Frontiers

OPEN ACCESS
Articles are free to read for greatest visibility and readership

FAST PUBLICATION
Around 90 days from submission to decision

HIGH QUALITY PEER-REVIEW
Rigorous, collaborative, and constructive peer-review

TRANSPARENT PEER-REVIEW
Editors and reviewers acknowledged by name on published articles

Frontiers
Avenue du Tribunal-Fédéral 34
1005 Lausanne | Switzerland

Visit us: www.frontiersin.org
Contact us: info@frontiersin.org | +41 21 510 17 00

REPRODUCIBILITY OF RESEARCH
Support open data and methods to enhance research reproducibility

DIGITAL PUBLISHING
Articles designed for optimal readership across devices

FOLLOW US
@frontiersin

IMPACT METRICS
Advanced article metrics track visibility across digital media

EXTENSIVE PROMOTION
Marketing and promotion of impactful research

LOOP RESEARCH NETWORK
Our network increases your article's readership